TOWARDS A CHARACTERISTIC EQUATION FOR PERMEABILITY

A Thesis

by

ADIL AHMED SIDDIQUI

Submitted to the Office of Graduate Studies of
Texas A&M University
in partial fulfillment of the requirements for the degree of

MASTER OF SCIENCE

August 2008

Major Subject: Petroleum Engineering

TOWARDS A CHARACTERISTIC EQUATION FOR PERMEABILITY

A Thesis

by

ADIL AHMED SIDDIQUI

Submitted to the Office of Graduate Studies of
Texas A&M University
in partial fulfillment of the requirements for the degree of

MASTER OF SCIENCE

Approved by:

Chair of Committee,	Thomas A. Blasingame
Committee Member,	Walter B. Ayers
	Richard Gibson
Head of Department,	Stephen A. Holditch

August 2008

Major Subject: Petroleum Engineering

ABSTRACT

Towards a Characteristic Equation for Permeability. (August 2008)

Adil Ahmed Siddiqui, B.E., National University of Sciences & Technology, Pakistan

Chair of Advisory Committee: Dr. Thomas A. Blasingame

The characterization of reservoir permeability (k) remains the elusive challenge in reservoir engineering. This work considers prior developments in an evolutionary sense, and, as with prior work, our *goal* is the development of a "characteristic permeability relation" (*CPR*). To this end, we have developed 5 *CPR* formulations — 3 of which could be considered modifications of "historical" models and 2 of which are "weighted" power law-exponential models.

In this work, *we consider permeability to be only a function of two variables*; $k = f(\phi,z)$ — porosity (ϕ) and z, where z is <u>*either*</u> the water saturation (S_w) or the Archie Formation Factor (F). Our rationale in considering $k = f(\phi,z)$ is two-fold — first, such a formulation is a fundamental extension of the $k = f(\phi)$ correlation work by Archie (and countless others); and second, our validation datasets are limited to literature cases and cases obtained from industry sources — none of which would be considered suitable for extension beyond porosity and another variable.

We demonstrate and validate our concept of a characteristic permeability relation using various datasets obtained from the literature and from industry sources. In this work we show that each proposed relation has a unique character and performance — depending on primarily on the data, rather than the functional form of the permeability relation. Using the *characteristic permeability relations* developed in this work — the proposed permeability relations can be extended to other and other data types. It may also be possible to develop so-called "hydraulic flow unit" methods which segregate petrophysical data into depositional flow sequences.

DEDICATION

This thesis is dedicated to my family members and friends for their help and support.

There is no man living that can not do more than he thinks he can.
— Henry Ford

Patience and perseverance have a magical effect before which difficulties disappear and obstacles vanish.
— John Quincy Adams

ACKNOWLEDGEMENTS

I would like to express my gratitude to Dr. Tom Blasingame for his patience, support and guidance throughout my research and graduate studies at Texas A&M University. I would also like to thank Drs. Walter Ayers and Richard Gibson for serving as members of my advisory committee.

TABLE OF CONTENTS

Page

LIST OF FIGURES

FIGURE Page

FIGURE Page

FIGURE Page

CHAPTER I

INTRODUCTION

1.1. Statement of the Problem

There have been exhaustive attempts to correlate permeability with porosity and other variables — this is one of the most intractable problems in the petroleum industry. Our goal is not to provide a "universal" relation or concept, but rather, to provide "characteristic relations" that can accurately represent a correlation of permeability with other variables. A typical "characteristic relation" will use either the *power law* or *exponential* models proposed by Archie (1950).

$$k_{\text{Archie-PLM}} = a\phi^b \qquad \text{("Power Law Model")} \quad (1.1)$$

$$k_{\text{Archie-EM}} = \alpha \exp[\beta\phi] \qquad \text{("Exponential Relation")} \quad (1.2)$$

Our motivation for this work is our observation that many correlations of permeability, porosity, and other variables might yield inconsistent and/or inaccurate results, especially for low permeability rock samples. As we are pursuing opportunities in very low permeability (k<0.01 md) and ultra-low permeability (k<0.001 md) reservoirs, the potential for such correlations to establish/verify reservoir quality becomes significant. We believe that for ultra-low permeability samples, it will increasingly be difficult to measure permeability on a routine basis making the *correlation* of permeability a main concern (using a few key measurements of permeability).

Unfortunately, there is no single relation written primarily in terms of porosity that can be valid as a permeability estimator across different types of rocks and/or different scales. As part of our literature review, we found similar attempts — the most recent of which is a series of articles by Pape *et al.* (1999, 2000) which focus on a fractal-based derivation of permeability from porosity. The Pape *et al.* result is presented as an additive power law relation, typically of the form: $k = a\phi + b\phi^2 + c\phi^{10}$. We do not believe that the Pape *et al.* model will find significant utility in the petroleum industry, apart from unconsolidated materials and rocks of very uniform grain sizes. We do not wish to diminish the work of Pape *et al.* rather we just do not see the same behavior in our rock sample data (*i.e.*, extremely well-defined data trends where permeability is essentially only a function of porosity). For reference, we rederived the Pape *et al.* fractal model for permeability in **Appendix A**.

This thesis follows the style and format of the *SPE Journal*.

Another modified power law model written for permeability as a univariate function of porosity is the "Bryant-Finney" model (Finney (1970), Bryant *et al*. (1993a, 1993b), and Bryant *et al.* (1993c)).

The "Bryant-Finney" model is given as.

$$k = a(\phi - c)^b \qquad (1.3)$$

We labeled models such as Eq. 1.3 to be "modified power law" formulations, since these models employ a "correction" term in the original power law formula. As a side note, we also established the "Bryant-Finney" model independently when working on our own modified power law relations, but we did not consider the *c*-term to be constant. Regardless of origin, the Bryant-Finney model is one of our characteristic permeability relations. The negative (-) sign in front of the *c*-term is a minor issue (negative numbers must be avoided in the argument of the power law formulation), but we found a few cases where this model performs very well.

In general, applying the Bryant-Finney model with the power law straight line at the leftmost portion of the data, seems to be somewhat limiting as the negative *c*-term has a profound impact when the (ϕ-c) quantity approaches zero (and then negative numbers). We find that when Eq. 1.3 is recast using (ϕ+c), and then the straight-line power law trend is placed at the rightmost portion of the data, we instead achieve a "J" type of shape in the data function, which seems to mimic the behavior of the Pape *et al.* fractal model. This formulation (in terms of (ϕ+c)) is given by:

$$k = a(\phi + c)^b \qquad (1.4)$$

However — historically, engineers and geoscientists have by far preferred an *exponential* type relationship to *correlate* permeability as a function of porosity — as given below:

$$k = \alpha \exp[\beta\phi] \qquad (1.5)$$

Eq. 1.5 has been used almost exclusively in the correlation of permeability, based primarily on the rationalization that "permeability is a logarithmically-scaled variable." We are concerned that Eq. 1.5 is uniquely an empirical result — as opposed to the generalized power law scaling of permeability and porosity (Eq. 1.1), which has had considerable validation by theory and by experimental study — primarily with unconsolidated sediments/materials and very uniform pore distributions.

We cite references by Beard and Weyl (1973), Berg (1970), and Morrow *et al.* (1969) to support our contention of a power law formulation for the permeability of unconsolidated sediments, and we note (without references) that this characteristic behavior has also been observed in fluidized beds, powders, ceramics, cements, and sintered metals. The power law scaling of permeability is widely accepted (under specific conditions), but the exponential scaling has, to our knowledge, never been proven theoretically.

There are suggestions that the exponential scaling of permeability has to do with the tendency for permeability to be logarithmically distributed, and perhaps this is sufficient as "validation." We believe that the exponential correlation of permeability and porosity is most likely an empirical representation of a more complex process — one where the power law model is not directly applicable due to "non-ideal" conditions (*e.g.*, shaliness, poor grain sorting, diagenesis, *etc*.). However; we employ the exponential model in two of our *CPR* models.

Based on the discussion, we presently know (or accept) the following points:

1. Power Law Model for Permeability: *Unconsolidated Sediments/Materials*

   Eq. 1.1 provides the base relation for a power law scaling of permeability using porosity (*i.e.*, $k=a\phi^b$). This formulation is validated in a form that includes the square of grain size by Beard and Weyl (1973) and Morrow *et al.* (1969) for unconsolidated sediments and for (theoretical) packings of perfect spheres [Berg (1970)].

   $k_{\text{Berg}} = a\phi^b d_p^2$ ("Berg Equation" (general form))..(1.6)

   Further, variations of the simple power law formulation have been given which include saturation as a correlation variable by Timur (1968) (referencing his own relation) and Ahmed *et al*. (1989) (referencing the Coates-Denoo (1981) permeability relation) — these relations are:

   $k_{\text{Timur}} = a\phi^b S_w^c$ ("Timur Model")..(1.7)

   $k_{\text{Coates}} = \left[100\phi^2 \frac{(1-S_w)}{S_w}\right]^2$ ("Coates-Denoo Model")..(1.8)

2. Modified Power Law Model for Permeability: *Proposed for Consolidated Sediments*

   Eqs. 1.3 and 1.4 are proposed intuitively as "modifications" of the power law model for permeability (*i.e.*, Eq. 1.1) — where these formulations are intended to compensate for non-ideal behavior due to the *influence of variables other than porosity*. Eqs. 1.3 and 1.4 are repeated for clarity in this discussion:

   $k_{\text{Bryant-1}} = a(\phi-c)^b$ (Bryant-Finney Model (straight-line on left of data)) ....(1.3)

   $k_{\text{Bryant-2}} = a(\phi+c)^b$ (Modified Bryant-Finney Model (straight-line on right of data)) ....(1.4)

   As we do not believe that the Pape *et al.* model ($k = a\phi + b\phi^2 + c\phi^{10}$) is viable in practice, we mention this model as only as a possible (analytical) solution for relating permeability to porosity in near-ideal situations.

3. Modified Exponential Model for Permeability: *Proposed for Consolidated Sediments*

Eq. 1.5 is the "basis" formulation for the exponential model, where Eq. 1.5 is repeated for clarity.

$$k = \alpha \exp[\beta\phi] \qquad \text{("Exponential Model")} \quad \text{.......(1.5)}$$

Our contention is that the slope term (β) is constant, but the intercept term varies from an original value to a maximum value. For convenience, we write this modified exponential form as.

$$k = c(\phi, F, V_{sh}, \text{etc.}) \ \exp[\beta\phi] \quad \text{.......(1.9)}$$

A "$c_{\min}$ to $c_{\max}$" formulation could be developed using the "error function" (erf[x]), and would be written as:

$$k = c\exp[\beta\phi] \quad \text{where} \quad c = c_{\min} + (c_{\max} - c_{\min})\,\text{erf}[c_1\phi^{c_2} z^{c_3}] \quad \text{.......(1.10)}$$

However, the erf[x] term would be potentially difficult to resolve as the *c*-function may not be particularly similar to erf[x]. We have found that the following "exponential" form for the *c*-function is well-behaved and generally provides accurate estimates:

$$k = c\exp[\beta\phi] \quad c = c_{\max}\exp[-c_1\phi^{c_2} z^{c_3}] \quad \text{.......(1.11)}$$

In addition to the (somewhat) theoretical relations proposed by Eqs. 1.3-1.11, we also employ a "hybrid" relationship between the Archie power law and exponential models (Eqs. 1.1 and 1.2, respectively). We have labeled this the *Weighted Power Law-Exponential Model*, which is *defined* as:

$$k = xa\phi^{b} + (1-x)\alpha\exp[\beta\phi] \quad [0 \le x \le 1] \quad \text{(basic form)} \quad \text{.......(1.12)}$$

1.2. Objectives

The objectives of this work are:

- To *propose and develop* a family of "characteristic permeability relations" — specifically, functional forms based on the original observations of Archie (power law and exponential behavior of numerous permeability-porosity data sets).
- To *validate* these "characteristic permeability relations" using data from literature and industry sources for consolidated rocks, as well as data for other materials.
- To *provide a general methodology* for applying the "characteristic permeability relations" in practice, including methods to distinguish poor data from correlation efforts.

1.3. Validation

Data obtained from the literature and industry resources were used to validate the models (*i.e*., "characteristic permeability relations") proposed in this work. The (measured) permeability of the samples (from both carbonate and sandstone reservoirs) ranges from low (tight gas sands) to high permeability reservoir rocks. One example validation case (the "Lower Wilcox" Well, located in South Texas (USA) is presented in the next chapter and the other nine example validation cases are presented in the appendices (see **Appendix B** — **Appendix J**). We present the characteristic plots for each validation case where we attempt to validate the "power law" and/or "exponential" nature of the data corresponding to the characteristic permeability relations. In each validation case, the proposed characteristic permeability relations (*CPRs*) *A-D* are applied. In addition, we use the "Alternating Conditional Expectations" (*ACE*) algorithm (see Xue *et al.* 1997), which is a non-parametric regression method to obtain the optimum correlation, to check the consistency of the proposed models (*i.e*., *CPRs*).

1.4 Summary and Conclusions

In this work we attempt to develop, demonstrate and validate our concept of a characteristic permeability relation (*CPR*) for various different models where we allow the reservoir permeability to be a function of only two variables — namely, porosity and water saturation or Archie Formation Factor.

We evaluate each characteristic permeability relation systematically to identify the strengths of each proposed relation. Specifically, our objective is to demonstrate the characteristic (or dominant) behavior of each characteristic permeability relation.

In conclusion, we recognize that each characteristic permeability relation has a distinctive "signature," and we note that some *CPRs* perform better than others depending on the nature of the problem. It is also worth to note that the systematic application of the *CPRs* as proposed and demonstrated in this work should be functional in the correlation of a given set of permeability data with other variables.

1.5 Organization of the Thesis

The outline of the proposed research thesis is as follows:

- Chapter I — Introduction
  - Statement of the Problem
  - Objectives
  - Validation
  - Summary and Conclusions
  - Organization of the Thesis
- Chapter II — Characteristic Permeability Relations
  - Development
  - Characteristic Behavior
  - Validation
  - Results and Discussion
- Chapter III — Summary, Conclusions, and Recommendations for Future Work
  - Summary
  - Conclusions
  - Recommendation for Future Work
- Nomenclature
- References
- Appendices
  - Appendix A — Derivation of the "Pape" Multi Power Law Formulation for Permeability
  - Appendix B — Results for Howell Well (E. Texas — USA)
  - Appendix C — Results Miocene Sand (S. Louisiana — USA)
  - Appendix D — Results for Vicksburg Sand (S. Texas — USA)
  - Appendix E — Results for Wilcox Sand (S. Texas — USA)
  - Appendix F — Results for Hazlett Well 103
  - Appendix G — Results for Devonian Limestone (Texas — USA)
  - Appendix H — Results for Frio Shaly Sandstone (Texas — USA)
  - Appendix I — Results for Lower Wilcox Shaly Sandstone (Texas — USA)
  - Appendix J — Results for Paluxy Clean Sandstone (Texas — USA)
- Vita

CHAPTER II

CHARACTERISTIC PERMEABILITY RELATIONS

2.1. Development

In this section we present the five characteristic permeability relations that we have developed in this work. As stated before, three of the proposed characteristic permeability relations could be considered as modifications of "historical" models and two of the characteristic permeability relations are hybrid formulations which use both exponential and power law relations. The characteristic permeability relations are given by:

CPR-A — Modified Archie "Clean Sand" Model: (Bryant-Finney Model)

$$k = a(\phi - c)^b \quad c = c_{\max} \exp[-c_1 \phi^{c_2} z^{c_3}] \text{ ....(2.1)}$$

CPR-B — Modified Archie "Dirty Sand" Model: (Power-Law Basis)

$$k = a(\phi + c)^b \quad c = c_{\max} \exp[-c_1 \phi^{c_2} z^{c_3}] \text{ ....(2.2)}$$

CPR-C — Modified Archie "Dirty Sand" Model: (Exponential Basis)

$$k = c \exp[\beta\phi] \quad c = c_{\max} \exp[-c_1 \phi^{c_2} z^{c_3}] \text{ ....(2.3)}$$

CPR-DxL — Weighted Power Law-Exponential Model: (Linear logarithmic weights model)

$$k = xa\phi^b + (1-x)\alpha \exp[\beta\phi] \quad [0 \le x \le 1] \quad x = \exp[-\ln(x_0) + x_1 \ln(\phi) + x_2 \ln(z) + x_3 \ln(\phi)\ln(z)]$$

$$\text{..........(2.4)}$$

CPR-DxQ — Weighted Power Law-Exponential Model: (Quadratic logarithmic weights model)

$$k = xa\phi^b + (1-x)\alpha \exp[\beta\phi] \quad [0 \le x \le 1]$$

$$x = \exp\begin{bmatrix} -\ln(x_0) + x_1 \ln(\phi) + x_2 \ln(z) + x_3 \ln(\phi)\ln(z) + x_4 \ln(\phi)^2 \\ + x_5 \ln(z)^2 + x_6 \ln(\phi)^2 \ln(z) + x_7 \ln(\phi)\ln(z)^2 + x_8 \ln(\phi)^2 \ln(z)^2 \end{bmatrix}$$

$$\text{..........(2.5)}$$

2.2. Characteristic Behavior

In our next effort we consider the "characteristic behavior" of Eqs. 2.1-2.5 which is the so-called "characteristic permeability relations" (*CPRs*). Our goal is to establish the characteristic or dominant behavior of each relation — but not the behavior of the individual "*c* or *x*-functions," these function will be illustrated in the "Validation" section.

We utilize field examples to illustrate the behavior of the characteristic permeability relations (*CPRs*) (*i.e.*, Eqs. 2.1-2.5) — and we attempt to "connect" each relation to an aspect of theory or accepted empirical behavior. Our "historical" characteristic permeability relations (*i.e.*, *CPR-A*, *CPR-B*, and *CPR-C*) were formulated using the work by others as follows:

- Archie (1950): Logarithm of permeability as a function of porosity (exponential model) and permeability as a function of the Archie Formation Factor, which leads directly to a power law relationship of permeability with porosity (*i.e.*, Eq. 1.1). *According to the data presented by Archie*, the power law relationship of permeability with porosity is primarily valid for unconsolidated/weakly consolidated rocks.
- Morrow *et al.* (1969): Correlation of permeability with porosity and grain size for unconsolidated sediments using statistical representations of the grain size distribution.
- Berg (1970): Correlation of permeability with porosity and grain size using theoretical (systematic) packings of perfect spheres.
- Beard and Weyl (1973): Correlation of permeability with porosity and grain size for unconsolidated sediments using sieved sand samples to represent the influence of both grain size and sorting.
- Pape *et al.* (1999): Correlation of permeability with porosity using a "multiple power law" model based on fractal theory.

These contributions lead us to the definition of characteristic power law permeability-porosity relations based on modifications of the Archie "Clean Sand" model (Eq. 1.1). In particular, relations *CPR-A* (Eq. 3.1) and *CPR-B* (Eq. 3.2) are direct modifications of the Archie "Clean Sand" model. As a coincidence, Bryant (1993a, 1993b, 1993c) and Finney (1970) also proposed the *CPR-A* formulation (Eq. 2.1), so we will also refer to the *CPR-A* model as the Bryant-Finney model. We note that Eqs. 1.1 and 2.1 are both "clean sand" models, *implying that the Archie* (*clean sand*) *power law trend will lie to the left of the data body* (see **Fig. 2.1**). Also the "c_{max}" trend is constructed by substitution of a constant value of "c_{max}" into Eq. 2.1 until trend lies along the rightmost portion of the data (see **Fig. 2.1**).

In order to use the *CPR-A* equation, first we plot log(k) versus log(ϕ). Then we locate the Archie "Clean Sand" trend — we use the graphical method (*i.e.*, hand analysis) to establish the a and b parameters. We establish the $c_{\max}$ trend by substitution of $c_{\max}$ values, and the $c_{\max}$ trend should be just beyond the rightmost body of data. Next, we use regression methods to estimate the c_1, c_2, and c_3 parameters.

It is worth to note that regression methods should not be used to estimate the *a* and *b* parameters. As c_{max} is *subtracted* in this model, care must be taken to avoid negative values in the solution. For many cases, the *b*-parameter is on the order of 8 [suggested from the work of Morrow *et al* (1969) and Beard and Weyl (1974)].

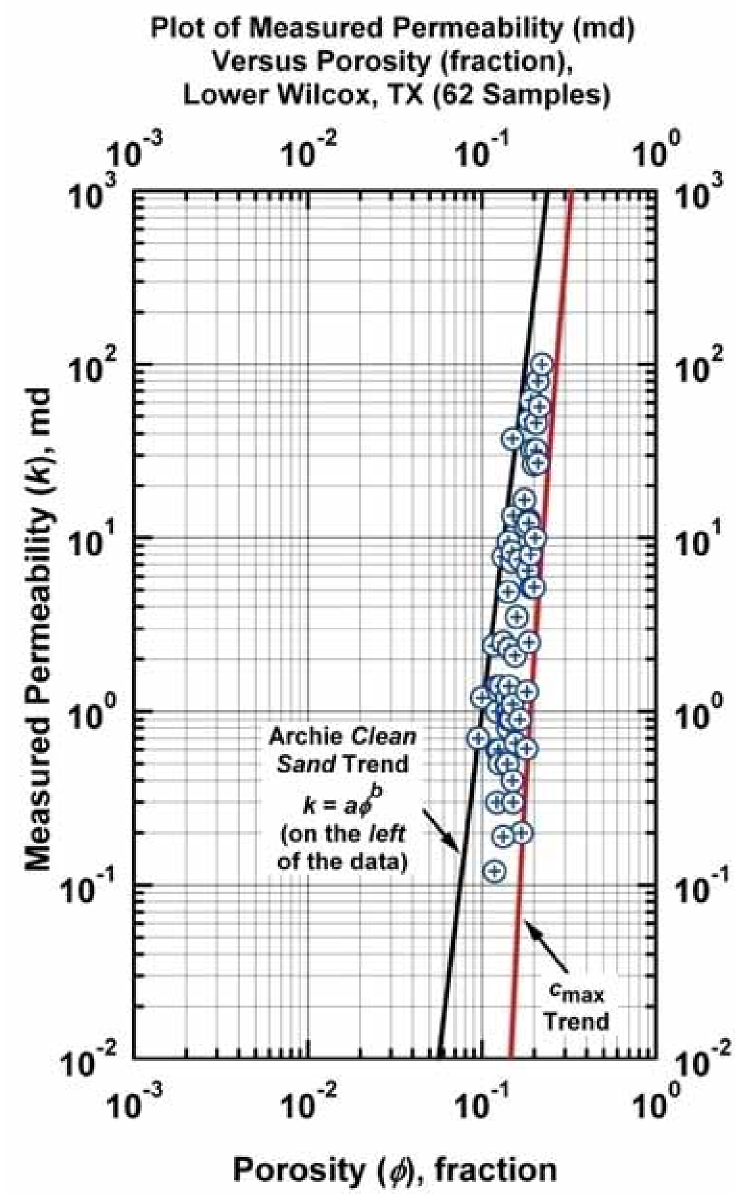

Figure 2.1— Model *CPR-A*: $k = a(\phi - c)^b$ $(c = c_{\max} \exp[-c_1 \phi^{c_2} z^{c_3}])$ — Log-log correlation of permeability (k) and porosity (ϕ). Archie "clean sand" trend is constructed to the left of the body of data.

Generally speaking, *we strongly recommend against using statistical methods for locating the base trends for all CPR models* — these trends should be constructed (carefully) by the analyst. Regression can and should be used to estimate the model parameters (*e.g.*, the c_i and x_i coefficients), but *never* to locate the base trends (*i.e.*, the power law or exponential trends).

Our rationale behind the *CPR-A*/Bryant-Finney model is that the Archie "clean sand" trend represents the highest permeability value for a given value of porosity, hence the position of this line to the left of the data body. By induction, any point not lying on the "clean sand" trend must be affected by some factor(s) which mitigate permeability — for example: shaliness, poor sorting, diagenesis, etc.

In contrast, we define *CPR-B* (Eq. 2.2) as the Archie "dirty sand" *power law* model and *CPR-C* (Eq. 2.3) as the Archie "dirty sand" exponential model. *CPR-B* implies that the "dirty sand" trend on a log-log plot of permeability versus porosity will lie along the far *rightmost* trend of data (see **Fig. 2.2**).

In order to use the *CPR-B* equation first we plot log(k) versus log(ϕ). Then we locate the Archie "Dirty Sand" trend — we use the graphical method (*i.e.*, hand analysis) to establish the a and b parameters. The c_{max} trend is established by substitution of c_{max} values, we note that the c_{max} trend should be just beyond the leftmost body of data. We finally use regression methods to estimate the c_1, c_2, and c_3 parameters.

We should not use regression methods to estimate the a and b parameters. As c_{max} is *added* in this model, you can note the unique "J"-shape of the c_{max} trend towards the left. A best "hand fit" of the b-parameter should always work well.

Similarly, *CPR-C* implies that the "dirty sand" trend on a plot of logarithm of permeability versus porosity will also lie along the far *rightmost* trend of data (see **Fig. 2.3**). Archie (1950) showed some of the first correlations of log(k) versus ϕ, and although Archie provided an average trend through the data, we can infer that (perhaps) the exponential trend ($k=\alpha \exp[\beta\phi]$) could represent the lowest (*i.e.*, far rightmost) correlation of permeability and porosity on the semilog plot. The "dirty sand" trend illustrated in **Fig. 2.3** is plausible in all of the cases we consider.

In order to use the *CPR-C* equation first we plot log(k) versus ϕ. Then we locate the Archie "Dirty Sand" trend — we use the graphical method (*i.e.*, hand analysis) to establish the β-parameter (*i.e.*, the slope). We establish the c_{max} (straight-line) trend by substitution of c_{max} values, similarly, the c_{max} trend should be just beyond the leftmost body of data. We finally use regression methods to estimate the c_1, c_2, and c_3 parameters.

It is very important to note that regression methods to should not be employed to estimate the β-parameter. c_{max} simply represents a "shift" of the straight-line (exponential) trend to the left-most portion of the data. An alternate formulation of this problem could be written as:

$$k = c\exp[\beta\phi]$$
$$c = c_{\min} + (c_{\max} - c_{\min})\, erf[c_1\phi^{c_2} z^{c_3}] \quad \text{...}(2.6)$$

Although we do not believe that such a form will be necessary in practice, it does have certain attractive features (*e.g.*, $c_{min} < c < c_{max}$ is explicitly stated).

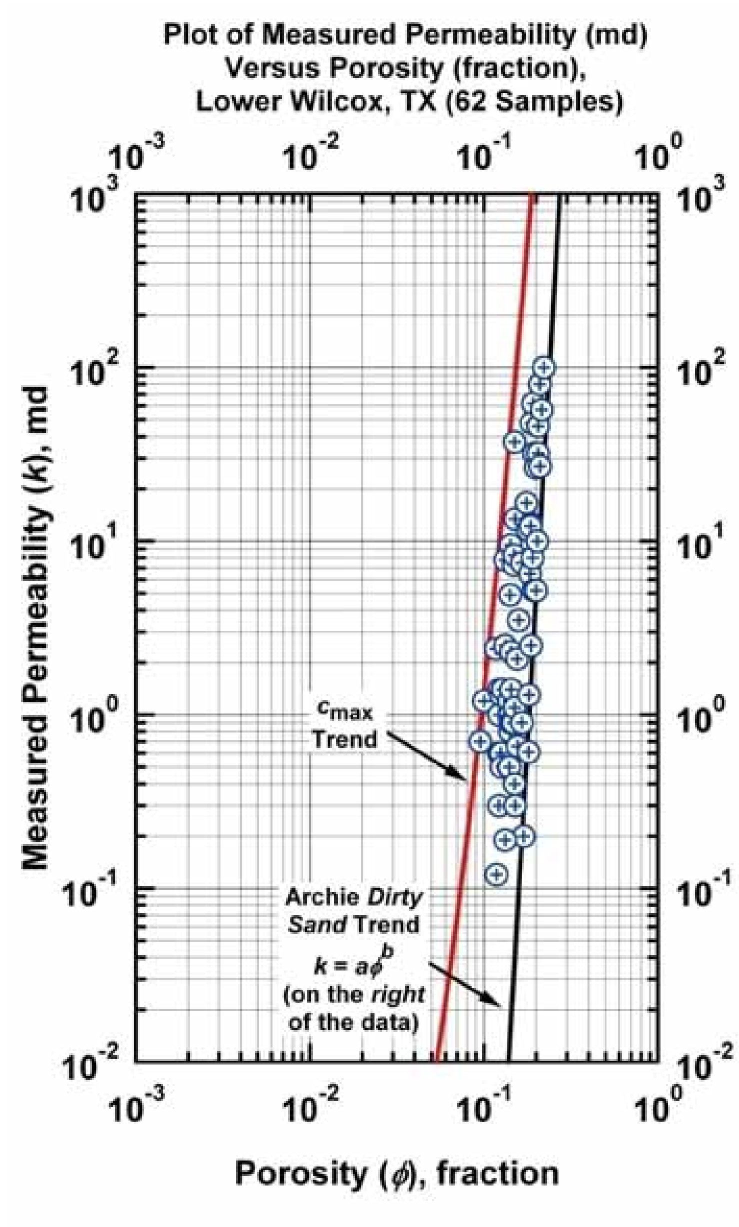

Figure 2.2— Model *CPR-B*: $k = a(\phi + c)^b$ ($c = c_{\max}\exp[-c_1\phi^{c_2} z^{c_3}]$) — Log-log correlation of permeability (k) and porosity (ϕ). Archie "dirty sand" trend is constructed to the right of the body of data.

Our final approach, the *Weighted Power Law-Exponential Model* is a simple weighting of the historical power law and exponential trends, the generic form of this "weighted" model is given as:

$$k = xa\phi^b + (1-x)\alpha \exp[\beta\phi] \quad [0 \le x \le 1] \quad \text{.......}(2.7)$$

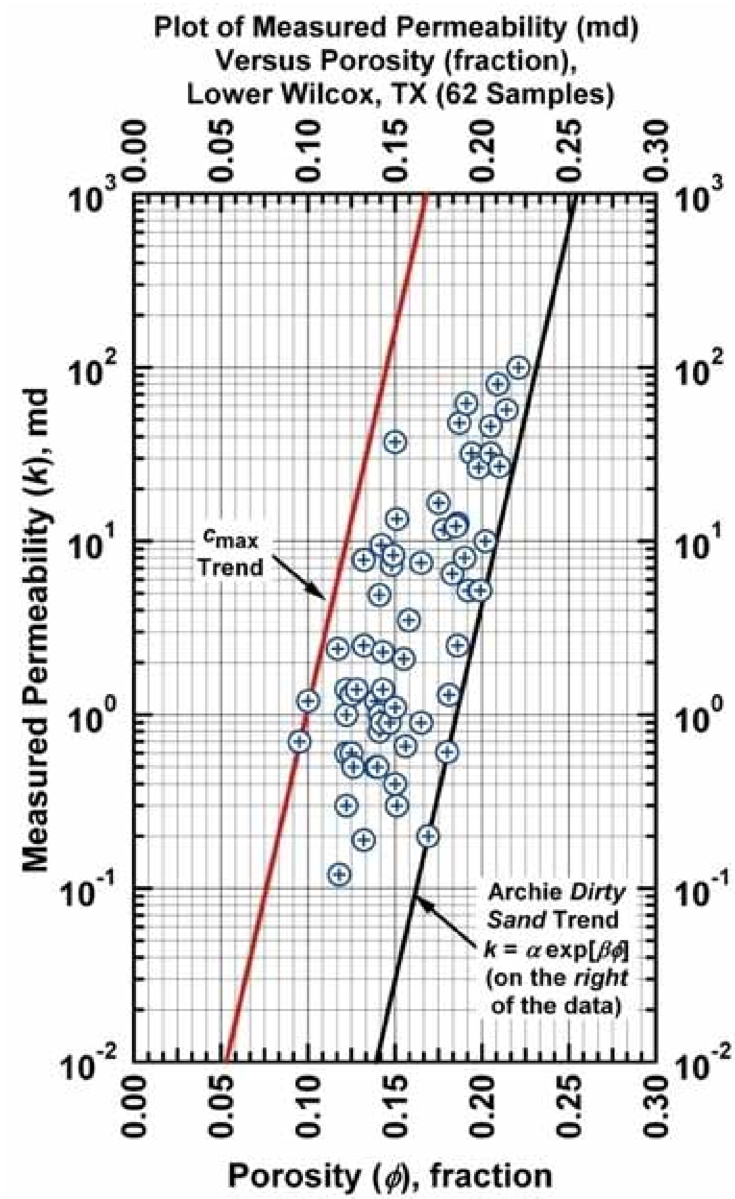

Figure 2.3— Model *CPR-C*: $k = c\exp[\beta\phi] \quad c = c_{\max}\exp[-c_1\phi^{c_2} z^{c_3}]$ — Semilog correlation plot of permeability (k) and porosity (ϕ). Archie "dirty sand" trend is constructed to the right of the body of data.

Our approach has been to define the power law relation ($a\phi^b$) as the Archie "clean sand" trend (the same as using *CPR-A* (Eq. 2.1) on the leftmost portion of the data on a log(k) versus log(ϕ) plot); and to define the exponential relation (αexp[$\beta\phi$]) as the Archie "dirty sand" trend (the same as in *CPR-C* (Eq. 2.3) on the rightmost portion of the data on a log(k) versus ϕ plot)). Once the trends are defined, and the parameters (a,b,α,β) are known, we then solve Eq. 2.7 for the weights (x-values). This process gives us a basis for establishing the weights (somewhat) directly from the data. Obviously, the weights (x-values) then must be correlated with independent variables (*e.g.*, ϕ, S_w, F, V_{sh}, etc.). Solving Eq. 2.7 for the weights (*i.e.*, the x-values), we have:

$$x = \frac{(k - \alpha \exp[\beta\phi])}{(a\phi^b - \alpha \exp[\beta\phi])} \quad \text{.......... (2.8)}$$

Our procedure is to estimate x using data, and then to attempt a correlation of $x = f(\phi, S_w, F, V_{sh}$, etc.). As such, our best effort to correlate the x-values has led to the following logarithmic polynomial forms:

1. *CPR-DxL*: (Linear logarithmic weights model)

$$x = \exp[-\ln(x_0) + x_1 \ln(\phi) + x_2 \ln(z) + x_3 \ln(\phi)\ln(z)]$$

.... (2.9)

2. *CPR-DxL*: (Quadratic logarithmic weights model)

$$x = \exp\begin{bmatrix} -\ln(x_0) + x_1 \ln(\phi) + x_2 \ln(z) + x_3 \ln(\phi)\ln(z) + x_4 \ln(\phi)^2 \\ + x_5 \ln(z)^2 + x_6 \ln(\phi)^2 \ln(z) + x_7 \ln(\phi)\ln(z)^2 + x_8 \ln(\phi)^2 \ln(z)^2 \end{bmatrix}$$

.... (2.10)

As noted earlier in Eqs. 2.9 and 2.10, the z-variable represents S_w or F, as prescribed by available data. The z-variable could also be V_{sh}, well log responses, *etc*. As comment, there are certainly other forms that could be used to represent the x-variable, but for the purposes of this work, we are quite satisfied with the performance of the logarithmic polynomial forms (Eqs. 2.9 and 2.10) as correlating functions.

Our rationale in creating the *Weighted Power Law-Exponential Model* was to "capture" the most significant features of the power law (Archie "clean sand") and the exponential (Archie "dirty sand") models. We recognize that such a "hybrid" model may not have a strong theoretical basis, but our intention is to provide this model *as a mechanism to correlate permeability*. A graphical presentation of the *Weighted Power Law-Exponential Model* is illustrated in **Fig. 2.4**. We note that the power law and exponential relations form an "envelope" around the permeability-porosity data (the log-log format is shown in **Fig. 2.4a** and the semilog format is shown in **Fig. 2.4b**). The construction of the envelope is by design as we wish to capture all of the data (or at least, all of the relevant data). The weighting function (x) is then used to correlate the "interior" behavior of the data envelope.

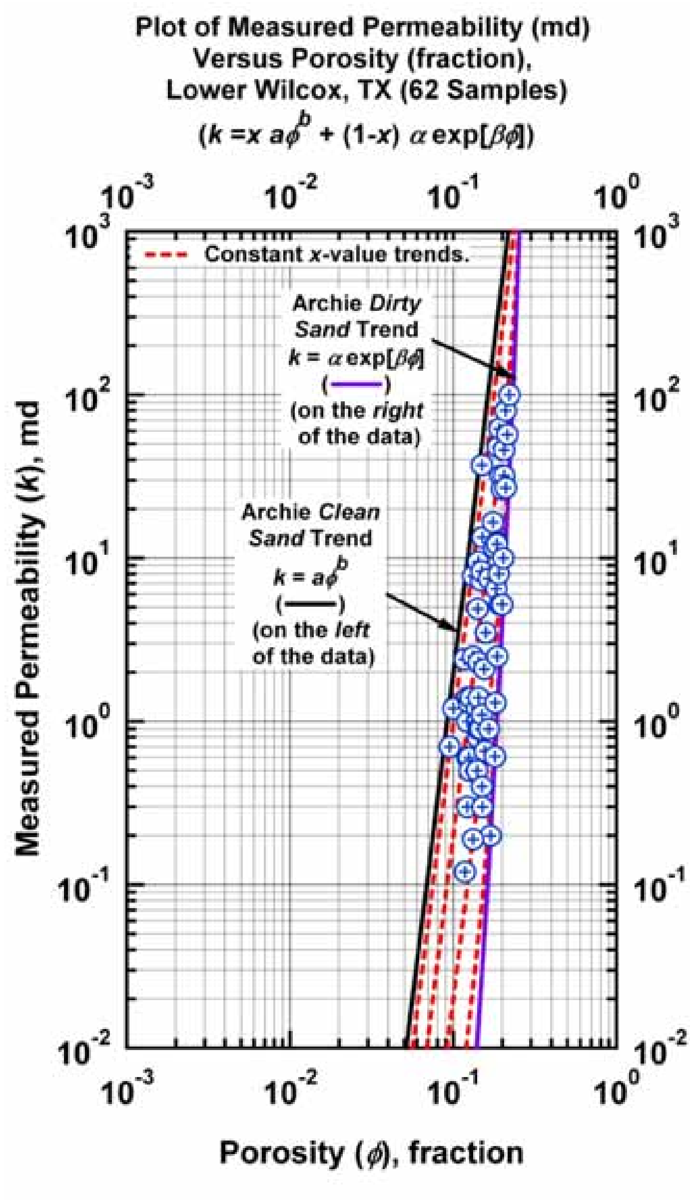

Figure 2.4a — "Clean Sand" Plot — Archie "Clean Sand" trend is given by the straight-line trend at the far left of the data (power law model).

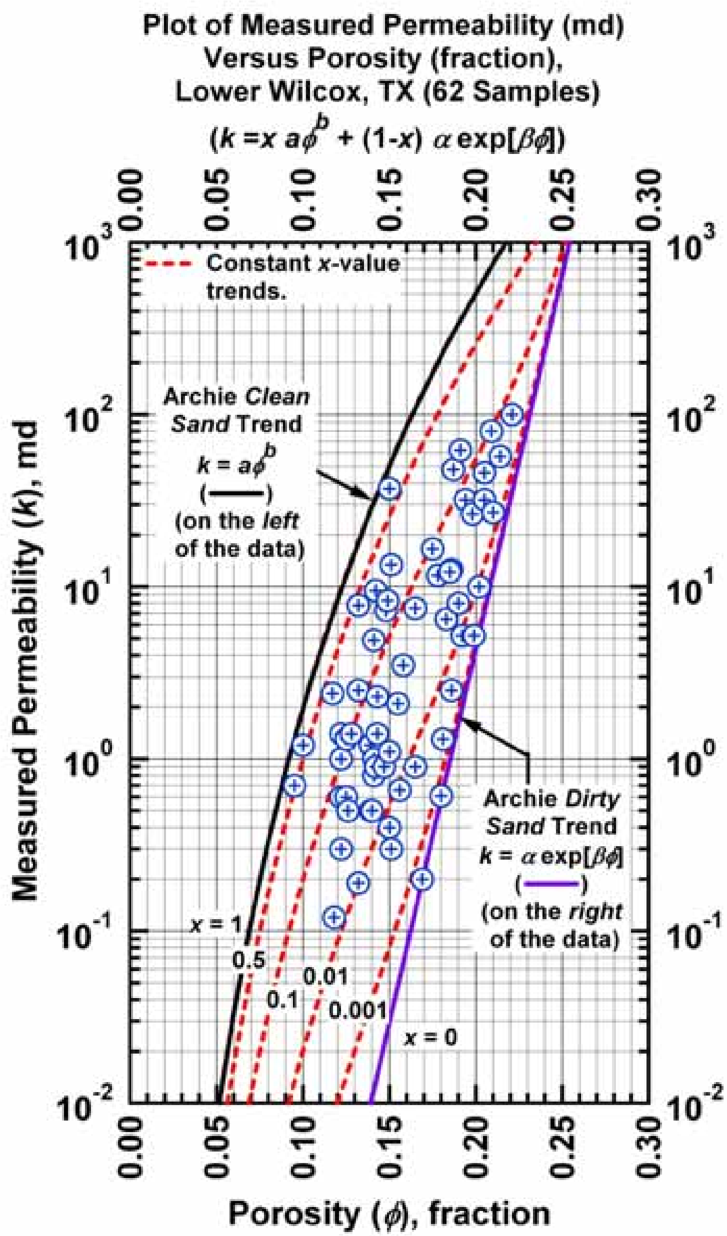

Figure 2.4b — "Dirty Sand" Plot — Archie "Dirty Sand" trend is given by the straight-line trend at the far right of the data (exponential model)

Because of the Cartesian scaling of the porosity axis in **Fig. 2.4b**, this plot provides perhaps the best resolution of the power law and exponential "boundaries" of the data envelope, as well as the selected values of the *x*-function, which illustrate the interior behavior.

2.3. Validation

In this section we present an example validation — in particular, the "Lower Wilcox" Well, located in South Texas (USA), where this is a tight gas reservoir system comprised of shaly (clastic) sediments (Ellis, 1987). The characteristic plots for this case were shown in **Figs. 2.5-2.7**, where "characteristic" implies that we attempted to validate the "power law" and/or "exponential" nature of the data relative to the characteristic permeability relations (*CPRs*) *A-D* (*i.e.*, Eqs. 2.1-2.5).

As in every validation case, we apply *CPRs A-D* (and the *Archie "Clean Sand" Model*) to the field data, in this case the field data were obtained from the "Lower Wilcox" Well:

For completeness, we also use a modification of the "Timur" model (Timur, 1968) — where this model is optimized to a particular dataset using non-linear regression methods. *For this case* (*i.e.*, and other cases where we have F but not S_w), the "Modified Timur Model" is defined as:

$$k_{\text{Timur}} = a\phi^b F^c \quad \text{("Modified Timur Model")} \qquad (2.11)$$

In this work we also utilize the so-called "Alternating Conditional Expectations" (or ACE) algorithm (see Xue *et al*, 1997) — this is a non-parametric regression method referred to in this work as the "*GRACE*" solution.

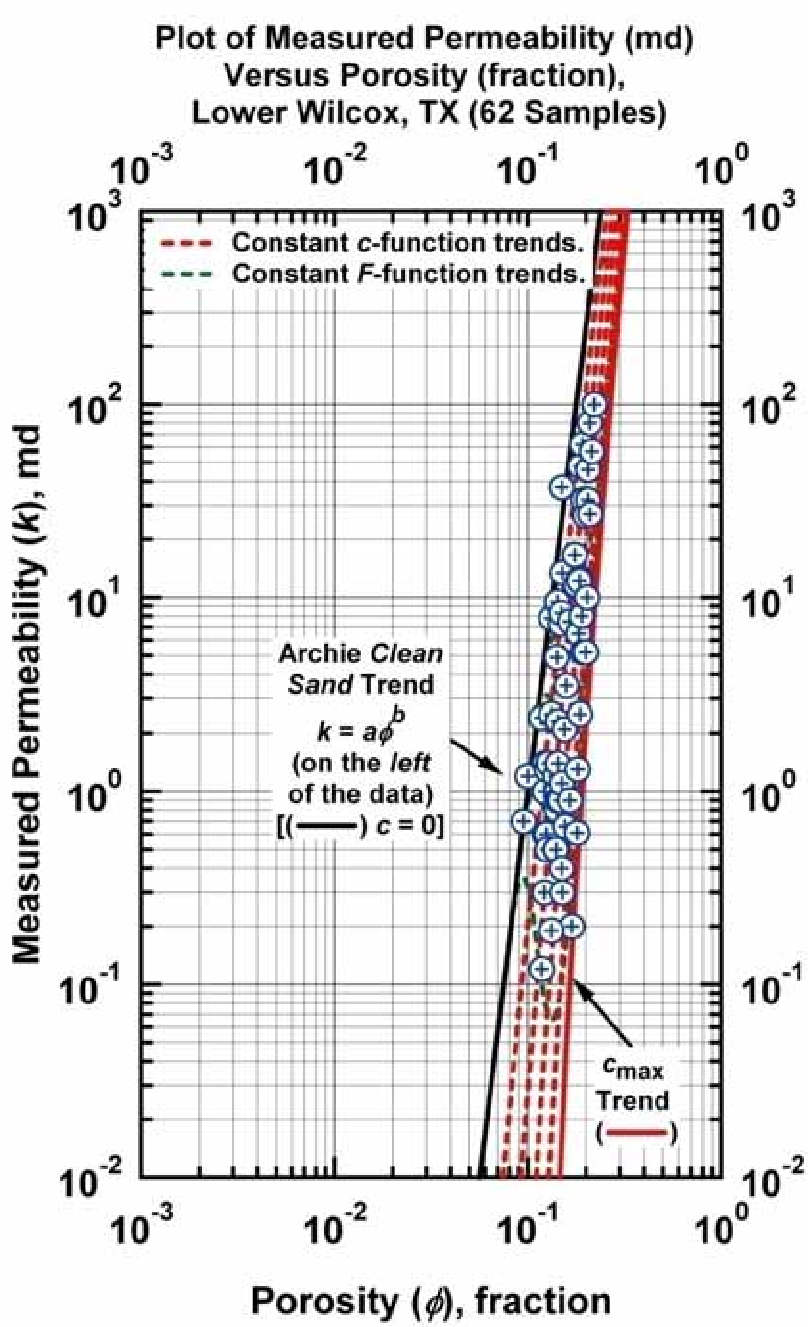

Figure 2.5a — Model *CPR-A*: $k = a(\phi - c)^b$ ($c = c_{max} \exp[-c_1 \phi^{c_2} F^{c_3}]$) — "Clean Sand" Plot (log-log format) — Archie "Clean Sand" trend is given by the straight-line trend at the far left of the data (power law model). [*Case*: Lower Wilcox S. TX (USA)]

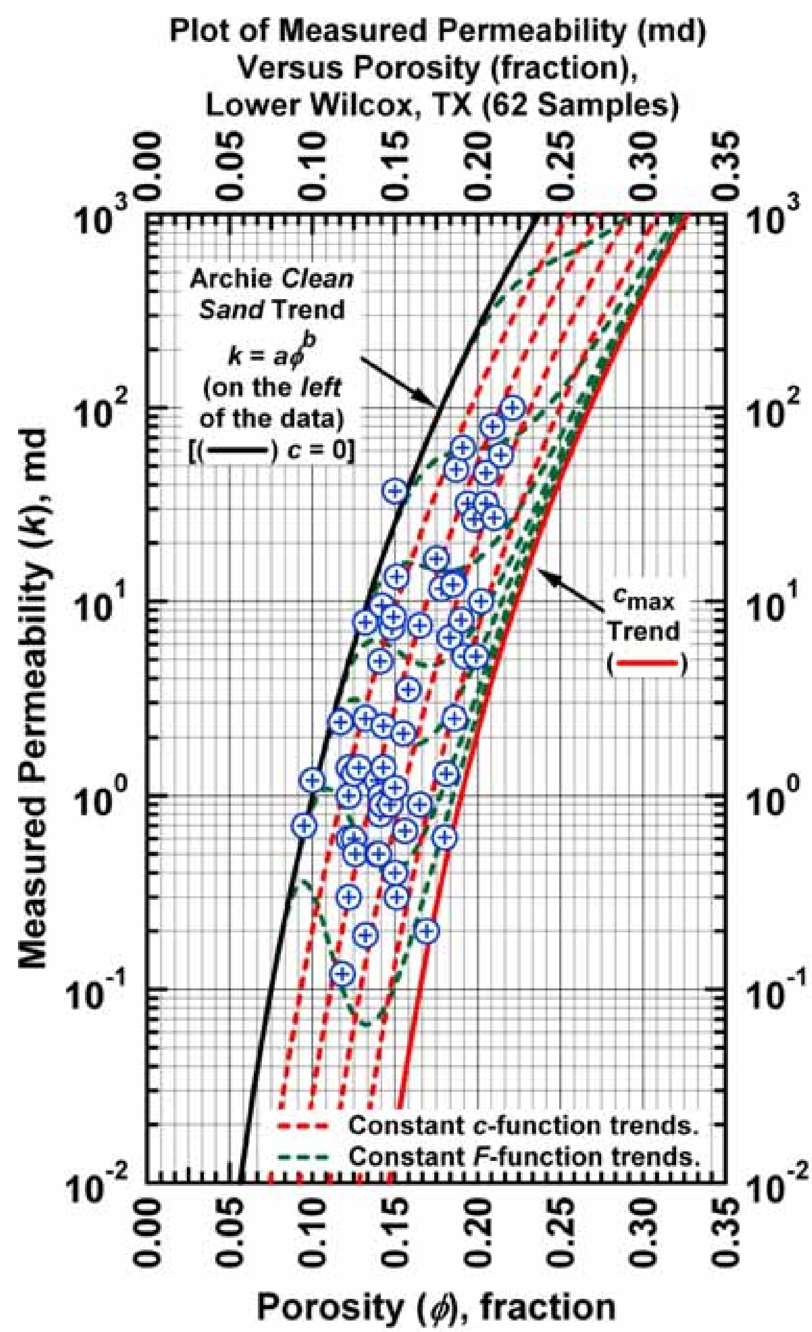

Figure 2.5b — Model *CPR-A*: $k = a(\phi - c)^b$ ($c = c_{\max} \exp[-c_1\phi^{c2} F^{c3}]$) — "Dirty Sand" Plot (semilog format). Archie "Clean Sand" trend is given by the curved trend at the far left of the data (power law model). [*Case*: Lower Wilcox S. TX (USA)]

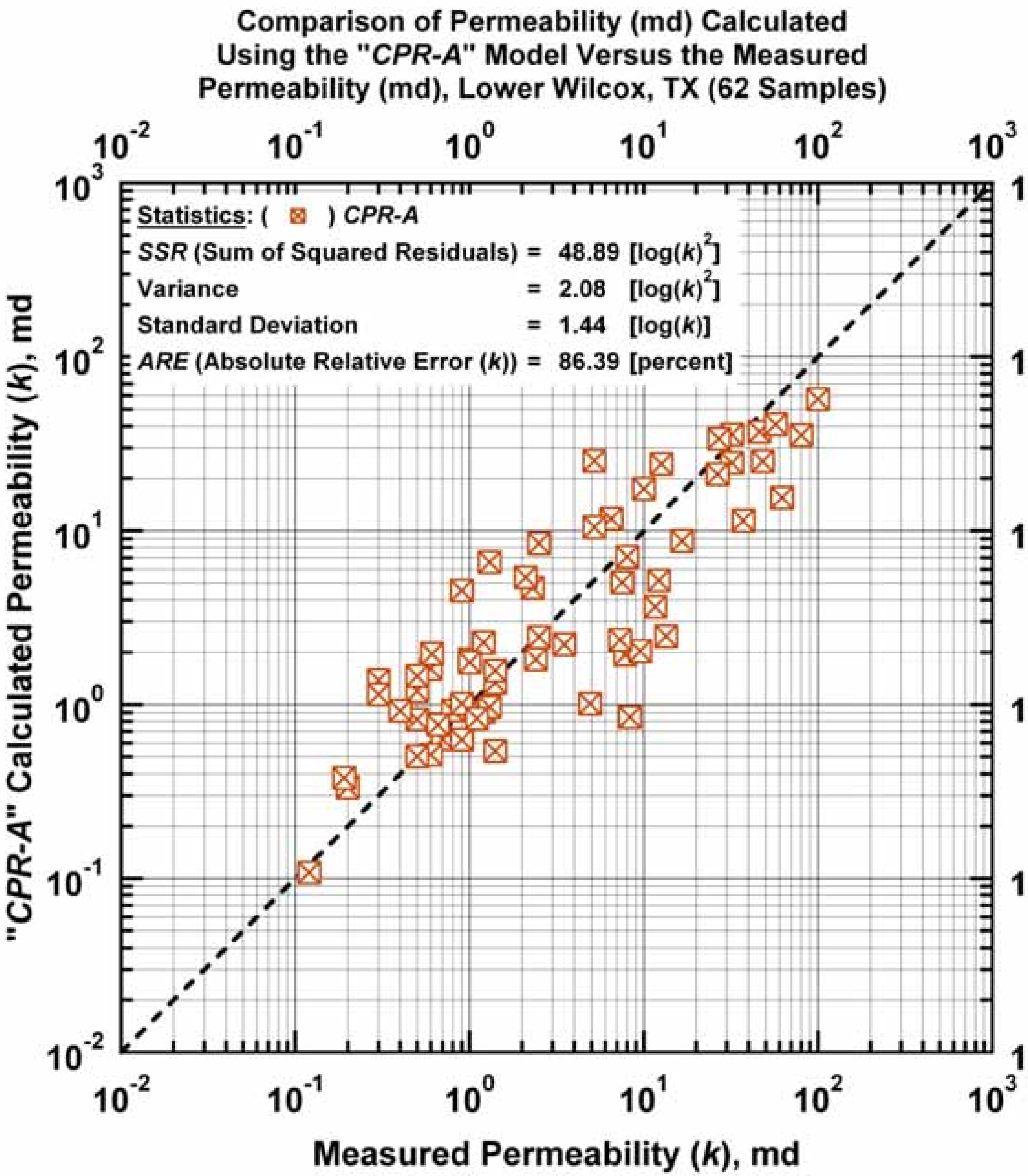

Figure 2.6a — Model *CPR-A*: calculated versus measured permeability. [*Case*: Lower Wilcox S. TX (USA)]

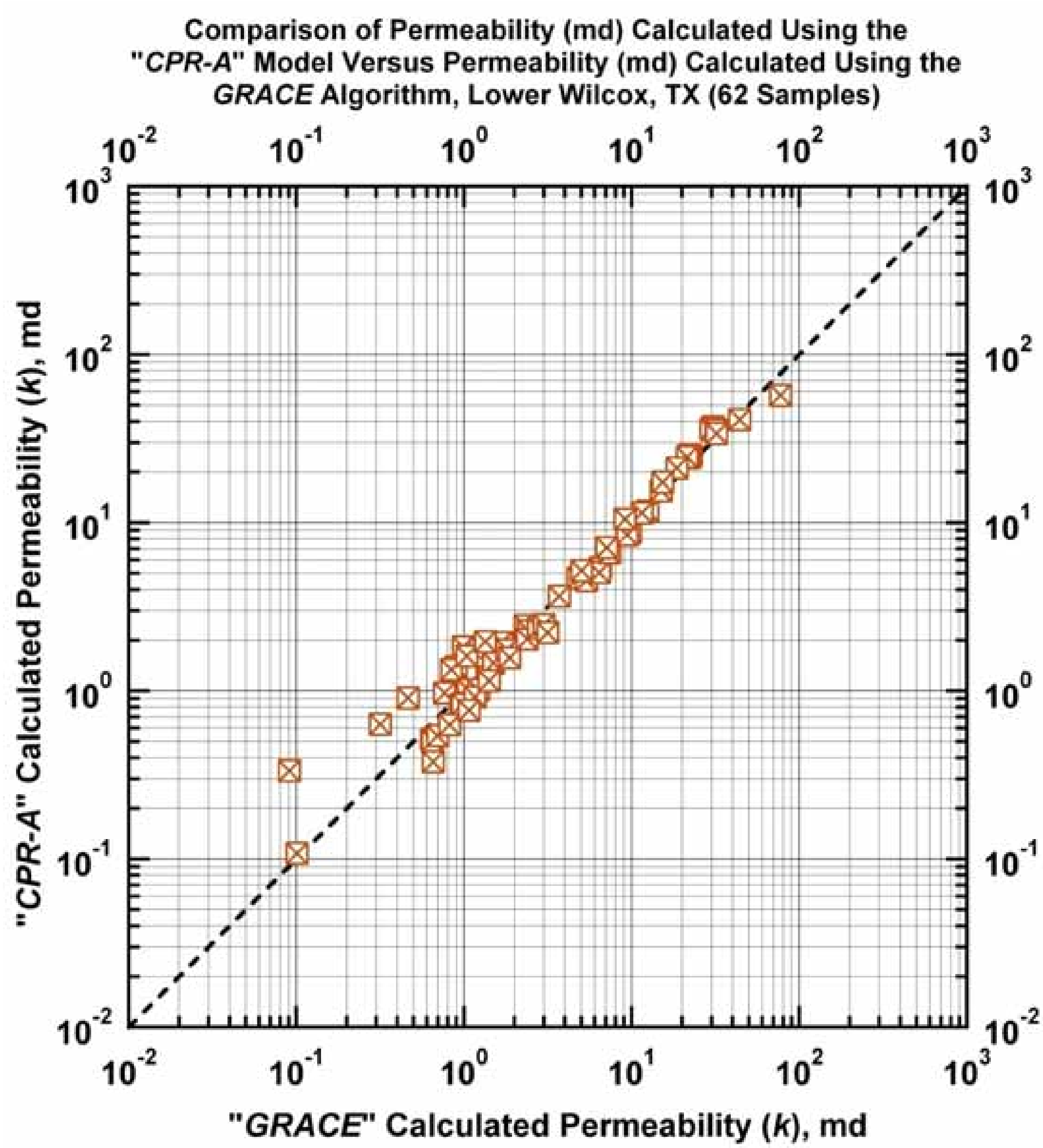

Figure 2.6b — Model *CPR-A*: Permeability calculated using Model *CPR-A* versus permeability calculated using the *GRACE* Algorithm. [*Case*: Lower Wilcox S. TX (USA)]

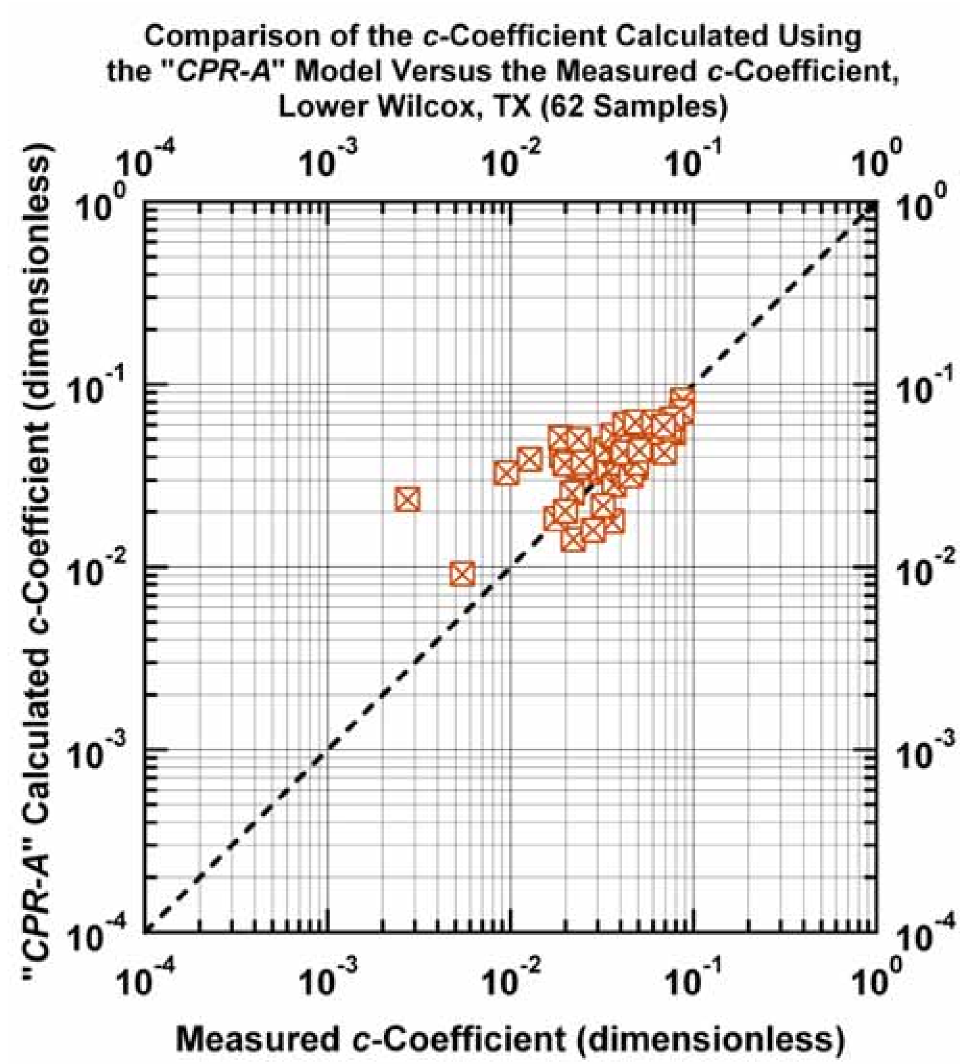

Figure 2.6c — Model *CPR-A*: Calculated *c*-function values versus measured *c*-function values. [*Case*: Lower Wilcox S. TX (USA)]

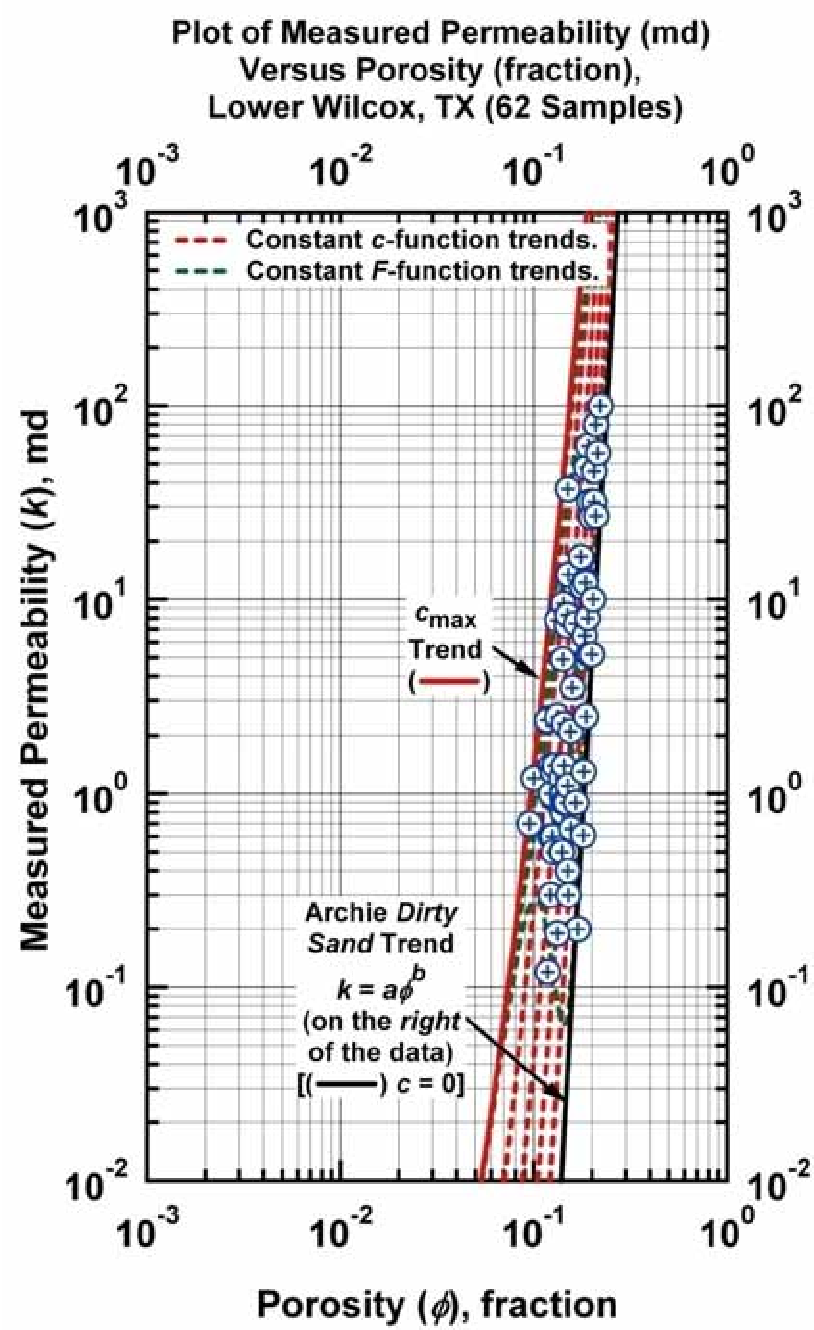

Figure 2.7a — Model *CPR-B*: $k = a(\phi + c)^b \quad c = c_{max} \exp[-c_1 \phi^{c_2} F^{c_3}]$ — "Clean Sand" Plot (log-log format) — Archie "Dirty Sand" trend is given by the straight-line trend at the far right of the data (power law model). [*Case*: Lower Wilcox S. TX (USA)]

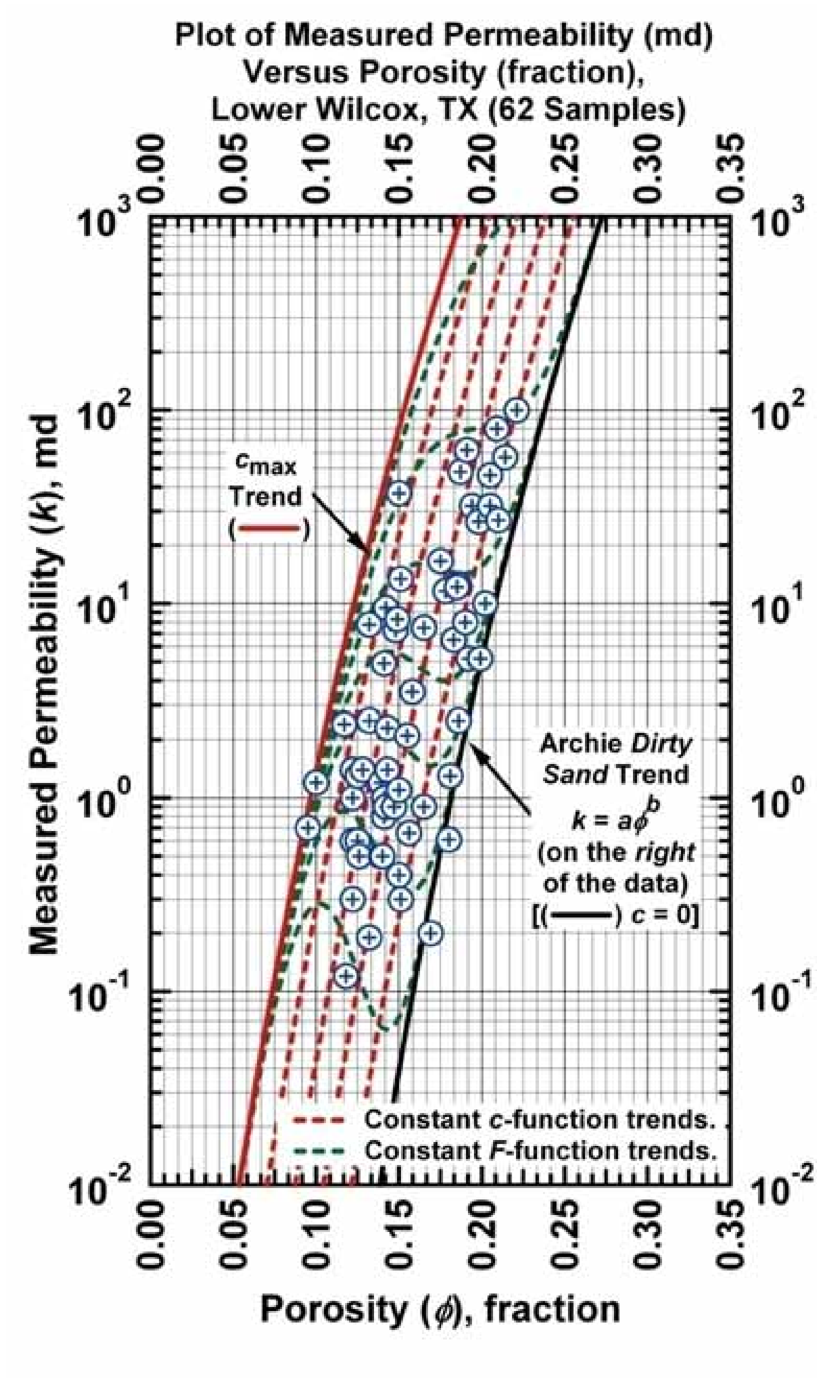

Figure 2.7b — Model *CPR-B*: $k = a(\phi + c)^b \quad c = c_{max} \exp[-c_1 \phi^{c2} F^{c3}]$ — "Dirty Sand" Plot (semilog format) — Archie "Dirty Sand" trend is given by the curved trend at the far right of the data (power law model). [*Case*: Lower Wilcox S. TX (USA)]

2.4. Results and Discussion

In **Fig. 2.5** we observe very good behavior of the *CPR-A* model for this case — we clearly note the power law straight-line trend in **Fig. 2.5a** (log-log format), as well as the clarity and uniqueness of the fit in **Fig. 2.5b** (semilog format). In **Fig. 2.6** we provide the "error" plots for this case, where measured and computed data are compared systematically. Of particular value is **Fig. 2.6b** (*GRACE* comparison), a very good correlation.

We now consider the case of *CPR-B* — the *Modified Archie "Dirty Sand" Model* (power law base). In this case the *c*-function is *added* to the power law relation, and *the rightmost data become the basis for the power law straight-line*, and the leftmost data are used to define c_{max}. The results for this case are presented in **Figs. 2.7 and 2.8**. In **Fig. 2.7a** (log-log format) we note a very good "envelope" is formed by the *CPR-B* model, essentially all of the data on the right and left flanks are well-matched (*i.e.*, the "dirty sand" power law relation and its correction function, respectively). Similarly, in **Fig. 2.7b** (semilog format), we observe an excellent distribution of the power law model across the body of the data. We can also note the "constant *c*-function" lines which provide orientation as to the influence of the *c*-function, as well as the constant "*F*-function" lines which indicate the behavior of the Formation Factor relative to this correlation and data set. The error analysis for this case is shown in **Fig. 2.8** and all of the component plots suggest that the *CPR-B* model has given excellent performance with the only significant errors/deviations in the lower permeability values.

The *CPR-C* model — the *Modified Archie "Dirty Sand" Model* (exponential base) is shown in **Figs. 2.9 and 2.10** and, as with the *CPR-B* model, we note very good performance of the base function — in this case an exponential relation. In particular, **Fig. 2.9b** illustrates the excellent conformance of the *CPR-C* model for this case (again recalling that this model has an exponential relationship with porosity as its basis). In **Fig. 2.10** we review the error analyses plots for this case, and we note good performance (visually) in terms of the correlation of the results using model *CPR-C*. We do note that in this case, the overall (statistical) error is somewhat high, but we have to remember that we are proposing "characteristic models" in this work, and as such, this case appears (again, based on visual inspections) to have good clustering of the correlated results. Also, the *c*-function in this case (see **Fig. 2.10c**) is not a correction term, but rather the instantaneous intercept for the exponential basis. Again, we are approaching this work from the perspective that the primary value is the characteristic model, not the statistical "best fit" correlation. We believe that the *CPR-C* model has performed well for this case, and the plots in **Fig. 2.10** confirm the value of this model as a characteristic relation.

We next apply the *Weighted Power Law-Exponential Models* — Model *CPR-DxL* (linear weights) and Model *CPR-DxQ* (quadratic weights). The base results using Models *CPR-DxL* and *CPR-DxQ* are presented in **Fig. 2.11** — where the power law and exponential basis functions are simply fitted to the appropriate portion of the data. The power law equation represents the "Archie clean sand" trend and is fitted to the leftmost data as shown in **Fig. 2.11a**. In contrast, the exponential equation is thought to represent the "Archie dirty sand" trend and the exponential is fitted to the far rightmost portion of the data (see **Fig. 2.11b**).

In **Figs. 2.12 and 2.13** we present the error analysis which includes the weighting functions (Eqs. 2.9 or 2.10) as appropriate. In **Fig. 2.12a** we note a fairly good correlation of permeability, and in **Fig. 2.12b** we note that the results obtained using Model *CPR-DxL* does "drift" slightly from the *GRACE* solution, indicating some inconsistency. The computed weight function (x) shown for the *CPR-DxL* model in **Fig. 2.12c** does have more scatter than expected, but the trend is centered on the perfect correlation line. The results obtained using Model *CPR-DxQ* are presented in **Fig. 2.13**, and we note substantially improved behavior over that of Model *CPR-DxL*.

In **Fig. 2.14** we present the results of the "Modified Timur Model" which is essentially just a generalized power function relation in terms of k, ϕ, and F. Somewhat surprisingly, as shown in **Figs. 2.14a and 2.14b**, the "Modified Timur Model" provides the best correlation of the data for this case.

In **Fig. 2.15** we present the results predicted by the *GRACE* algorithm, which is a non-parametric regression approach (see Xue, *et al* (1997) for details). In theory, the *GRACE* algorithm should provide the most *unbiased* correlation of the data — *i.e.*, the *GRACE* algorithm is designed not to "fit the errors" as other regression approaches may. It is our contention that the *GRACE* algorithm is the statistical standard — and any algorithm/approach/model which achieves better regression statistics than the *GRACE* algorithm is actually "fitting the errors" in the data. The only case which has significantly better regression statistics than the GRACE algorithm is the "Modified Timur Model" — hence, we must label this case as "*over-fitted*" in a statistical sense.

Our final graphic, **Fig. 2.16**, illustrates all of the models on a single plot of calculated versus measured permeability. We also present a table of all statistical results in **Table 2.1** below.

Table 2.1 — Statistical Results for all Models (Lower Wilcox Case, n=62).

Model	Sum of Squared Residuals [log(k)^2]	Variance [log(k)^2]	Standard Deviation [log(k)]	Absolute Relative Error [percent]
CPR-A	48.89	2.08	1.44	86.39
CPR-B	48.78	2.11	1.45	90.10
CPR-C	57.32	2.20	1.48	99.03
CPR-DxL	51.74	2.36	1.54	102.77
CPR-DxQ	49.10	2.15	1.46	93.05
Modified Timur	47.83	2.11	1.45	84.41
GRACE Algorithm	50.47	2.17	1.47	88.14

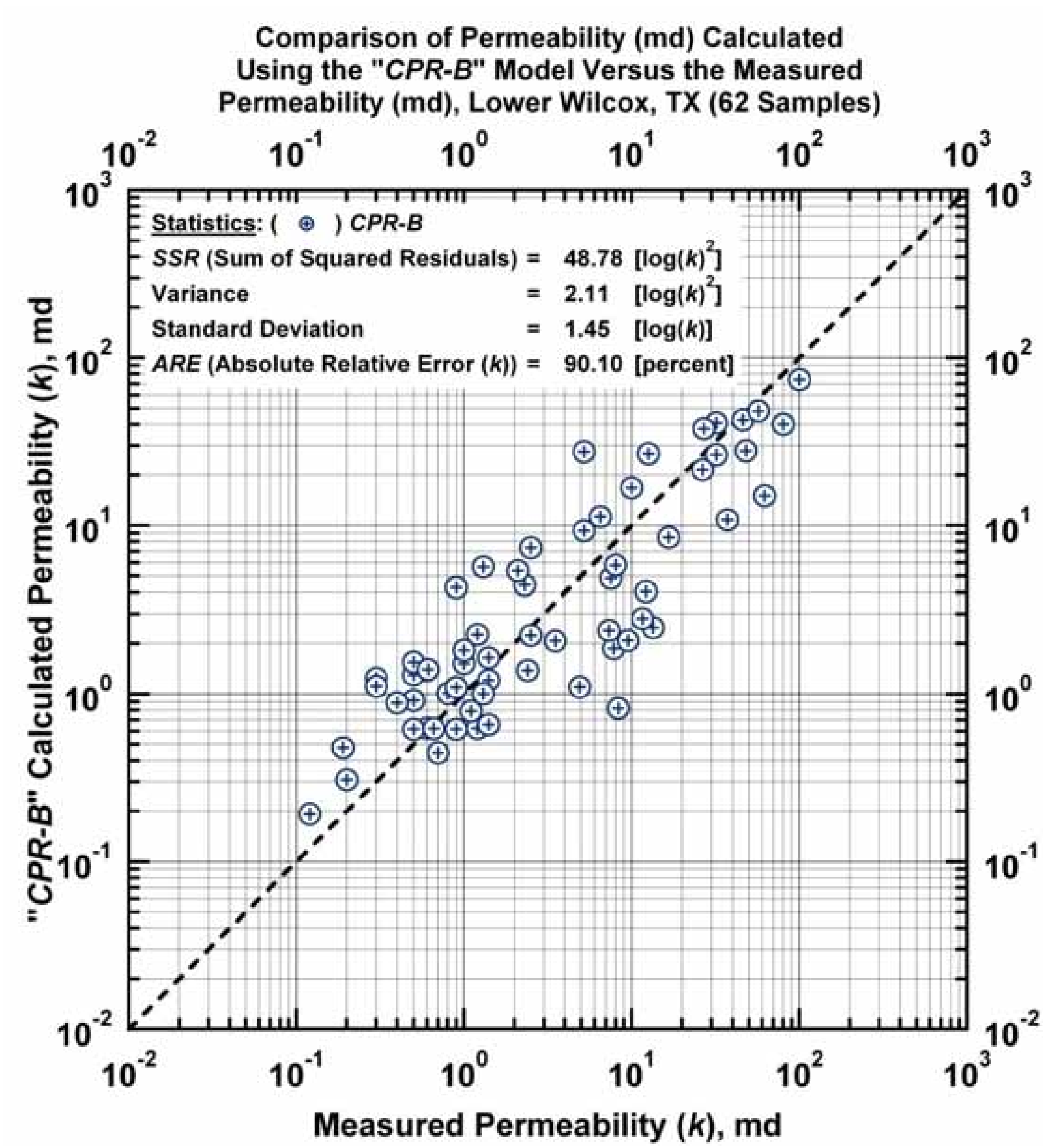

Figure 2.8a — Model *CPR-B*: calculated versus measured permeability. [*Case*: Lower Wilcox S. TX (USA)]

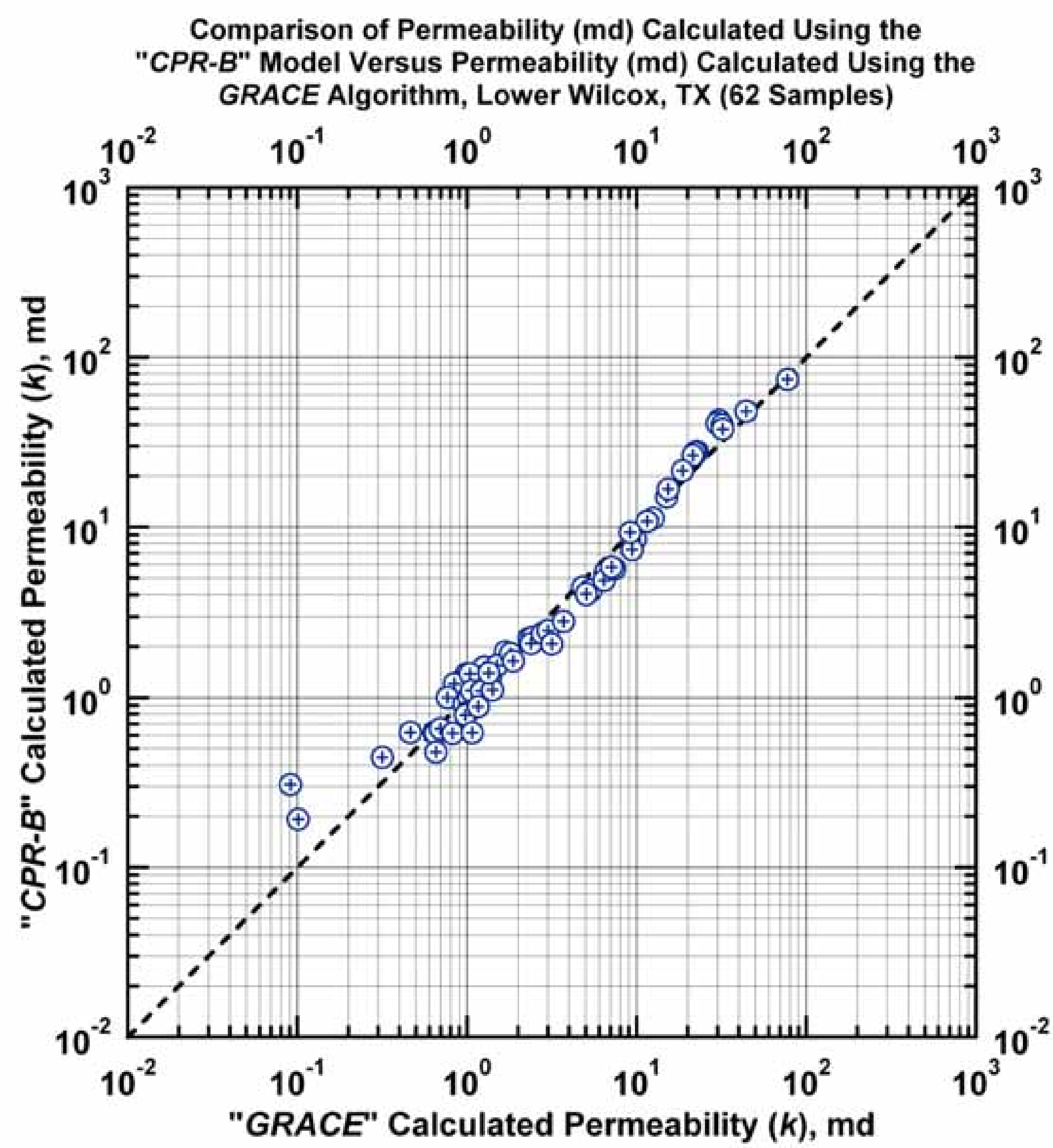

Figure 2.8b — Model *CPR-B*: Permeability calculated using Model *CPR-B* versus permeability calculated using the *GRACE* Algorithm. [*Case*: Lower Wilcox S. TX (USA)]

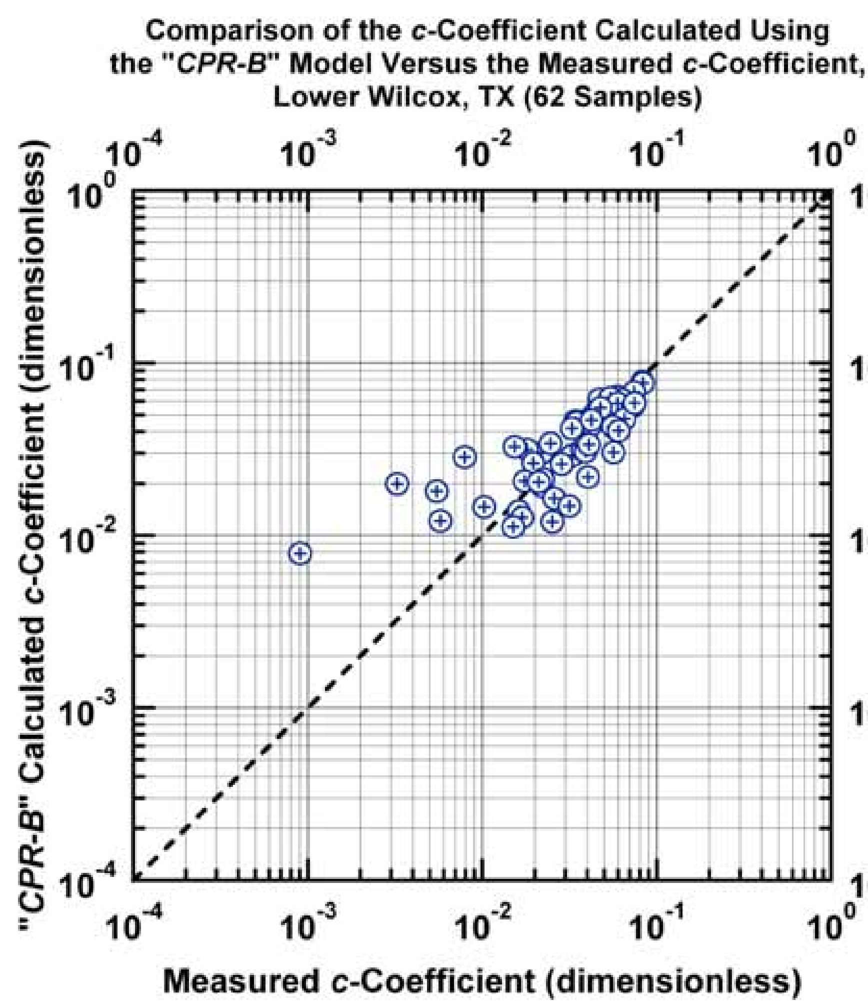

Figure 2.8c — Model *CPR-B*: Calculated *c*-function values versus measured *c*-function values. [*Case*: Lower Wilcox S. TX (USA)]

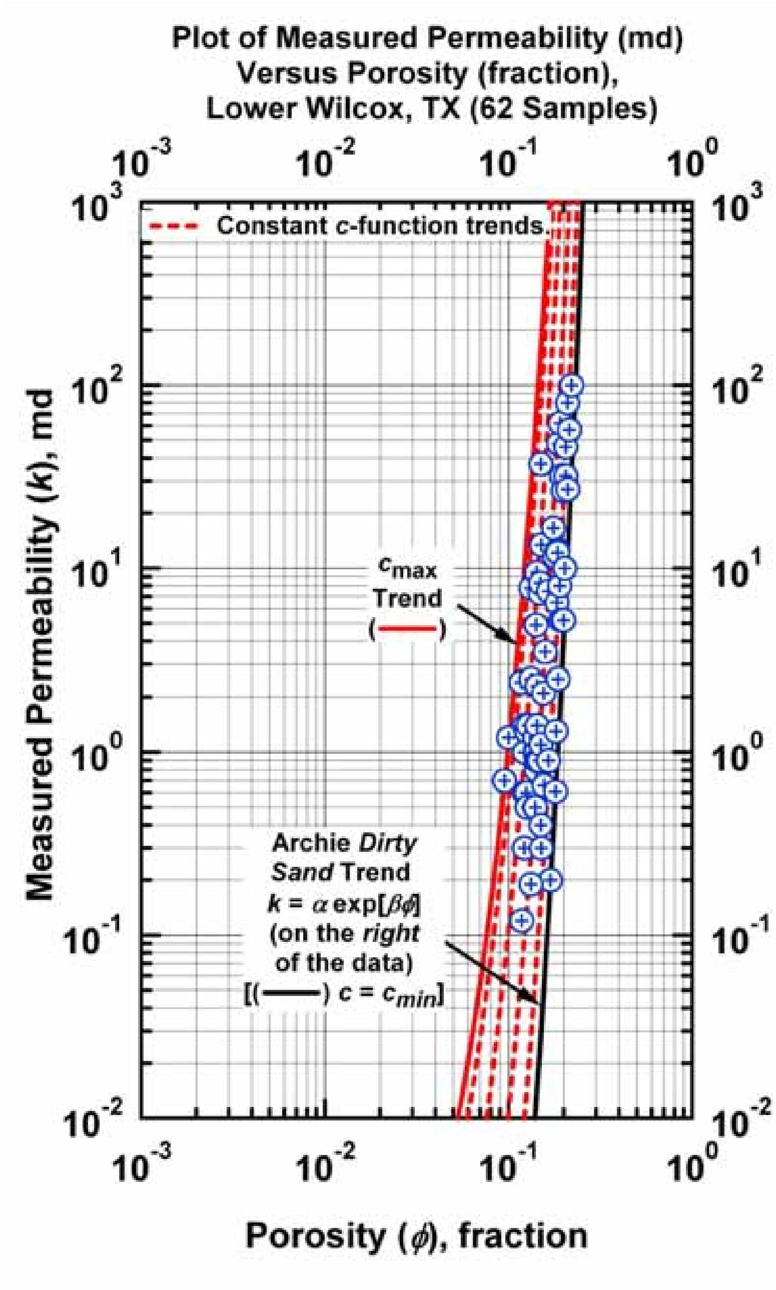

Figure 2.9a — Model *CPR-C*: $k = c\exp[\beta\phi]$ $\quad c = c_{\max}\exp[-c_1\phi^{c2}F^{c3}]$ — "Clean Sand" Plot (log-log format) — Archie "Dirty Sand" trend is given by the curved trend at the far right of the data (exponential model). [*Case*: Lower Wilcox S. TX (USA)]

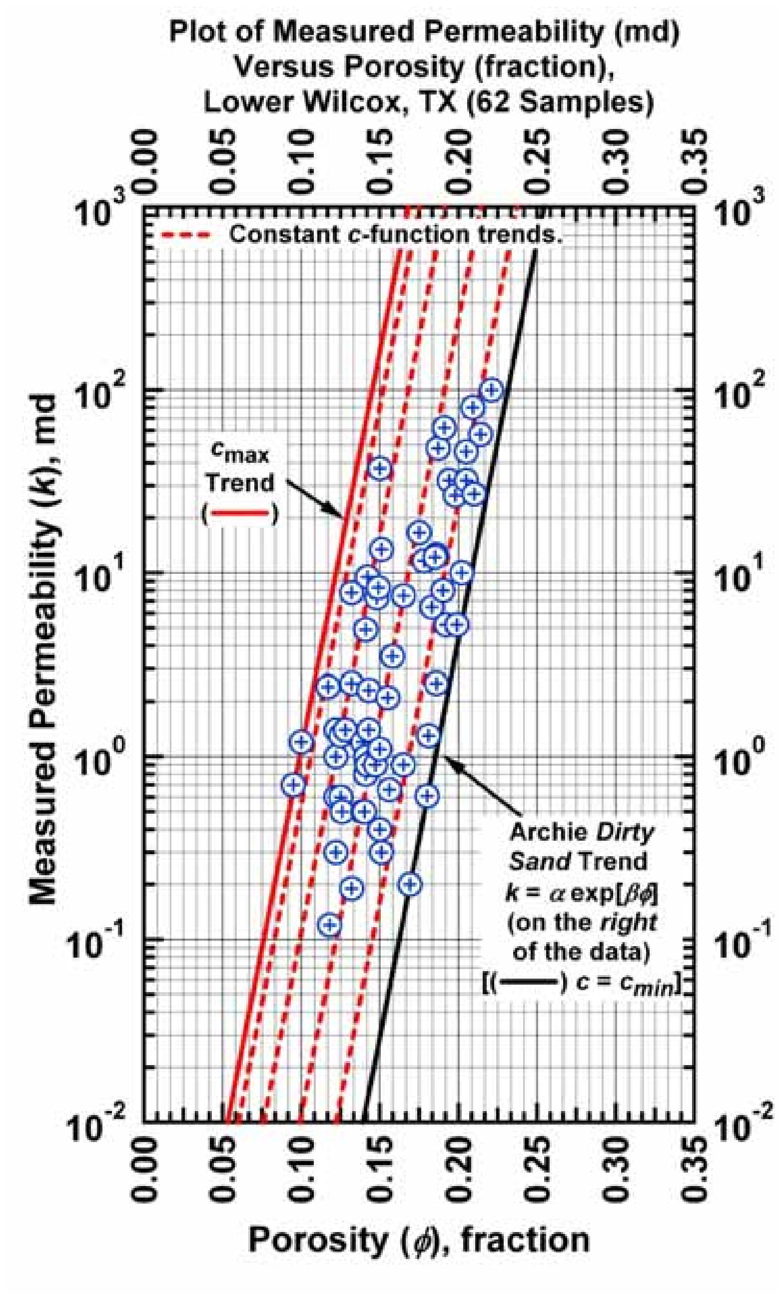

Figure 2.9b — Model *CPR-C*: $k = c\exp[\beta\phi]$ $c = c_{\max}\exp[-c_1\phi^{c_2}F^{c_3}]$ — "Dirty Sand" Plot (semilog format) — Archie "Dirty Sand" trend is given by the straight-line trend at the far right of the data (exponential model). [*Case*: Lower Wilcox S. TX (USA)]

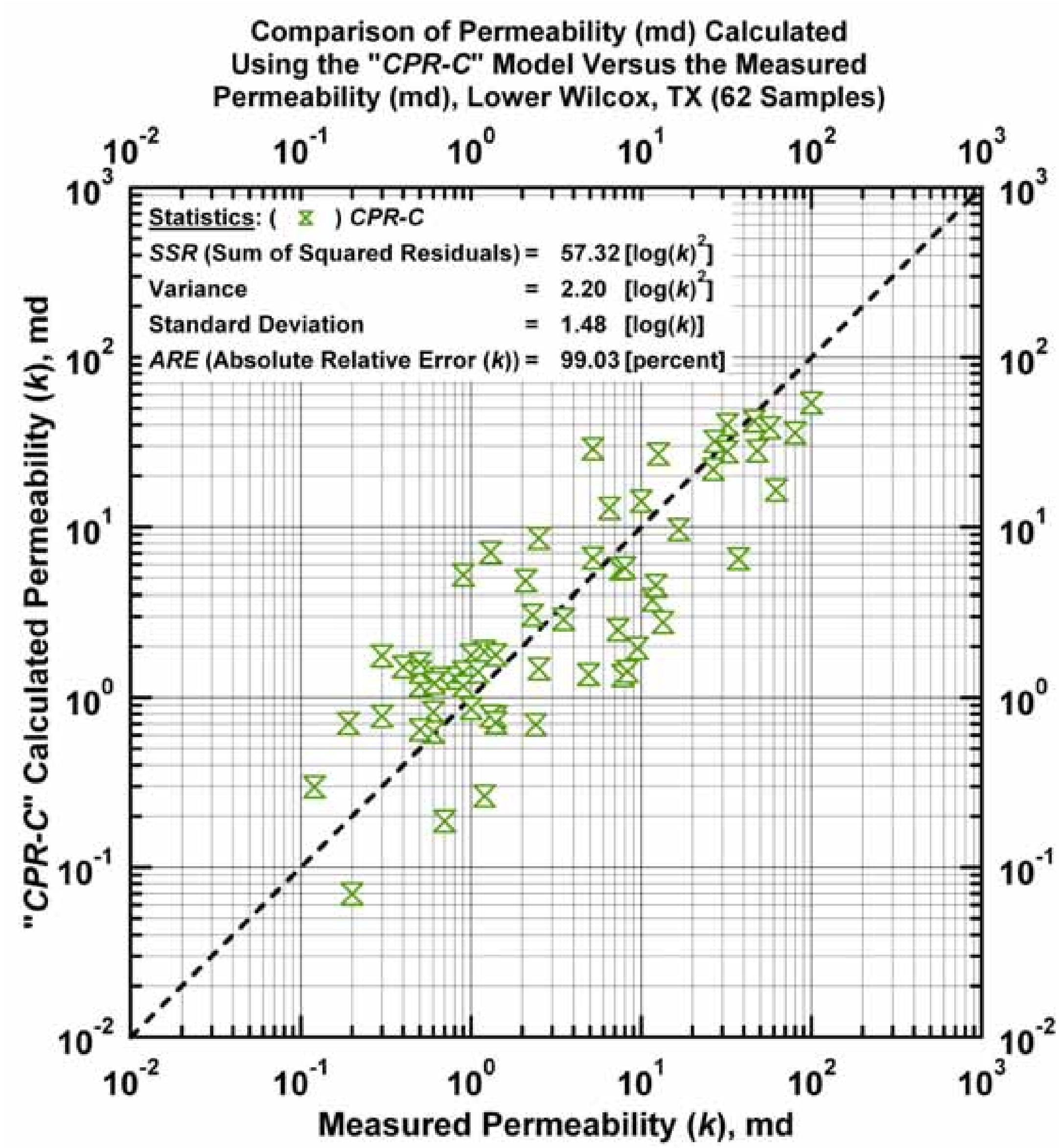

Figure 2.10a — Model *CPR-C*: calculated versus measured permeability. [*Case*: Lower Wilcox S. TX (USA)]

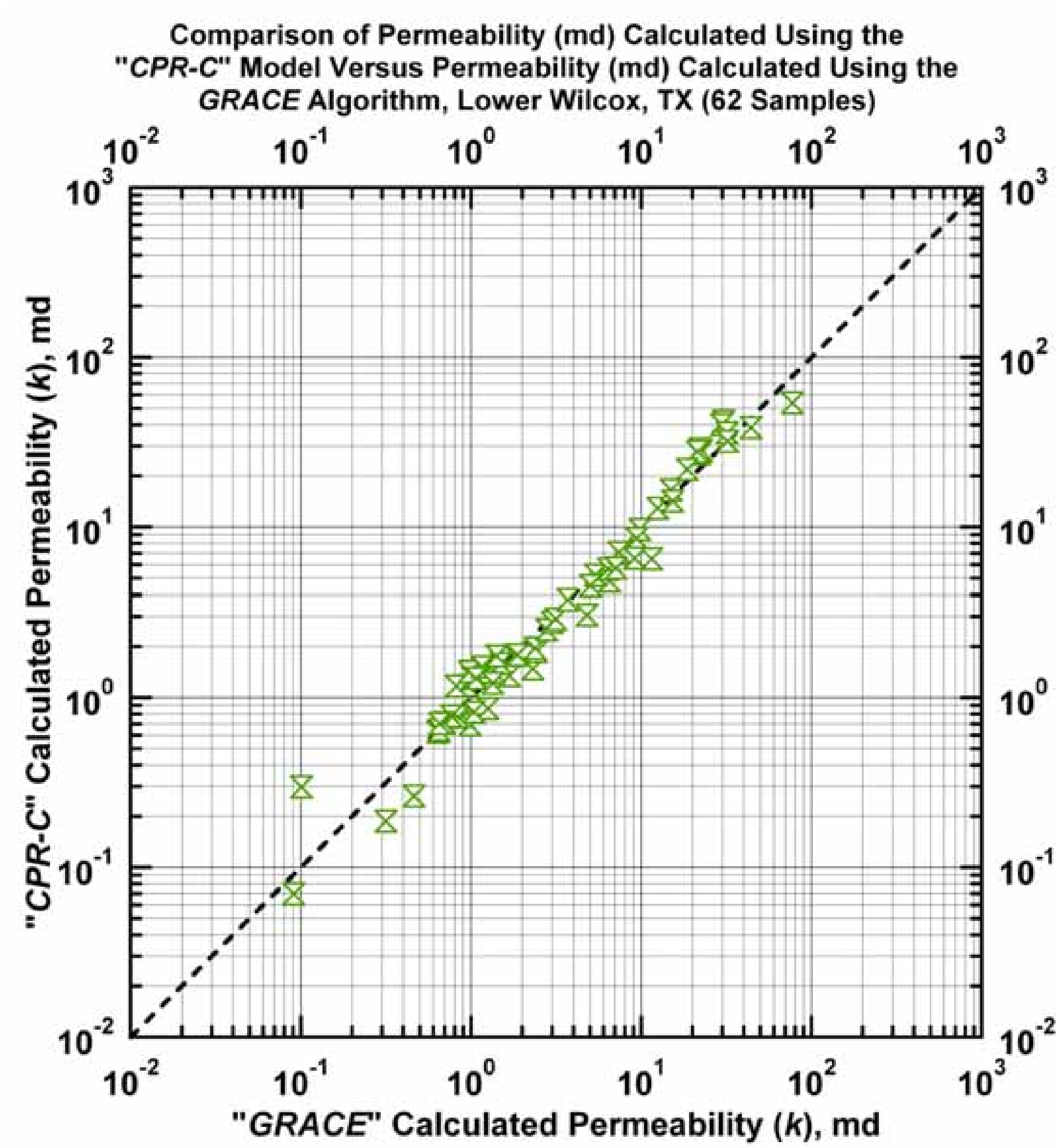

Figure 2.10b — Model *CPR-C*: Permeability calculated using Model *CPR-C* versus permeability calculated using the *GRACE* Algorithm. [*Case*: Lower Wilcox S. TX (USA)]

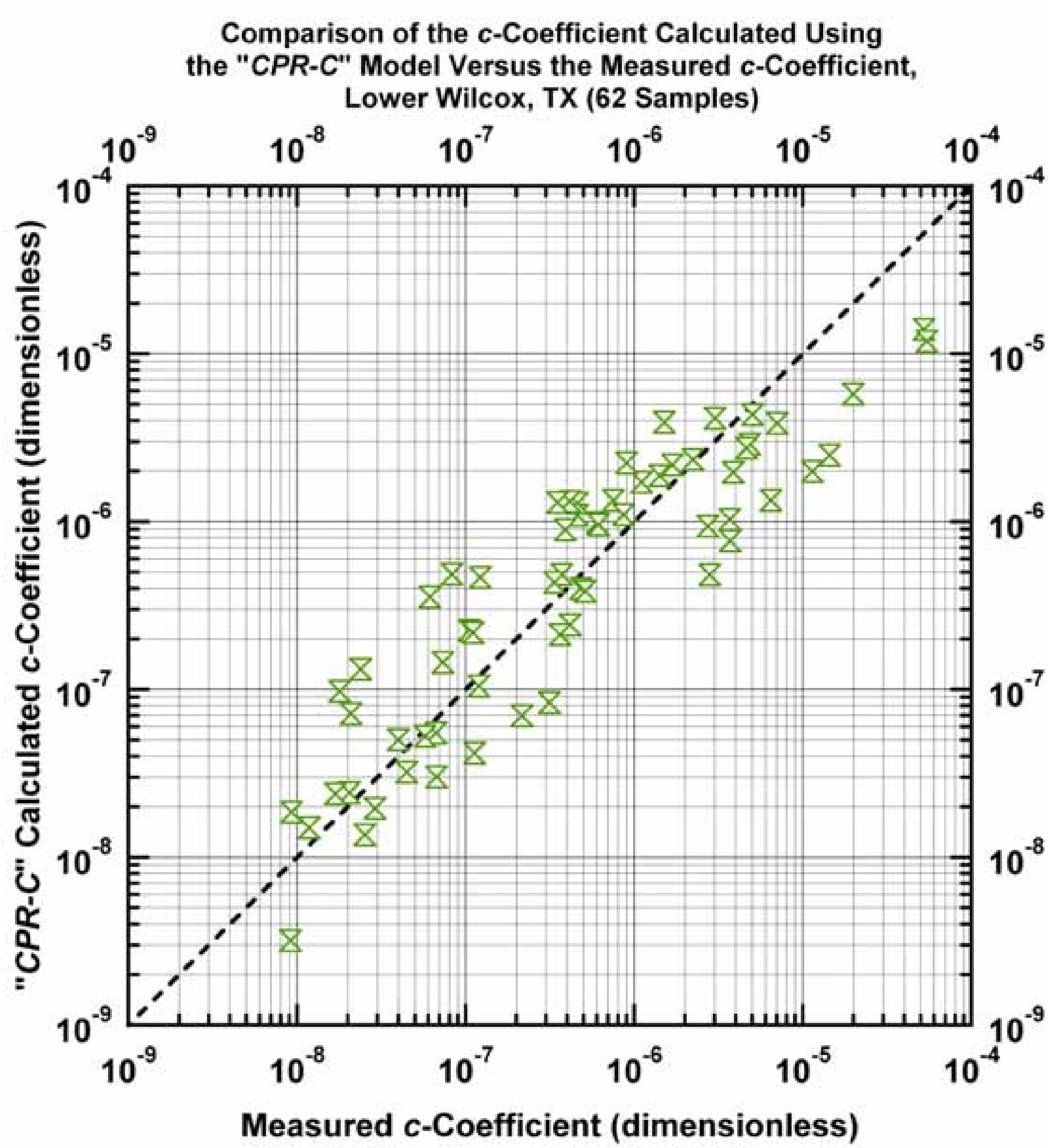

Figure 2.10c — Model *CPR-C*: Calculated *c*-function values versus measured *c*-function values. [*Case*: Lower Wilcox S. TX (USA)]

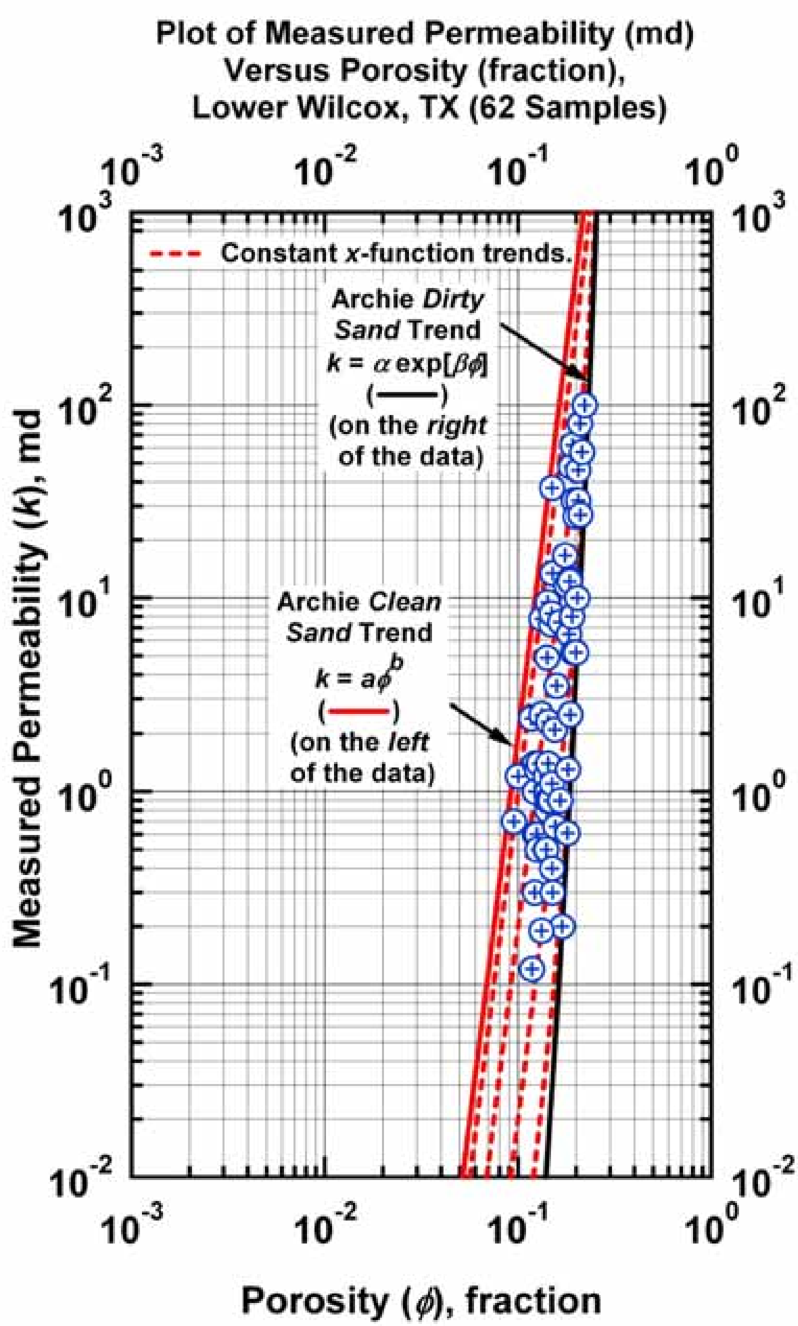

Figure 2.11a — Model *CPR-D*: $k = xa\phi^{b} + (1-x)\alpha\exp[\beta\phi]$ $[0 \le x \le 1]$ — *Weighted Power Law-Exponential Model* used to correlate permeability (k) and porosity (ϕ). "Clean Sand" Plot — Archie "Clean Sand" trend is given by the straight-line trend at the far left of the data (power law model). [*Case*: Lower Wilcox S. TX (USA)]

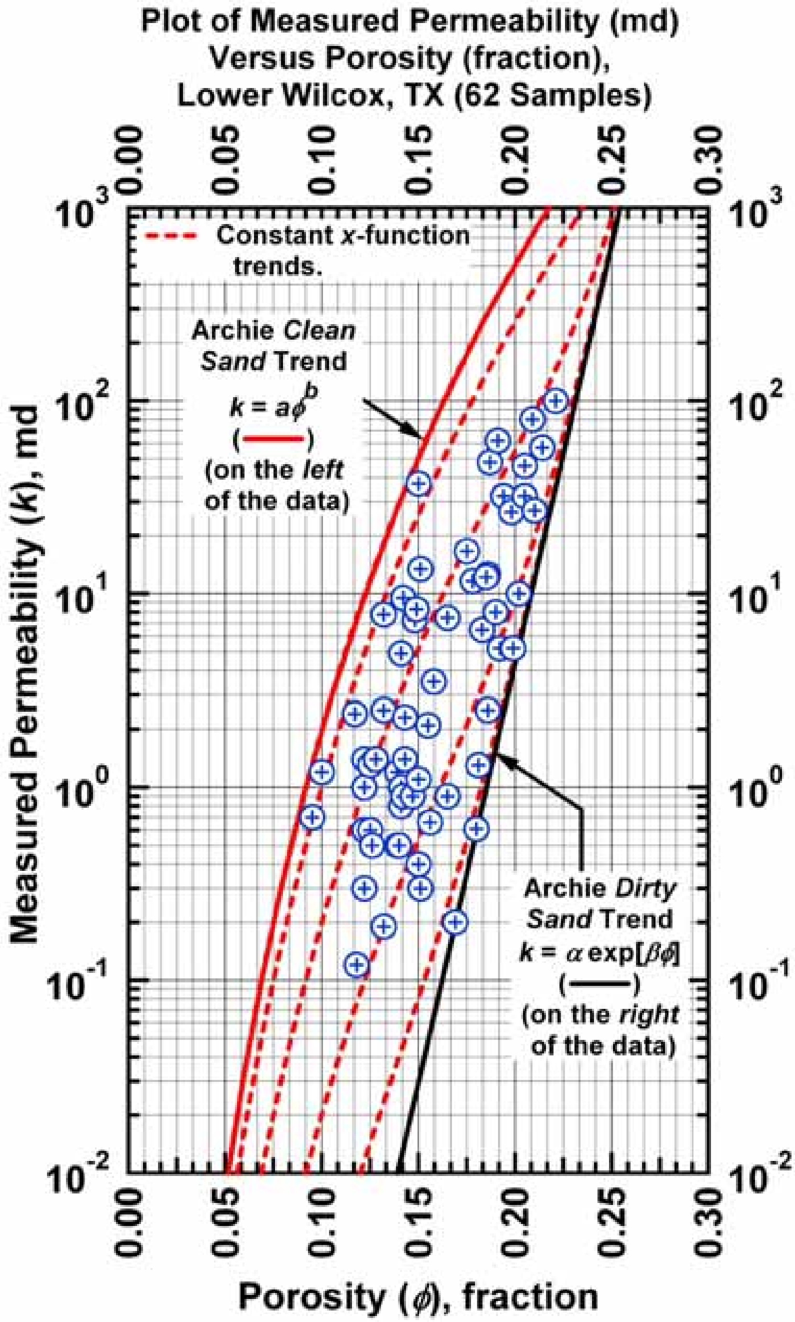

Figure 2.11b — Model *CPR-D*: $k = xa\phi^b + (1-x)\alpha\exp[\beta\phi]$ $[0 \le x \le 1]$ — *Weighted Power Law-Exponential Model* used to correlate permeability (k) and porosity (ϕ). "Dirty Sand" Plot — Archie "Dirty Sand" trend is given by the straight-line trend at the far right of the data (exponential model). [*Case*: Lower Wilcox S. TX (USA)]

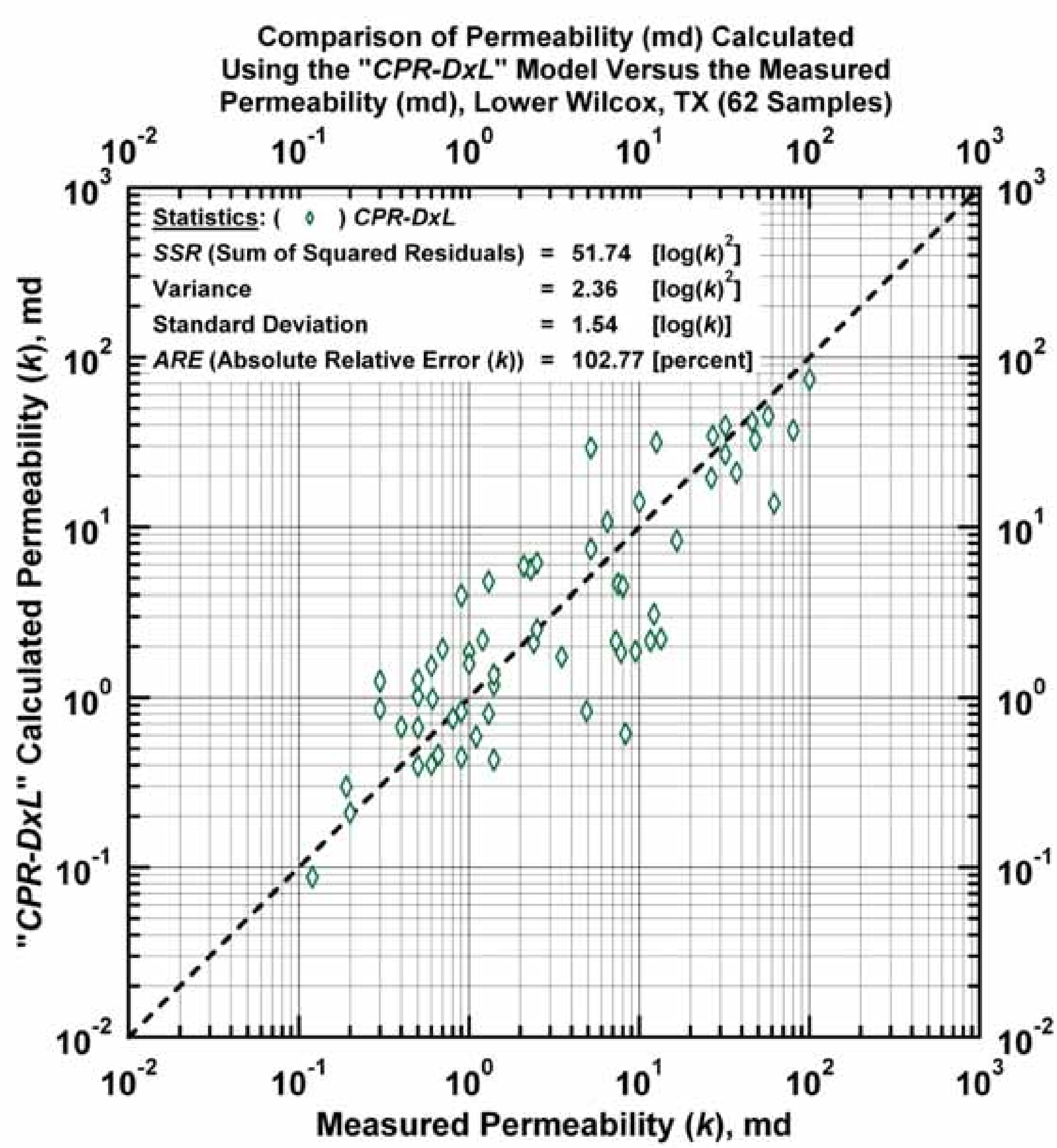

Figure 2.12a — Model *CPR-DxL*: Calculated versus measured permeability. [*Case*: Lower Wilcox S. TX (USA)]

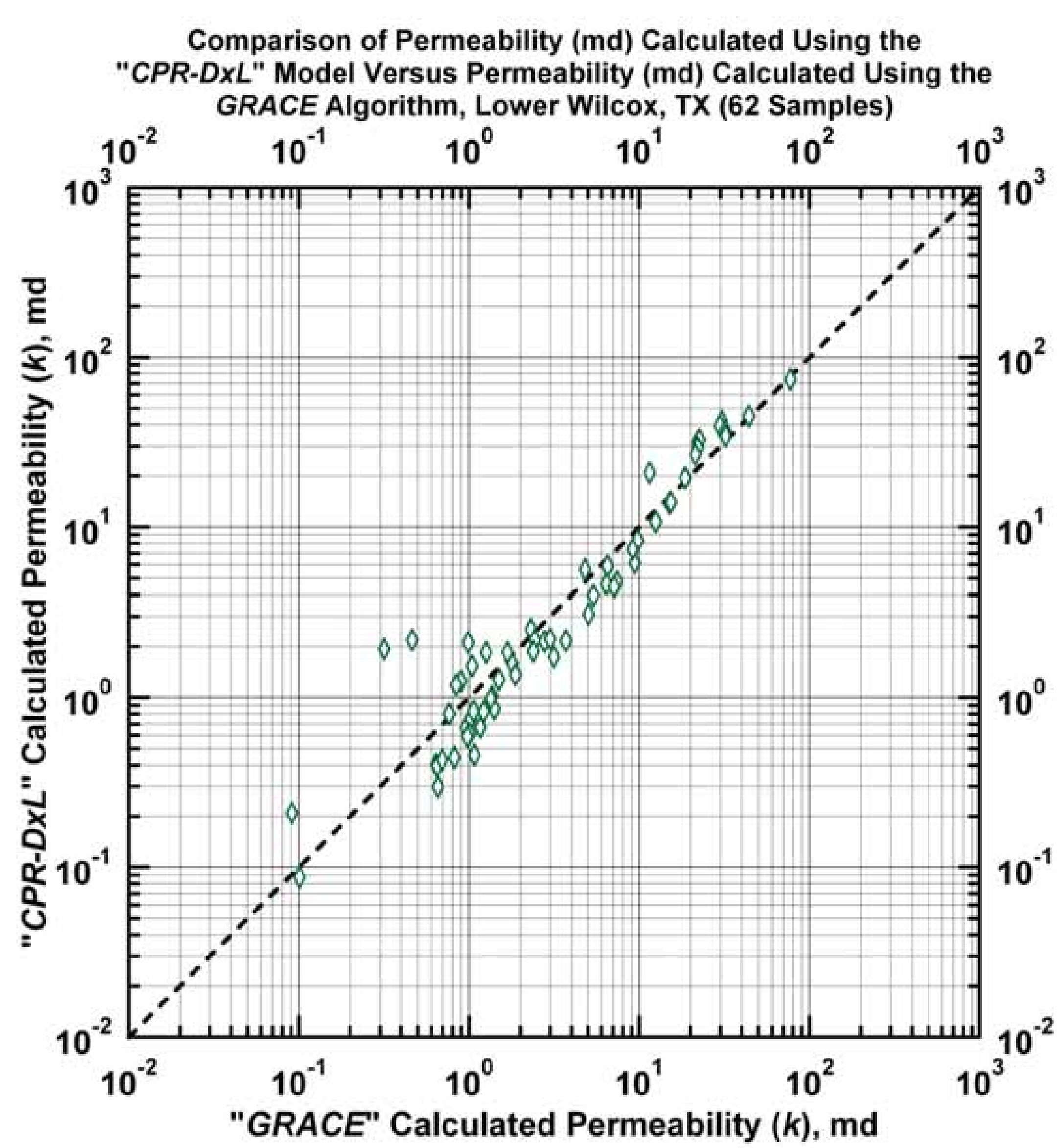

Figure 2.12b — Model *CPR-DxL*: Permeability calculated using Model *CPR-C* versus permeability calculated using the *GRACE* Algorithm. [*Case*: Lower Wilcox S. TX (USA)]

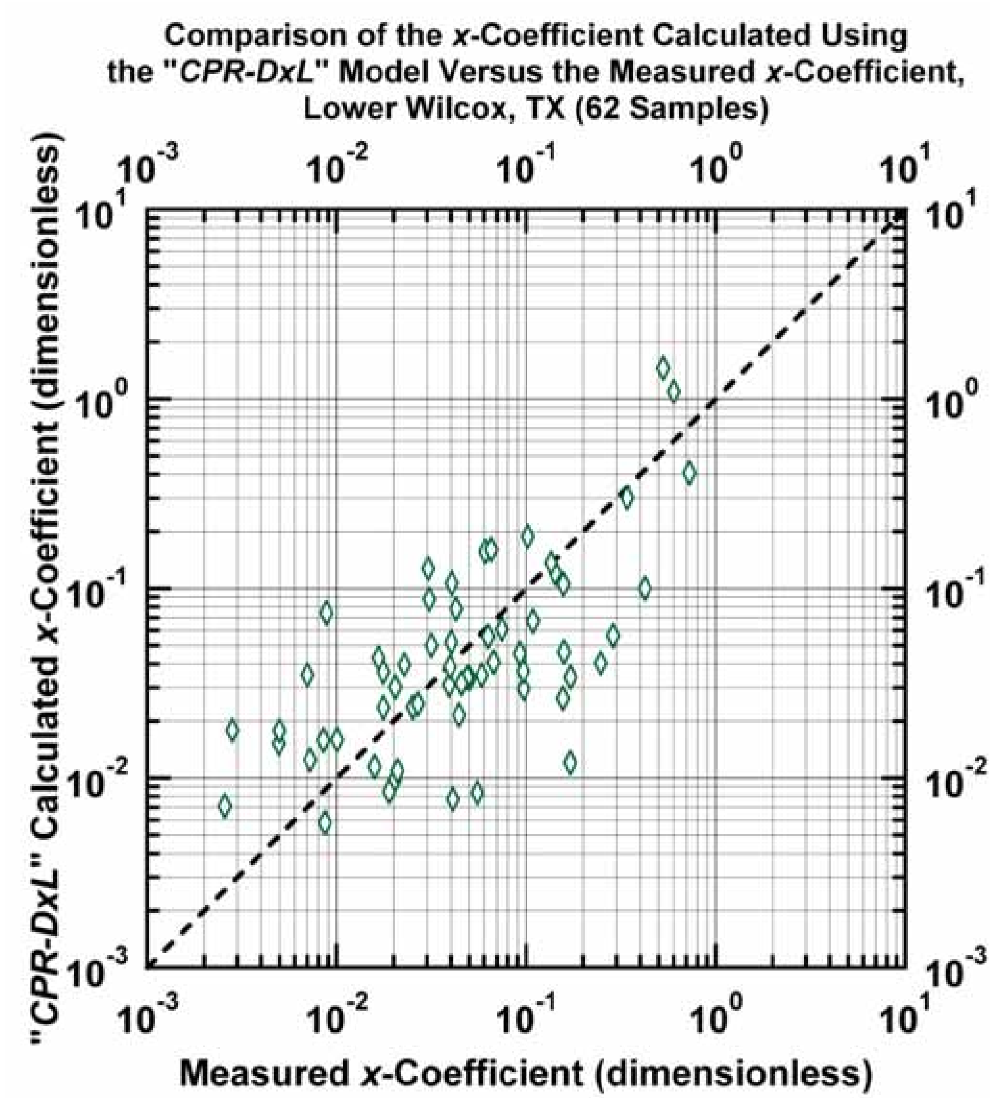

Figure 2.12c — Model *CPR-DxL*: Calculated *x*-function weight values versus measured *x*-function weight values. [*Case*: Lower Wilcox S. TX (USA)]

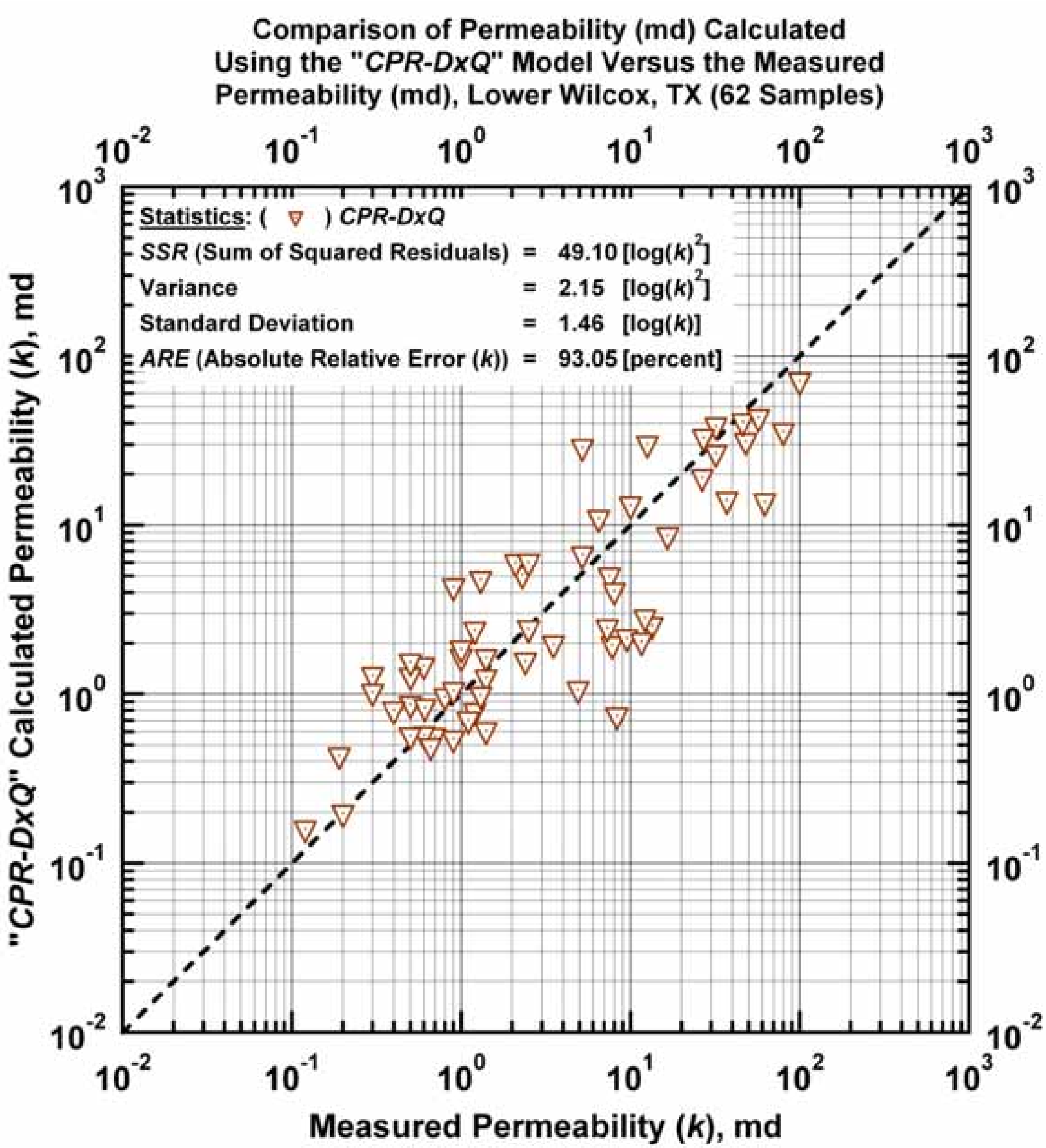

Figure 2.13a — Model *CPR-DxQ*: Calculated versus measured permeability. [*Case*: Lower Wilcox S. TX (USA)]

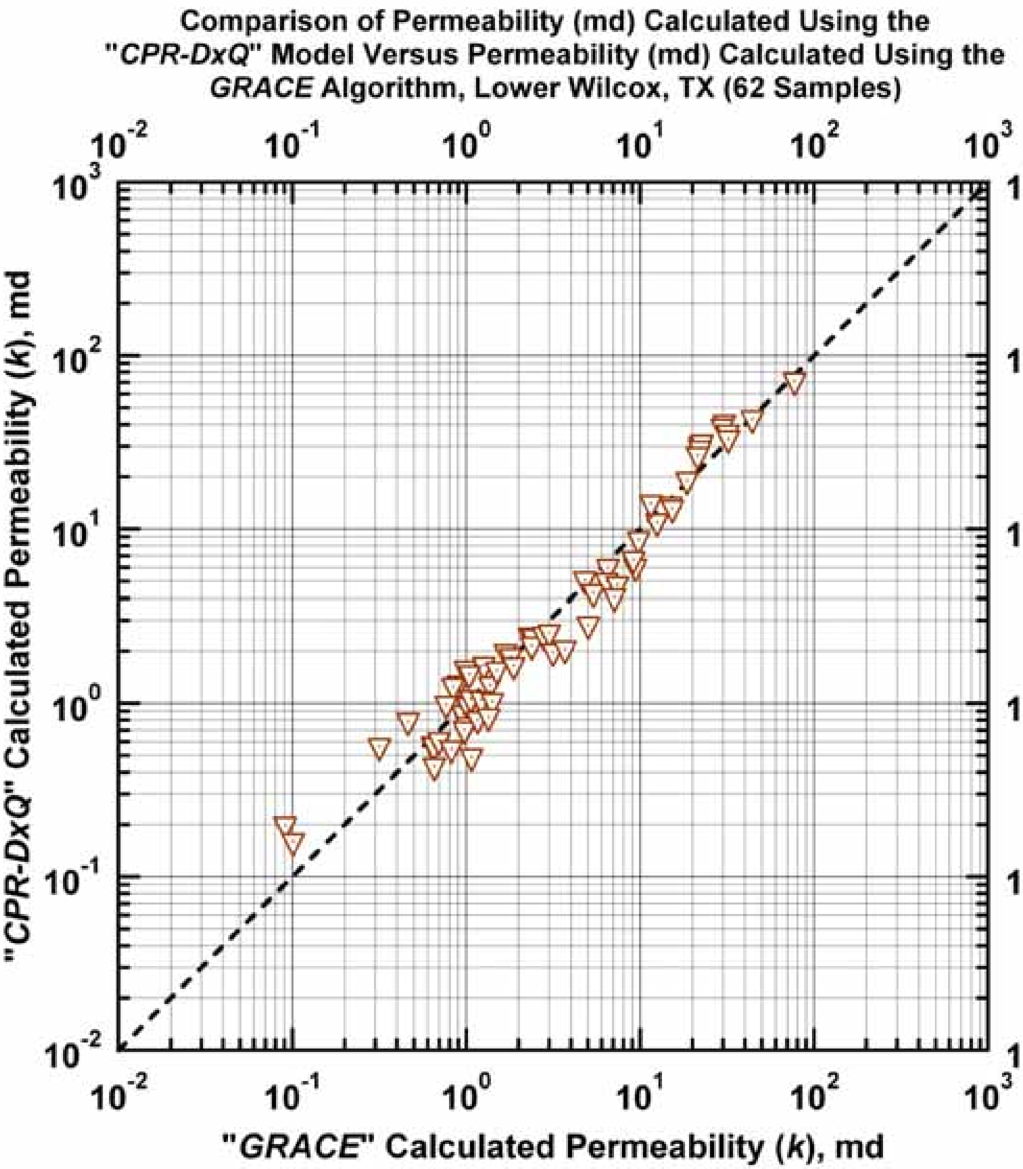

Figure 2.13b — Model *CPR-DxQ*: Permeability calculated using Model *CPR-C* versus permeability calculated using the *GRACE* Algorithm. [*Case*: Lower Wilcox S. TX (USA)]

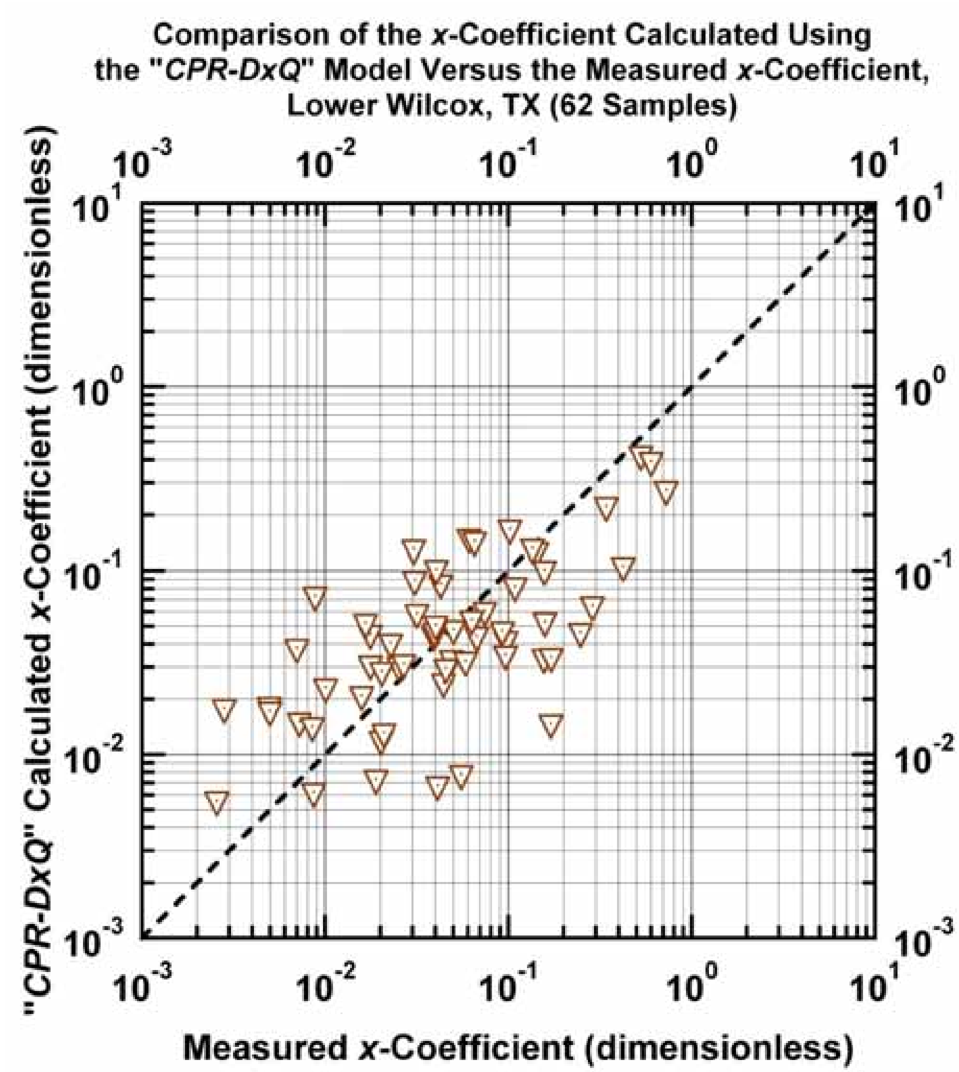

Figure 2.13c — Model *CPR-DxQ*: Calculated *x*-function weight values versus measured *x*-function weight values. [*Case*: Lower Wilcox S. TX (USA)]

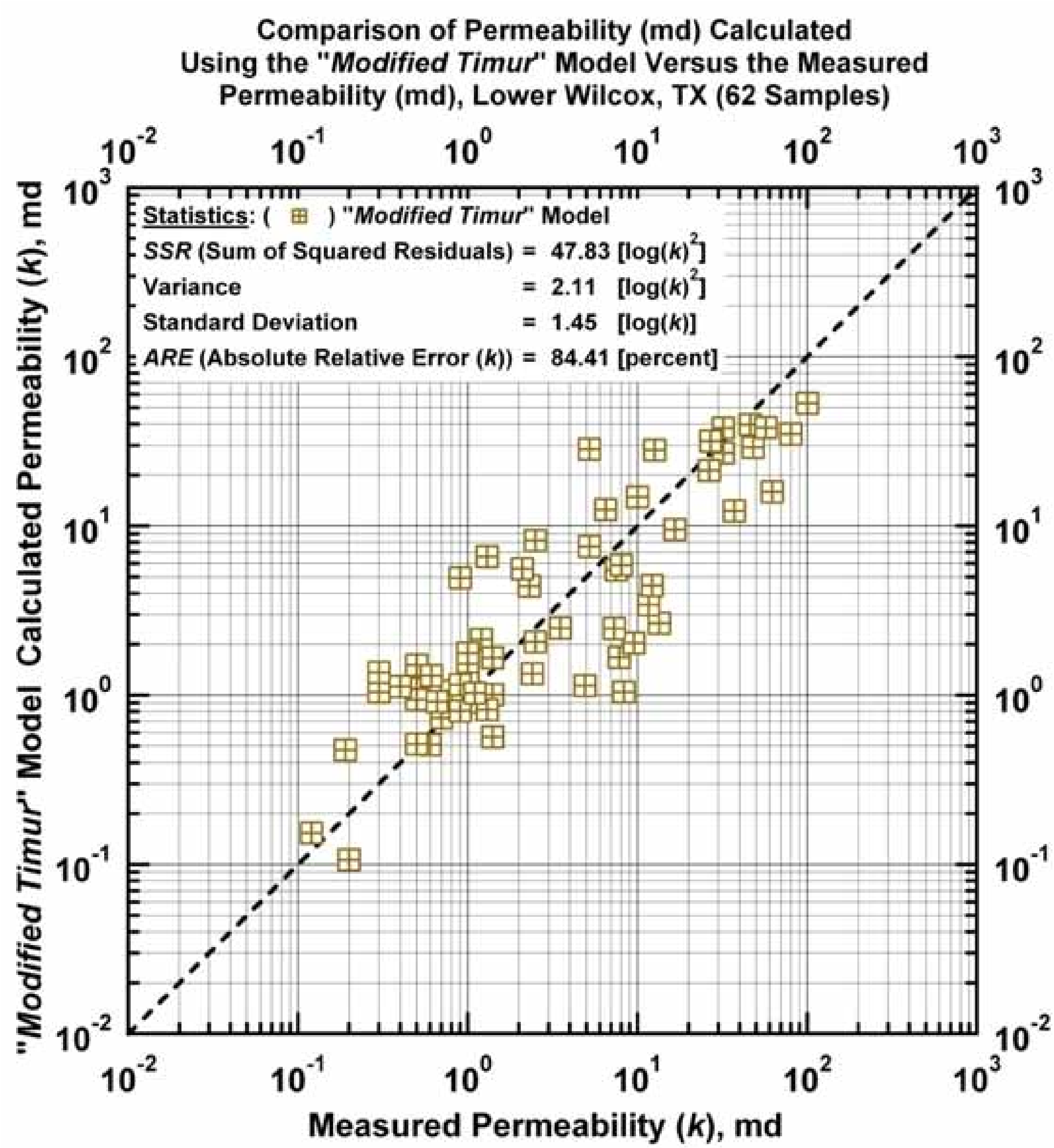

Figure 2.14a — "Modified Timur Model:" Calculated versus measured permeability. [*Case*: Lower Wilcox S. TX (USA)]

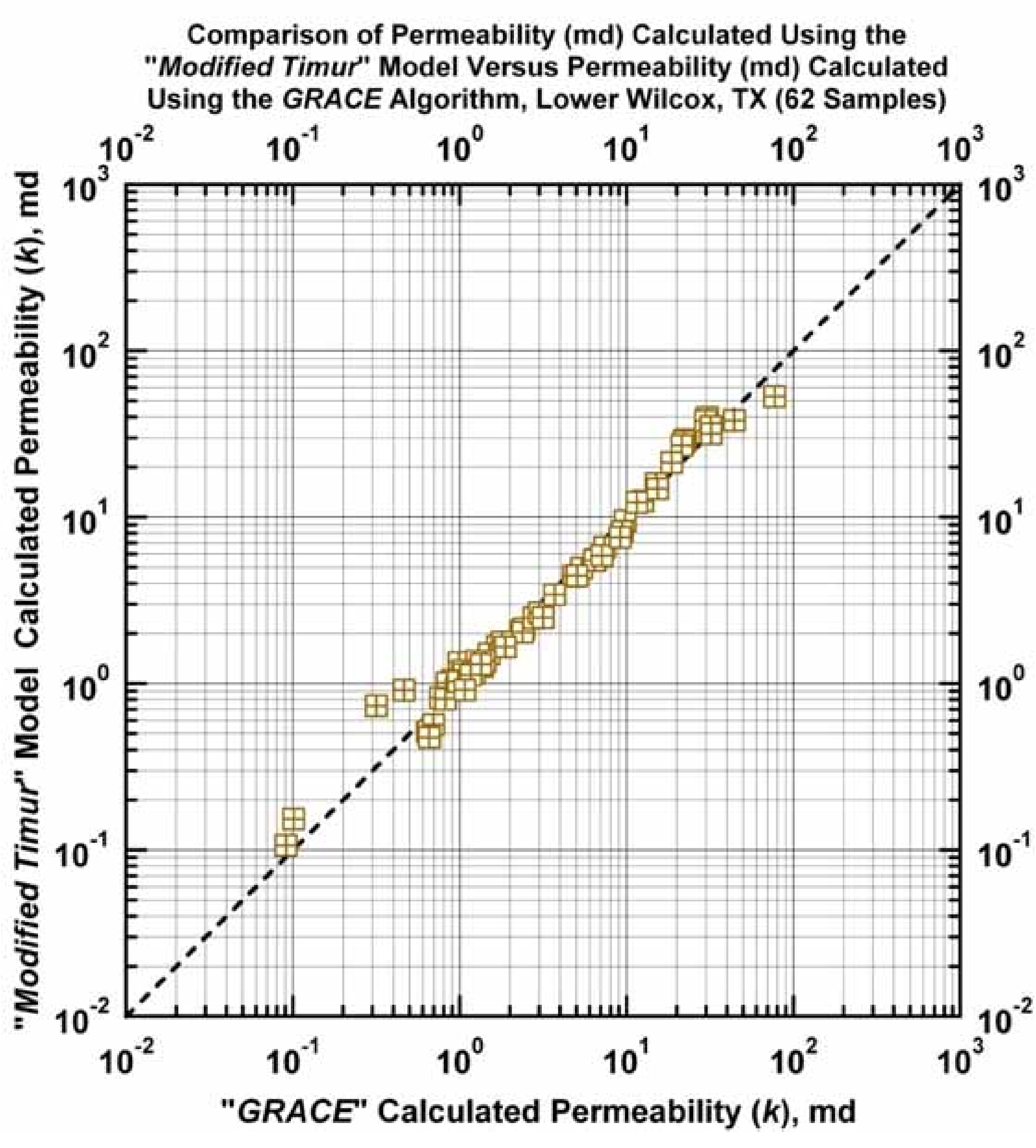

Figure 2.14b — "Modified Timur Model:" Permeability calculated using the "Modified Timur Model" versus permeability calculated using the *GRACE* Algorithm. [*Case*: Lower Wilcox S. TX (USA)]

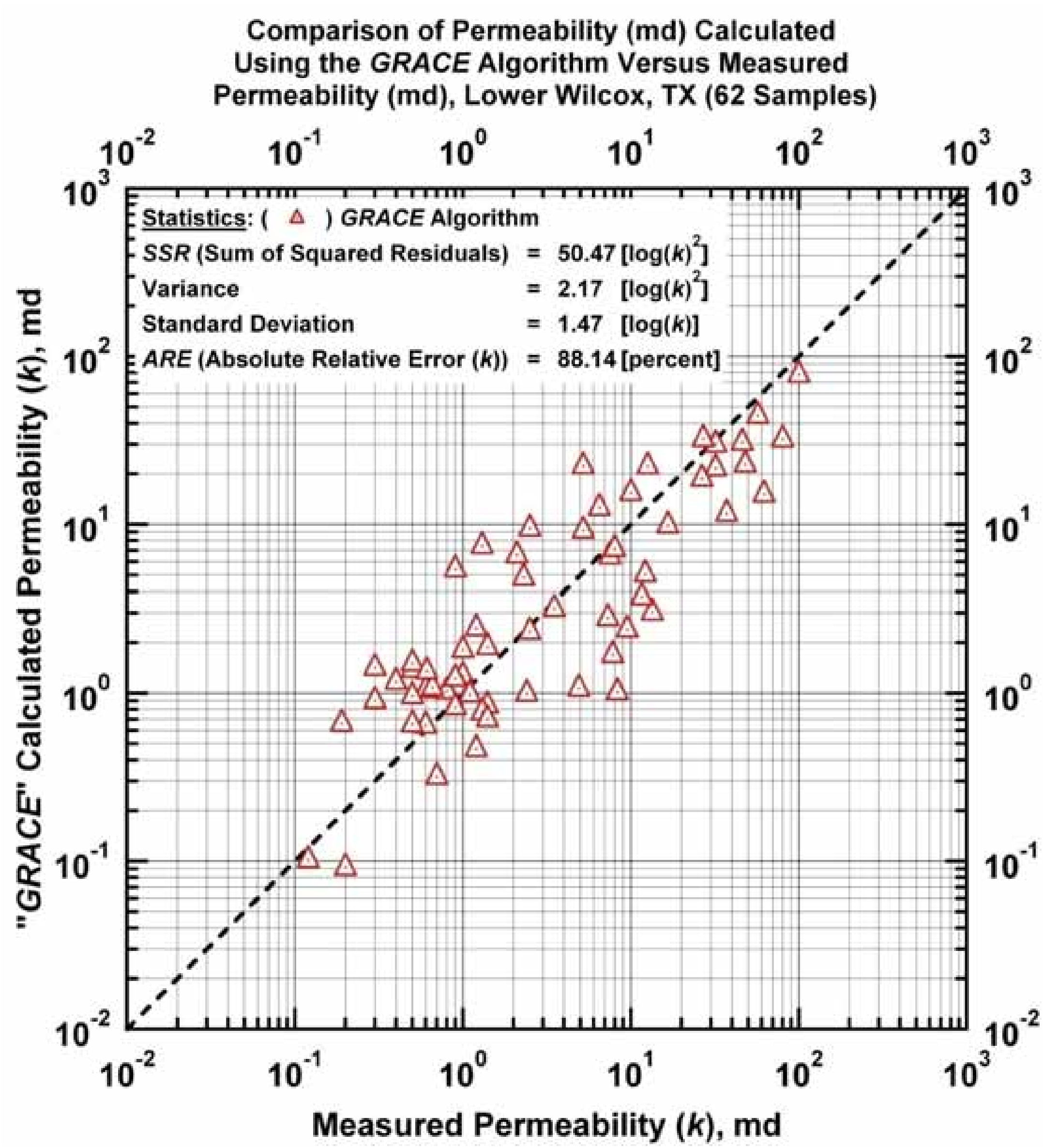

Figure 2.15 — *GRACE* Model: Calculated versus measured permeability. [*Case*: Lower Wilcox S. TX (USA)]

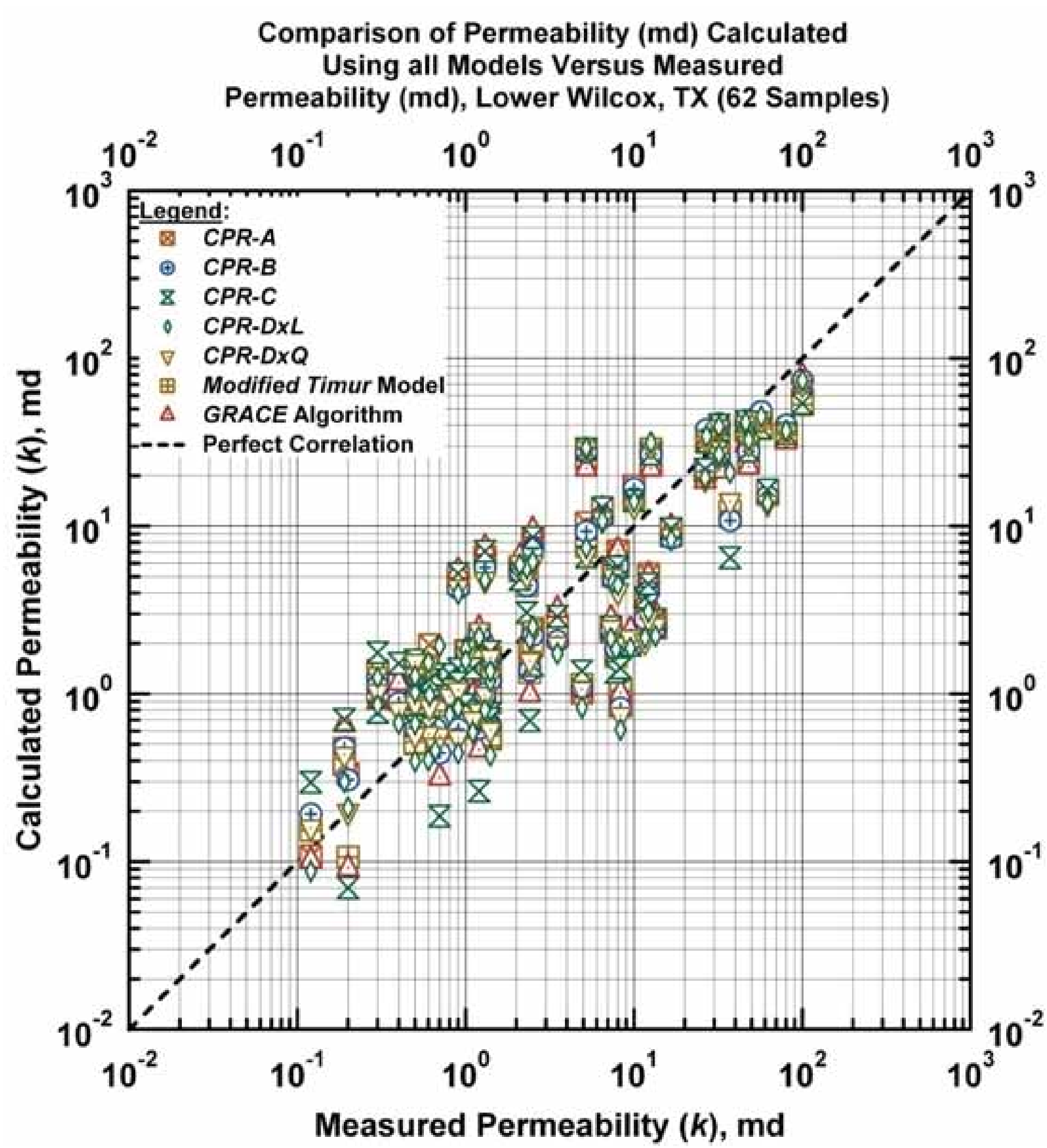

Figure 2.16 — All Models: Calculated versus measured permeability. [*Case*: Lower Wilcox S. TX (USA)]

CHAPTER III

SUMMARY, CONCLUSIONS, AND RECOMMENDATIONS FOR FUTURE WORK

3.1 Summary

In this work, we have successfully developed, demonstrated, and validated our concept of a characteristic permeability relation (*CPR*) for several different models where $k = f(\phi, S_w \text{ or } F)$. Our goal was not to achieve a "universal" *CPR*, but to identify the strengths of each of our proposed relations. Perhaps the most important contribution of this work is the systematic evaluation of each *CPR* — in particular, the illustration of the dominant (or characteristic) behavior of each *CPR*.

3.2 Conclusions

We present the following conclusions for our characteristic permeability relations (*CPRs*) (*i.e.*, permeability models):

- *Archie "Clean Sand" Model*:

  $$k = a\phi^b \qquad (1.1)$$

  - Base Plot: log(k) versus log(ϕ).
  - This is the basis relation for all "power law" *CPRs*.
  - This *CPR* is uniquely suited to highly-sorted unconsolidated sediments.

- *CPR-A — Modified Archie "Clean Sand" Model*: (Bryant-Finney Model)

  $$k = a(\phi - c)^b \quad \text{where} \quad c = c_{\max}\exp[-c_1\phi^{c_2} z^{c_3}] \qquad (2.1)$$

  - Base Plot: log(k) versus log(ϕ).
  - This *CPR* represents *negative* deviation from the Archie "Clean Sand" power law model — *i.e.*, the permeability profile is less than the Archie "Clean Sand" *CPR*.
  - The straight-line power law trend (c=0) must be placed just to the *left* of the data.
  - This *CPR* has the potential for negative values in the power law argument — therefore, $c_{\max}$ must be chosen carefully.

● *CPR-B — Modified Archie "Dirty Sand" Model*: (Power-Law Basis)

$$k = a(\phi + c)^{b} \quad \text{where} \quad c = c_{\max} \exp[-c_1 \phi^{c2} z^{c3}] \qquad (2.2)$$

■ Base Plot: log(k) versus log(ϕ).

■ This *CPR* represents *positive* deviation from a straight-line power law trend (*i.e.*, c=0), placed just beyond the far rightmost portion of the data trend.

■ The straight-line power law trend (c=0) must be placed just to the *right* of the data.

■ For our data sets, this *CPR* was the most "universal" in terms of the proposed "simple" power law or exponential relations (*CPR-DxL* and *CPR-DxQ* were often quite comparable to this relation).

● *CPR-C — Modified Archie "Dirty Sand" Model*: (Exponential Basis)

$$k = c \exp[\beta\phi] \quad \text{where} \quad c = c_{\max} \exp[-c_1 \phi^{c2} z^{c3}] \qquad (2.3)$$

■ Base Plot: log(k) versus ϕ.

■ This *CPR* is initiated with a straight-line placed on the *rightmost* data trend, and only the intercept (c) changes (as prescribed by Eq. 2.3).

■ For our data sets, this *CPR* also performed very well in general.

● *CPR-DxL — Weighted Power Law-Exponential Model*: (Linear logarithmic weights model)

$$k = xa\phi^{b} + (1-x)\alpha \exp[\beta\phi] \quad [0 \le x \le 1] \quad x = \exp[-\ln(x_0) + x_1 \ln(\phi) + x_2 \ln(z) + x_3 \ln(\phi)\ln(z)] \qquad (2.4)$$

■ Base Plots: log(k) versus log(ϕ) *and* log(k) versus ϕ.

■ This *CPR* performed well for most cases, the x-function model prescribed in Eq. 2.8 was, in a few cases, insufficient to model the character of the x-function defined by data.

● *CPR-DxQ — Weighted Power Law-Exponential Model*: (Quadratic logarithmic weights model)

$$k = xa\phi^{b} + (1-x)\alpha\exp[\beta\phi] \qquad [0 \le x \le 1]$$
$$x = \exp\begin{bmatrix} -\ln(x_0) + x_1\ln(\phi) + x_2\ln(z) + x_3\ln(\phi)\ln(z) + x_4\ln(\phi)^2 \\ + x_5\ln(z)^2 + x_6\ln(\phi)^2\ln(z) + x_7\ln(\phi)\ln(z)^2 + x_8\ln(\phi)^2\ln(z)^2 \end{bmatrix}$$
.... (2.5)

■ Base Plots: log(k) versus log(ϕ) *and* log(k) versus ϕ.

■ This *CPR* performed well for all cases, often providing the best correlation. We have some concern that the flexible character of the x-function model prescribed in Eq. 2.5 may be "over-fitting" the data (*i.e.*, fitting the errors in the data). This should not be a significant issue, but the analyst should be aware of the possibility of this condition.

In addition to the conclusions given above — we note the following generic conclusions:

● The proposed "characteristic permeability relations" each have a unique "signature," and clearly some *CPRs* provide better correlation of data than others — this is a problem-dependent issue, there is no single best or worst *CPR*.

● The systematic application of the *CPRs* as proposed and demonstrated in this work should provide the ability to correlate a given set of permeability data with other variables (*e.g.*, porosity, water saturation, Archie Formation Factor, shale fraction, individual well log responses, etc.).

3.3 Recommendations for Future Work

We put forward the following recommendations to extend this work:

● Application/validation of the *CPRs* to samples from specific carbonate reservoirs.

● Application/validation of the *CPRs* to samples from low to ultra-low permeability reservoirs.

● Extension of the *CPRs* to the identification and analysis of "hydraulic flow units."

● Integration of the *CPRs* with relations for capillary pressure and relative permeability.

● Utilization of the *CPRs* for reservoir scaling (heterogeneity).

NOMENCLATURE

a = Constant coefficient in the characteristic permeability relation
b = Constant coefficient in the characteristic permeability relation
c = Function in the characteristic permeability relation
d_p = Average grain diameter, m (or appropriate consistent units)
F = Archie Formation Factor (dimensionless)
k = Formation Permeability, md (or any consistent units)
S_w = Water Saturation (fraction)
V_{sh} = Shale Volume (fraction)
x = Weighting Function
z = Variable (Water saturation or Archie Formation Factor)
α = Constant coefficient in the characteristic permeability relation (*CPR-C*, *CPR-DxL*, *CPR-DxQ*)
β = Constant coefficient in the characteristic permeability relation (*CPR-C*, *CPR-DxL*, *CPR-DxQ*)
ϕ = Porosity, fraction

REFERENCES

Ahmed, U., Crary, S.F., and Coates, G.R. 1989. Permeability Estimation: The Various Sources and Their Interrelationship. Paper SPE 19604 presented at the SPE Annual Technical Conference and Exhibition, San Antonio, Texas, 8-11 October.

Archie, G.E. 1942. Electrical Resistivity Log as an Aid in Determining Some Reservoir Characteristics. *Trans*., AIME **146**: 54-62.

Archie, G.E. 1950. Introduction to Petrophysics of Reservoir Rocks. *Bull*. AAPG **34**: 943-961.

Beard, D.C., and Weyl, P.K. 1973. Influence of Texture on Porosity and Permeability of Unconsolidated Sand. *Bull.*, AAPG **57**: 349-69.

Berg, R.R. Method for Determining Permeability from Reservoir Rock Properties. 1970. *Trans.*, GCAGS **20:** 303-317.

Bryant, S., Cade, C., and Mellor, D. 1993a. Permeability Prediction from Geologic Models. *Bull.*, AAPG **77**: 1338-1350.

Bryant, S., Cade, C., and Mellor, D. 1993b. Physically Representative Network Models of Transport in Porous Media. *AIChE* **39**: 387-396.

Bryant, S.C., King, P.R., and Mellor, D.W. 1993c. Network Model Evaluation of Permeability and Spatial Correlation in a Real Random Sphere Packing. *Transport in Porous Media* **11**: 53-70.

Coates, G.R., and Denoo, S. 1981. The Producibility Answer Product. *Schlumberger Technical Review* **29** (2): 55-63.

Ellis, K.W. 1987. Extended Correlations of Porosity, Permeability, and Formation Resistivity Factor. MS thesis, Texas A&M U., College Station, Texas.

Finney, J. 1970. Random Packings and the Structure of Simple Liquids: I. The Geometry of Random Close Packing. Proceedings of the Royal Society of London Series A-Mathematical & Physical Sciences **319**: 479–493.

Hazlett, W.G. 1989. Correlation of Reservoir Rock Properties in Porous Media. PhD dissertation, Texas A&M U., College Station, Texas.

Jennings, J.W., and Lucia, J. 2001. Predicting Permeability from Well Logs in Carbonates with a Link to Geology for Interwell Permeability Mapping. Paper SPE 71336 presented at the SPE Annual Technical Conference and Exhibition, New Orleans, Louisiana, September 30-October 3.

Morrow, N.M, Huppler, J.D., and Simmons III, A.B. 1969. Porosity and Permeability of Unconsolidated, Upper Miocene Sands from Grain-Size Analysis. *J. Sed. Pet.* **39** (1): 312-321.

Pape, H., Clauser, C., Iffland, J. 1999. Permeability Prediction Based on Fractal Pore-Space Geometry. *Geophysics* **64:** 1447–1460.

Pape, H., Clauser, C., Iffland, J. 2000. Variation of Permeability with Porosity in Sandstone Diagenesis Interpreted with a Fractal Pore Space Model. *Pure Applied Geophysics* **157**: 603–619.

Timur, A. An Investigation of Permeability, Porosity, and Residual Water Saturation Relationships. 1968. *Trans.*, SPWLA Symposium Paper I.

Travis Peak Formation Core Report — Well Howell No. 5, S.A. Holditch, (1986).

Travis Peak Formation Core Report — Well Cargill No. 15, Mobil Exploration & Production Company, (1989).

Xue, G., Datta-Gupta, A., Valko, P., and Blasingame, T.A. 1997. Optimal Transformations for Multiple Regression: Application to Permeability Estimation from Well Logs. *SPEFE*, 85-93.

APPENDIX A

DERIVATION OF THE "PAPE" MULTI POWER LAW FORMULATION FOR PERMEABILITY

Pape *et al.* (1999) developed a fractal model to predict the permeability of sedimentary as well as metamorphic rocks. The Pape *et al.* permeability model consists of a number of power law relations (typically with integer exponents) simply added together (usually 3). This approach is theoretically based on a fractal model for the internal structure of a porous medium [Pape *et al.* (1984, 1987a, 1987b) Pape and Schopper (1988), and Pape *et al.* 1999)]. The proposed "fractal" permeability relation is a completely general formulation that links porosity to permeability — where permeability can be estimated using either porosity data, or from the pore-radius distribution. Pape *et al.* (1999) propose that this general relation can be *tuned* to the entire range of sandstones — from clean to shaly sands.

A.1 Tortuosity

The expression for the permeability of a porous medium is given by the modified Kozeny–Carman equation [Carman (1956) and Kozeny (1927)]:

$$k = \frac{r_{eff}^2}{8} \frac{1}{F} \qquad \text{(A.1)}$$

Where F is the formation factor as defined by Archie (1942) — and is defined as the ratio of *tortuosity* (T) and the porosity (ϕ):

$$F = \frac{T}{\phi} \qquad \text{(A.2)}$$

The formation (resistivity) factor was defined as the ratio of the electrical resistivity of a porous medium saturated (100 percent) with an electrolyte compared to the resistivity of the electrolyte, and is written as:

$$F = \frac{R_o}{R_w} \qquad \text{(A.3)}$$

Considering Eq. A-3, it is obvious that R_o will always be greater than R_w, hence F will always be greater than unity. F can be related to permeability via the Kozeny–Carman relation (*i.e.*, Eq. A-1). An empirical relationship between F and ϕ is given by "Archie's first law" — which is given as:

$$F = \frac{a}{\phi^m} \qquad \text{(A.4)}$$

In Eq. A-4, a is a factor depending on lithology and m is the cementation (or tortuosity) factor, which depends on rock structure. From Serra (1984) the parameters a and m typically vary along the ranges:

$$0.6 < a < 2$$
$$1 \quad < m < 3$$

Pape *et al* (1987b) showed that the tortuosity behaves as a *fractal* and depends on the ratio of r_{eff} and r_{grain}, with an exponent involving the fractal dimension (D). The Pape *et al* (1987b) formulation is given as:

$$T = 1.34\left[\frac{r_{grain}}{r_{eff}}\right]^{0.67(D-2)} \quad \text{.....(A.5)}$$

Eq. A-5 implies that the tortuosity *increases* with *increasing* fractal dimension. Pape *et al* (1987b) suggest that Eq. A-5 is only valid for the range: $2 < D < 2.4$ (common rock samples). Pape and Schopper (1988) suggest that strongly fractured rocks (and/or claystones) demonstrate fractal dimensions in the range of $2.4 < D < 3$ — Pape and Schopper note that these rocks are characterized by a high degree of connectivity within the pore system, which in turn reduces the tortuosity.

At this stage r_{eff} is unknown, so we replace r_{eff} in Eq. A-5 by the pore radius at the 50th-percentile (r_{50}) and the r_{grain} variable is replaced by the median grain radius d_m. Also, as noted by Kulenkampff (1994), reservoir sandstones are limited in tortuosity — therefore Eq. A-5 is modified such that for large pore radii (r_{eff} or r_{50}), then we set $T = T_{\max} = 10$ as the limit when r_{eff} (or r_{50}) approaches zero. This substitution avoids extreme and unrealistic tortuosity values. Making these substitutions into Eq. A-5, and solving for the reciprocal of tortuosity using data taken on Rotliegend sandstones in northwestern Germany, Köhler *et al* (1993) presented the following result:

$$\frac{1}{T} = 0.1 + 0.5\left[\frac{r_{50}}{d_m}\right]^{0.67(D-2)} \quad \text{.....(A.6)}$$

A.2 Permeability-Porosity Relationship

Consider again the Kozeny–Carman (Eq. A-1) and the expression for the Archie Formation Factor (Eq. A-2), if we combine Eqs. A-1 and A-2, then we can express permeability as a function of the effective pore radius(r_{eff}), the tortuosity (T), and the porosity (ϕ) as:

$$k = \frac{r_{eff}^2}{8}\frac{1}{F} = \frac{r_{eff}^2}{8}\frac{1}{(T/\phi)} = \frac{r_{eff}^2}{8}\frac{\phi}{T} \quad \text{.....(A.7)}$$

Using Eq. A-5, and assuming that D=2.36 (the "average" value for hydrocarbon-bearing formations in northwestern German), Pape *et al* (1984) present the following relations for T and ϕ:

$$T = 1.34\left[\frac{r_{grain}}{r_{eff}}\right]^{0.67(D-2)} = 1.34\left[\frac{r_{grain}}{r_{eff}}\right]^{0.24} \quad \text{.....(A.8)}$$

and

$$\phi = 0.534\left[\frac{r_{grain}}{r_{eff}}\right]^{0.39(D-3)} = 0.5\left[\frac{r_{grain}}{r_{eff}}\right]^{-0.25} \quad \text{.......................................(A.9)}$$

If we neglect the slight differences in the exponents, solving Eqs. A-8 and A-9 for an approximation only in terms of tortuosity and porosity, we have:

$$T \approx \frac{0.67}{\phi} \quad \text{.......................................(A.10)}$$

and solving A-9 as an identity for r_{eff} and r_{grain} in terms of ϕ, we obtain:

$$r_{eff}^2 = r_{grain}^2 (2\phi)^8 \quad \text{.......................................(A.11)}$$

Substituting Eqs. A-2, A-10, and A-11 into Eq. A-1 — and using a default value of r_{grain} =200,000 nm (again, an average grain radius in the German sandstone data sets), k can now be written as

$$\begin{aligned} k &= \frac{r_{eff}^2}{8}\frac{1}{F} \\ &= \frac{r_{grain}^2}{8}\frac{(2\phi)^8}{(T/\phi)} \\ &= \frac{r_{grain}^2}{8}\frac{(2\phi)^8}{\left[\dfrac{0.67}{\phi^2}\right]} \\ &= \frac{(200{,}000\ \text{nm})^2}{8}\frac{(2)^8}{(0.67)}\phi^{10} \\ &= 1.91045\times 10^{12}\ \phi^{10}\ \text{nm}^2 \end{aligned}$$

$$\text{.......................................(A.12)}$$

Eq. A-12 defines a linear trend of slope 10 on a log–log plot of k versus ϕ. Eq. A-12 is presumed to be valid for porosities larger than 0.1 — Pape *et al* (1987a) and Pape *et al* (1987b) noted that the effective pore radii of the samples they considered do not decrease as rapidly with decreasing porosity as suggested by Eq. A-11. Pape *et al* suggest that the permeability estimates can be improved for cases where $0.01 < \phi < 0.1$ by assigning a fixed value to the effective hydraulic pore radius in Eq. A-1 — *i.e.*, $r_{eff} = r_{eff,fix} = 200$ nm. This substitution is equal or near to the mean of r_{eff} value determined from measured permeabilities and porosities using Eqs. A-1, A-2, and A-10 for $0.01 < \phi < 0.1$. Substituting $r_{eff,fix}$ =200 nm into the combination of Eqs. A-1, A-2, and A-10 yields

$$k = \frac{r_{eff}^2}{8}\frac{1}{F}$$
$$= \frac{(200\text{ nm})^2}{8}\frac{1}{\left[\frac{0.67}{\phi^2}\right]}$$
$$= 7462.69\,\phi^2\text{ nm}^2 \qquad \text{(A.13)}$$

However, for $\phi < 0.01$ this expression still yields permeabilities which are *much lower* than the measured data. A limiting value for r_{eff} in this range is $r_{eff,min}$ = 50 nm — substituting $r_{eff,min}$ = 50 nm as r_{50} into Eq. A-6 yields a maximum value for tortuosity, $T_{\max} = 10$. Using $r_{eff} = r_{eff,min}$ = 50 nm and $T = T_{\max} = 10$; substituting into Eqs. A-1 and A-2 and solving for permeability yields:

$$k = \frac{r_{eff}^2}{8}\frac{1}{F}$$
$$= \frac{r_{eff,\min}^2}{8}\frac{1}{(T_{\max}/\phi)}$$
$$= \frac{r_{eff,\min}^2}{8}\frac{1}{T_{\max}}\phi$$
$$= \frac{(50\text{ nm})^2}{8}\frac{1}{(10)}\phi$$
$$= 31.25\,\phi\text{ nm}^2 \qquad \text{(A.14)}$$

Pape *et al* (1999) propose a generalized expression for permeability as a *summation* of Eqs. A-12, A-13, and A-14 — *with the rationale that this definition provides an "average permeability-porosity" relationship for the entire porosity range*. The generalized Pape *et al* (1999) result is:

$$k = 31.25\,\phi + 7462.69\,\phi^2 + 1.91045\times10^{12}\,\phi^{10}\ \text{nm}^2\ \ (\textit{Pape Analytical}) \qquad \text{(A.15)}$$

Pape *et al* (1999) state that the addition of the expressions for the low-, medium-, and high-porosity ranges is reasonable because, for a given porosity, the expressions for the other two porosity ranges do not contribute significantly due to the difference in the exponents of porosity used in Eq. A-15.

Obviously, Eq. A-15 is an idealized formulation, and the coefficients of the three power law terms in Eq. A-15 must be calibrated when applied to a specific formation or reservoir. For the case of Rotliegend samples (northeastern Germany), Pape *et al* (1999) provide the following result, obtained by regression:

$$k = 155\,\phi + 37315\,\phi^2 + 6.30\times10^{12}\,\phi^{10}\ \text{nm}^2\ \ (\textit{Rotliegend}) \qquad \text{(A.16)}$$

Recall that the "analytical" relations where derived assuming a fractal dimension of D =2.36 — obviously, if the fractal dimension changes, so must the exponents (as well as the multiplicative constants). As such, Pape *et al* (1987a) propose the following general result:

$$k = A\phi + B\phi^{m} + C\phi^{\frac{m+2}{c_1(3-D)}} \ \text{nm}^2 \quad (\text{where } 0.39 < c_1 < 1) \text{ ......} \tag{A.17}$$

Where D is the fractal dimension, and m is the exponent (cementation factor) in Archie's first law (*i.e.*, Eq. A-4). The parameter c_1 relates the effective pore radius r_{eff} to the pore radius r_p and the grain radius r_{grain} as follows:

$$\frac{r_{grain}}{r_p} = \left[\frac{r_{grain}}{r_{eff}}\right]^{c_1} \text{ with } c_1 = 0.39, \text{ if } \frac{r_{grain}}{r_{eff}} > 30 \text{ ......} \tag{A.18}$$

Pape *et al* (1987a) propose Eq. A-18 as an empirical result, for which Pape *et al* suggest Eq. A-18 is valid for a wide variety of sandstones.

Another formulation, the "shaly sandstone" relation is developed by Pape *et al* (1999) to represent shaly sand samples. This result is given as:

$$k = 6.2\phi + 1493\,\phi^2 + 5.8\times10^{11}\,\phi^{10} \ \text{nm}^2 \ (\textit{Shaly Sandstone}) \text{ ......} \tag{A.19}$$

Finally, Pape *et al* (1999) present a formulation that matches data measured on high-porosity kaolinite samples and on low-porosity shales, this is the so-called "shale" equation, and is given below:

$$k = 0.1\phi + 26\,\phi^2 + 1\times10^{11}\,\phi^{10} \ \text{nm}^2 \ (\textit{Shale}) \text{ ......} \tag{A.20}$$

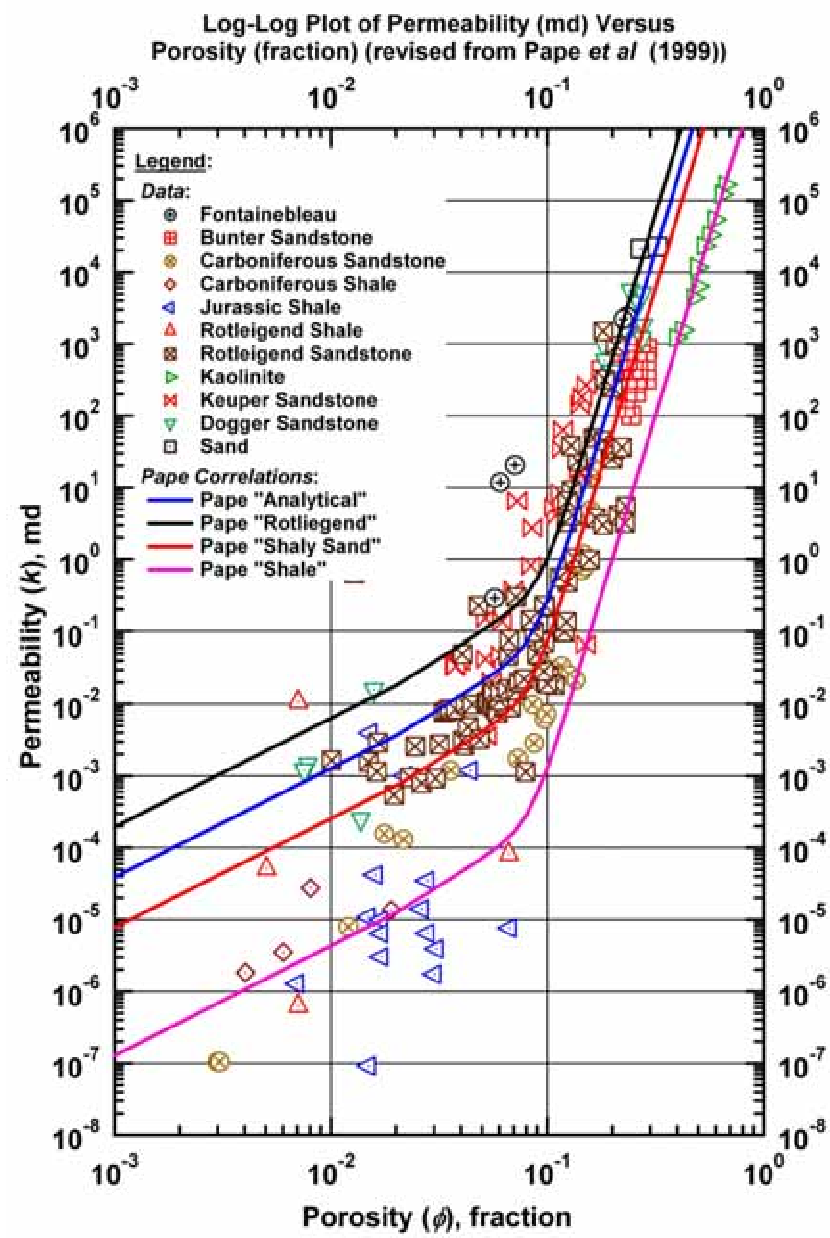

Figure A.1 — Pape *et al* (1999) fractal correlation of permeability and porosity — various data sources (modified from Pape *et al* (1999)).

Nomenclature: Pape Derivation

a = Intercept term in Archie's First Law (dimensionless)
D = Fractal dimension (dimensionless)
d_m = Median grain radius, nm
F = Archie Formation Factor (dimensionless)
k = Formation Permeability, nm^2
m = Slope term in Archie's First Law (*i.e.*, the "cementation factor") (dimensionless)
S_w = Water Saturation (fraction)
r_p = Pore radius, nm
r_{eff} = Effective pore radius, nm
r_{grain}= Effective grain radius, nm
r_{50} = Pore radius at the 50th-percentile, nm
R_o = Resistivity of the sample at $S_w = 1$, ohm-m
R_w = Resistivity of the electrolyte (usually salt water), ohm-m
T = Tortuosity (dimensionless)
ϕ = Porosity, fraction

References: Pape Derivation

Archie, G. E. 1942. The Electrical Resistivity Log as an Aid in Determining Some Reservoir Characteristics. *Trans.* AIME. **146**: 54–61.

Carman, P. C. 1956. Flow of Gases Through Porous Media. *Butterworth Scientific Publication*

Köhler, M., Pape, H., Pasternak, M., and Schmidt, R. 1993. Natural Gas Reserves in the Ems Estuary Region, Part I. Reservoir engineering (*in German*): Geological Survey of Lower Saxony, internal report no. 110986, Hannover, Germany.

Kozeny, J. 1927. Über die kapillare Leitung des Wassers im Boden (Aufstieg Versickerung und Anwendung auf die Bewässerung). *Sitz. Ber. Akad. Wiss. Wien, Math. Nat. (Abt. IIa).* **136a**: 271–306.

Kulenkampff, J. 1994. Die komplexe elektrische Leitfähigkeit poröser Gesteine im Frequenz-bereich von 10 Hz bis 1 Mhz: Einflüsse von Porenstruktur und Porenfüllung. Ph.D. dissertation, Tech. U. Clausthal.

Pape, H., Riepe, L., and Schopper, J. R. 1984. The Role of Fractal Quantities, as Specific Surface and Tortuosities, for Physical Properties of Porous Media. *Particle Character* **1**: 66–73.

Pape, H., Riepe, L., and Schopper, J. R. 1987a. Interlayer Conductivity of Rocks—a Fractal Model of Interface Irregularities for Calculating Interlayer Conductivity of Natural Porous Mineral Systems. *Colloids and Surfaces* **27**: 97–122.

Pape, H., Riepe, L., and Schopper, J. R. 1987b. Theory of self-similar network structures in sedimentary and igneous rocks and their investigation with microscopical methods. *J. Microscopy* **148**: 121–147 (1987b).

Pape, H., and Schopper, J. R. 1988. Relations Between Physically Relevant Geometrical Properties of a Multifractal Porous System. In *Characterization of porous solids*, eds. K. K. Unger, J. Rouquerol, K.S.W. Sing, and H. Kral, 473–482, Elsevier Science Publ. Co., Inc.

Pape, H., Clauser, C., And Iffland, J. 1999. Permeability Prediction Based on Fractal Pore Space Geometry. *Geophysics* **64** (5): 1447–1460.

Serra, O. 1984. Fundamentals of Well-Log Interpretation: 1. The Acquisition of Data. *Elsevier Science Publ. Co., Inc.*

APPENDIX B

RESULTS FOR HOWELL WELL

(E. TEXAS — USA)

In this Appendix we present the "Howell" Well, located in East Texas (USA), where this is a sandstone reservoir (Holditch (1986)). First we do the correlation taking the entire interval in the correlation then we divide the interval into two zones based on the depositional environment. The correlation works good for all the cases but as expected it performs better when we divide the interval into different zones.

Model *CPR-A*: (Appendix B)

The "characteristic permeability relation" (or *CPR*) Model *CPR-A* (*i.e.*, the modified Archie "Clean Sand" Model) is given as:

$$k = a(\phi - c)^{b} \quad c = c_{max} \exp[-c_1 \phi^{c_2} S_w^{c_3}] \text{ .... (B-1)}$$

Where a plot of log(k) versus log(ϕ) is used to graphically calibrate Eq. B-1 in terms of the coefficients — a, b, and c_{max}. **Fig. B.1** shows that the *CPR-A* model performs quite well for this case. **Figs. B.1a and b** show the log-log and the semilog format of permeability versus porosity, respectively. In **Fig. B.2** we provide the "error" plots for this case, where the measured and computed data are compared systematically. In **Fig. B.2a** we note a good correlation of the results obtained using Model *CPR-A* versus the measured permeability data — there is good agreement with the perfect correlation trend (*i.e.*, the 45-degree line). In **Fig. B.2b** we provide a comparison with the *GRACE* algorithm correlation (Xue *et al*, 1997)), and we note that the *CPR-A* model results correlate very well with the *GRACE* algorithm results for this case. In **Fig. B.2c** we present the calculated and measure c-function — and again we note a very good correlation of the data about the perfect correlation trend. Lastly, in **Fig. B.2d and e** we present the measured and calculated permeability with depth.

Model *CPR-B*: (Appendix B)

The "characteristic permeability relation" (or *CPR*) Model *CPR-B* (*i.e.*, the modified Archie "Dirty Sand" Model (power-law basis)) is given as:

$$k = a(\phi + c)^{b} \quad c = c_{max} \exp[-c_1 \phi^{c_2} S_w^{c_3}] \text{ .... (B-2)}$$

Where a plot of log(k) versus log(ϕ) is used to graphically calibrate Eq. B-2 in terms of the coefficients — a, b, and c_{max}. The results for this case are presented in **Figs. B.3 and 4**. In **Fig. B.3a** (log-log format) we note that a very distinct "envelope" is formed by the *CPR-B* model, essentially all of the data on the right and left flanks are well-matched (*i.e.*, the "dirty sand" power law relation (applied on the right portion of the data) and its correction function (applied on the left portion of the data). Similarly, in **Fig. B.3b** (semilog format), we observe an excellent distribution of the power law model across the body of the data. The error analyses for this case are shown in **Fig. B.4**. In **Fig. B.4a** we present the results obtained using Model *CPR-B* versus the measured permeability data and in this case there is good agreement with the perfect correlation trend (*i.e.*, the 45-degree line). We provide a comparison with the *GRACE* algorithm correlation in **Fig. B.4b** — the results using Model *CPR-B* and the *GRACE* algorithm compare very well for this case. We compare the computed and data-derived values of the *c*-function for this case in **Fig. B.4c** and we note a reasonably "tight" correlation, except for few outliers of the *c*-function. Lastly, in **Fig. B.4d and e** we present the measured and calculated permeability with depth. In summary, we believe that Model *CPR-B* is a very effective correlation model for this particular data case.

Model *CPR-C*: (Appendix B)

The "characteristic permeability relation" (or *CPR*) Model *CPR-C* (*i.e.*, the modified Archie "Dirty Sand" Model (exponential basis)) is given as:

$$k = c\exp[\beta\phi] \quad c = c_{\max}\exp[-c_1\phi^{c_2} S_w^{c_3}] \text{ .... (B-3)}$$

Where a plot of log(k) versus ϕ is used to graphically calibrate Eq. B-3 in terms of the coefficients — β and $c_{\max}$. Model *CPR-C* is fundamentally different than Models *CPR-A* and *CPR-B*, as the basis for Model *CPR-C* is an exponential function, not a power law relation. In **Figs. B.5 and 6** we present the results of applying Model *CPR-B* for this case, and in general, we observe a very consistent performance of Model *CPR-B*. **Fig. B.5b** illustrates the excellent conformance of Model *CPR-C* for this case — again recalling that this model has an exponential relationship with porosity as its basis.

In **Figs. B.6a, B.6b, and B.6c** we review the error analyses plots for this case, and we note good performance (visually) in terms of the correlation of the results using Model *CPR-C*. In this case, the *c*-function (in Eq. B-3) is not a correction term, but rather the instantaneous intercept for the exponential basis. The correlation of the *c*-function (see **Fig. B.6c**) appears to be consistent — but scatter and a slight off-center trend is evident. However, as we are approaching this work from the perspective that the primary value of the work is the characteristic model, not the statistical "best fit" correlation, we believe that the *CPR-C* model has performed well for this case, and the plots in **Fig. B.6** confirm the value of this model as a "characteristic relation" for permeability.

Model *CPR-D*: (Appendix B)

The "characteristic permeability relation" (or *CPR*) Model *CPR-D* (*i.e.*, the weighted power law-exponential model) is given in its fundamental form as:

$$k = xa\phi^b + (1-x)\alpha\exp[\beta\phi] \quad [0 \le x \le 1]] \text{ .... (B-4a)}$$

For Eq. B-4 there are two proposed models for the *x*-function (*i.e.*, the weighting function) — these are:

$$x = \exp[-\ln(x_0) + x_1\ln(\phi) + x_2\ln(S_w) + x_3\ln(\phi)\ln(S_w)] \text{ (Model } CPR\text{-}DxL\text{) .... (B-4b)}$$

$$x = \exp\begin{bmatrix} -\ln(x_0) + x_1 \ln(\phi) + x_2 \ln(S_w) + x_3 \ln(\phi)\ln(S_w) \\ + x_4 \ln(\phi)^2 + x_5 \ln(S_w)^2 + x_6 \ln(\phi)^2 \ln(S_w) \\ + x_7 \ln(\phi)\ln(S_w)^2 + x_8 \ln(\phi)^2 \ln(S_w)^2 \end{bmatrix} \text{(Model } \mathit{CPR\text{-}DxL}\text{)} \ldots\ldots\ldots\ldots\text{(B-4c)}$$

As noted in Eq. B-4b, Model *CPR-DxL* utilizes a logarithmic linear model for the weights (*x*-values) and as seen in Eq. B-4c, Model *CPR-DxQ* utilizes a logarithmic quadratic model for the weights (*x*-values). While these models (Eqs. B-4b and B-4c) are *empirical*, we have found generally good application of these relations for all cases. In this case, the base results using Models *CPR-DxL* and *CPR-DxQ* are presented in **Fig. B.7** — where the power law and exponential basis functions are fitted to the appropriate portion of the data. The power law equation represents the "Archie clean sand" trend and is fitted to the leftmost data as shown in **Fig. B.7a** and in contrast, the exponential equation is thought to represent the "Archie dirty sand" trend and the exponential is fitted to the far rightmost portion of the data (see **Fig. B.7b**).

In **Figs. B.8 and 9** we present the error analyses for this case, where we have employed the weighting functions (Eqs. B-4b and B-4c) as appropriate. In **Fig. B.8a** we find a good correlation of permeability (with the out-lying points noted in the middle of the trend). The comparison of the Model *CPR-DxL* results are compared to the results obtained from the *GRACE* algorithm in **Fig. B.8b**, we note that the results obtained using Model *CPR-DxL* does "drift" slightly from the *GRACE* solution at middle values of permeability, indicating some inconsistency. The computed weight function (*x*-values) shown for the *CPR-DxL* model in **Fig. B.8c** does exhibit more scatter than expected, but the trend is (relatively) centered about the perfect correlation line. **Fig. B.8d and e** provide the measured and calculated permeability versus depth.

The results obtained using Model *CPR-DxQ* are presented in **Fig. B.9**, and we note substantially improved behavior over that of Model *CPR-DxL*. In particular, the base correlation of computed and measured permeabilities (**Fig. B.9a**) for Model *CPR-DxQ* does indicate a slightly better correlation than that of Model *CPR-DxL*. Also, the comparison of Model *CPR-DxQ* with the results from the *GRACE* algorithm (**Fig. B.9b**) exhibits better agreement than the results of Model *CPR-DxL*. Finally, the correlation of the *x*-function (**Fig. B.9c**) for Model *CPR-DxQ* is better than the correlation for Model *CPR-DxL*. These comparisons suggest that Model *CPR-DxQ* (*i.e.*, the combination of Eqs. B-4a and B-4c) has provided a better correlation of data, for this case, than Model *CPR-DxL*. **Fig. B.9d and e** provide the measured and calculated permeability versus depth.

"Timur Model": (Appendix B)

The "Timur Model" [Timur (1968)] is given as:

$$k_{\text{Timur}} = a\phi^b S_w^c \quad \text{(B-5)}$$

In **Fig. B.10** we present the results of the "Timur Model" (Eq. B-5) which is essentially just a generalized power function relation in terms of k, ϕ, and S_w. As shown in **Figs. B.10a and b**, the "Timur Model" also provides a good correlation of the data for this case. The comparison of results using the "Timur Model" with the results of the *GRACE* algorithm (**Fig. B.10b**).

"Coates Model": (Appendix B)

The "Coates Model" [referenced by Ahmed *et al* (1989)] is given as:

$$k_{\text{Coates}} = \left[100\phi^2 \frac{(1-S_w)}{S_w}\right]^2 \quad \text{(B-6)}$$

In **Fig. B.11** we present the results of the "Coates Model" (Eq. B-6) which is essentially just a modified power function relation in terms of k, ϕ, and S_w. The results are shown in **Figs. B.11a and b** of the data for this case. The comparison of results using the "Coates Model " with the results of the *GRACE* algorithm (**Fig. B.11b**) is also shown.

***GRACE* Algorithm: (Appendix B)**

In **Fig. B.12** we present the results predicted by the *GRACE* algorithm, which is a non-parametric regression approach (see Xue, *et al* (1997) for details). In theory, the *GRACE* algorithm should provide the most *unbiased* correlation of the data — *i.e.*, the *GRACE* algorithm is designed not "fit the errors" as other regression approaches may. It is our contention that the *GRACE* algorithm is the statistical standard — and any algorithm/approach/model which achieves better regression statistics than the *GRACE* algorithm is actually "fitting the errors" in the data. Since none of the cases are better statistically than the *GRACE* algorithm so none of the cases are "over-fitted" in a statistical sense.

***Comparison of All Models*: (Appendix B)**

Fig. B.13, illustrates all of the models on a single plot of calculated versus measured permeability. We also present a table of all statistical results in **Table B.1**.

As mentioned before we perform the same procedure but this time we make two zones of the entire interval and the results are presented from **Figs. B.14 to B.39**, and we note substantially improvement in the correlation.

We present a table of all statistical results taking into account all of the interval in **Tables B.1**.

Table B.1 — Statistical Results for all Models (Howell Well, E. TX (USA), *n*=352).

Model	Sum of Squared Residuals [log(k)^2]	Variance [log(k)^2]	Standard Deviation [log(k)]	Absolute Relative Error [percent]
CPR-A	813.37	5.46	2.34	291.48
CPR-B	806.50	4.95	2.23	278.37
CPR-C	795.47	5.45	2.33	288.73
CPR-DxL	781.67	5.46	2.34	274.74
CPR-DxQ	696.09	5.63	2.37	288.62
Timur	878.58	5.24	2.29	310.91
Coates	1085.36	4.69	2.16	352.45
GRACE Algorithm	779.84	5.31	2.30	267.90

The coefficients for the models used in this case are provided in **Table B.2**.

Table B.2a — Model Coefficients (Howell Well, E. TX (USA), *n*=352).

Model	a or α	b or β	c or c_{max}	c_1	c_2	c_3
CPR-A	7.00×10^{9}	8.00	0.100	7.55×10^{-3}	-1.79	-0.42
CPR-B	4.00×10^{9}	12.00	0.090	77.17	1.61	1.02
CPR-C	5.00×10^{-8}	100.00	0.006	48.74	0.73	0.42
Timur	1.41×10^{2}	3.71	2.574	–	–	–
Coates	6.27×10^{4}	5.54	0.781	–	–	–

Table B.2b — Model Coefficients (Howell Well, E. TX (USA), *n*=352).

Model	a	b	α	β
CPR-DxL	7.00×10^{9}	8.00	5.00×10^{-8}	100.00
CPR-DxQ	7.00×10^{9}	8.00	5.00×10^{-8}	100.00

Model	c_0	c_1	c_2	c_3	c_4	c_5	c_6	c_7	c_8
CPR-DxL	2.85×10^{9}	-5.88	-9.00	-2.68	–	–	–	–	–
CPR-DxQ	1.75×10^{7}	-0.08	-12.22	2.14	1.47	-5.05	2.51	0.06	0.92

These are the results for Zone 1.

Table B.3 — Statistical Results for all Models (Howell Well, E. TX (USA), *n*=228).

Model	Sum of Squared Residuals [log(k)^2]	Variance [log(k)^2]	Standard Deviation [log(k)]	Absolute Relative Error [percent]
CPR-A	408.58	5.56	2.36	133.32
CPR-B	438.75	5.40	2.32	138.72
CPR-C	423.02	5.50	2.34	132.08
CPR-DxL	431.05	5.48	2.34	131.80
CPR-DxQ	368.09	5.61	2.37	119.80
Timur	535.73	5.22	2.28	167.91
Coates	622.28	4.83	2.20	180.68
GRACE Algorithm	431.32	5.69	2.39	115.13

The coefficients for the models used in this case are provided in **Table B.4**.

Table B.4a — Model Coefficients (Howell Well, E. TX (USA), *n*=228).

Model	a or α	b or β	c or c_{max}	c_1	c_2	c_3
CPR-A	$1.00\text{x}10^{11}$	9.00	0.100	0.010	-1.83	-0.22
CPR-B	$4.80\text{x}10^{10}$	12.50	0.050	5970.45	3.36	1.25
CPR-C	$5.00\text{x}10^{-8}$	100.00	0.001	40.00	0.76	0.31
Timur	$7.38\text{x}10^{2}$	4.27	1.908	–	–	–
Coates	$4.05\text{x}10^{9}$	11.34	0.426	–	–	–

Table B.4b — Model Coefficients (Howell Well, E. TX (USA), *n*=228).

Model	a	b	α	β
CPR-DxL	$1.00\text{x}10^{11}$	9.00	$5.00\text{x}10^{-8}$	100.00
CPR-DxQ	$1.00\text{x}10^{11}$	9.00	$5.00\text{x}10^{-8}$	100.00

Model	c_0	c_1	c_2	c_3	c_4	c_5	c_6	c_7	c_8
CPR-DxL	$9.71\text{x}10^{9}$	-6.45	-10.71	-3.88	–	–	–	–	–
CPR-DxQ	$3.00\text{x}10^{6}$	1.17	-31.63	-14.51	1.75	-6.22	-0.63	0.03	1.27

These are the results for Zone 2.

Table B.5 — Statistical Results for all Models (Howell Well, E. TX (USA), *n*=124).

Model	Sum of Squared Residuals [log(k)^2]	Variance [log(k)^2]	Standard Deviation [log(k)]	Absolute Relative Error [percent]
CPR-A	302.72	2.30	1.52	133.30
CPR-B	281.99	2.52	1.59	129.49
CPR-C	275.54	2.53	1.59	121.95
CPR-DxL	278.43	2.60	1.61	126.13
CPR-DxQ	251.05	2.67	1.63	137.16
Timur	330.38	2.13	1.46	120.01
Coates	363.65	2.30	1.52	144.04
GRACE Algorithm	277.97	2.29	1.51	114.20

The coefficients for the models used in this case are provided in **Table B.6**.

Table B.6a — Model Coefficients (Howell Well, E. TX (USA), *n*=124).

Model	a or α	b or β	c or c_{max}	c_1	c_2	c_3
CPR-A	$7.00\text{x}10^{9}$	8.00	0.060	$5.26\text{x}10^{-4}$	-2.47	-0.82
CPR-B	$1.00\text{x}10^{20}$	21.00	0.060	1193.25	2.55	0.65
CPR-C	$5.00\text{x}10^{-8}$	130.00	0.001	112.62	1.01	0.53
Timur	$8.33\text{x}10^{-1}$	1.87	3.336	–	–	–
Coates	$1.68\text{x}10^{2}$	2.62	1.441	–	–	–

Table B.6b — Model Coefficients (Howell Well, E. TX (USA), n=124).

Model	a	b	α	β
CPR-DxL	7.00×10^{9}	8.00	5.00×10^{-8}	130.00
CPR-DxQ	7.00×10^{9}	8.00	5.00×10^{-8}	130.00

Model	c_0	c_1	c_2	c_3	c_4	c_5	c_6	c_7	c_8
CPR-DxL	7.16×10^{10}	-7.05	-13.04	-4.07	–	–	–	–	–
CPR-DxQ	8.17×10^{8}	0.75	3.46	19.02	2.13	-4.80	6.03	0.10	0.58

Nomenclature: (Appendix B)

S_w = Water Saturation (fraction)
k = Formation Permeability, md (or any consistent units)
ϕ = Porosity, fraction

References: (Appendix B)

Ahmed, U., Crary, S.F., and Coates, G.R: "Permeability Estimation: The Various Sources and Their Interrelationship," paper SPE 19604 presented at the 1989 SPE Annual Technical Conference and Exhibition, San Antonio, TX, 8-11 Oct., 649-662.

Timur, A.: "An Investigation of Permeability, Porosity, and Residual Water Saturation Relation-ships," *Trans.*, SPWLA Symposium (1968) paper I.

Travis Peak Formation Core Report — Well Howell No. 5, S.A. Holditch, (1986).

Xue, G., Datta-Gupta, A., Valko, P., and Blasingame, T.A.: "Optimal Transformations for Multiple Regression: Application to Permeability Estimation from Well Logs," *SPEFE* (June 1997), 85-93.

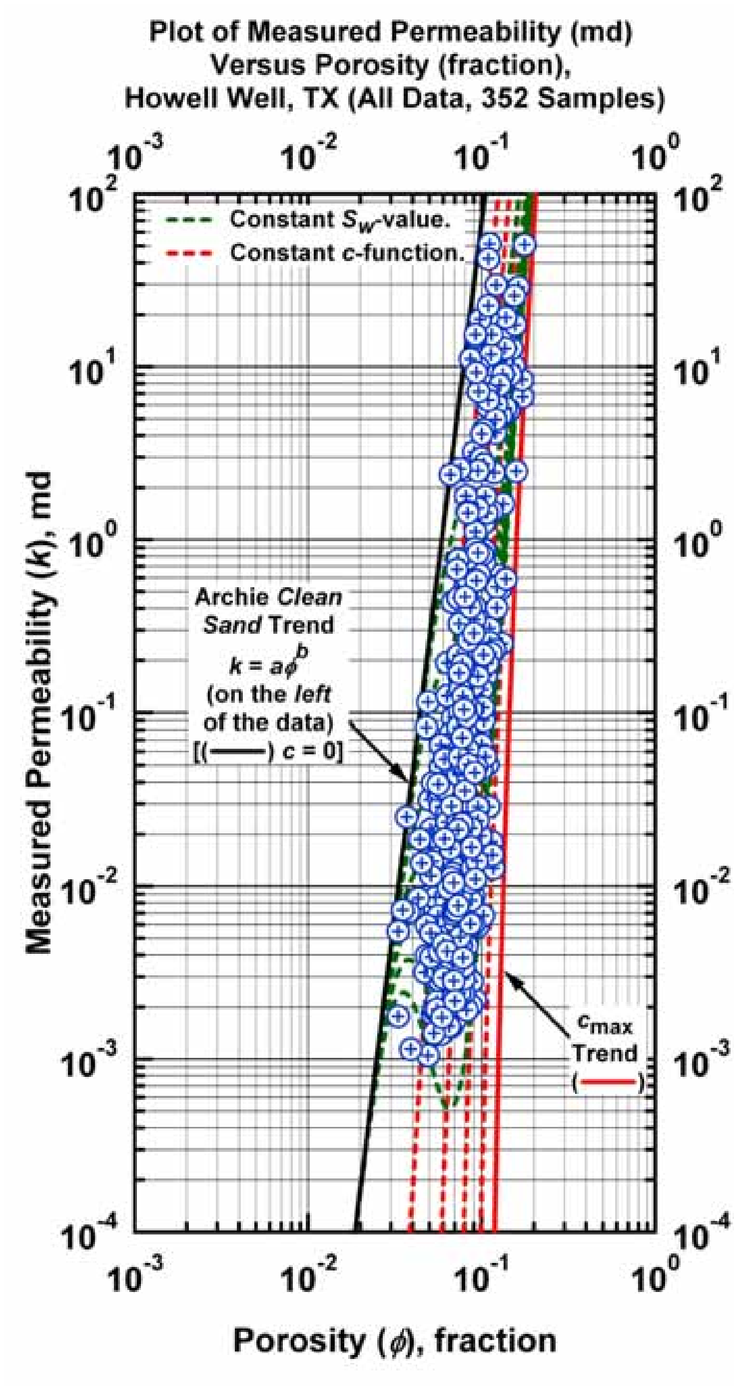

Figure B.1a — Model *CPR-A*: $k = a(\phi - c)^b \quad c = c_{max}\exp[-c_1\phi^{c_2} S_w^{c_3}]$ — "Clean Sand" Plot (log-log format) — Archie "Clean Sand" trend is given by the straight-line trend at the far left of the data (power law model). [*Case*: Howell Well, E. TX (USA)]

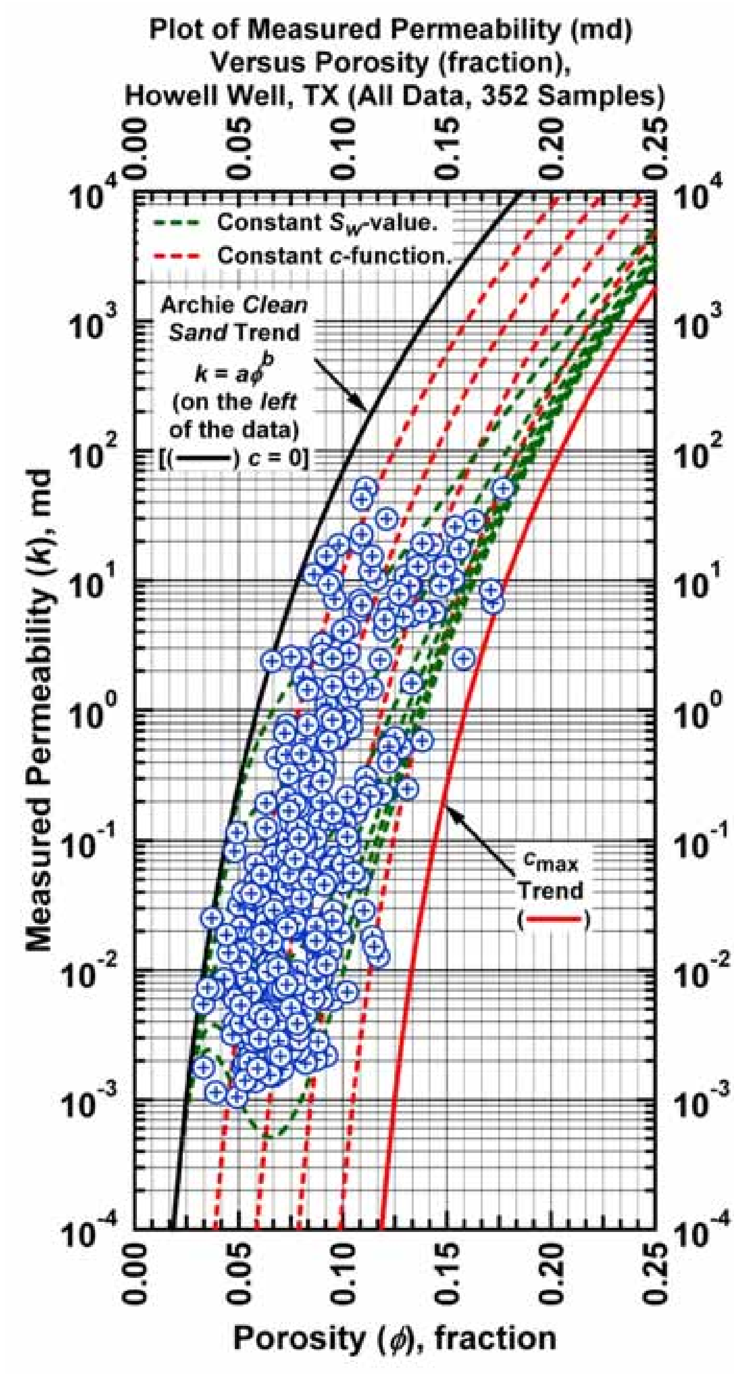

Figure B.1b — Model *CPR-A*: $k = a(\phi - c)^b \quad c = c_{max} \exp[-c_1 \phi^{c_2} S_w^{c_3}]$ — "Dirty Sand" Plot (semilog format). Archie "Clean Sand" trend is given by the curved trend at the far left of the data (power law model). [*Case*: Howell Well, E. TX (USA)]

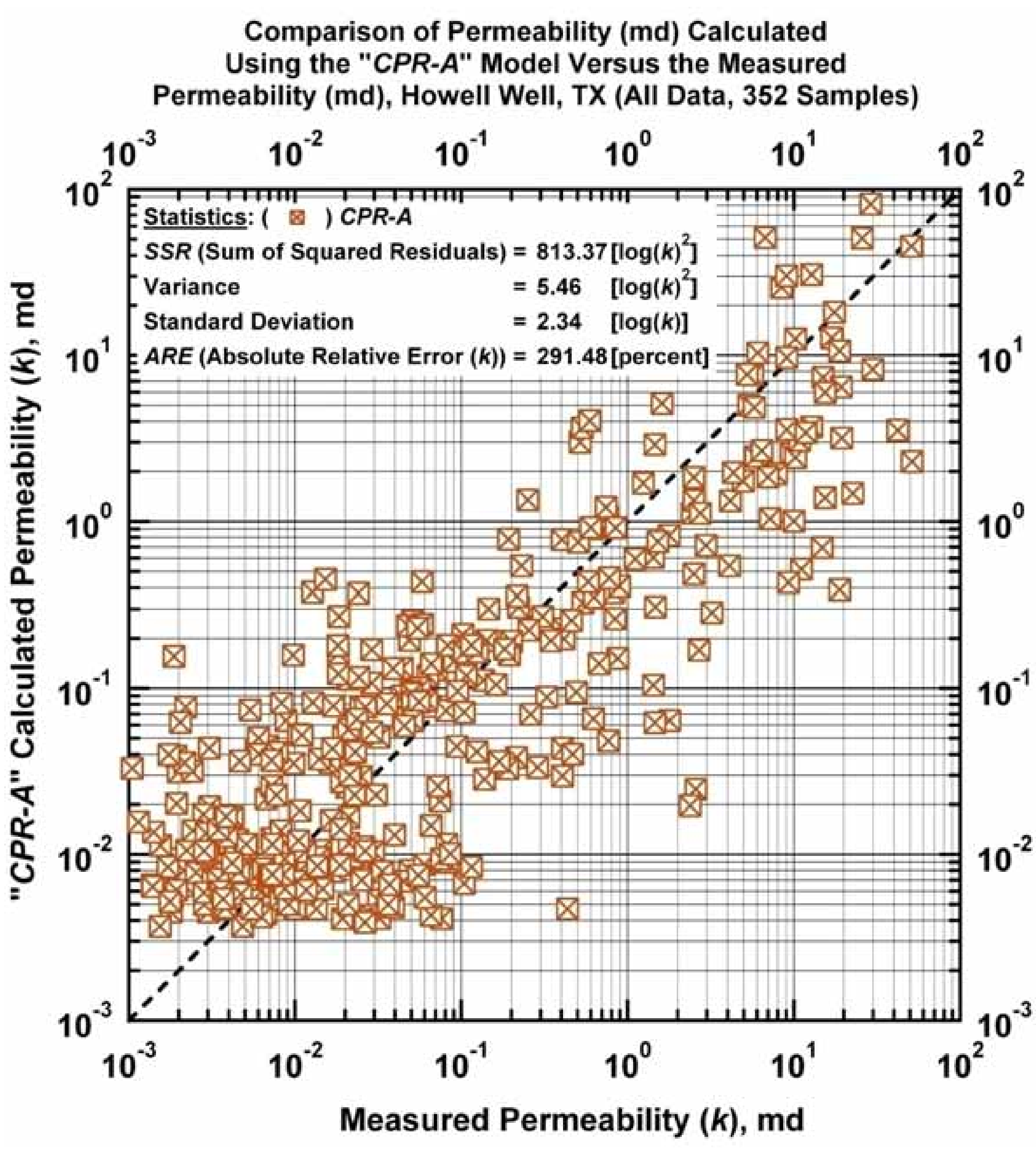

Figure B.2a — Model *CPR-A*: calculated versus measured permeability. [*Case*: Howell Well, E. TX (USA)]

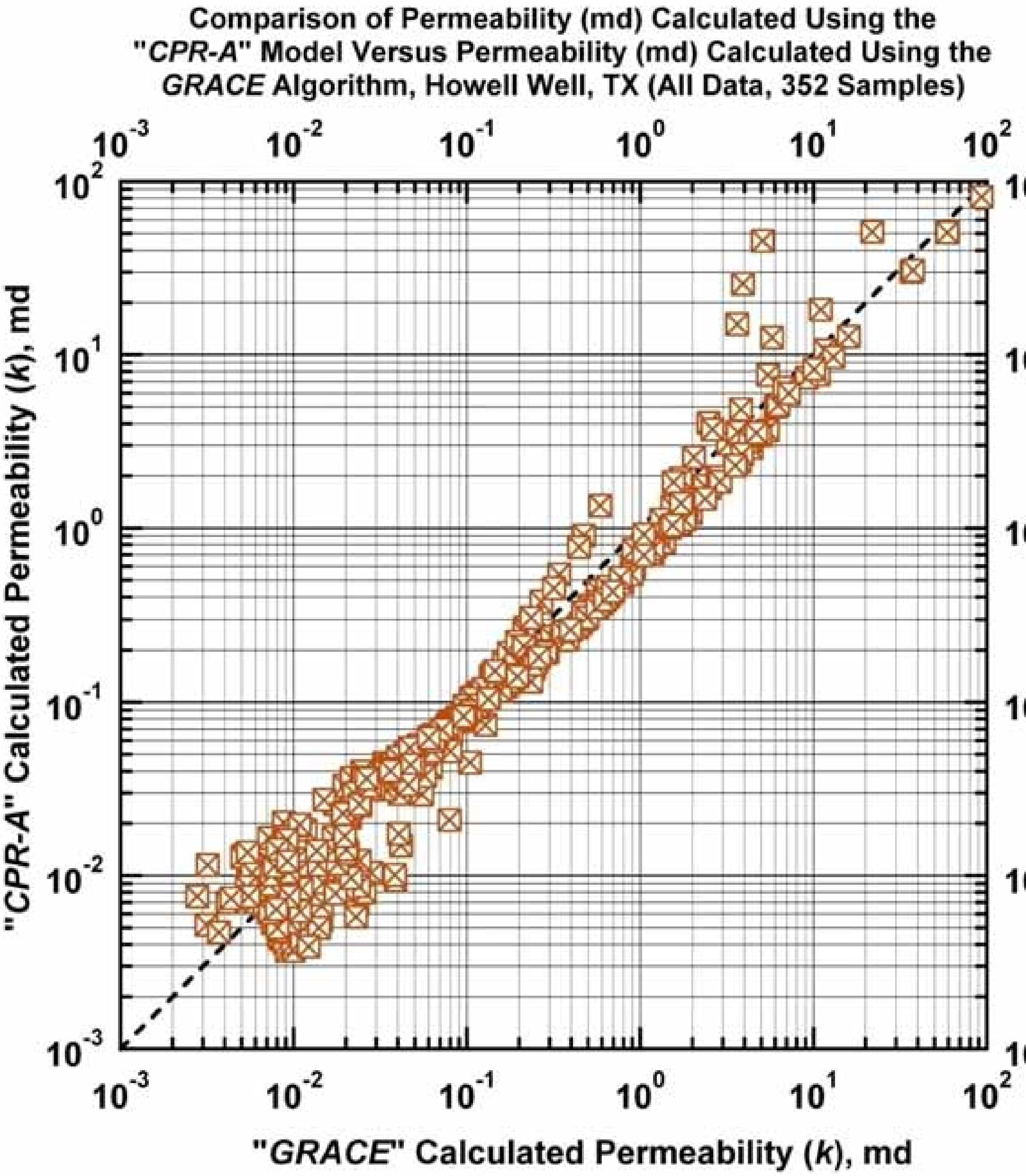

Figure B.2b — Model *CPR-A*: Permeability calculated using Model *CPR-A* versus permeability calculated using the *GRACE* Algorithm. [*Case*: Howell Well, E. TX (USA)]

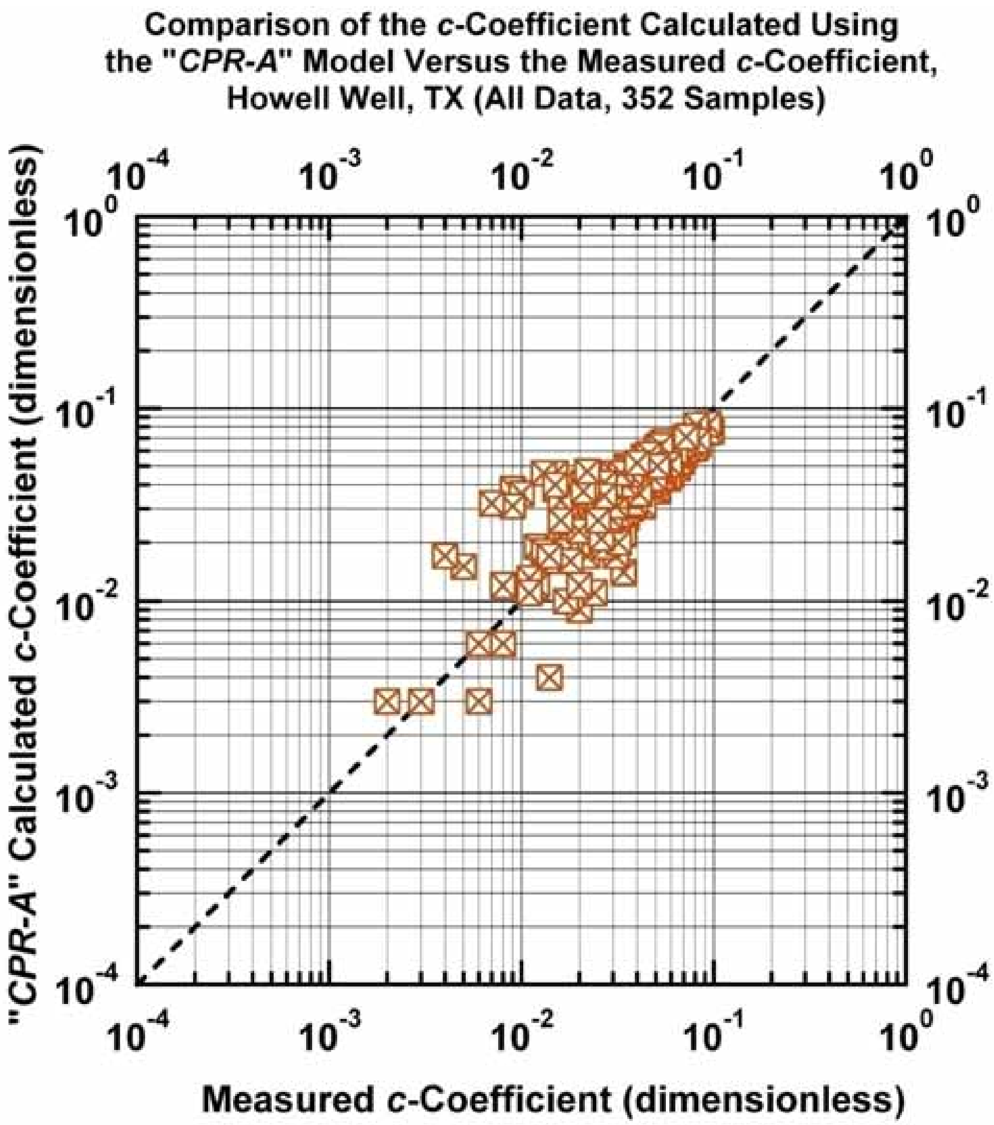

Figure B.2c — Model *CPR-A*: Calculated *c*-function values versus measured *c*-function values. [*Case*: Howell Well, E. TX (USA)]

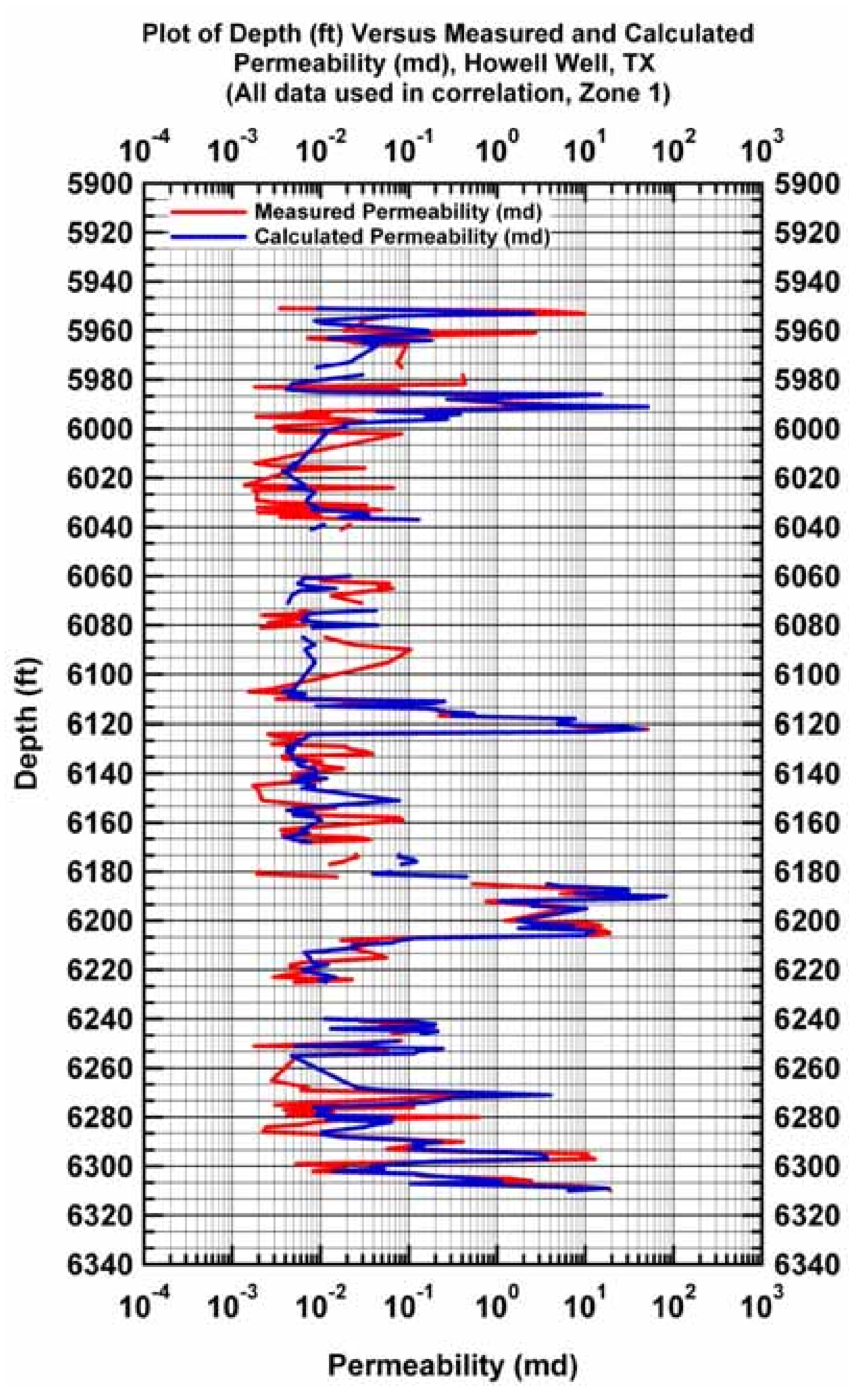

Figure B.2d — Model *CPR-A*: Calculated and measured permeability values versus depth. [*Case*: Howell Well, E. TX (USA)]

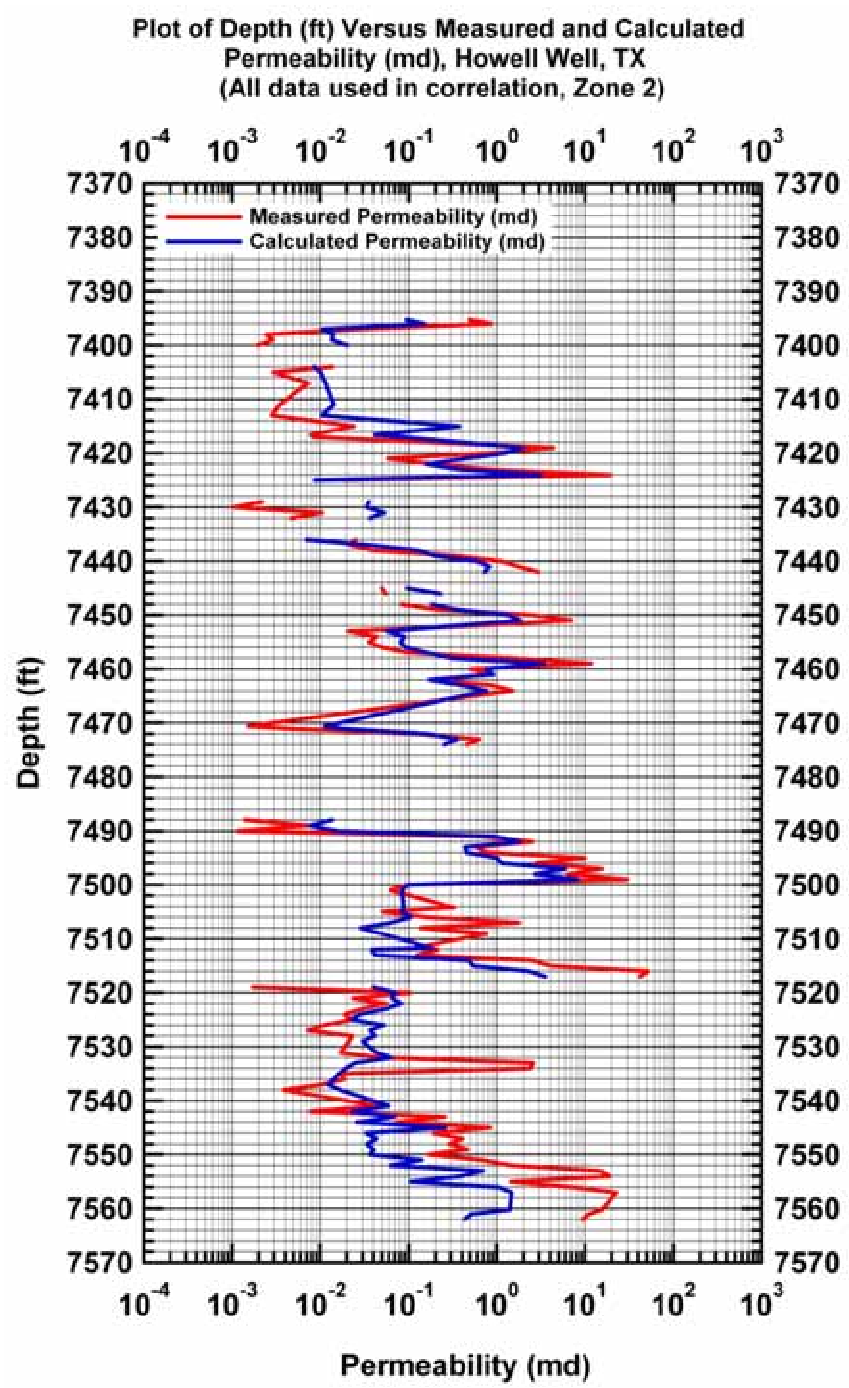

Figure B.2e — Model *CPR-A*: Calculated and measured permeability values versus depth. [*Case*: Howell Well, E. TX (USA)]

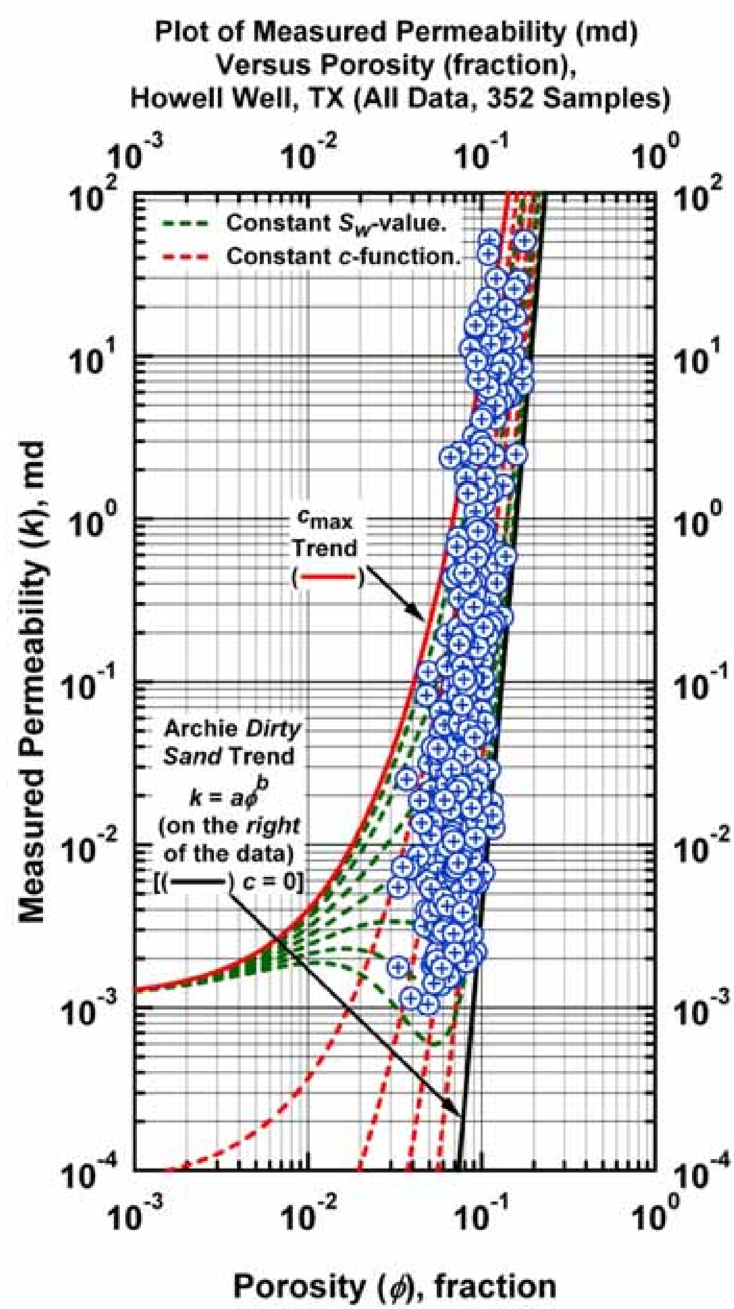

Figure B.3a — Model *CPR-B*: $k = a(\phi + c)^b$ $c = c_{max} \exp[-c_1 \phi^{c_2} S_w^{c_3}]$ — "Clean Sand" Plot (log-log format) — Archie "Dirty Sand" trend is given by the straight-line trend at the far right of the data (power law model). [*Case*: Howell Well, E. TX (USA)]

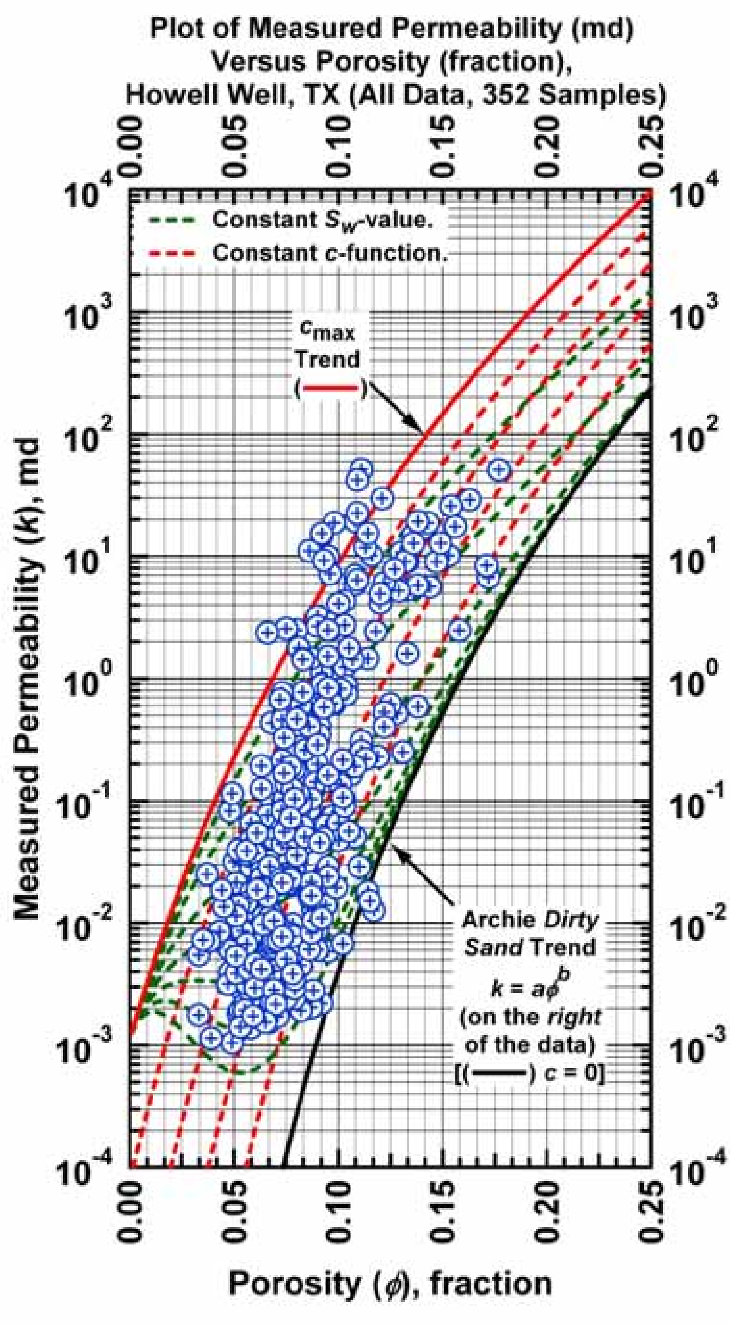

Figure B.3b — Model *CPR-B*: $k = a(\phi + c)^b \quad c = c_{max} \exp[-c_1 \phi^{c_2} S_w^{c_3}]$ — "Dirty Sand" Plot (semilog format) — Archie "Dirty Sand" trend is given by the curved trend at the far right of the data (power law model). [*Case*: Howell Well, E. TX (USA)]

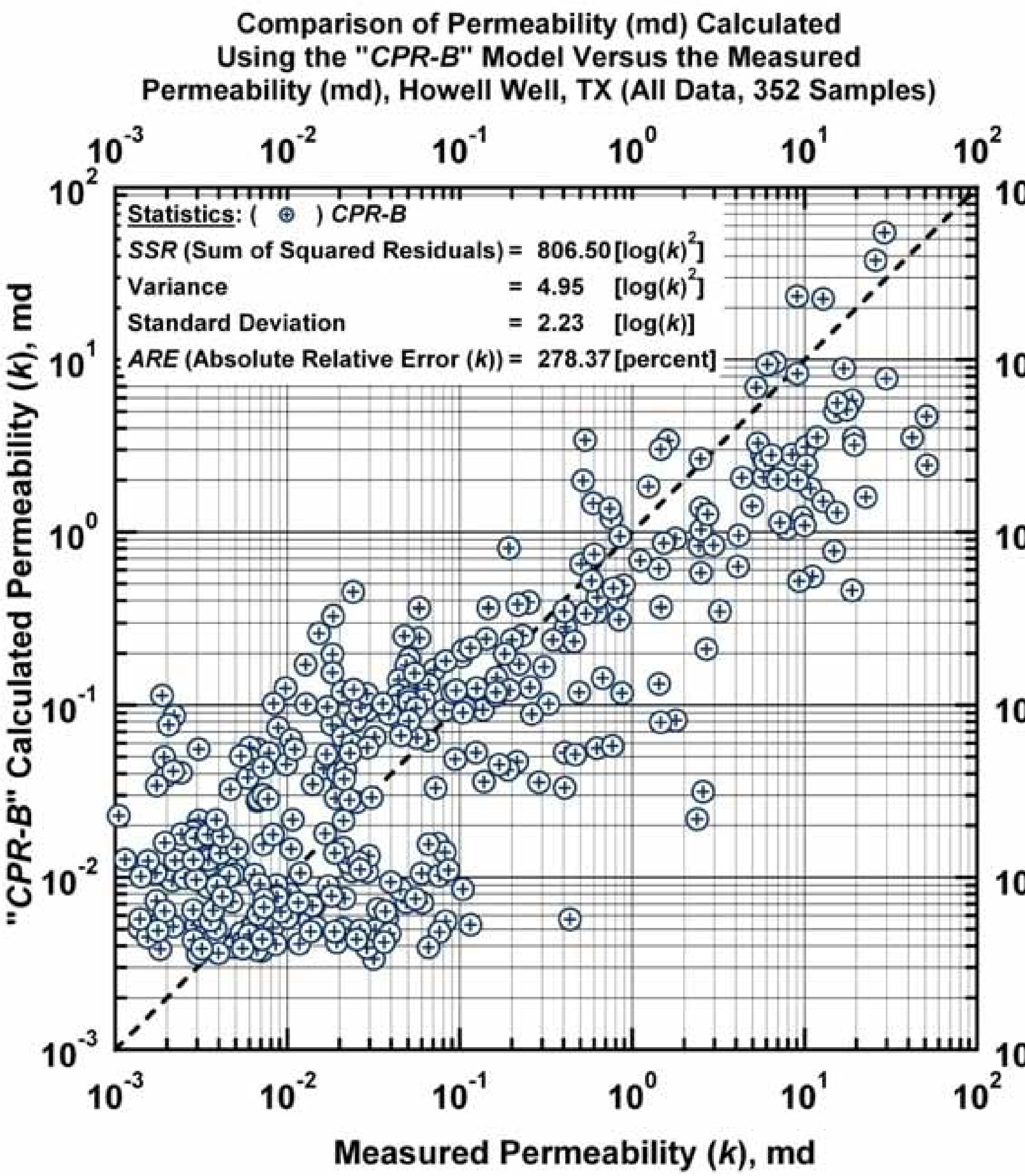

Figure B.4a — Model *CPR-B*: calculated versus measured permeability. [*Case*: Howell Well, E. TX (USA)]

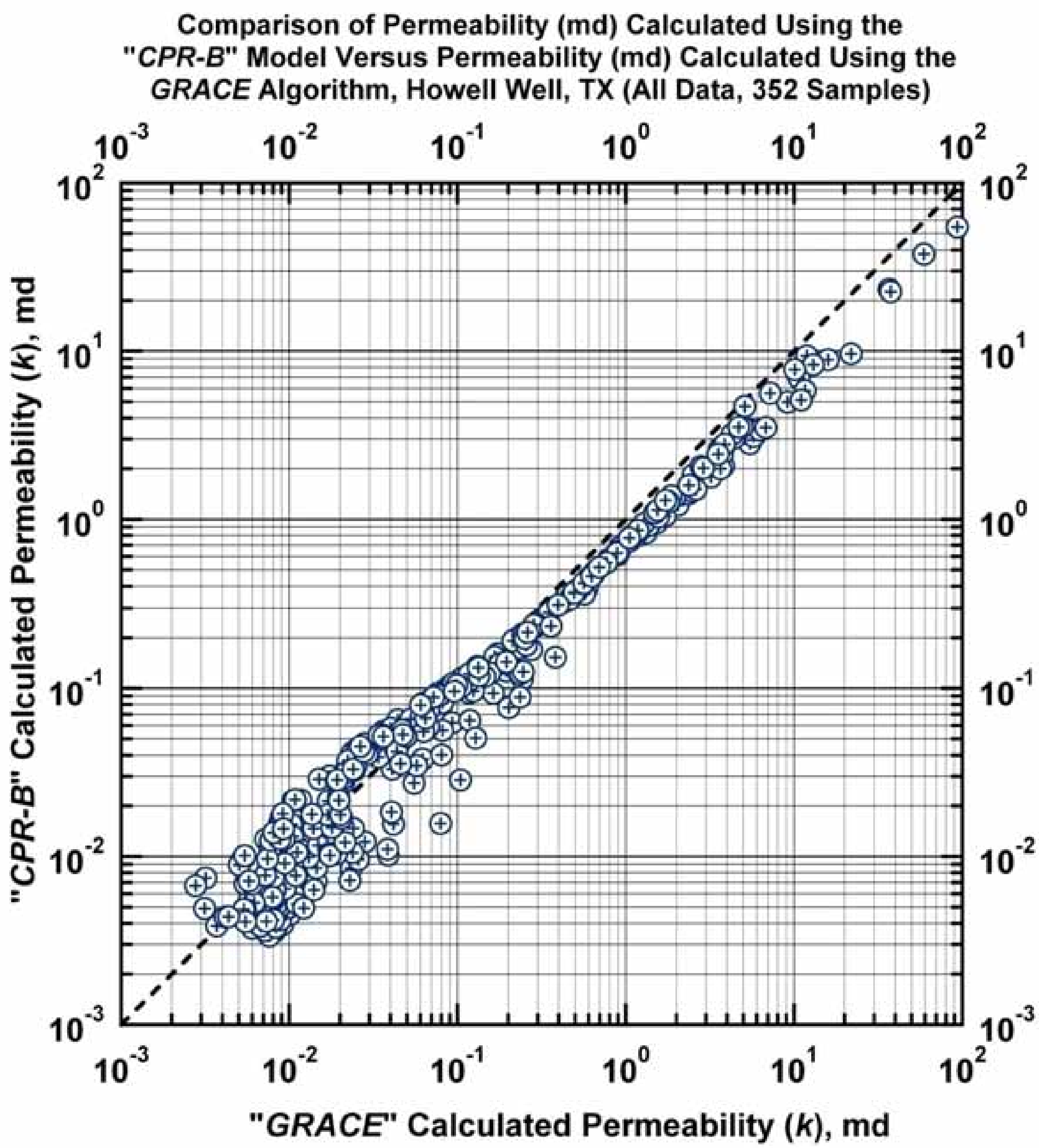

Figure B.4b — Model *CPR-B*: Permeability calculated using Model *CPR-B* versus permeability calculated using the *GRACE* Algorithm. [*Case*: Howell Well, E. TX (USA)]

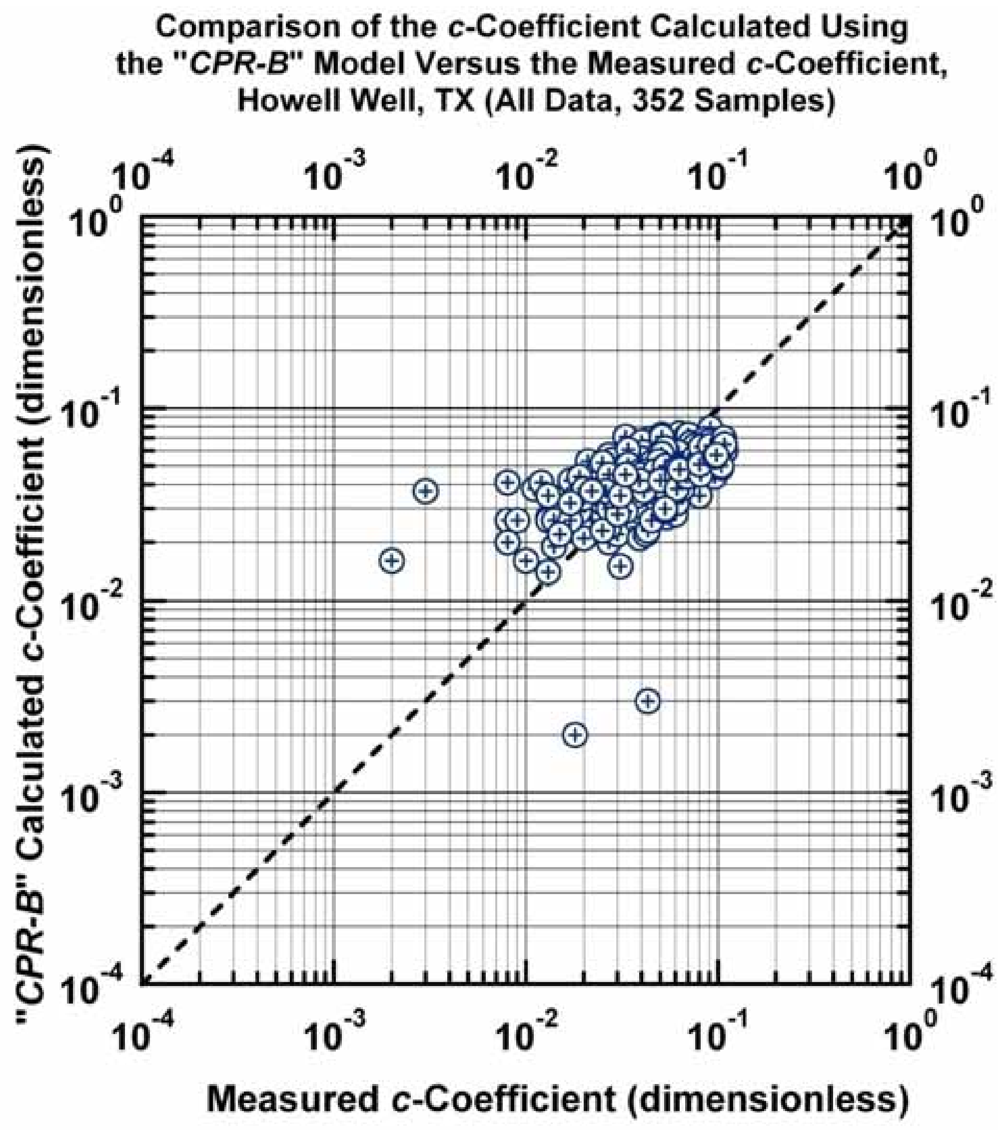

Figure B.4c — Model *CPR-B*: Calculated *c*-function values versus measured *c*-function values. [*Case*: Howell Well, E. TX (USA)]

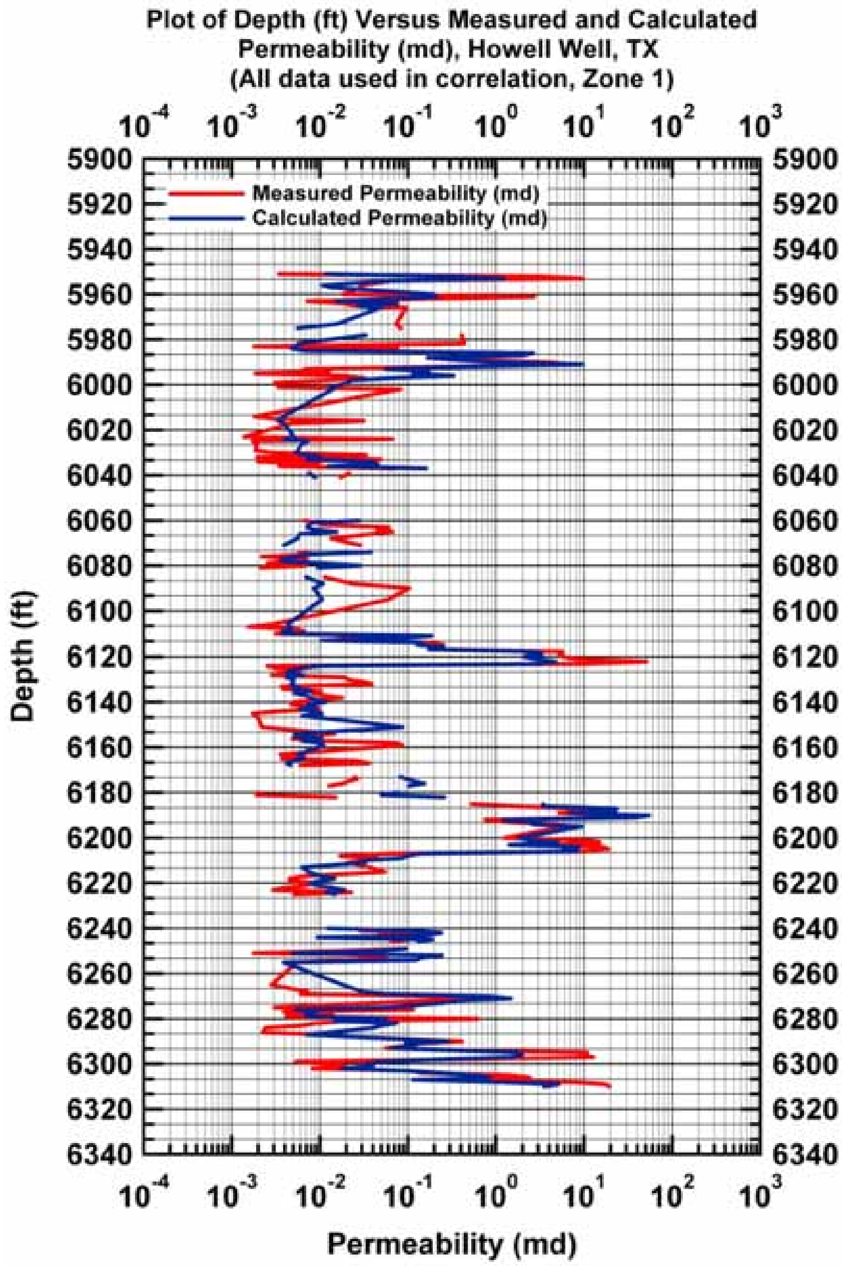

Figure B.4d — Model *CPR-B*: Calculated and measured permeability values versus depth. [*Case*: Howell Well, E. TX (USA)]

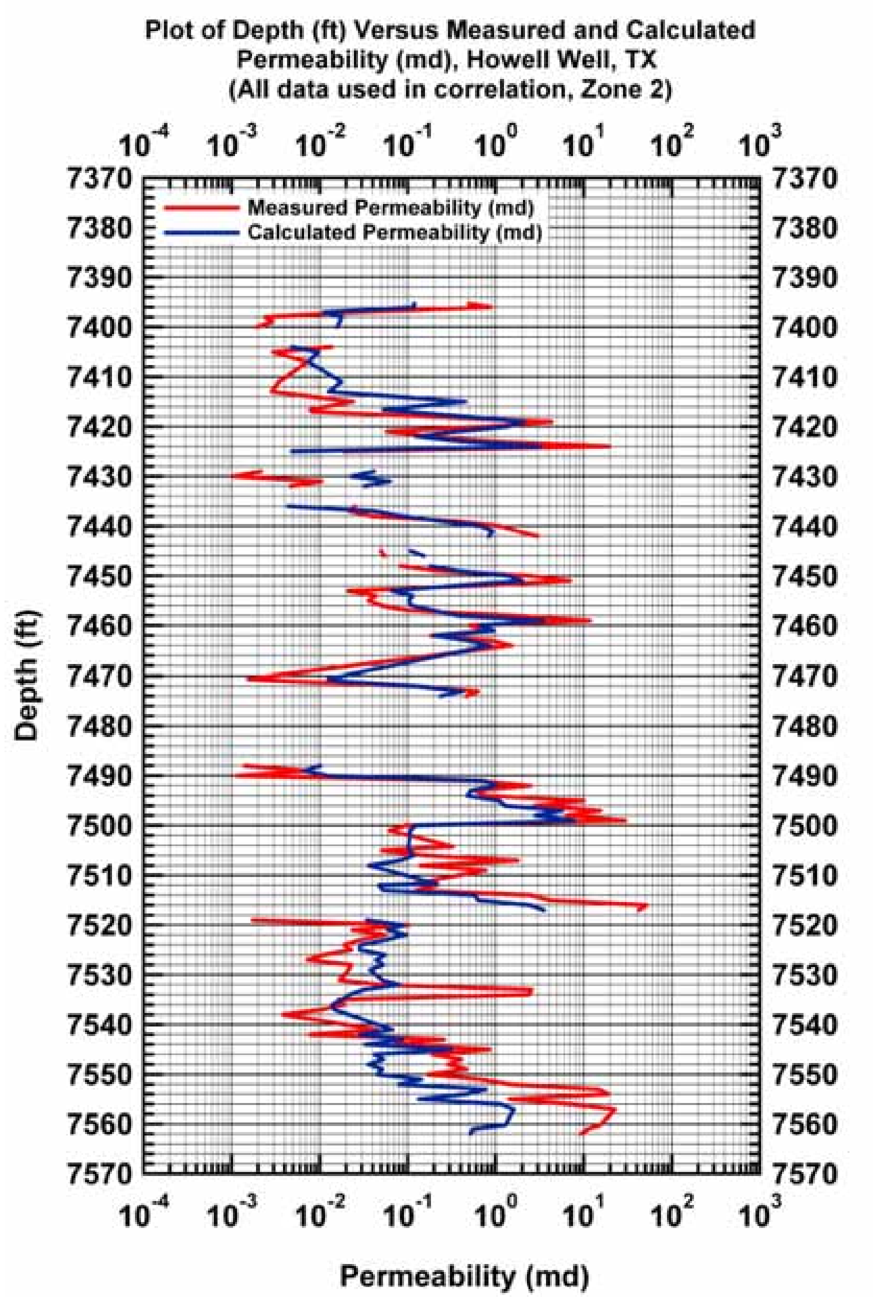

Figure B.4e — Model *CPR-B*: Calculated and measured permeability values versus depth. [*Case*: Howell Well, E. TX (USA)]

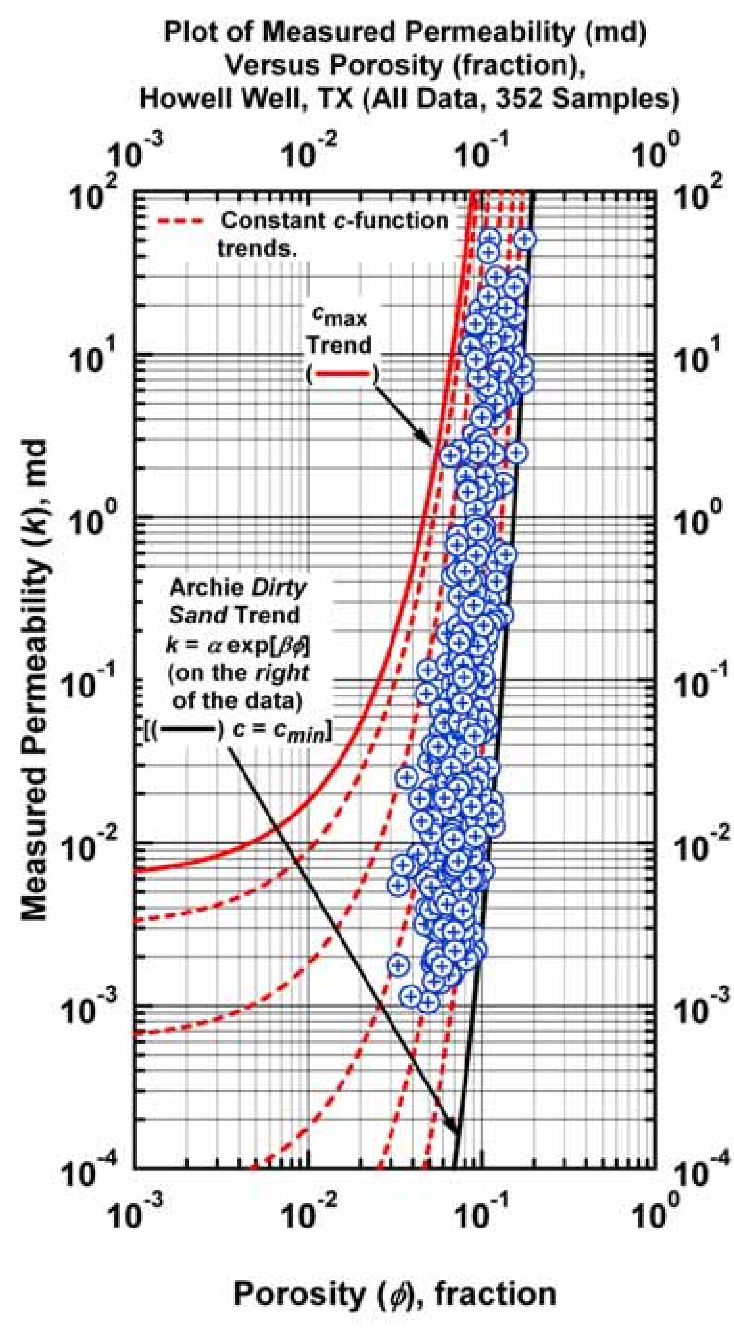

Figure B.5a — Model *CPR-C*: $k = c\exp[\beta\phi]$ $\quad c = c_{\max}\exp[-c_1\phi^{c_2} S_w^{c_3}]$ — "Clean Sand" Plot (log-log format) — Archie "Dirty Sand" trend is given by the curved trend at the far right of the data (exponential model). [*Case*: Howell Well, E. TX (USA)]

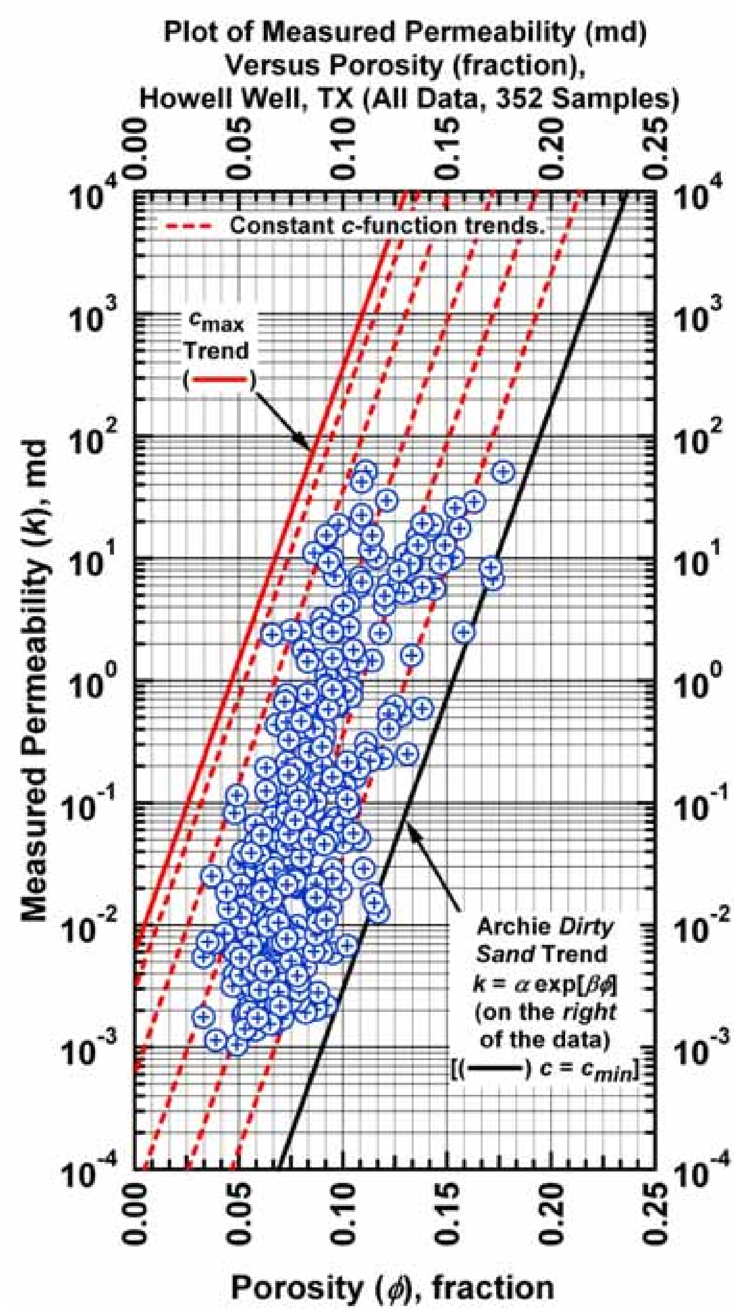

Figure B.5b — Model *CPR-C*: $k = c\exp[\beta\phi]$ $\quad c = c_{\max}\exp[-c_1\phi^{c_2} S_w^{c_3}]$ — "Dirty Sand" Plot (semilog format) — Archie "Dirty Sand" trend is given by the straight-line trend at the far right of the data (exponential model). [*Case*: Howell Well, E. TX (USA)]

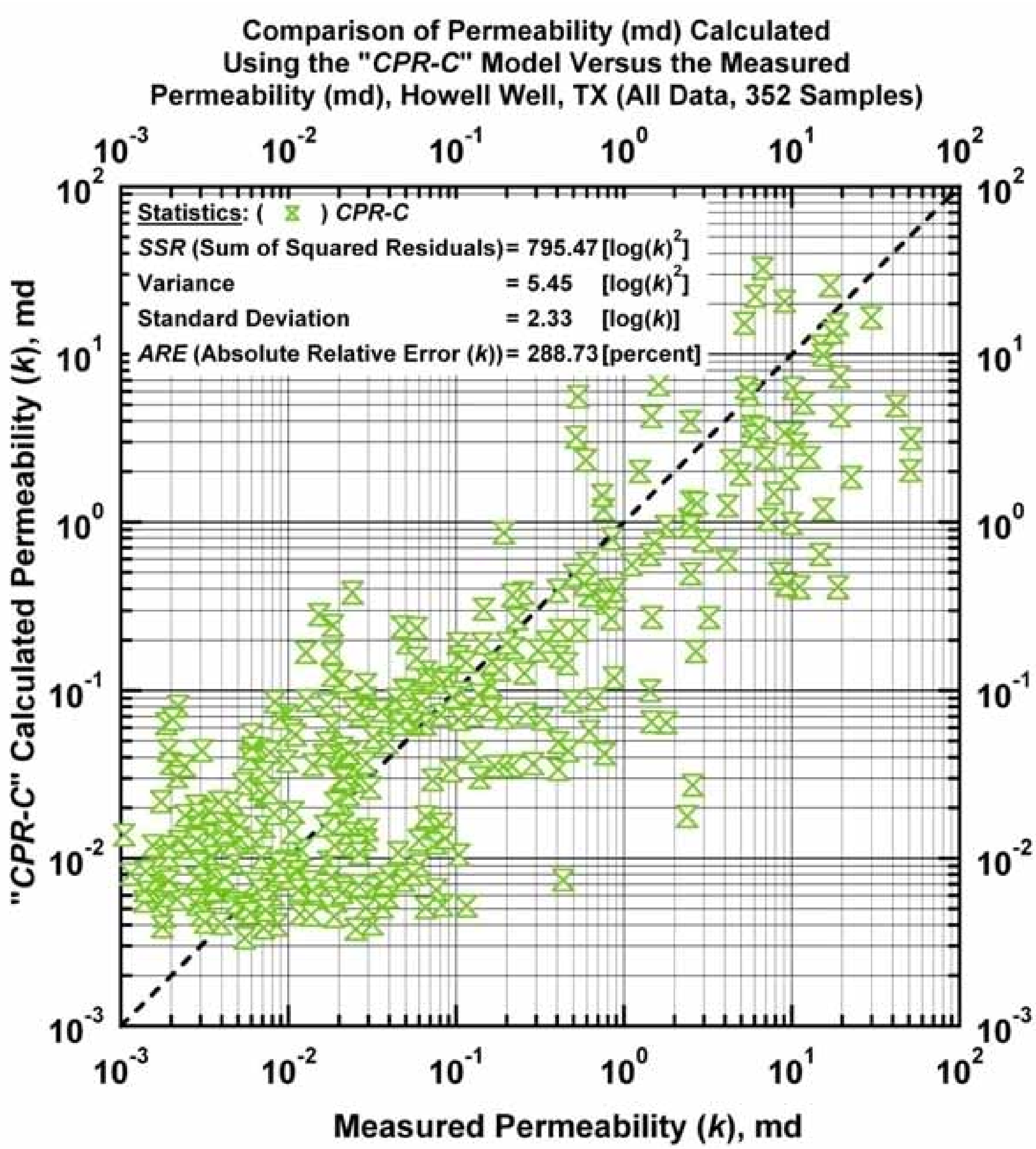

Figure B.6a — Model *CPR-C*: calculated versus measured permeability. [*Case*: Howell Well, E. TX (USA)]

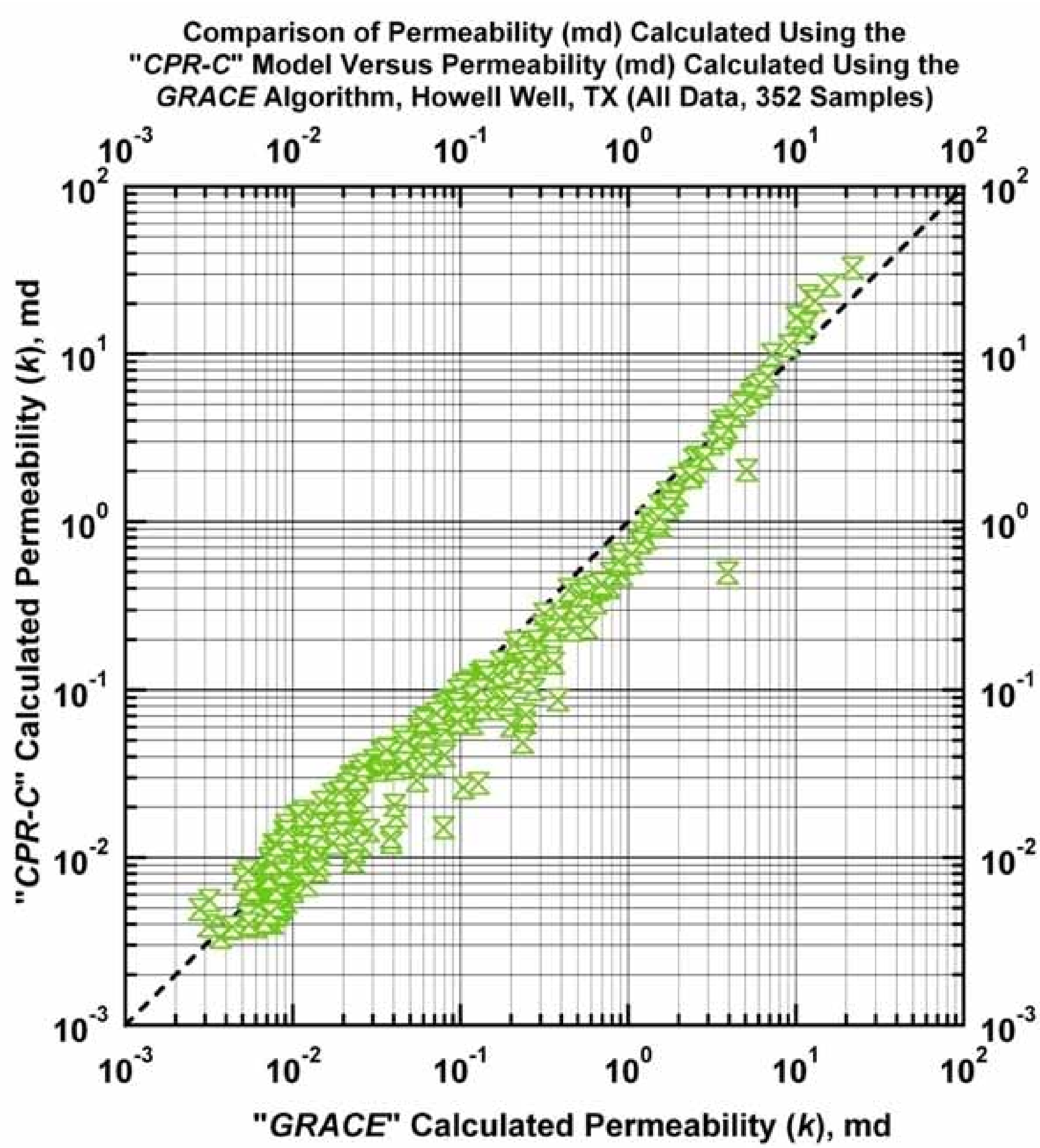

Figure B.6b — Model *CPR-C*: Permeability calculated using Model *CPR-C* versus permeability calculated using the *GRACE* Algorithm. [*Case*: Howell Well, E. TX (USA)]

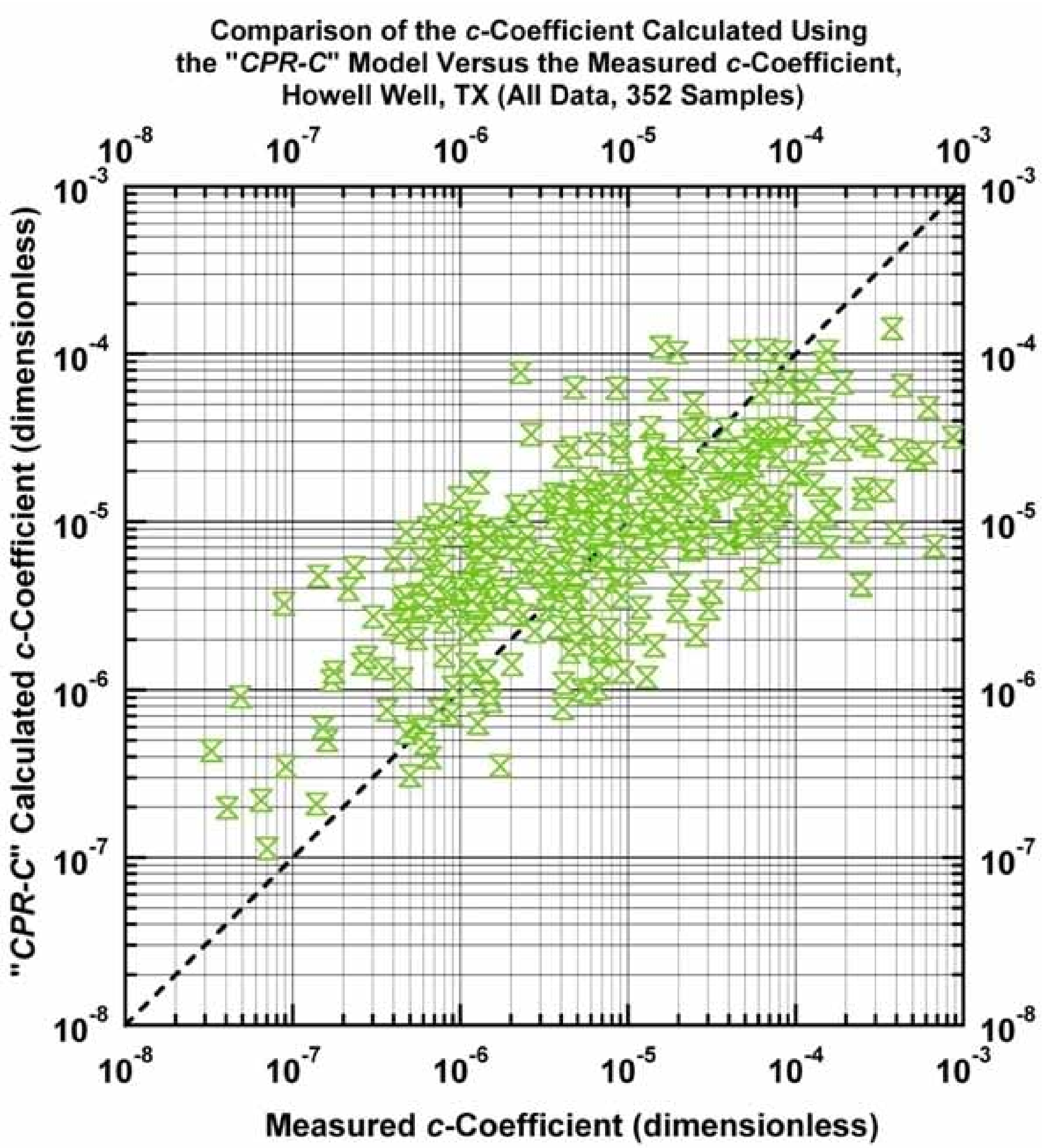

Figure B.6c — Model *CPR-C*: Calculated *c*-function values versus measured *c*-function values. [*Case*: Howell Well, E. TX (USA)]

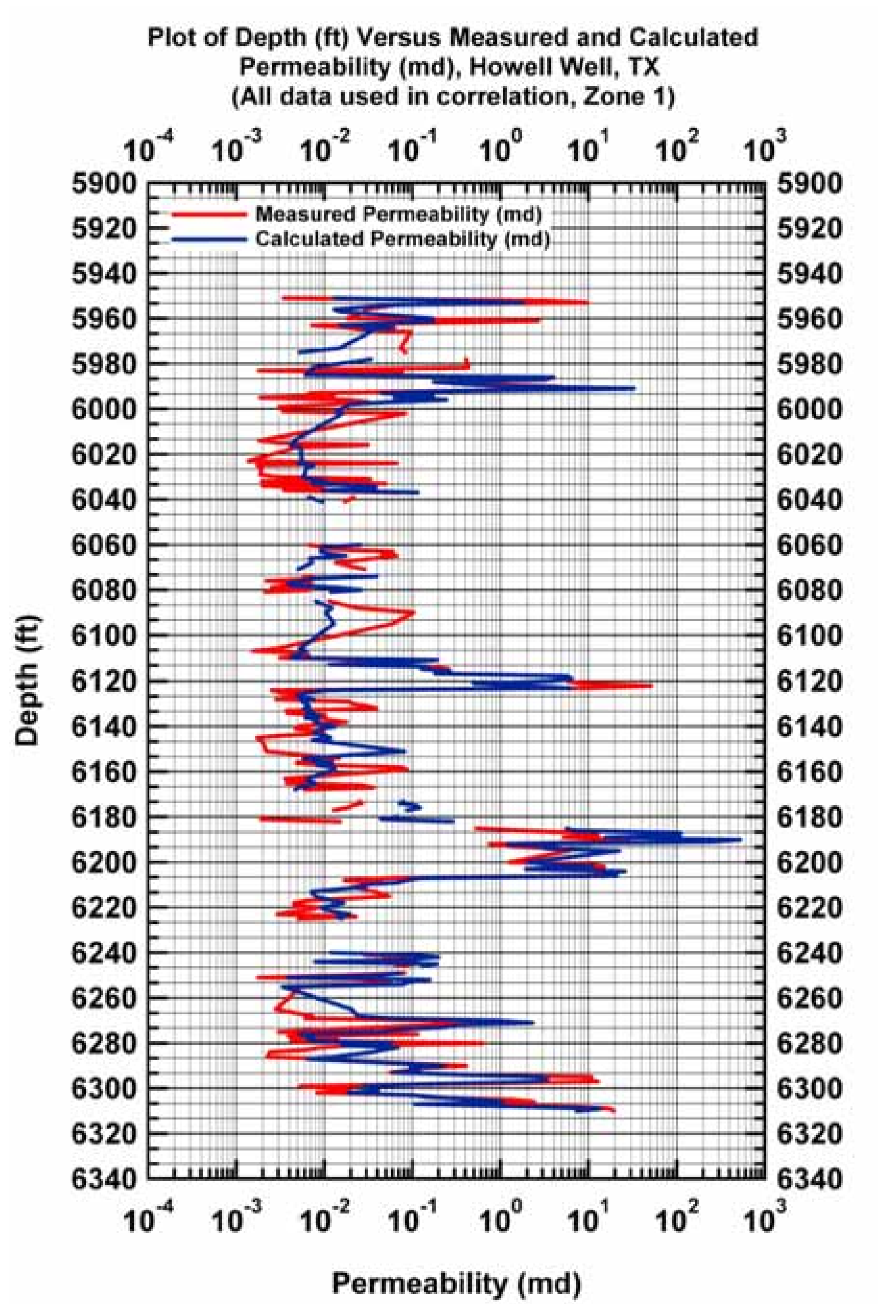

Figure B.6d — Model *CPR-C*: Calculated and measured permeability values versus depth. [*Case*: Howell Well, E. TX (USA)]

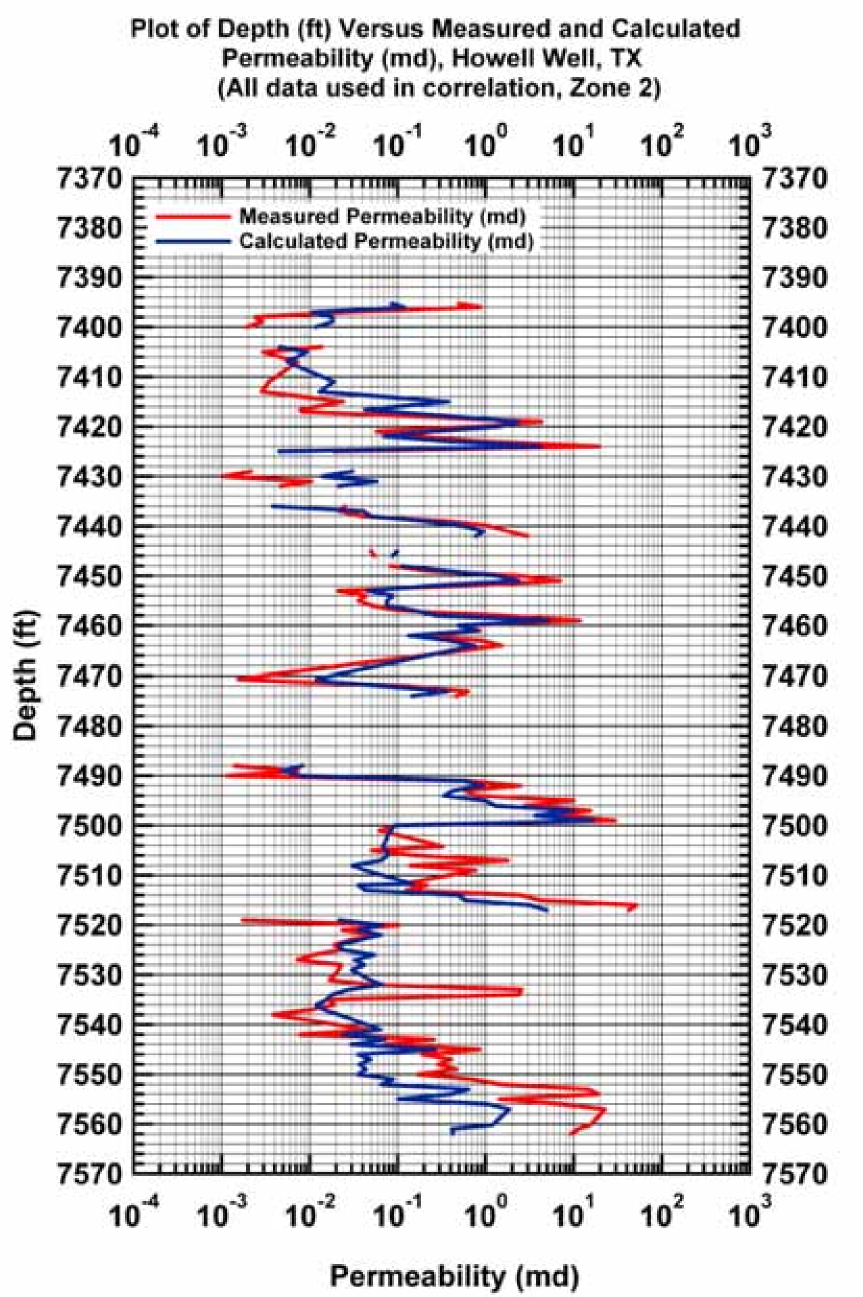

Figure B.6e — Model *CPR-C*: Calculated and measured permeability values versus depth. [*Case*: Howell Well, E. TX (USA)]

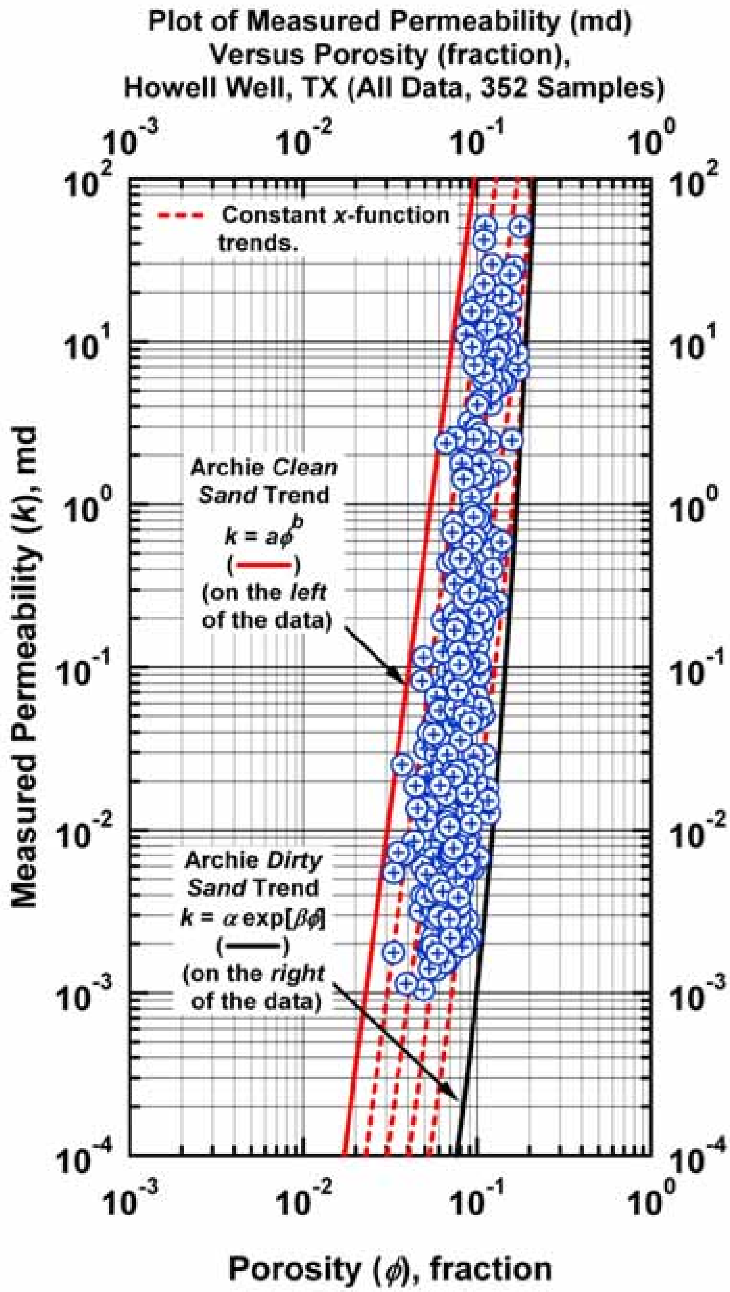

Figure B.7a — Model *CPR-D*: $k = xa\phi^b + (1-x)\alpha\exp[\beta\phi] \quad [0 \le x \le 1]$ — *Weighted Power Law-Exponential Model* used to correlate permeability (k) and porosity (ϕ). "Clean Sand" Plot — Archie "Clean Sand" trend is given by the straight-line trend at the far left of the data (power law model). [*Case*: Howell Well, E. TX (USA)]

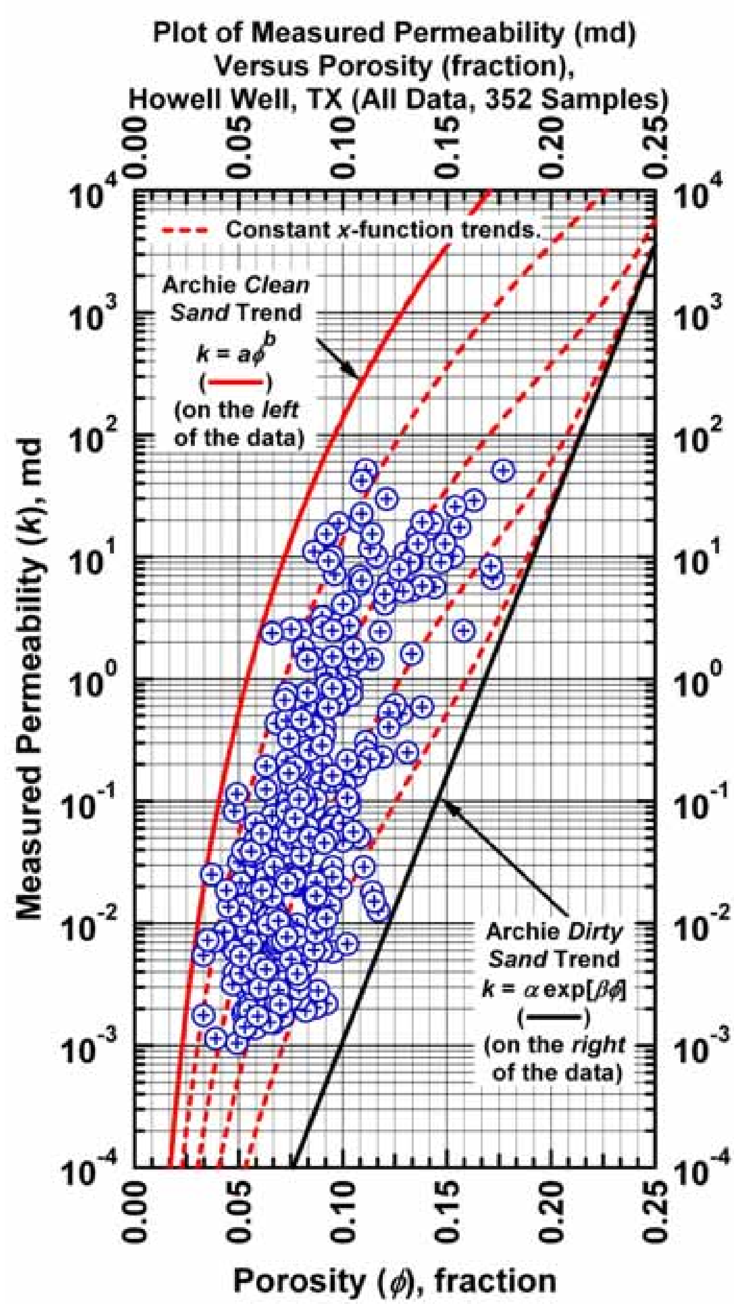

Figure B.7b — Model *CPR-D*: $k = xa\phi^{b} + (1-x)\alpha\exp[\beta\phi] \quad [0 \le x \le 1]$ — *Weighted Power Law-Exponential Model* used to correlate permeability (k) and porosity (ϕ). "Dirty Sand" Plot — Archie "Dirty Sand" trend is given by the straight-line trend at the far right of the data (exponential model). [*Case*: Howell Well, E. TX (USA)]

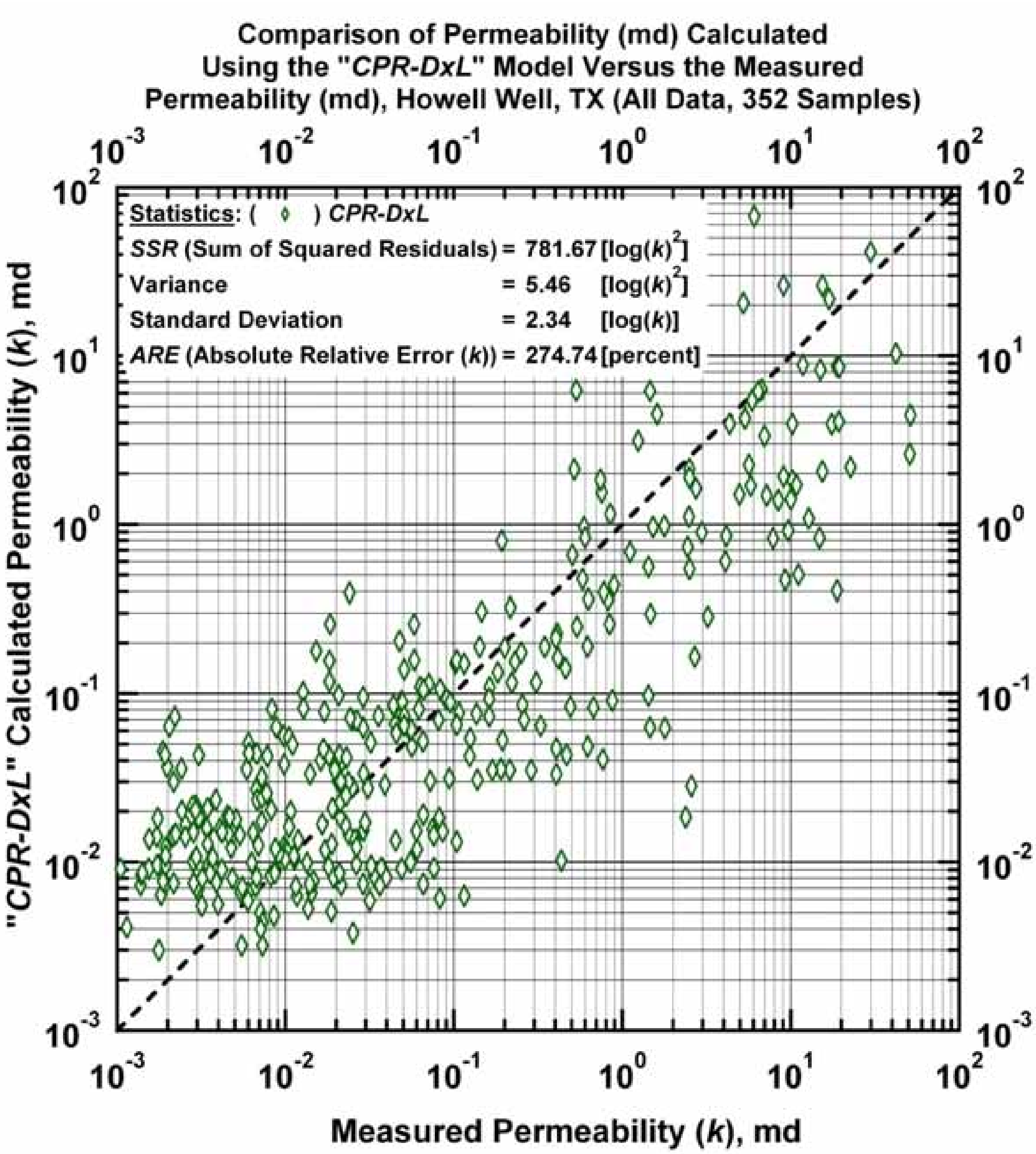

Figure B.8a — Model *CPR-DxL*: Calculated versus measured permeability. [*Case*: Howell Well, E. TX (USA)]

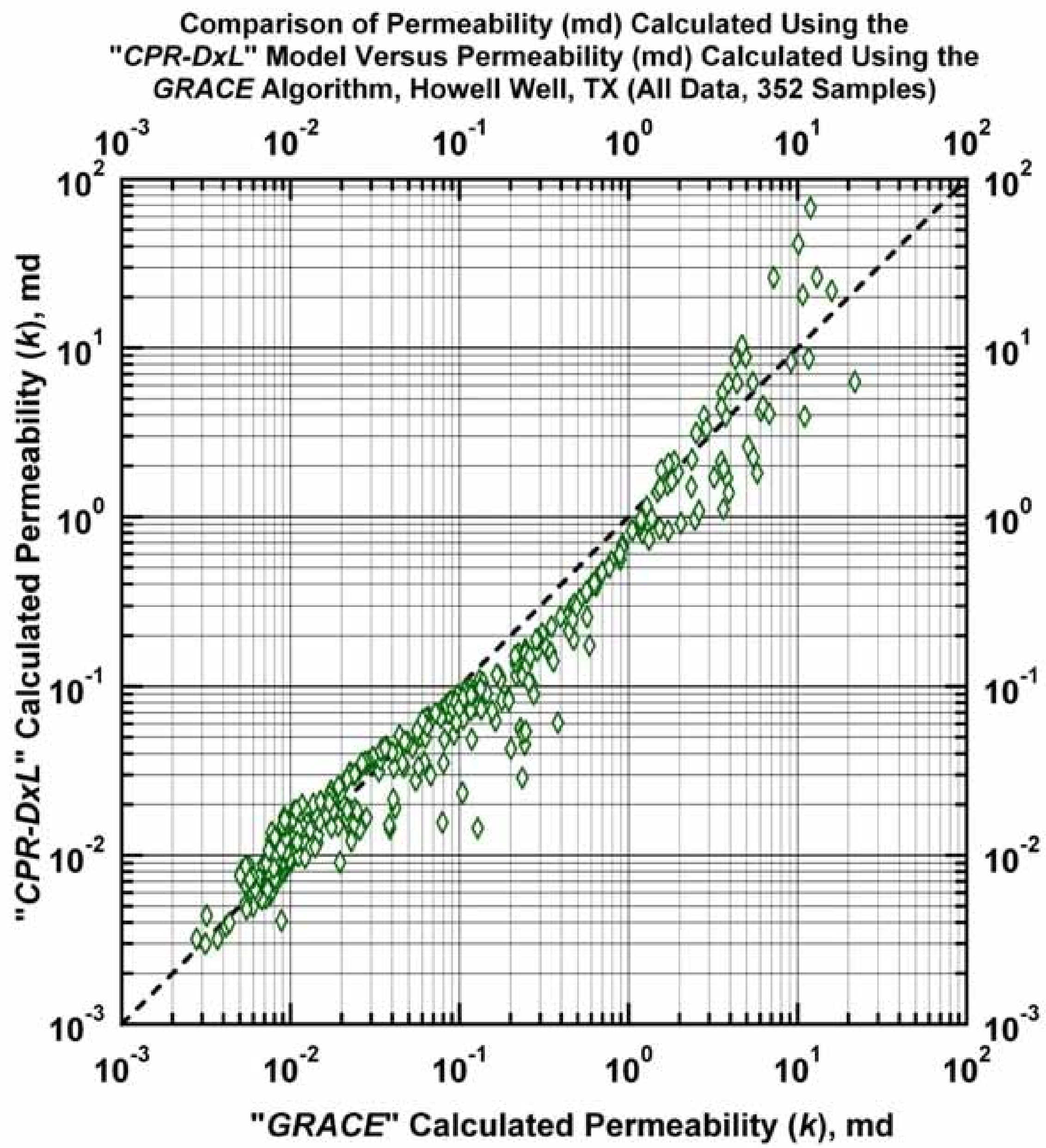

Figure B.8b — Model *CPR-DxL*: Permeability calculated using Model *CPR-C* versus permeability calculated using the *GRACE* Algorithm. [*Case*: Howell Well, E. TX (USA)]

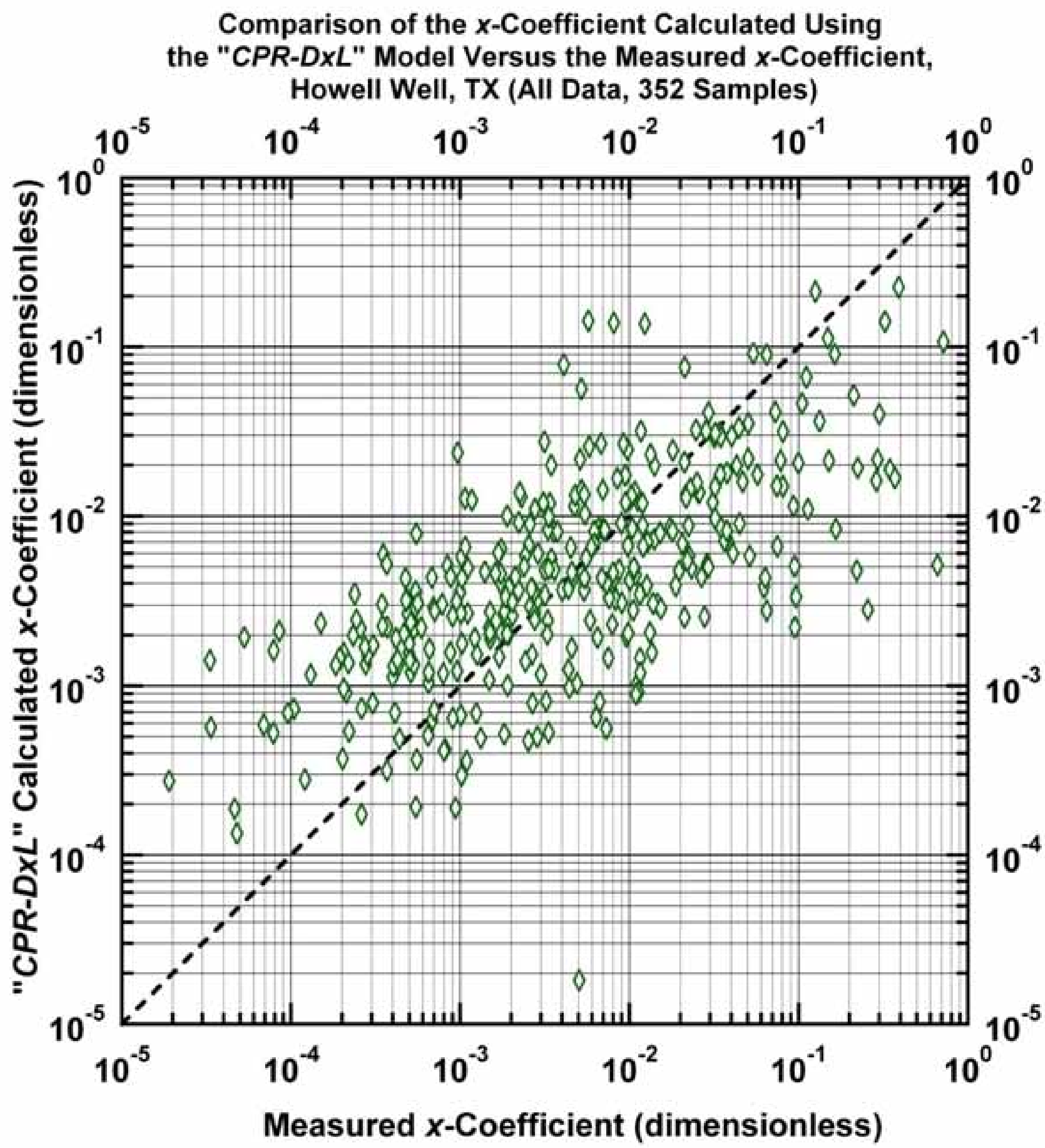

Figure B.8c — Model *CPR-DxL*: Calculated *x*-function weight values versus measured *x*-function weight values. [*Case*: Howell Well, E. TX (USA)]

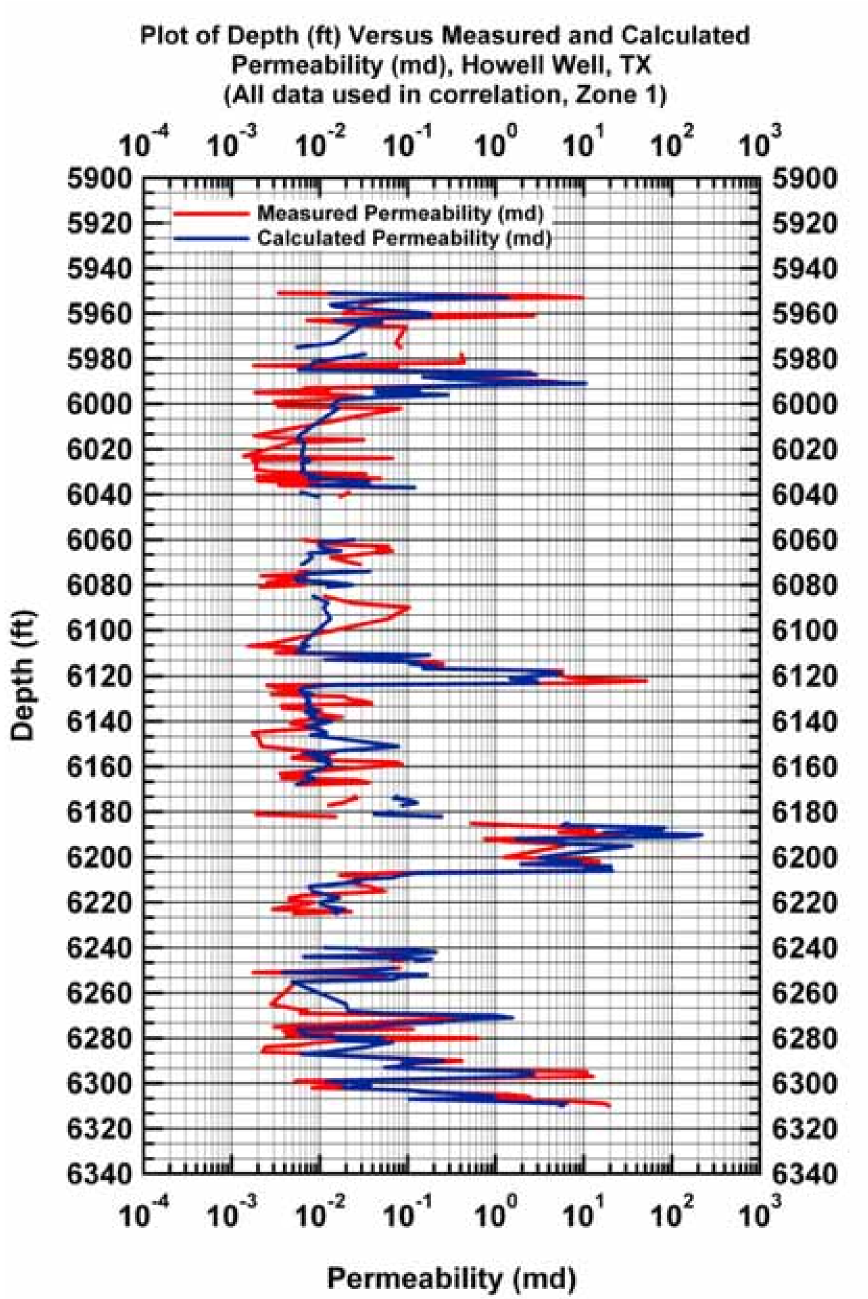

Figure B.8d — Model *CPR-DxL*: Calculated and measured permeability values versus depth. [*Case*: Howell Well, E. TX (USA)]

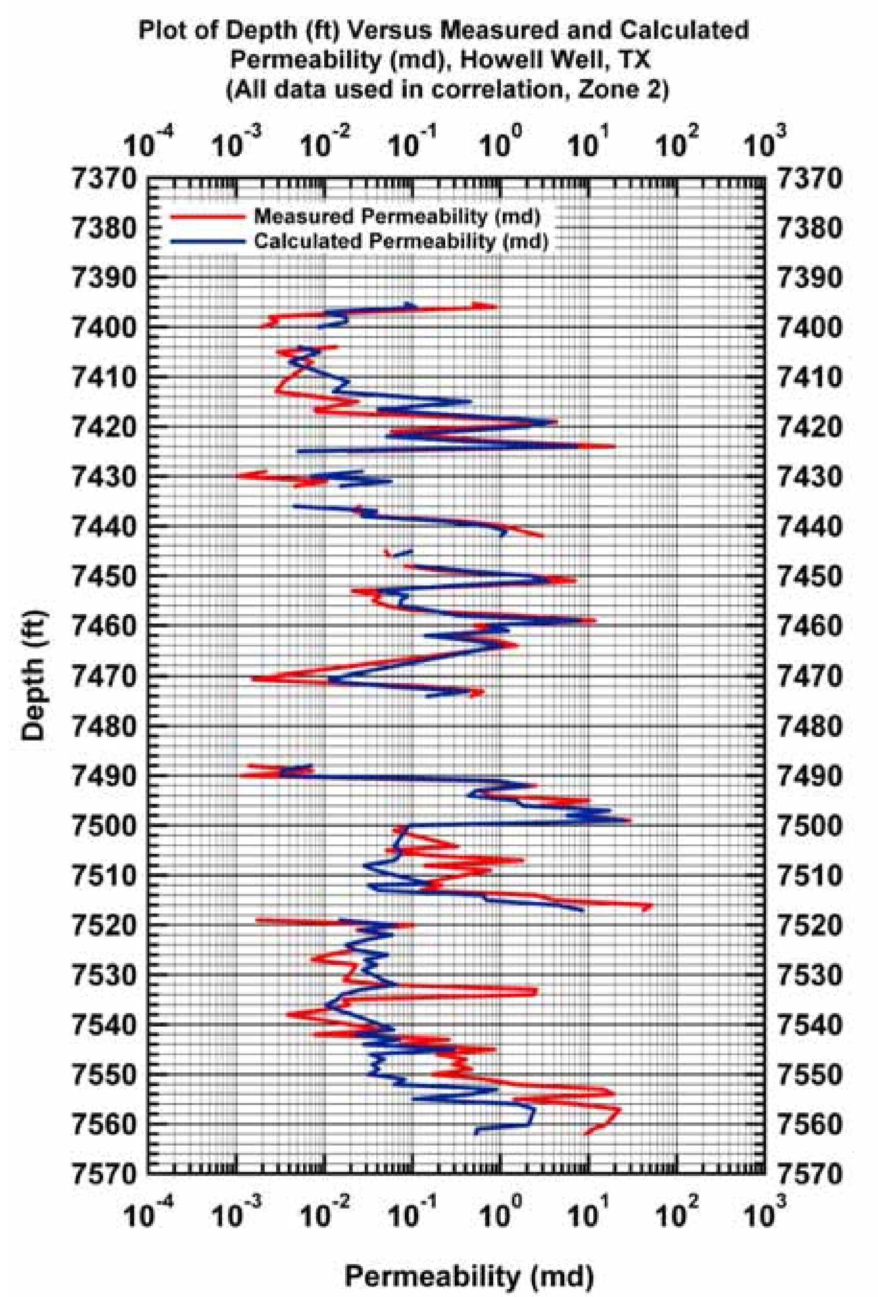

Figure B.8e — Model *CPR-DxL*: Calculated and measured permeability values versus depth. [*Case*: Howell Well, E. TX (USA)]

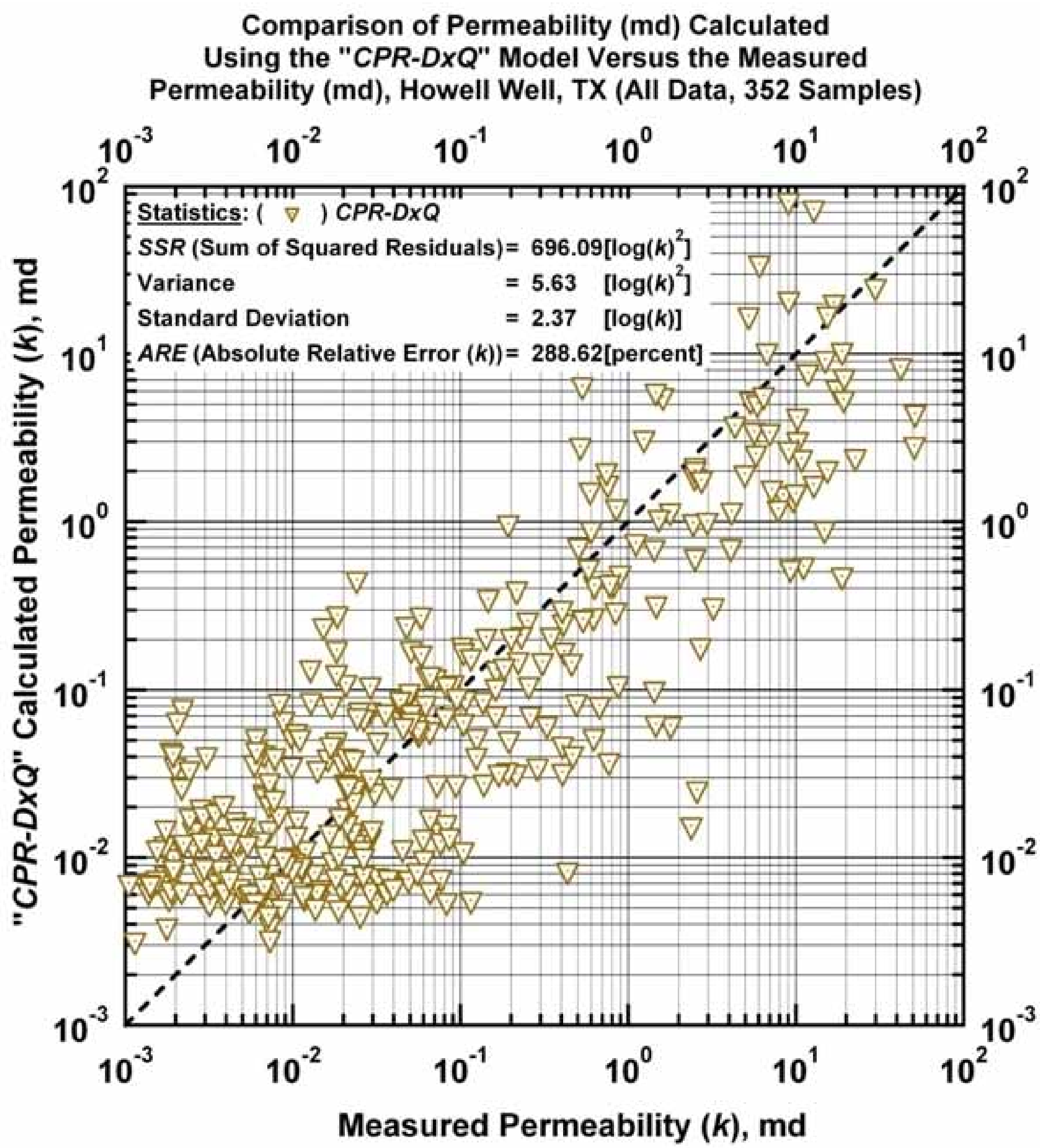

Figure B.9a — Model *CPR-DxQ*: Calculated versus measured permeability. [*Case*: Howell Well, E. TX (USA)]

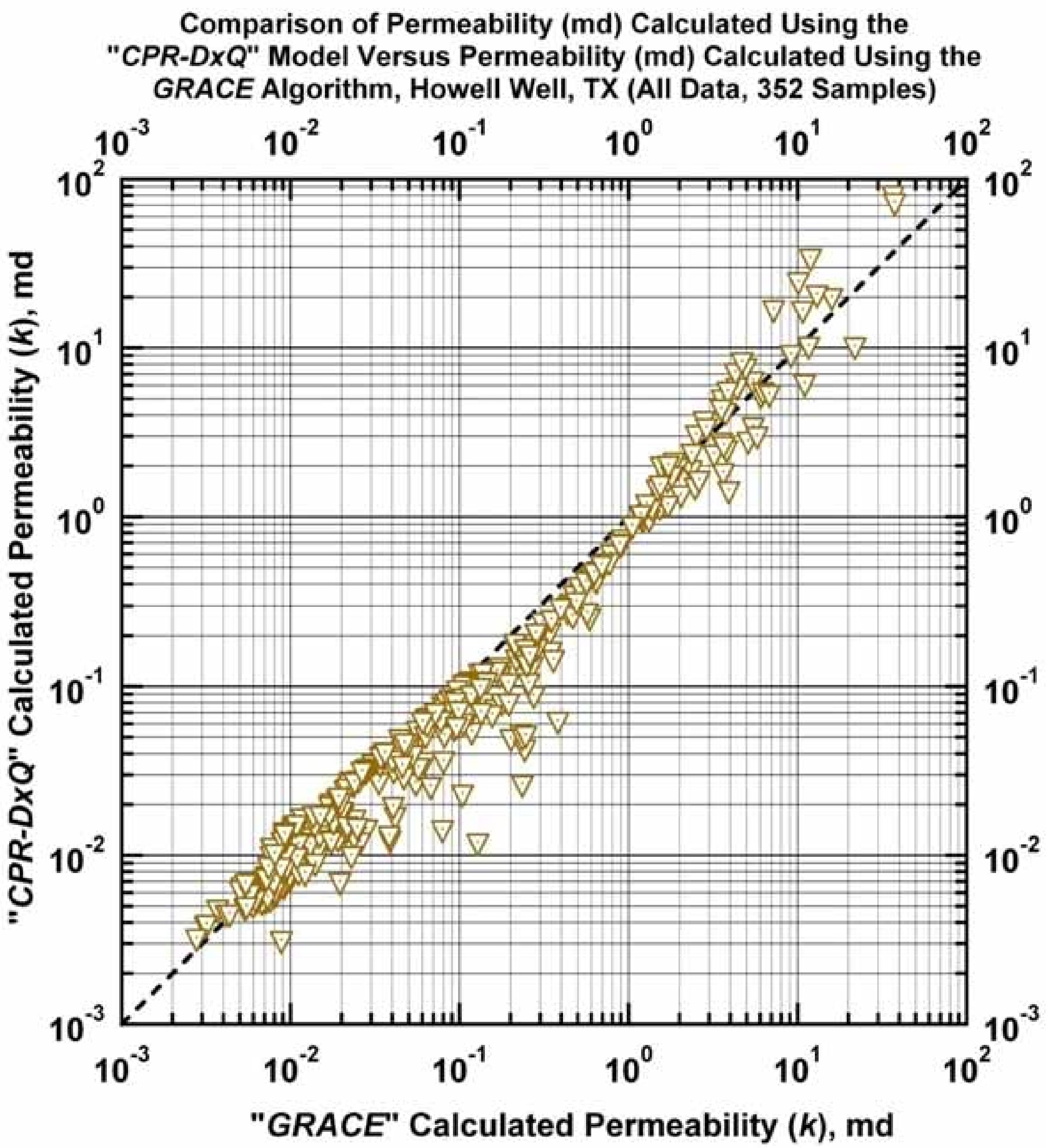

Figure B.9b — Model *CPR-DxQ*: Permeability calculated using Model *CPR-C* versus permeability calculated using the *GRACE* Algorithm. [*Case*: Howell Well, E. TX (USA)]

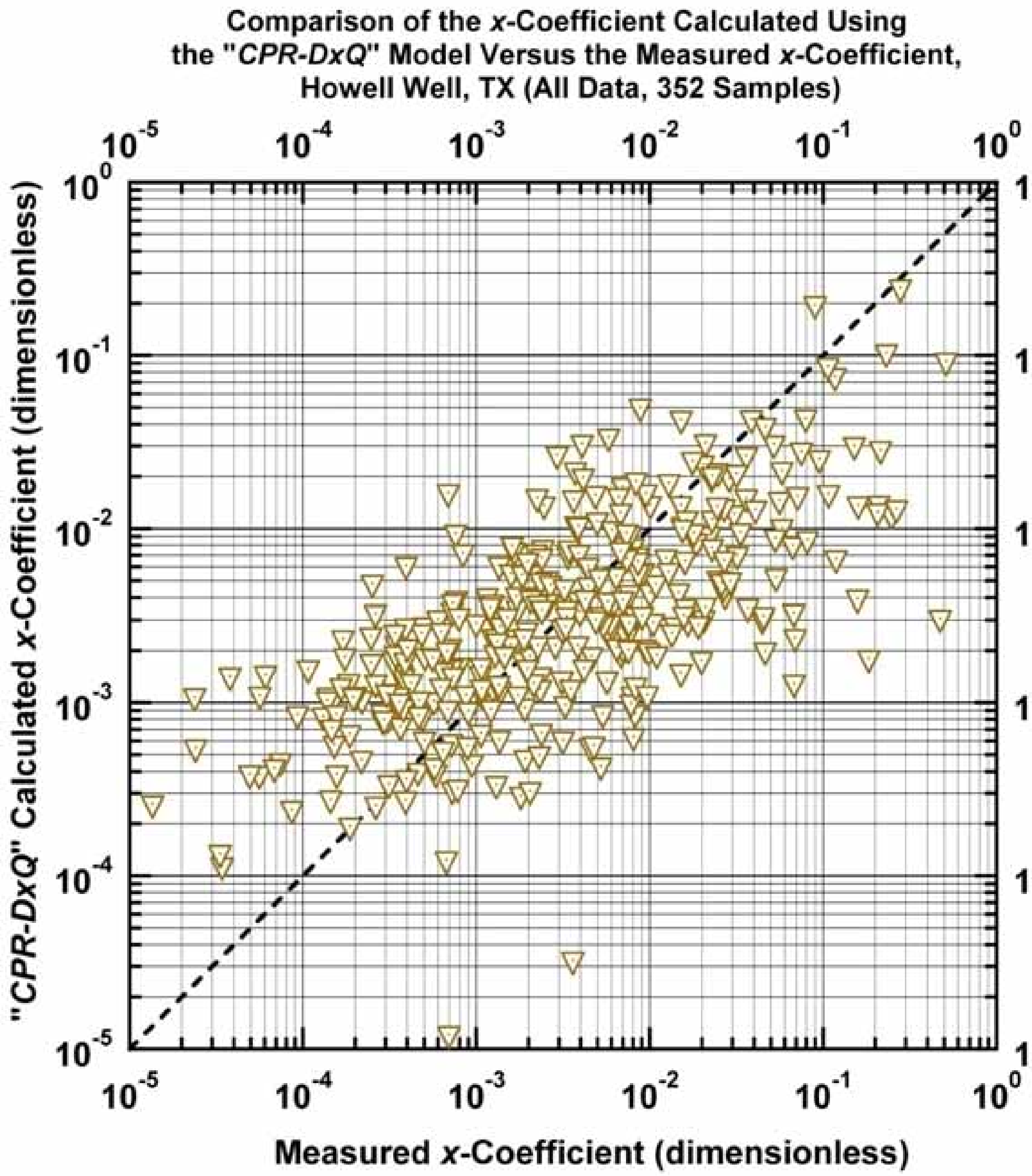

Figure B.9c — Model *CPR-DxQ*: Calculated *x*-function weight values versus measured *x*-function weight values. [*Case*: Howell Well, E. TX (USA)]

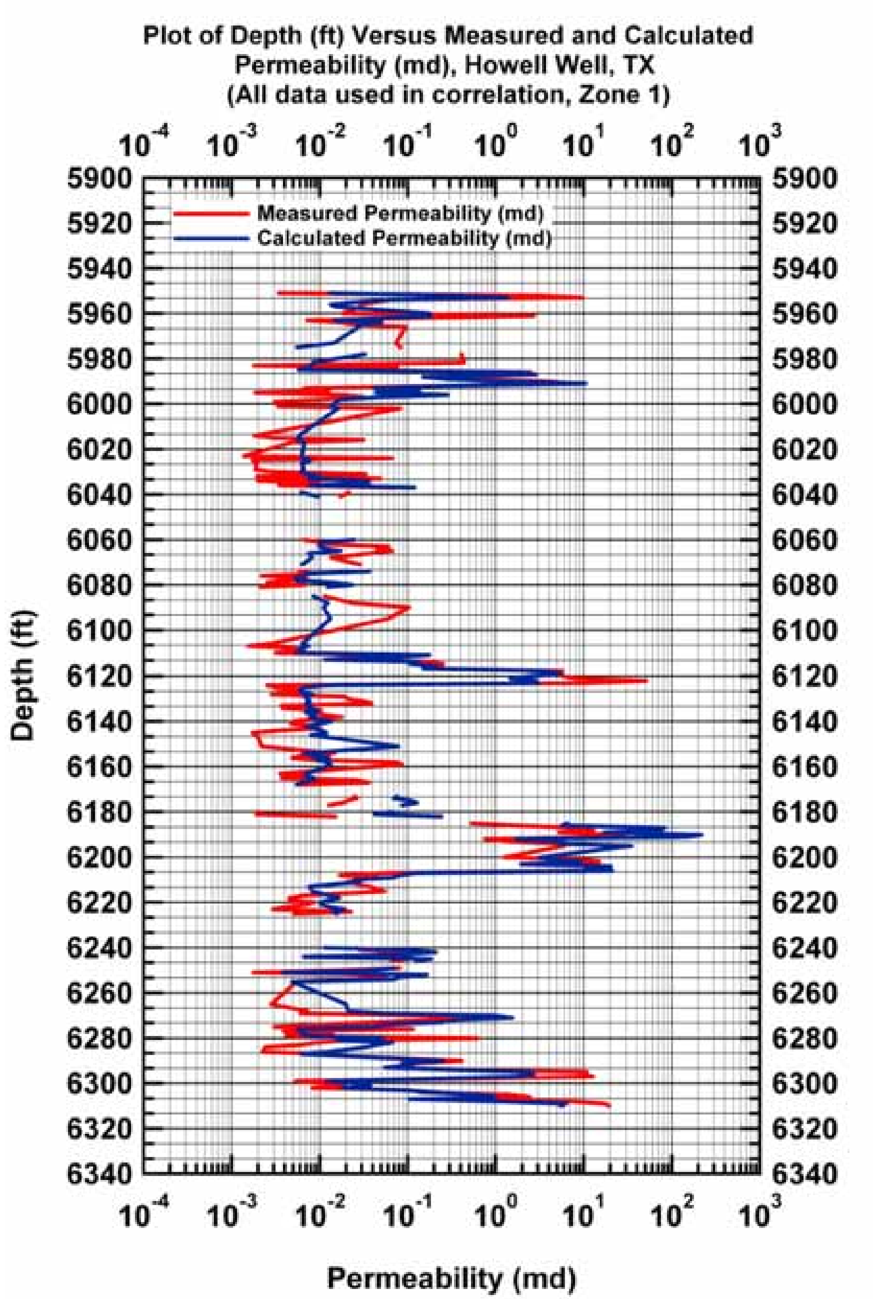

Figure B.9d — Model *CPR-DxQ*: Calculated and measured permeability values versus depth. [*Case*: Howell Well, E. TX (USA)]

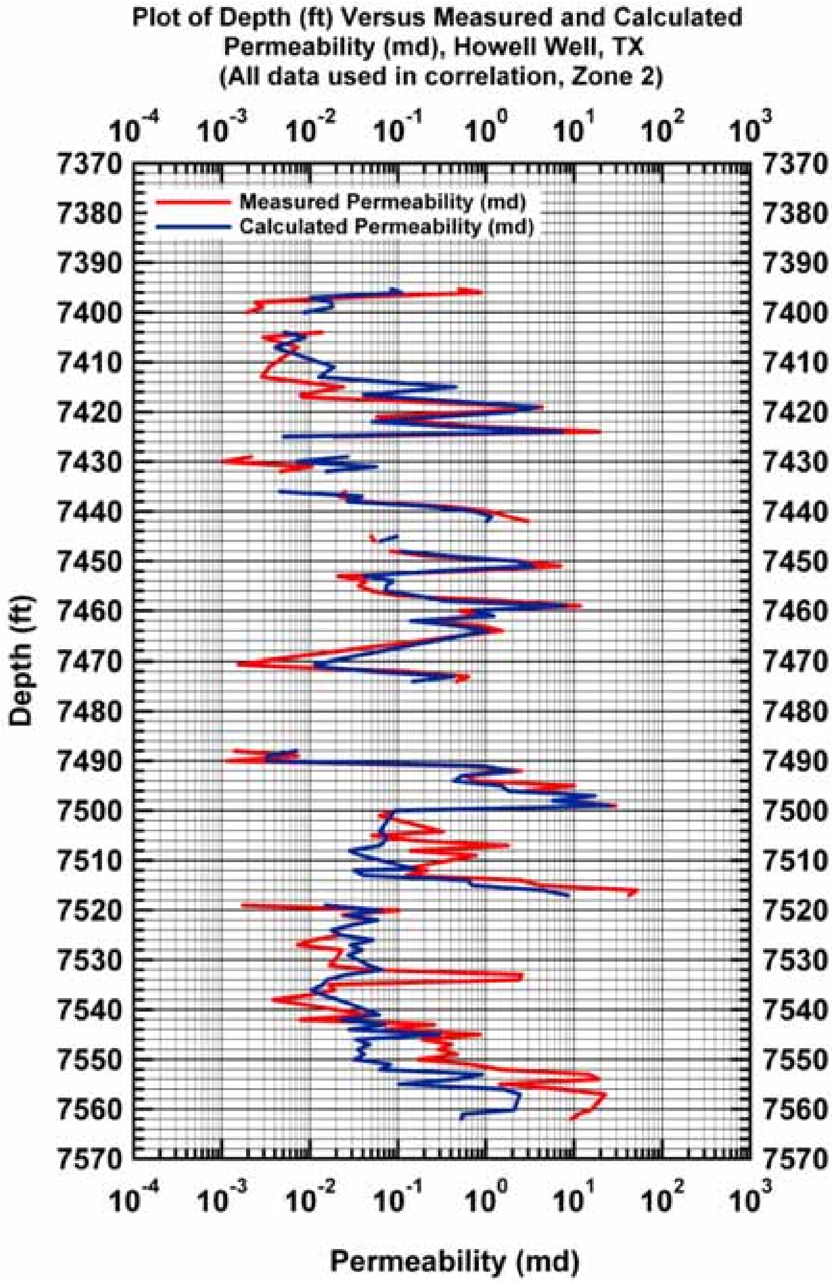

Figure B.9e — Model *CPR-DxQ*: Calculated and measured permeability values versus depth. [*Case*: Howell Well, E. TX (USA)]

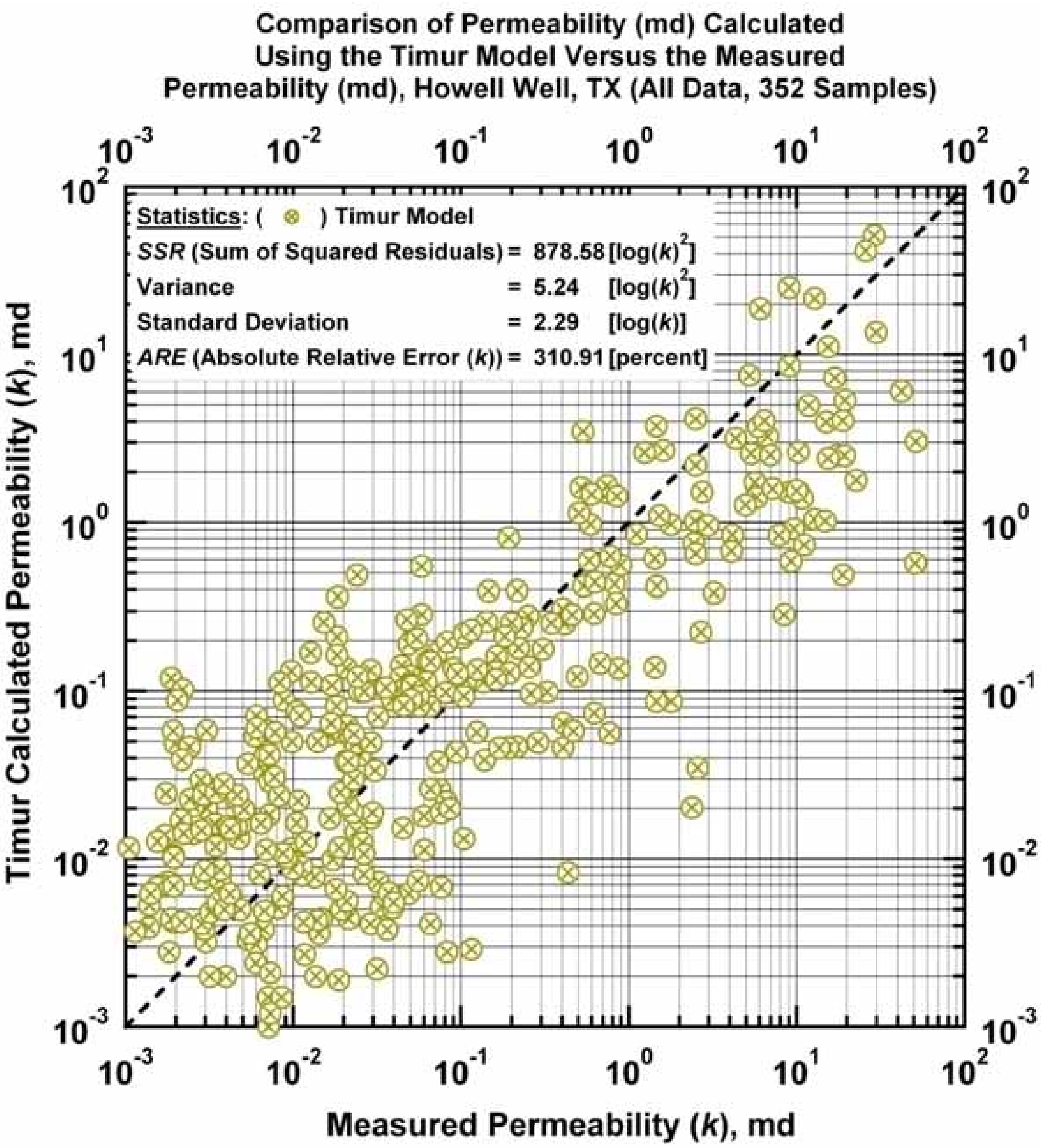

Figure B.10a — "Timur Model:" Calculated versus measured permeability. [*Case*: Howell Well, E. TX (USA)]

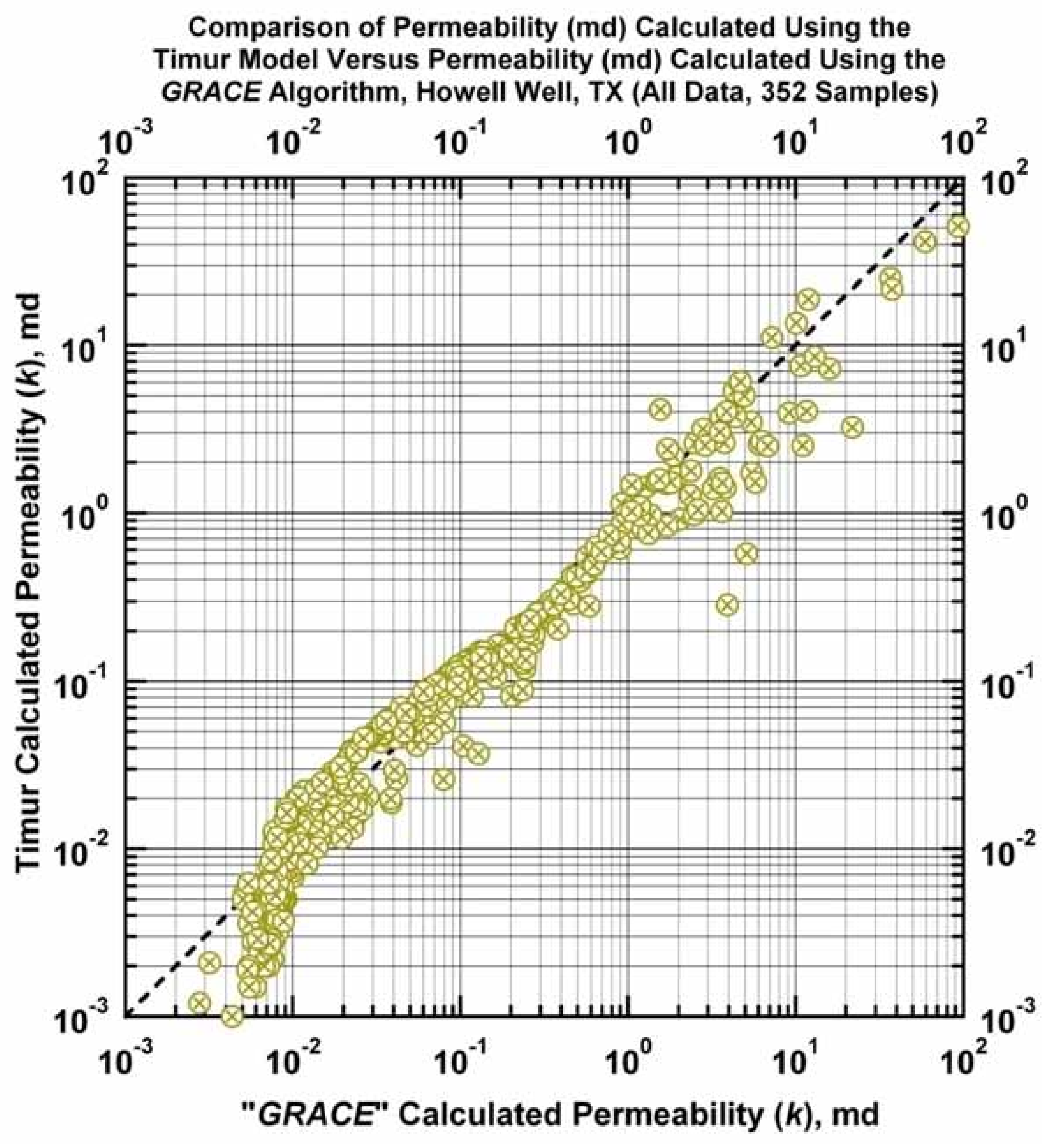

Figure B.10b — "Timur Model:" Permeability calculated using the "Timur Model" versus permeability calculated using the *GRACE* Algorithm. [*Case*: Howell Well, E. TX (USA)]

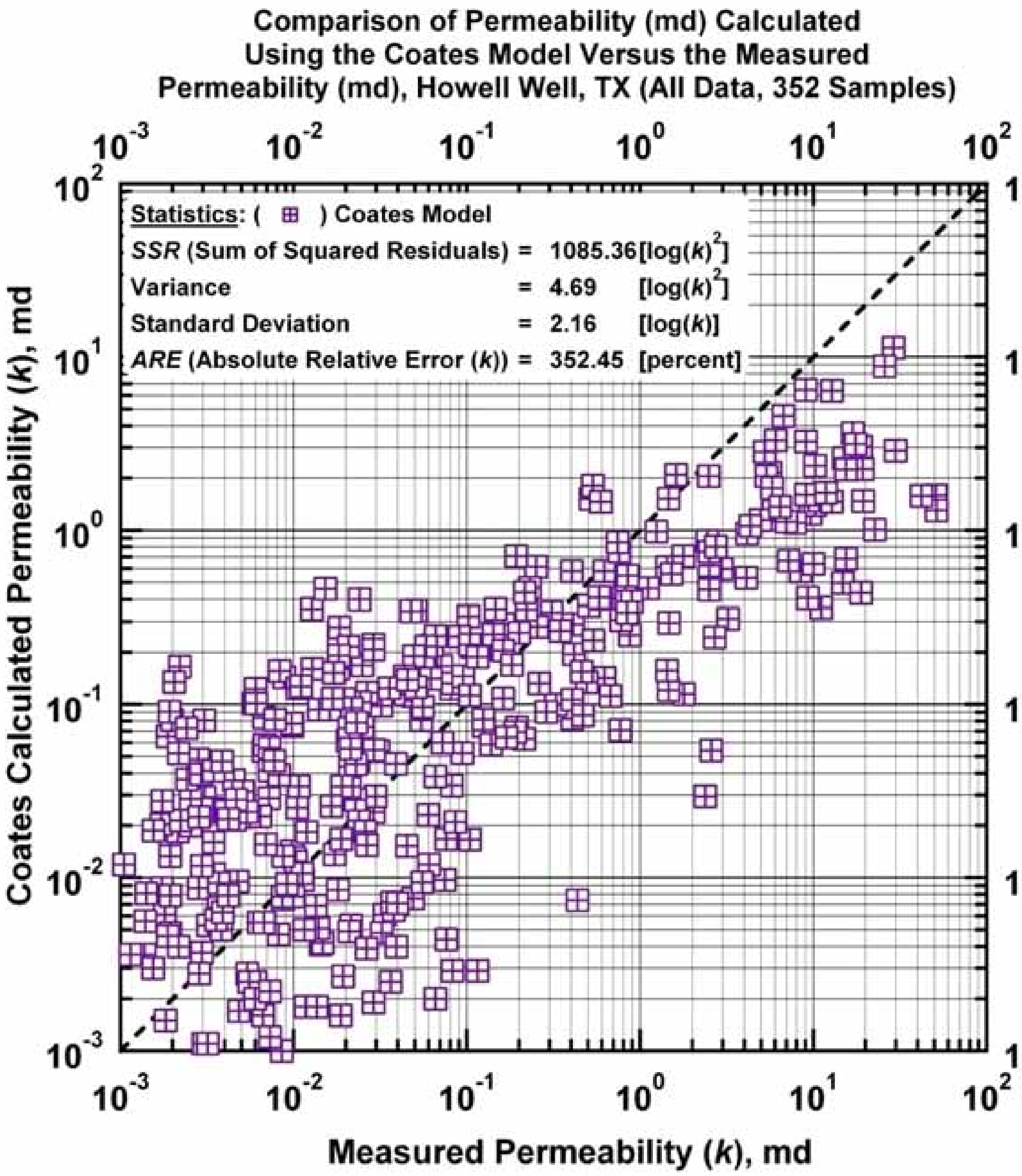

Figure B.11a — "Coates Model:" Calculated versus measured permeability. [*Case*: Howell Well, E. TX (USA)]

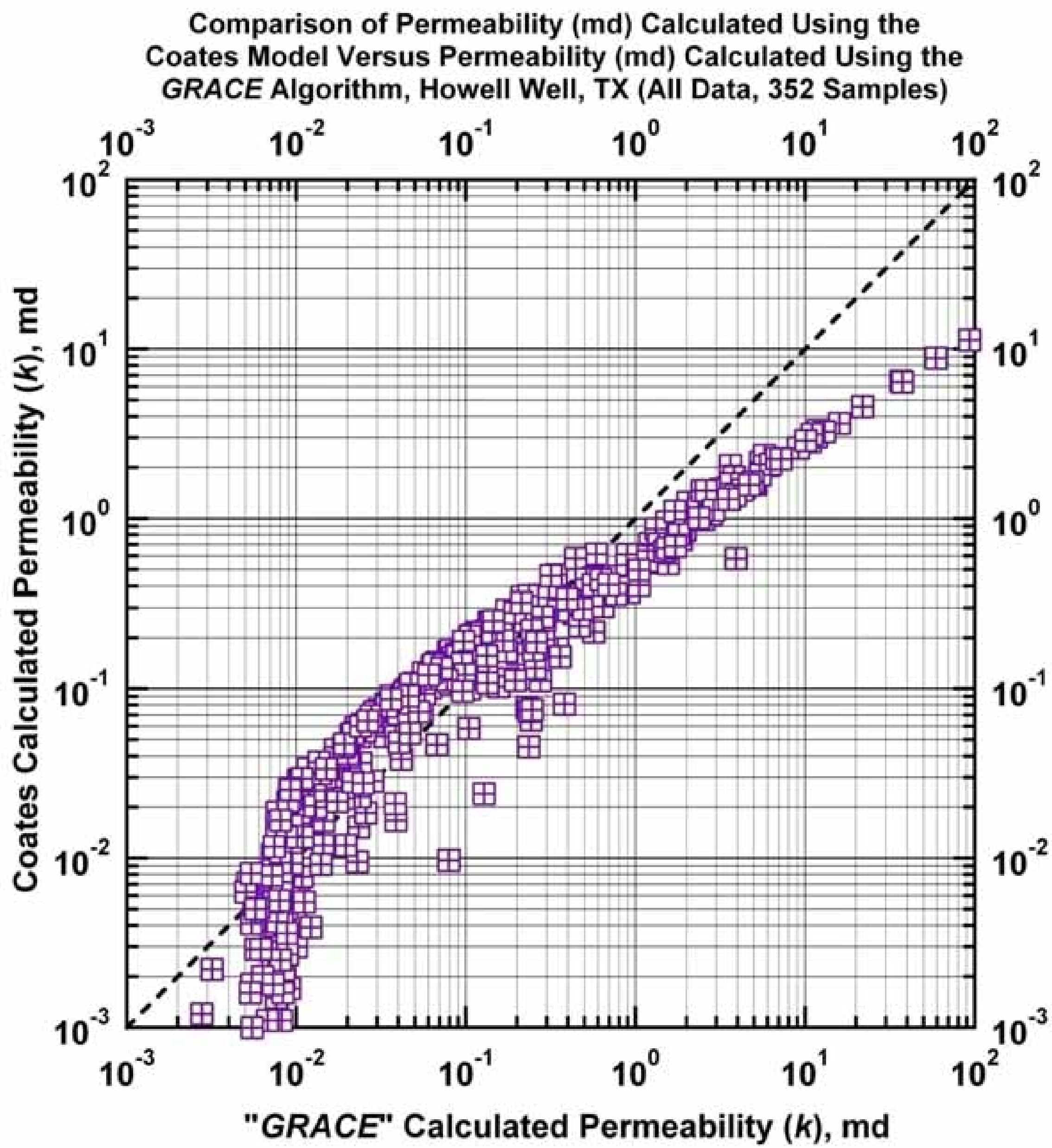

Figure B.11b — "Coates Model:" Permeability calculated using the "Coates Model " versus permeability calculated using the *GRACE* Algorithm. [*Case*: Howell Well, E. TX (USA)]

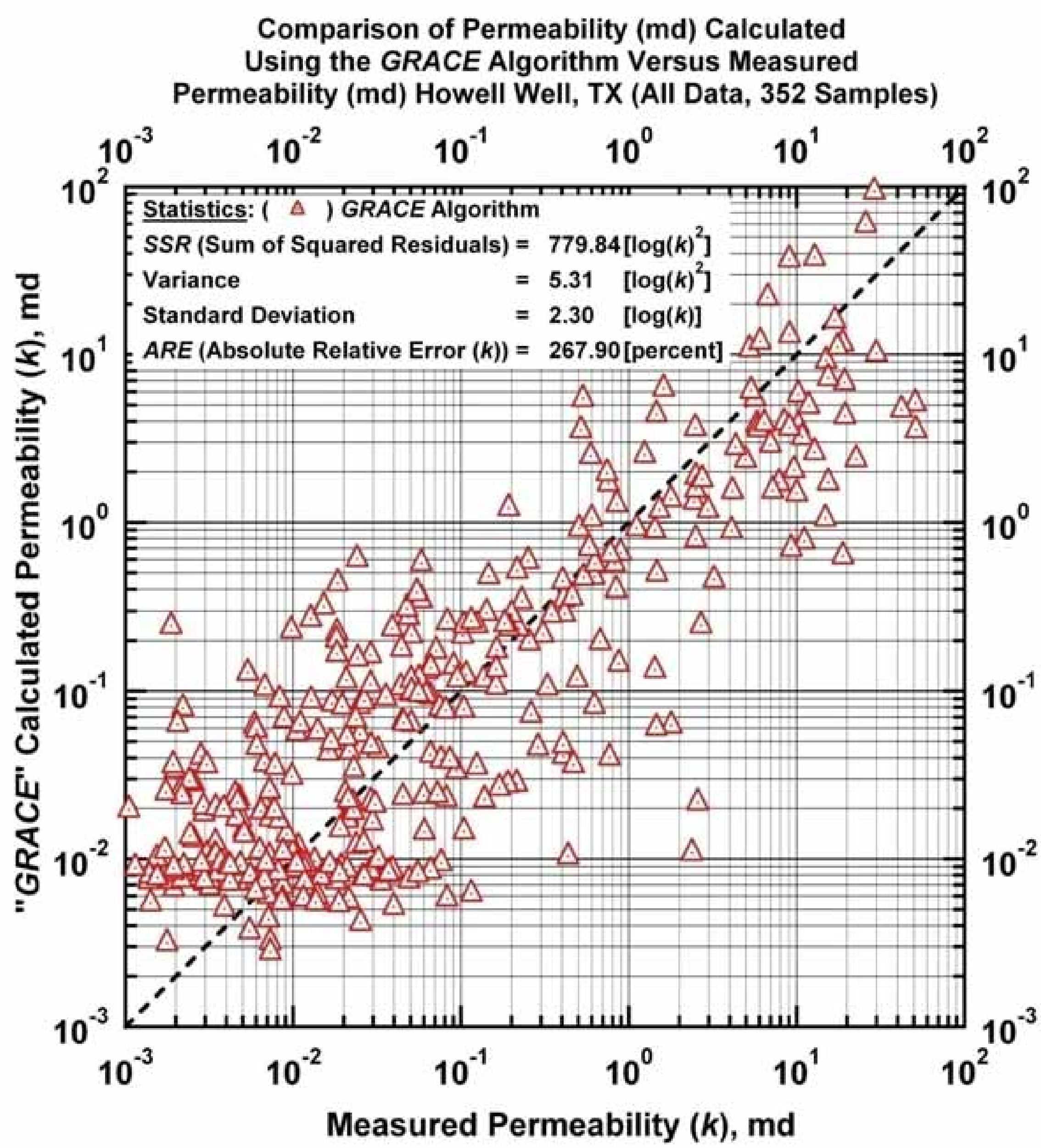

Figure B.12 — *GRACE* Model: Calculated versus measured permeability. [*Case*: Howell Well, E. TX (USA)]

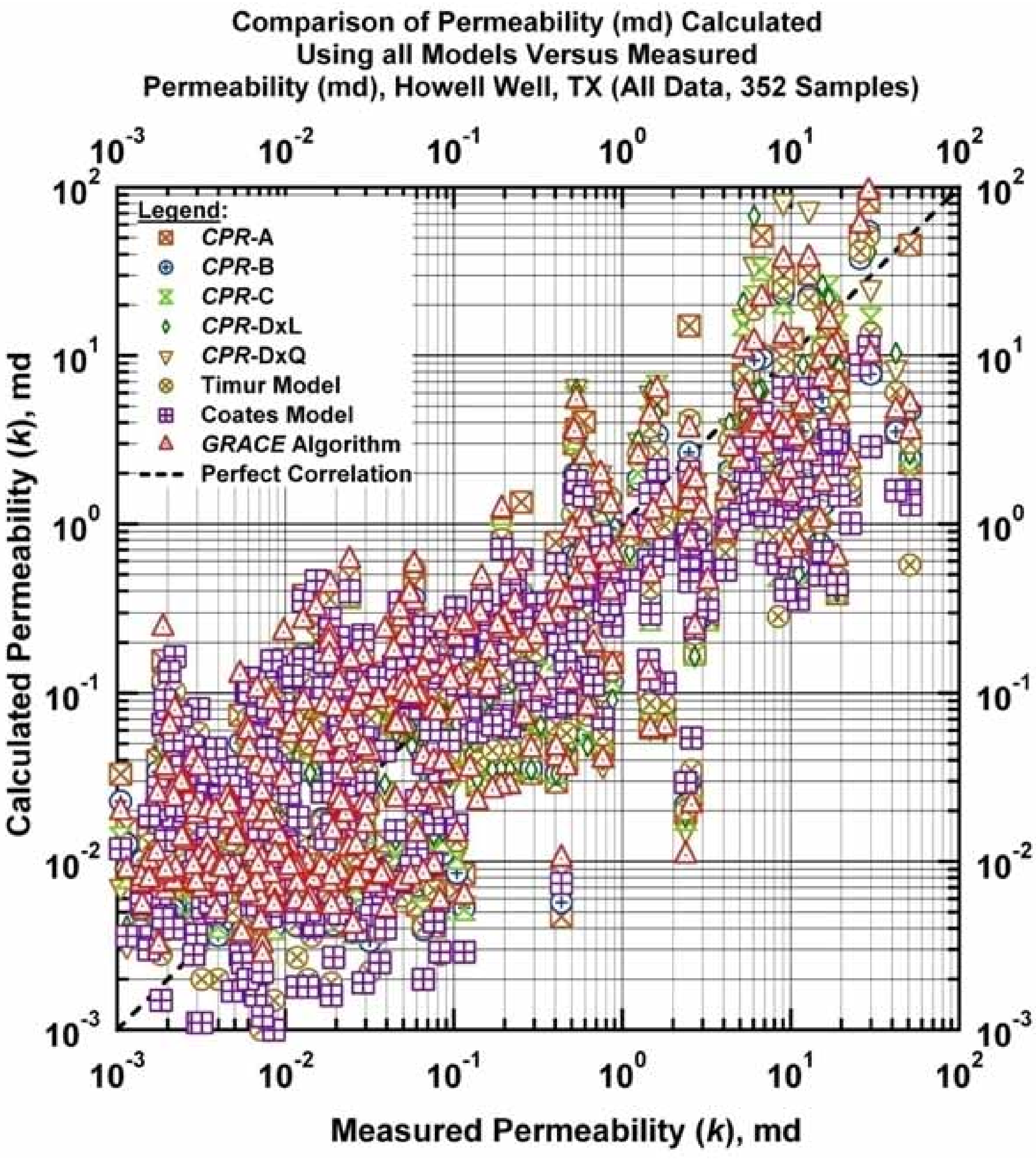

Figure B.13 — All Models: Calculated versus measured permeability. [*Case*: Howell Well, E. TX (USA)]

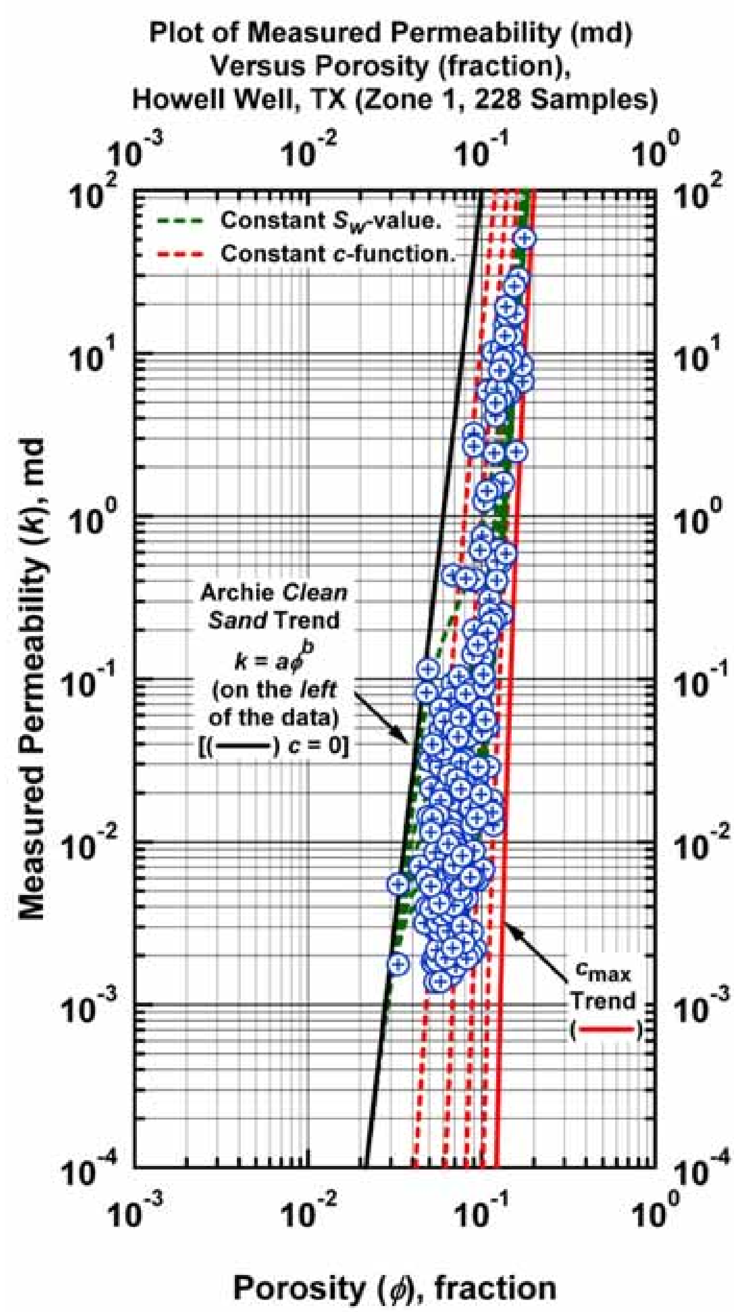

Figure B.14a — Model *CPR-A*: $k = a(\phi - c)^b$ $c = c_{\max}\exp[-c_1\phi^{c_2} S_w^{c_3}]$ — "Clean Sand" Plot (log-log format) — Archie "Clean Sand" trend is given by the straight-line trend at the far left of the data (power law model). [*Case*: Howell Well, E. TX (USA)]

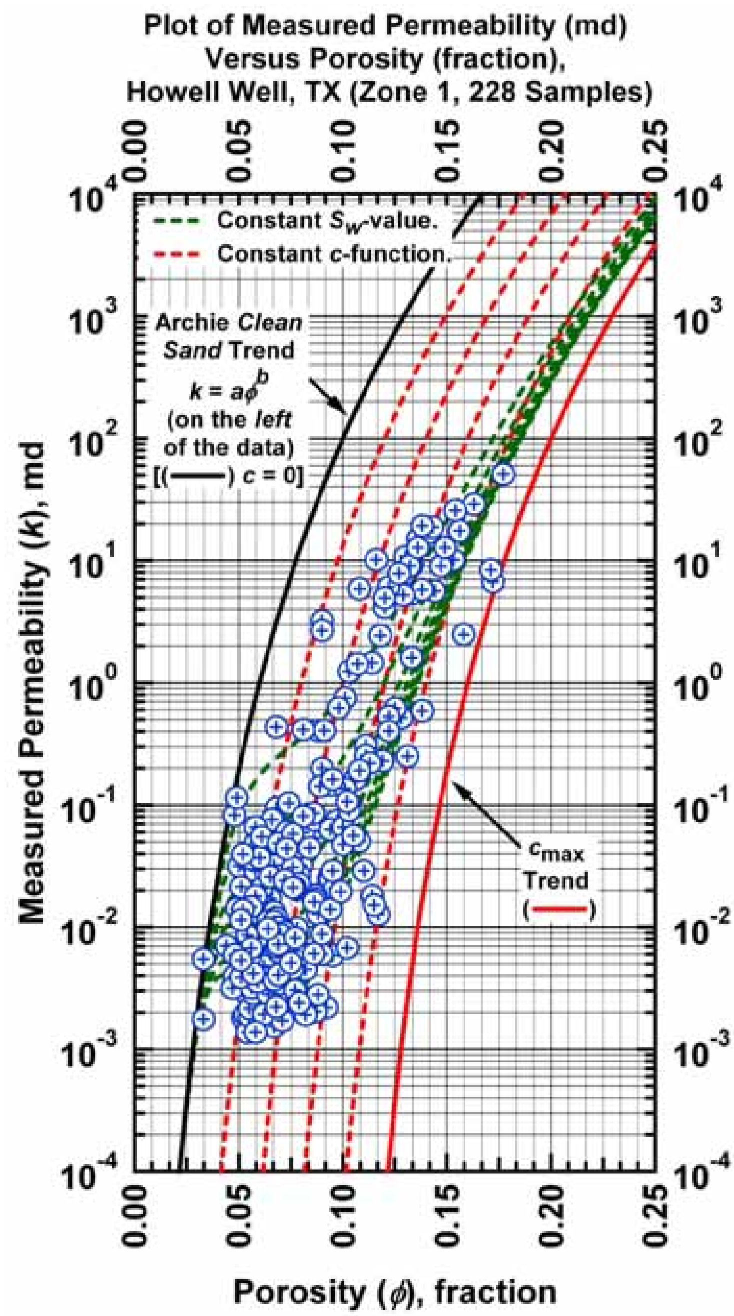

Figure B.14b — Model *CPR-A*: $k = a(\phi - c)^b$ $c = c_{max} \exp[-c_1 \phi^{c_2} S_w^{c_3}]$ — "Dirty Sand" Plot (semilog format). Archie "Clean Sand" trend is given by the curved trend at the far left of the data (power law model). [*Case*: Howell Well, E. TX (USA)]

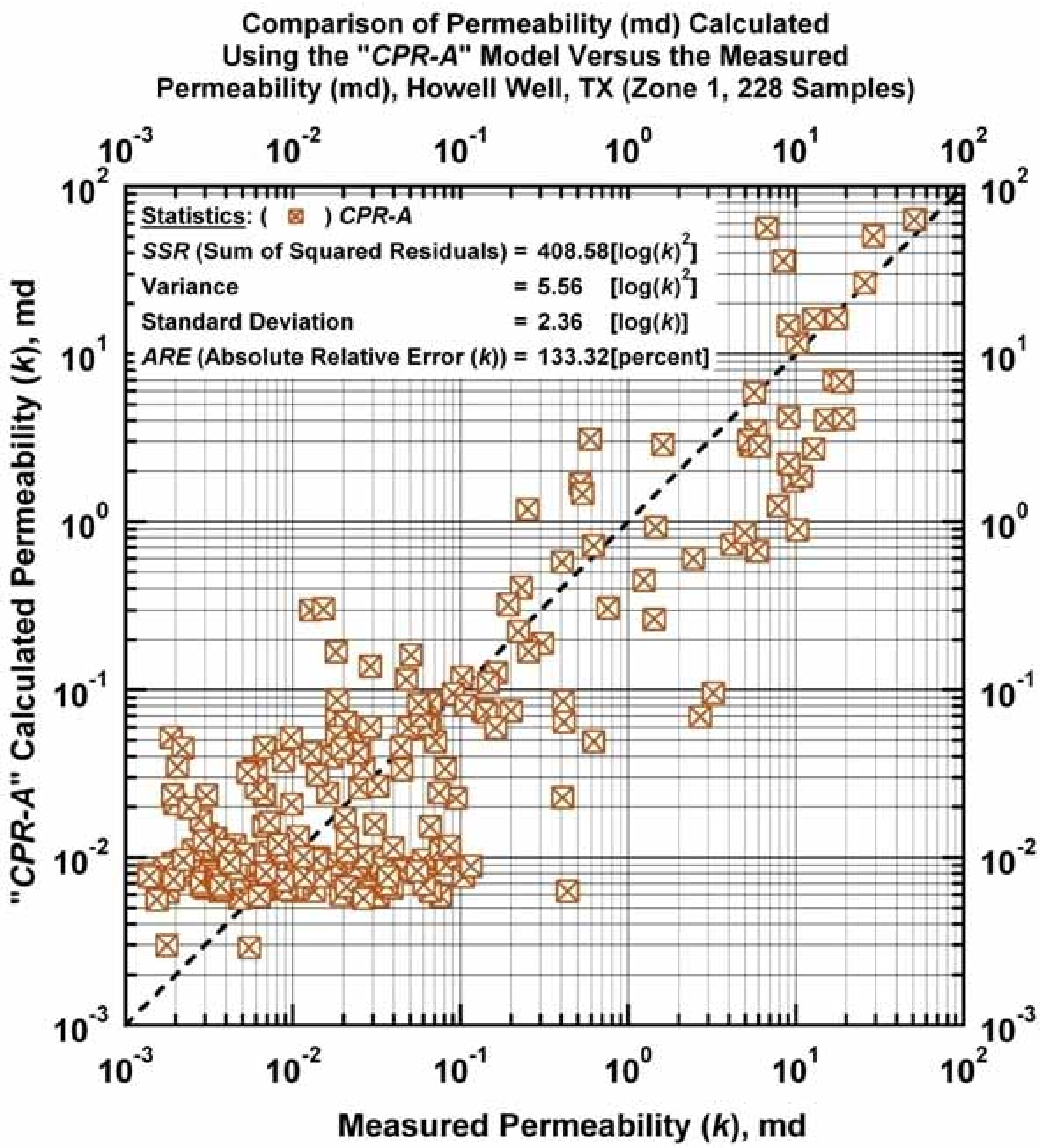

Figure B.15a — Model *CPR-A*: calculated versus measured permeability. [*Case*: Howell Well, E. TX (USA)]

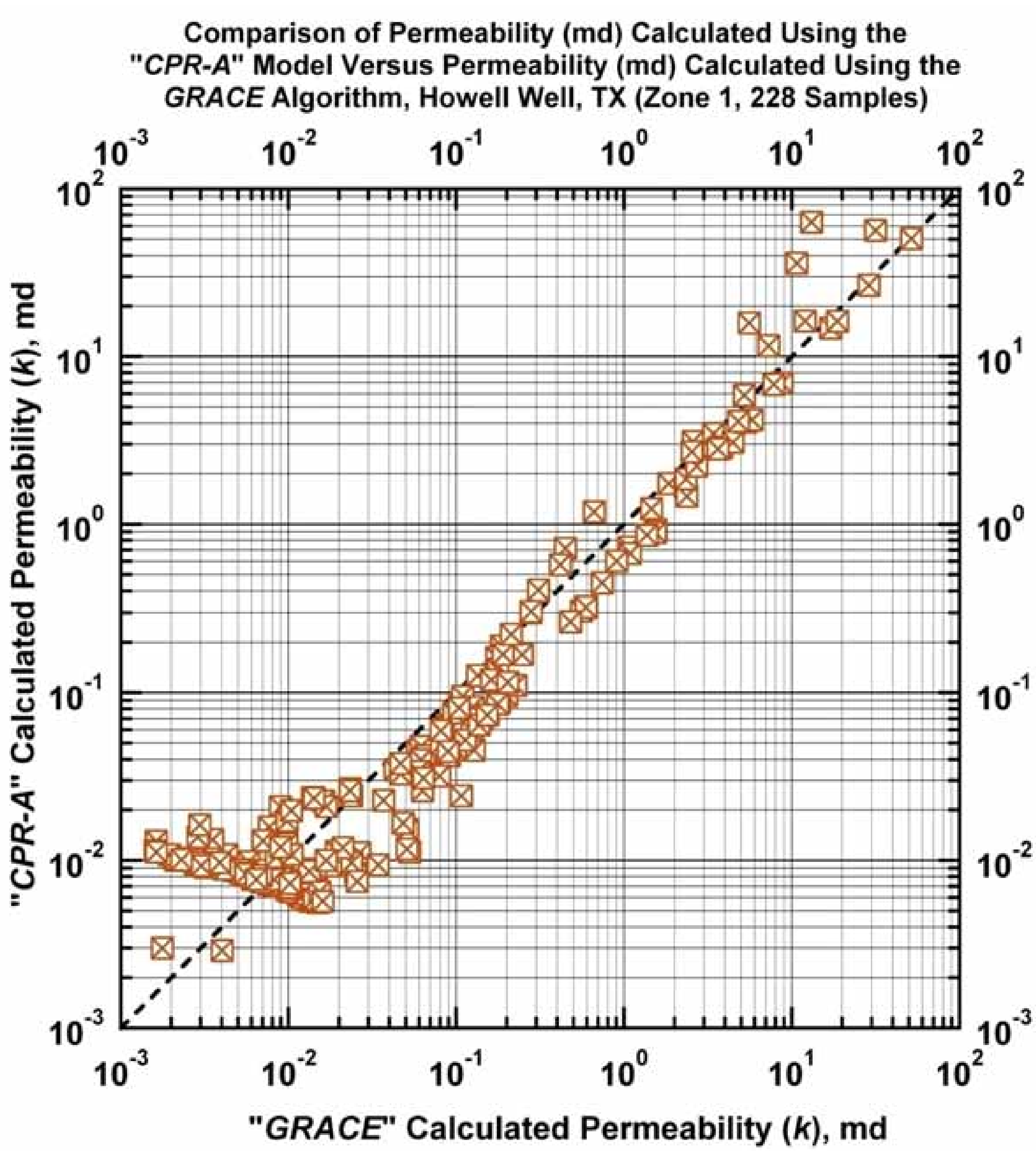

Figure B. 15b — Model *CPR-A*: Permeability calculated using Model *CPR-A* versus permeability calculated using the *GRACE* Algorithm. [*Case*: Howell Well, E. TX (USA)]

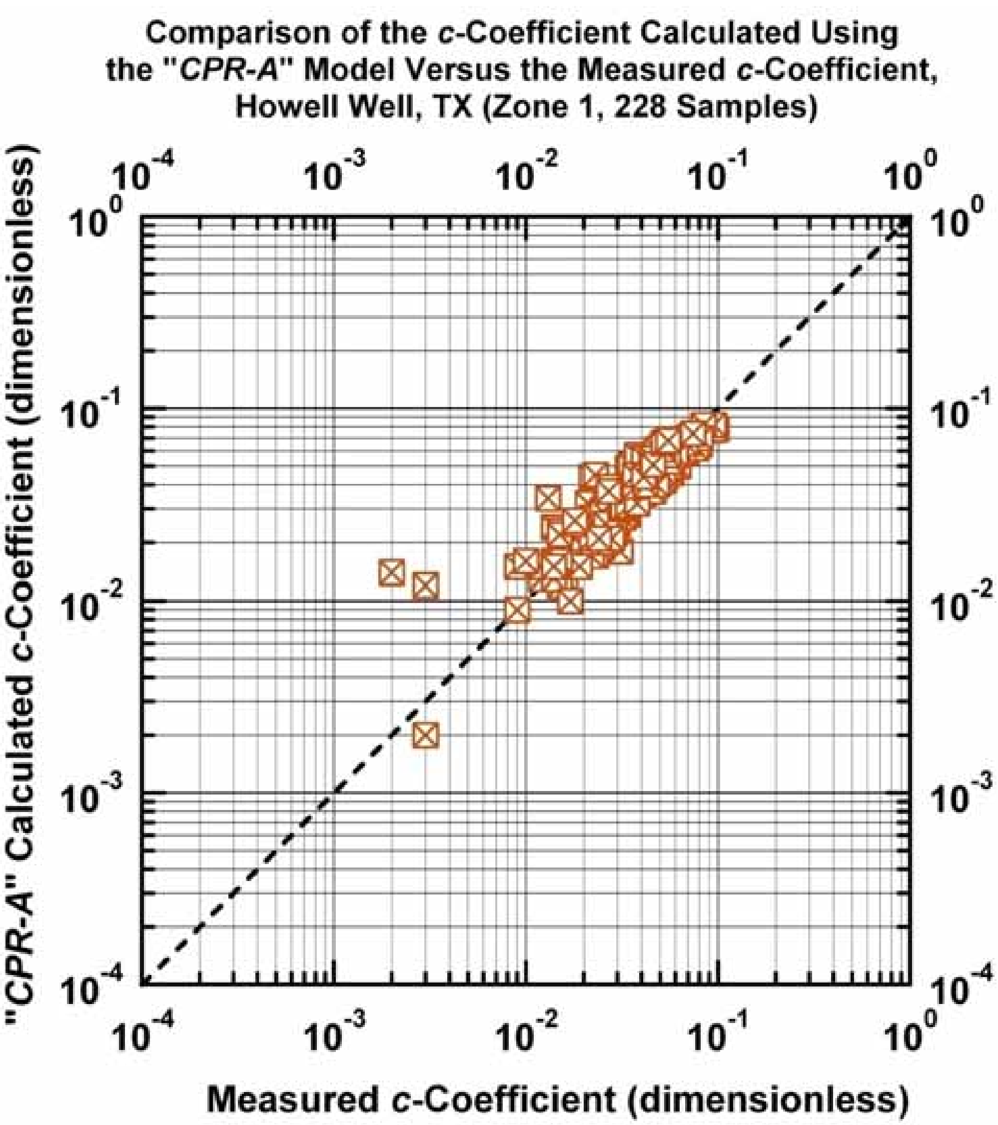

Figure B. 15c — Model *CPR-A*: Calculated *c*-function values versus measured *c*-function values. [*Case*: Howell Well, E. TX (USA)]

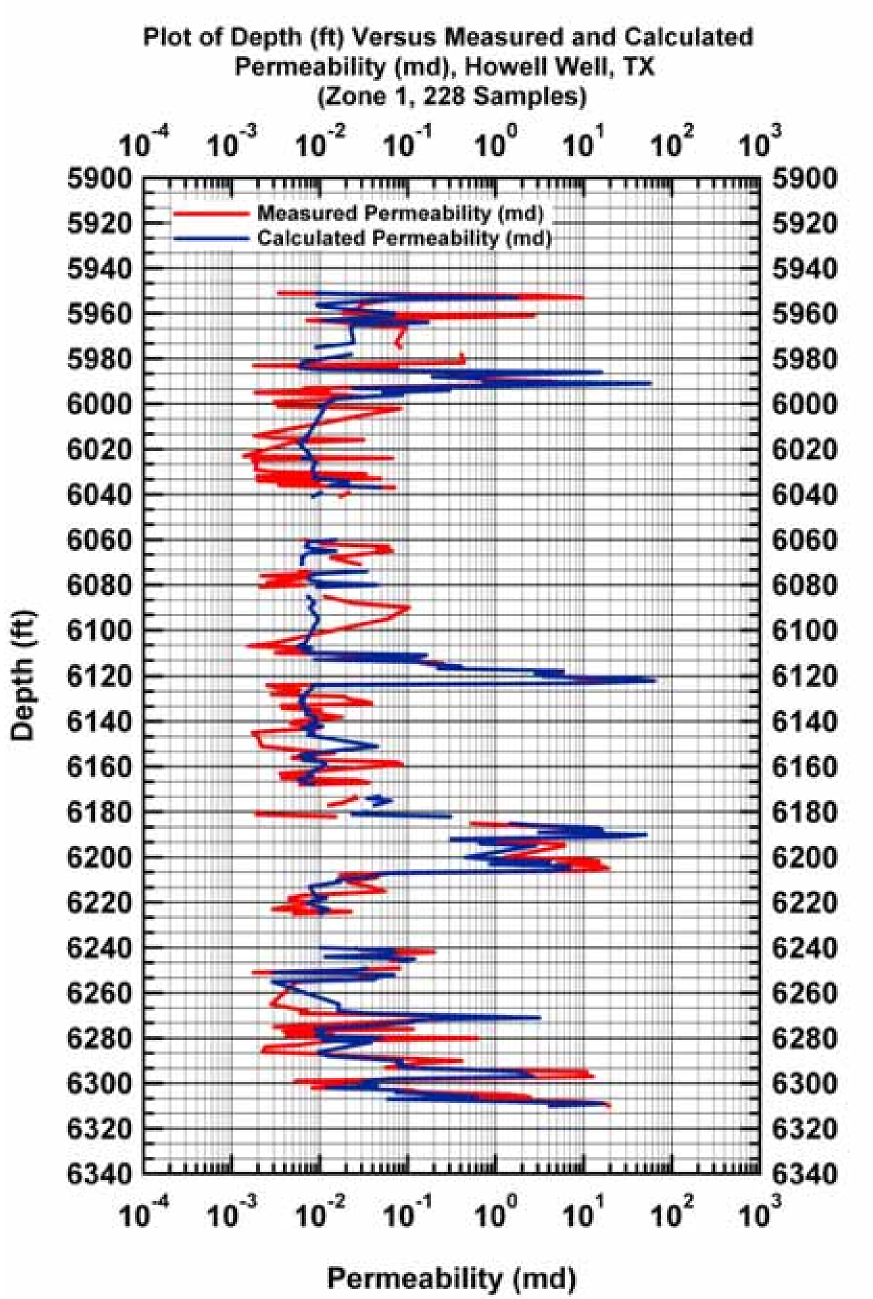

Figure B. 15d — Model *CPR-A*: Calculated and measured permeability values versus depth. [*Case*: Howell Well, E. TX (USA)]

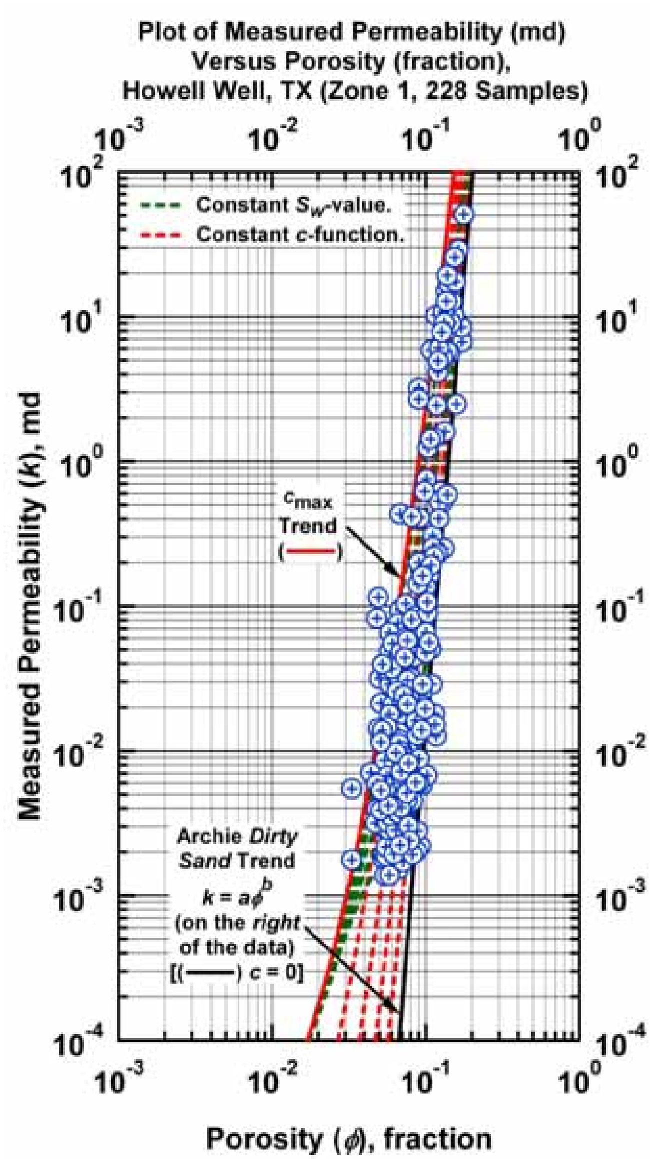

Figure B.16a — Model *CPR-B*: $k = a(\phi + c)^b$ $c = c_{max} \exp[-c_1 \phi^{c_2} S_w^{c_3}]$ — "Clean Sand" Plot (log-log format) — Archie "Dirty Sand" trend is given by the straight-line trend at the far right of the data (power law model). [*Case*: Howell Well, E. TX (USA)]

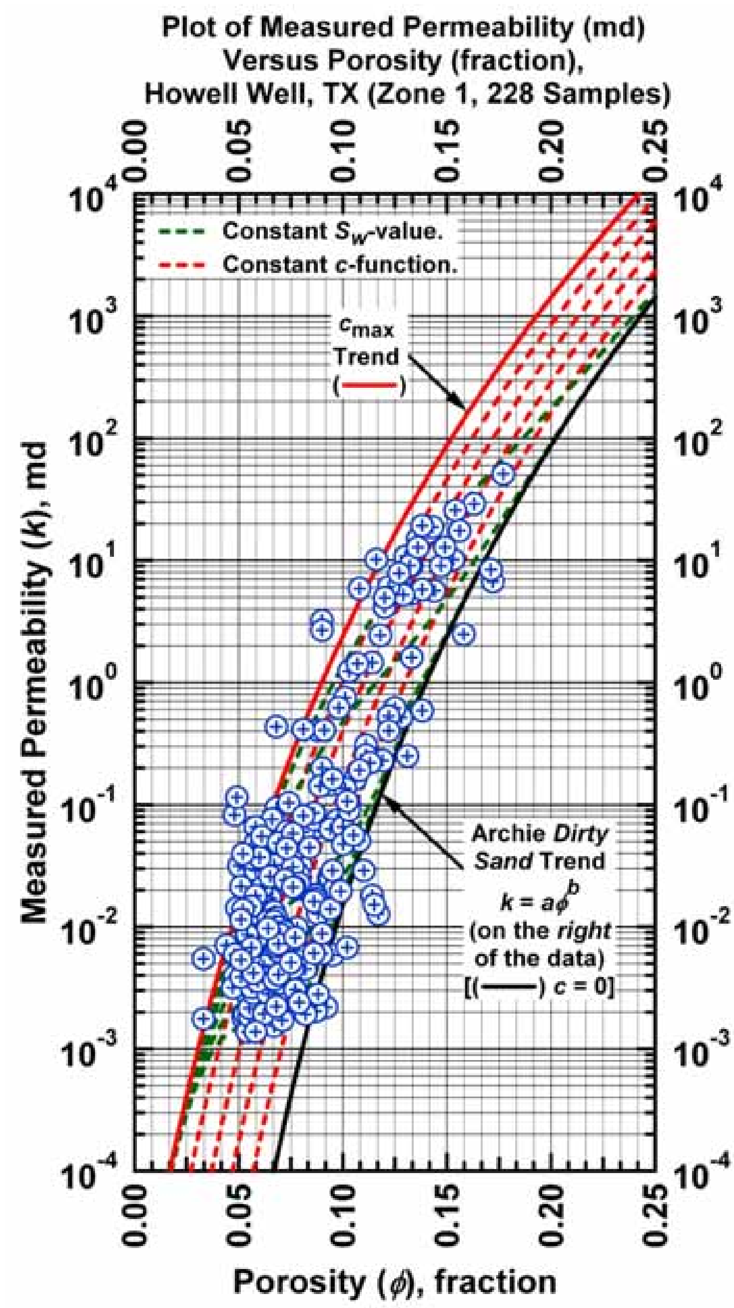

Figure B.16b — Model *CPR-B*: $k = a(\phi + c)^b \quad c = c_{\max} \exp[-c_1 \phi^{c_2} S_w^{c_3}]$ — "Dirty Sand" Plot (semilog format) — Archie "Dirty Sand" trend is given by the curved trend at the far right of the data (power law model). [*Case*: Howell Well, E. TX (USA)]

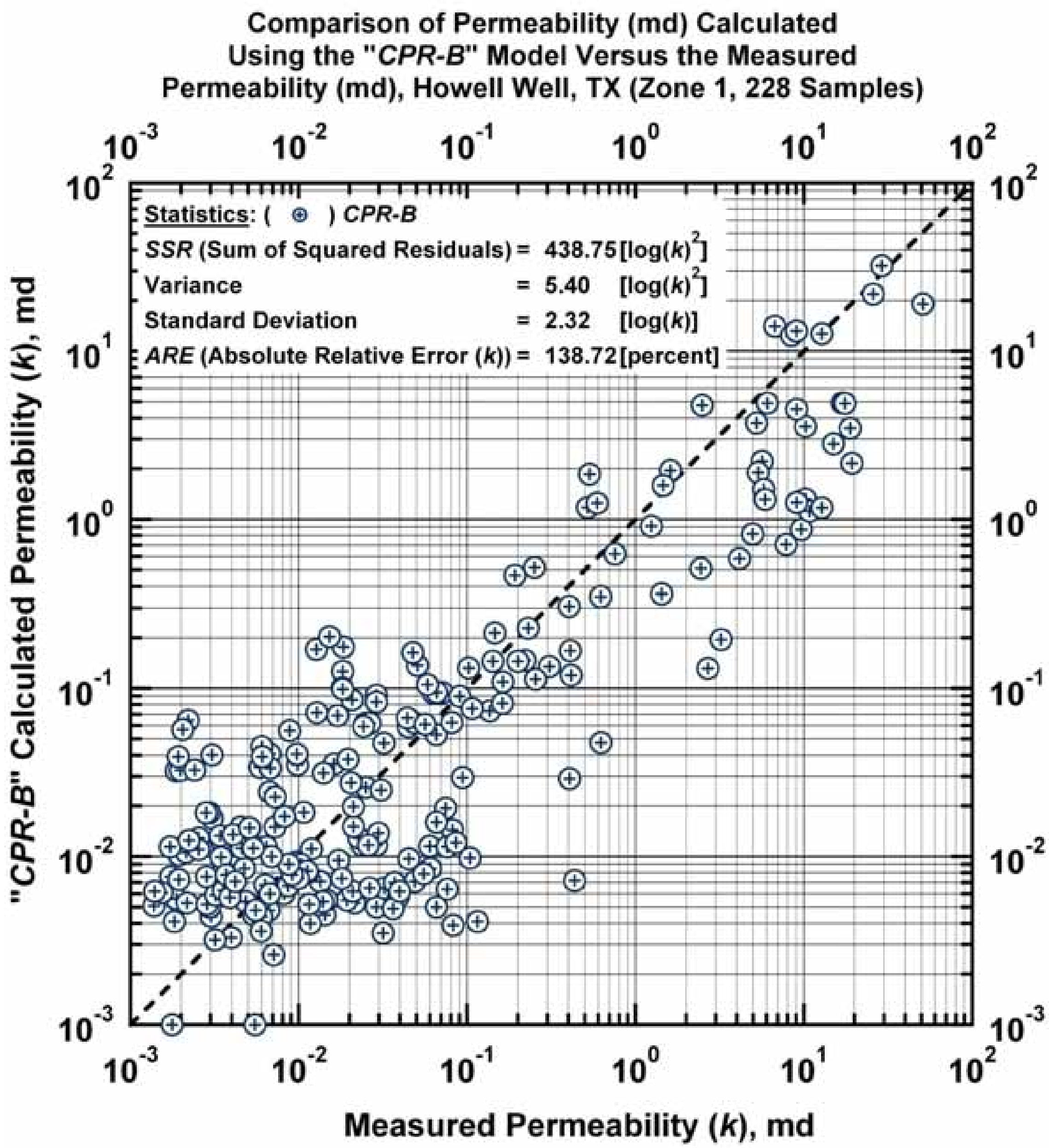

Figure B.17a — Model *CPR-B*: calculated versus measured permeability. [*Case*: Howell Well, E. TX (USA)]

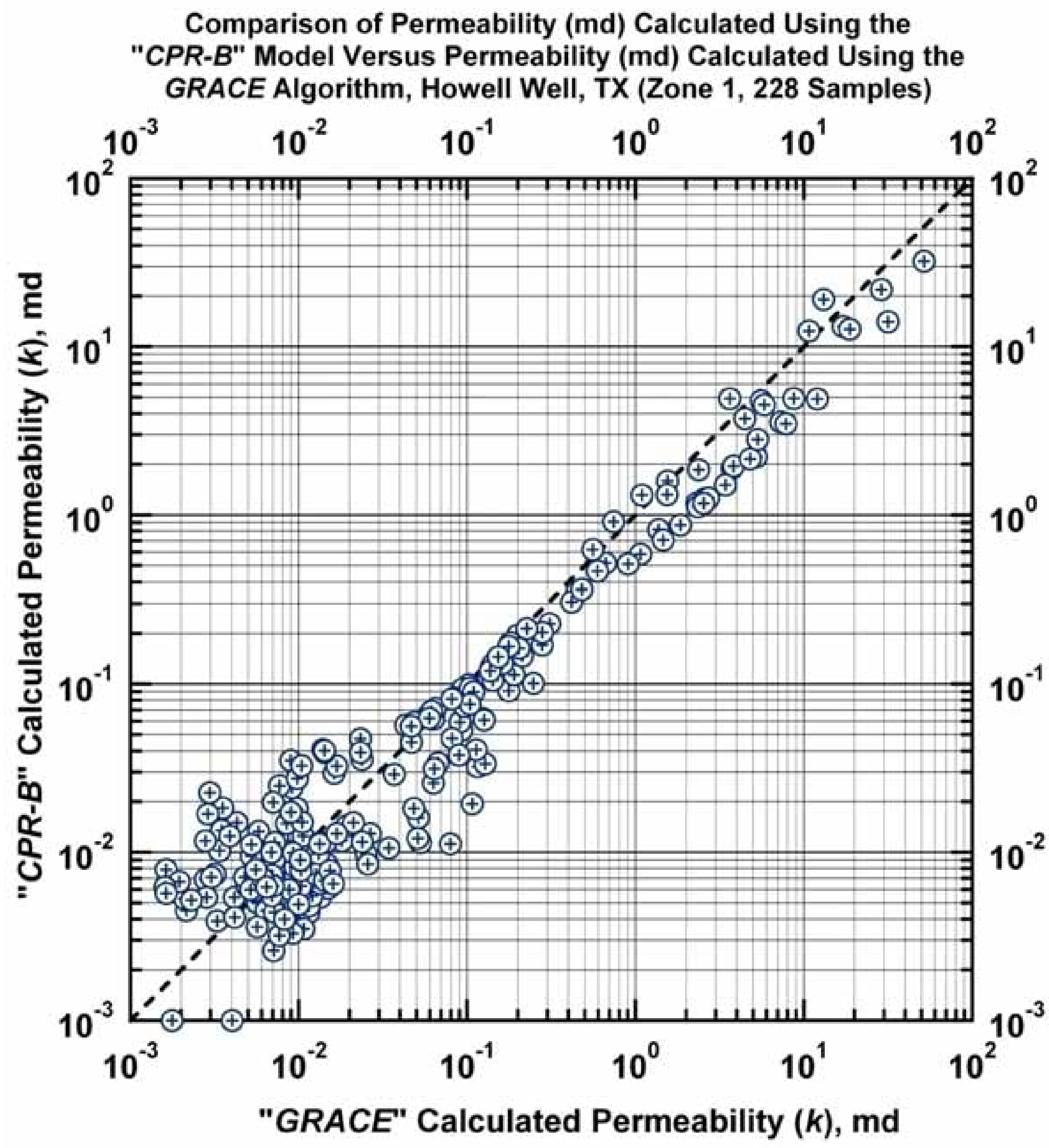

Figure B. 17b — Model *CPR-B*: Permeability calculated using Model *CPR-B* versus permeability calculated using the *GRACE* Algorithm. [*Case*: Howell Well, E. TX (USA)]

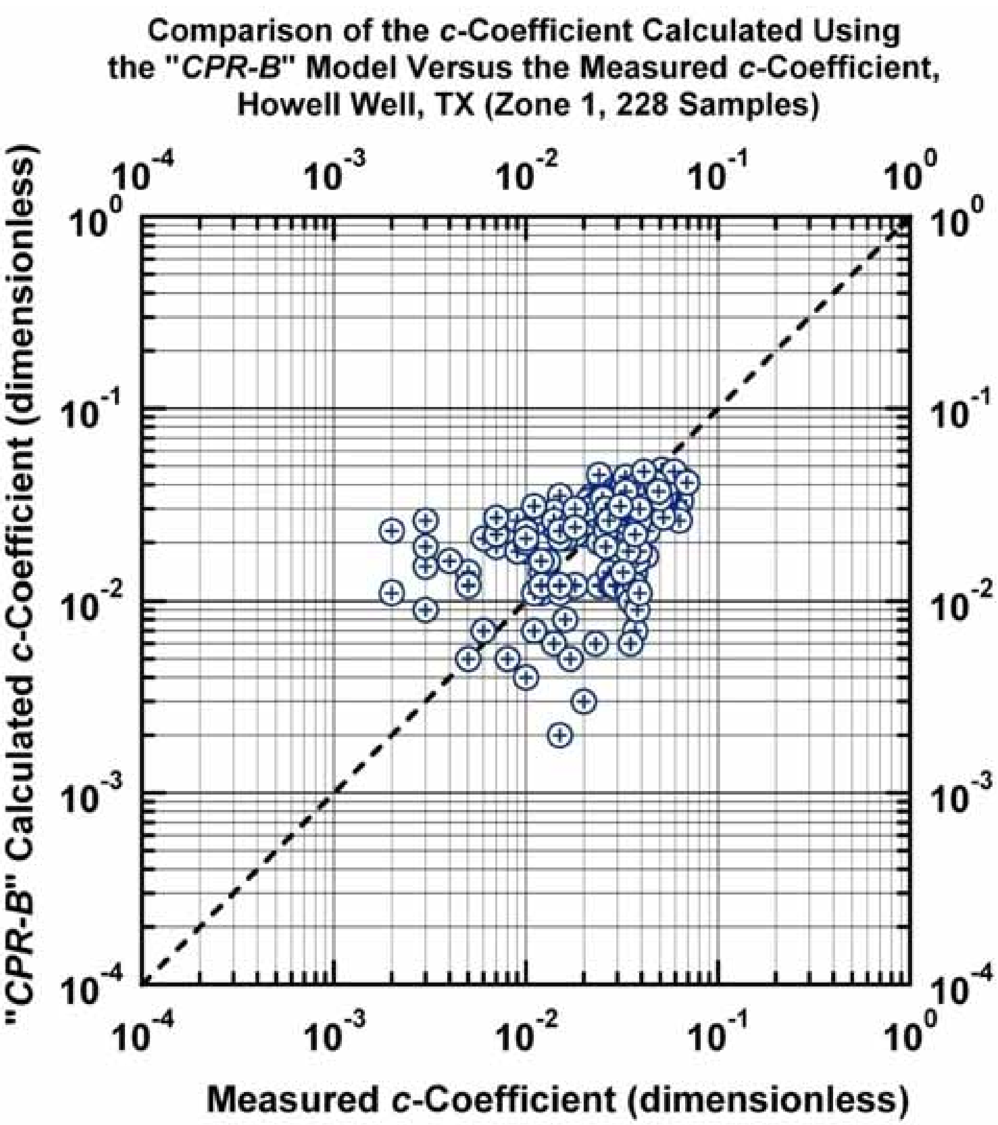

Figure B. 17c — Model *CPR-B*: Calculated *c*-function values versus measured *c*-function values. [*Case*: Howell Well, E. TX (USA)]

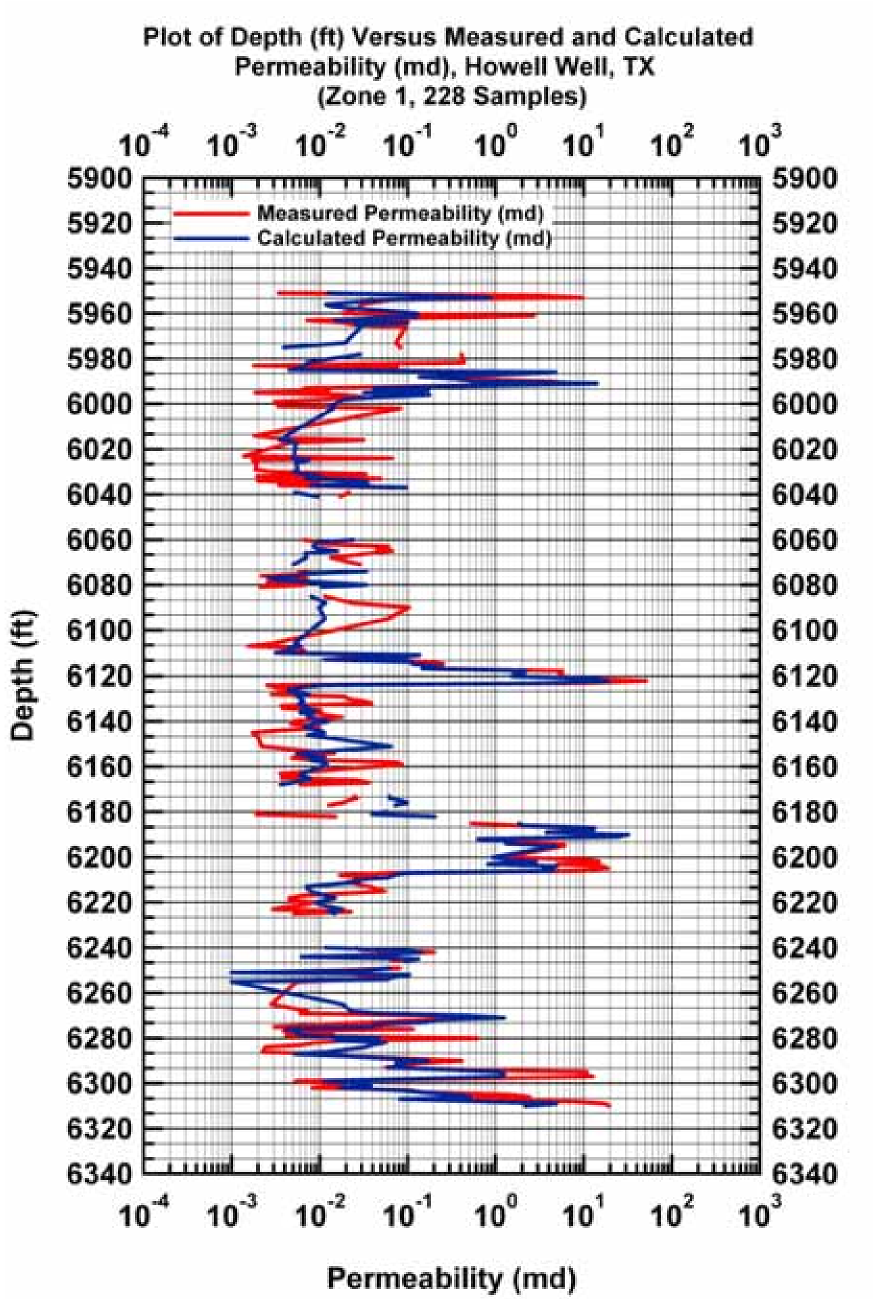

Figure B. 17d — Model *CPR-B*: Calculated and measured permeability values versus depth. [*Case*: Howell Well, E. TX (USA)]

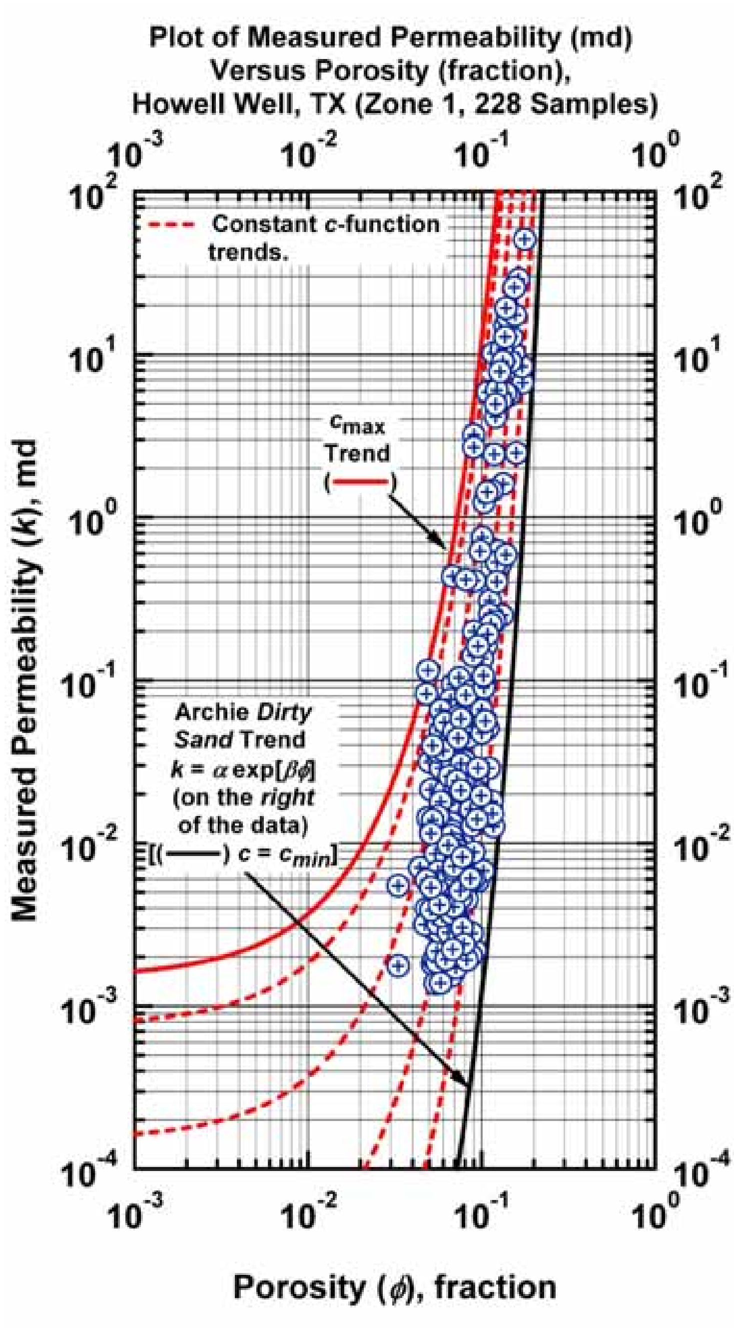

Figure B.18a — Model *CPR-C*: $k = c\exp[\beta\phi]$ $\quad c = c_{\max}\exp[-c_1\phi^{c_2} S_w^{c_3}]$ — "Clean Sand" Plot (log-log format) — Archie "Dirty Sand" trend is given by the curved trend at the far right of the data (exponential model). [*Case*: Howell Well, E. TX (USA)]

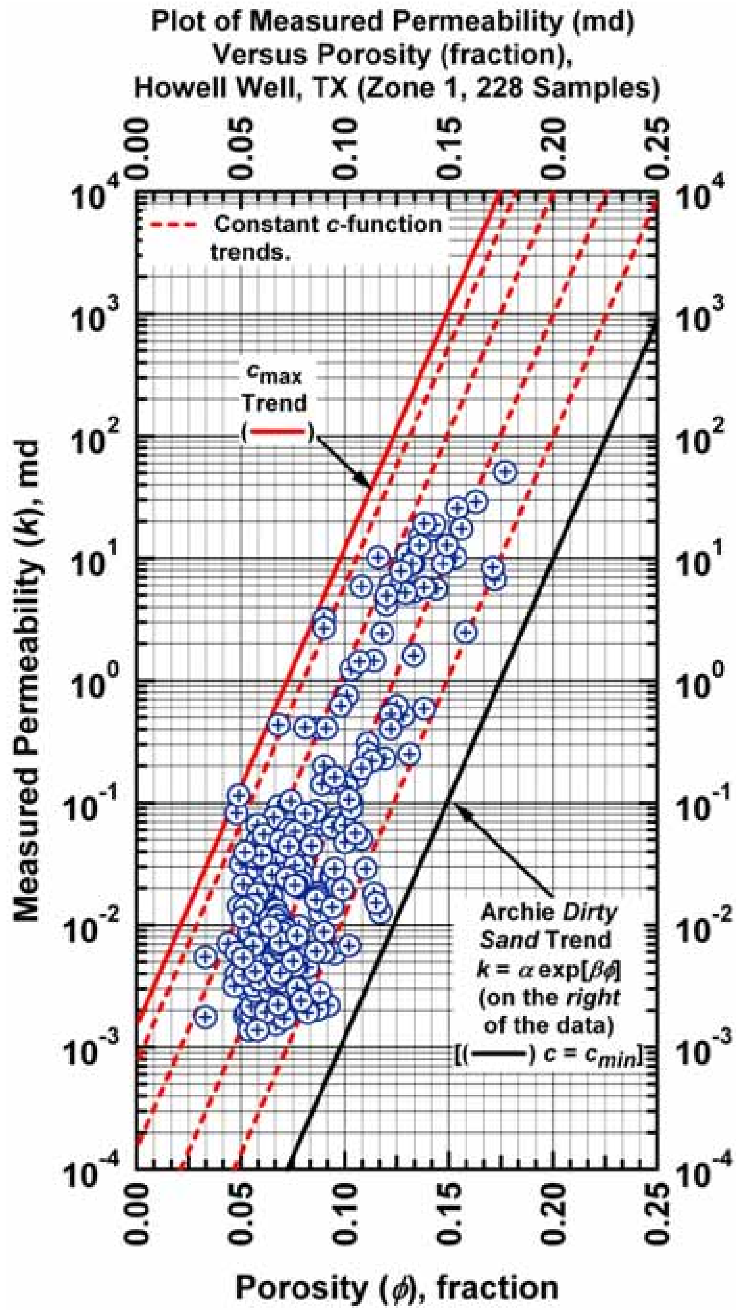

Figure B.18b — Model *CPR-C*: $k = c\exp[\beta\phi]$ $\quad c = c_{\max}\exp[-c_1\phi^{c_2} S_w^{c_3}]$ — "Dirty Sand" Plot (semilog format) — Archie "Dirty Sand" trend is given by the straight-line trend at the far right of the data (exponential model). [*Case*: Howell Well, E. TX (USA)]

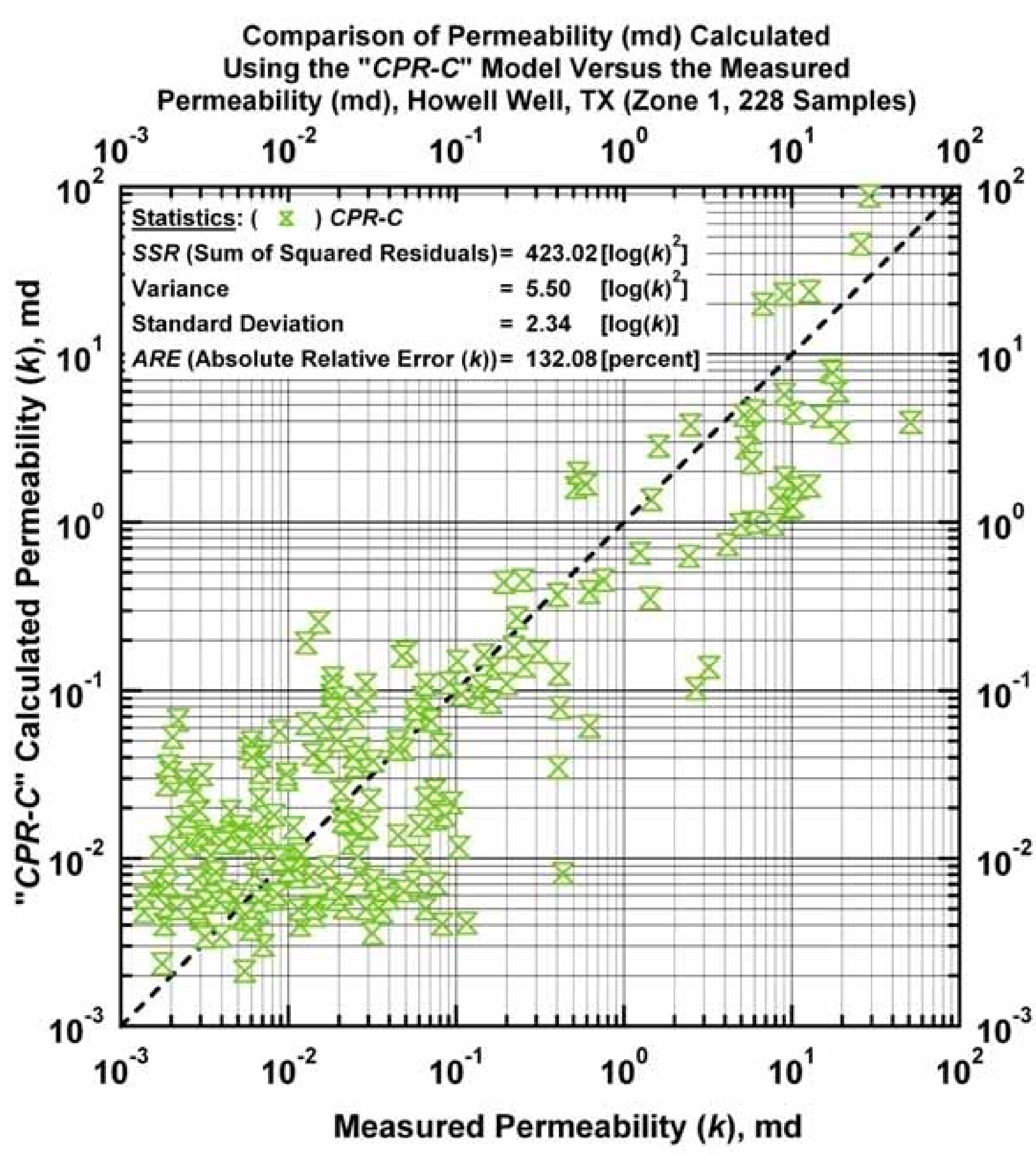

Figure B.19a — Model *CPR-C*: calculated versus measured permeability. [*Case*: Howell Well, E. TX (USA)]

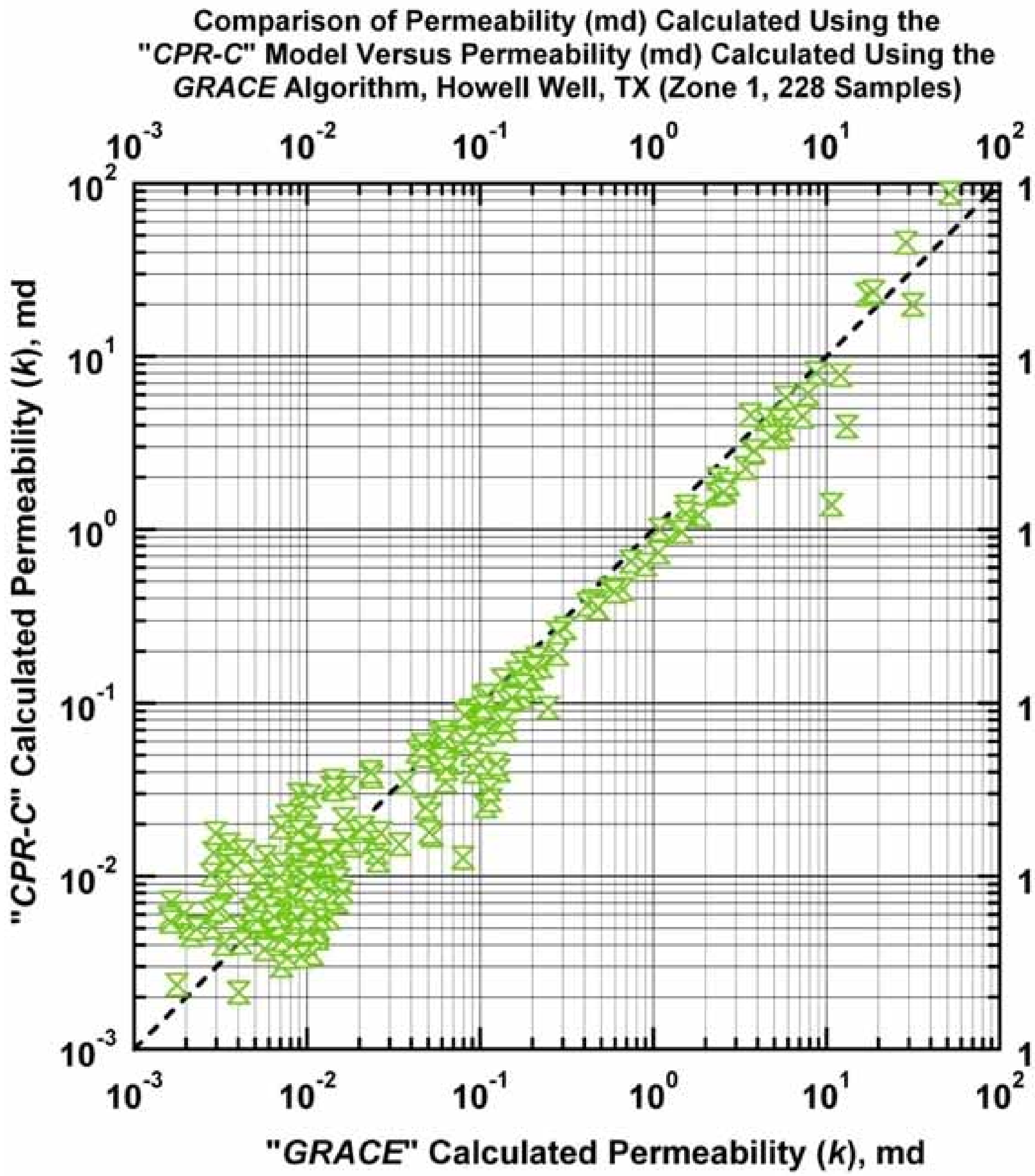

Figure B. 19b — Model *CPR-C*: Permeability calculated using Model *CPR-C* versus permeability calculated using the *GRACE* Algorithm. [*Case*: Howell Well, E. TX (USA)]

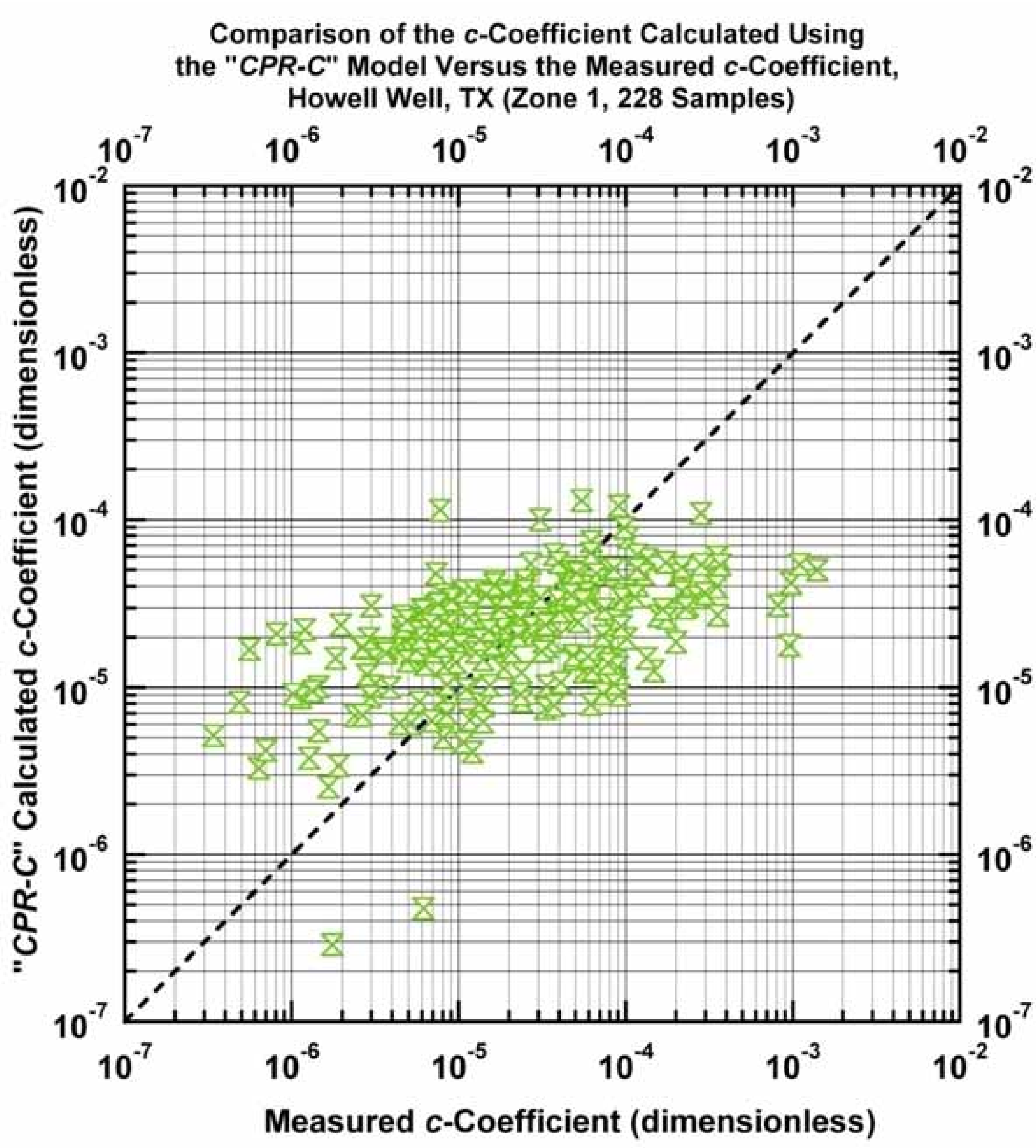

Figure B. 19c — Model *CPR-C*: Calculated *c*-function values versus measured *c*-function values. [*Case*: Howell Well, E. TX (USA)]

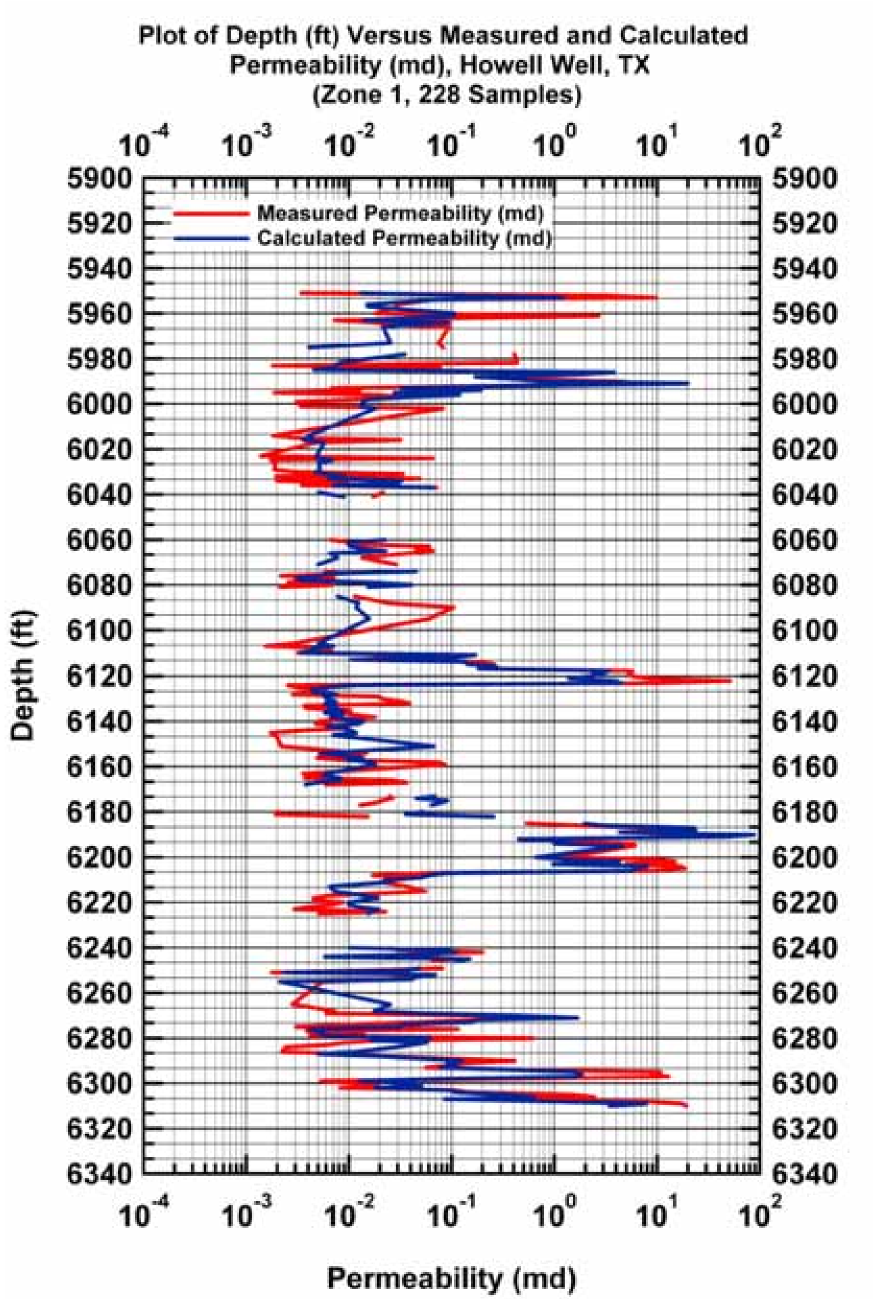

Figure B. 19d — Model *CPR-C*: Calculated and measured permeability values versus depth. [*Case*: Howell Well, E. TX (USA)]

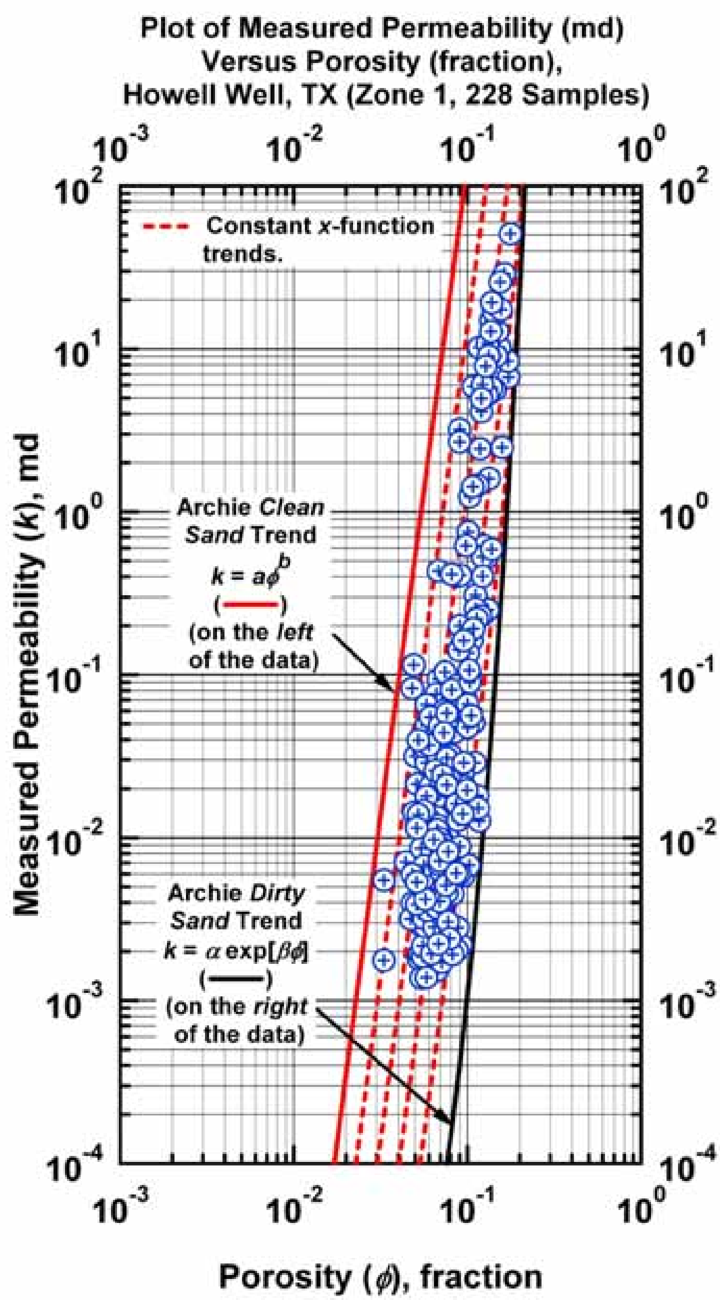

Figure B.20a — Model *CPR-D*: $k = xa\phi^b + (1-x)\alpha \exp[\beta\phi] \quad [0 \le x \le 1]$ — *Weighted Power Law-Exponential Model* used to correlate permeability (k) and porosity (ϕ). "Clean Sand" Plot — Archie "Clean Sand" trend is given by the straight-line trend at the far left of the data (power law model). [*Case*: Howell Well, E. TX (USA)]

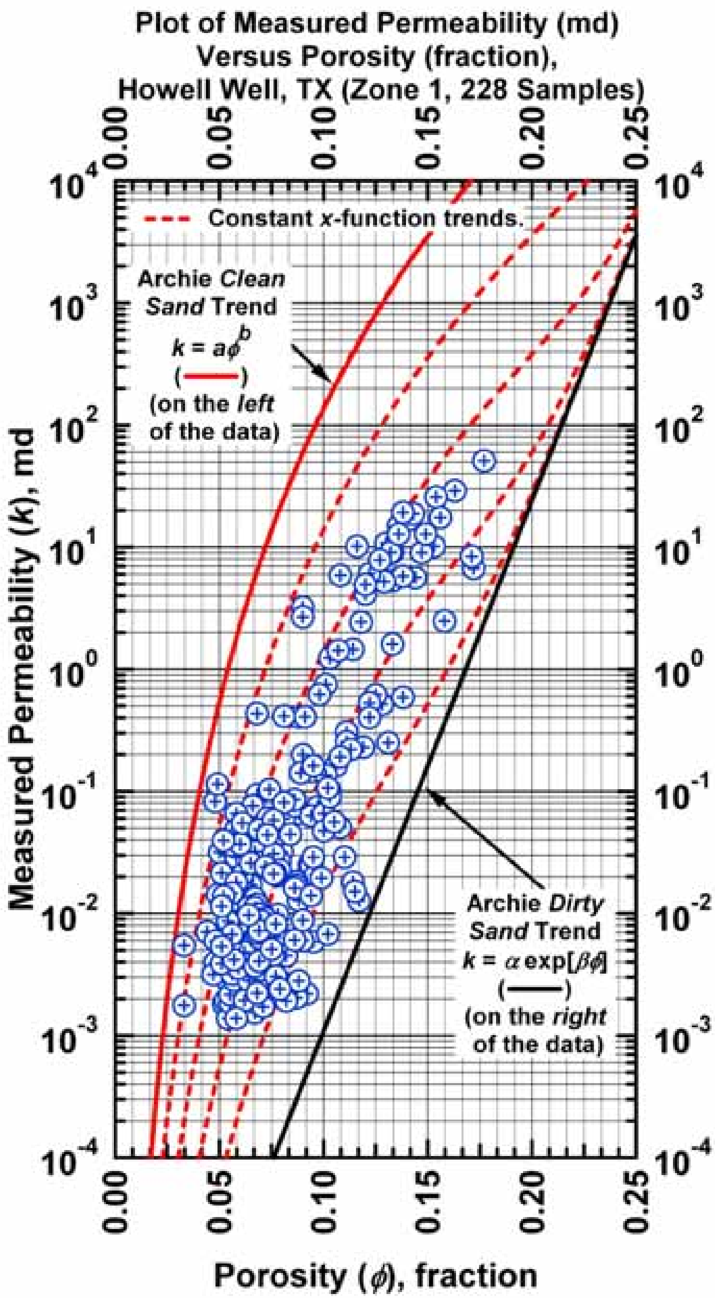

Figure B.20b — Model *CPR-D*: $k = xa\phi^{b} + (1-x)\alpha \exp[\beta\phi]$ $[0 \le x \le 1]$ — *Weighted Power Law-Exponential Model* used to correlate permeability (k) and porosity (ϕ). "Dirty Sand" Plot — Archie "Dirty Sand" trend is given by the straight-line trend at the far right of the data (exponential model). [*Case*: Howell Well, E. TX (USA)]

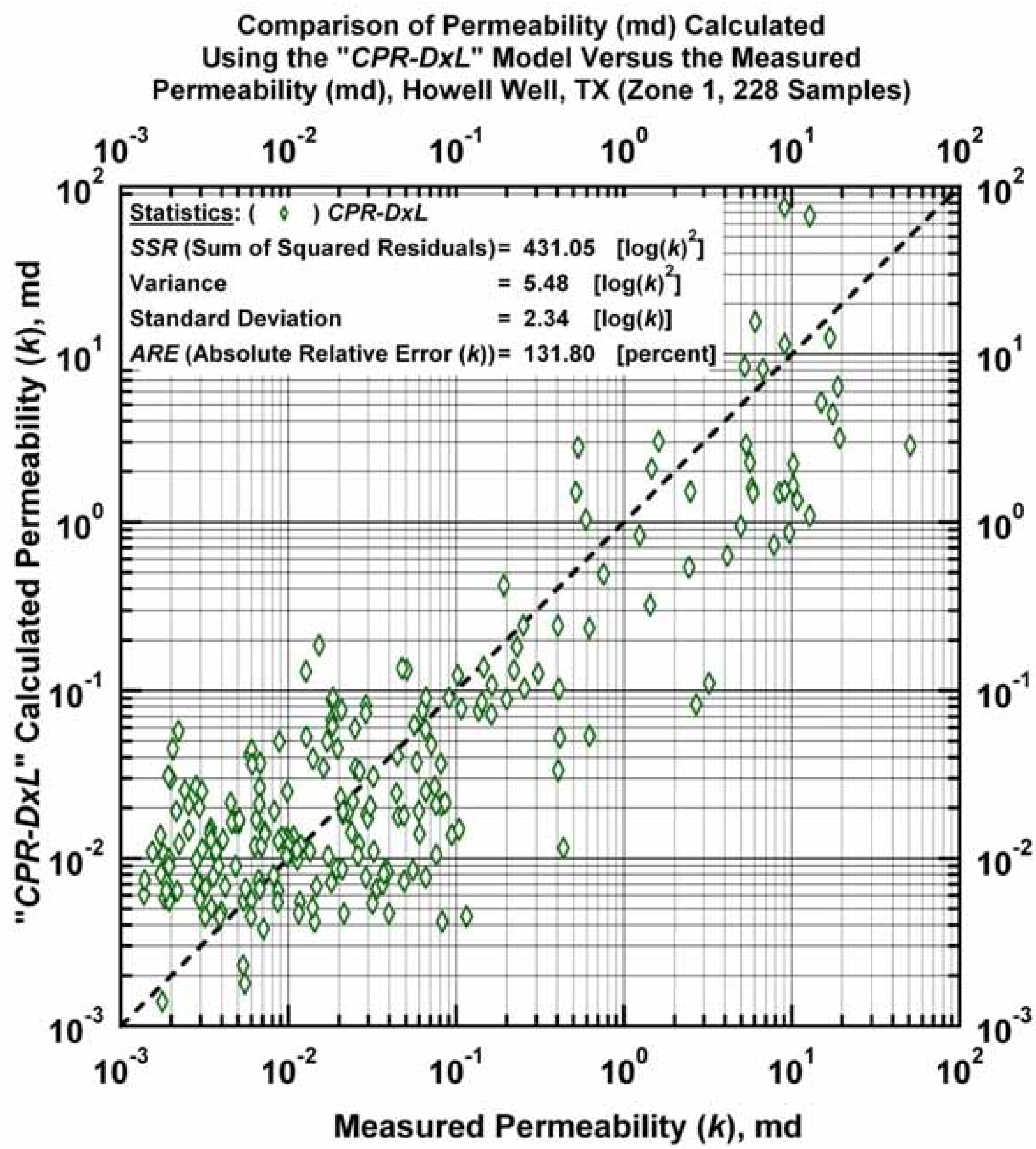

Figure B.21a — Model *CPR-DxL*: Calculated versus measured permeability. [*Case*: Howell Well, E. TX (USA)]

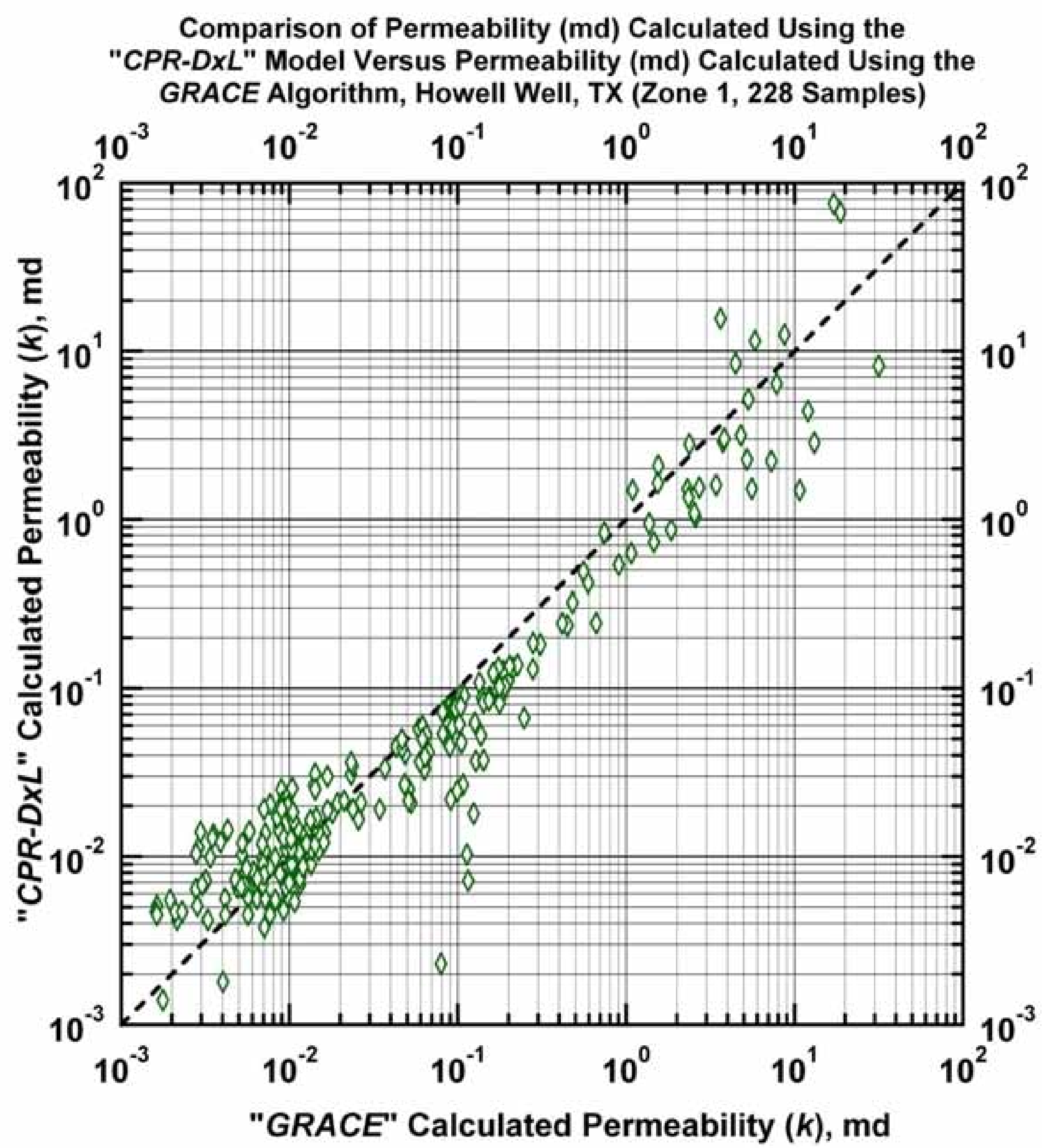

Figure B. 21b — Model *CPR-DxL*: Permeability calculated using Model *CPR-C* versus permeability calculated using the *GRACE* Algorithm. [*Case*: Howell Well, E. TX (USA)]

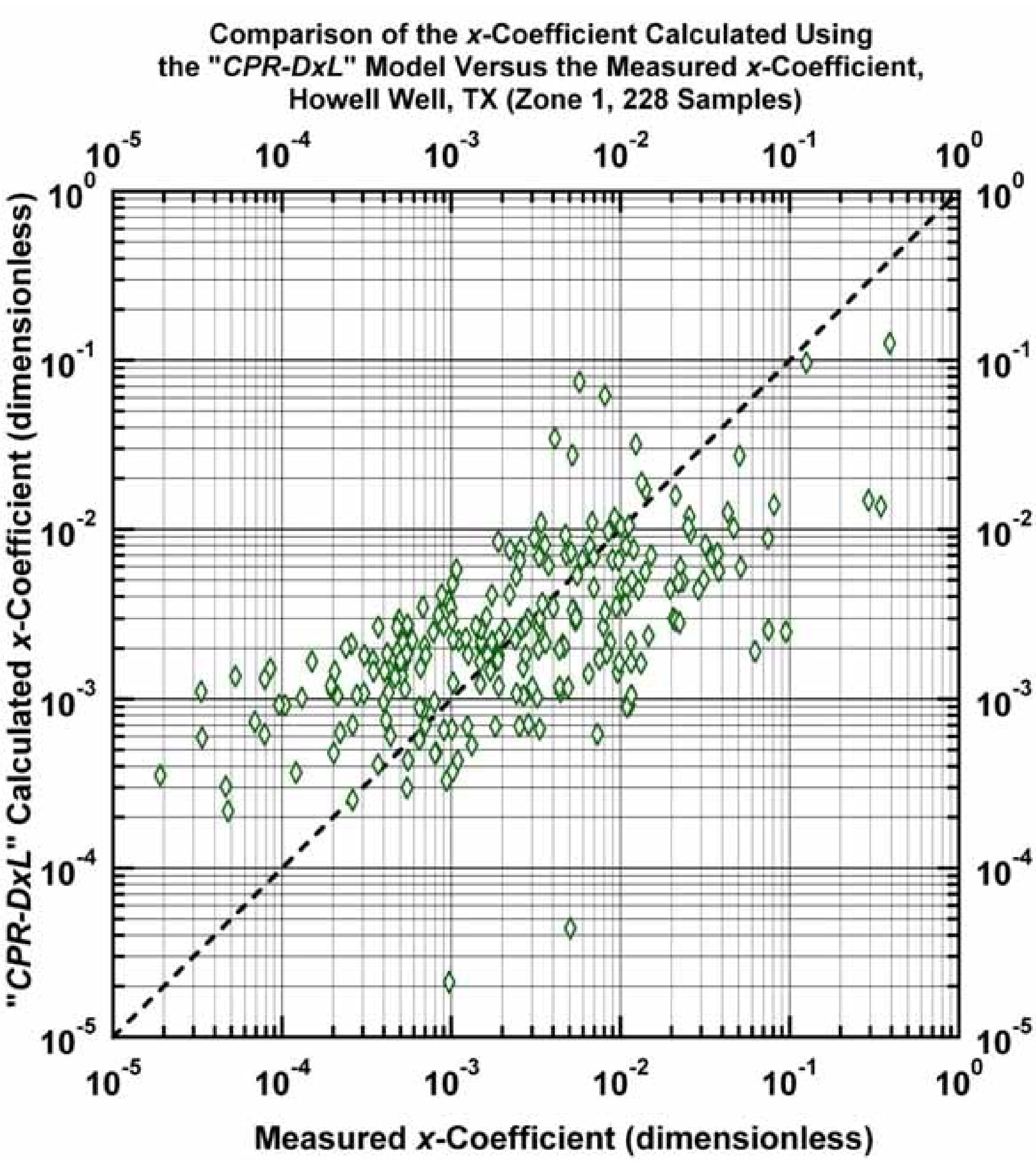

Figure B. 21c — Model *CPR-DxL*: Calculated *x*-function weight values versus measured *x*-function weight values. [*Case*: Howell Well, E. TX (USA)]

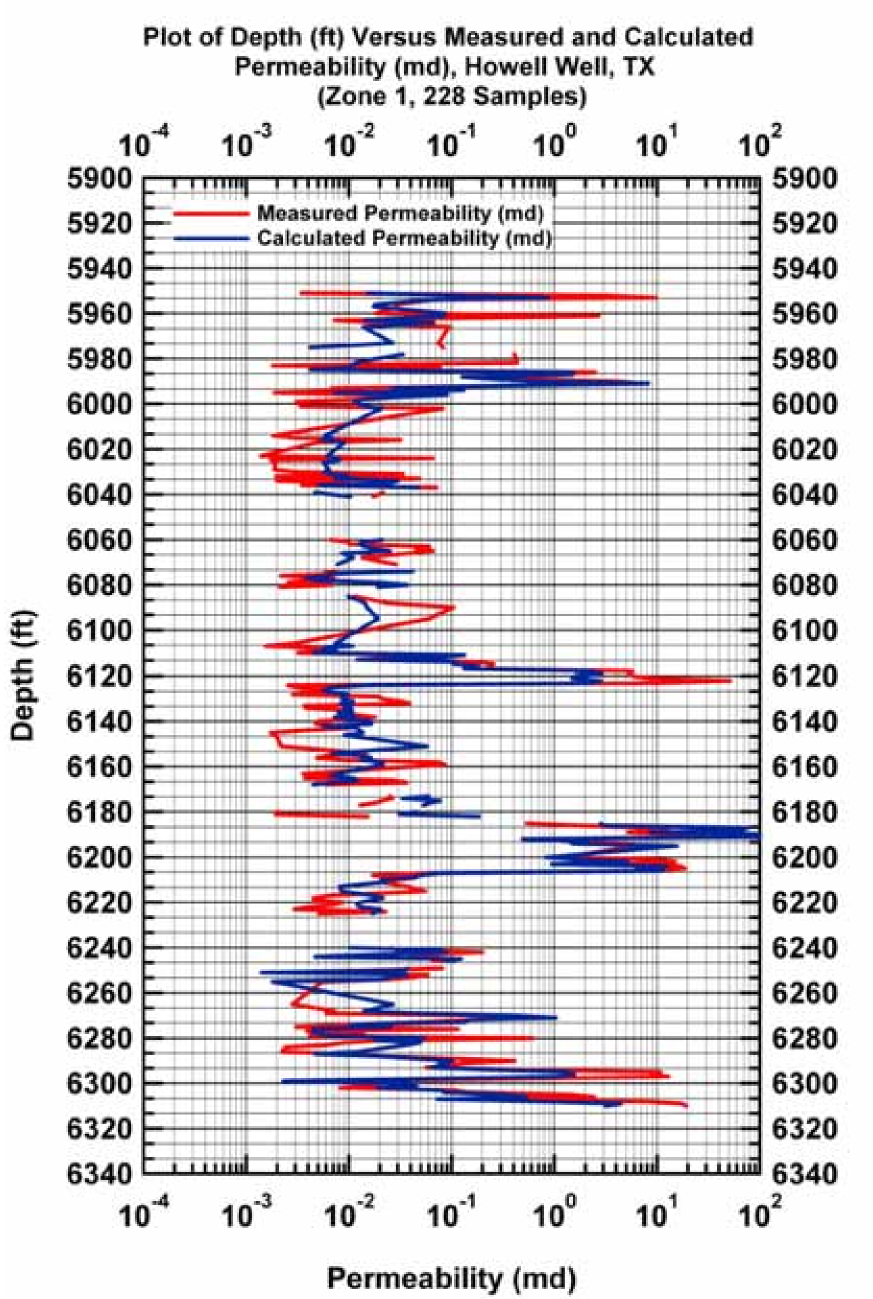

Figure B. 21d — Model *CPR-DxL*: Calculated and measured permeability values versus depth. [*Case*: Howell Well, E. TX (USA)]

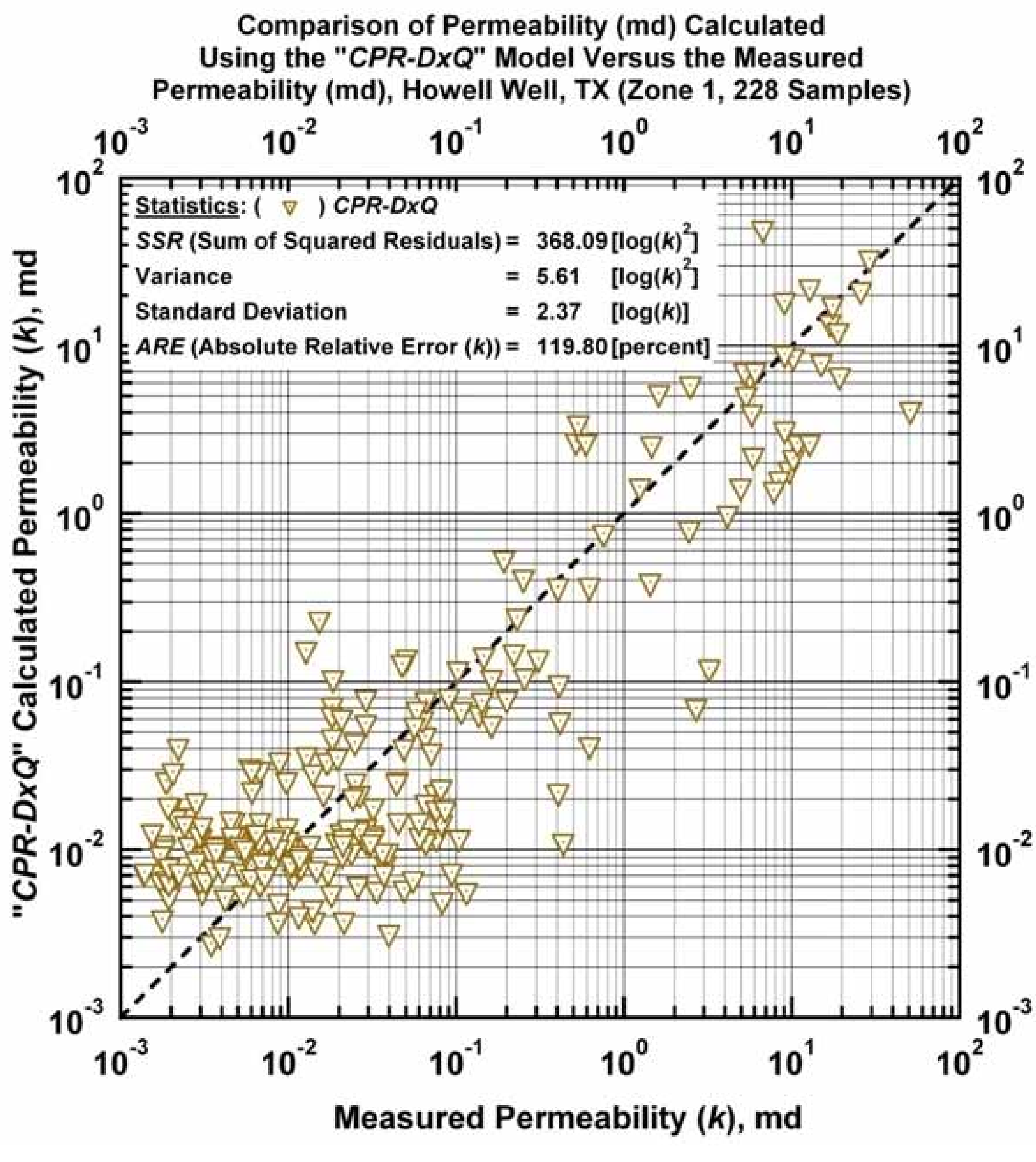

Figure B.22a — Model *CPR-DxQ*: Calculated versus measured permeability. [*Case*: Howell Well, E. TX (USA)]

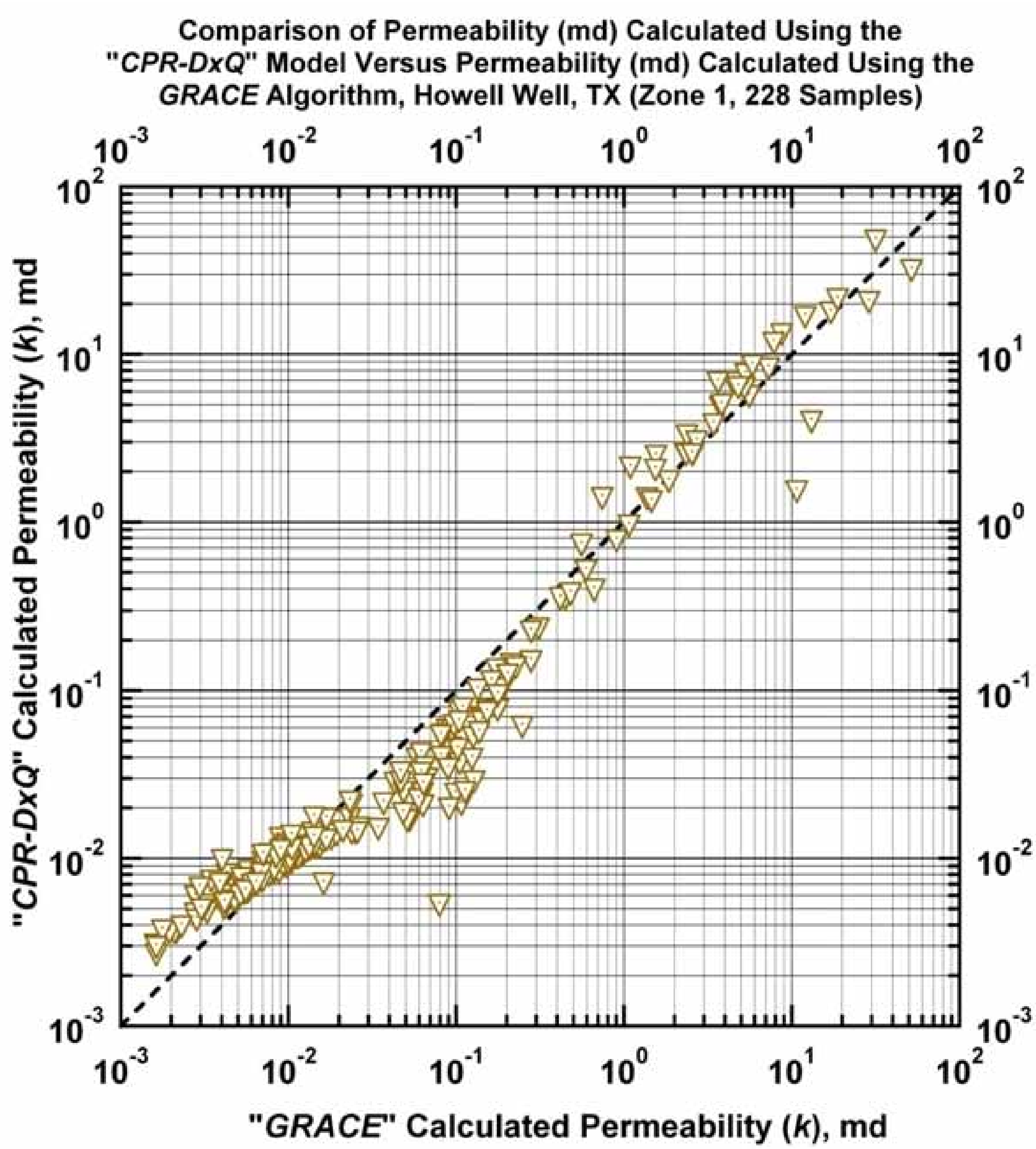

Figure B.22b — Model *CPR-DxQ*: Permeability calculated using Model *CPR-C* versus permeability calculated using the *GRACE* Algorithm. [*Case*: Howell Well, E. TX (USA)]

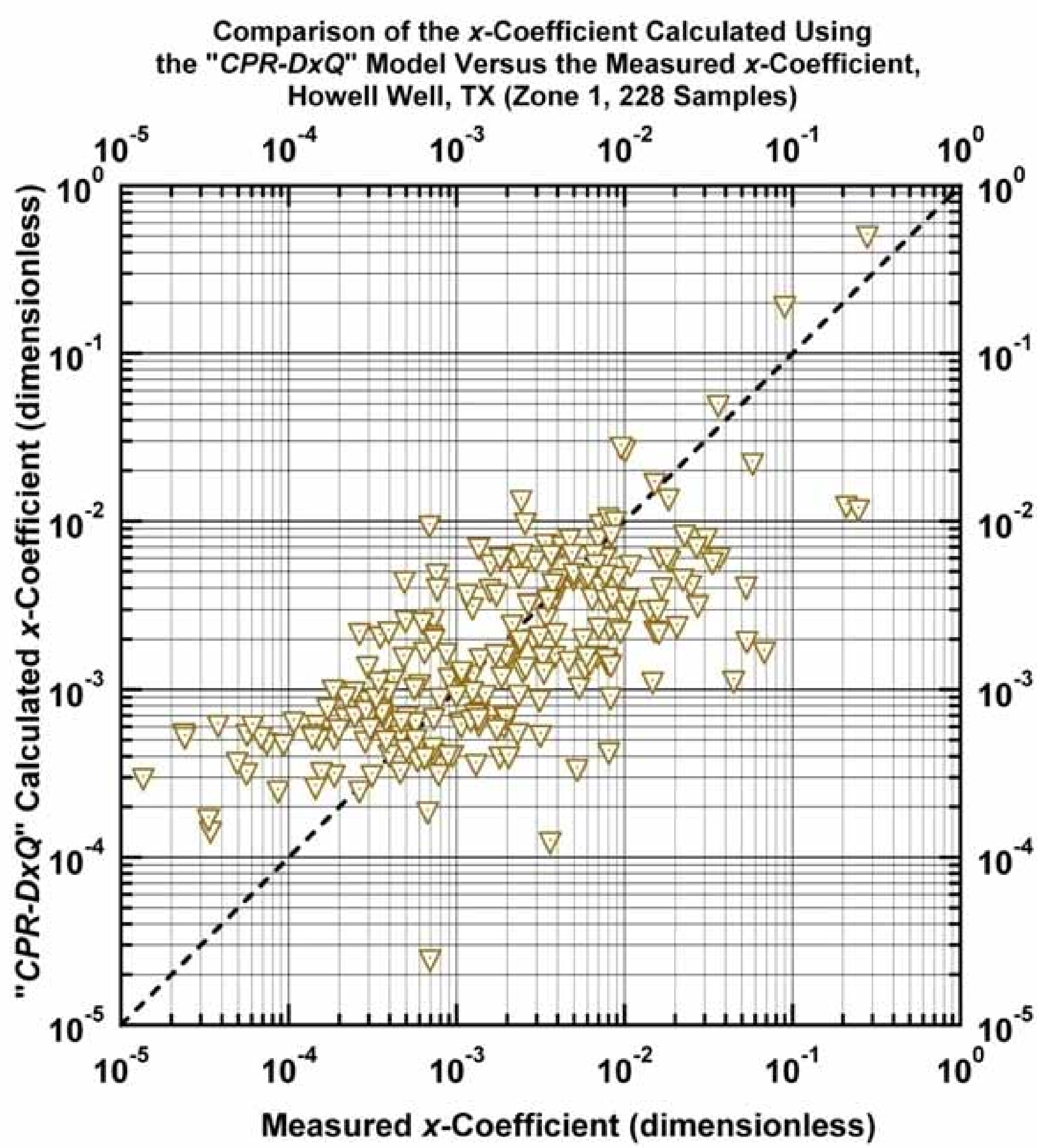

Figure B.22c — Model *CPR-DxQ*: Calculated *x*-function weight values versus measured *x*-function weight values. [*Case*: Howell Well, E. TX (USA)]

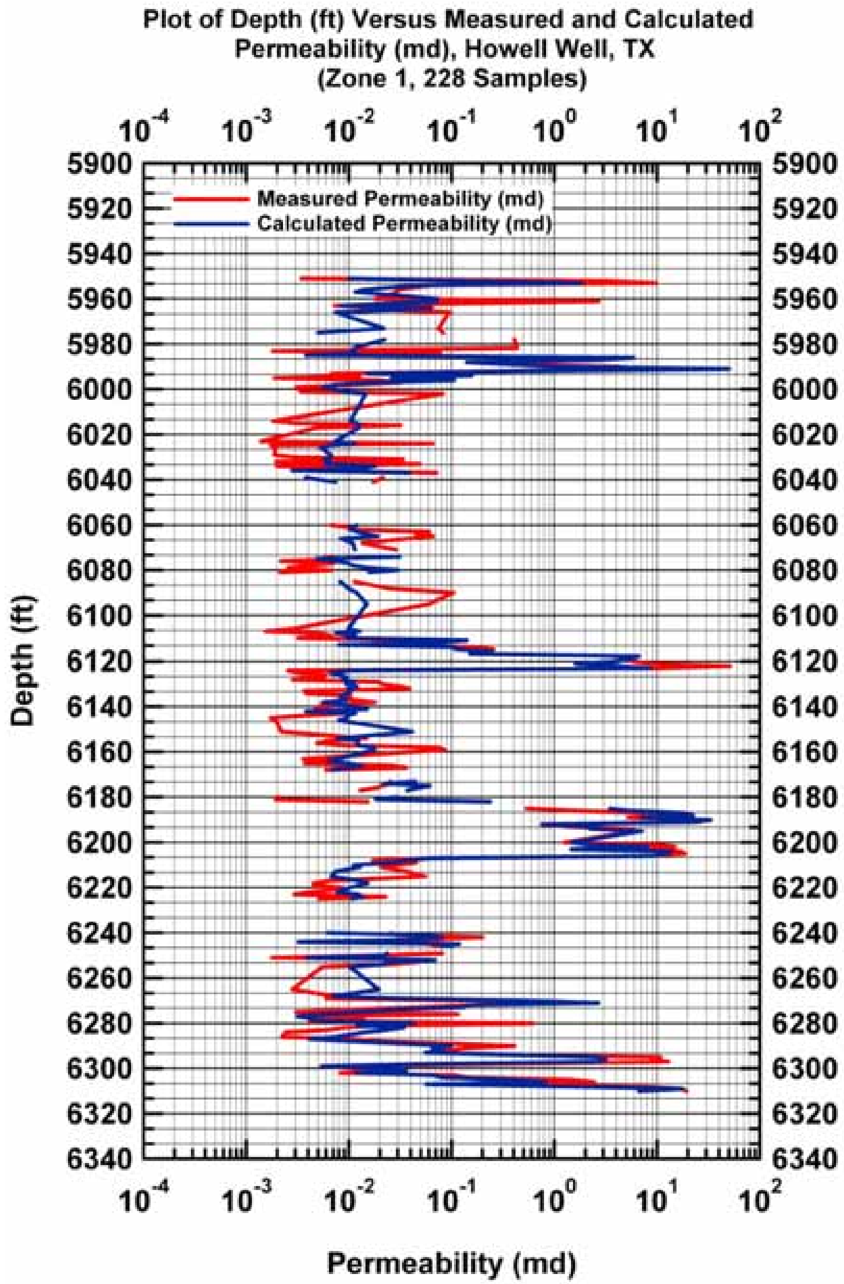

Figure B.22d — Model *CPR-DxQ*: Calculated and measured permeability values versus depth. [*Case*: Howell Well, E. TX (USA)]

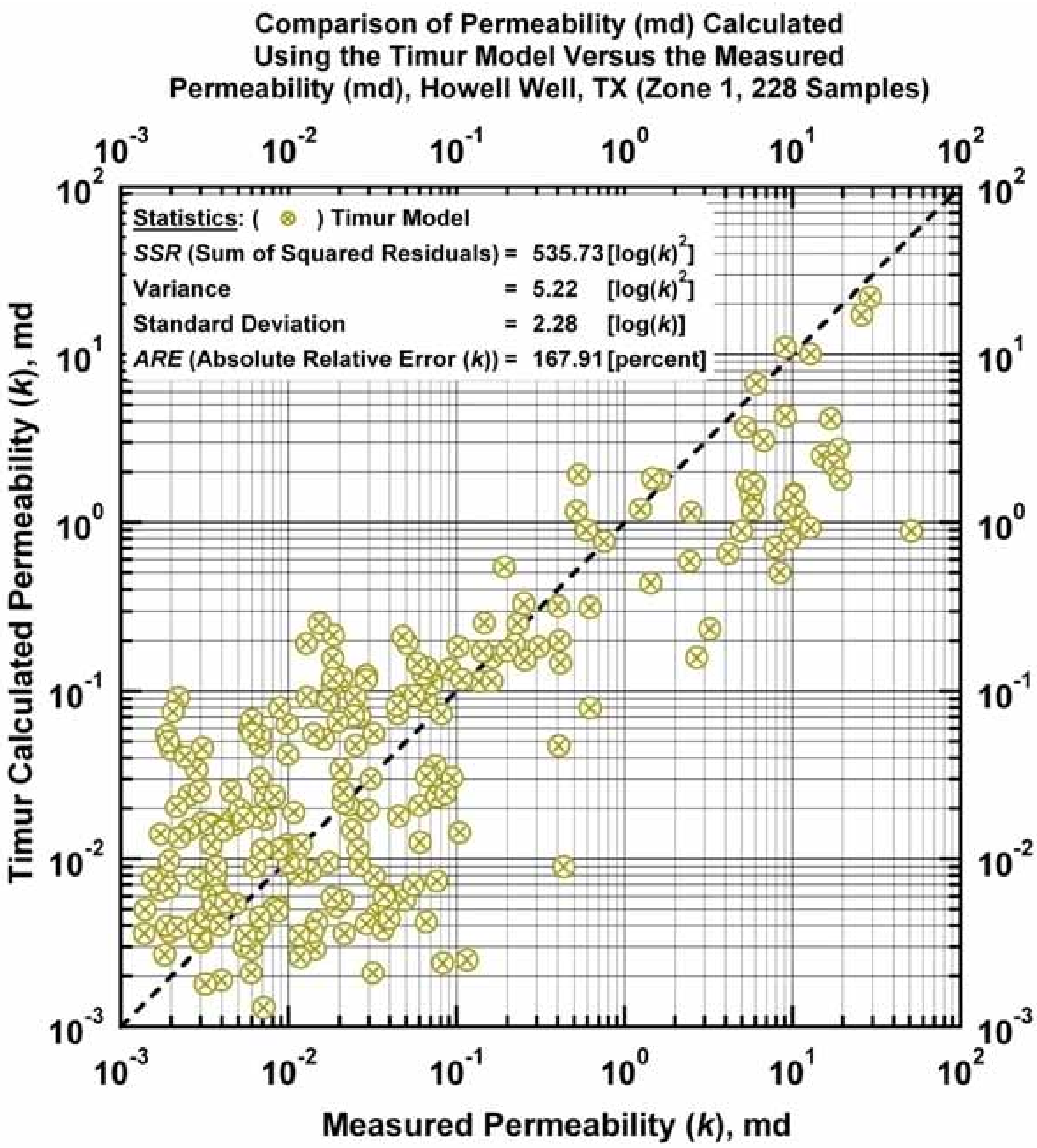

Figure B.23a — "Timur Model:" Calculated versus measured permeability. [*Case*: Howell Well, E. TX (USA)]

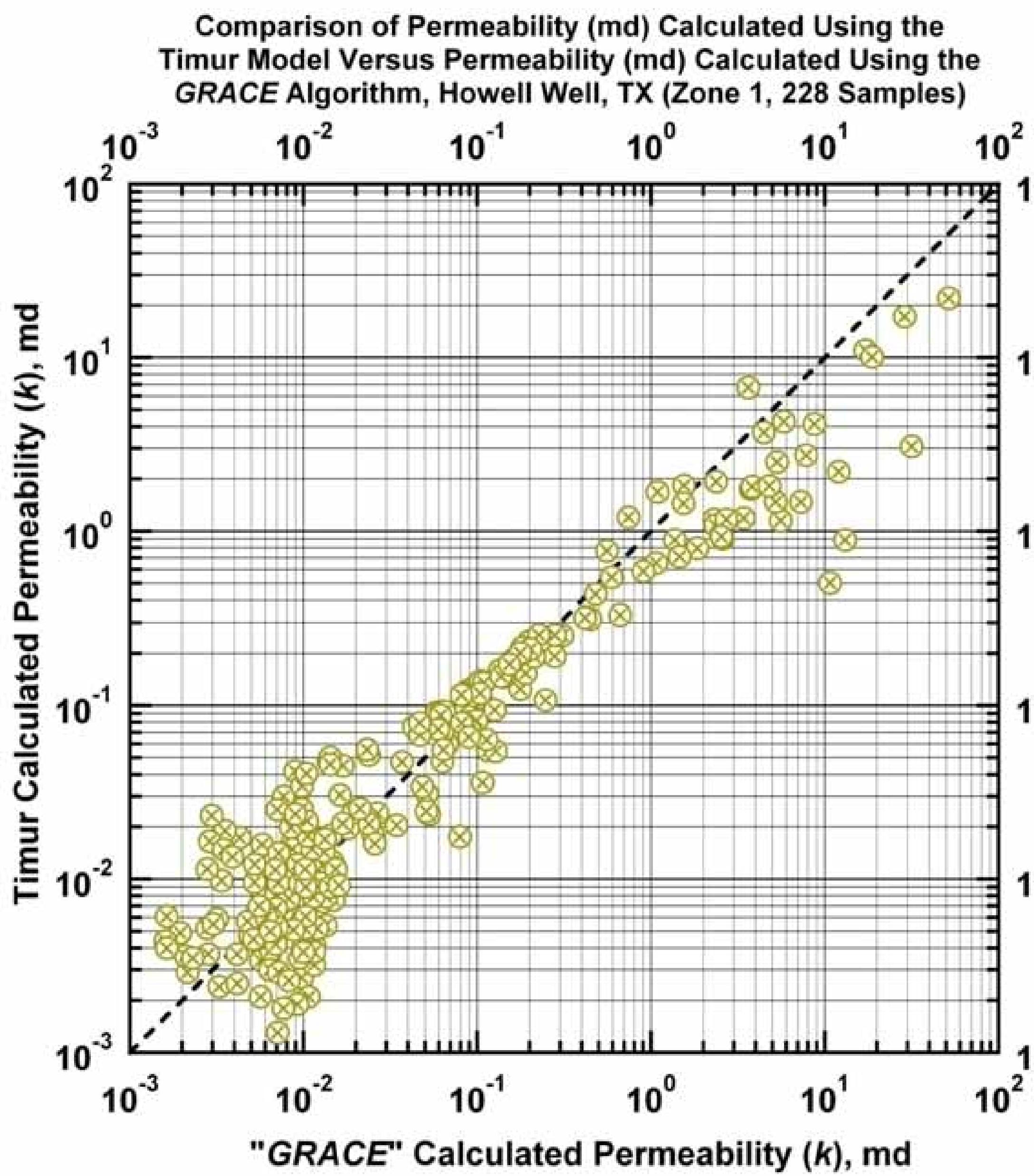

Figure B.23b — "Timur Model:" Permeability calculated using the "Timur Model" versus permeability calculated using the *GRACE* Algorithm. [*Case*: Howell Well, E. TX (USA)]

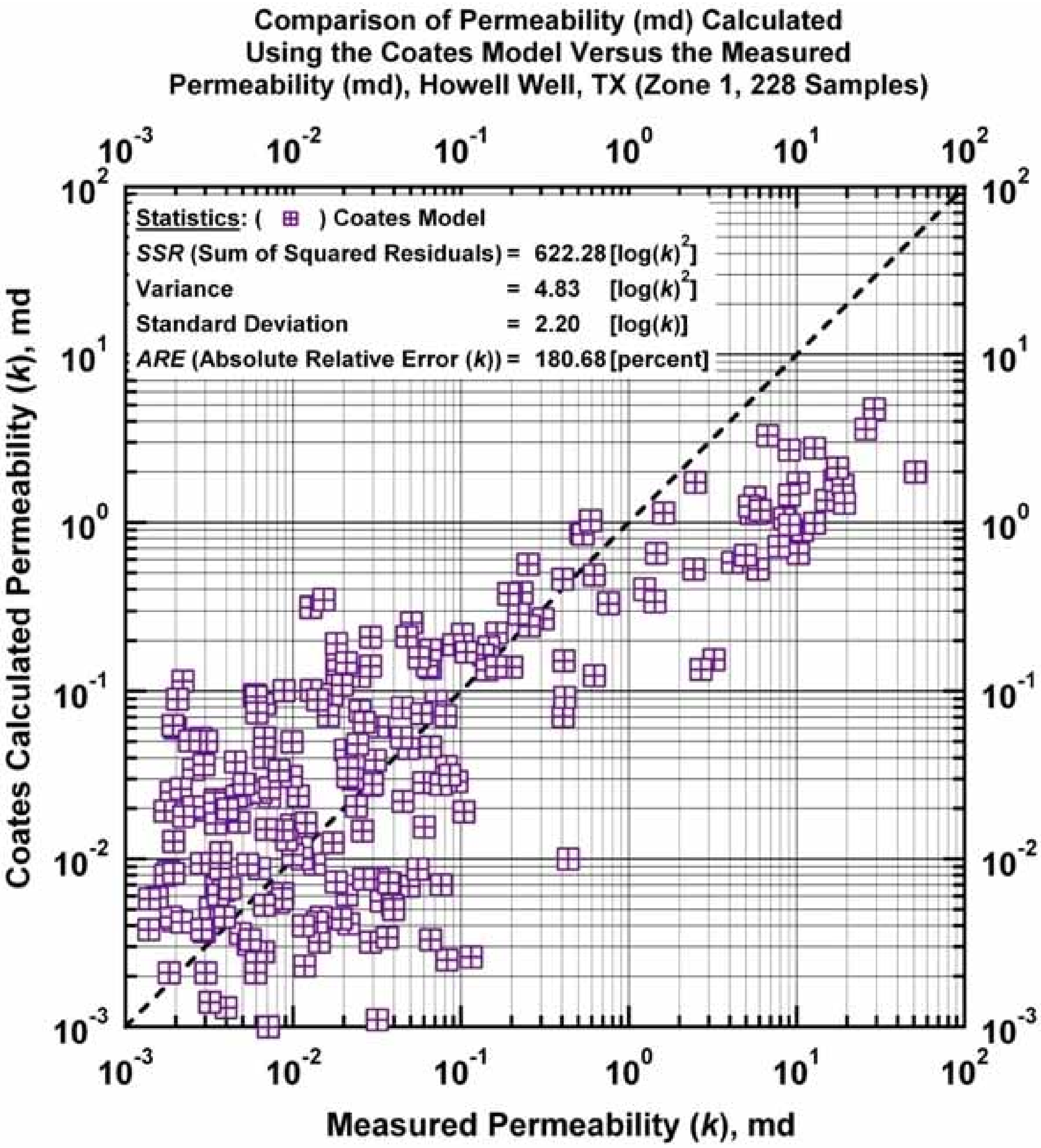

Figure B.24a — "Coates Model:" Calculated versus measured permeability. [*Case*: Howell Well, E. TX (USA)]

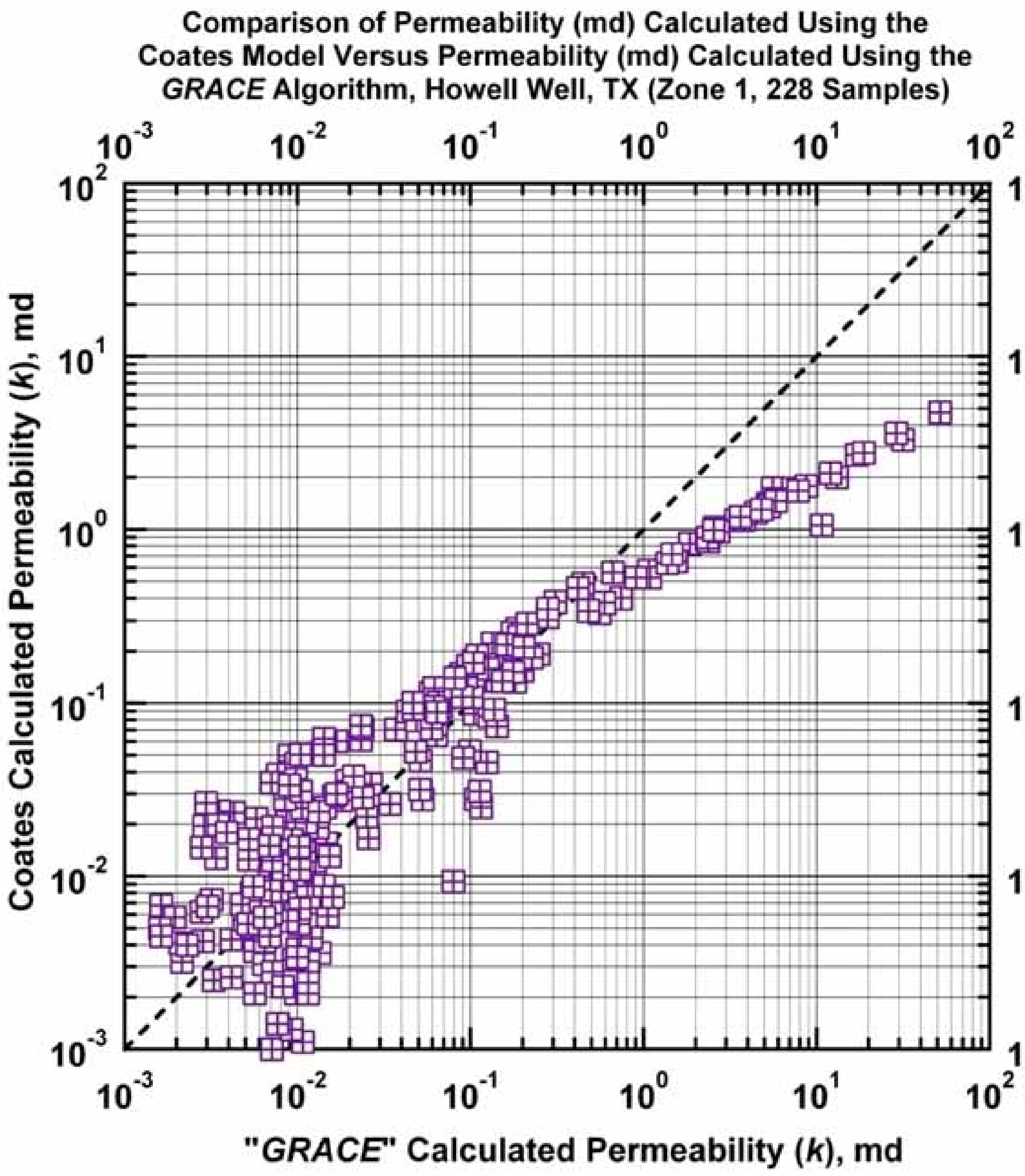

Figure B.24b — "Coates Model:" Permeability calculated using the "Coates Model" versus permeability calculated using the *GRACE* Algorithm. [*Case*: Howell Well, E. TX (USA)]

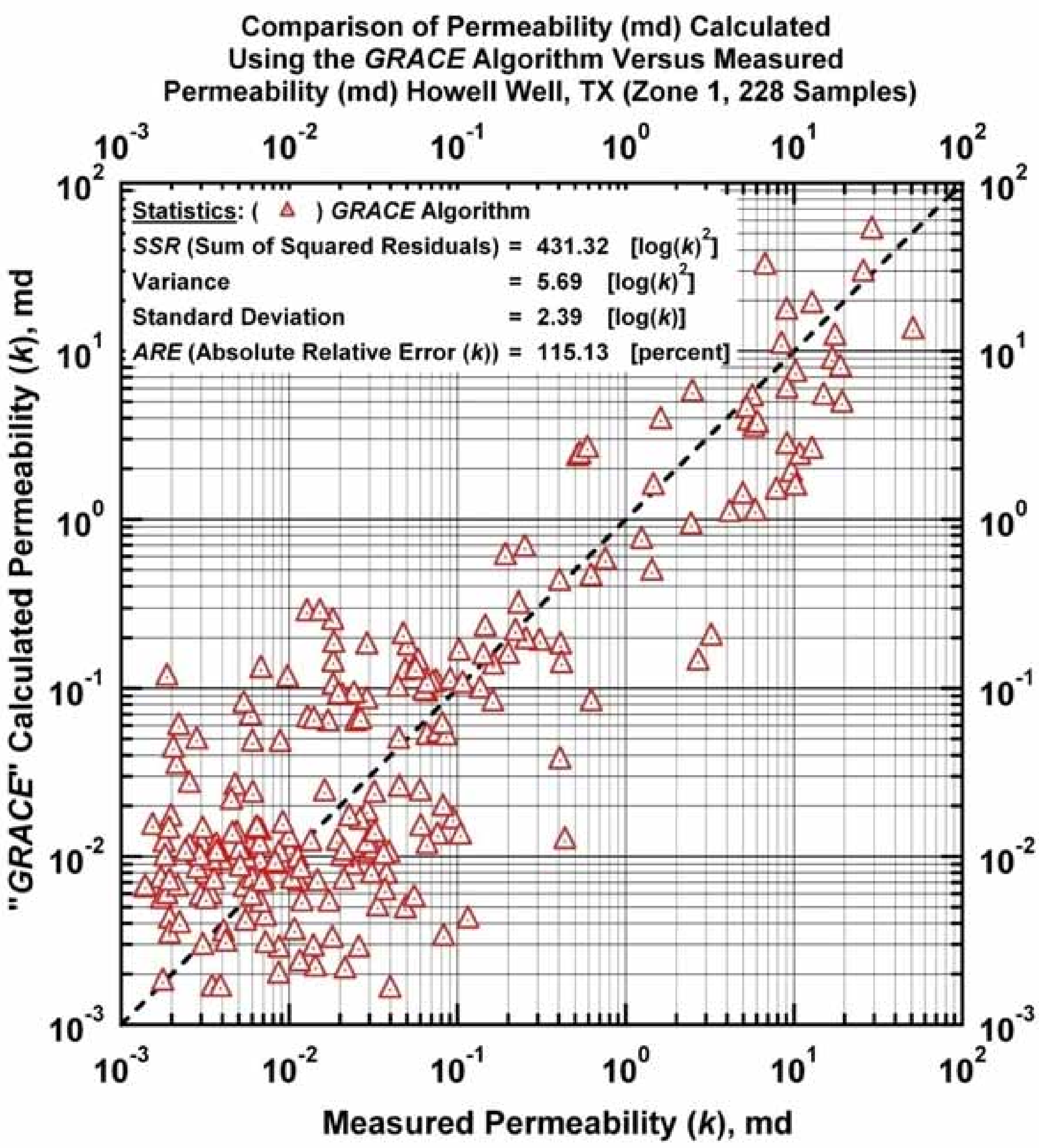

Figure B.25 — *GRACE* Model: Calculated versus measured permeability. [*Case*: Howell Well, E. TX (USA)]

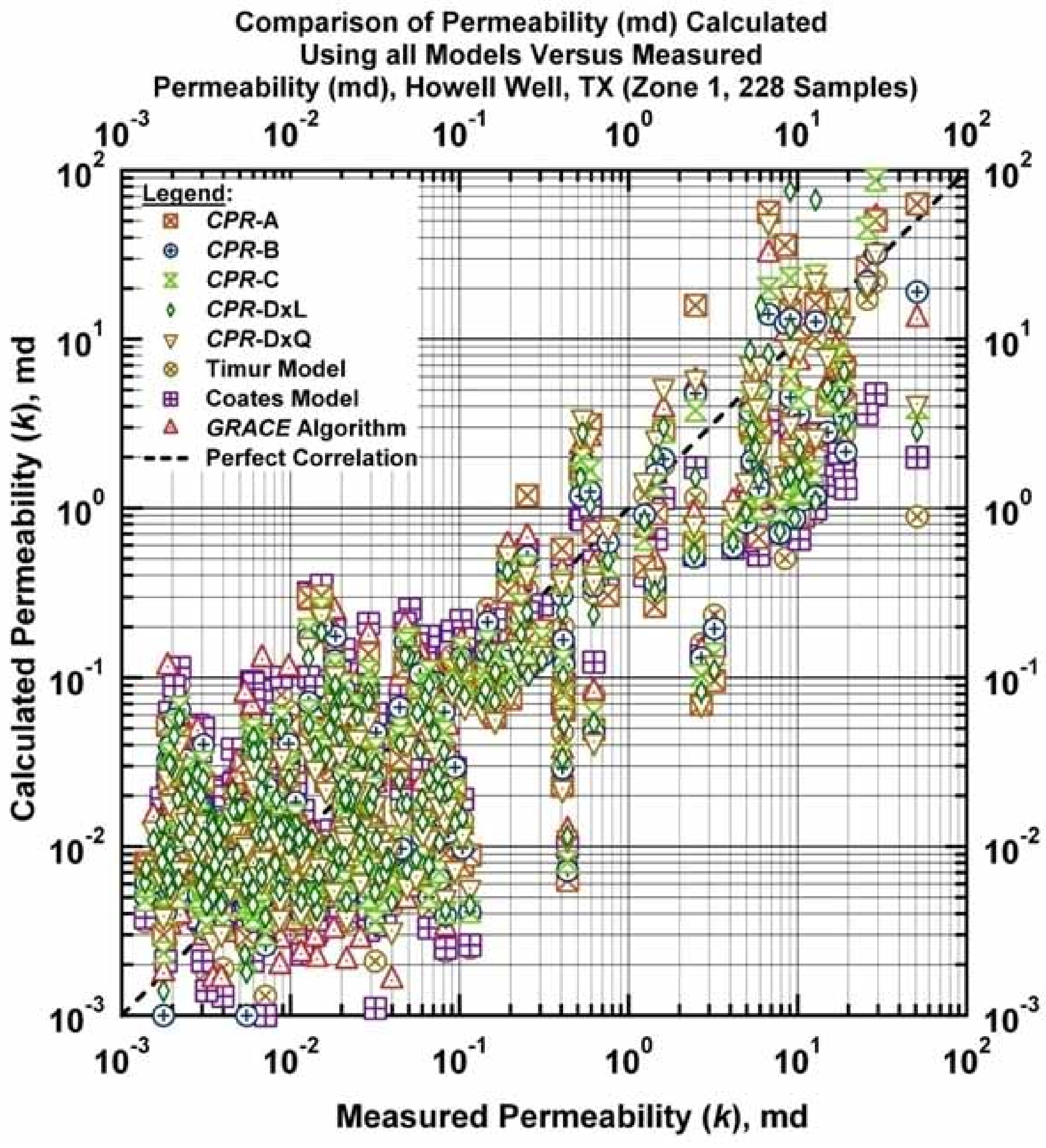

Figure B.26 — All Models: Calculated versus measured permeability. [*Case*: Howell Well, E. TX (USA)]

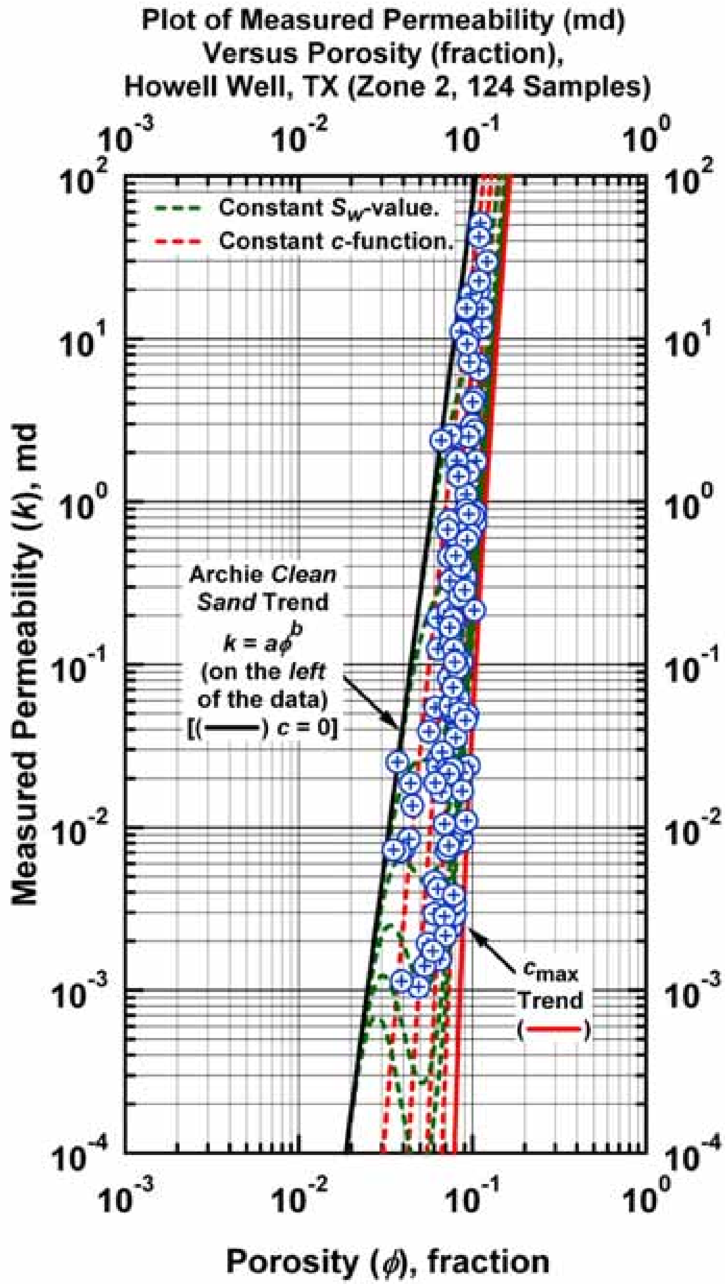

Figure B.27a — Model *CPR-A*: $k = a(\phi - c)^b \quad c = c_{\max}\exp[-c_1\phi^{c_2} S_w^{c_3}]$ — "Clean Sand" Plot (log-log format) — Archie "Clean Sand" trend is given by the straight-line trend at the far left of the data (power law model). [*Case*: Howell Well, E. TX (USA)]

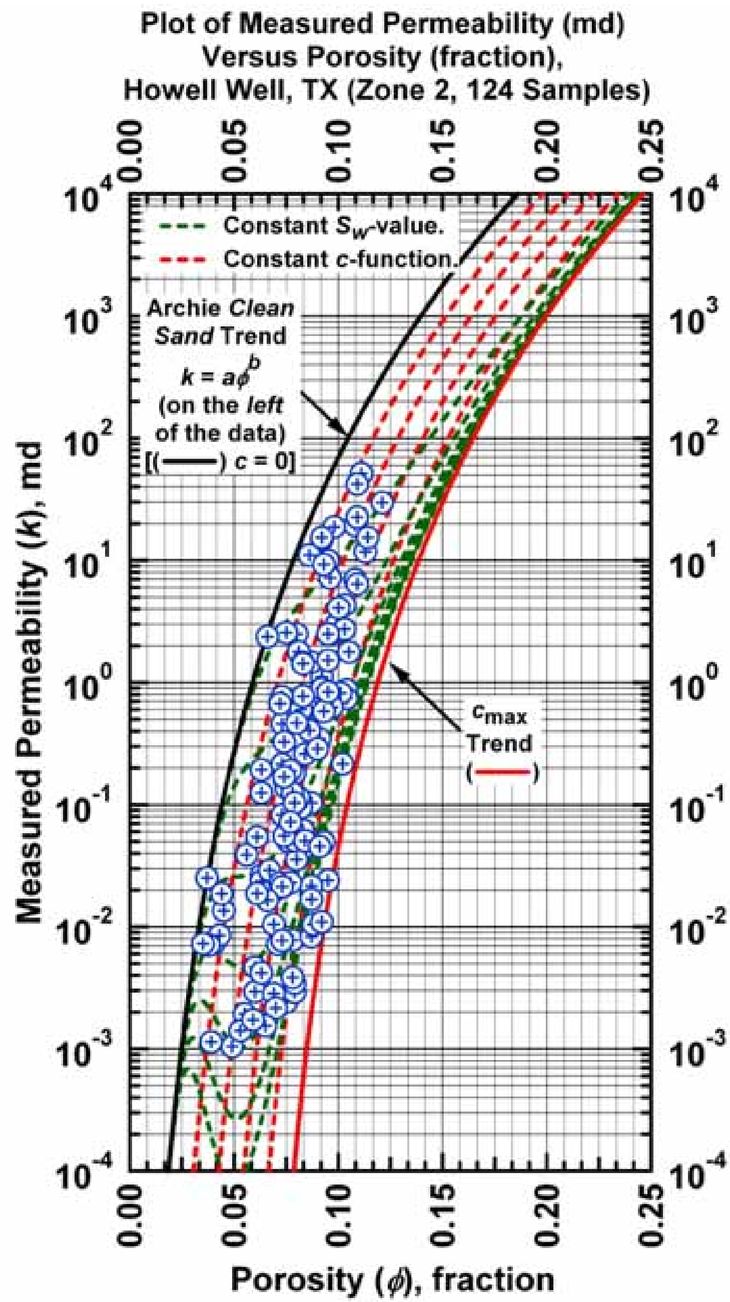

Figure B.27b — Model *CPR-A*: $k = a(\phi - c)^b$ $\quad c = c_{max} \exp[-c_1 \phi^{c_2} S_w^{c_3}]$ — "Dirty Sand" Plot (semilog format). Archie "Clean Sand" trend is given by the curved trend at the far left of the data (power law model). [*Case*: Howell Well, E. TX (USA)]

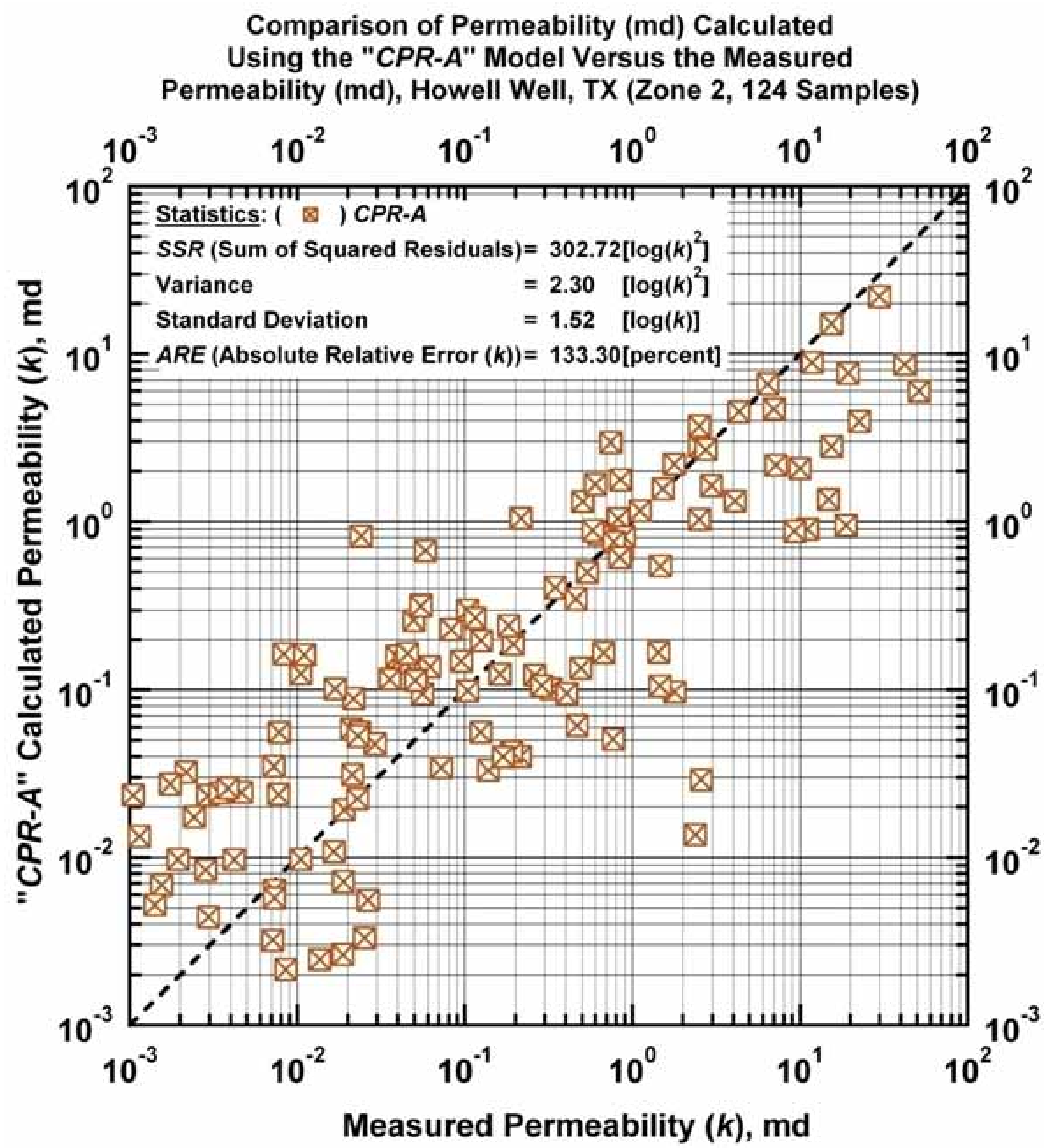

Figure B.28a — Model *CPR-A*: calculated versus measured permeability. [*Case*: Howell Well, E. TX (USA)]

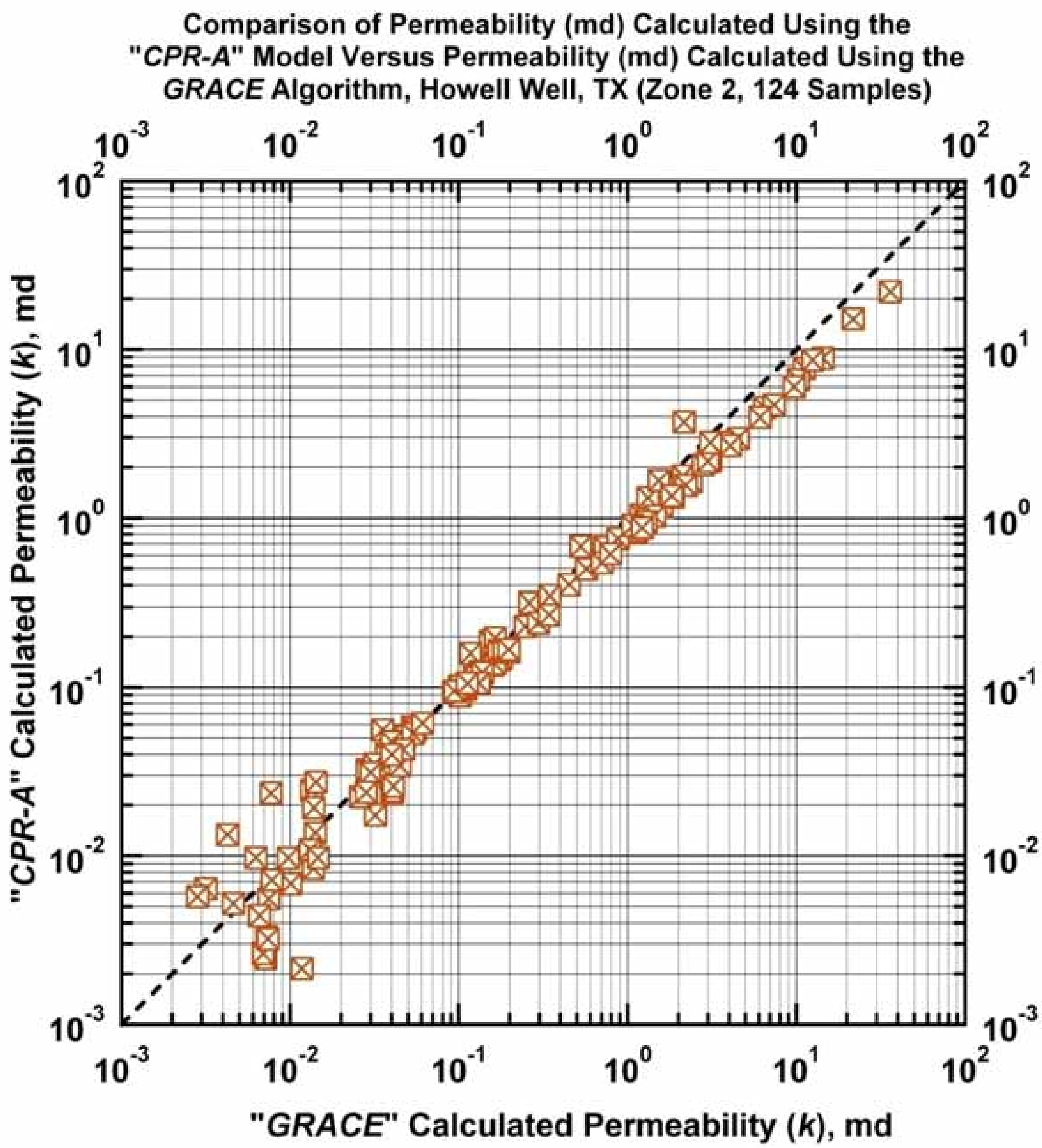

Figure B. 28b — Model *CPR-A*: Permeability calculated using Model *CPR-A* versus permeability calculated using the *GRACE* Algorithm. [*Case*: Howell Well, E. TX (USA)]

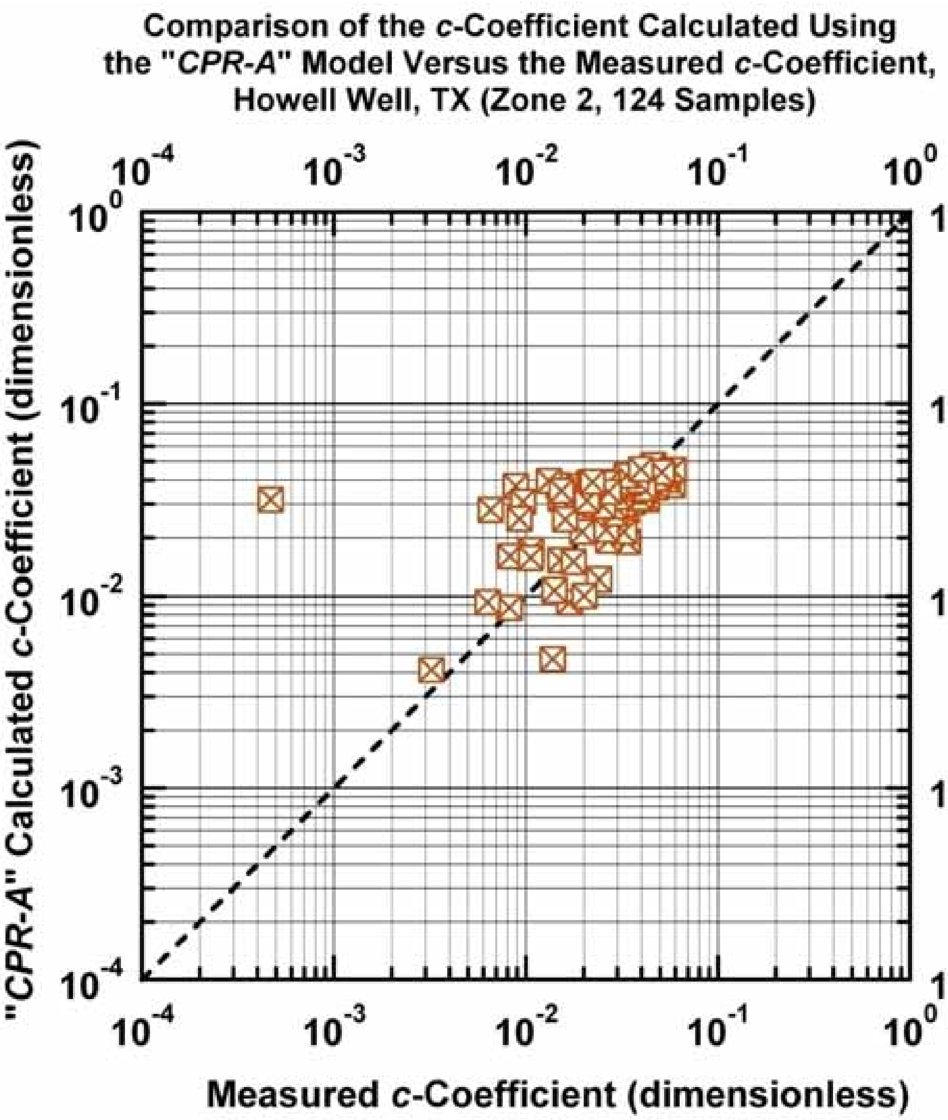

Figure B. 28c — Model *CPR-A*: Calculated *c*-function values versus measured *c*-function values. [*Case*: Howell Well, E. TX (USA)]

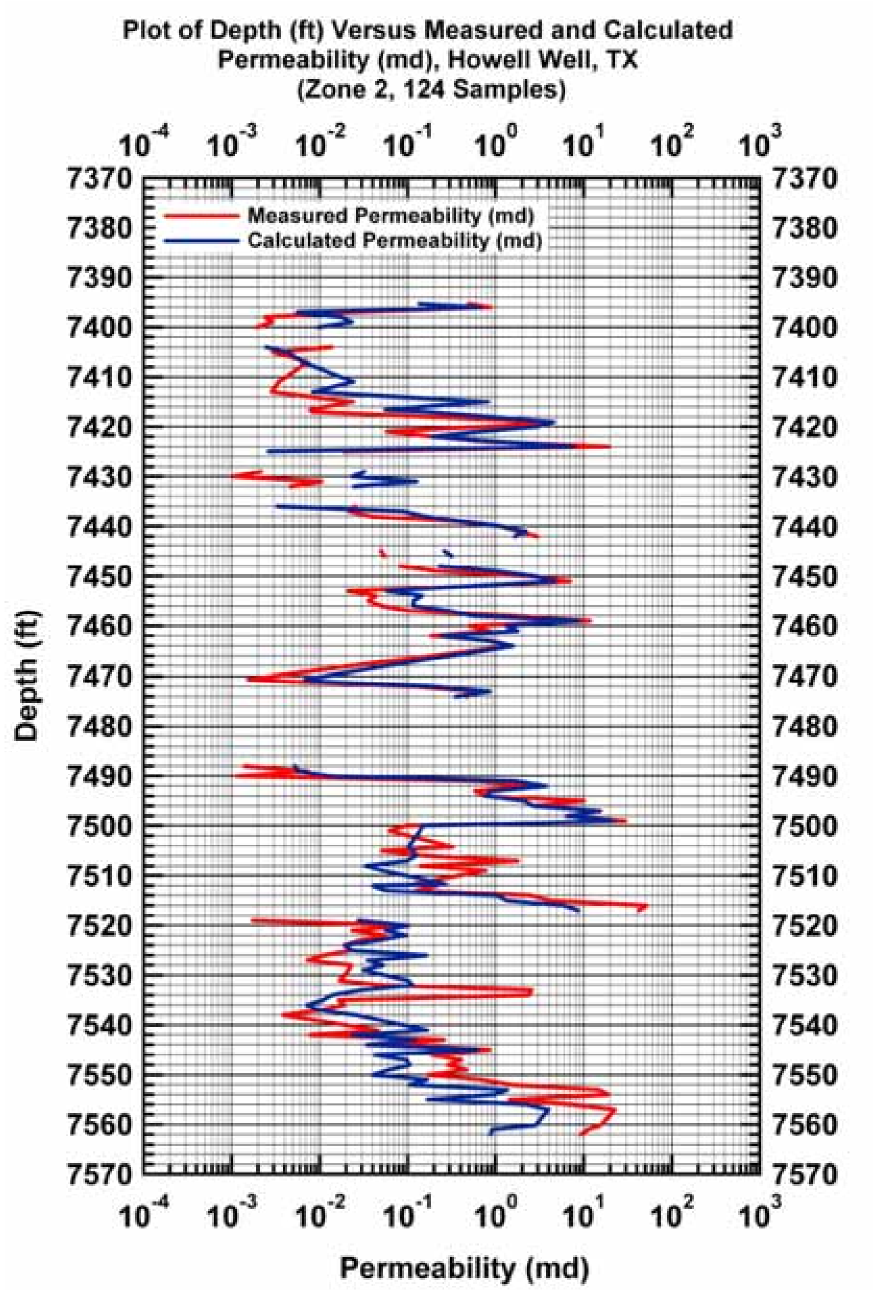

Figure B. 28d — Model *CPR-A*: Calculated and measured permeability values versus depth. [*Case*: Howell Well, E. TX (USA)]

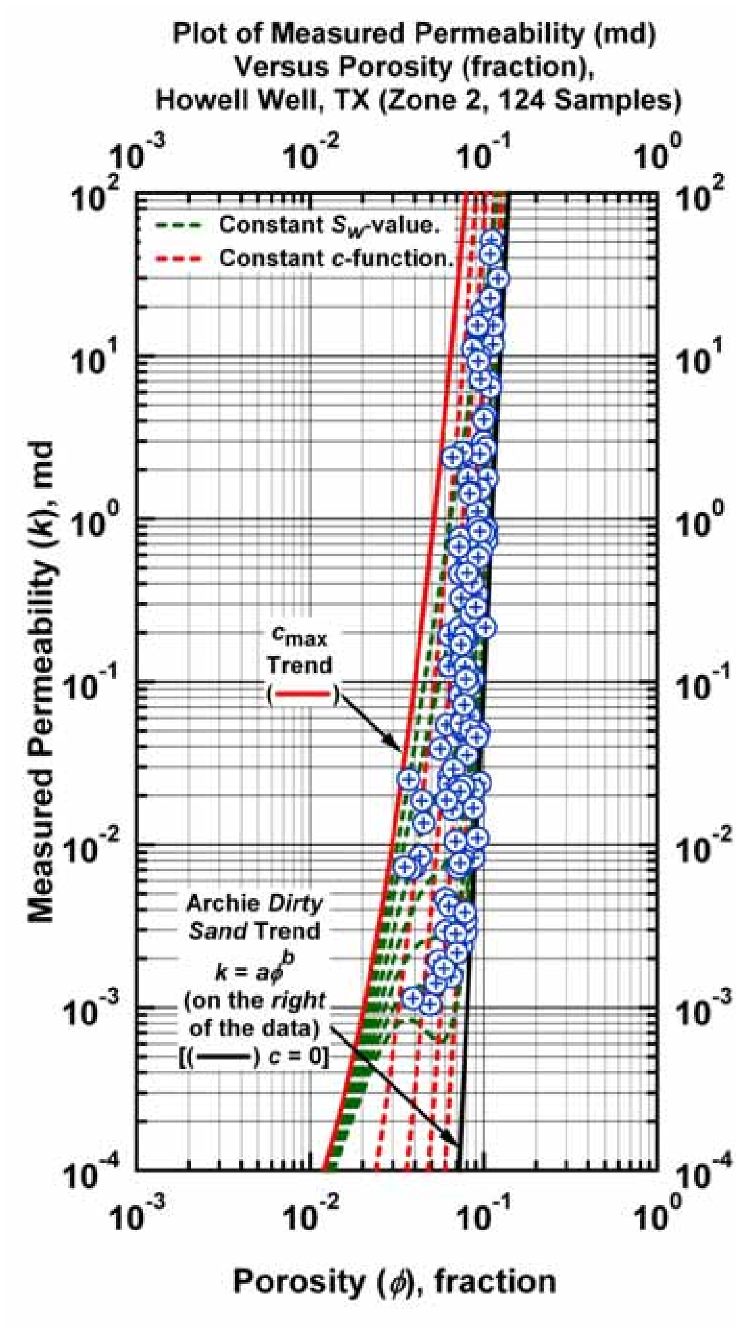

Figure B.29a — Model *CPR-B*: $k = a(\phi + c)^b$ $c = c_{max} \exp[-c_1 \phi^{c_2} S_w^{c_3}]$ — "Clean Sand" Plot (log-log format) — Archie "Dirty Sand" trend is given by the straight-line trend at the far right of the data (power law model). [*Case*: Howell Well, E. TX (USA)]

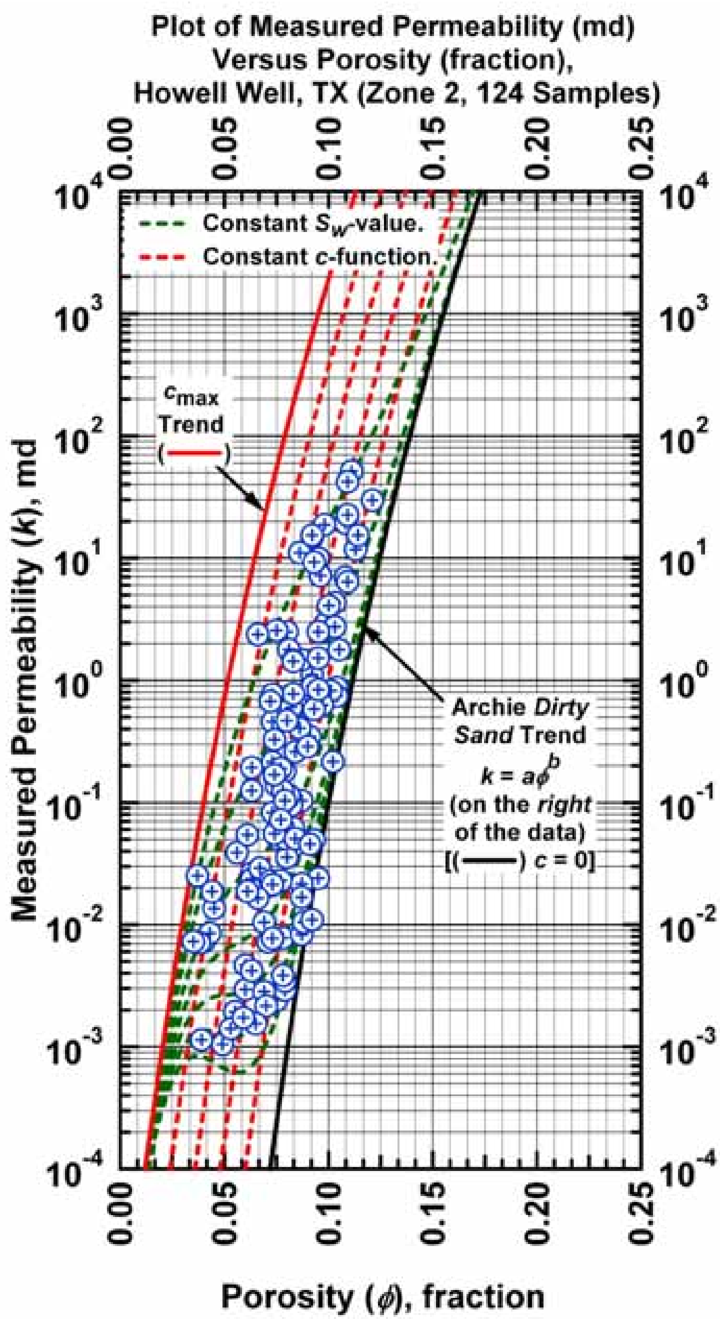

Figure B.29b — Model *CPR-B*: $k = a(\phi + c)^b \quad c = c_{\max} \exp[-c_1 \phi^{c_2} S_w^{c_3}]$ — "Dirty Sand" Plot (semilog format) — Archie "Dirty Sand" trend is given by the curved trend at the far right of the data (power law model). [*Case*: Howell Well, E. TX (USA)]

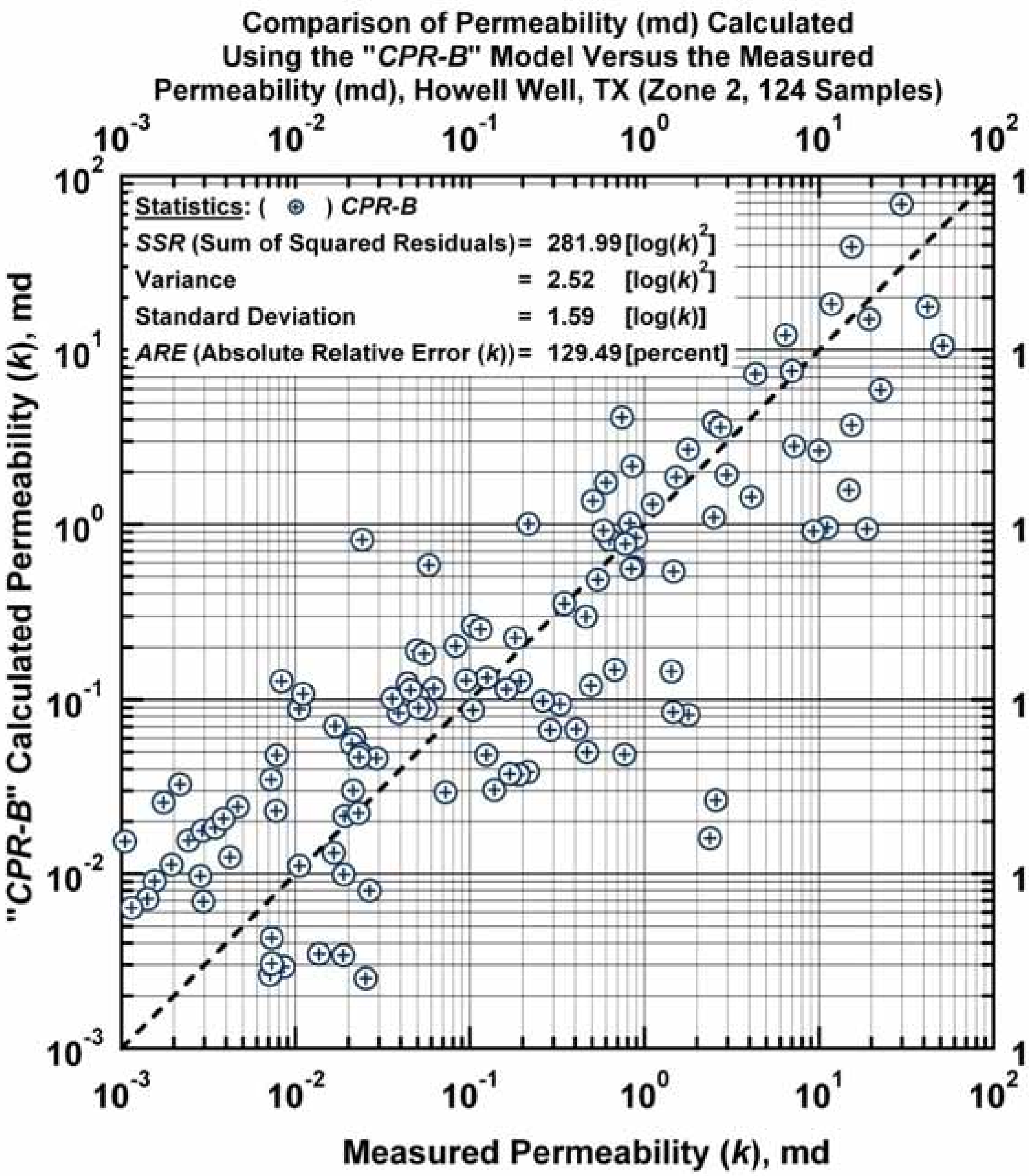

Figure B.30a — Model *CPR-B*: calculated versus measured permeability. [*Case*: Howell Well, E. TX (USA)]

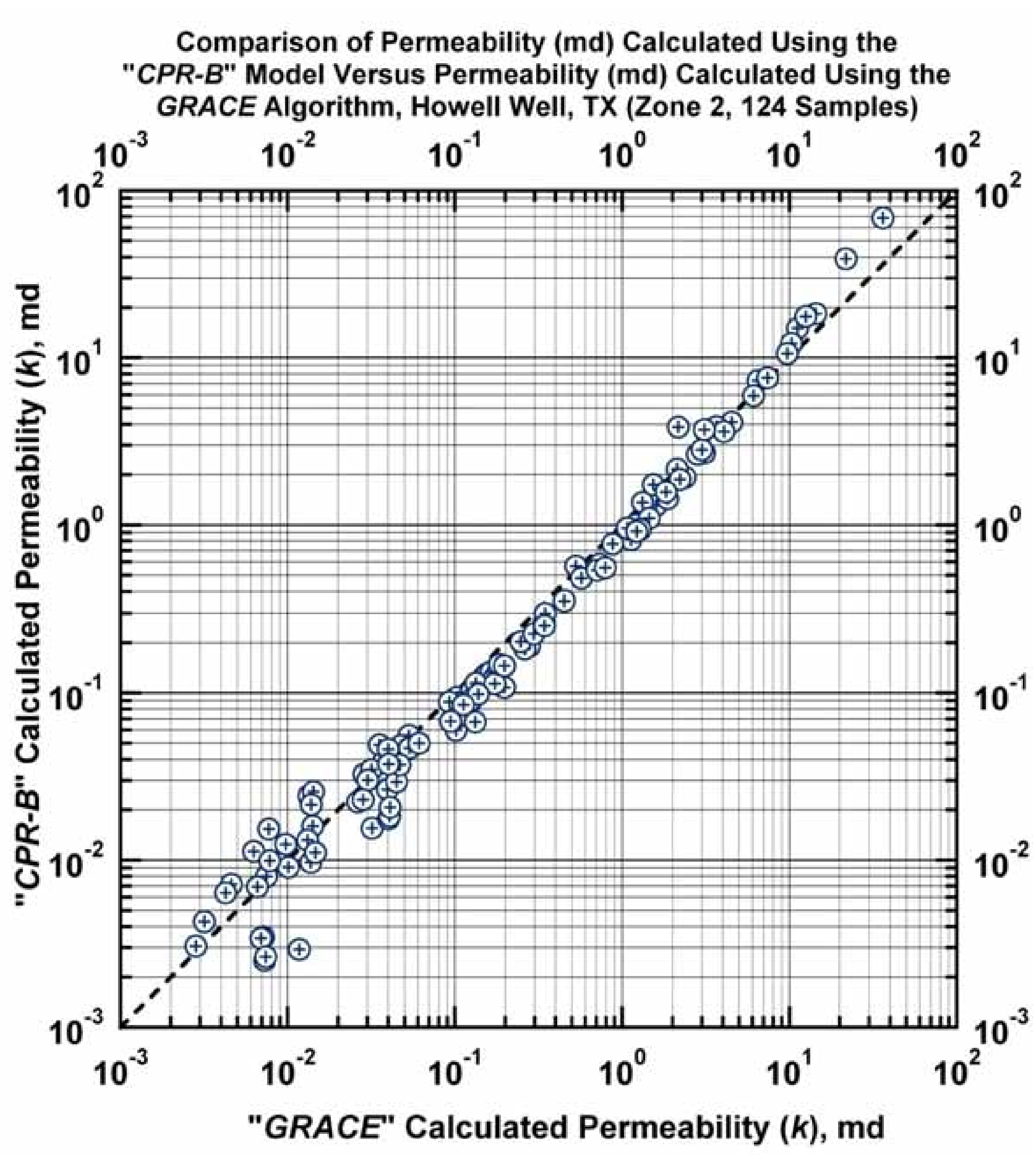

Figure B. 30b — Model *CPR-B*: Permeability calculated using Model *CPR-B* versus permeability calculated using the *GRACE* Algorithm. [*Case*: Howell Well, E. TX (USA)]

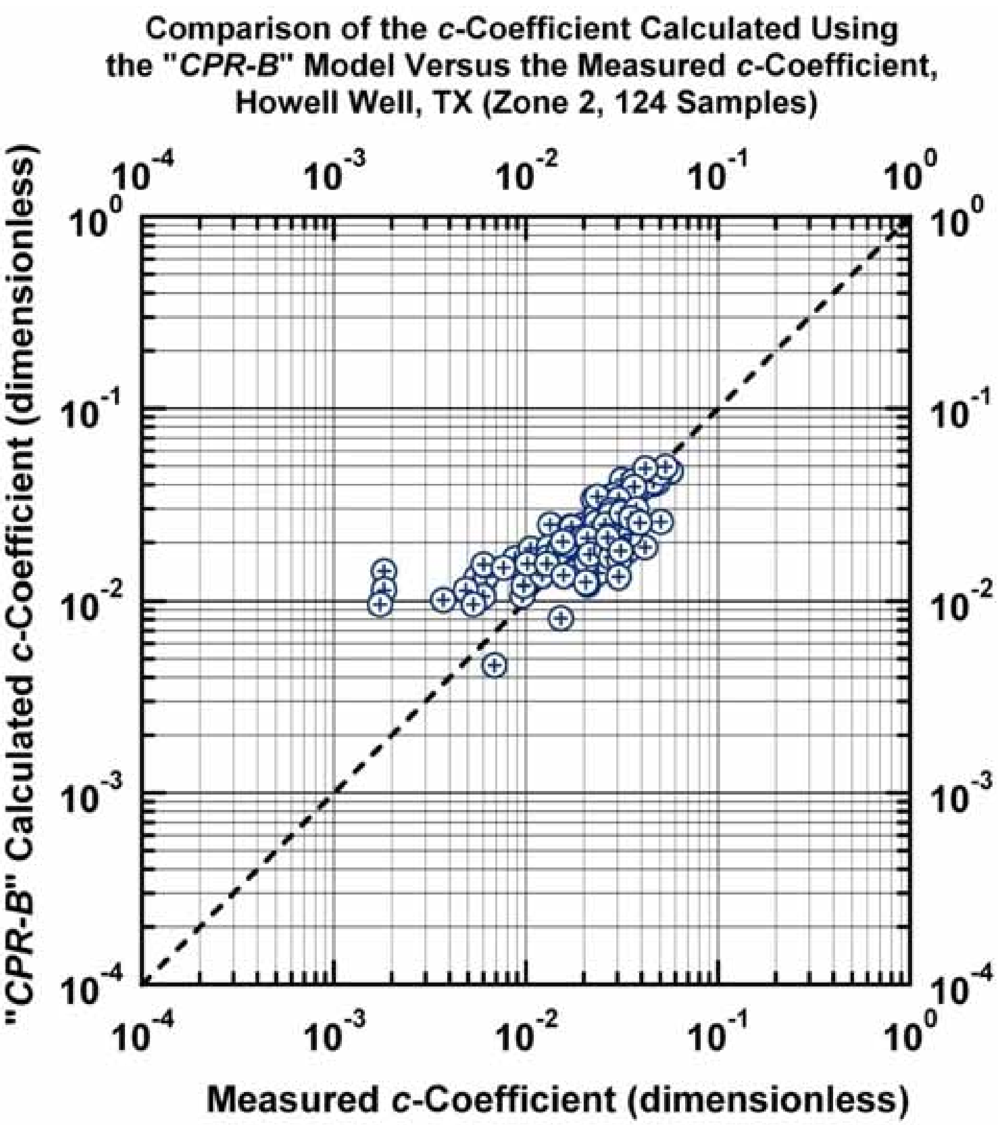

Figure B. 30c — Model *CPR-B*: Calculated *c*-function values versus measured *c*-function values. [*Case*: Howell Well, E. TX (USA)]

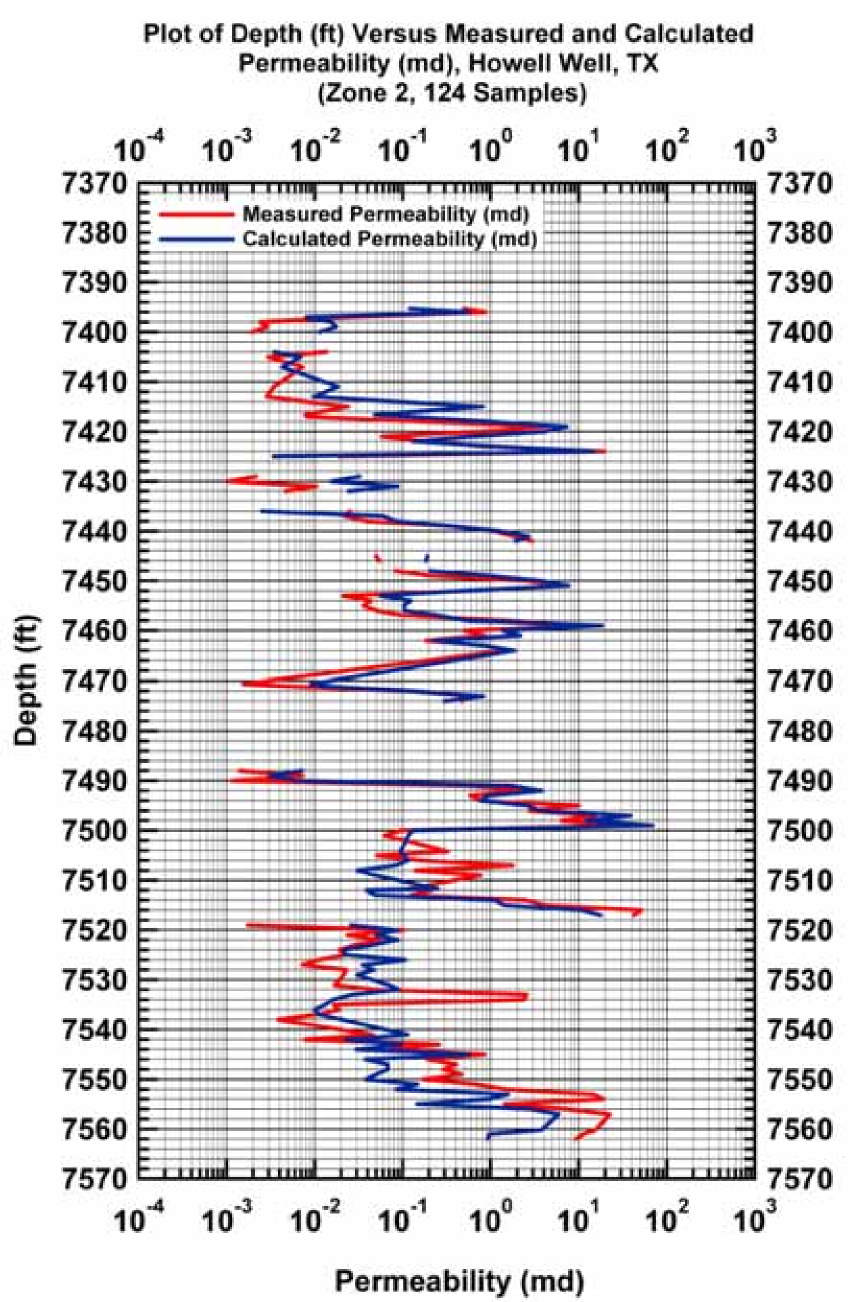

Figure B. 30d — Model *CPR-B*: Calculated and measured permeability values versus depth. [*Case*: Howell Well, E. TX (USA)]

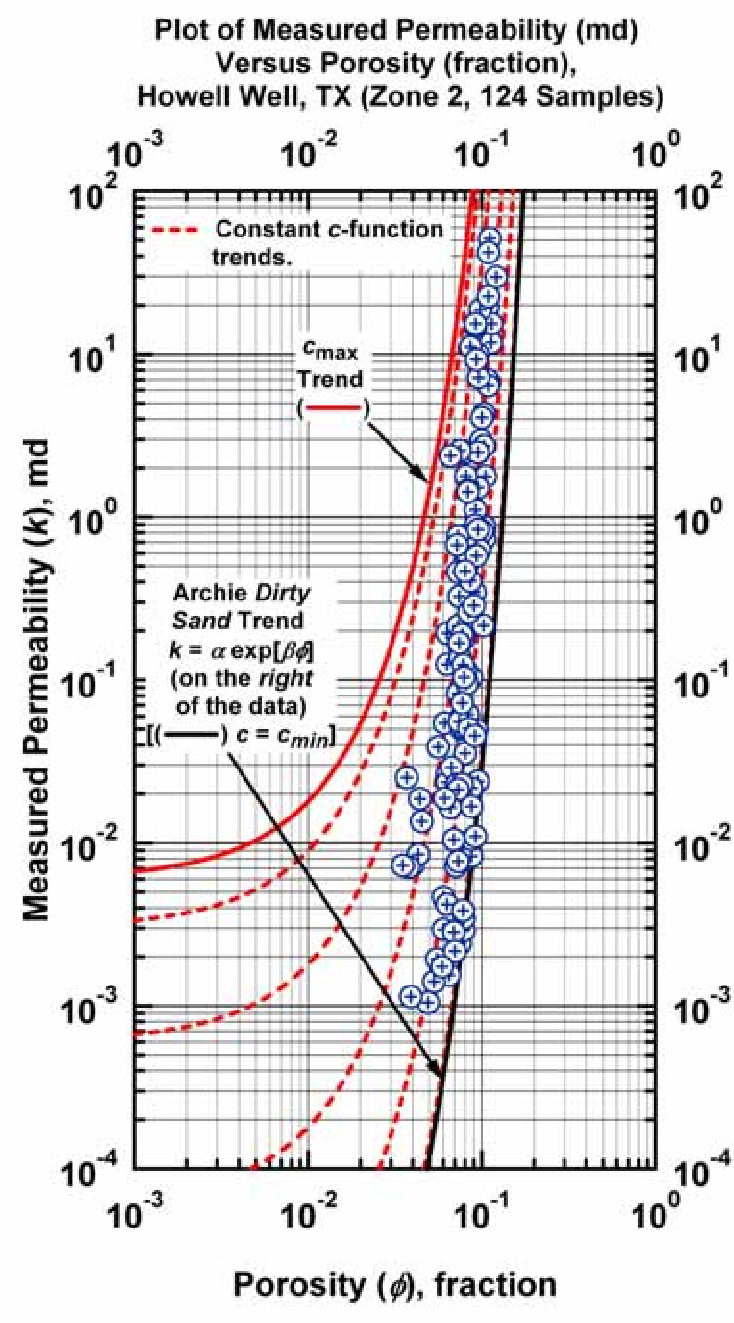

Figure B.31a — Model *CPR-C*: $k = c\exp[\beta\phi] \quad c = c_{\max}\exp[-c_1\phi^{c_2} S_w^{c_3}]$ — "Clean Sand" Plot (log-log format) — Archie "Dirty Sand" trend is given by the curved trend at the far right of the data (exponential model). [*Case*: Howell Well, E. TX (USA)]

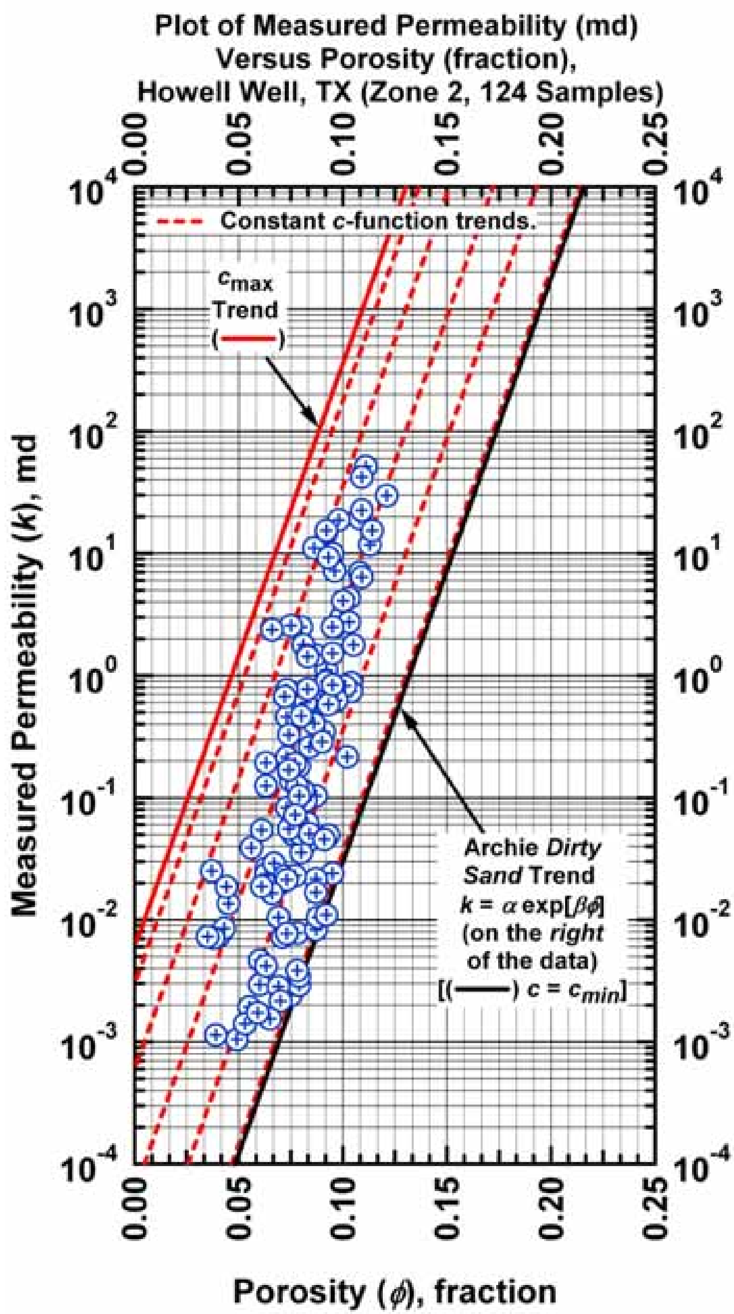

Figure B.31b — Model *CPR-C*: $k = c\exp[\beta\phi]$ $\quad c = c_{\max}\exp[-c_1\phi^{c_2} S_w^{c_3}]$ — "Dirty Sand" Plot (semilog format) — Archie "Dirty Sand" trend is given by the straight-line trend at the far right of the data (exponential model). [*Case*: Howell Well, E. TX (USA)]

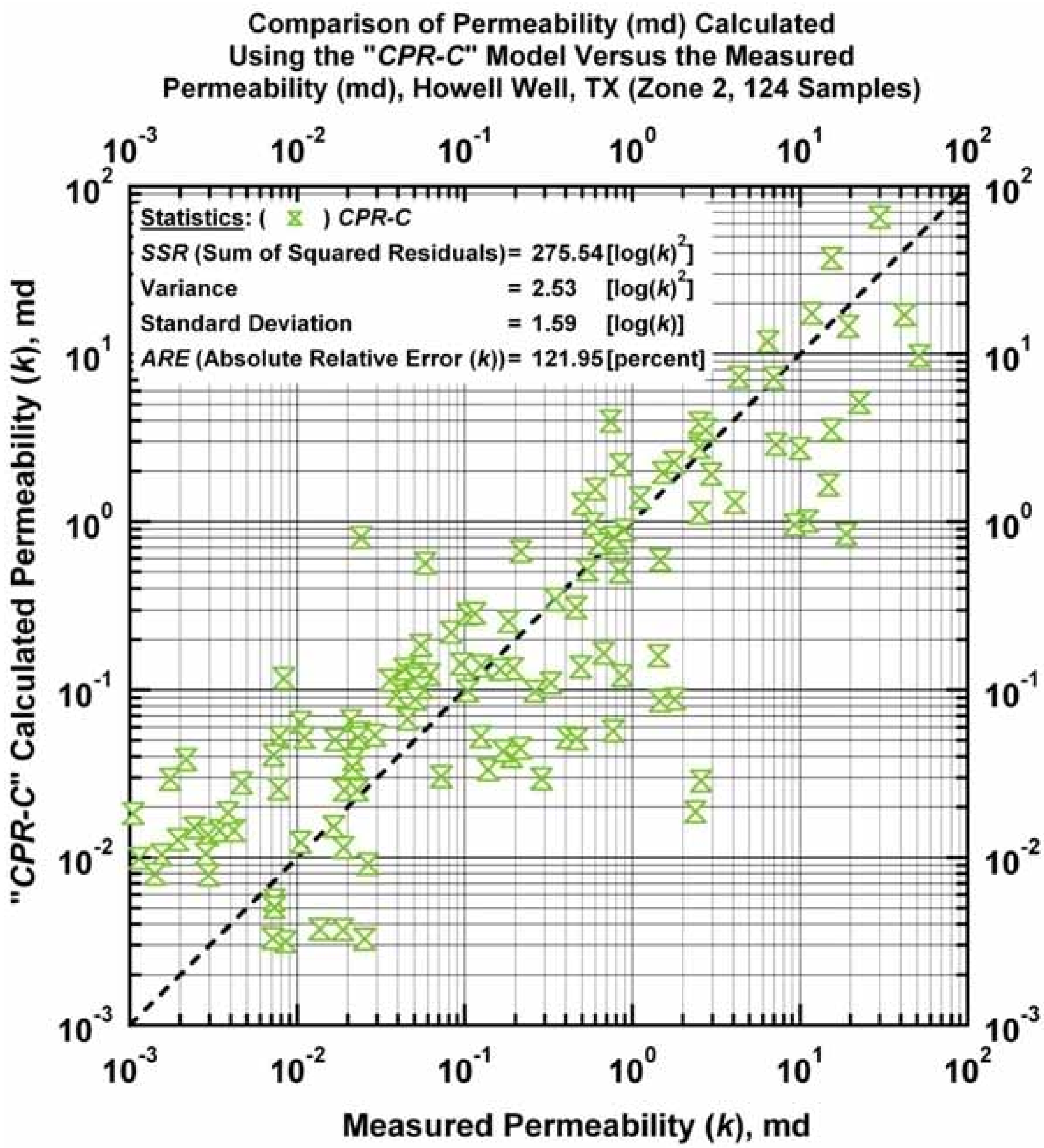

Figure B.32a — Model *CPR-C*: calculated versus measured permeability. [*Case*: Howell Well, E. TX (USA)]

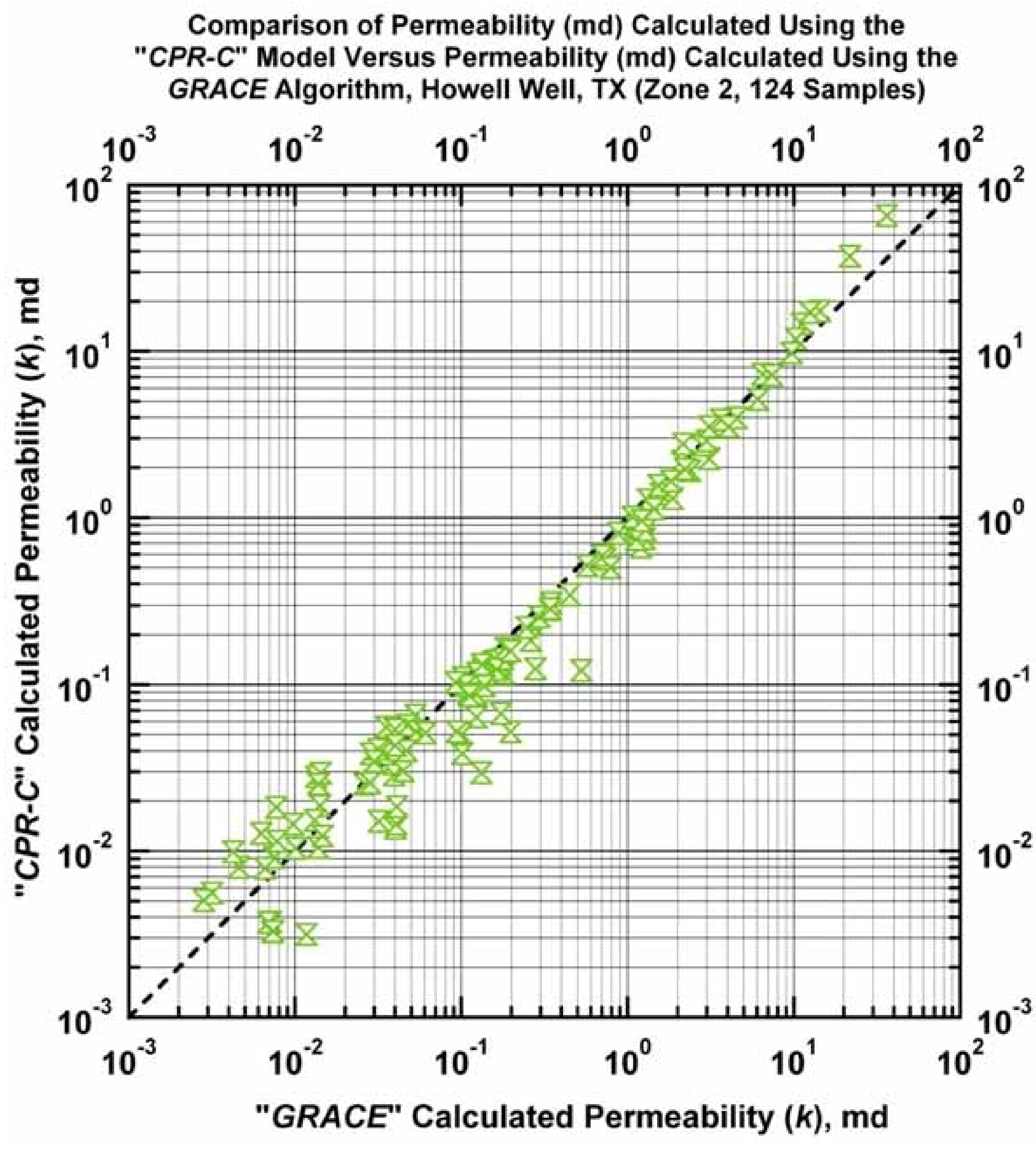

Figure B. 32b — Model *CPR-C*: Permeability calculated using Model *CPR-C* versus permeability calculated using the *GRACE* Algorithm. [*Case*: Howell Well, E. TX (USA)]

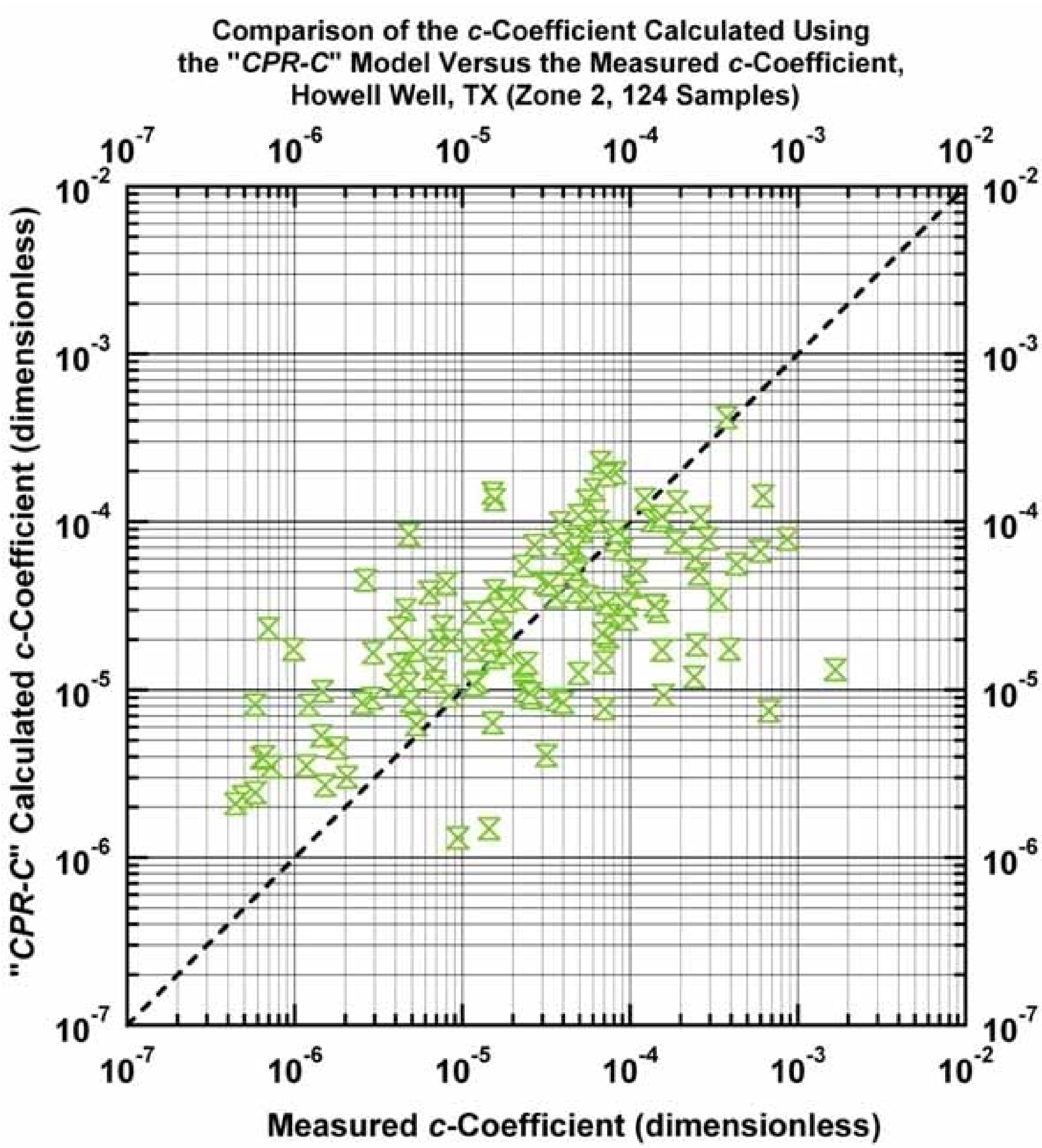

Figure B. 32c — Model *CPR-C*: Calculated *c*-function values versus measured *c*-function values. [*Case*: Howell Well, E. TX (USA)]

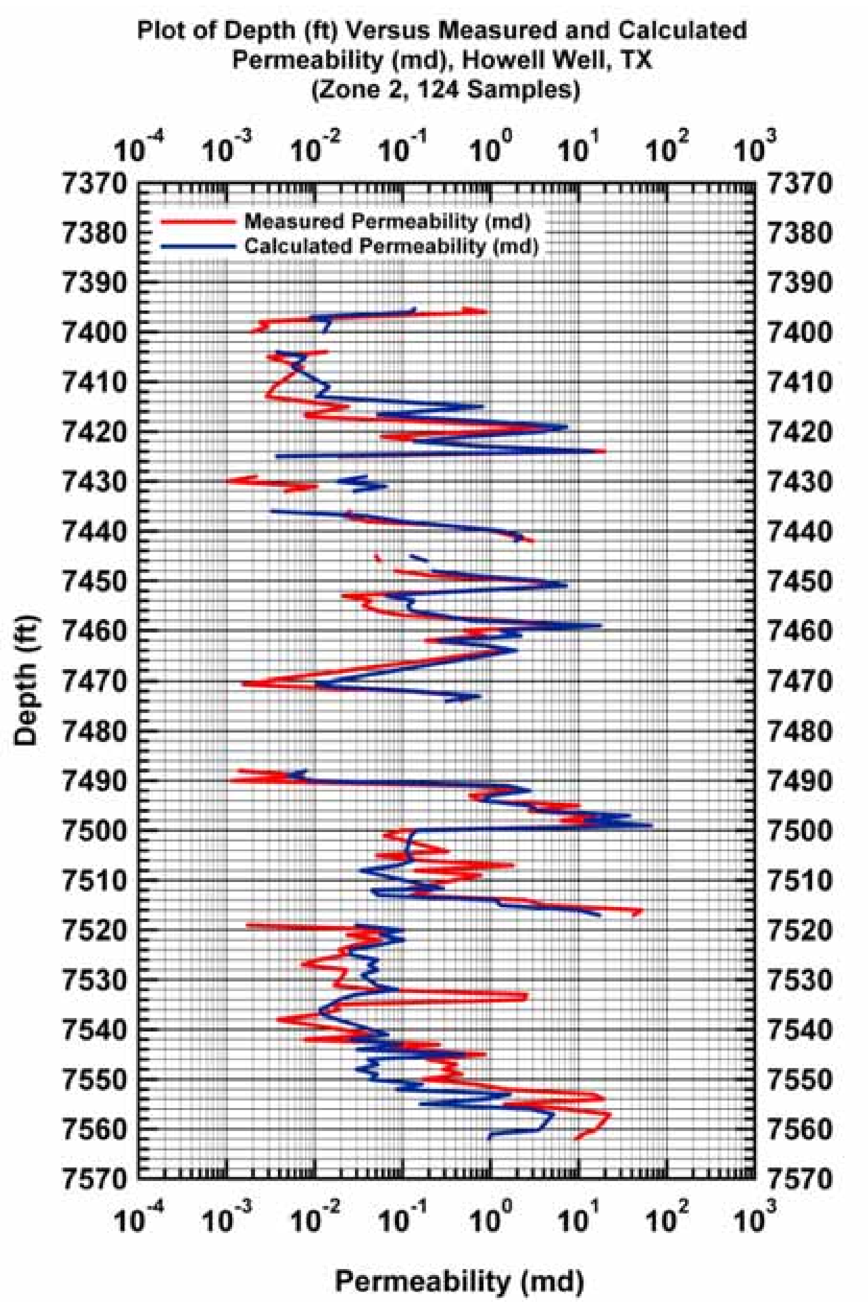

Figure B. 32d — Model *CPR-C*: Calculated and measured permeability values versus depth. [*Case*: Howell Well, E. TX (USA)]

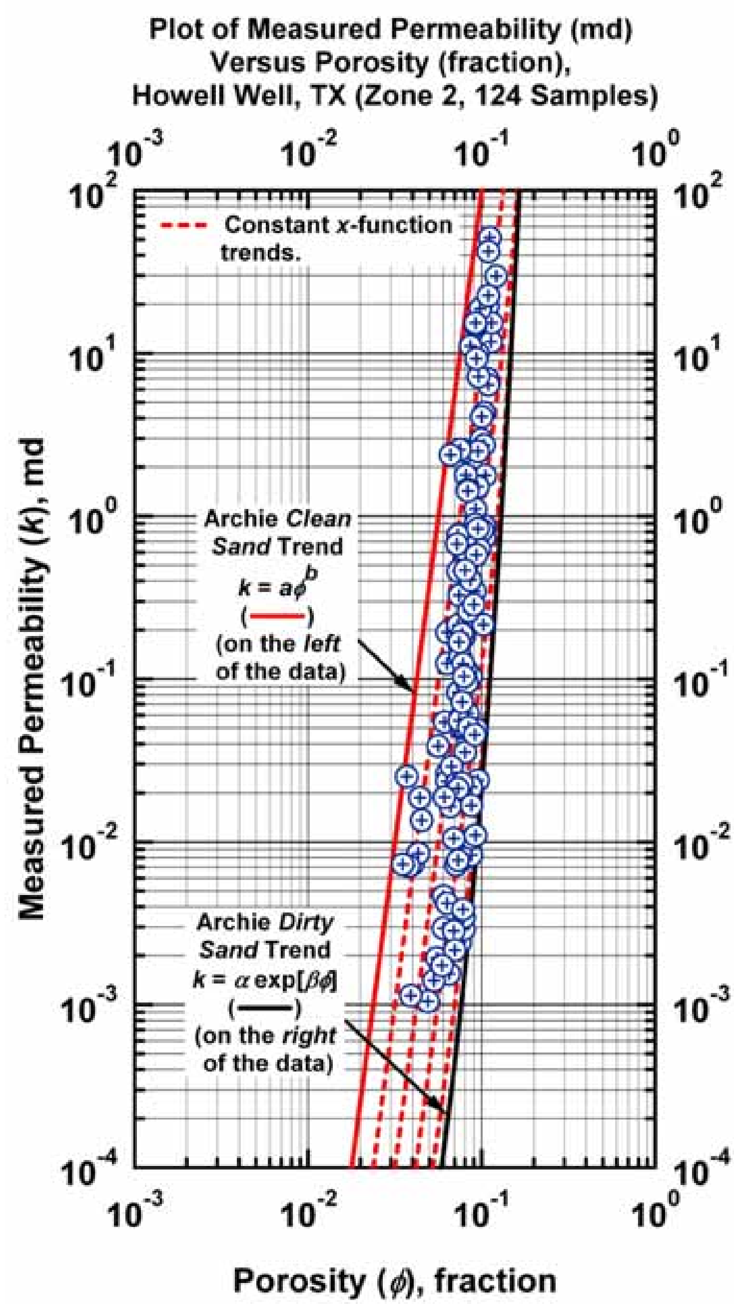

Figure B.33a — Model *CPR-D*: $k = xa\phi^{b} + (1-x)\alpha\exp[\beta\phi]$ $[0 \le x \le 1]$ — *Weighted Power Law-Exponential Model* used to correlate permeability (k) and porosity (ϕ). "Clean Sand" Plot — Archie "Clean Sand" trend is given by the straight-line trend at the far left of the data (power law model). [*Case*: Howell Well, E. TX (USA)]

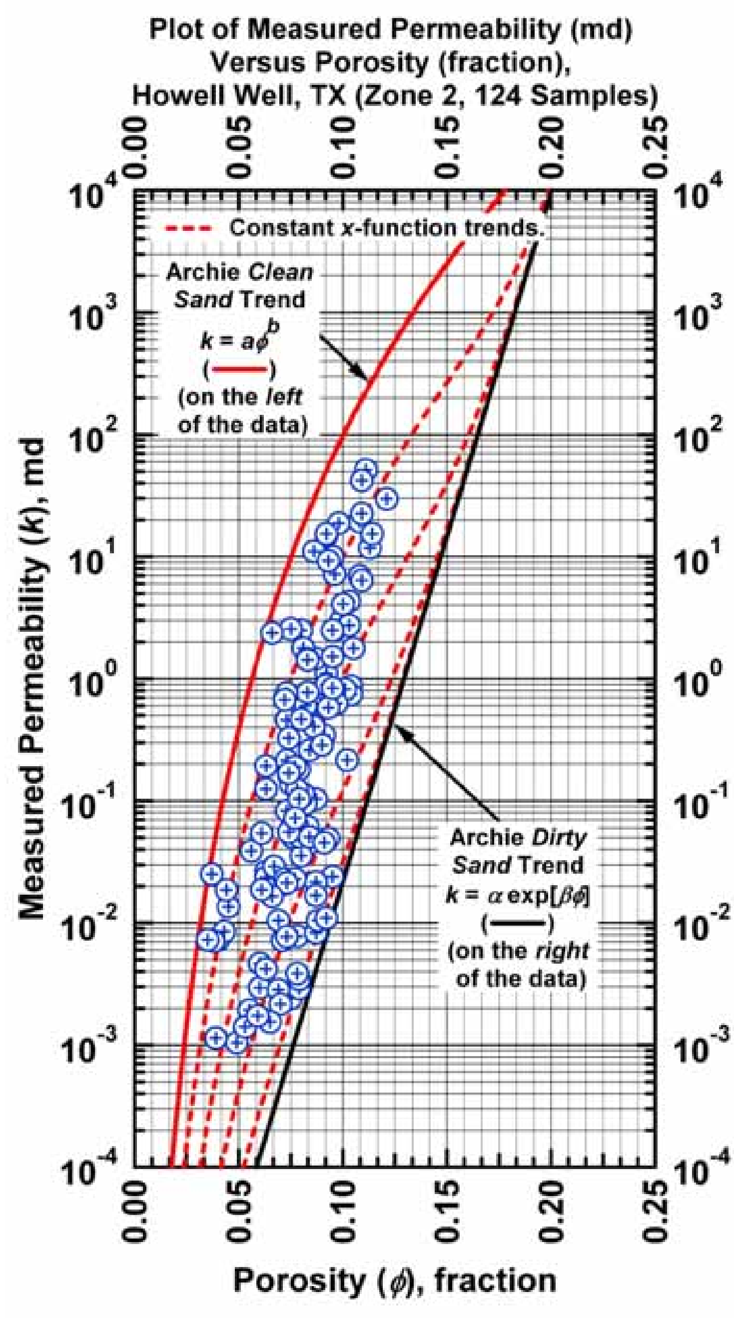

Figure B.33b — Model *CPR-D*: $k = xa\phi^b + (1-x)\alpha\exp[\beta\phi] \quad [0 \le x \le 1]$ — *Weighted Power Law-Exponential Model* used to correlate permeability (k) and porosity (ϕ). "Dirty Sand" Plot — Archie "Dirty Sand" trend is given by the straight-line trend at the far right of the data (exponential model). [*Case*: Howell Well, E. TX (USA)]

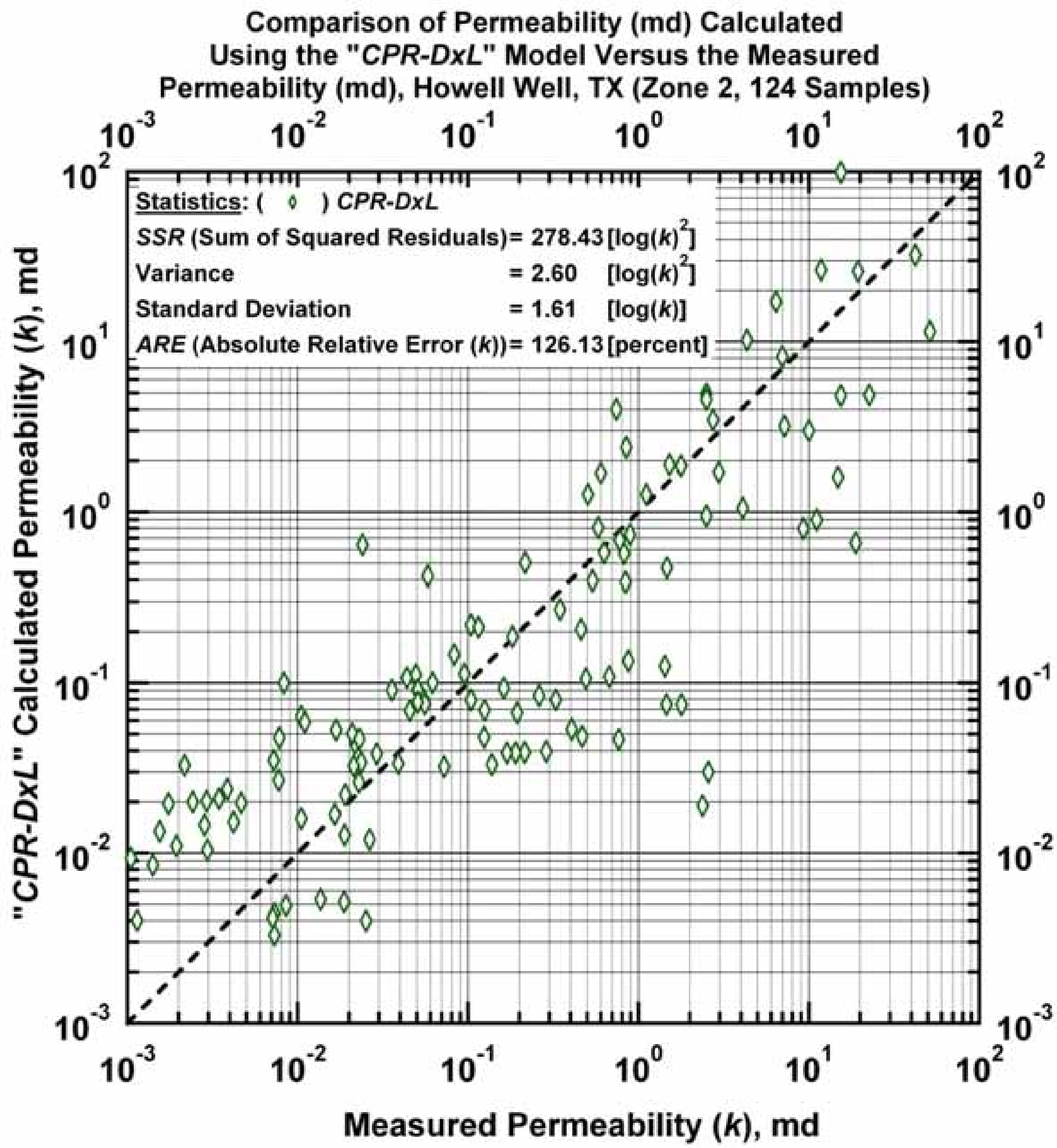

Figure B.34a — Model *CPR-DxL*: Calculated versus measured permeability. [*Case*: Howell Well, E. TX (USA)]

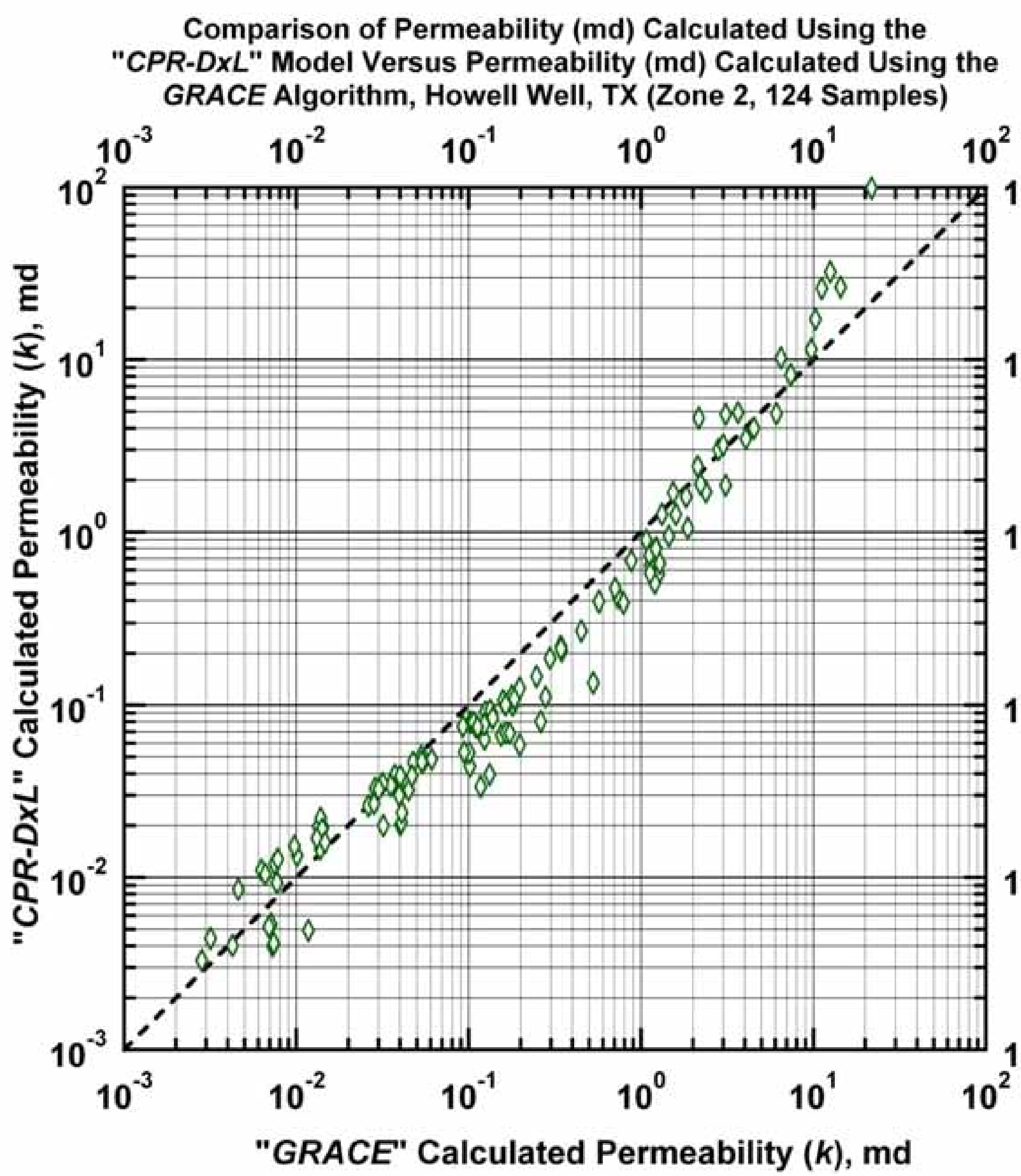

Figure B. 34b — Model *CPR-DxL*: Permeability calculated using Model *CPR-C* versus permeability calculated using the *GRACE* Algorithm. [*Case*: Howell Well, E. TX (USA)]

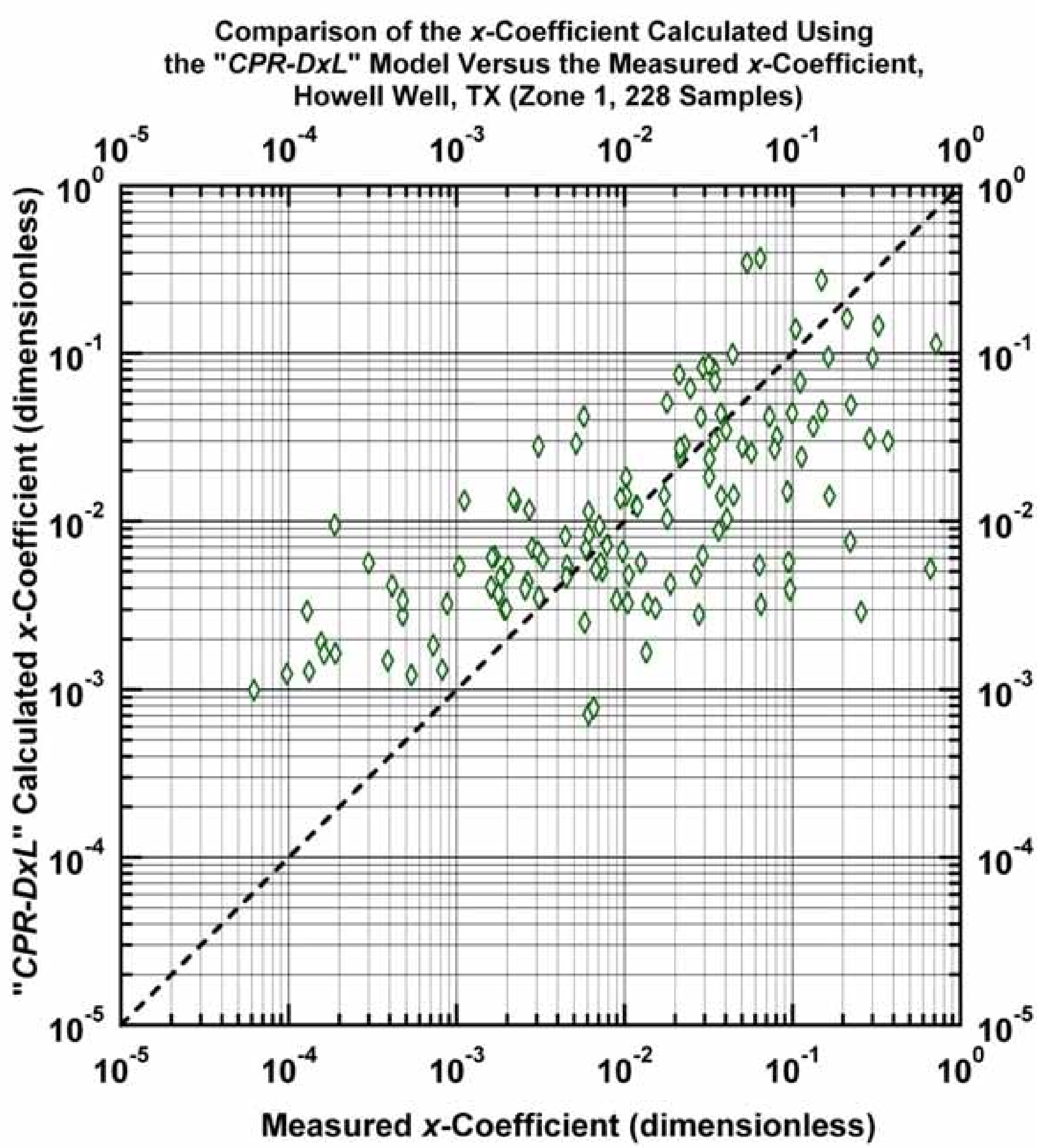

Figure B. 34c — Model *CPR-DxL*: Calculated *x*-function weight values versus measured *x*-function weight values. [*Case*: Howell Well, E. TX (USA)]

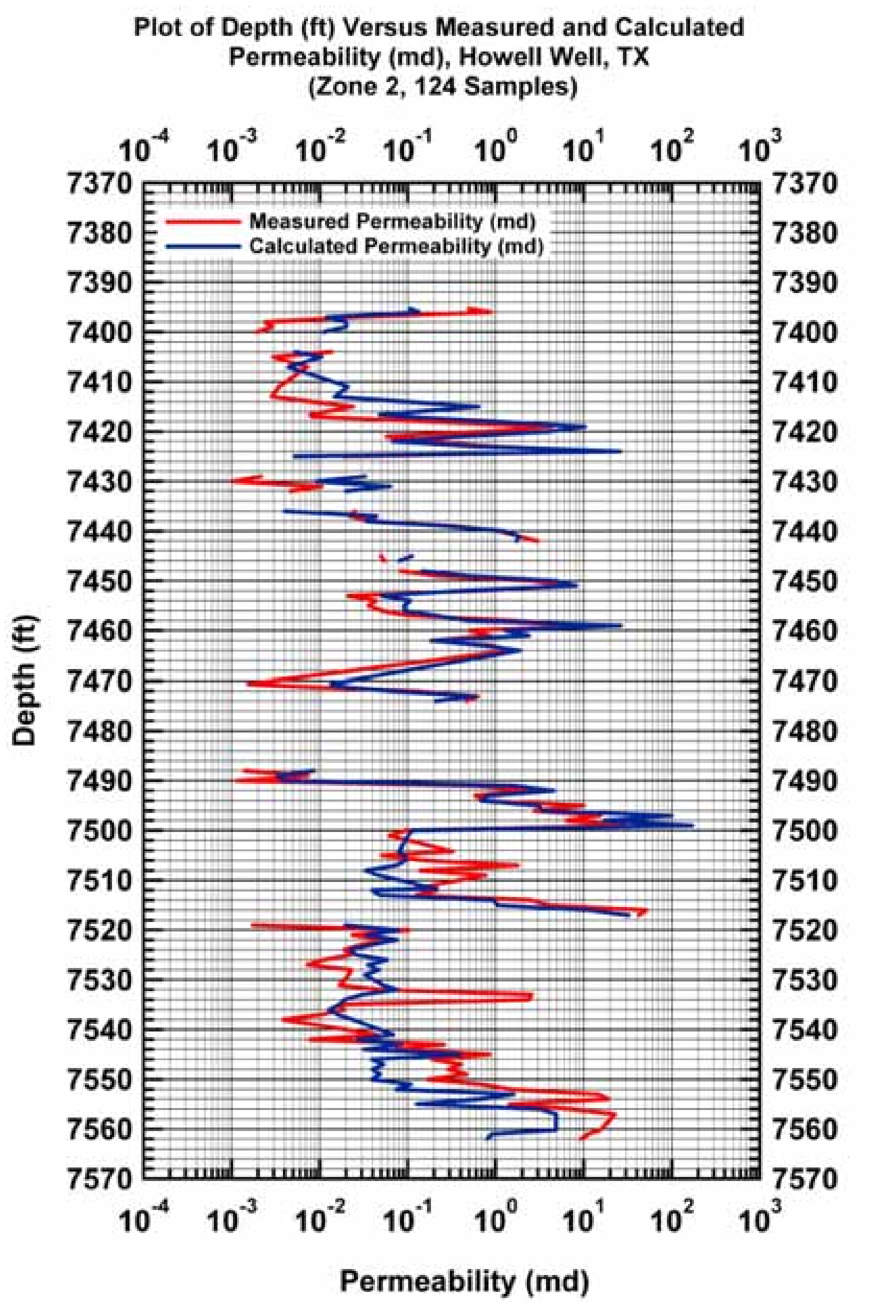

Figure B. 34d — Model *CPR-DxL*: Calculated and measured permeability values versus depth. [*Case*: Howell Well, E. TX (USA)]

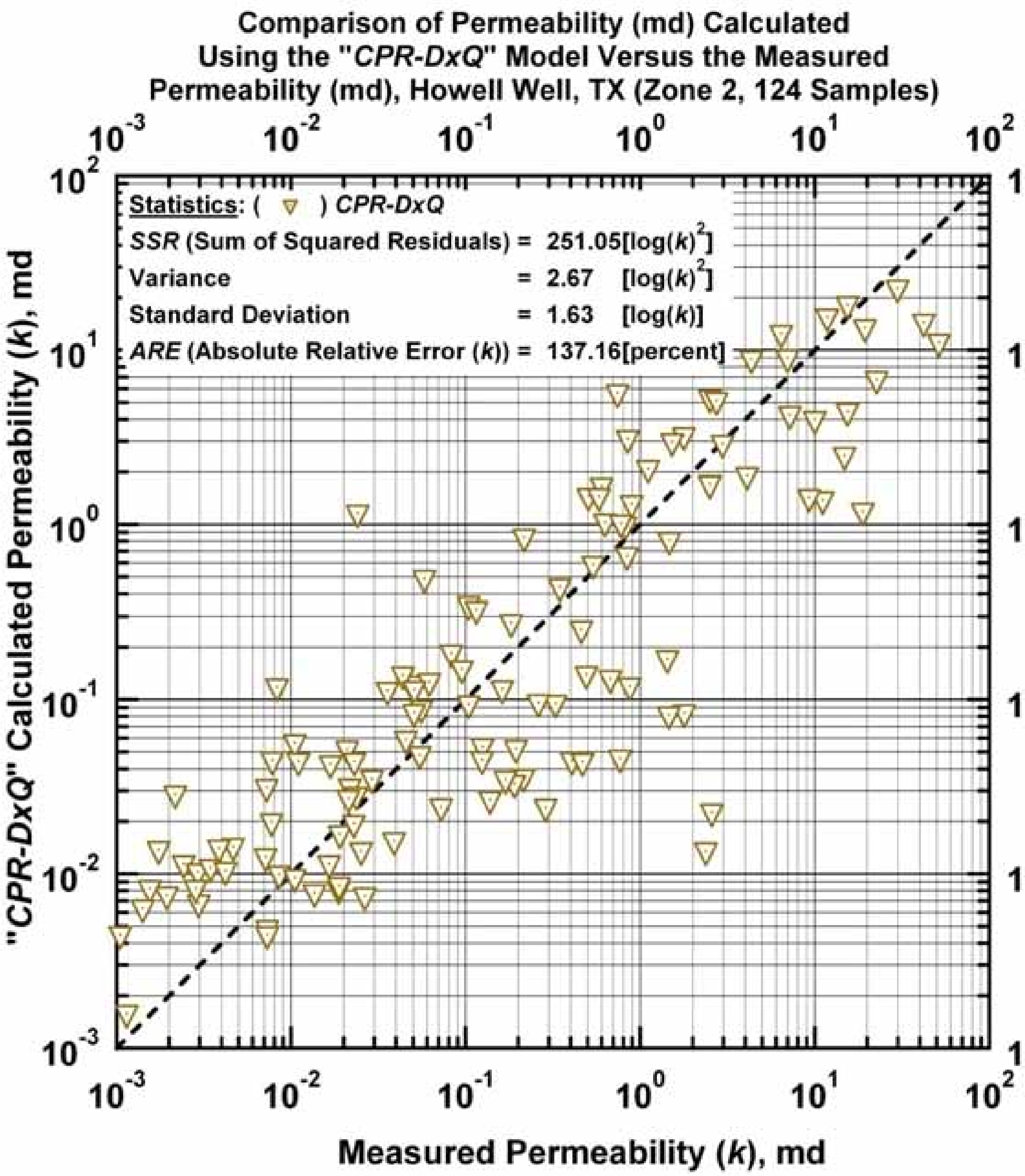

Figure B.35a — Model *CPR-DxQ*: Calculated versus measured permeability. [*Case*: Howell Well, E. TX (USA)]

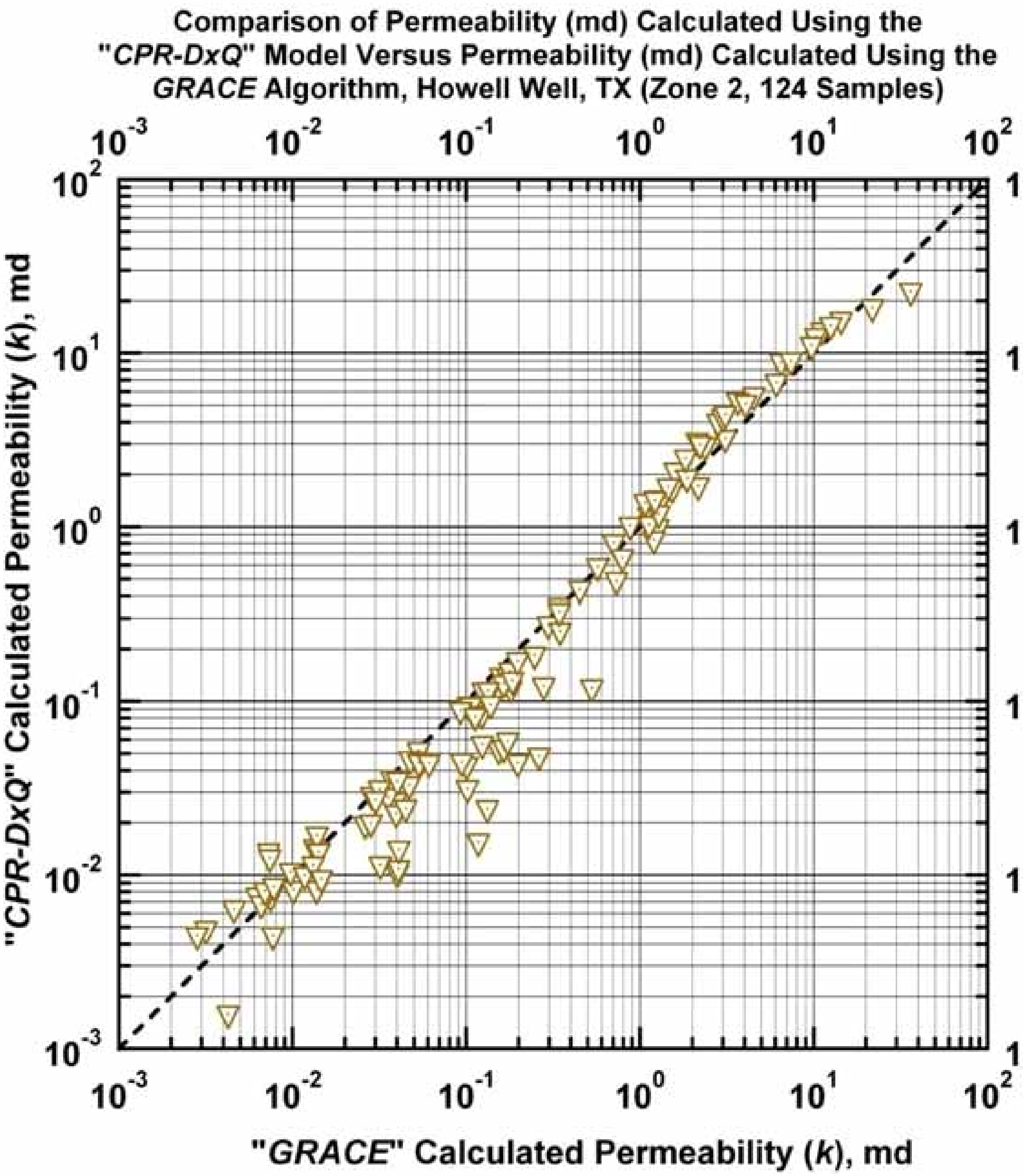

Figure B.35b — Model *CPR-DxQ*: Permeability calculated using Model *CPR-C* versus permeability calculated using the *GRACE* Algorithm. [*Case*: Howell Well, E. TX (USA)]

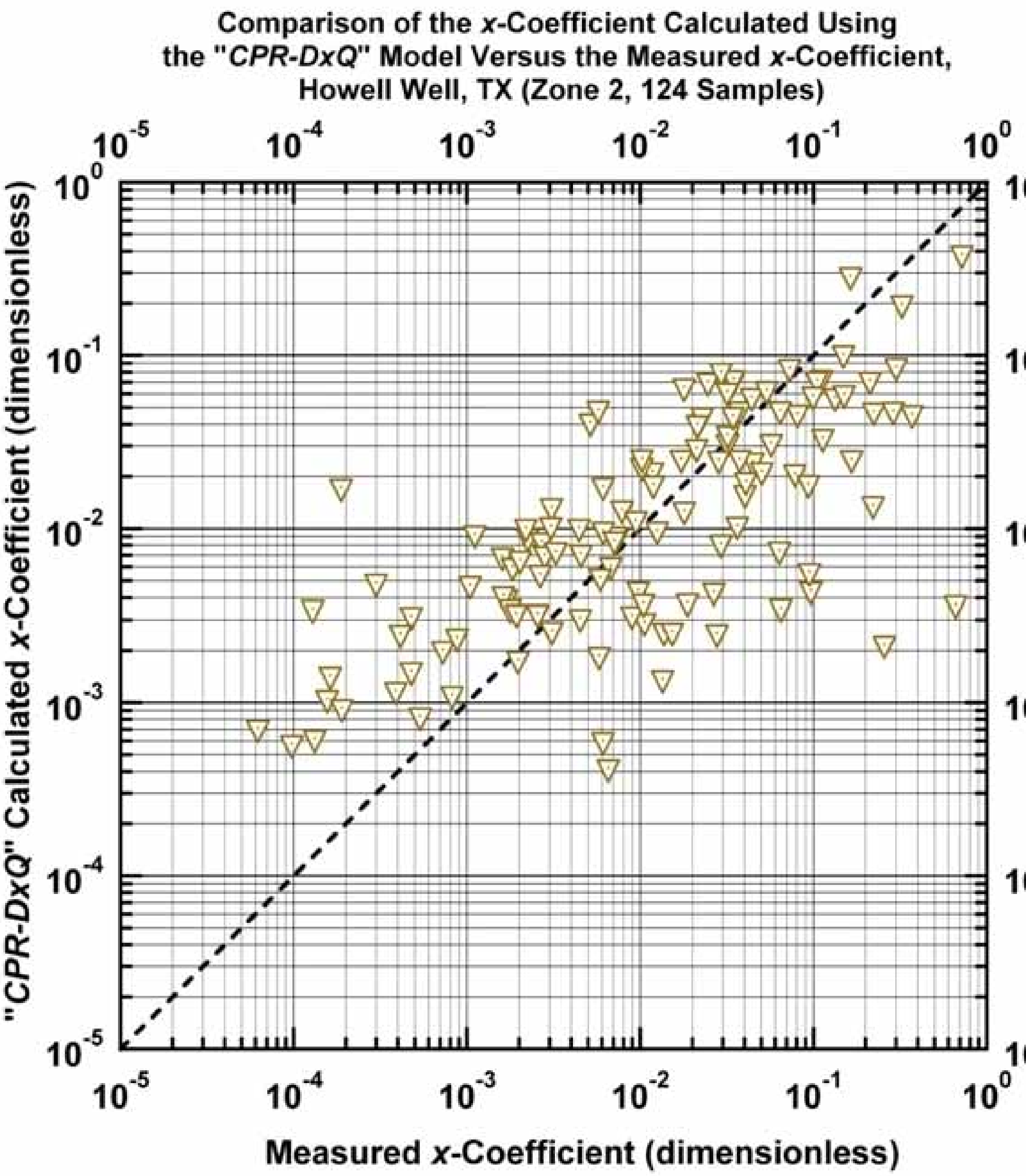

Figure B.35c — Model *CPR-DxQ*: Calculated *x*-function weight values versus measured *x*-function weight values. [*Case*: Howell Well, E. TX (USA)]

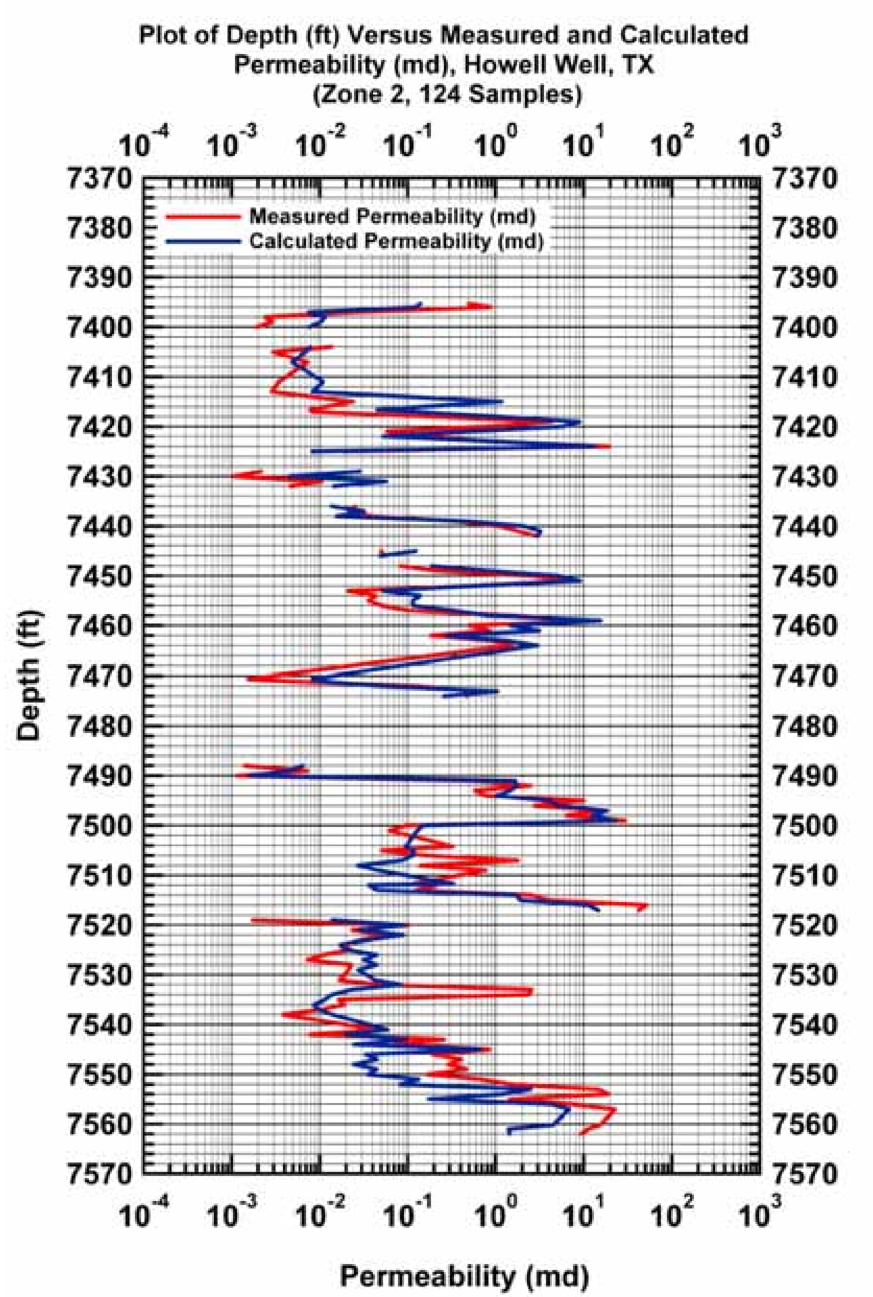

Figure B.35d — Model *CPR-DxQ*: Calculated and measured permeability values versus depth. [*Case*: Howell Well, E. TX (USA)]

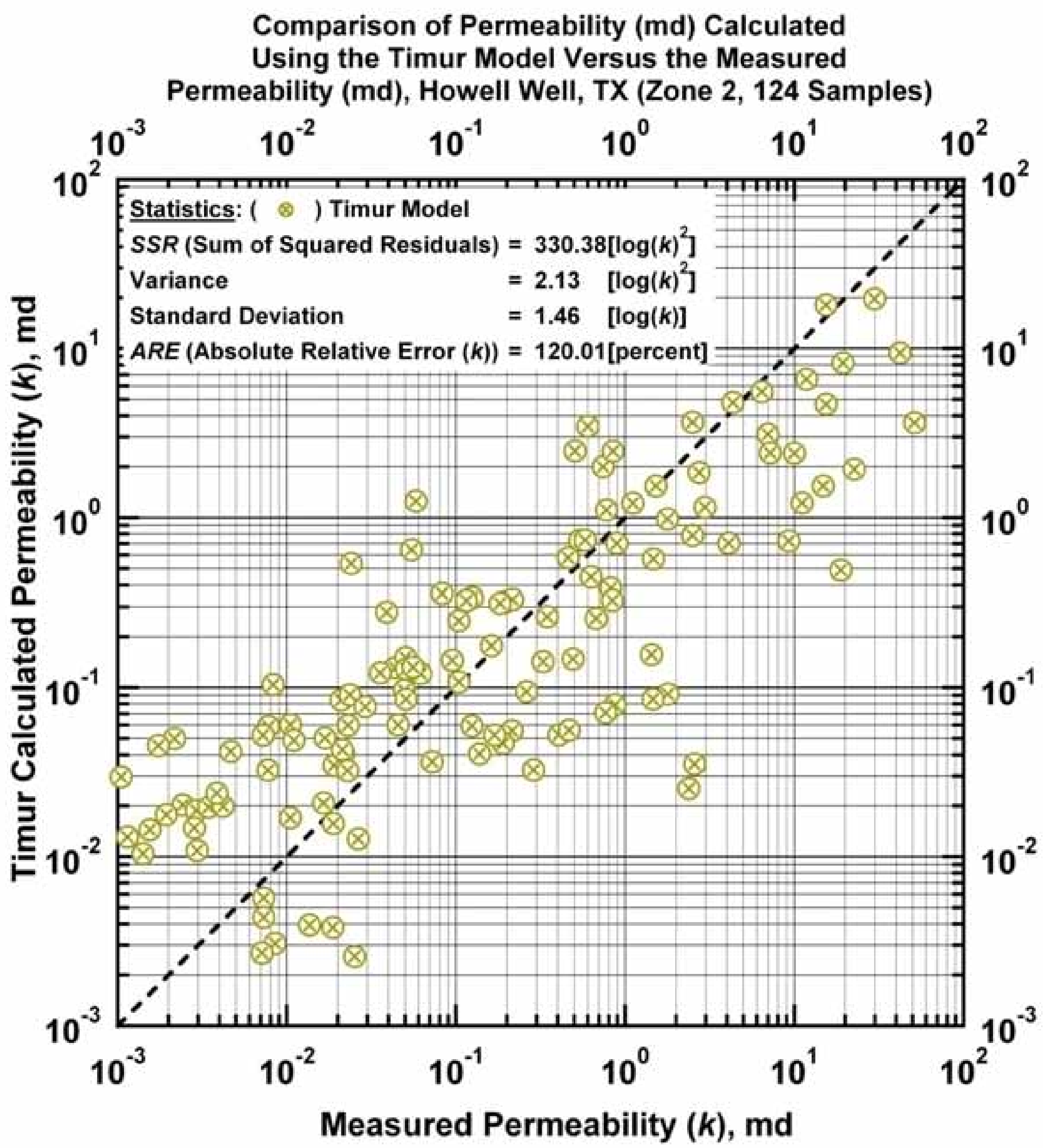

Figure B.36a — "Timur Model:" Calculated versus measured permeability. [*Case*: Howell Well, E. TX (USA)]

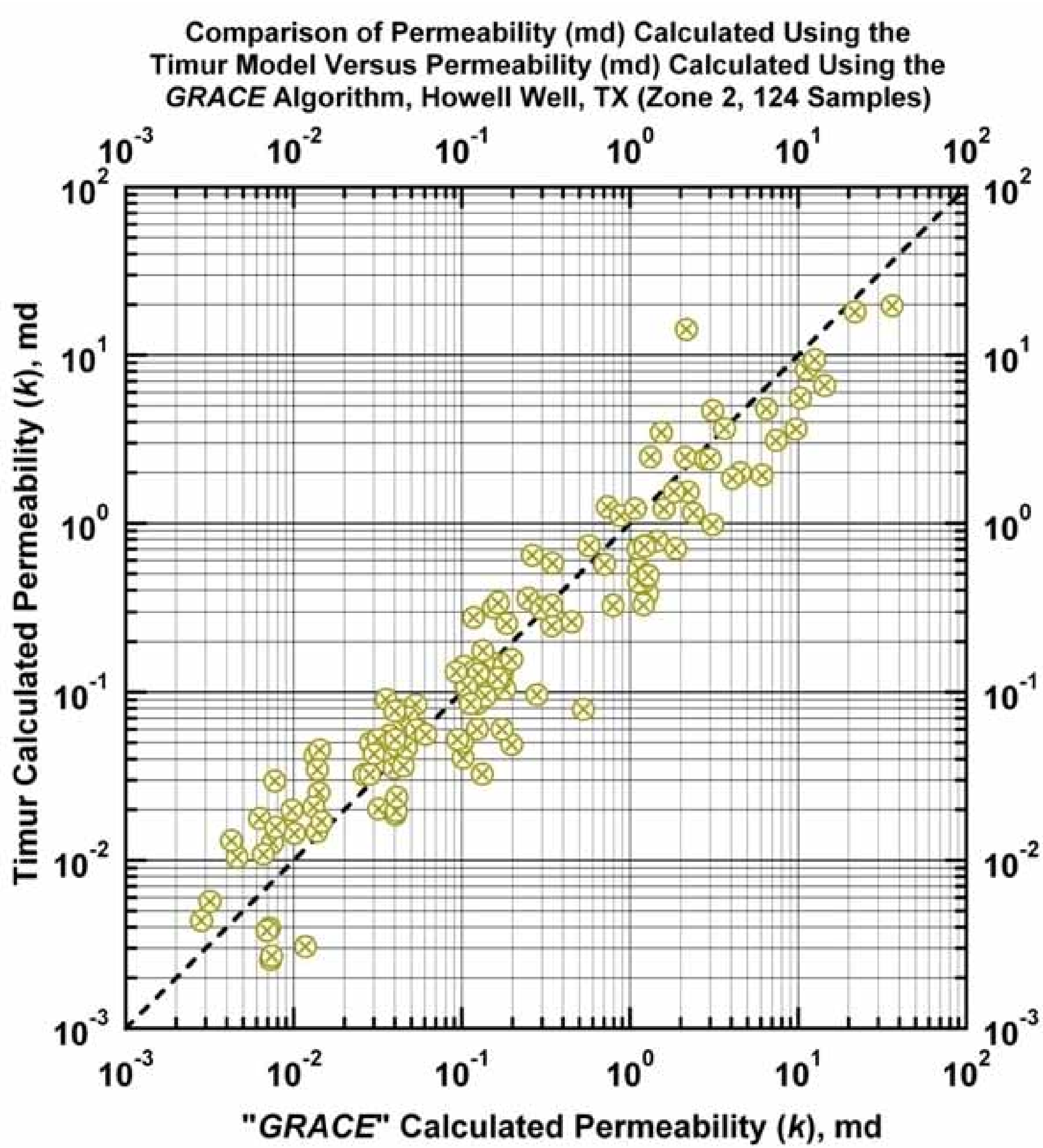

Figure B.36b — "Timur Model:" Permeability calculated using the "Timur Model" versus permeability calculated using the *GRACE* Algorithm. [*Case*: Howell Well, E. TX (USA)]

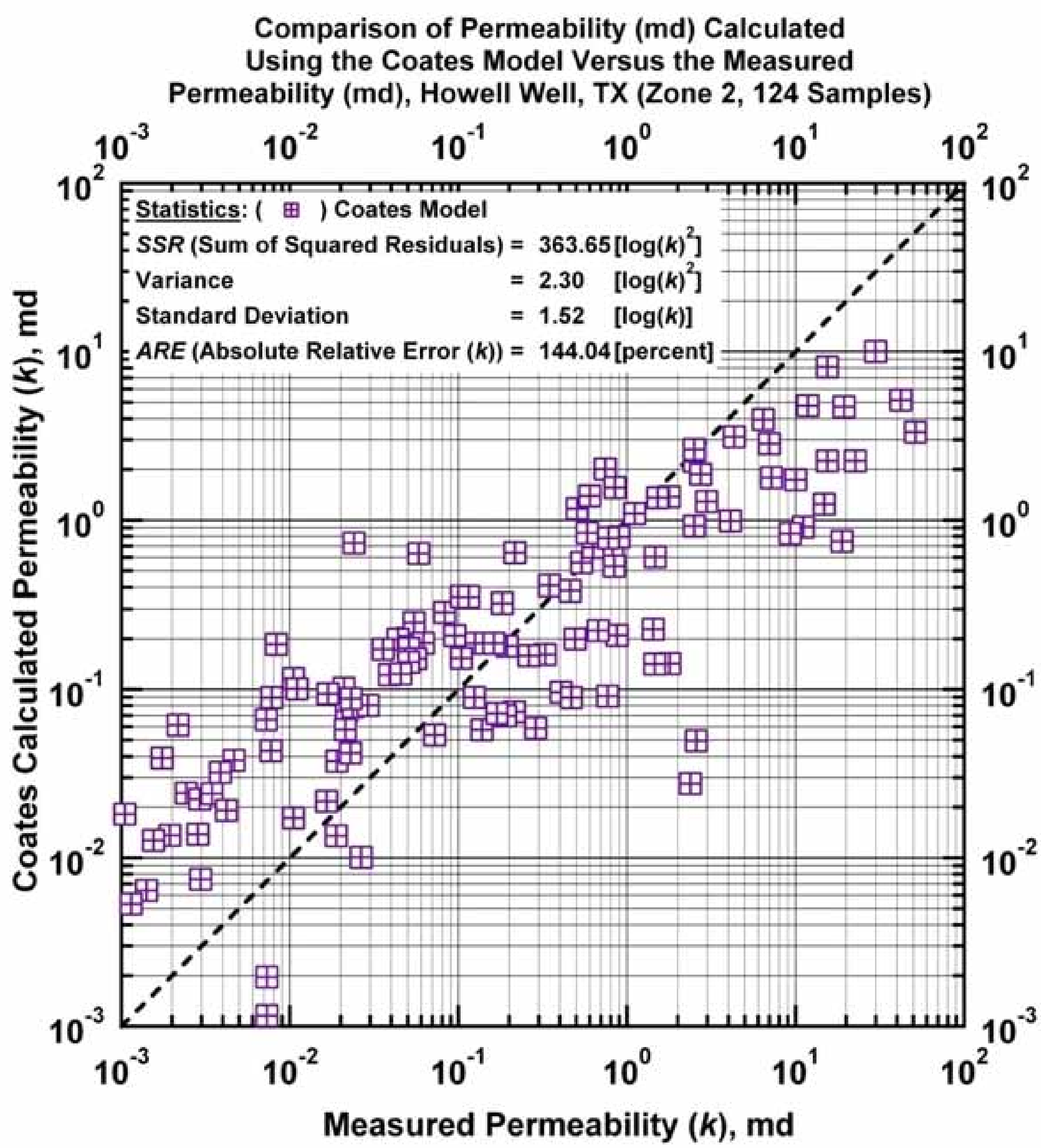

Figure B.37a — "Coates Model:" Calculated versus measured permeability. [*Case*: Howell Well, E. TX (USA)]

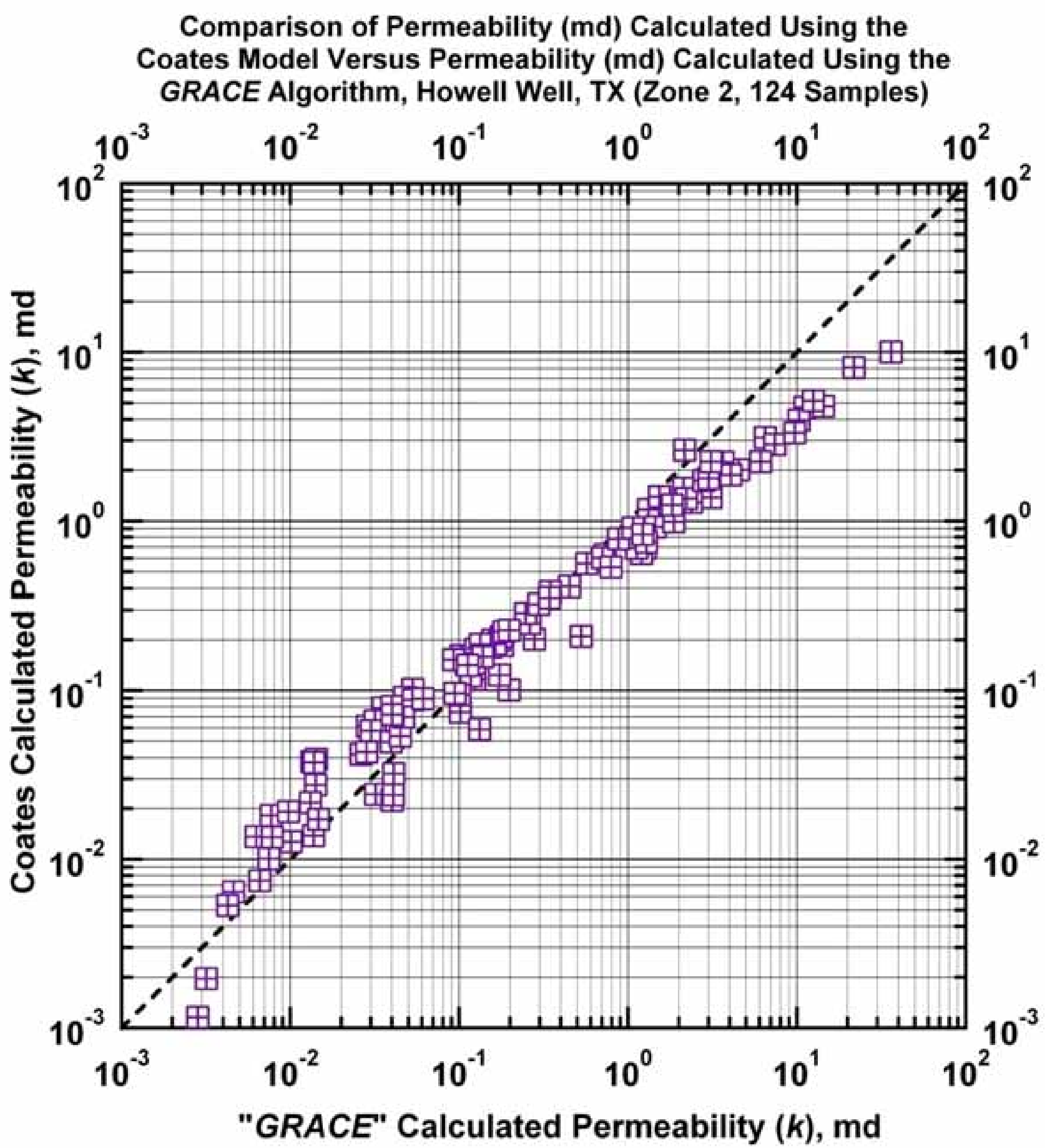

Figure B.37b — "Coates Model:" Permeability calculated using the "Coates Model" versus permeability calculated using the *GRACE* Algorithm. [*Case*: Howell Well, E. TX (USA)]

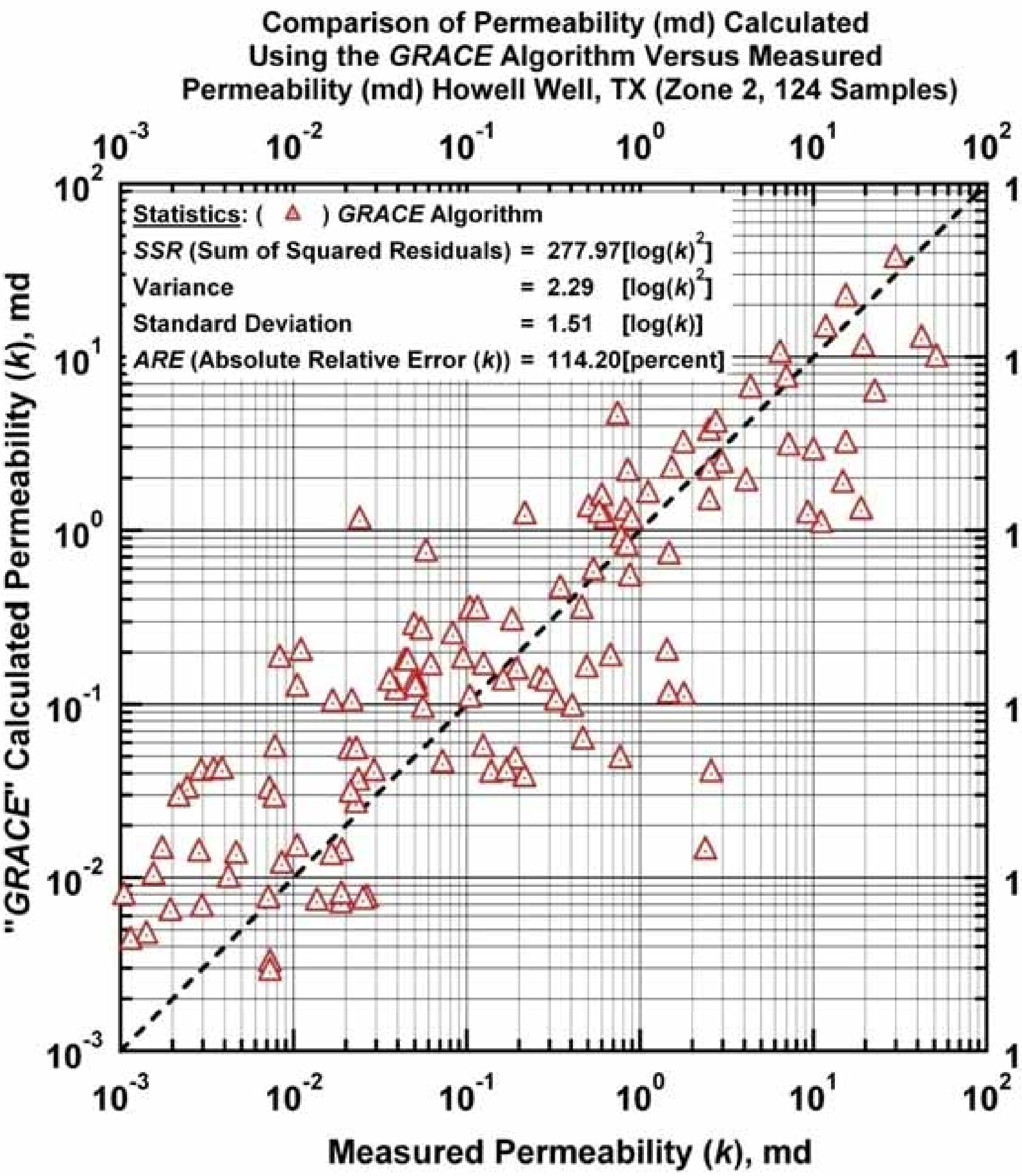

Figure B.38 — *GRACE* Model: Calculated versus measured permeability. [*Case*: Howell Well, E. TX (USA)]

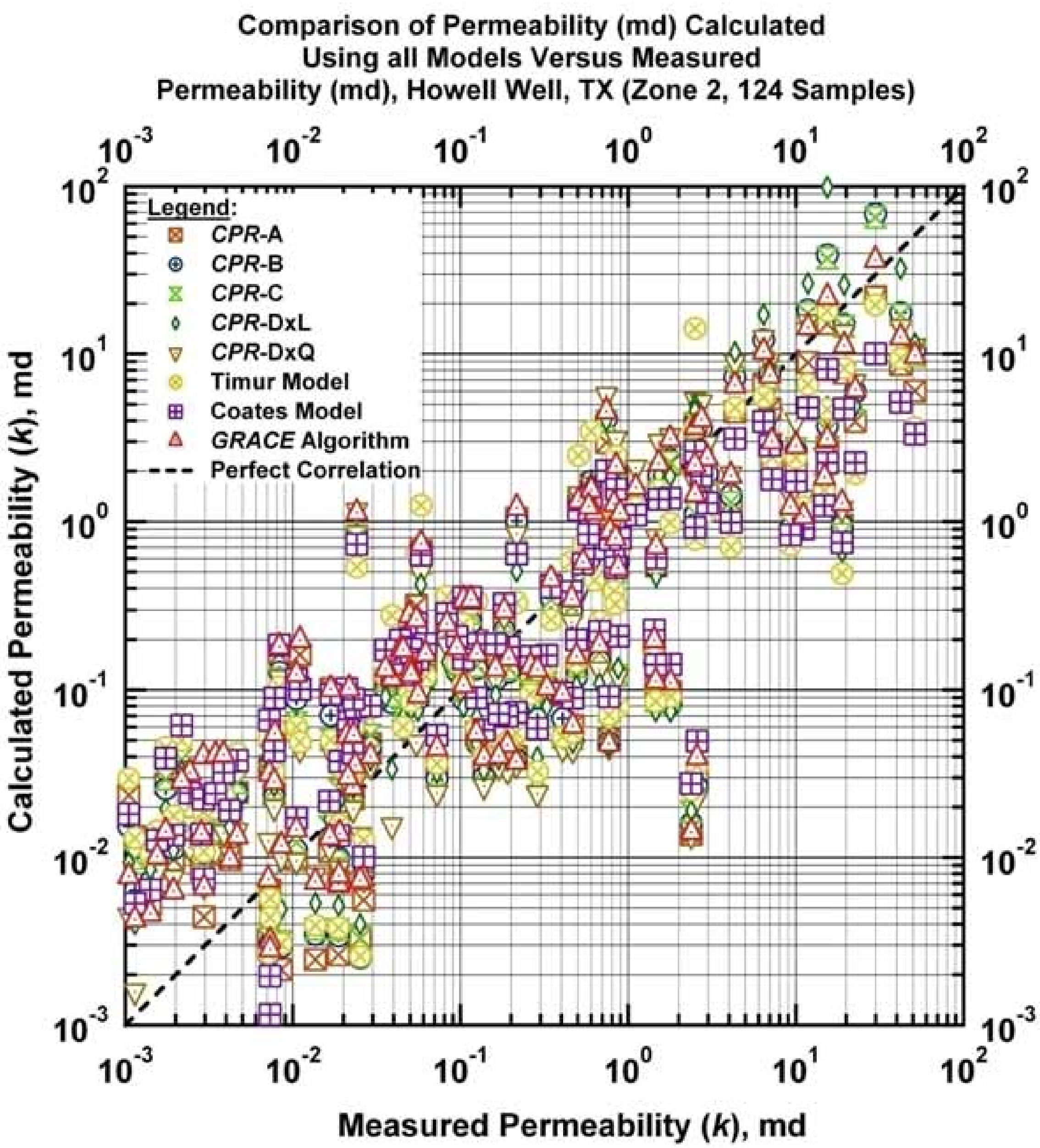

Figure B.39 — All Models: Calculated versus measured permeability. [*Case*: Howell Well, E. TX (USA)]

APPENDIX C

RESULTS FOR MIOCENE SAND

(S. LOUISIANA — USA)

In this Appendix we present the Miocene Sand, located in S. Louisiana (USA — this is a sandstone reservoir (Granberry and Wilshusen (1962)).

Model *CPR-A*: (Appendix C)

The "characteristic permeability relation" (or *CPR*) Model *CPR-A* (*i.e.*, the modified Archie "Clean Sand" Model) is given as:

$$k = a(\phi - c)^b \quad c = c_{max} \exp[-c_1 \phi^{c_2} S_w^{c_3}] \text{ ..... (C-1)}$$

Where a plot of log(k) versus log(ϕ) is used to graphically calibrate Eq. C-1 in terms of the coefficients — a, b, and c_{max}. **Fig. C.1** shows that the *CPR-A* model performs quite well for this case. **Figs. C.1a and b** show the log-log and the semilog format of permeability versus porosity, respectively. In **Fig. C.2** we provide the "error" plots for this case, where the measured and computed data are compared systematically. In **Fig. C.2a** we note a good correlation of the results obtained using Model *CPR-A* versus the measured permeability data — there is good agreement with the perfect correlation trend (*i.e.*, the 45-degree line). In **Fig. C.2b** we provide a comparison with the *GRACE* algorithm correlation (Xue *et al*. 1997)), and we note that the *CPR-A* model results correlate very well with the *GRACE* algorithm results for this case. In **Fig. C.2c** we present the calculated and measured c-function — and we note a deviation of the correlation of the data about the perfect correlation trend. Lastly, in **Fig. C.2d** we present the measured and calculated permeability with depth.

Model *CPR-B*: (Appendix C)

The "characteristic permeability relation" (or *CPR*) Model *CPR-B* (*i.e.*, the modified Archie "Dirty Sand" Model (power-law basis)) is given as:

$$k = a(\phi + c)^b \quad c = c_{max} \exp[-c_1 \phi^{c_2} S_w^{c_3}] \text{ ..... (C-2)}$$

Where a plot of log(k) versus log(ϕ) is used to graphically calibrate Eq. C-2 in terms of the coefficients — a, b, and c_{max}. The results for this case are presented in **Figs. C.3 and 4**. In **Fig. C.3a** (log-log format) we note that a very distinct "envelope" is formed by the *CPR-B* model, essentially all of the data on the right and left flanks are well-matched (*i.e.*, the "dirty sand" power law relation (applied on the right portion of the data) and its correction function (applied on the left portion of the data). Similarly, in **Fig. C.3b** (semilog format), we observe an excellent distribution of the power law model across the body of the data. The error analyses for this case are shown in **Fig. C.4**. In **Fig. C.4a** we present the results obtained using

Model *CPR-B* versus the measured permeability data and in this case there is good agreement with the perfect correlation trend (*i.e.*, the 45-degree line). We provide a comparison with the *GRACE* algorithm correlation in **Fig. C.4b** — the results using Model *CPR-B* and the *GRACE* algorithm compare very well for this case. We compare the computed and data-derived values of the *c*-function for this case in **Fig. C.4c** and we note a reasonably "tight" correlation. Lastly, in **Fig. C.4d** we present the measured and calculated permeability with depth. In summary, we believe that Model *CPR-B* is a very effective correlation model for this particular data case.

Model *CPR-C*: (Appendix C)

The "characteristic permeability relation" (or *CPR*) Model *CPR-C* (*i.e.*, the modified Archie "Dirty Sand" Model (exponential basis)) is given as:

$$k = c\exp[\beta\phi] \quad c = c_{\max}\exp[-c_1\phi^{c_2}S_w^{c_3}] \qquad \text{(C-3)}$$

Where a plot of log(*k*) versus ϕ is used to graphically calibrate Eq. C-3 in terms of the coefficients — β and $c_{\max}$. Model *CPR-C* is fundamentally different than Models *CPR-A* and *CPR-B*, as the basis for Model *CPR-C* is an exponential function, not a power law relation. In **Figs. C.5 and 6** we present the results of applying Model *CPR-C* for this case, and in general, we observe a very consistent performance of Model *CPR-C*. **Fig. C.5b** illustrates the excellent conformance of Model *CPR-C* for this case — again recalling that this model has an exponential relationship with porosity as its basis.

In **Figs. C.6a, C.6b, and C.6c** we review the error analyses plots for this case, and we note good performance (visually) in terms of the correlation of the results using Model *CPR-C*. We believe that the *CPR-C* model has performed well for this case, and **Fig. C.6** confirms the value of this model as a "characteristic relation" for permeability.

Model *CPR-D*: (Appendix C)

The "characteristic permeability relation" (or *CPR*) Model *CPR-D* (*i.e.*, the weighted power law-exponential model) is given in its fundamental form as:

$$k = xa\phi^b + (1-x)\alpha\exp[\beta\phi] \quad [0 \le x \le 1]] \qquad \text{(C-4a)}$$

For Eq. C-4 there are two proposed models for the *x*-function (*i.e.*, the weighting function) — these are:

$$x = \exp[-\ln(x_0) + x_1\ln(\phi) + x_2\ln(S_w) + x_3\ln(\phi)\ln(S_w)] \;\text{(Model } \textit{CPR-DxL}\text{)} \qquad \text{(C-4b)}$$

$$x = \exp\begin{bmatrix} -\ln(x_0) + x_1\ln(\phi) + x_2\ln(S_w) + x_3\ln(\phi)\ln(S_w) \\ + x_4\ln(\phi)^2 + x_5\ln(S_w)^2 + x_6\ln(\phi)^2\ln(S_w) \\ + x_7\ln(\phi)\ln(S_w)^2 + x_8\ln(\phi)^2\ln(S_w)^2 \end{bmatrix} \text{(Model } \textit{CPR-DxL}\text{)} \qquad \text{(C-4c)}$$

As noted in Eq. C-4b, Model *CPR-DxL* utilizes a logarithmic linear model for the weights (*x*-values) and as seen in Eq. C-4c, Model *CPR-DxQ* utilizes a logarithmic quadratic model for the weights (*x*-values). While these models (Eqs. C-4b and C-4c) are *empirical*, we have found generally good application of these relations for all cases. In this case, the base results using Models *CPR-DxL* and *CPR-DxQ* are presented in **Fig. C.7** — where the power law and exponential basis functions are fitted to the appropriate portion of the data. The power law equation represents the "Archie clean sand" trend and is fitted to the leftmost data as shown in **Fig. C.7a** and in contrast, the exponential equation is thought to represent the "Archie dirty sand" trend and the exponential is fitted to the far rightmost portion of the data (see **Fig. C.7b**).

In **Figs. C.8 and 9** we present the error analyses for this case, where we have employed the weighting functions (Eqs. C-4b and C-4c) as appropriate. In **Fig. C.8a** we find a good correlation of permeability (with the out-lying points noted in the middle of the trend). The comparison of the Model *CPR-DxL* results are compared to the results obtained from the *GRACE* algorithm in **Fig. C.8b**, we note the very good the results obtained using Model *CPR-DxL*. The computed weight function (*x*-values) shown for the *CPR-DxL* model in **Fig. C.8c** does exhibit deviation from the perfect correlation line. **Fig. C.8d** provides the measured and calculated permeability versus depth.

The results obtained using Model *CPR-DxQ* are presented in **Fig. C.9**, and we note substantially improved behavior over that of Model *CPR-DxL*. In particular, the base correlation of computed and measured permeabilities (**Fig. C.9a**) for Model *CPR-DxQ* does indicate a slightly better correlation than that of Model *CPR-DxL*. Also, the comparison of Model *CPR-DxQ* with the results from the *GRACE* algorithm (**Fig. C.9b**) exhibits better agreement than the results of Model *CPR-DxL*. Finally, the correlation of the *x*-function (**Fig. C.9c**) for Model *CPR-DxQ* is better than the correlation for Model *CPR-DxL*. These comparisons suggest that Model *CPR-DxQ* (*i.C.*, the combination of Eqs. C-4a and C-4c) has provided a better correlation of data, for this case, than Model *CPR-DxL*. **Fig. C.9d** provides the measured and calculated permeability versus depth.

"Timur Model": (Appendix C)

The "Timur Model" [Timur (1968)] is given as:

$$k_{\text{Timur}} = a\phi^b S_w^c \qquad \text{(C-5)}$$

In **Fig. C.10** we present the results of the "Timur Model" (Eq. C-5) which is essentially just a generalized power-law function relation in terms of k, ϕ, and S_w. As shown in **Figs. C.10a and b**, the "Timur Model" also provides a good correlation of the data for this case. The comparison of results using the "Timur Model" with the results of the *GRACE* algorithm is presented in **Fig. C.10b**.

"Coates Model": (Appendix C)

The "Coates Model" [referenced by Ahmed *et al.* (1989)] is given as:

$$k_{\text{Coates}} = \left[100\phi^2 \frac{(1-S_w)}{S_w}\right]^2 \qquad \text{(C-6)}$$

In **Fig. C.11** we present the results of the "Coates Model" (Eq. C-6) which is essentially just a modified power-law function relation in terms of k, ϕ, and S_w. The results are shown in **Figs. C.11a and b** of the data for this case. The comparison of results using the "Coates Model" with the results of the *GRACE* algorithm (**Fig. C.11b**) is also shown in the same plot.

***GRACE* Algorithm: (Appendix C)**

In **Fig. C.12** we present the results predicted by the *GRACE* algorithm, which is a non-parametric regression approach (see Xue *et al.* (1997) for details). In theory, the *GRACE* algorithm should provide the most *unbiased* correlation of the data — *i.e.*, the *GRACE* algorithm is designed not "fit the errors" as other regression approaches may. It is our contention that the *GRACE* algorithm is the statistical standard — and any algorithm/approach/model which achieves better regression statistics than the *GRACE* algorithm is actually "fitting the errors" in the data. *The only cases which have significantly better regression statistics than the GRACE algorithm are the CPR-A, CPR-DxQ, and "Timur Model"* — hence, we must label these cases as "over-fitted" in a statistical sense.

***Comparison of All Models*: (Appendix C)**

Fig. C.13, illustrates all of the models on a single plot of calculated versus measured permeability. We also present a table of all statistical results in **Table C.1**. Our final plot, **Fig. C.14** shows the source of the original data set.

Table C.1 — Statistical Results for all Models (Miocene Sand, S. LA (USA), *n*=24).

Model	Sum of Squared Residuals [log(k)^2]	Variance [log(k)^2]	Standard Deviation [log(k)]	Absolute Relative Error [percent]
CPR-A	7.18	3.50	1.87	48.68
CPR-B	7.37	3.43	1.85	50.71
CPR-C	7.54	3.74	1.93	50.03
CPR-DxL	7.56	3.35	1.83	55.51
CPR-DxQ	6.30	3.42	1.85	48.03
Timur	7.16	3.72	1.93	45.13
Coates	8.05	3.56	1.89	54.08
GRACE Algorithm	11.02	2.02	1.42	49.81

The coefficients for the models used in this case are provided in **Table C.2**.

Table C.2a — Model Coefficients (Miocene Sand, S. LA (USA), *n*=24).

Model	a or α	b or β	c or c_{max}	c_1	c_2	c_3
CPR-A	$3.00\text{x}10^{8}$	9.00	0.060	1.38	1.44	-0.97
CPR-B	$5.00\text{x}10^{6}$	8.00	0.100	$3.71\text{x}10^{-4}$	-6.60	1.38
CPR-C	$5.00\text{x}10^{-8}$	83.00	$2.00\text{x}10^{-6}$	576.54	3.77	0.44
Timur	$8.49\text{x}10^{9}$	12.93	0.738	–	–	–
Coates	$5.67\text{x}10^{6}$	8.74	1.383	–	–	–

Table C.2b — Model Coefficients (Miocene Sand, S. LA (USA), *n*=24).

Model	a	b	α	β
CPR-DxL	3.00×10^{8}	9.00	5.00×10^{-8}	83.00
CPR-DxQ	3.00×10^{8}	9.00	5.00×10^{-8}	83.00

Model	c_0	c_1	c_2	c_3	c_4	c_5	c_6	c_7	c_8
CPR-DxL	1.00×10^{7}	-8.45	-16.93	-10.38	–	–	–	–	–
CPR-DxQ	1.00×10^{4}	-89.82	33.70	-107.30	-51.68	54.75	-76.99	-0.09	-19.92

Nomenclature: (Appendix C)

S_w = Water Saturation (fraction)
k = Formation Permeability, md (or any consistent units)
ϕ = Porosity, fraction

References: (Appendix C)

Ahmed, U., Crary, S.F., and Coates, G.R: "Permeability Estimation: The Various Sources and Their Interrelationship," paper SPE 19604 presented at the 1989 SPE Annual Technical Conference and Exhibition, San Antonio, TX, 8-11 Oct., 649-662.

Granberry, R.J., and Wilshusen, R.C.: "Improved Interpretation of Formation Productivity by Combined Use of Core Analysis and Electronic Log Data," *Trans.*, Gulf Coast Association of Geological Societies (1962) 13, 213-221.

Timur, A.: "An Investigation of Permeability, Porosity, and Residual Water Saturation Relation-ships," *Trans.*, SPWLA Symposium (1968) paper I.

Xue, G., Datta-Gupta, A., Valko, P., and Blasingame, T.A.: "Optimal Transformations for Multiple Regression: Application to Permeability Estimation from Well Logs," *SPEFE* (June 1997), 85-93.

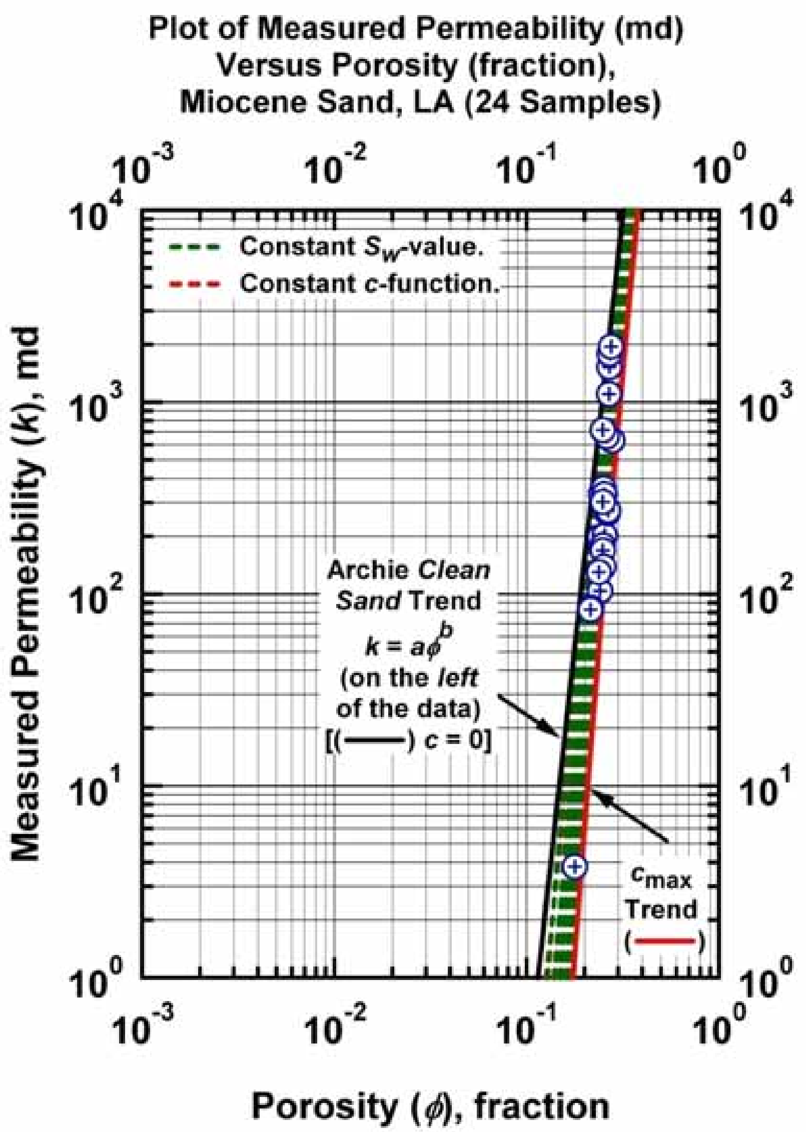

Figure C.1a — Model *CPR-A*: $k = a(\phi - c)^b \quad c = c_{\max}\exp[-c_1\phi^{c_2} S_w^{c_3}]$ — "Clean Sand" Plot (log-log format) — Archie "Clean Sand" trend is given by the straight-line trend at the far left of the data (power law model). [*Case*: Miocene Sand, S. LA (USA)]

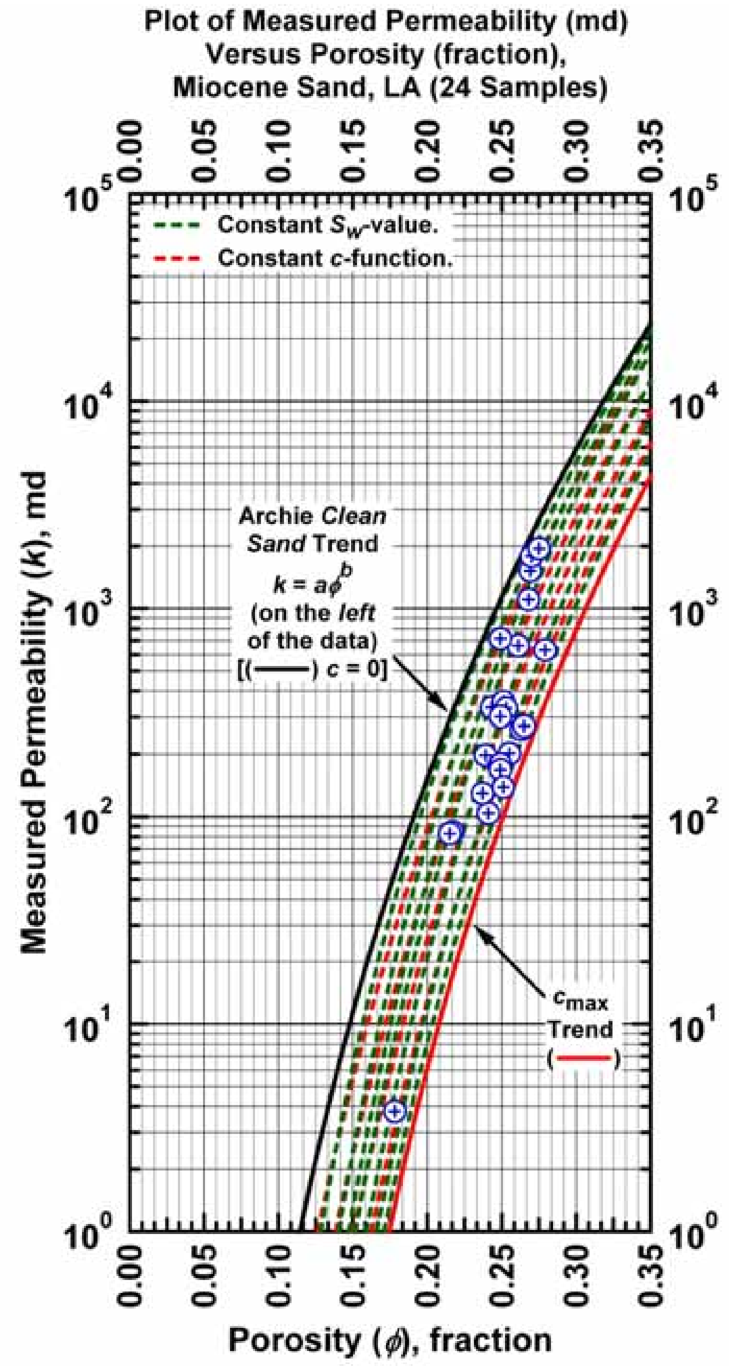

Figure C.1b — Model *CPR-A*: $k = a(\phi - c)^b$ $\quad c = c_{\max}\exp[-c_1\phi^{c_2} S_w^{c_3}]$ — "Dirty Sand" Plot (semilog format). Archie "Clean Sand" trend is given by the curved trend at the far left of the data (power law model). [*Case*: Miocene Sand, S. LA (USA)]

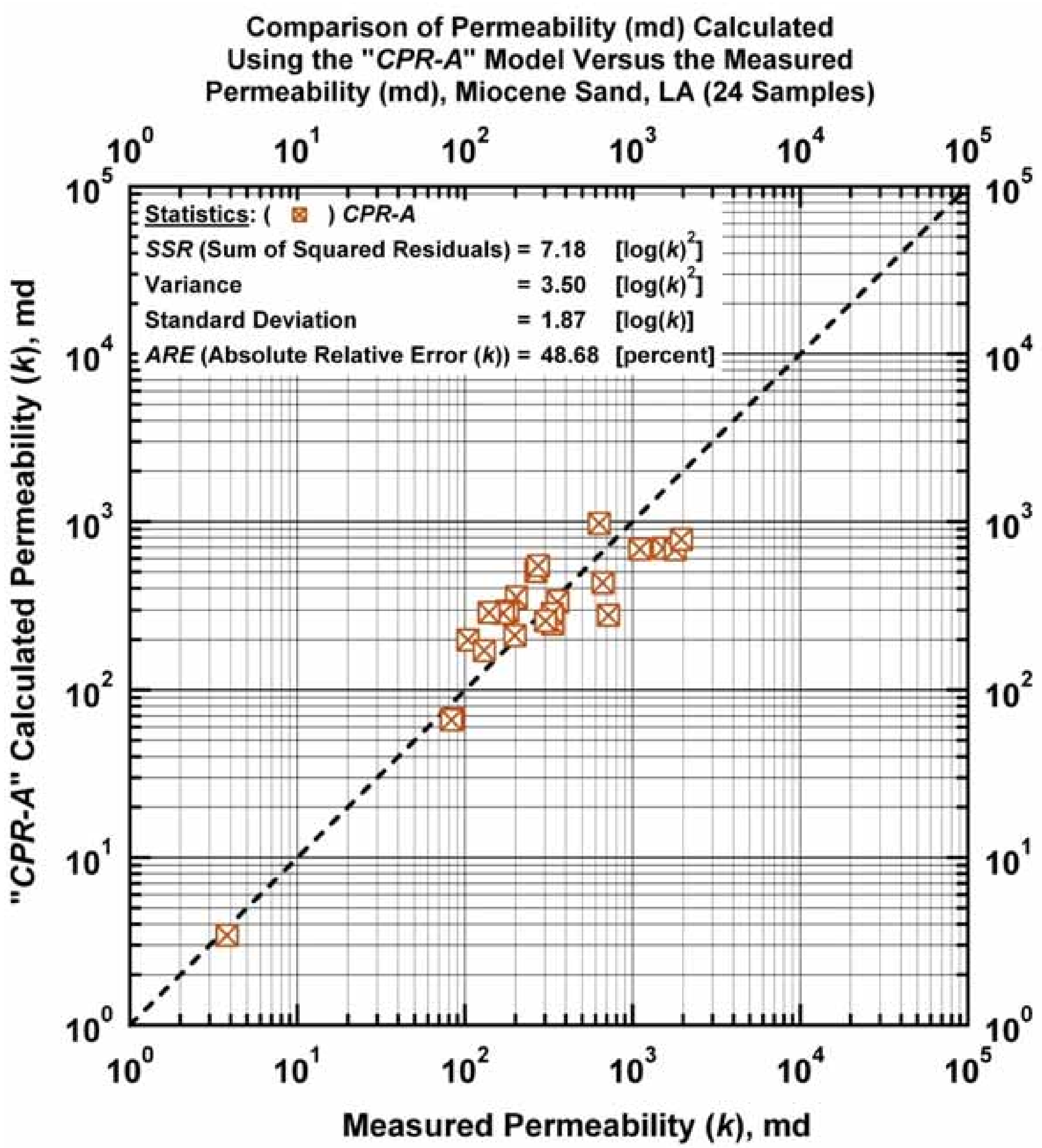

Figure C.2a — Model *CPR-A*: calculated versus measured permeability. [*Case*: Miocene Sand, S. LA (USA)]

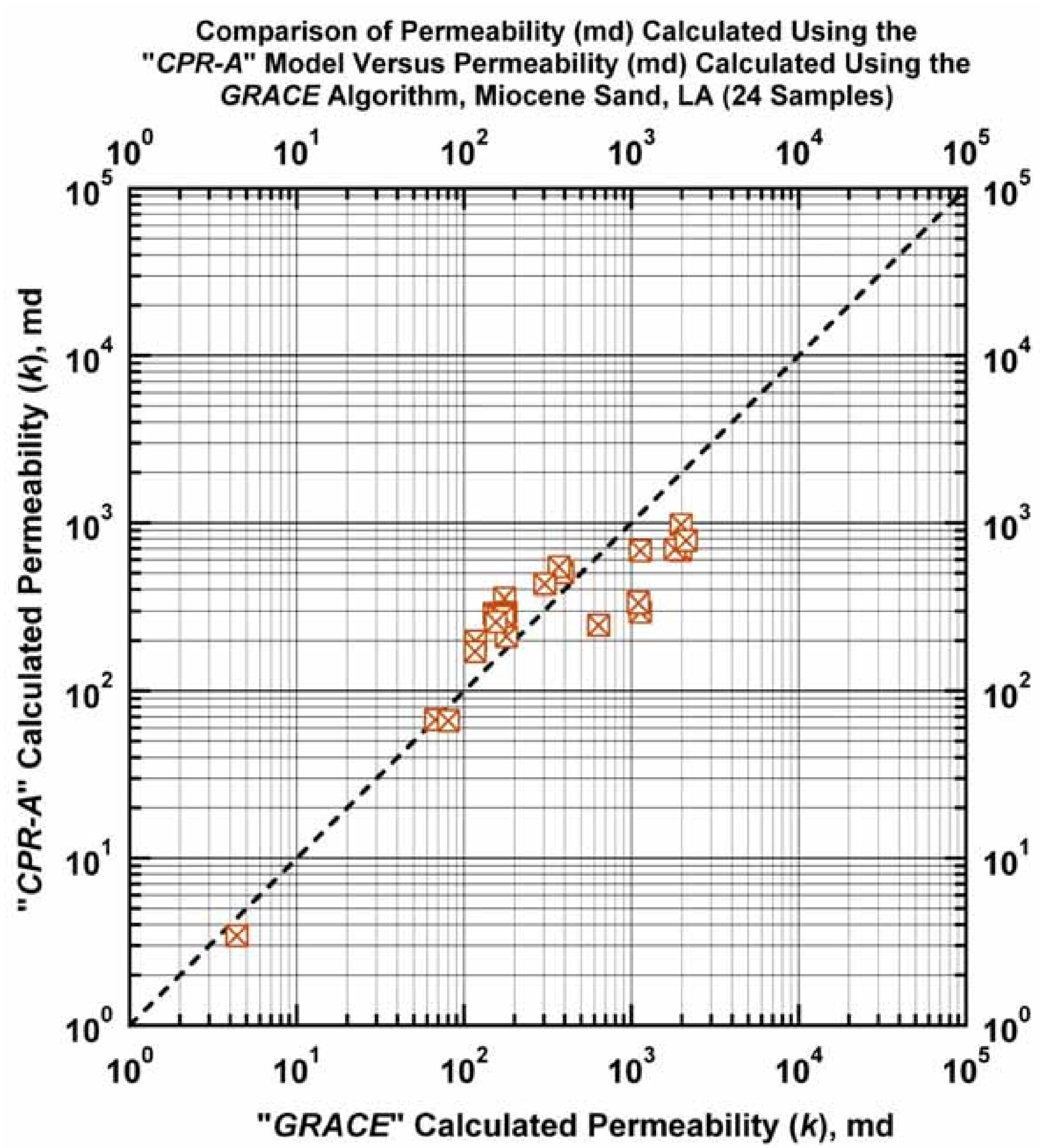

Figure C.2b — Model *CPR-A*: Permeability calculated using Model *CPR-A* versus permeability calculated using the *GRACE* Algorithm. [*Case*: Miocene Sand, S. LA (USA)]

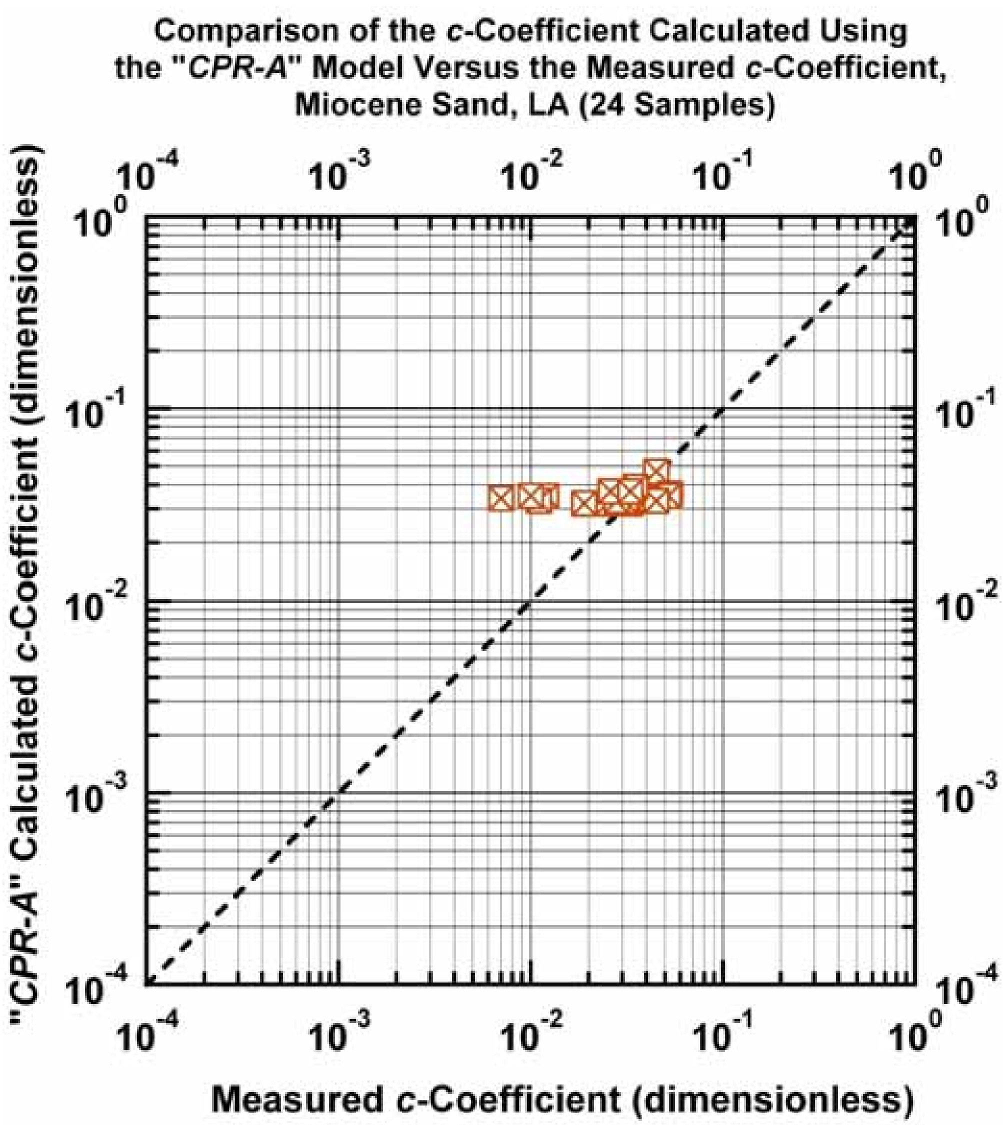

Figure C.2c — Model *CPR-A*: Calculated *c*-function values versus measured *c*-function values. [*Case*: Miocene Sand, S. LA (USA)]

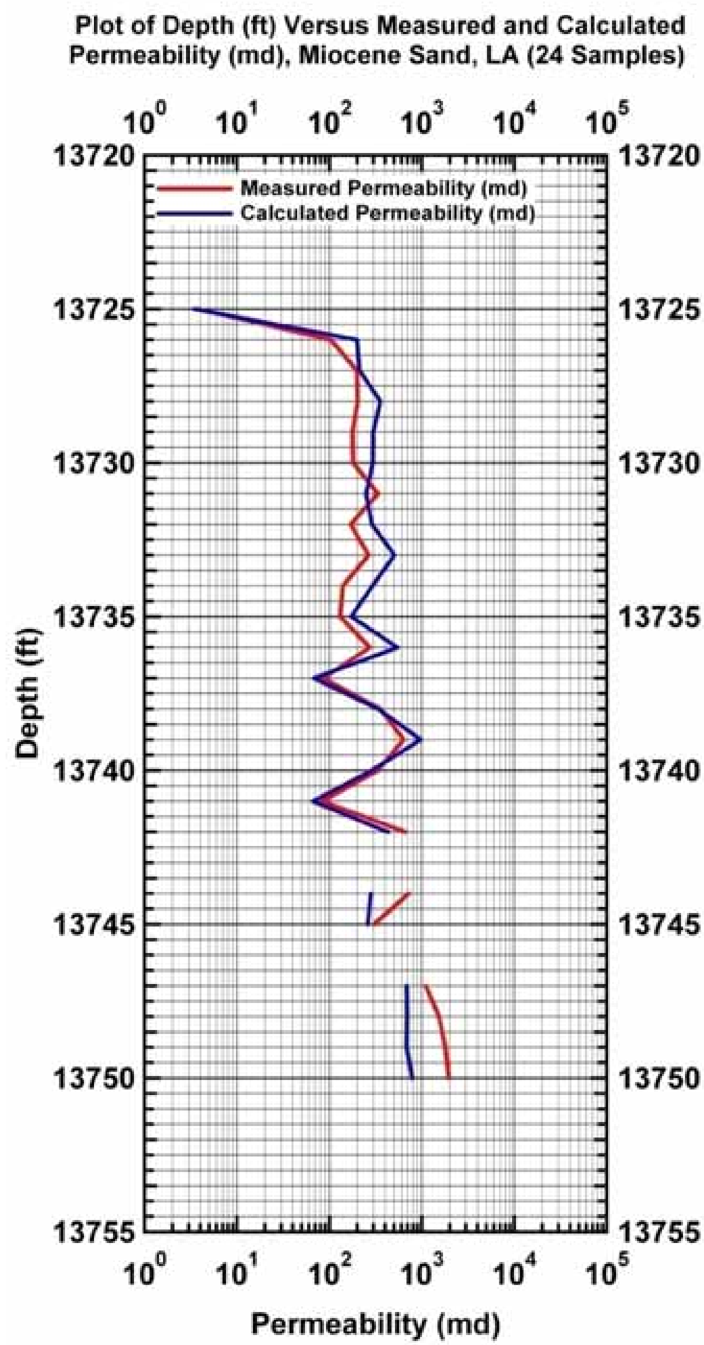

Figure C.2d — Model *CPR-A*: Calculated and measured permeability values versus depth. [*Case*: Miocene Sand, S. LA (USA)]

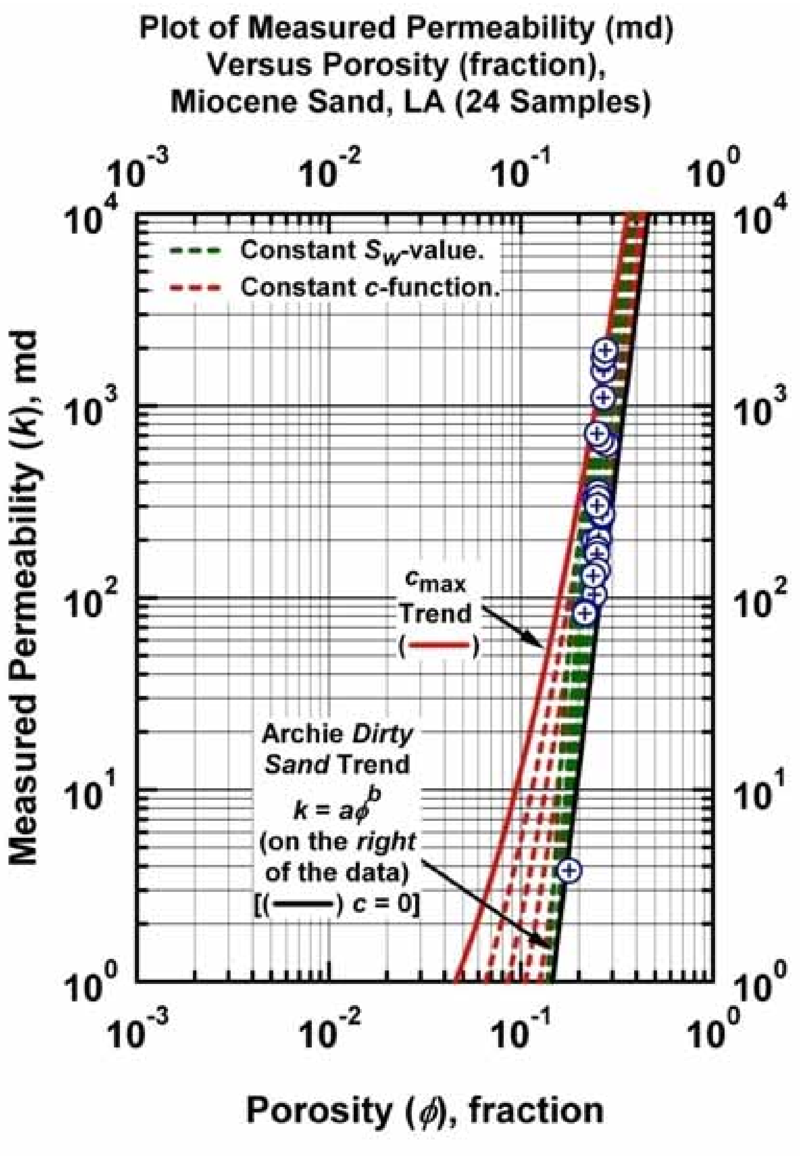

Figure C.3a — Model *CPR-B*: $k = a(\phi + c)^b$ $\quad c = c_{max} \exp[-c_1 \phi^{c_2} S_w^{c_3}]$ — "Clean Sand" Plot (log-log format) — Archie "Dirty Sand" trend is given by the straight-line trend at the far right of the data (power law model). [*Case*: Miocene Sand, S. LA (USA)]

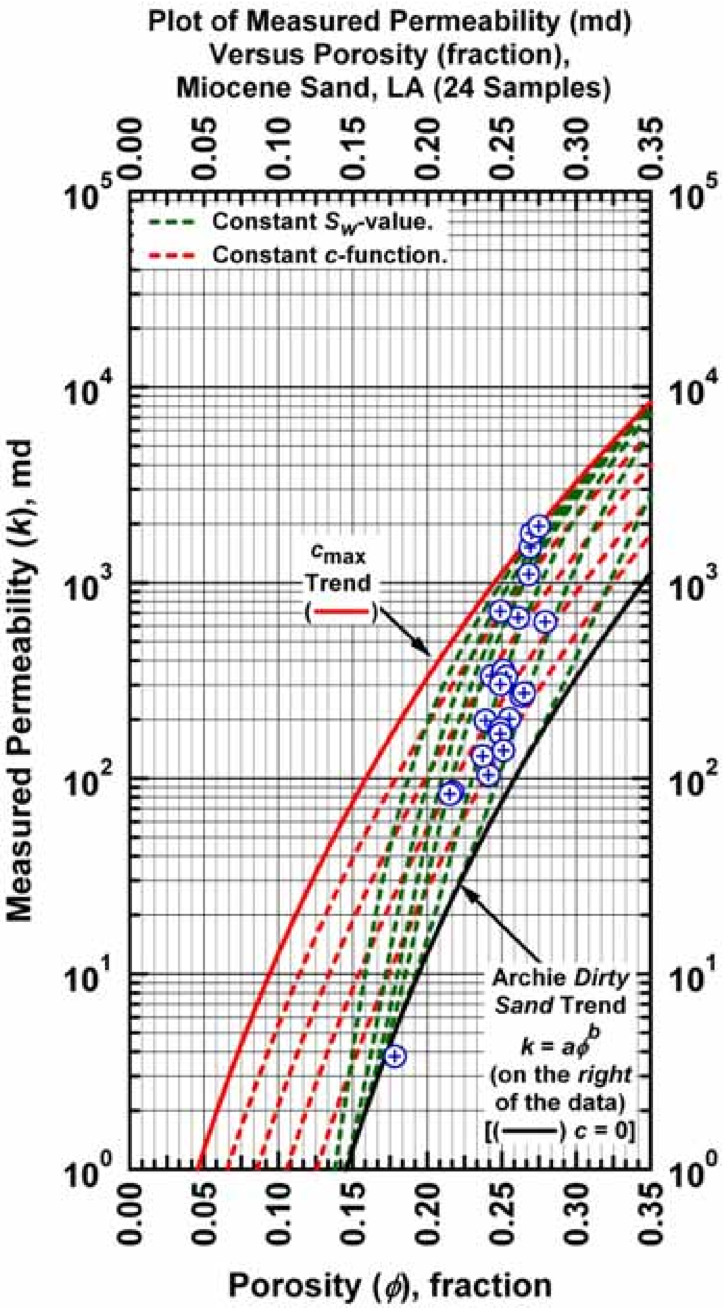

Figure C.3b — Model *CPR-B*: $k = a(\phi + c)^b$ $\quad c = c_{\max} \exp[-c_1 \phi^{c_2} S_w^{c_3}]$ — "Dirty Sand" Plot (semilog format) — Archie "Dirty Sand" trend is given by the curved trend at the far right of the data (power law model). [*Case*: Miocene Sand, S. LA (USA)]

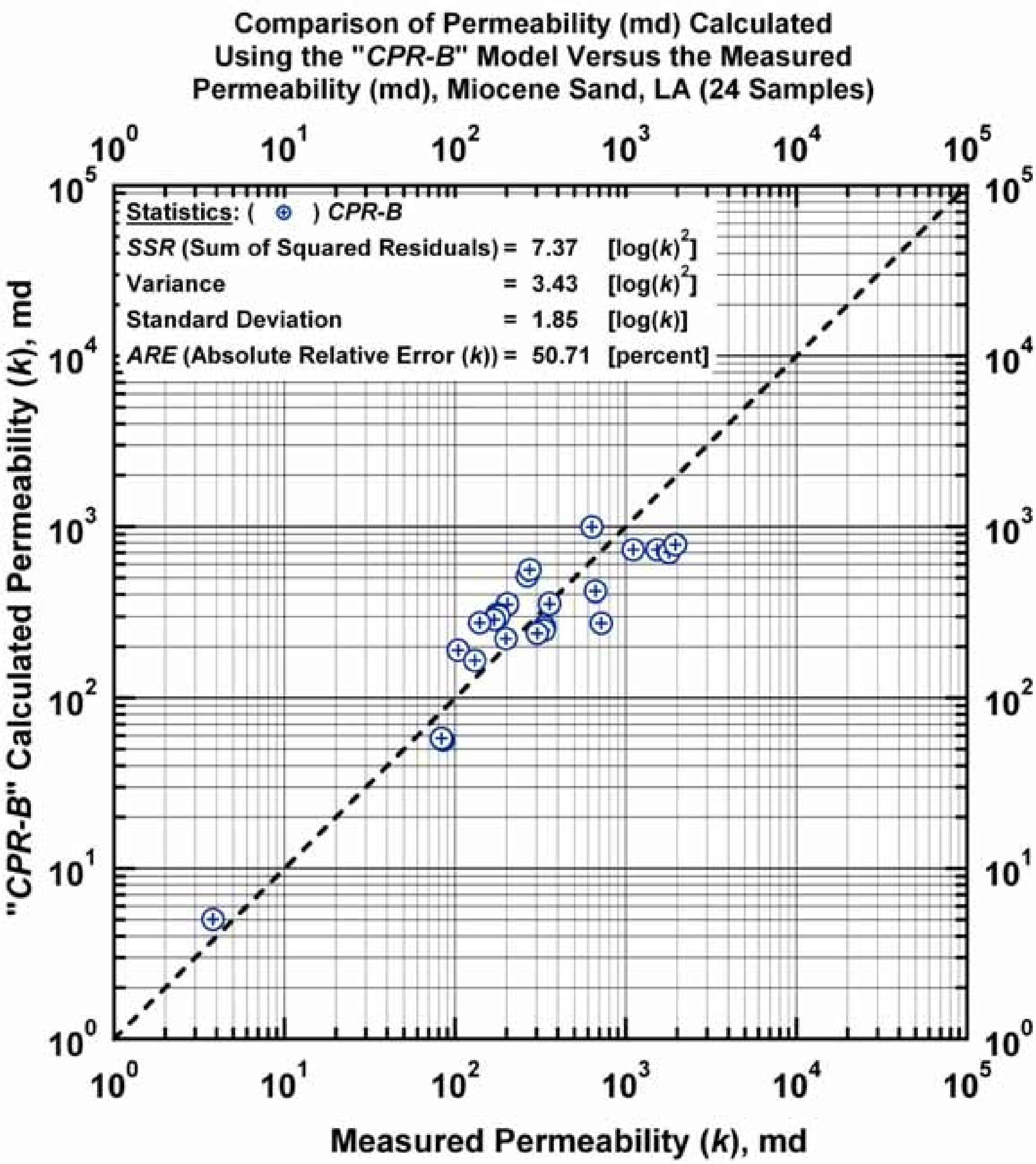

Figure C.4a — Model *CPR-B*: calculated versus measured permeability. [*Case*: Miocene Sand, S. LA (USA)]

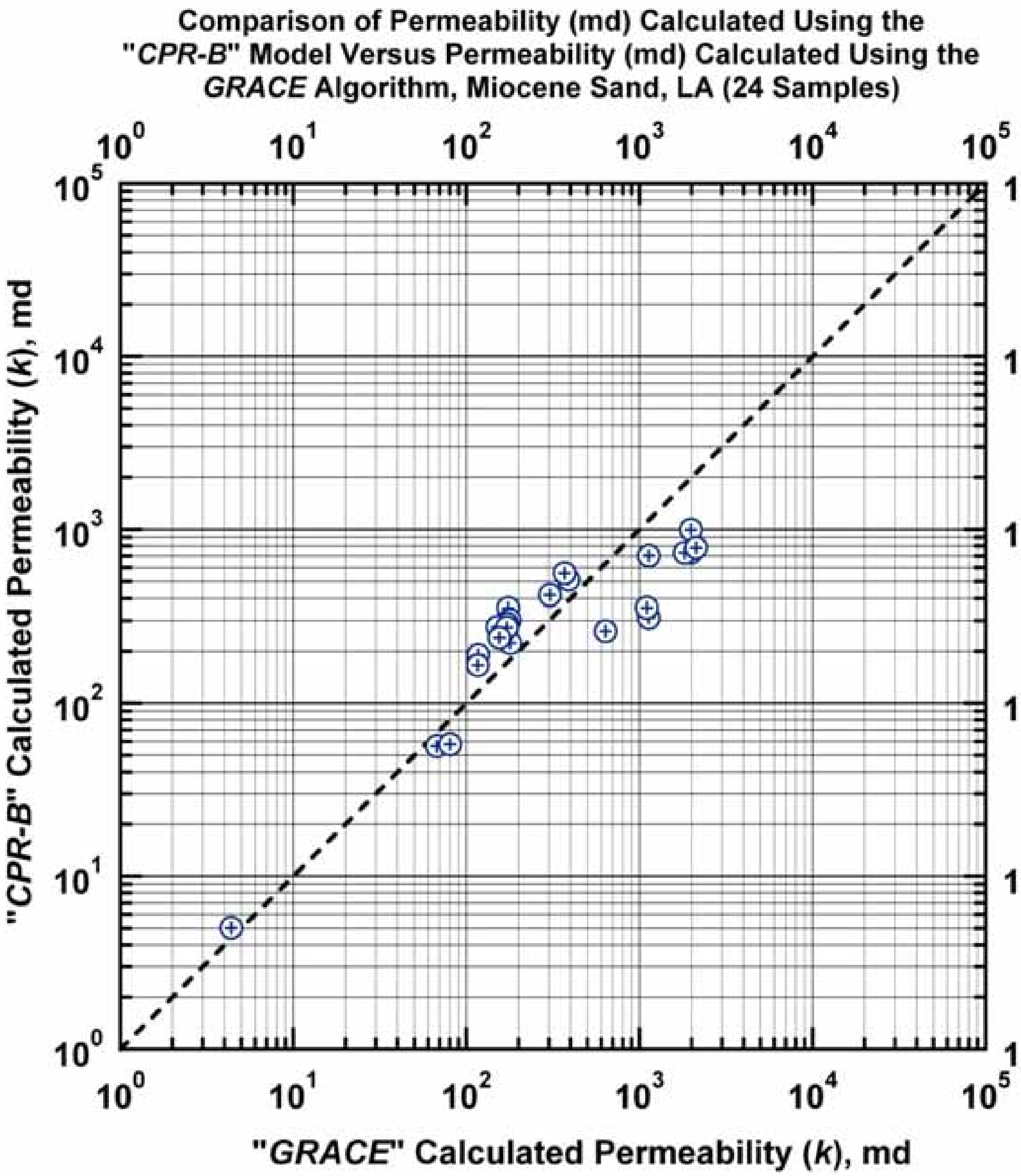

Figure C.4b — Model *CPR-B*: Permeability calculated using Model *CPR-B* versus permeability calculated using the *GRACE* Algorithm. [*Case*: Miocene Sand, S. LA (USA)]

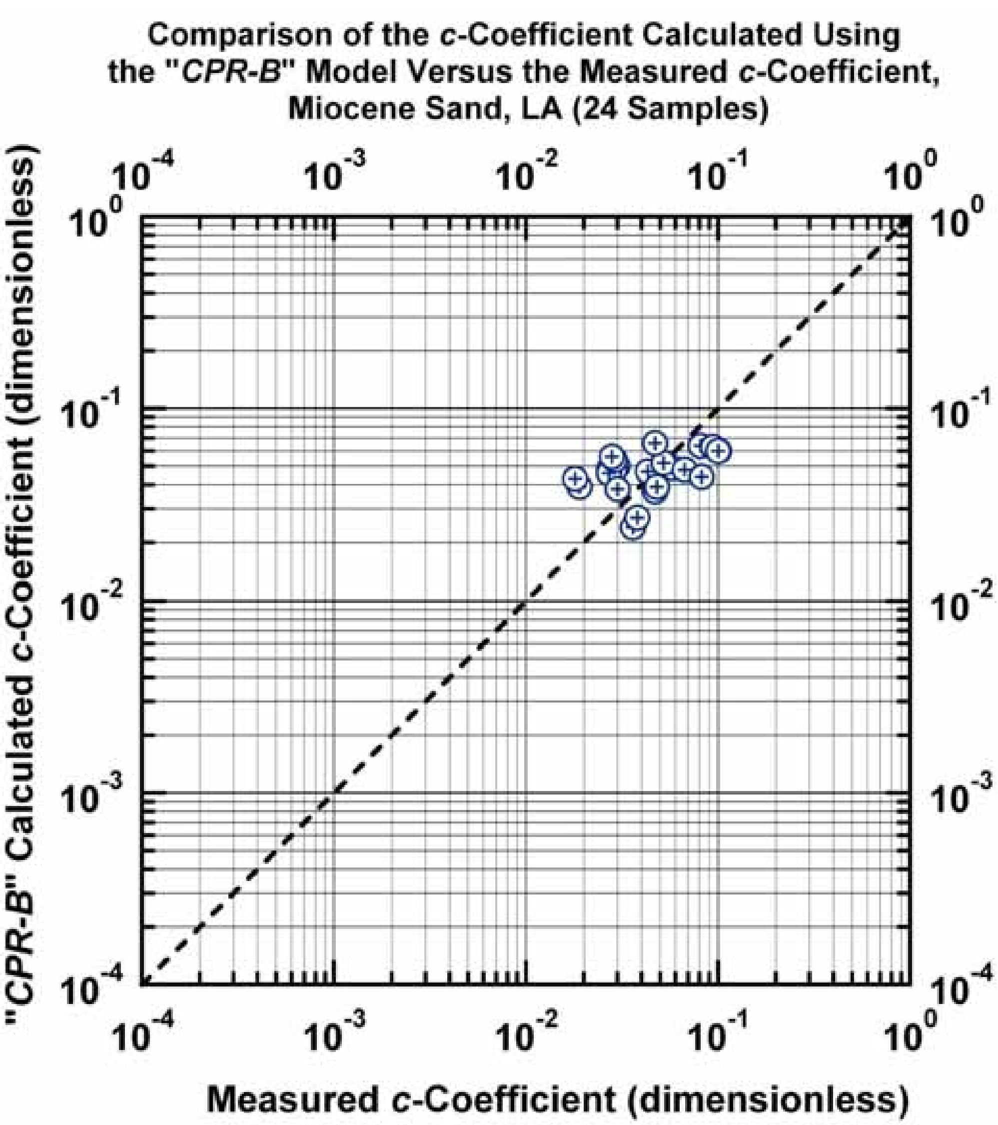

Figure C.4c — Model *CPR-B*: Calculated *c*-function values versus measured *c*-function values. [*Case*: Miocene Sand, S. LA (USA)]

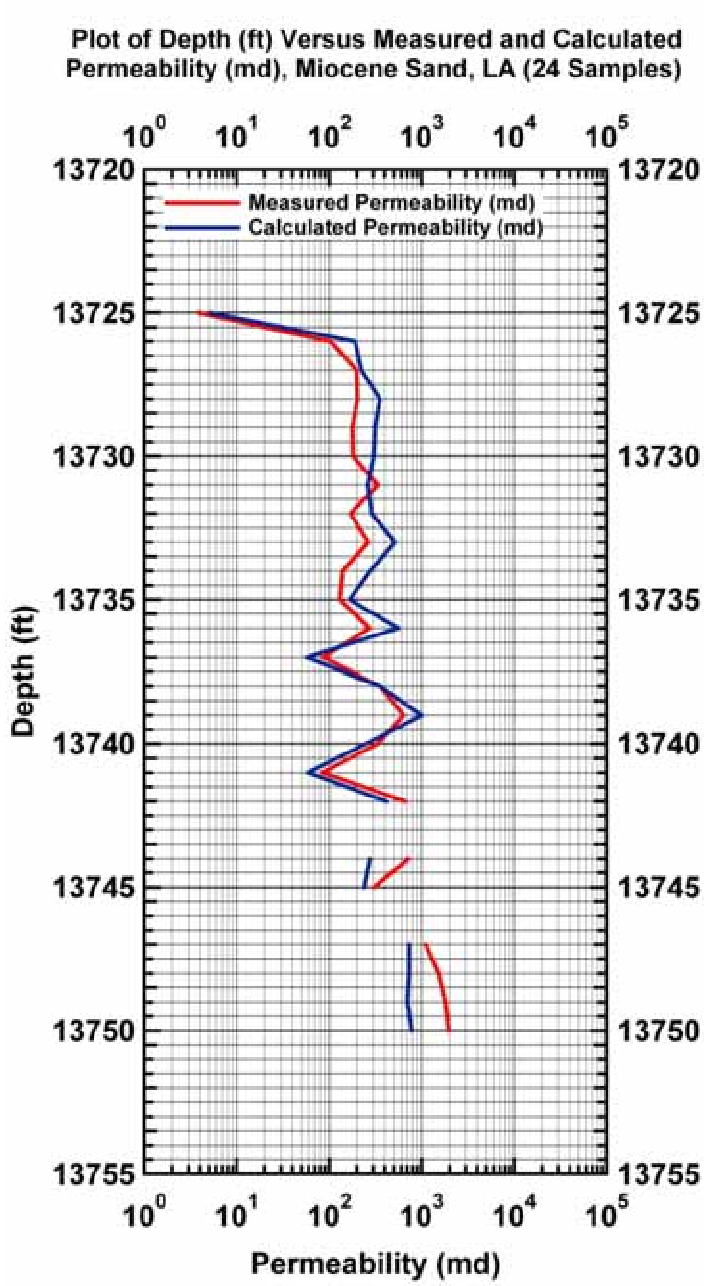

Figure C.4d — Model *CPR-A*: Calculated and measured permeability values versus depth. [*Case*: Miocene Sand, S. LA (USA)]

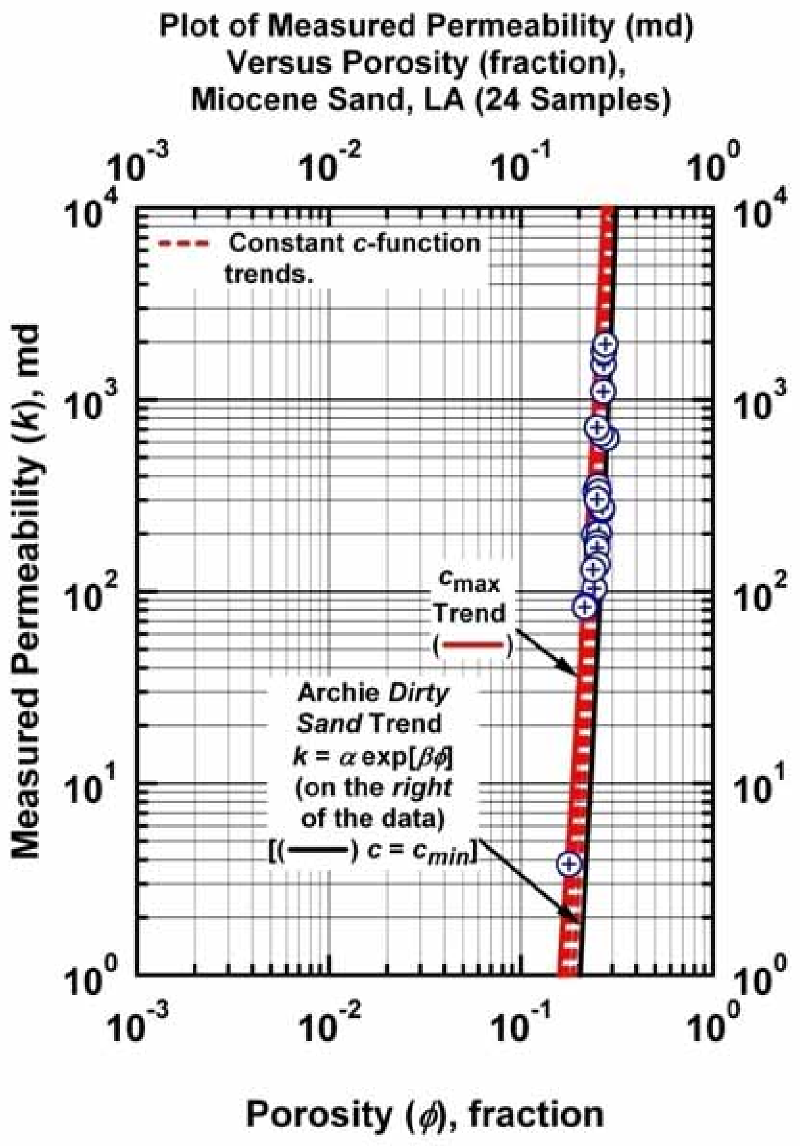

Figure C.5a — Model *CPR-C*: $k = c\exp[\beta\phi]$ $\quad c = c_{\max}\exp[-c_1\phi^{c_2} S_w^{c_3}]$ — "Clean Sand" Plot (log-log format) — Archie "Dirty Sand" trend is given by the curved trend at the far right of the data (exponential model). [*Case*: Miocene Sand, S. LA (USA)]

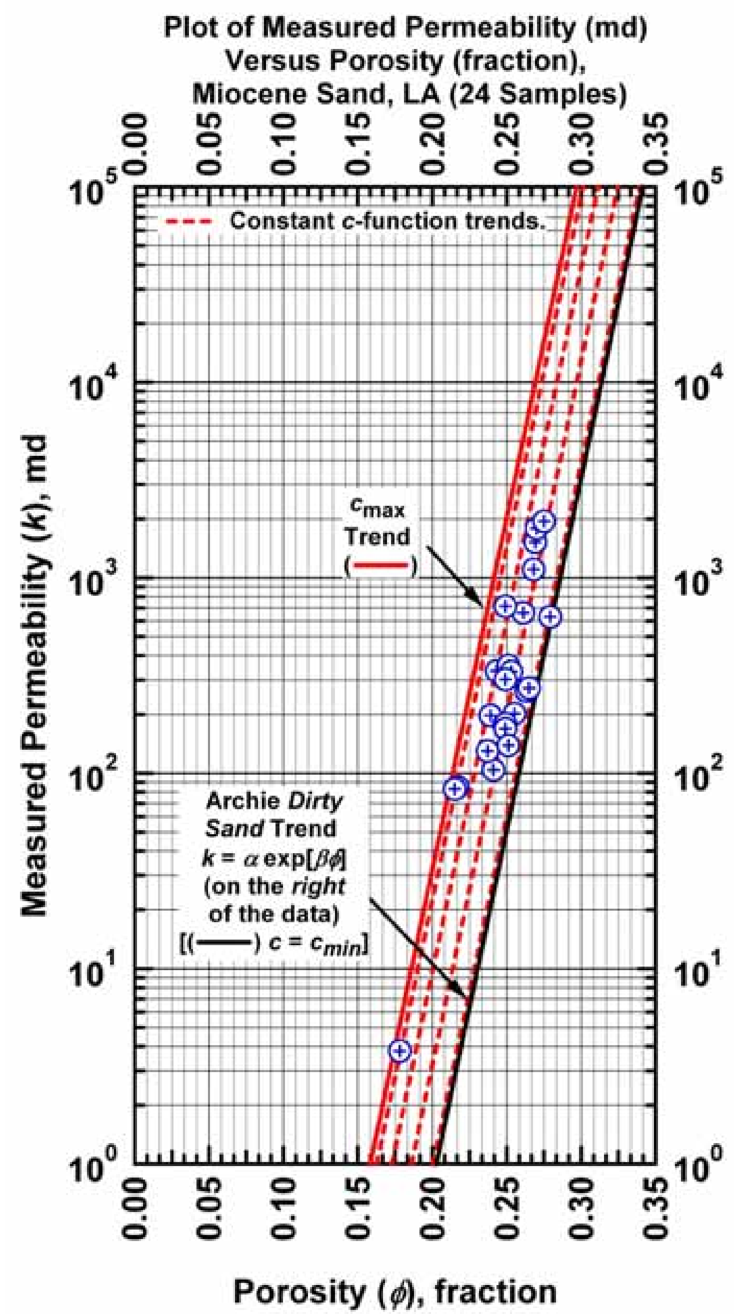

Figure C.5b — Model *CPR-C*: $k = c\exp[\beta\phi]$ $\quad c = c_{\max}\exp[-c_1\phi^{c_2} S_w^{c_3}]$ — "Dirty Sand" Plot (semilog format) — Archie "Dirty Sand" trend is given by the straight-line trend at the far right of the data (exponential model). [*Case*: Miocene Sand, S. LA (USA)]

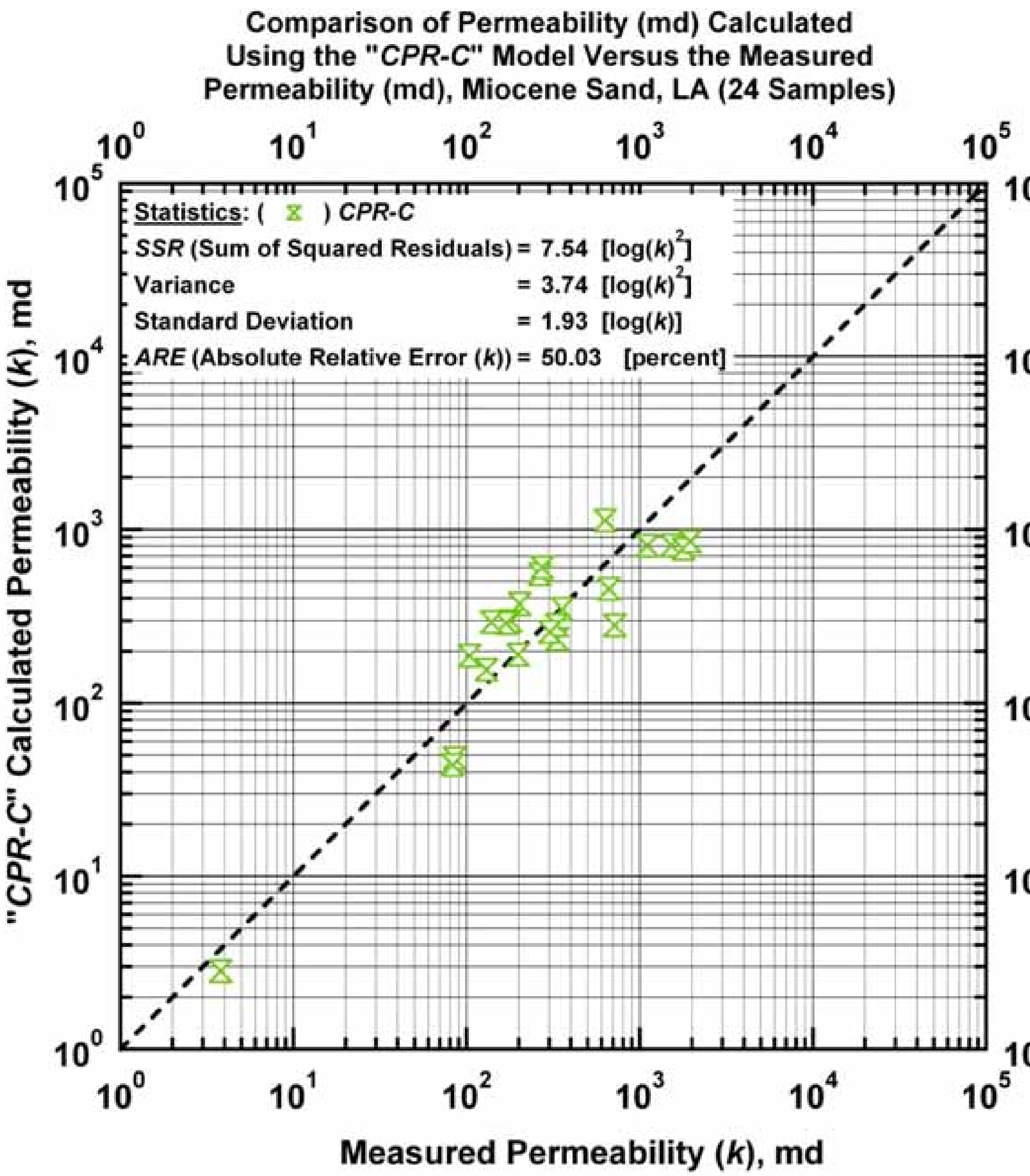

Figure C.6a — Model *CPR-C*: calculated versus measured permeability. [*Case*: Miocene Sand, S. LA (USA)]

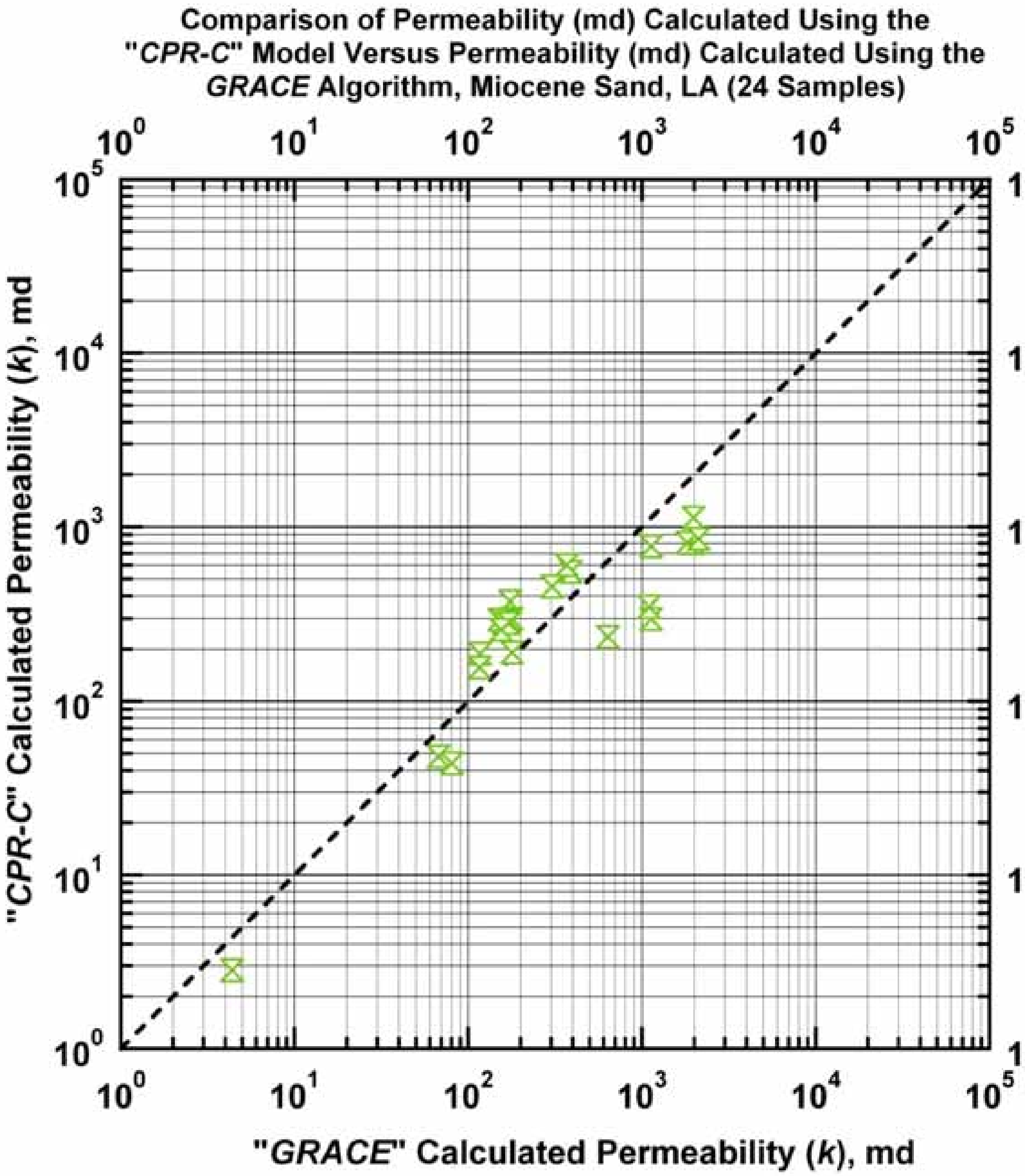

Figure C.6b — Model *CPR-C*: Permeability calculated using Model *CPR-C* versus permeability calculated using the *GRACE* Algorithm. [*Case*: Miocene Sand, S. LA (USA)]

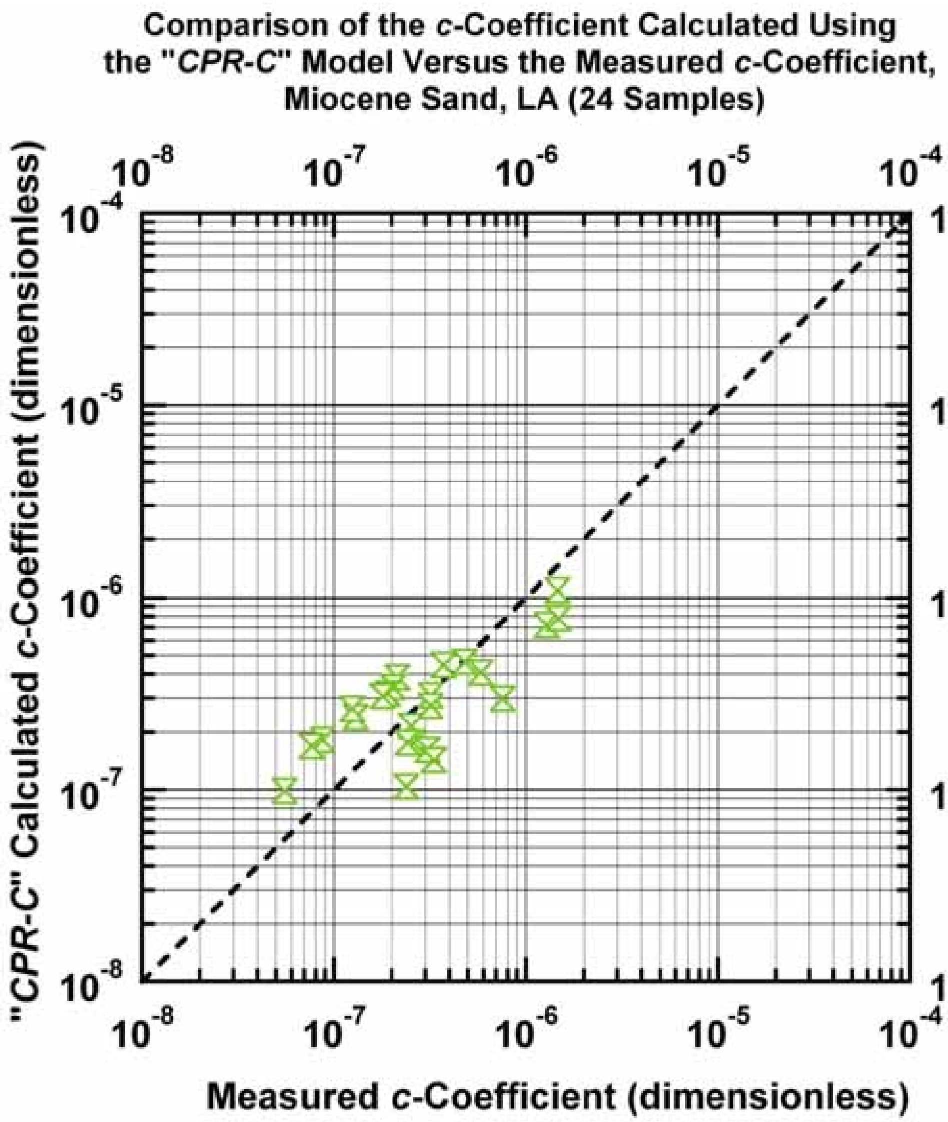

Figure C.6c — Model *CPR-C*: Calculated *c*-function values versus measured *c*-function values. [*Case*: Miocene Sand, S. LA (USA)]

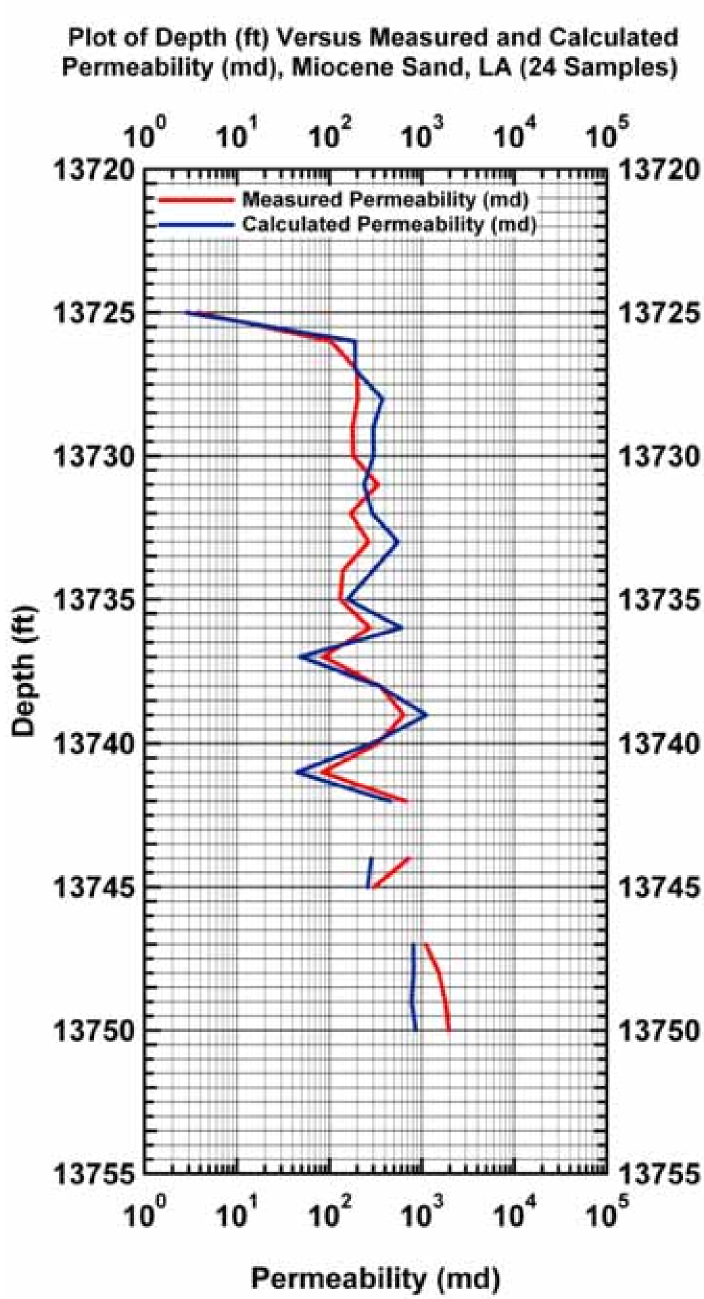

Figure C.6d — Model *CPR-A*: Calculated and measured permeability values versus depth. [*Case*: Miocene Sand, S. LA (USA)]

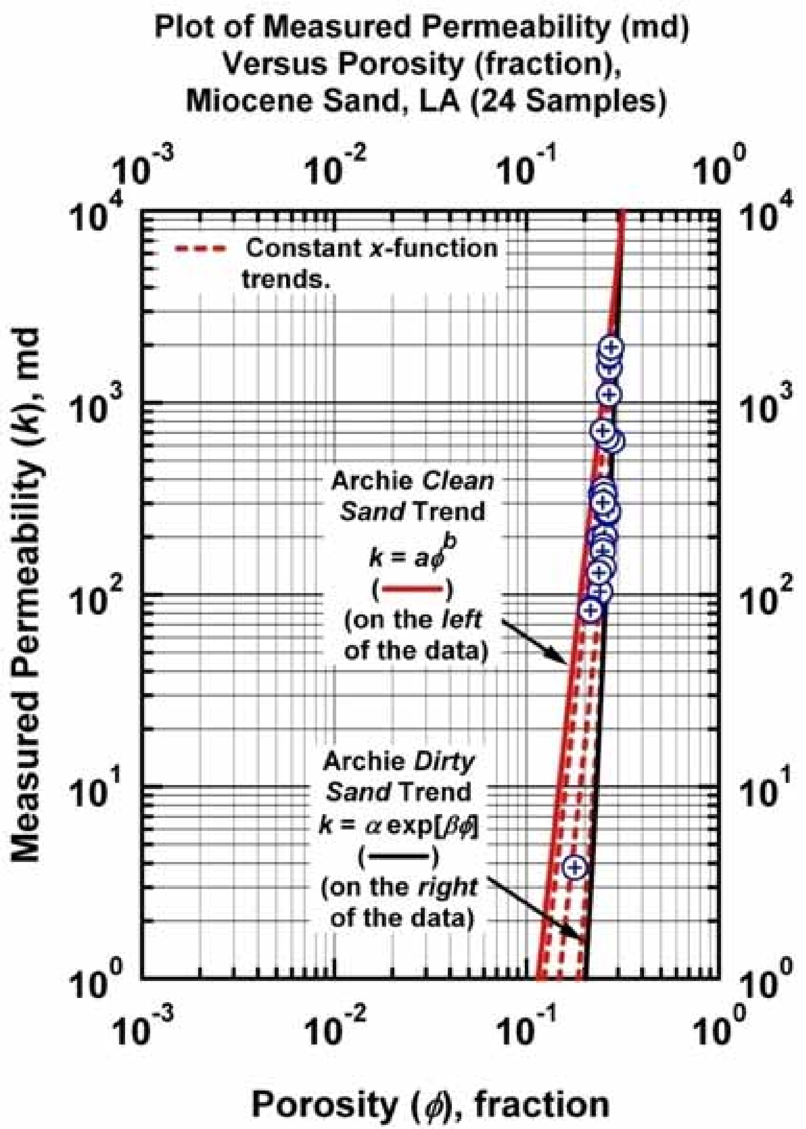

Figure C.7a — Model *CPR-D*: $k = xa\phi^b + (1-x)\alpha\exp[\beta\phi]$ $[0 \le x \le 1]$ — *Weighted Power Law-Exponential Model* used to correlate permeability (k) and porosity (ϕ). "Clean Sand" Plot — Archie "Clean Sand" trend is given by the straight-line trend at the far left of the data (power law model). [*Case*: Miocene Sand, S. LA (USA)]

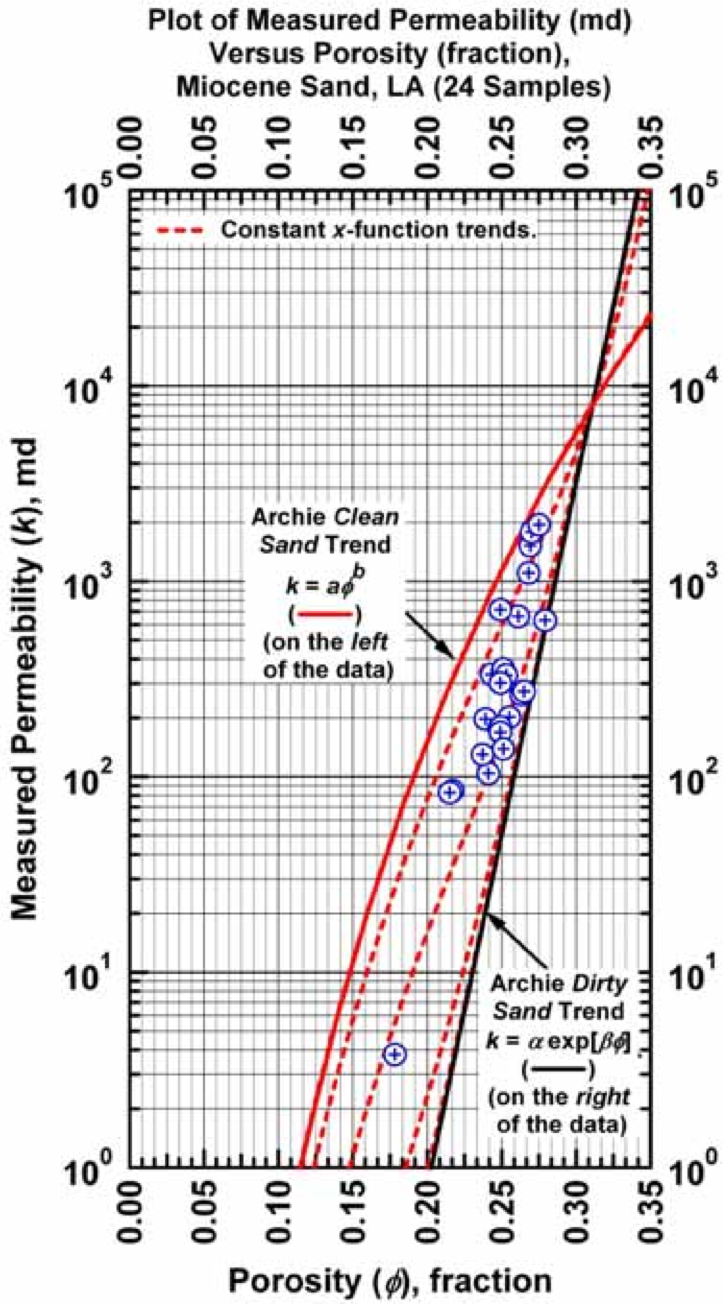

Figure C.7b — Model *CPR-D*: $k = xa\phi^b + (1-x)\alpha \exp[\beta\phi] \quad [0 \le x \le 1]$ — *Weighted Power Law-Exponential Model* used to correlate permeability (k) and porosity (ϕ). "Dirty Sand" Plot — Archie "Dirty Sand" trend is given by the straight-line trend at the far right of the data (exponential model). [*Case*: Miocene Sand, S. LA (USA)]

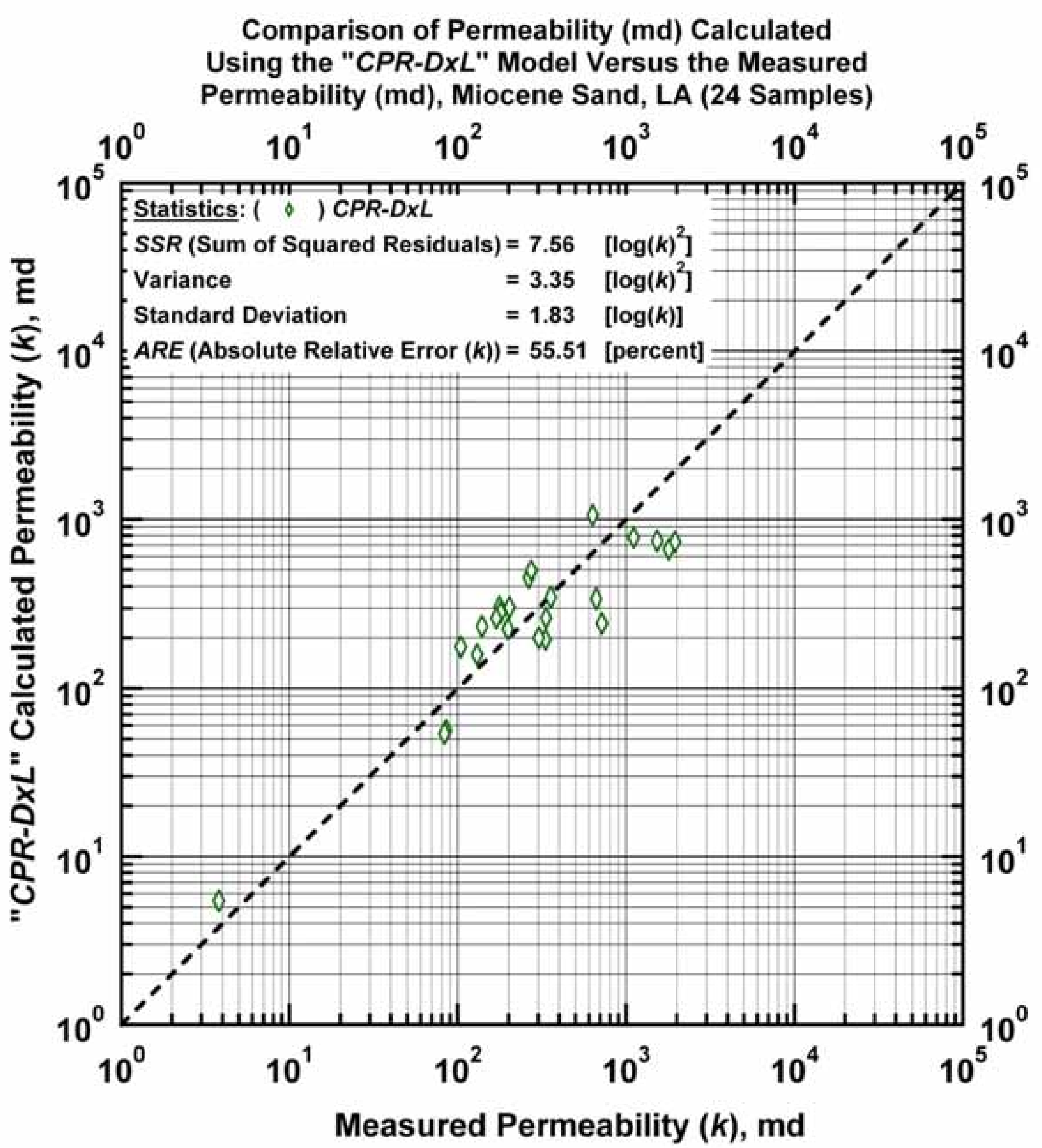

Figure C.8a — Model *CPR-DxL*: Calculated versus measured permeability. [*Case*: Miocene Sand, S. LA (USA)]

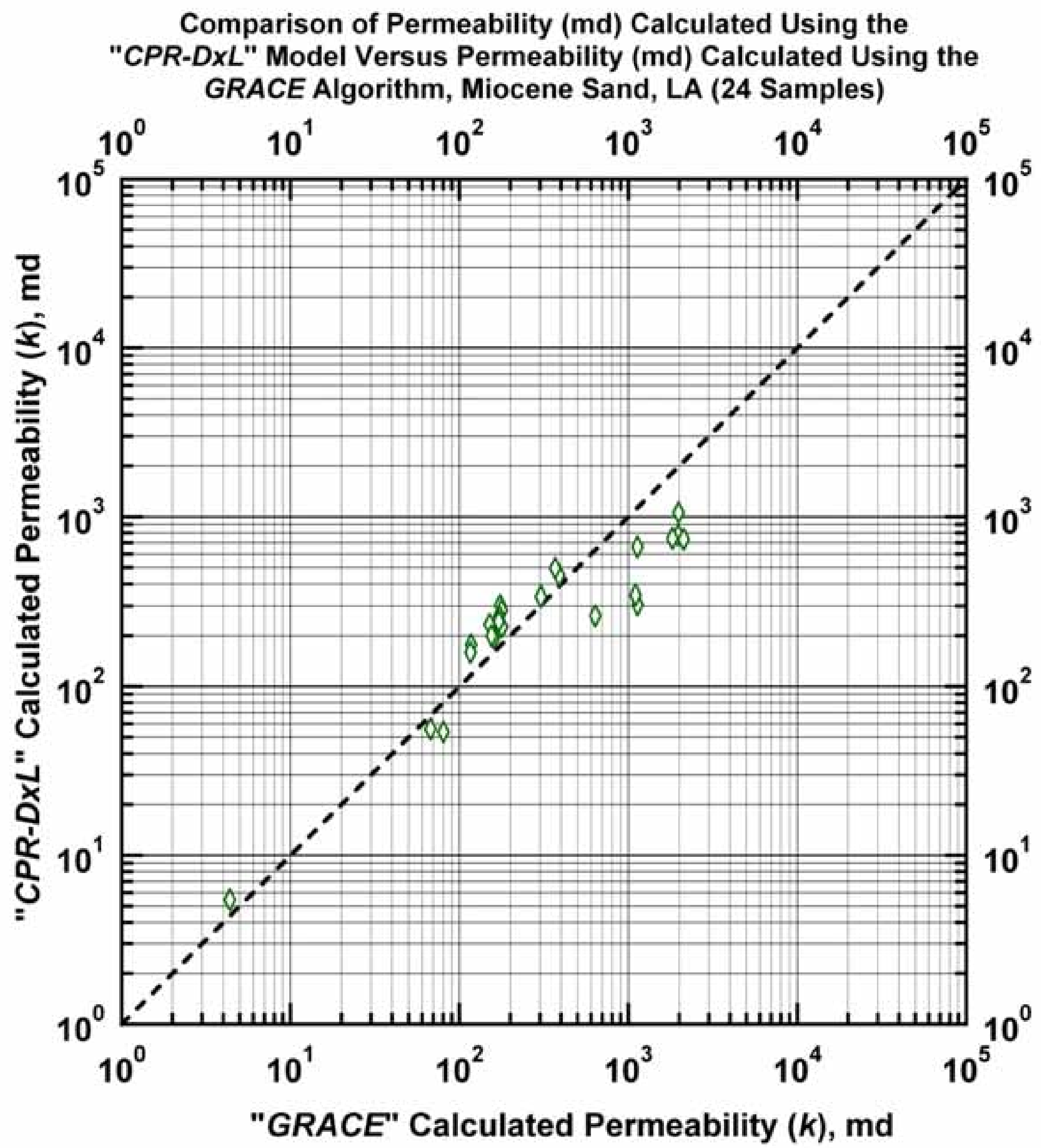

Figure C.8b — Model *CPR-DxL*: Permeability calculated using Model *CPR-C* versus permeability calculated using the *GRACE* Algorithm. [*Case*: Miocene Sand, S. LA (USA)]

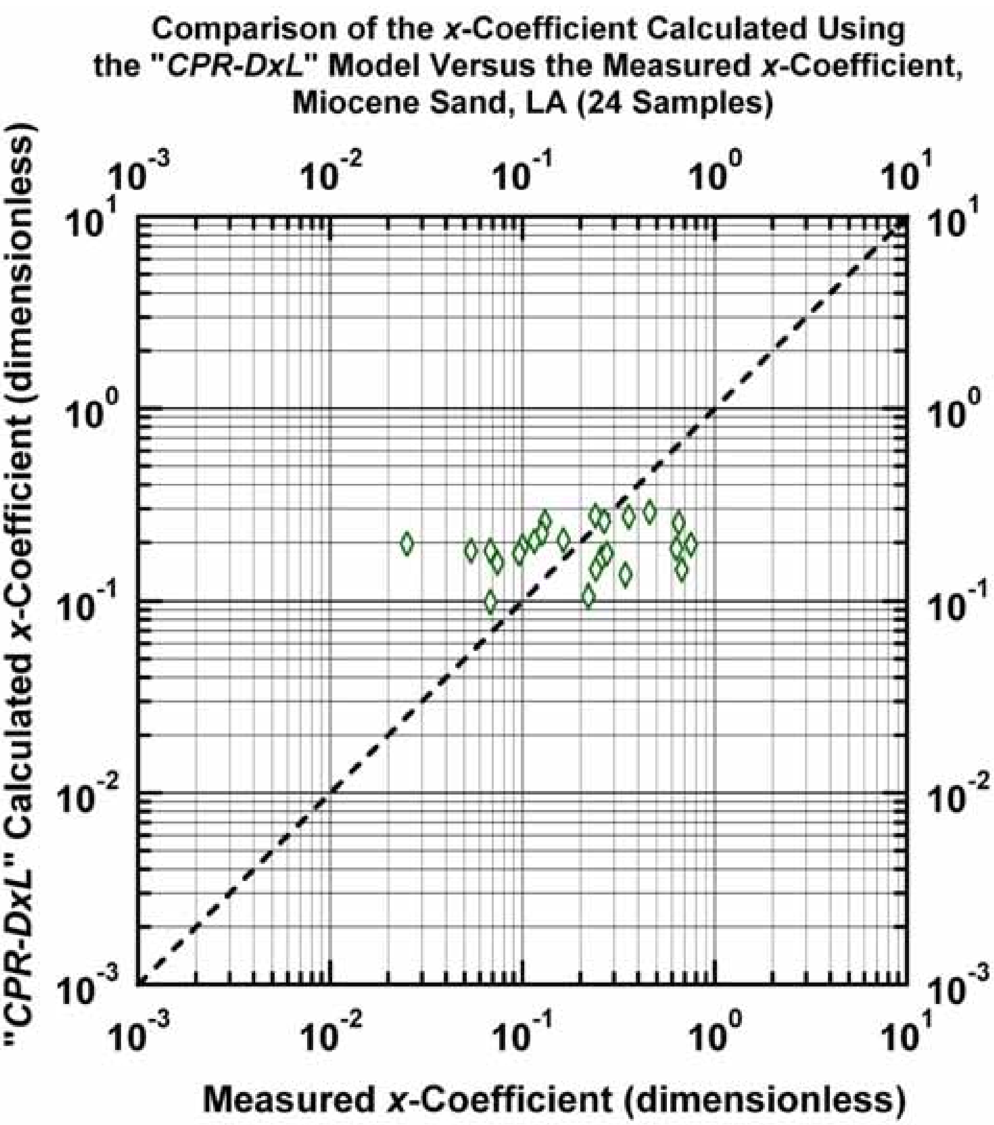

Figure C.8c — Model *CPR-DxL*: Calculated *x*-function weight values versus measured *x*-function weight values. [*Case*: Miocene Sand, S. LA (USA)]

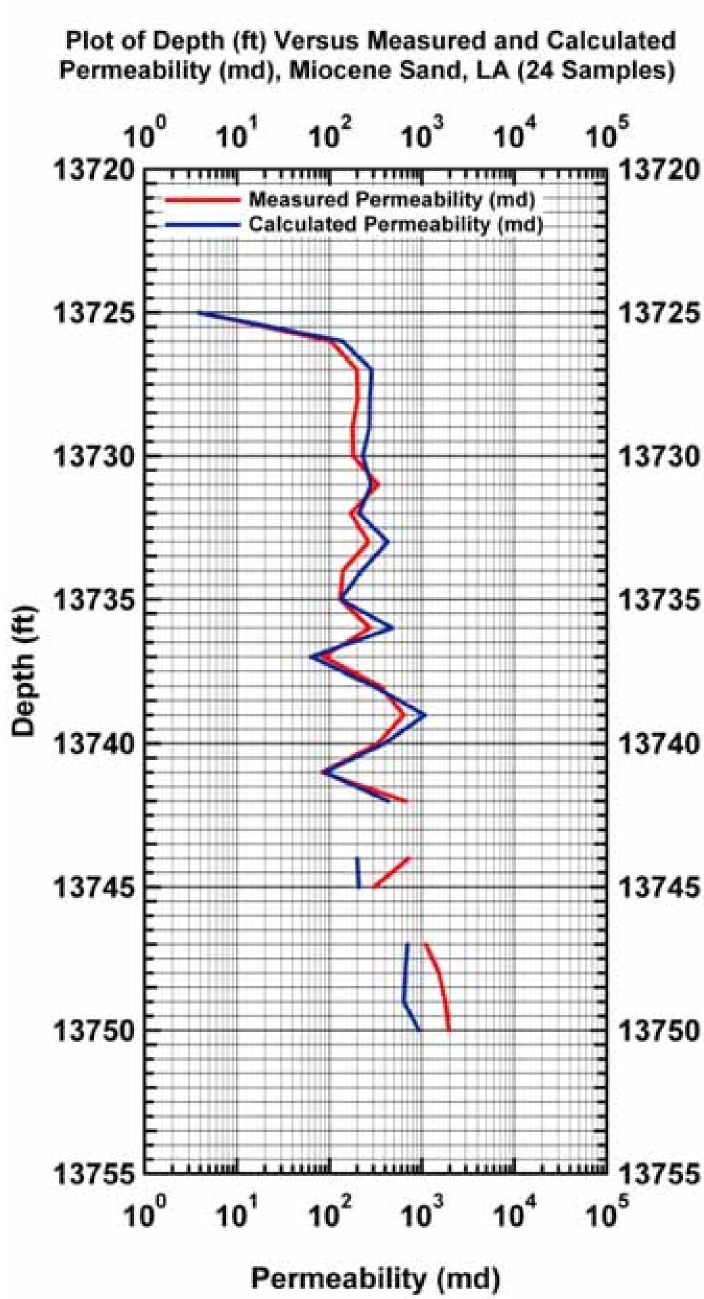

Figure C.8d — Model *CPR-A*: Calculated and measured permeability values versus depth. [*Case*: Miocene Sand, S. LA (USA)]

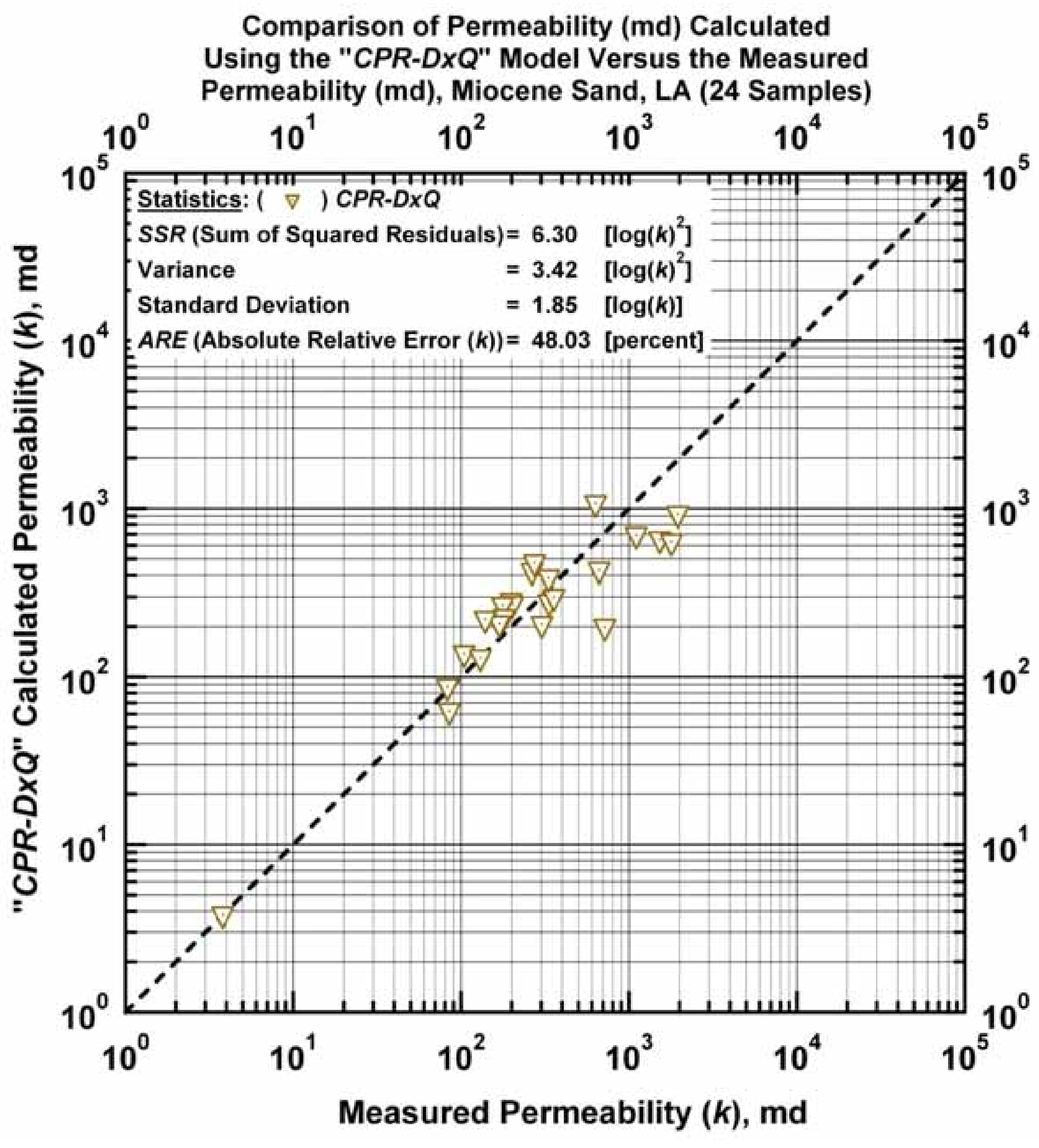

Figure C.9a — Model *CPR-DxQ*: Calculated versus measured permeability. [*Case*: Miocene Sand, S. LA (USA)]

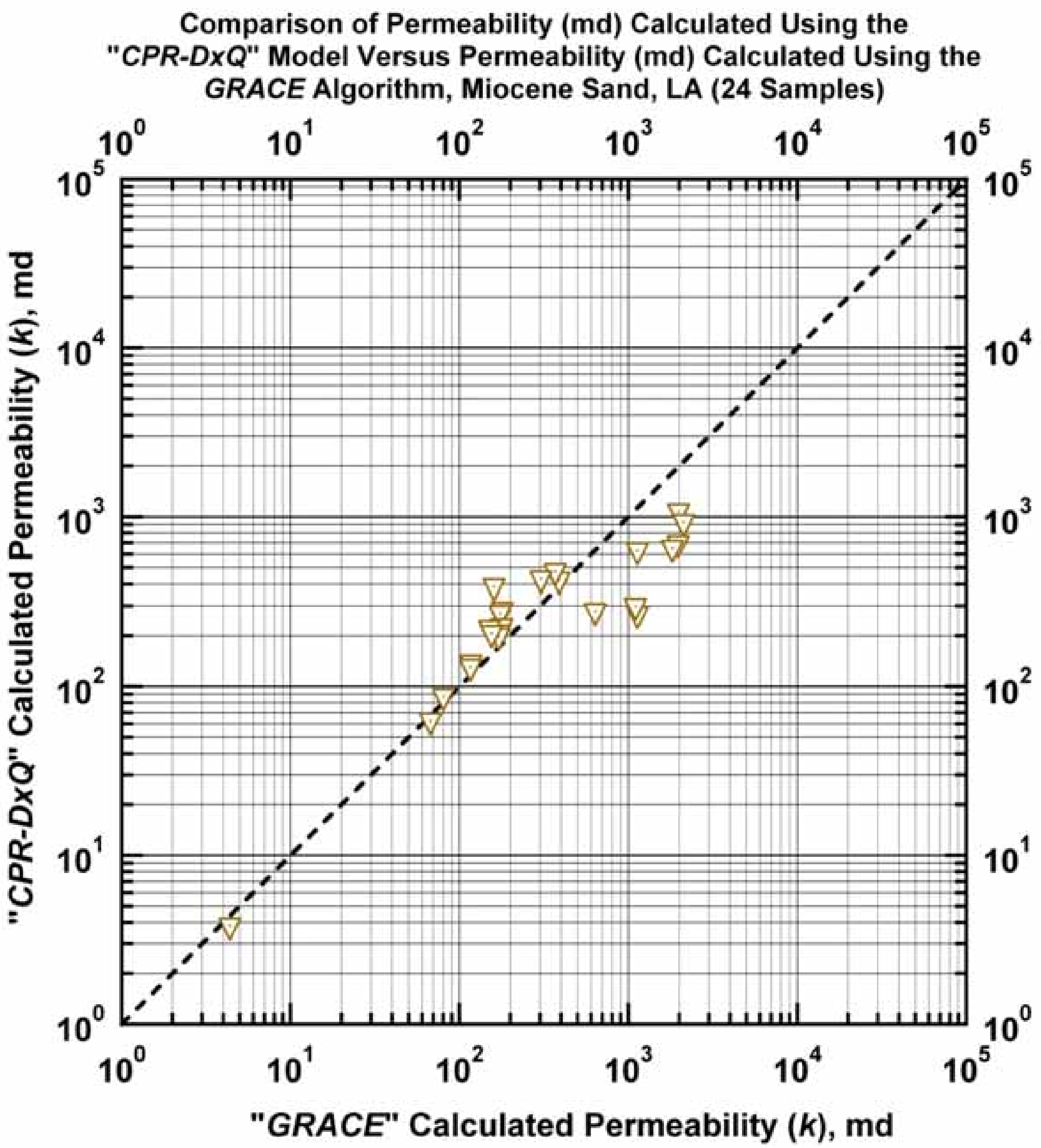

Figure C.9b — Model *CPR-DxQ*: Permeability calculated using Model *CPR-C* versus permeability calculated using the *GRACE* Algorithm. [*Case*: Miocene Sand, S. LA (USA)]

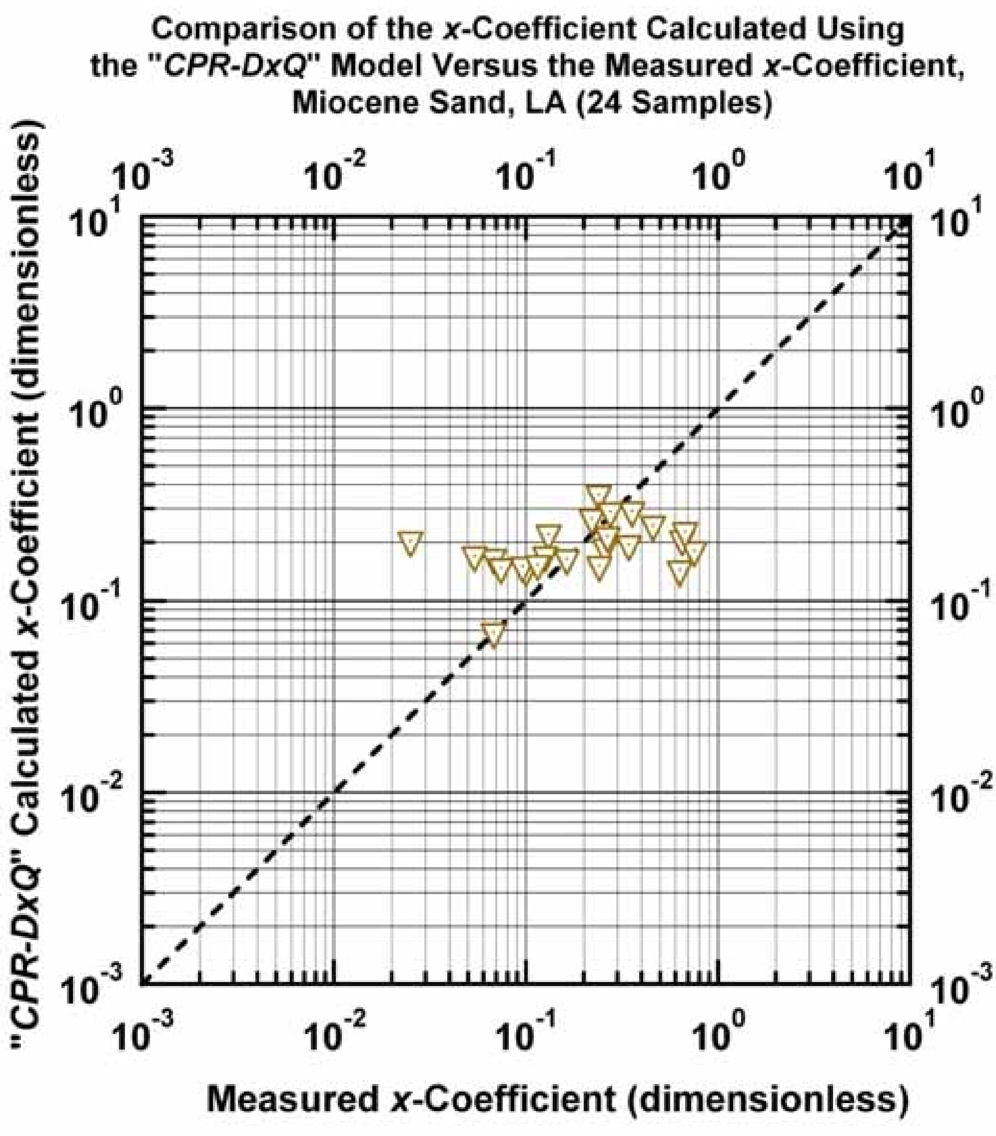

Figure C.9c — Model *CPR-DxQ*: Calculated *x*-function weight values versus measured *x*-function weight values. [*Case*: Miocene Sand, S. LA (USA)]

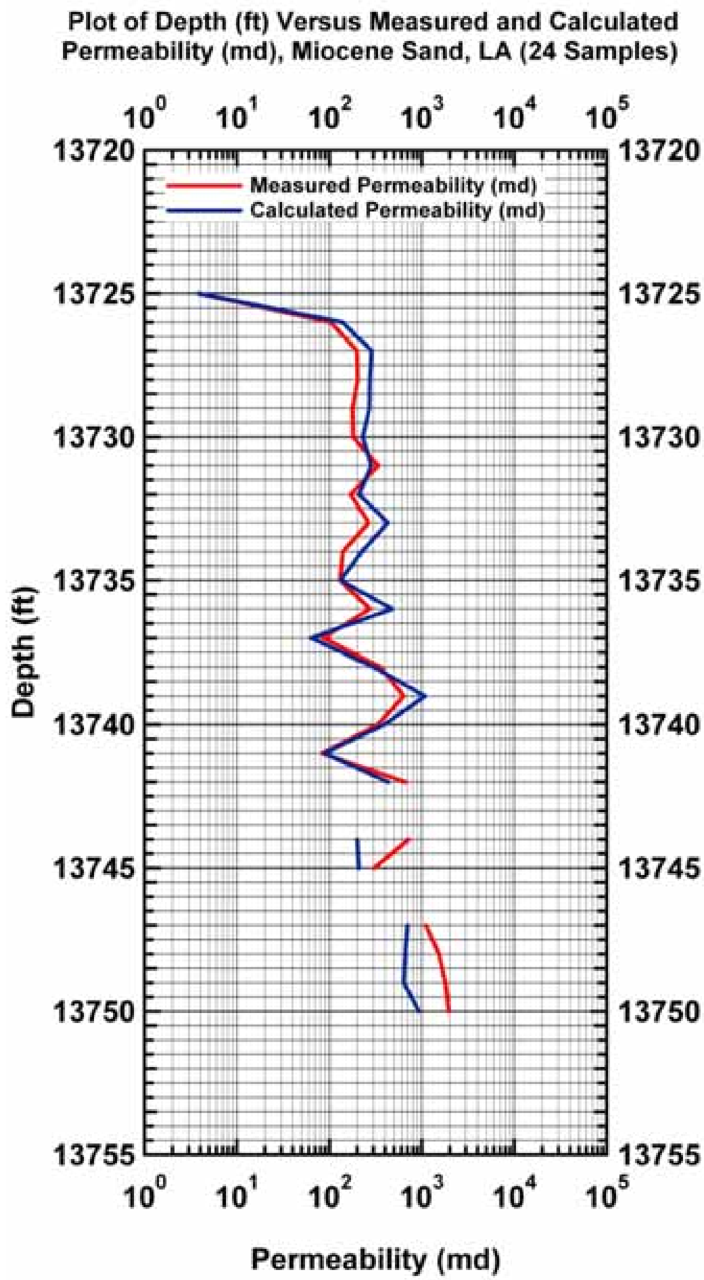

Figure C.9d — Model *CPR-A*: Calculated and measured permeability values versus depth. [*Case*: Miocene Sand, S. LA (USA)]

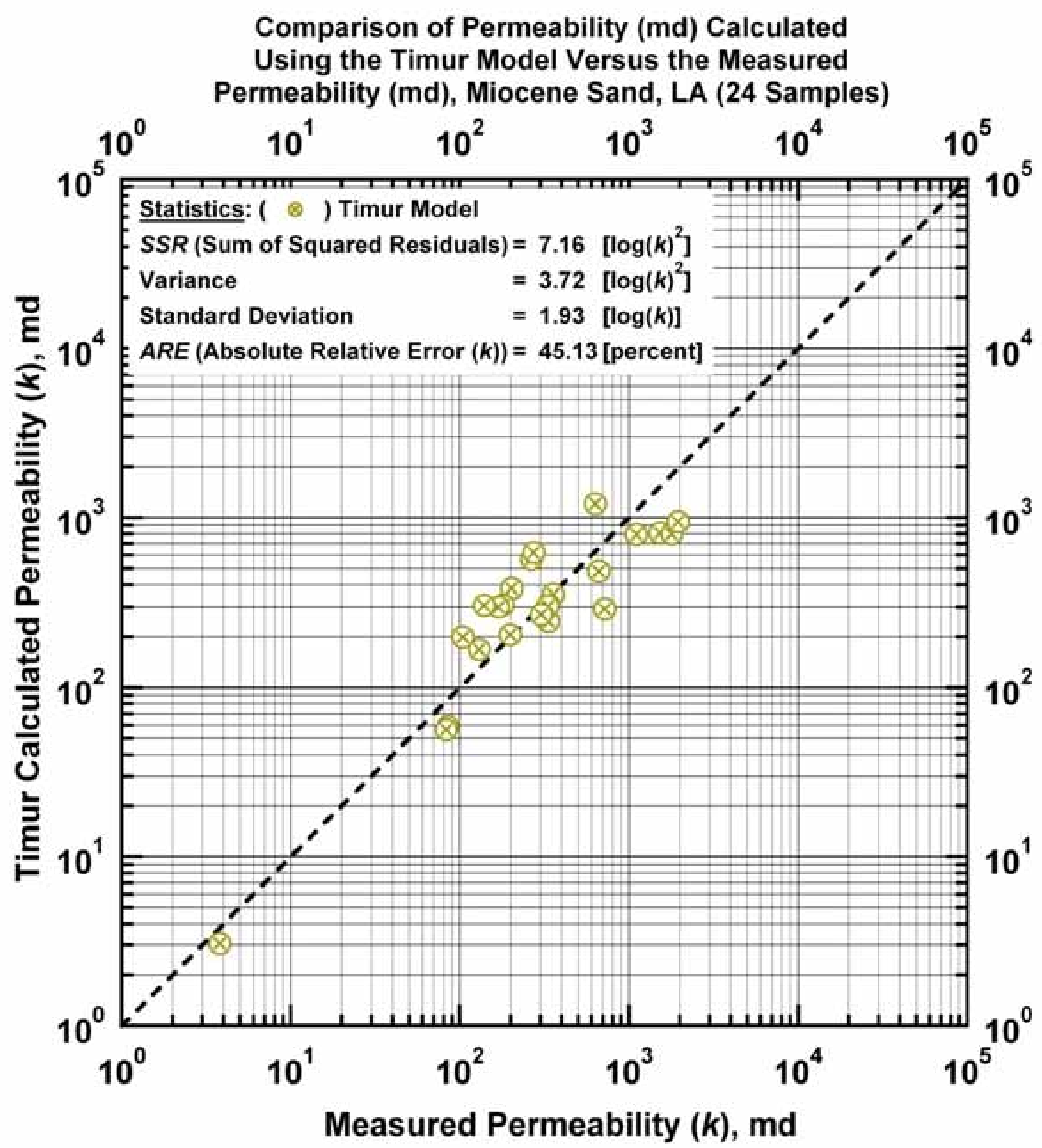

Figure C.10a — "Timur Model:" Calculated versus measured permeability. [*Case*: Miocene Sand, S. LA (USA)]

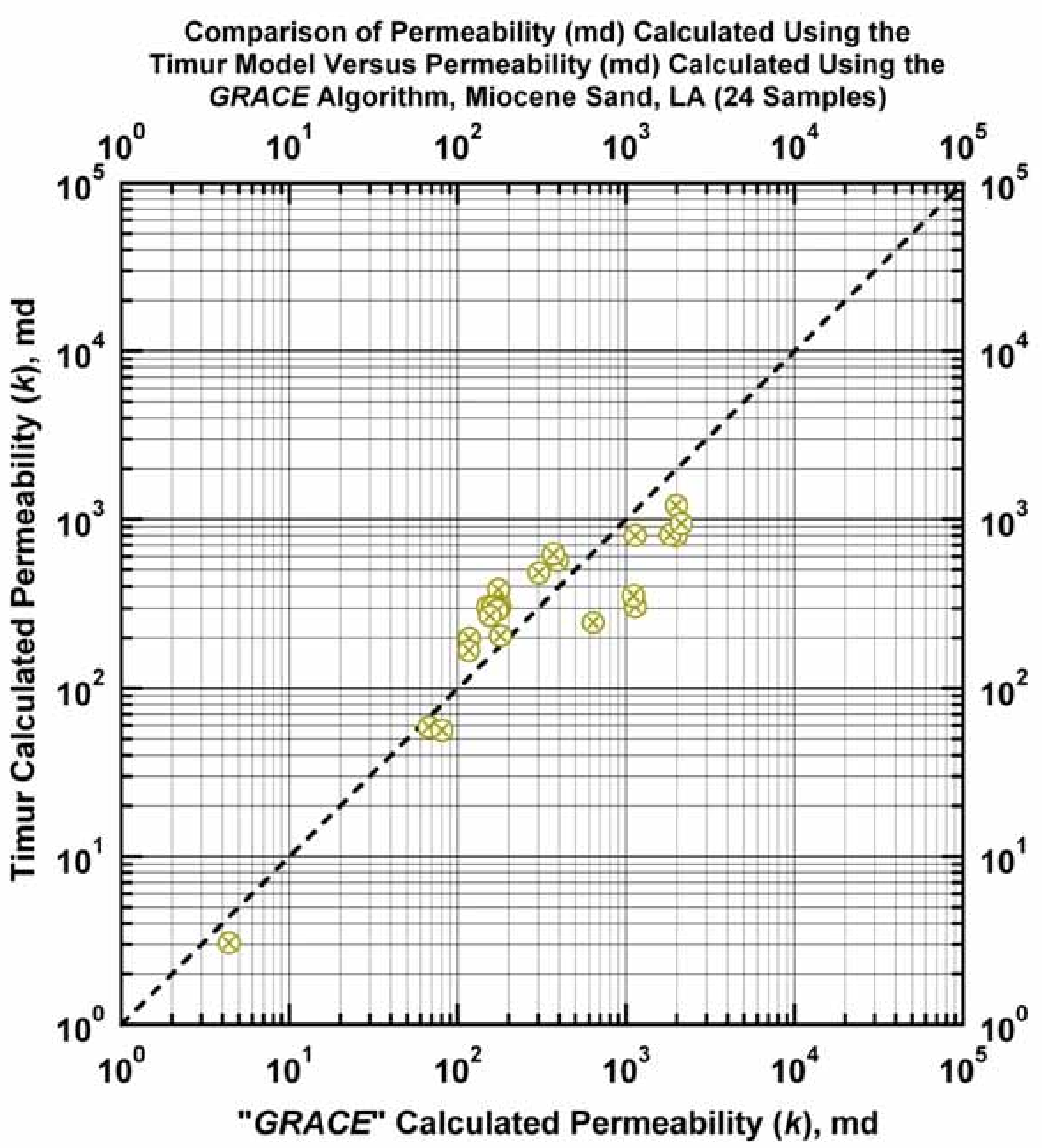

Figure C.10b — "Timur Model:" Permeability calculated using the "Timur Model" versus permeability calculated using the *GRACE* Algorithm. [*Case*: Miocene Sand, S. LA (USA)]

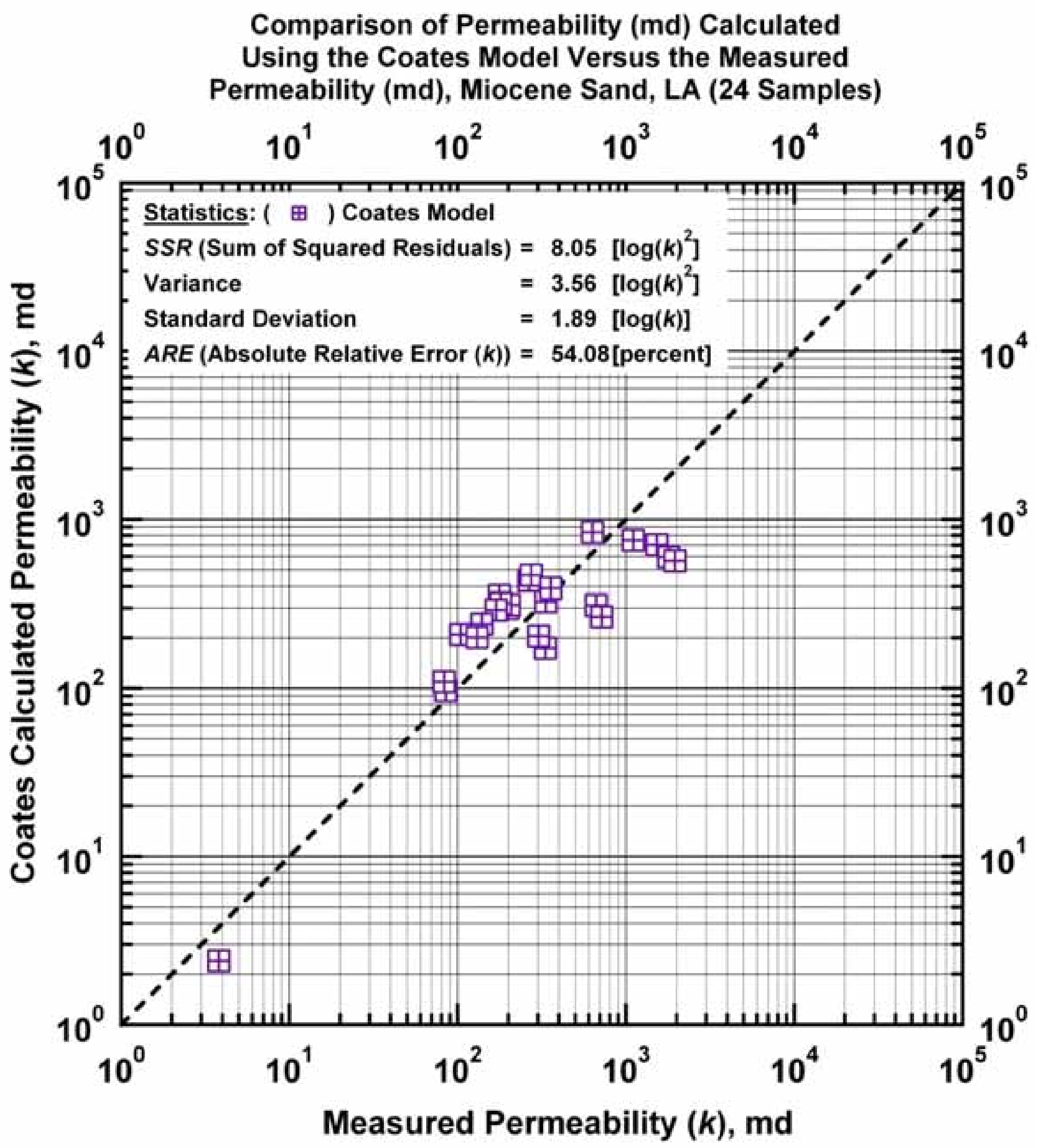

Figure C.11a — "Coates Model:" Calculated versus measured permeability. [*Case*: Miocene Sand, S. LA (USA)]

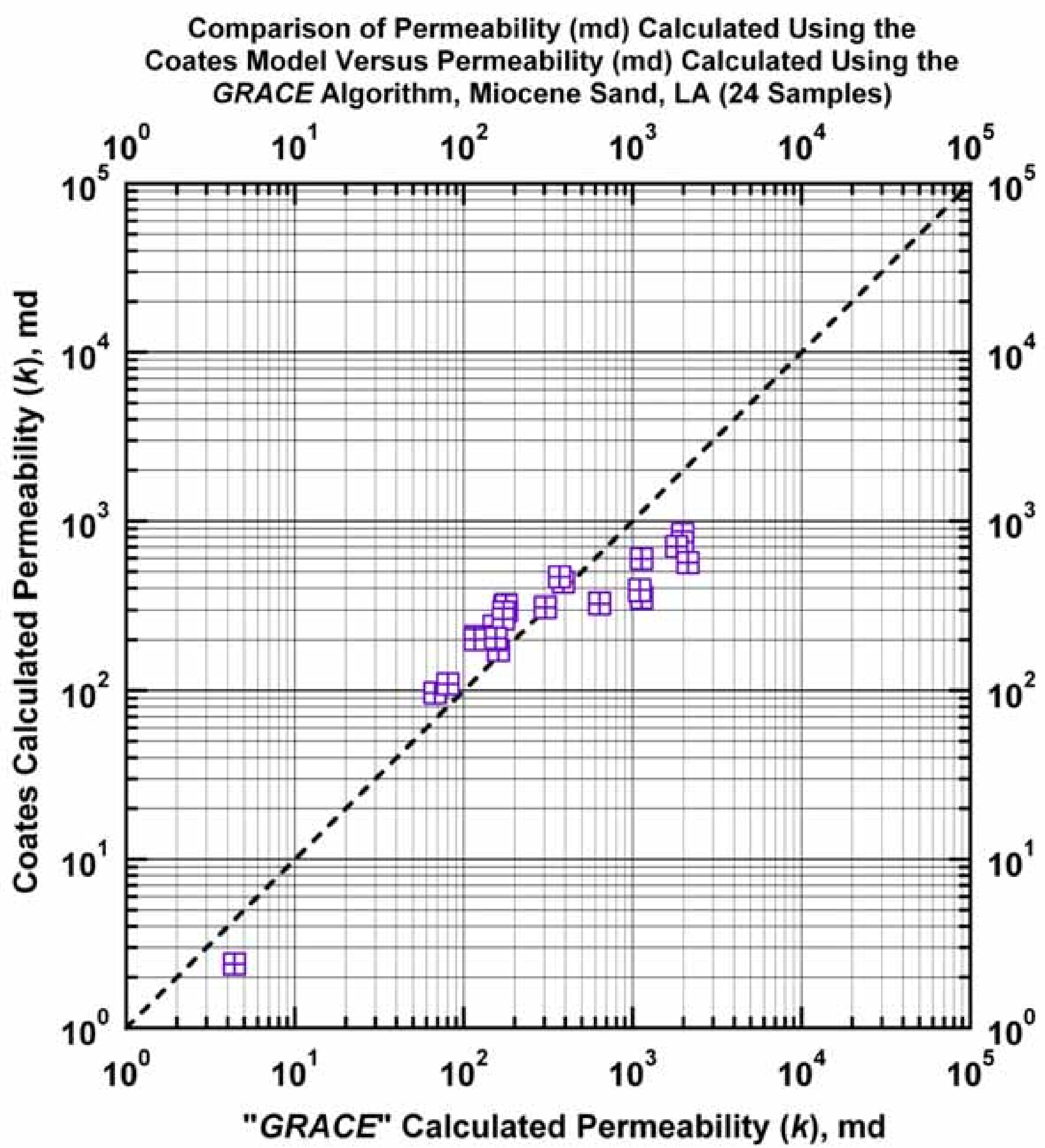

Figure C.11b — "Coates Model:" Permeability calculated using the "Coates Model" versus permeability calculated using the *GRACE* Algorithm. [*Case*: Miocene Sand, S. LA (USA)]

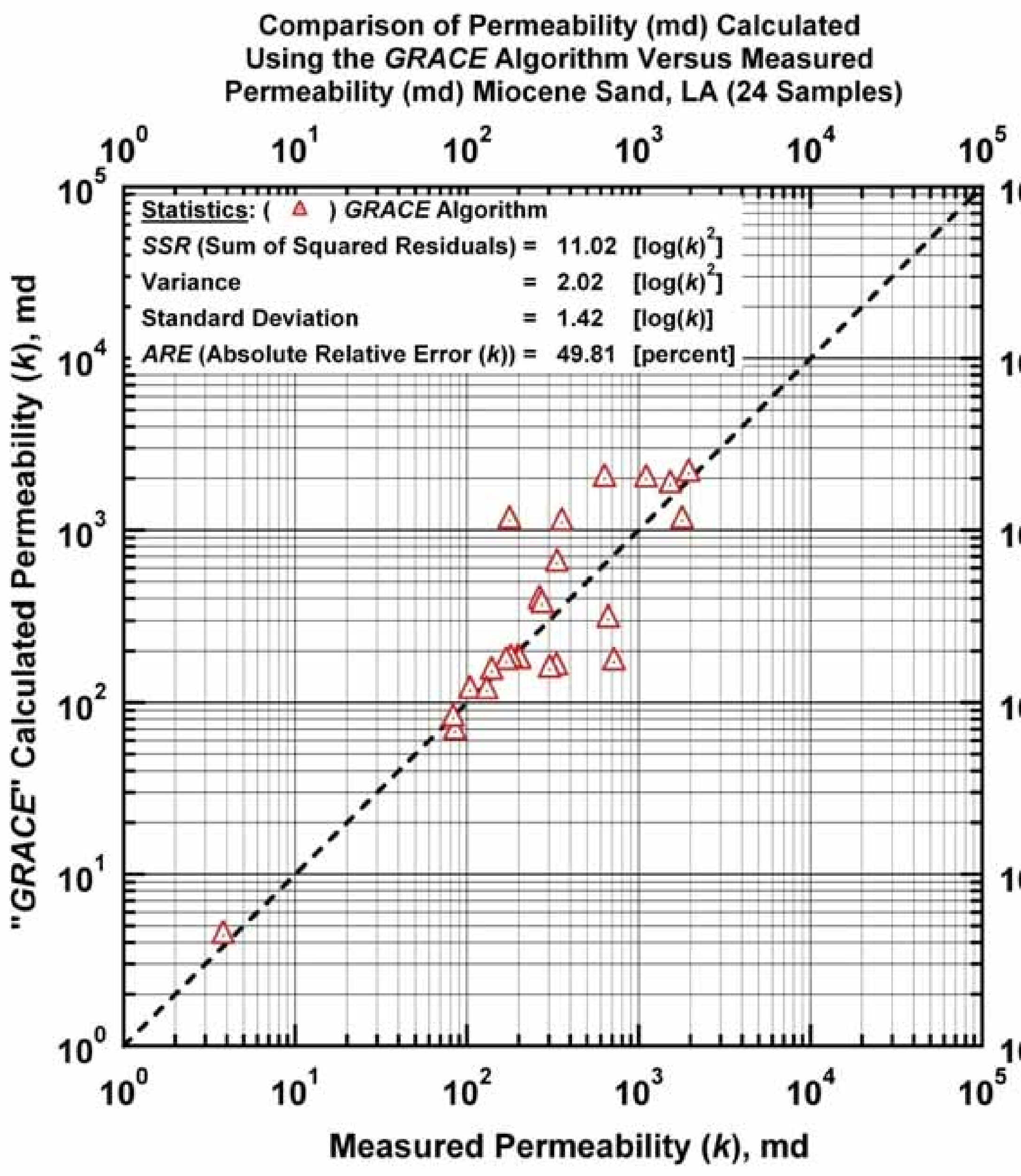

Figure C.12 — *GRACE* Model: Calculated versus measured permeability. [*Case*: Miocene Sand, S. LA (USA)]

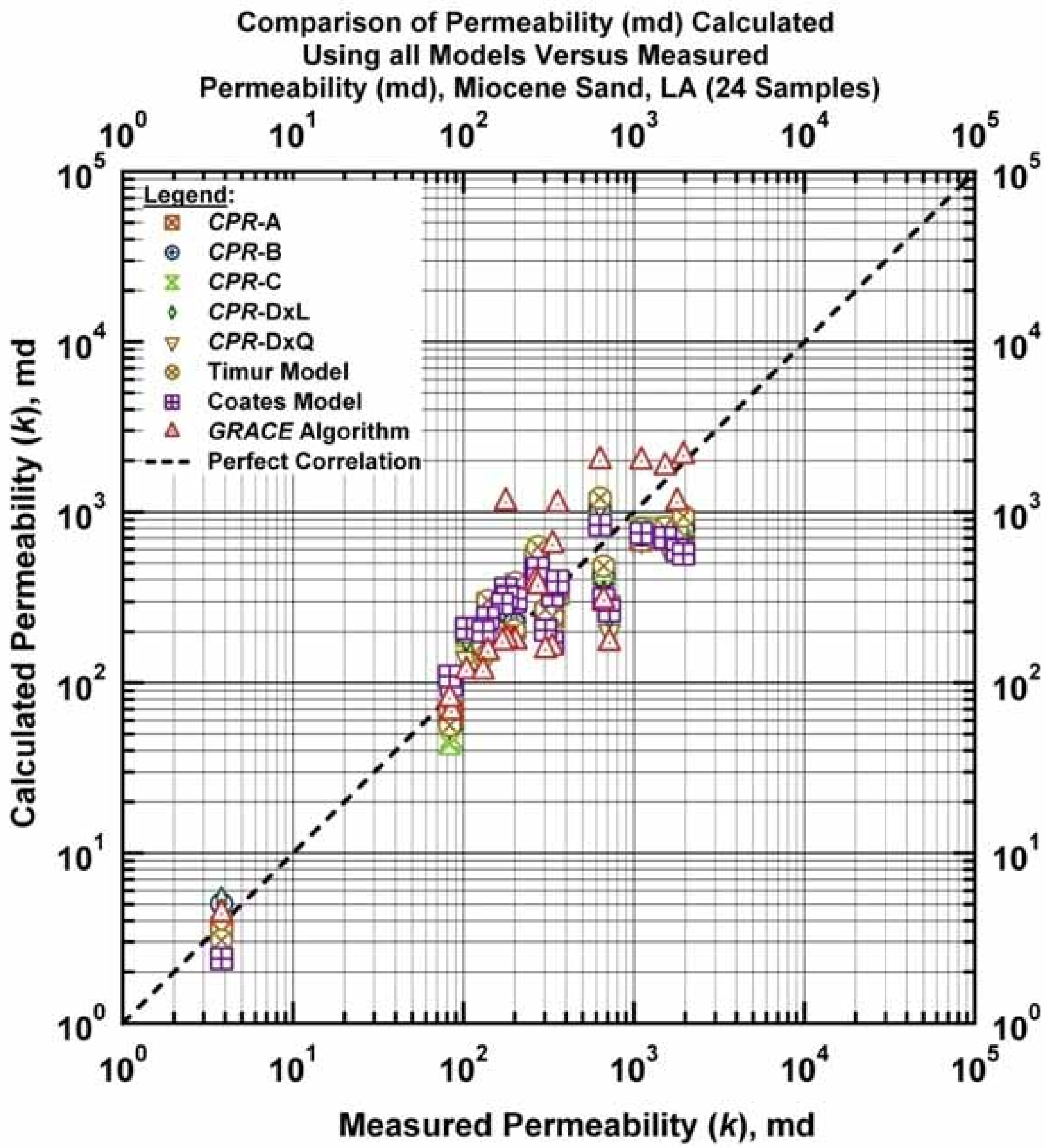

Figure C.13 — All Models: Calculated versus measured permeability. [*Case*: Miocene Sand, S. LA (USA)]

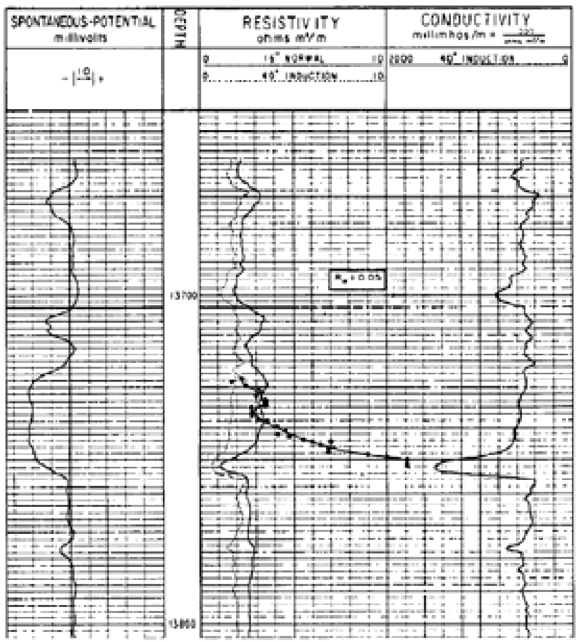

SAMP NO.	DEPTH FEET	PERM. Md.	POR. %	% POR. SAT OIL	% POR. SAT TOTAL WATER	PROB. PROD	% OIL VOL.	% GAS VOL.	%Pi
CONVENTIONAL DIAMOND CORE-DEPTHS CORRECTED TO ELECTRIC LOG									
1	13722-23	0.0	10.3	0.0	38.8			6.3	
2	23-24	0.0	15.3	0.0	58.7			6.3	
3	24-25	3.8	17.8	0.0	45.6	COND		9.7	
4	25-26	104	24.1	0.8	32.3	COND		16.1	
5	26-27	198	23.9	0.8	26.7	COND		17.3	
6	27-28	202	25.5	0.8	35.7	COND		16.2	
7	28-29	177	24.8	1.6	29.8	COND		17.0	
8	29-30	180	24.9	0.8	31.7	COND		16.8	
9	30-31	334	24.3	2.0	27.9	COND		17.0	
10	31-32	169	24.9	2.0	32.9	COND		16.2	
11	32-33	264	26.3	1.9	36.1	COND		16.3	
12	33-34	139	25.1	2.0	36.7	COND		15.4	
13	34-35	130	23.7	0.8	30.3	COND		16.3	
14	35-36	273	26.5	0.8	36.3	COND		16.7	
15	36-37	85.	21.7	0.9	26.7	COND		15.7	
16	37-38	356	25.1	0.8	30.3	COND		17.3	
17	38-39	632	27.9	0.7	36.5	COND		17.5	
18	39-40	332	25.3	0.8	42.7	COND		14.3	
19	40-41	83.	21.5	0.9	24.1	COND		16.1	
20	41-42	663	26.1	0.8	39.5	COND		15.6	
21	42-43	800	26.7	1.9	26.3	COND		19.2	
22	43-44	716	24.9	0.8	34.1	COND		16.2	
23	44-45	302	24.9	0.8	37.7	COND		15.3	
24	45-46	1000	26.4	0.8	25.0	COND		19.6	
25	46-47	1105	26.8	1.8	31.7	COND		17.8	
26	47-48	1524	26.9	0.7	33.1	COND		17.8	
27	48-49	1790	27.0	1.8	35.9	COND		16.8	
28	13749-50	1950	27.5	0.7	39.6	COND		16.4	

FIGURE 6: Rmo - Rt COMPARISON FOR MIOCENE SAND IN SOUTH LOUISIANA

Figure C.14 — Original data from Granberry and Wilshusen (1962). [*Case*: Miocene Sand, S. LA (USA)]

APPENDIX D

RESULTS FOR VICKSBURG SAND

(S. TEXAS — USA)

In this Appendix we present the Vicksburg Sand, located in S. Texas (USA), — this is a sandstone reservoir (Granberry and Wilshusen (1962)).

Model *CPR-A*: (Appendix D)

The "characteristic permeability relation" (or *CPR*) Model *CPR-A* (*i.e.*, the modified Archie "Clean Sand" Model) is given as:

$$k = a(\phi - c)^b \quad c = c_{max} \exp[-c_1 \phi^{c_2} S_w^{c_3}] \qquad \text{(D-1)}$$

Where a plot of log(k) versus log(ϕ) is used to graphically calibrate Eq. D-1 in terms of the coefficients — a, b, and c_{max}. **Fig. D.1** shows that the *CPR-A* model performs reasonably well for this case. **Figs. D.1a and b** show the log-log and the semilog format of permeability versus porosity, respectively. In **Fig. D.2** we provide the "error" plots for this case, where the measured and computed data are compared systematically. In **Fig. D.2a** we note a good correlation of the results obtained using Model *CPR-A* versus the measured permeability data — we observe good agreement with the perfect correlation trend (*i.e.*, the 45-degree line). In **Fig. D.2b** we provide a comparison with the *GRACE* algorithm correlation (Xue *et al*. 1997)), and we note that the *CPR-A* model results correlate very well with the *GRACE* algorithm results for this case. **Fig. D.2c** we present the calculated and measured c-function — and again we note a reasonable correlation of the data about the perfect correlation trend. Lastly, in **Fig. D.2d** we present the measured and calculated permeability with depth.

Model *CPR-B*: (Appendix D)

The "characteristic permeability relation" (or *CPR*) Model *CPR-B* (*i.e.*, the modified Archie "Dirty Sand" Model (power-law basis)) is given as:

$$k = a(\phi + c)^b \quad c = c_{max} \exp[-c_1 \phi^{c_2} S_w^{c_3}] \qquad \text{(D-2)}$$

Where a plot of log(k) versus log(ϕ) is used to graphically calibrate Eq. D-2 in terms of the coefficients — a, b, and c_{max}. The results for this case are presented in **Figs. D.3 and 4**. In **Fig. D.3a** (log-log format) we note that a very distinct "envelope" is formed by the *CPR-B* model, essentially all of the data on the right and left flanks are well-matched (*i.e.*, the "dirty sand" power law relation (applied on the right portion of the data) and its correction function (applied on the left portion of the data). Similarly, in **Fig. D.3b** (semilog format), we observe an excellent distribution of the power law model across the body of the data. The error analyses for this case are shown in **Fig. D.4**. In **Fig. D.4a** we present the results obtained using

Model *CPR-B* versus the measured permeability data and in this case there is good agreement with the perfect correlation trend (*i.e.*, the 45-degree line). We provide a comparison with the *GRACE* algorithm correlation in **Fig. D.4b** — the results using Model *CPR-B* and the *GRACE* algorithm compare very well for this case. We compare the computed and data-derived values of the *c*-function for this case in **Fig. D.4c** and we note a reasonably "tight" correlation, except for the very lowest values of the *c*-function. Finally, in **Fig. D.4d** we present the measured and calculated permeability with depth. In summary, we believe that Model *CPR-B* is a very effective correlation model for this particular data case.

Model *CPR-C*: (Appendix D)

The "characteristic permeability relation" (or *CPR*) Model *CPR-C* (*i.e.*, the modified Archie "Dirty Sand" Model (exponential basis)) is given as:

$$k = c\exp[\beta\phi] \quad c = c_{\max}\exp[-c_1\phi^{c_2} S_w^{c_3}] \quad \text{(D-3)}$$

Where a plot of log(k) versus ϕ is used to graphically calibrate Eq. D-3 in terms of the coefficients — β and $c_{\max}$. Model *CPR-C* is fundamentally different than Models *CPR-A* and *CPR-B*, as the basis for Model *CPR-C* is an exponential function, not a power law relation. In **Figs. D.5 and 6** we present the results of applying Model *CPR-B* for this case, and in general, we observe a very consistent performance of Model *CPR-B*. **Fig. D.5b** illustrates the excellent conformance of Model *CPR-C* for this case — again recalling that this model has an exponential relationship with porosity as its basis.

In **Figs. D.6a, D.6b, and D.6c** we review the error analyses plots for this case, and we note good performance (visually) in terms of the correlation of the results using Model *CPR-C*. The correlation of the *c*-function (see **Fig. D.6c**) appears to be consistent. We believe that the *CPR-C* model has performed well for this case, and **Fig. D.6** confirms the value of this model as a "characteristic relation" for permeability.

Model *CPR-D*: (Appendix D)

The "characteristic permeability relation" (or *CPR*) Model *CPR-D* (*i.e.*, the weighted power law-exponential model) is given in its fundamental form as:

$$k = xa\phi^b + (1-x)\alpha\exp[\beta\phi] \quad [0 \le x \le 1]] \quad \text{(D-4a)}$$

For Eq. D-4 there are two proposed models for the *x*-function (*i.e.*, the weighting function) — these are:

$$x = \exp[-\ln(x_0) + x_1\ln(\phi) + x_2\ln(S_w) + x_3\ln(\phi)\ln(S_w)] \ \text{(Model } \mathit{CPR\text{-}DxL}\text{)} \quad \text{(D-4b)}$$

$$x = \exp\begin{bmatrix} -\ln(x_0) + x_1\ln(\phi) + x_2\ln(S_w) + x_3\ln(\phi)\ln(S_w) \\ + x_4\ln(\phi)^2 + x_5\ln(S_w)^2 + x_6\ln(\phi)^2\ln(S_w) \\ + x_7\ln(\phi)\ln(S_w)^2 + x_8\ln(\phi)^2\ln(S_w)^2 \end{bmatrix} \text{(Model } \mathit{CPR\text{-}DxL}\text{)} \quad \text{(D-4c)}$$

As noted in Eq. D-4b, Model *CPR-DxL* utilizes a logarithmic linear model for the weights (*x*-values) and as seen in Eq. D-4c, Model *CPR-DxQ* utilizes a logarithmic quadratic model for the weights (*x*-values).

While these models (Eqs. D-4b and D-4c) are *empirical*, we have found generally good application of these relations for all cases. In this case, the base results using Models *CPR-DxL* and *CPR-DxQ* are presented in **Fig. D.7** — where the power law and exponential basis functions are fitted to the appropriate portion of the data. The power law equation represents the "Archie clean sand" trend and is fitted to the leftmost data as shown in **Fig. D.7a** and in contrast, the exponential equation is thought to represent the "Archie dirty sand" trend and the exponential is fitted to the far rightmost portion of the data (see **Fig. D.7b**).

In **Figs. D.8 and 9** we present the error analyses for this case, where we have employed the weighting functions (Eqs. D-4b and D-4c) as appropriate. In **Fig. D.8a** we find a good correlation of permeability. The comparison of the Model *CPR-DxL* results are compared to the results obtained from the *GRACE* algorithm in **Fig. D.8b**, we note the very good results obtained using Model *CPR-DxL*. The computed weight function (*x*-values) shown for the *CPR-DxL* model in **Fig. D.8c** does exhibit more scatter than expected, but the trend is (relatively) centered about the perfect correlation line. **Fig. D.8d** provide the measured and calculated permeability versus depth.

The results obtained using Model *CPR-DxQ* are presented in **Fig. D.9**, and we note substantially improved behavior over that of Model *CPR-DxL*. In particular, the base correlation of computed and measured permeabilities (**Fig. D.9a**) for Model *CPR-DxQ* does indicate a slightly better correlation than that of Model *CPR-DxL*. Also, the comparison of Model *CPR-DxQ* with the results from the *GRACE* algorithm (**Fig. D.9b**) exhibits better agreement than the results of Model *CPR-DxL*. Finally, the correlation of the *x*-function (**Fig. D.9c**) for Model *CPR-DxQ* is better than the correlation for Model *CPR-DxL*. These comparisons suggest that Model *CPR-DxQ* (*i.e.*, the combination of Eqs. D-4a and D-4c) has provided a better correlation of data, for this case, than Model *CPR-DxL*. **Fig. D.9d** provides the measured and calculated permeability versus depth.

"Timur Model": (Appendix D)

The "Timur Model" [Timur (1968)] is given as:

$$k_{\text{Timur}} = a\phi^b S_w^c \qquad \text{(D-5)}$$

In **Fig. D.10** we present the results of the "Timur Model" (Eq. D-5) which is essentially just a generalized power-law function relation in terms of k, ϕ, and S_w. As shown in **Figs. D.10a and b**, the "Timur Model" also provides a good correlation of the data for this case. The comparison of results using the "Timur Model" with the results of the *GRACE* algorithm (**Fig. D.10b**).

"Coates Model": (Appendix D)

The "Coates Model" [referenced by Ahmed *et al* (1989)] is given as:

$$k_{\text{Coates}} = \left[100\phi^2 \frac{(1-S_w)}{S_w}\right]^2 \text{ .... (D-6)}$$

In **Fig. D.11** we present the results of the "Coates Model" (Eq. D-6) which is essentially just a modified power-law function relation in terms of k, ϕ, and S_w. The results are shown in **Figs. D.11a and b** of the data for this case. The comparison of results using the "Coates Model" with the results of the *GRACE* algorithm is also shown in **Fig. D.11b**.

***GRACE* Algorithm: (Appendix G)**

In **Fig. D.12** we present the results predicted by the *GRACE* algorithm, which is a non-parametric regression approach (see Xue *et al.* (1997) for details). In theory, the *GRACE* algorithm should provide the most *unbiased* correlation of the data — *i.e.*, the *GRACE* algorithm is designed not to "fit the errors" as other regression approaches may. It is our contention that the *GRACE* algorithm is the statistical standard — and any algorithm/approach/model which achieves better regression statistics than the *GRACE* algorithm is actually "fitting the errors" in the data. *None of the cases have significantly better regression statistics than the GRACE algorithm* — hence, none of the cases are "over-fitted" in a statistical sense.

***Comparison of All Models*: (Appendix D)**

Fig. D.13, illustrates all of the models on a single plot of calculated versus measured permeability. We also present a table of all statistical results in **Table D.1**. Our last plot, **Fig. D.14**, illustrates the source of the original data set.

Table D.1 — Statistical Results for all Models (Vicksburg Sand, S. TX (USA), *n*=19).

Model	Sum of Squared Residuals [$\log(k)^2$]	Variance [$\log(k)^2$]	Standard Deviation [$\log(k)$]	Absolute Relative Error [percent]
CPR-A	8.26	3.18	1.78	46.25
CPR-B	5.13	2.73	1.65	38.79
CPR-C	6.36	2.76	1.66	40.14
CPR-DxL	5.42	2.62	1.62	41.06
CPR-DxQ	4.10	2.76	1.66	31.17
Timur	8.12	2.60	1.61	45.95
Coates	5.32	2.72	1.65	35.51
GRACE Algorithm	4.22	2.74	1.66	28.90

The coefficients for the models used in this case are provided in **Table D.2**.

Table D.2a — Model Coefficients (Vicksburg Sand, S. TX (USA), n=19).

Model	a or α	b or β	c or c_{max}	c_1	c_2	c_3
CPR-A	5.00×10^{7}	8.00	0.070	0.25	0.37	-1.44
CPR-B	2.00×10^{6}	8.00	0.100	958.97	1.03	4.71
CPR-C	5.00×10^{-8}	88.00	1.00×10^{-5}	3116.21	3.67	0.96
Timur	7.76×10^{7}	9.83	0.971	–	–	–
Coates	6.90×10^{1}	2.36	2.656	–	–	–

Table D.2b — Model Coefficients (Vicksburg Sand, S. TX (USA), n=19).

Model	a	b	α	β
CPR-DxL	5.00×10^{7}	8.00	5.00×10^{-8}	88.00
CPR-DxQ	5.00×10^{7}	8.00	5.00×10^{-8}	88.00

Model	c_0	c_1	c_2	c_3	c_4	c_5	c_6	c_7	c_8
CPR-DxL	1.00×10^{7}	-5.62	-7.63	-1.94	–	–	–	–	–
CPR-DxQ	6.66×10^{1}	0.04	33.70	-13.72	3.33	-15.54	8.65	-0.22	9.69

Nomenclature: (Appendix D)

S_w = Water Saturation (fraction)
k = Formation Permeability, md (or any consistent units)
ϕ = Porosity, fraction

References: (Appendix D)

Ahmed, U., Crary, S.F., and Coates, D.R: "Permeability Estimation: The Various Sources and Their Interrelationship," paper SPE 19604 presented at the 1989 SPE Annual Technical Conference and Exhibition, San Antonio, TX, 8-11 Oct., 649-662.

Granberry, R.J., and Wilshusen, R.C.: "Improved Interpretation of Formation Productivity by Combined Use of Core Analysis and Electronic Log Data," *Trans.*, Gulf Coast Association of Geological Societies (1962) 13, 213-221.

Timur, A.: "An Investigation of Permeability, Porosity, and Residual Water Saturation Relationships," *Trans.*, SPWLA Symposium (1968) paper I.

Xue, D., Datta-Gupta, A., Valko, P., and Blasingame, T.A.: "Optimal Transformations for Multiple Regression: Application to Permeability Estimation from Well Logs," *SPEFE* (June 1997), 85-93.

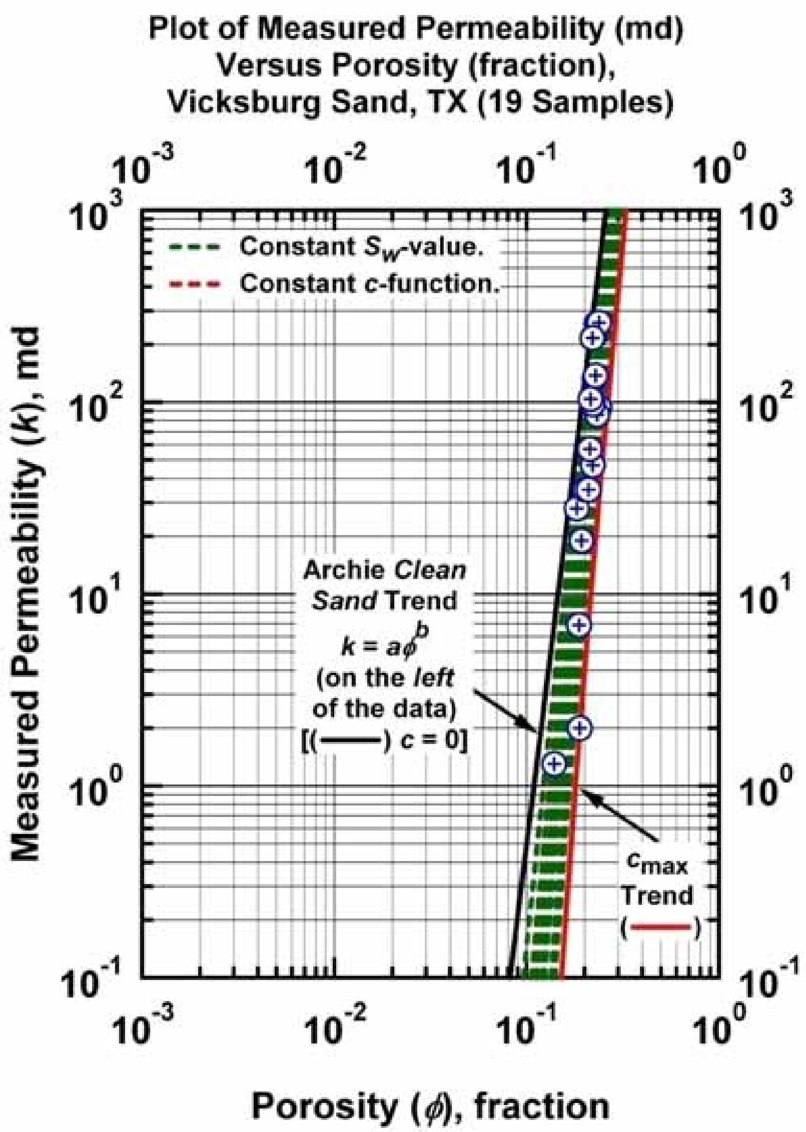

Figure D.1a — Model *CPR-A*: $k = a(\phi - c)^b \quad c = c_{\max} \exp[-c_1 \phi^{c_2} S_w^{c_3}]$ — "Clean Sand" Plot (log-log format) — Archie "Clean Sand" trend is given by the straight-line trend at the far left of the data (power law model). [*Case*: Vicksburg Sand, S. TX (USA)]

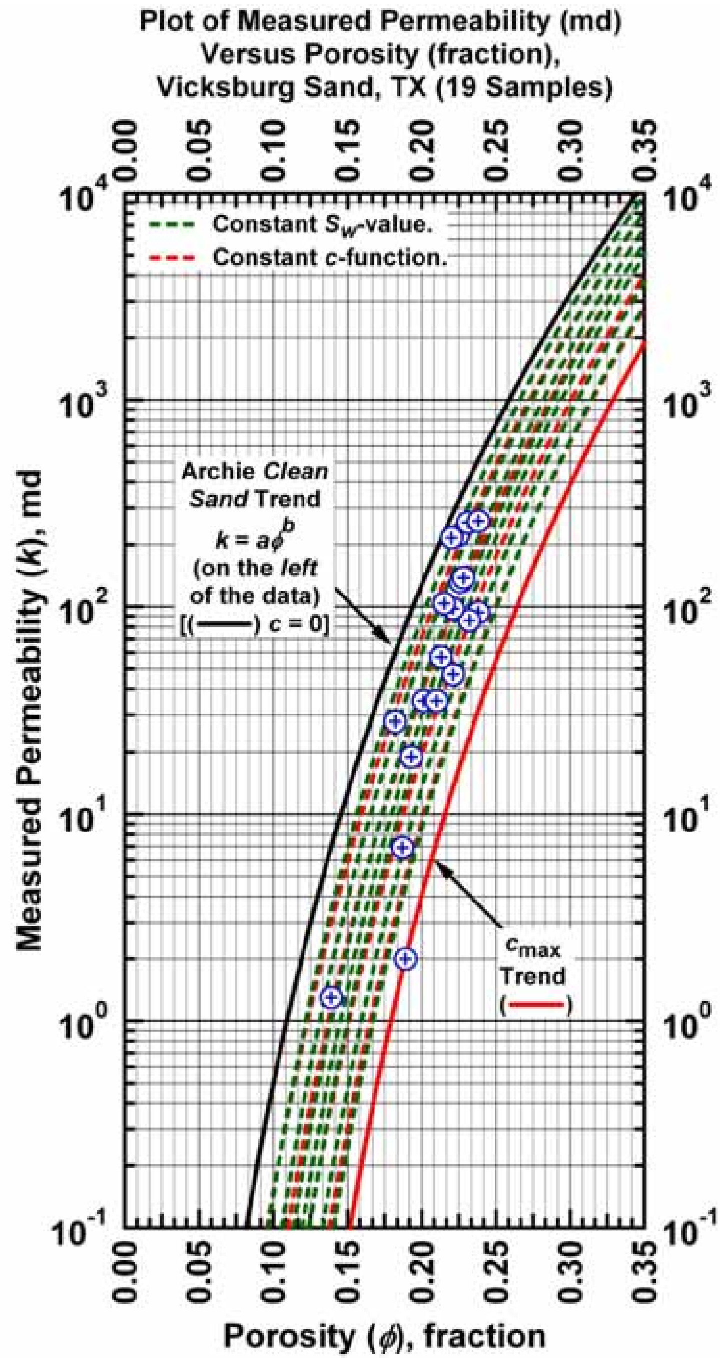

Figure D.1b — Model *CPR-A*: $k = a(\phi - c)^b \quad c = c_{\max}\exp[-c_1\phi^{c_2} S_w^{c_3}]$ — "Dirty Sand" Plot (semilog format). Archie "Clean Sand" trend is given by the curved trend at the far left of the data (power law model). [*Case*: Vicksburg Sand, S. TX (USA)]

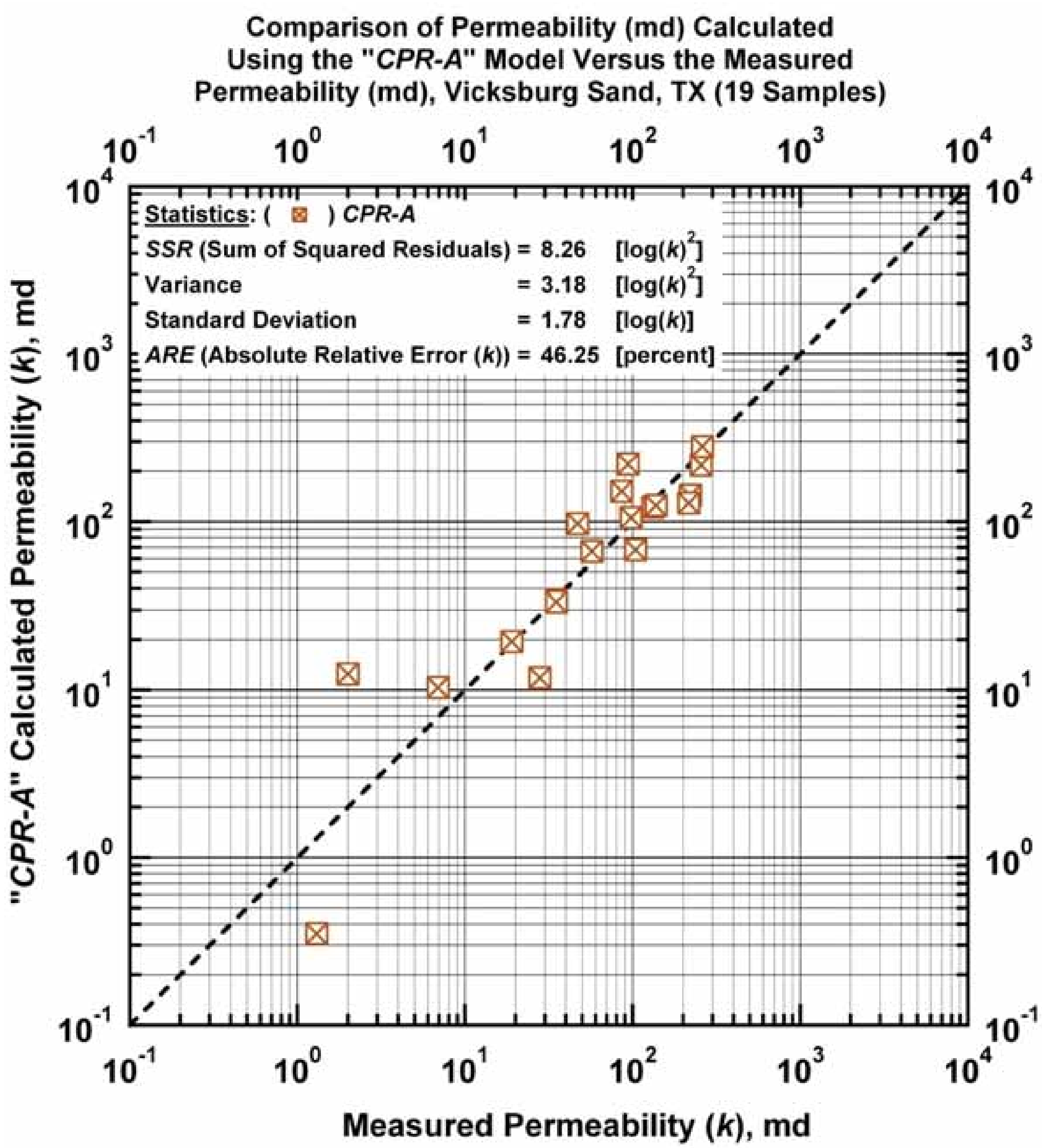

Figure D.2a — Model *CPR-A*: calculated versus measured permeability. [*Case*: Vicksburg Sand, S. TX (USA)]

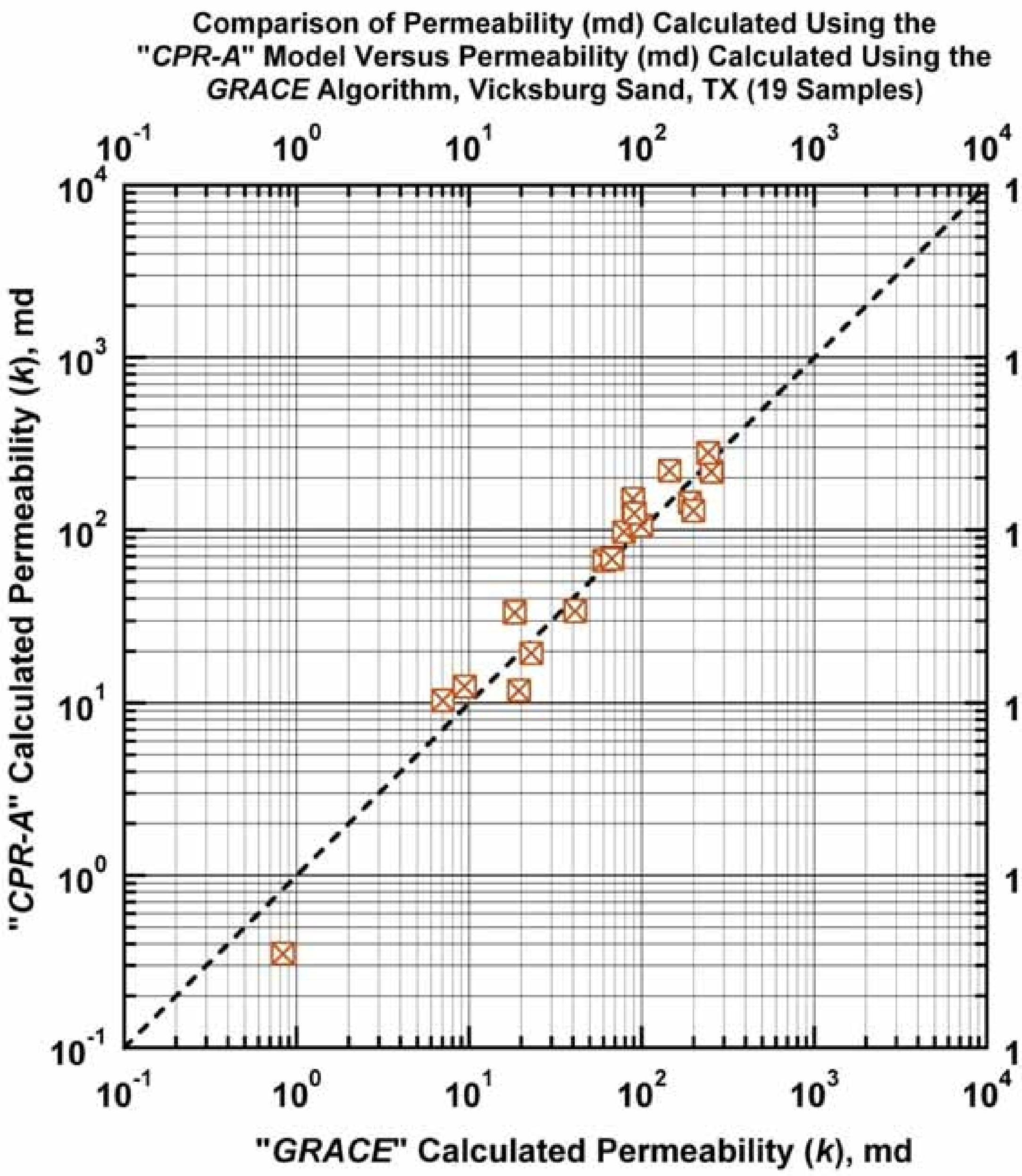

Figure D.2b — Model *CPR-A*: Permeability calculated using Model *CPR-A* versus permeability calculated using the *GRACE* Algorithm. [*Case*: Vicksburg Sand, S. TX (USA)]

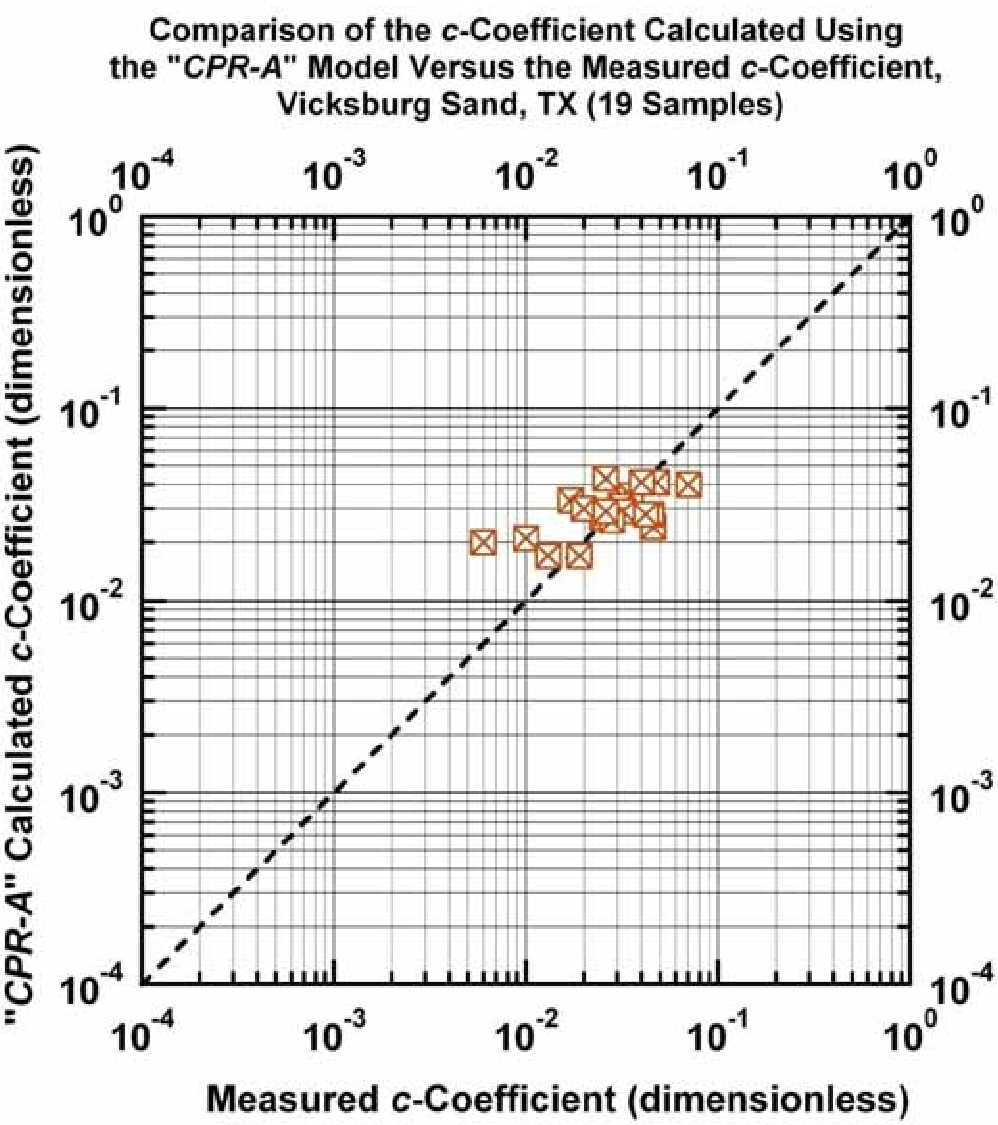

Figure D.2c — Model *CPR-A*: Calculated *c*-function values versus measured *c*-function values. [*Case*: Vicksburg Sand, S. TX (USA)]

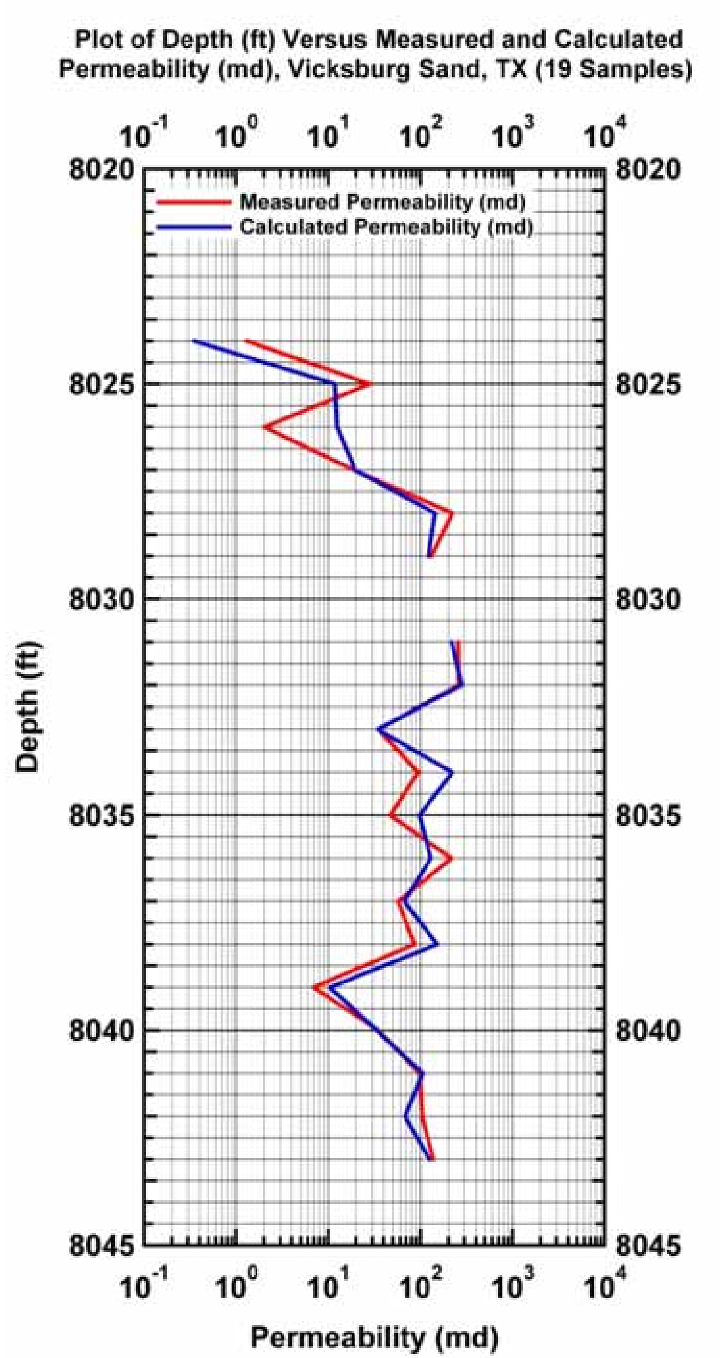

Figure D.2d — Model *CPR-A*: Calculated and measured permeability values versus depth. [*Case*: Vicksburg Sand, S. TX (USA)]

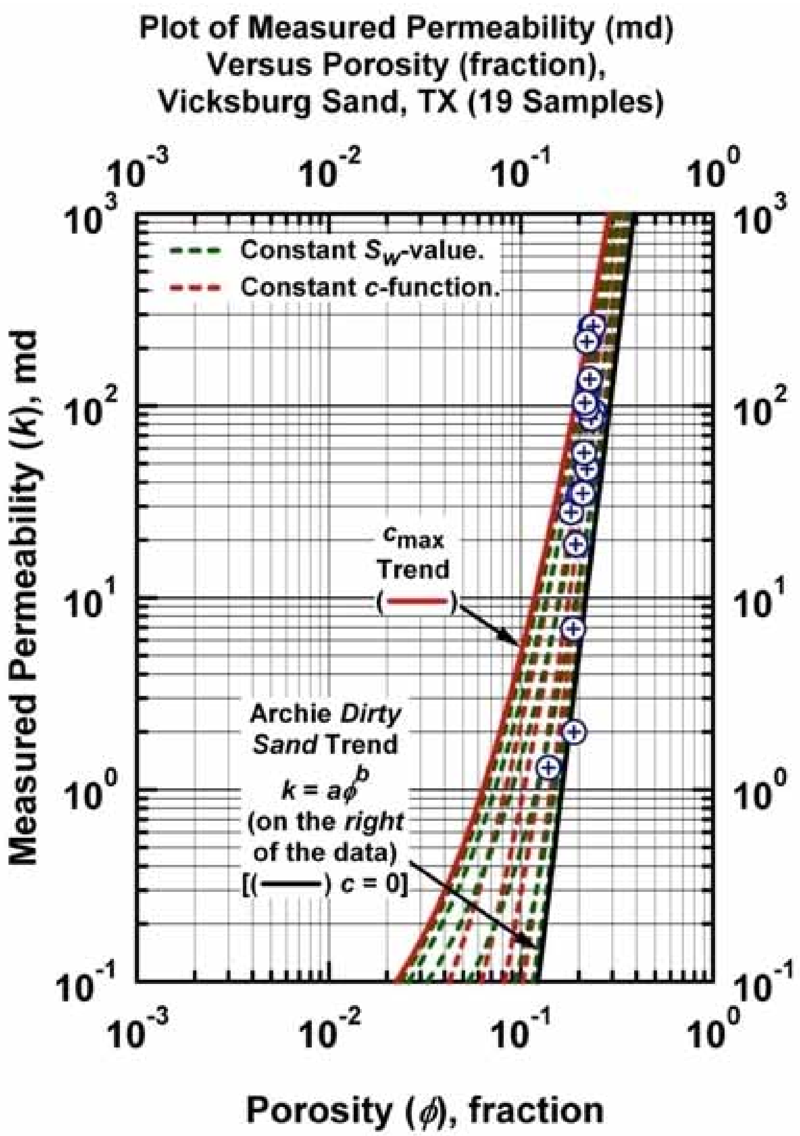

Figure D.3a — Model *CPR-B*: $k = a(\phi + c)^b \quad c = c_{\max} \exp[-c_1 \phi^{c_2} S_w^{c_3}]$ — "Clean Sand" Plot (log-log format) — Archie "Dirty Sand" trend is given by the straight-line trend at the far right of the data (power law model). [*Case*: Vicksburg Sand, S. TX (USA)]

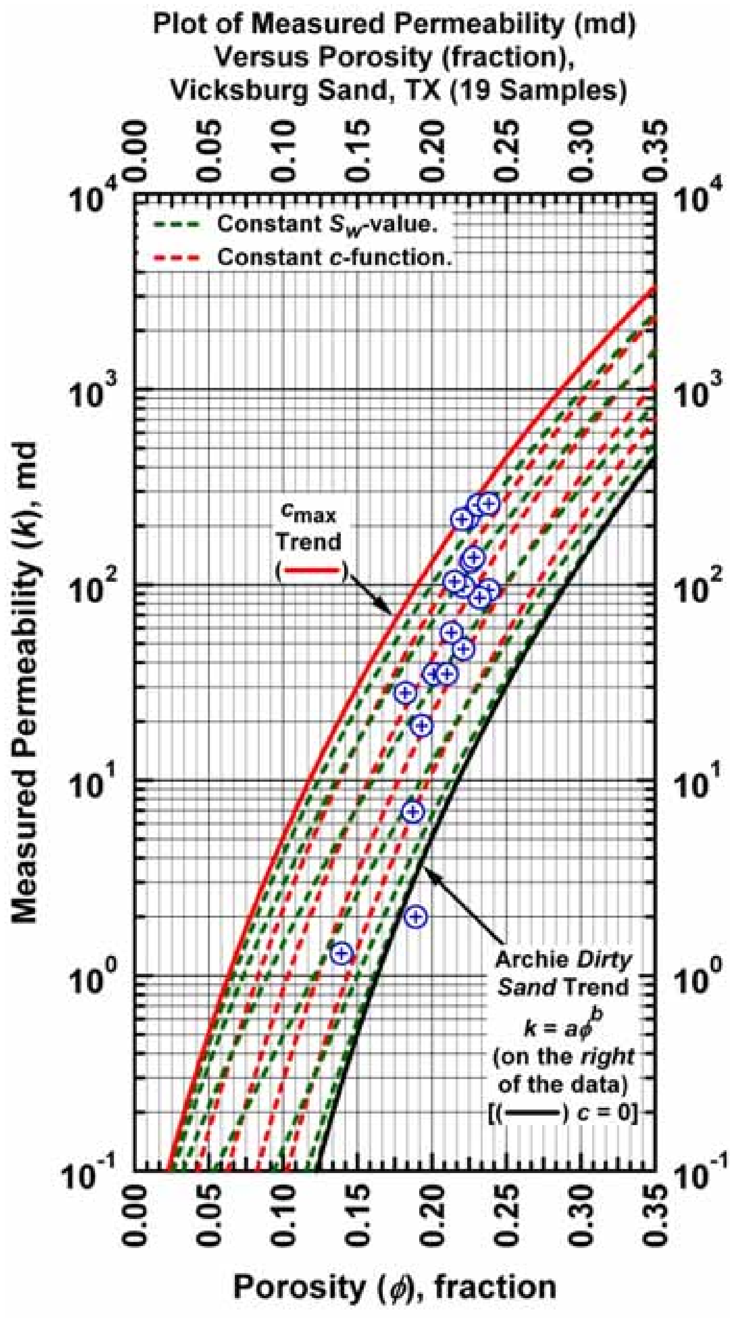

Figure D.3b — Model *CPR-B*: $k = a(\phi + c)^b \quad c = c_{\max}\exp[-c_1\phi^{c_2} S_w^{c_3}]$ — "Dirty Sand" Plot (semilog format) — Archie "Dirty Sand" trend is given by the curved trend at the far right of the data (power law model). [*Case*: Vicksburg Sand, S. TX (USA)]

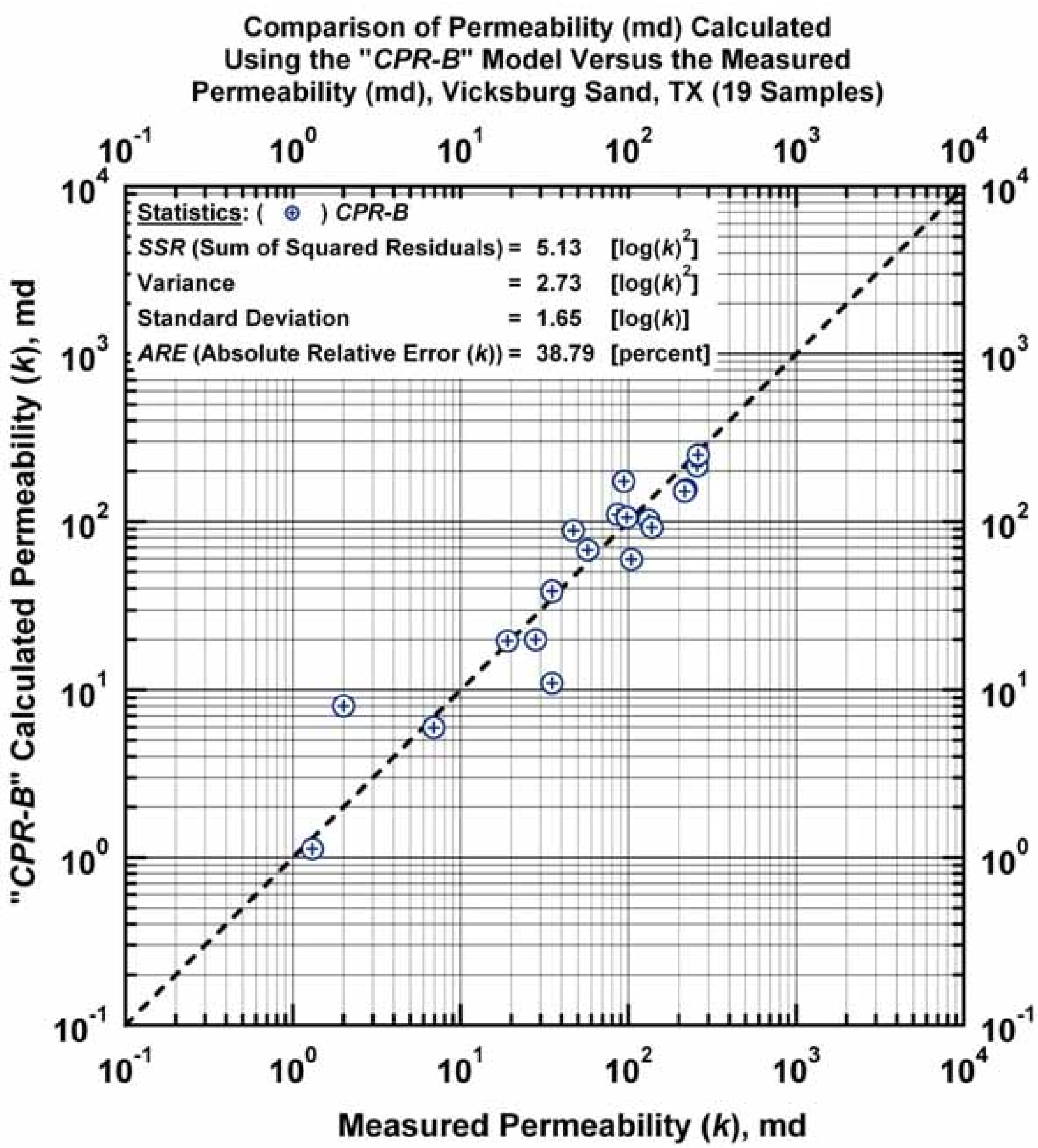

Figure D.4a — Model *CPR-B*: calculated versus measured permeability. [*Case*: Vicksburg Sand, S. TX (USA)]

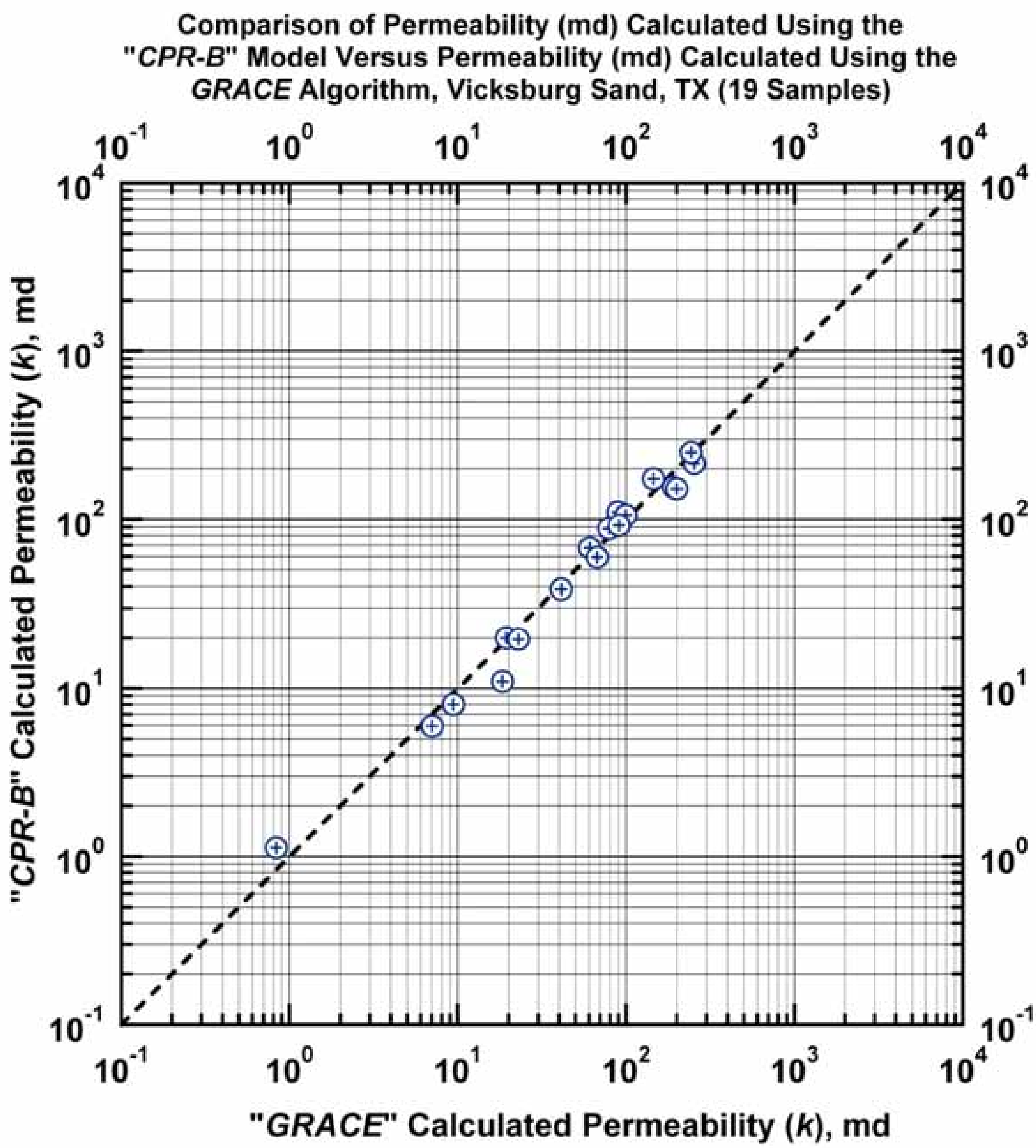

Figure D.4b — Model *CPR-B*: Permeability calculated using Model *CPR-B* versus permeability calculated using the *GRACE* Algorithm. [*Case*: Vicksburg Sand, S. TX (USA)]

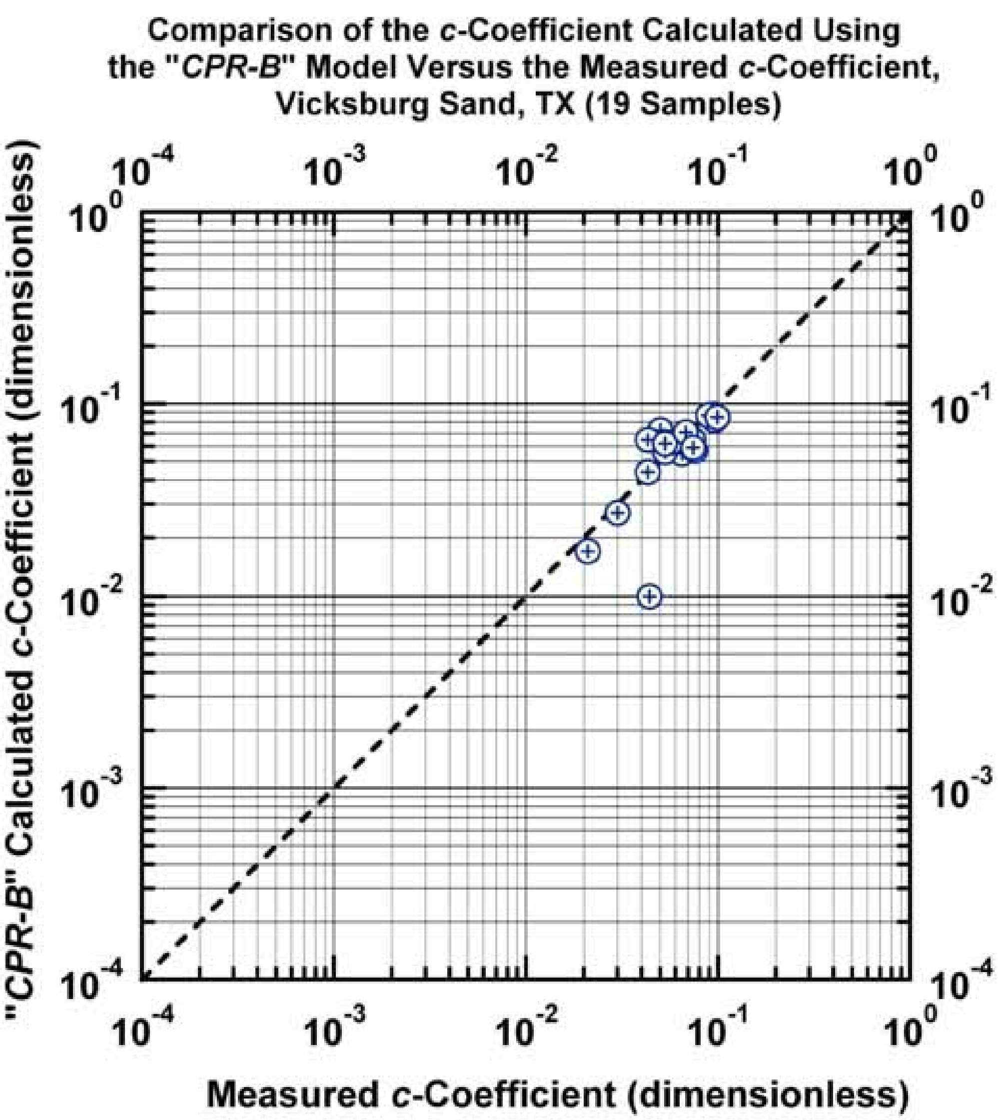

Figure D.4c — Model *CPR-B*: Calculated *c*-function values versus measured *c*-function values. [*Case*: Vicksburg Sand, S. TX (USA)]

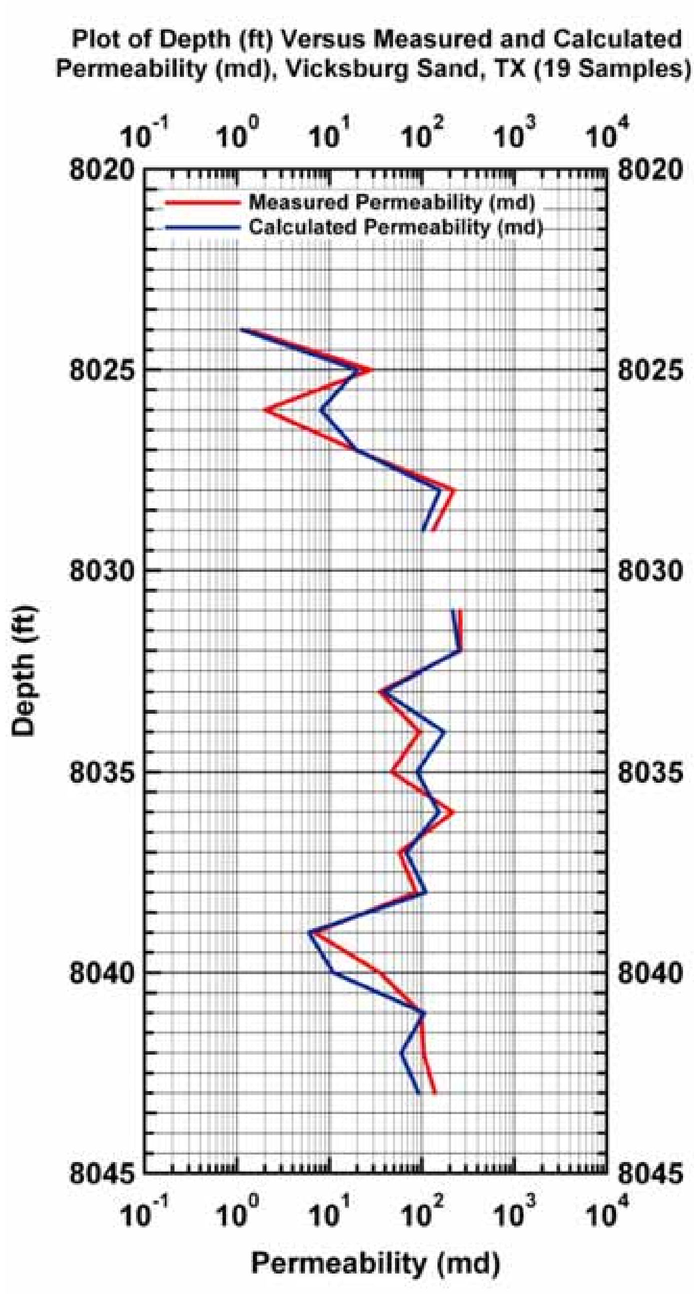

Figure D.4d — Model *CPR-A*: Calculated and measured permeability values versus depth. [*Case*: Vicksburg Sand, S. TX (USA)]

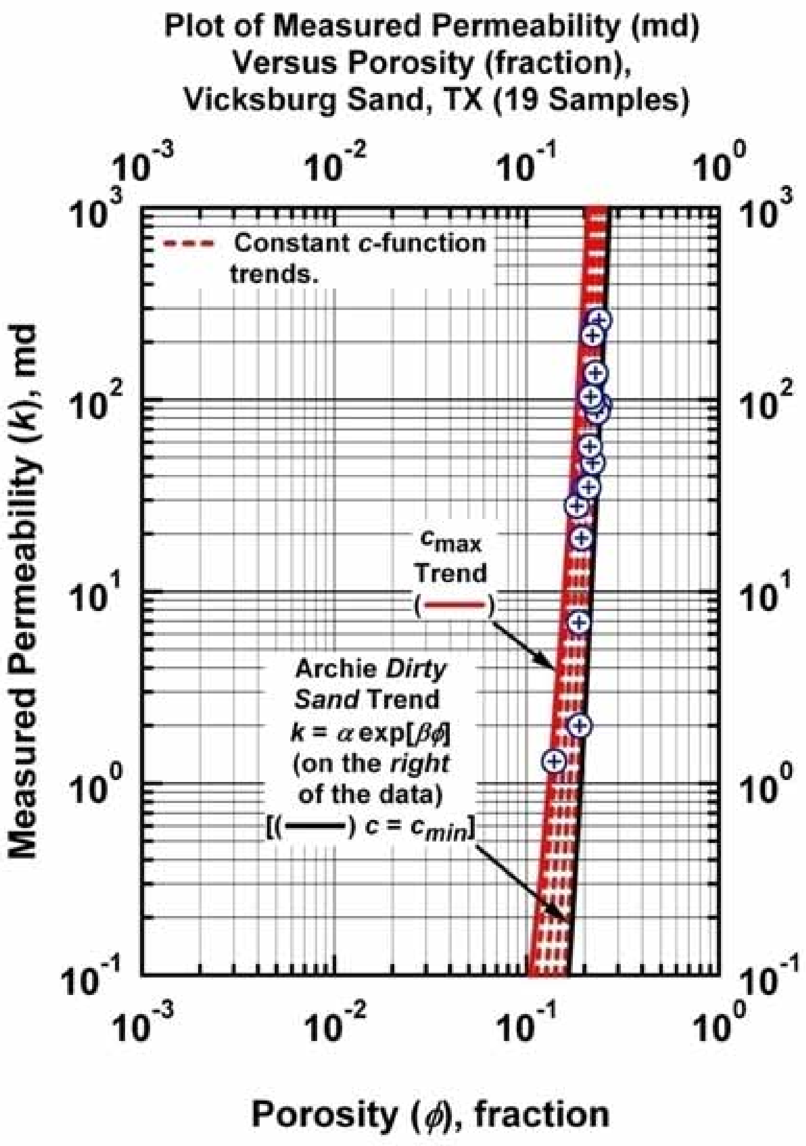

Figure D.5a — Model *CPR-C*: $k = c\exp[\beta\phi]$ $\quad c = c_{\max}\exp[-c_1\phi^{c_2} S_w^{c_3}]$ — "Clean Sand" Plot (log-log format) — Archie "Dirty Sand" trend is given by the curved trend at the far right of the data (exponential model). [*Case*: Vicksburg Sand, S. TX (USA)]

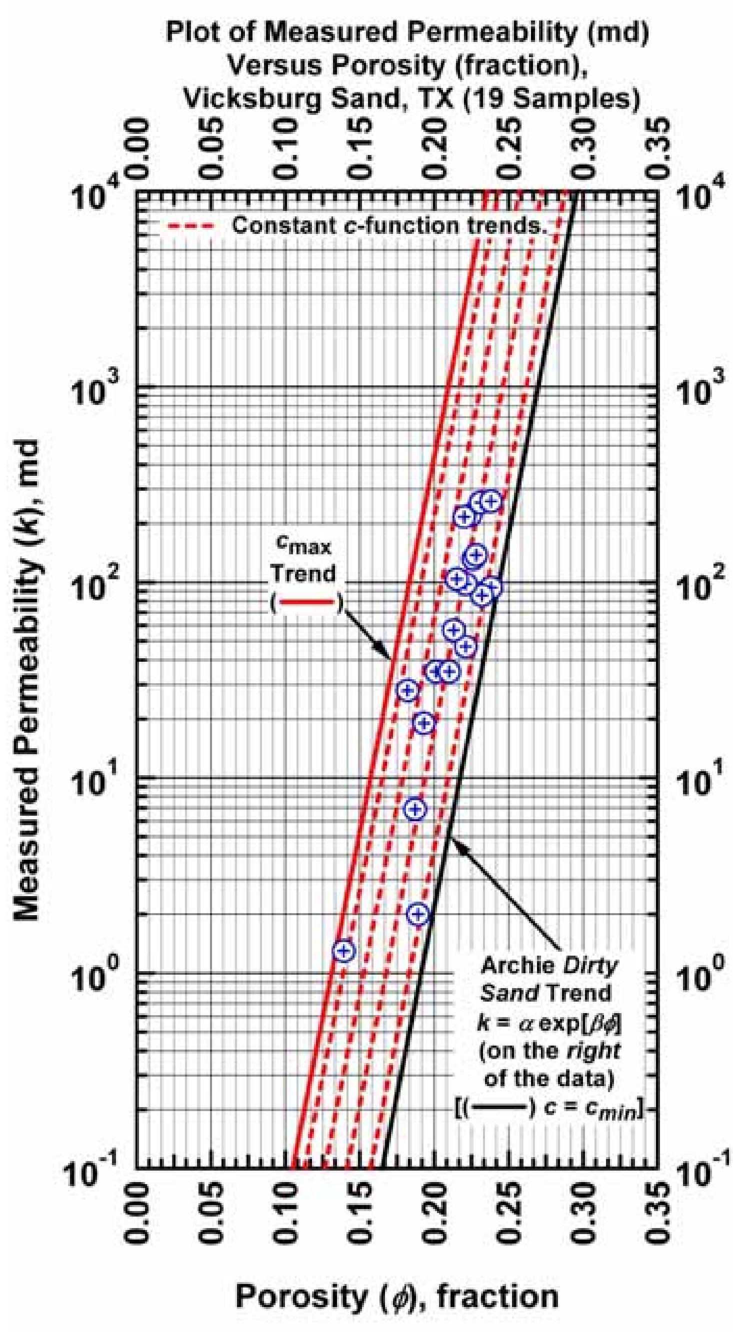

Figure D.5b — Model *CPR-C*: $k = c\exp[\beta\phi]$ $c = c_{\max}\exp[-c_1\phi^{c_2} S_w^{c_3}]$ — "Dirty Sand" Plot (semilog format) — Archie "Dirty Sand" trend is given by the straight-line trend at the far right of the data (exponential model). [*Case*: Vicksburg Sand, S. TX (USA)]

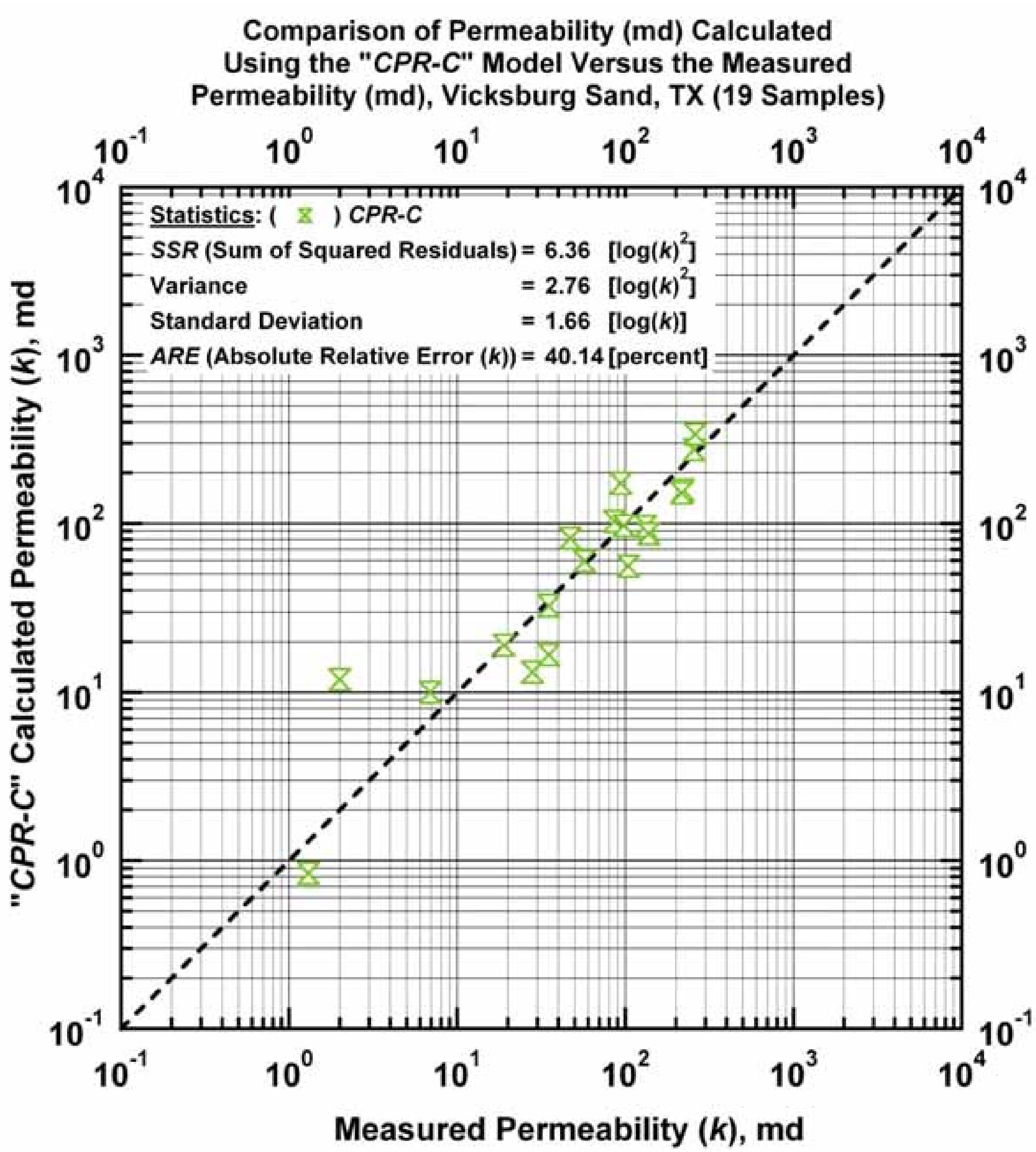

Figure D.6a — Model *CPR-C*: calculated versus measured permeability. [*Case*: Vicksburg Sand, S. TX (USA)]

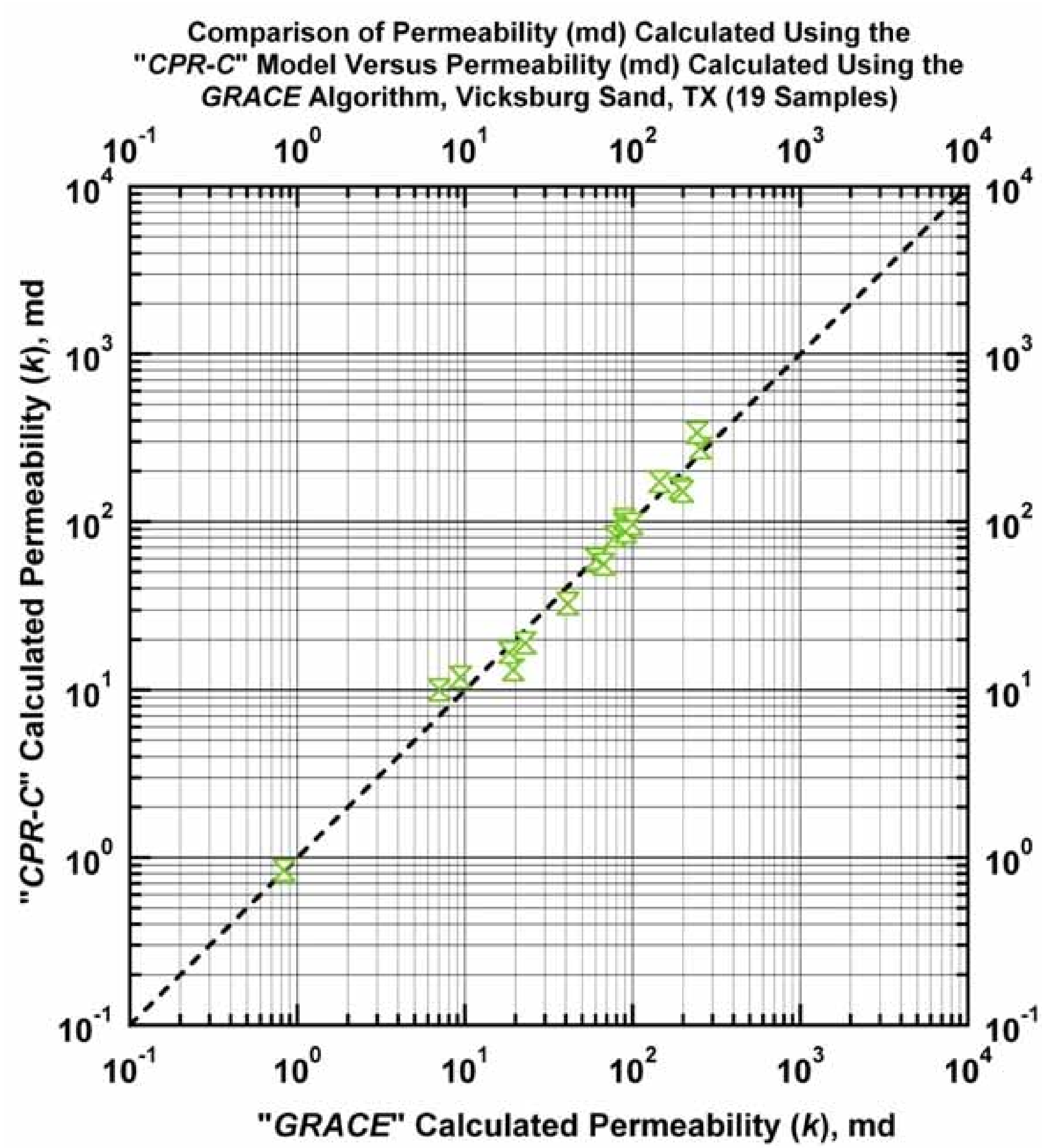

Figure D.6b — Model *CPR-C*: Permeability calculated using Model *CPR-C* versus permeability calculated using the *GRACE* Algorithm. [*Case*: Vicksburg Sand, S. TX (USA)]

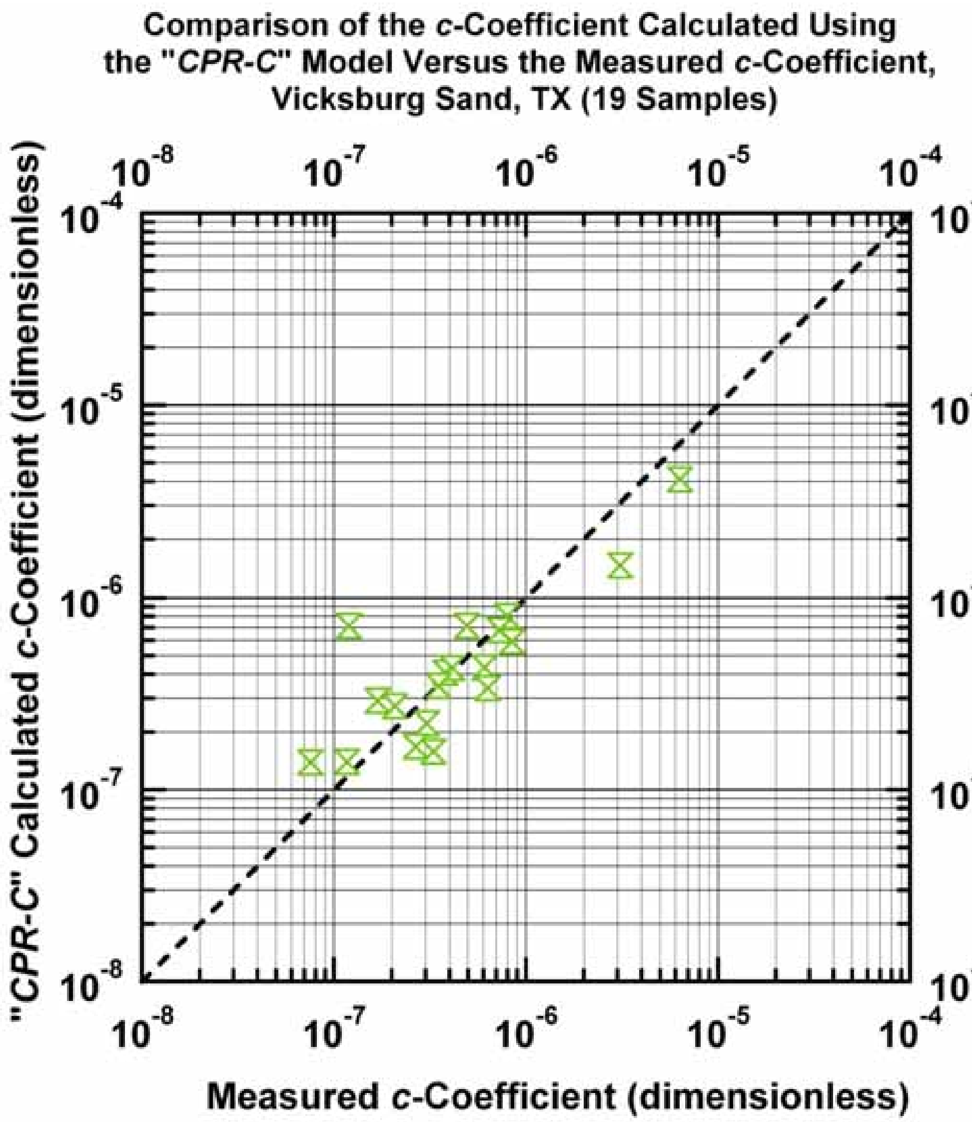

Figure D.6c — Model *CPR-C*: Calculated *c*-function values versus measured *c*-function values. [*Case*: Vicksburg Sand, S. TX (USA)]

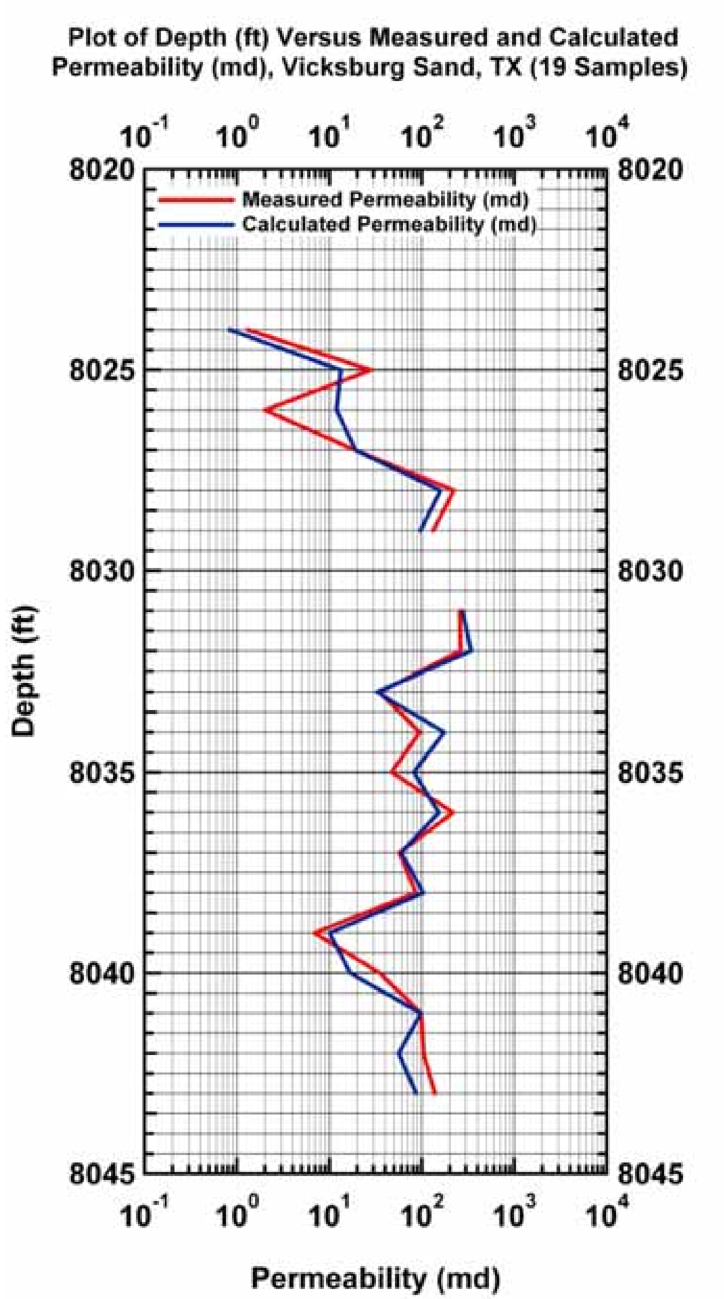

Figure D.6d — Model *CPR-A*: Calculated and measured permeability values versus depth. [*Case*: Vicksburg Sand, S. TX (USA)]

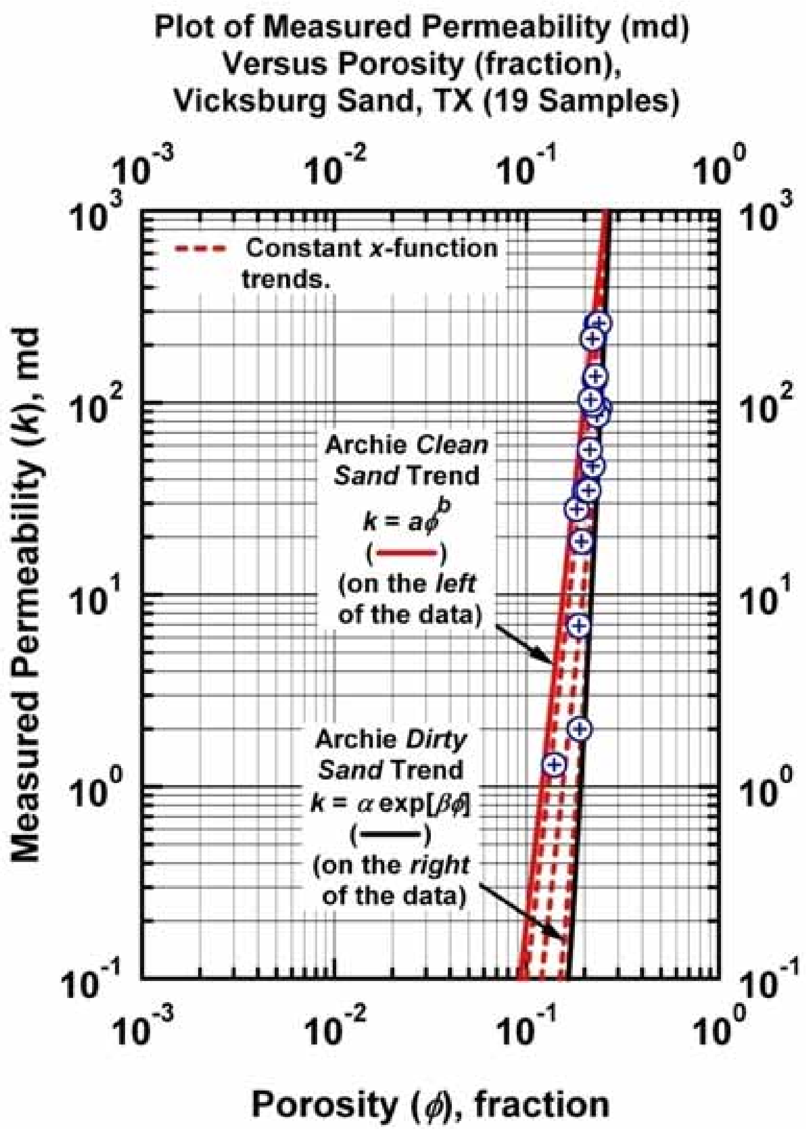

Figure D.7a — Model *CPR-D*: $k = xa\phi^{b} + (1-x)\alpha\exp[\beta\phi]\quad[0 \le x \le 1]$ — *Weighted Power Law-Exponential Model* used to correlate permeability (k) and porosity (ϕ). "Clean Sand" Plot — Archie "Clean Sand" trend is given by the straight-line trend at the far left of the data (power law model). [*Case*: Vicksburg Sand, S. TX (USA)]

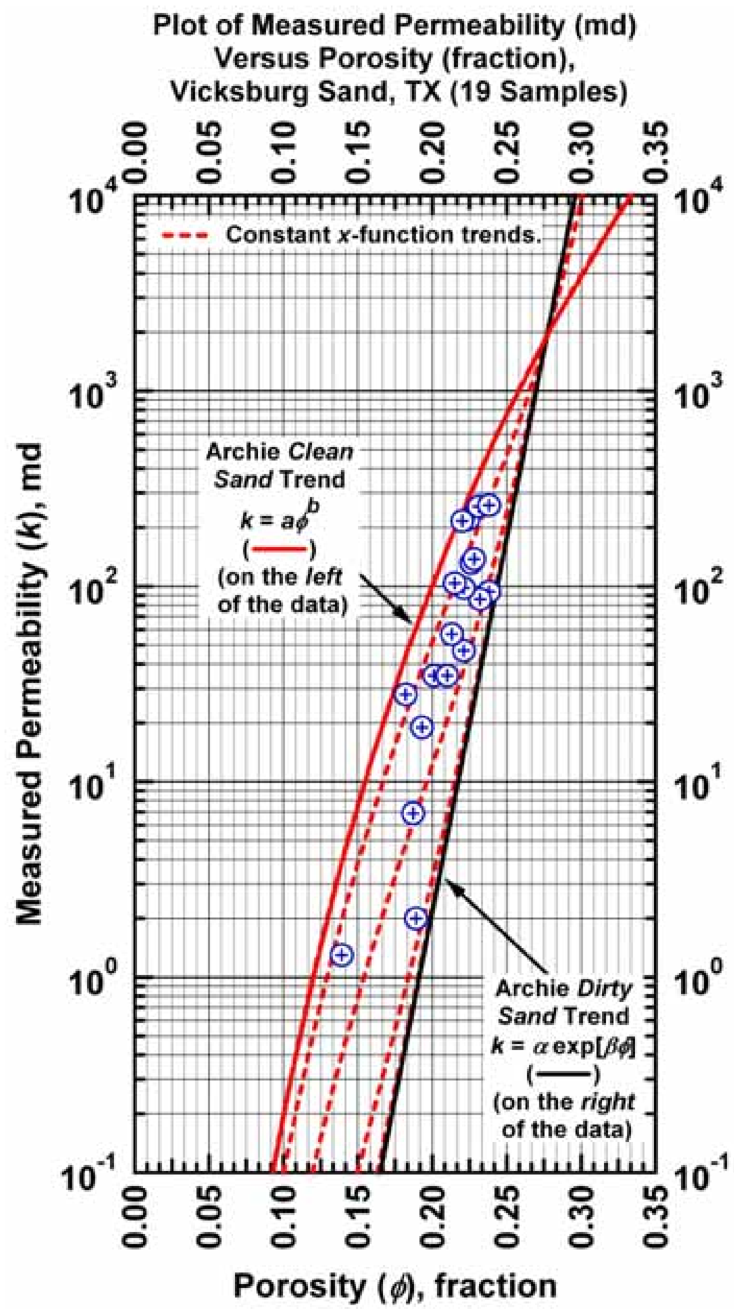

Figure D.7b — Model *CPR-D*: $k = xa\phi^b + (1-x)\alpha \exp[\beta\phi] \quad [0 \le x \le 1]$ — *Weighted Power Law-Exponential Model* used to correlate permeability (k) and porosity (ϕ). "Dirty Sand" Plot — Archie "Dirty Sand" trend is given by the straight-line trend at the far right of the data (exponential model). [*Case*: Vicksburg Sand, S. TX (USA)]

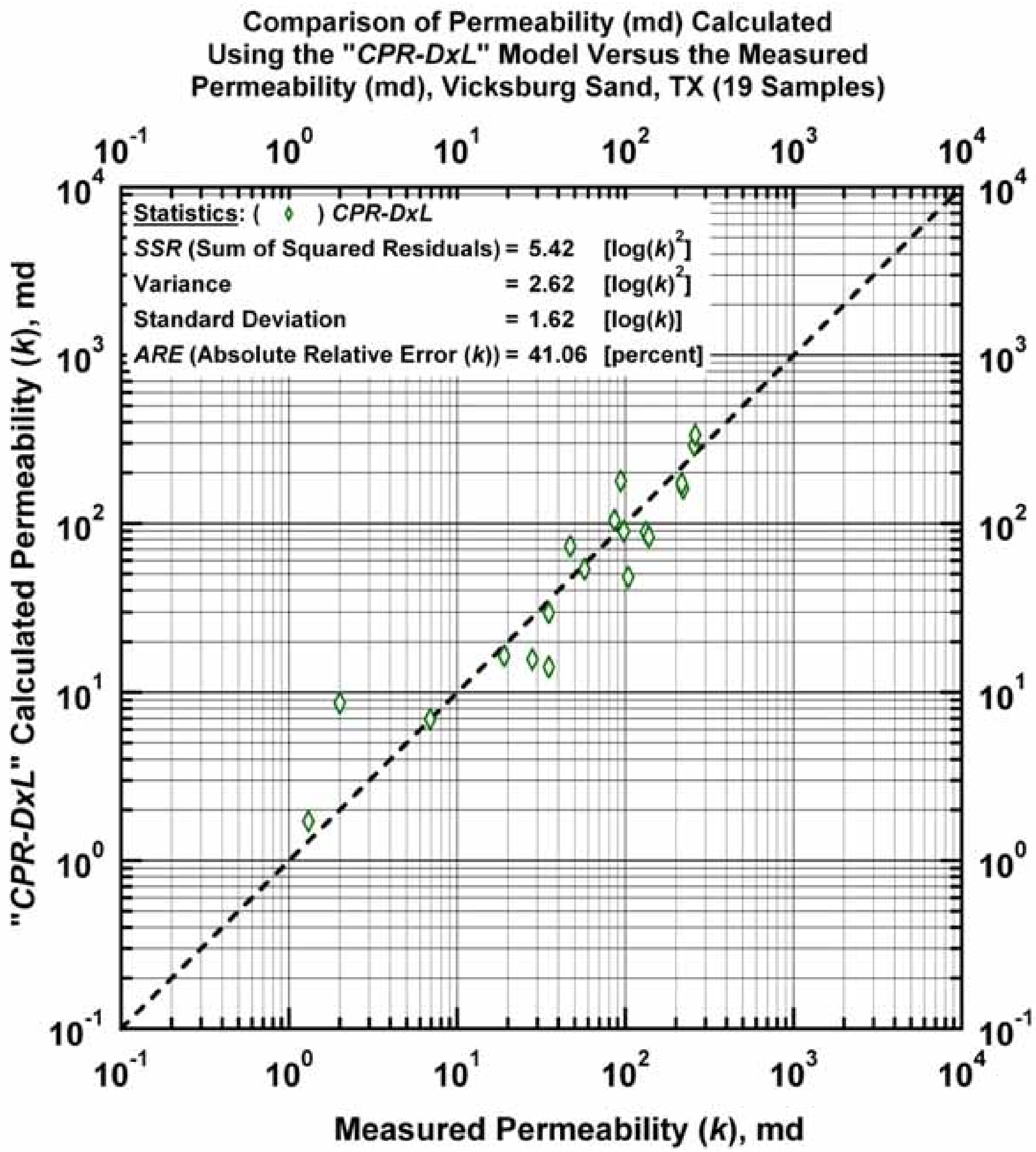

Figure D.8a — Model *CPR-DxL*: Calculated versus measured permeability. [*Case*: Vicksburg Sand, S. TX (USA)]

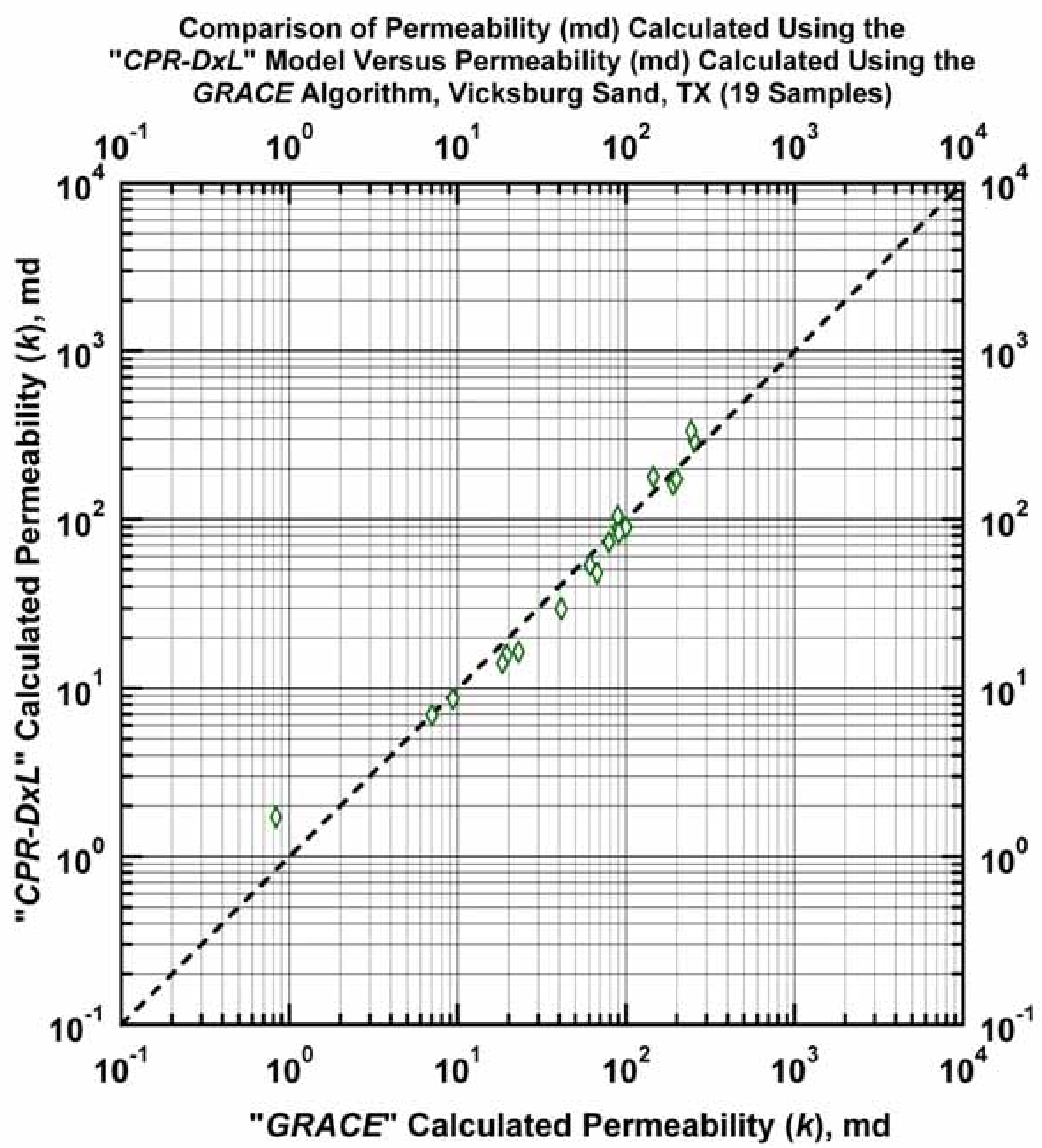

Figure D.8b — Model *CPR-DxL*: Permeability calculated using Model *CPR-C* versus permeability calculated using the *GRACE* Algorithm. [*Case*: Vicksburg Sand, S. TX (USA)]

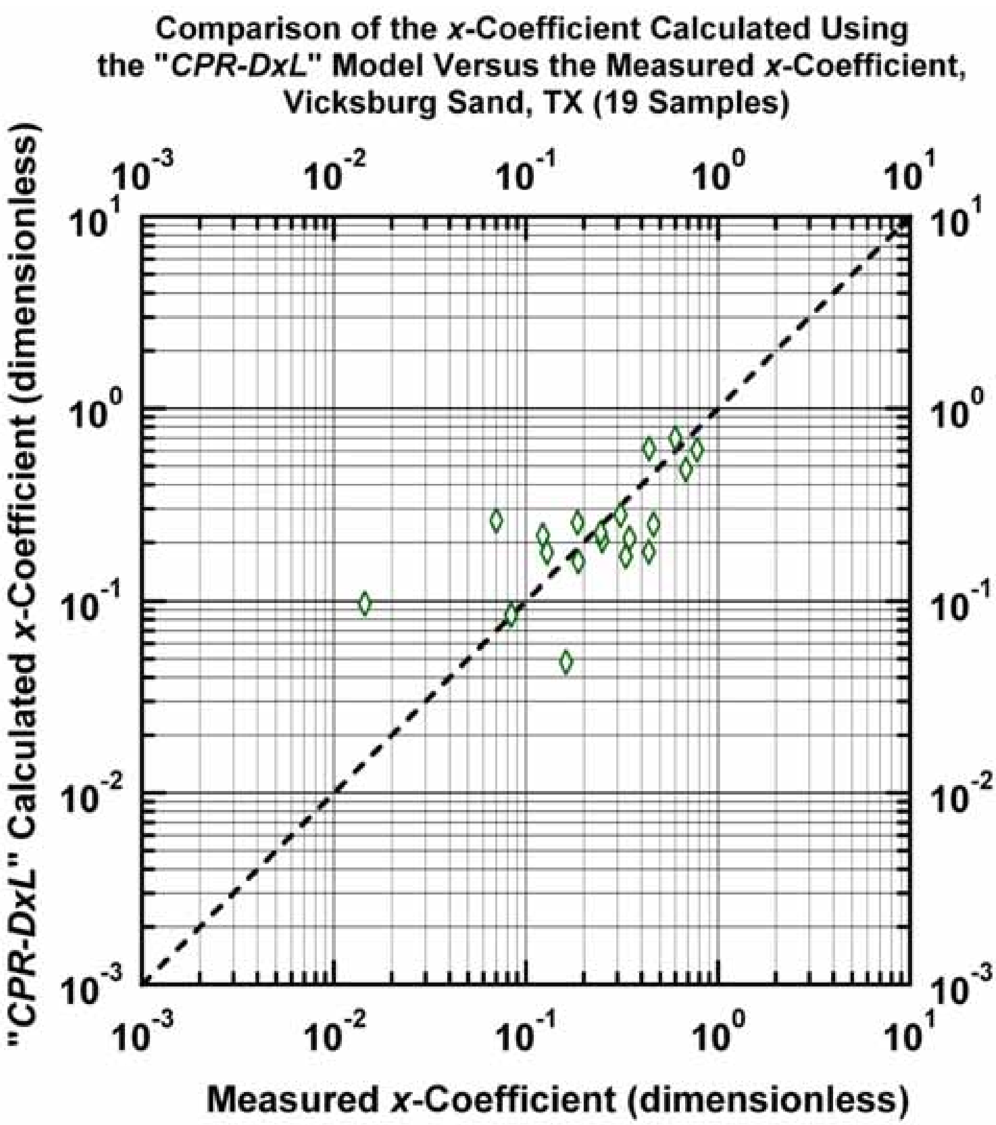

Figure D.8c — Model *CPR-DxL*: Calculated *x*-function weight values versus measured *x*-function weight values. [*Case*: Vicksburg Sand, S. TX (USA)]

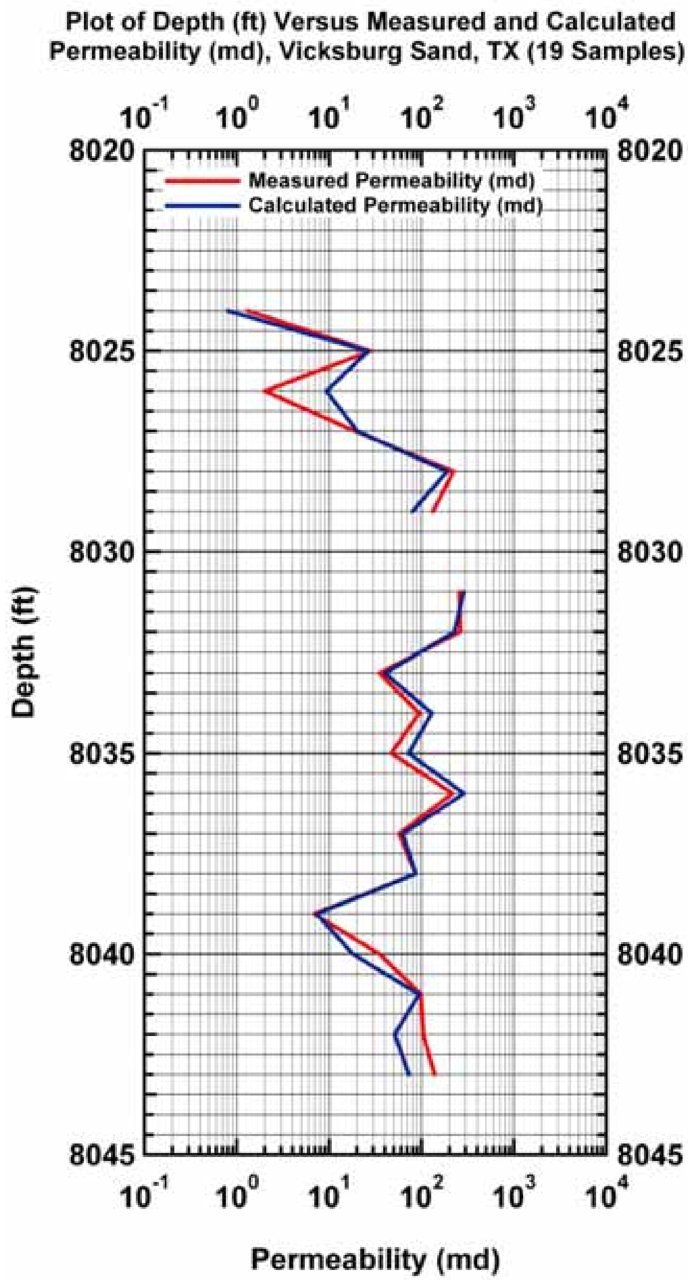

Figure D.8d — Model *CPR-A*: Calculated and measured permeability values versus depth. [*Case*: Vicksburg Sand, S. TX (USA)]

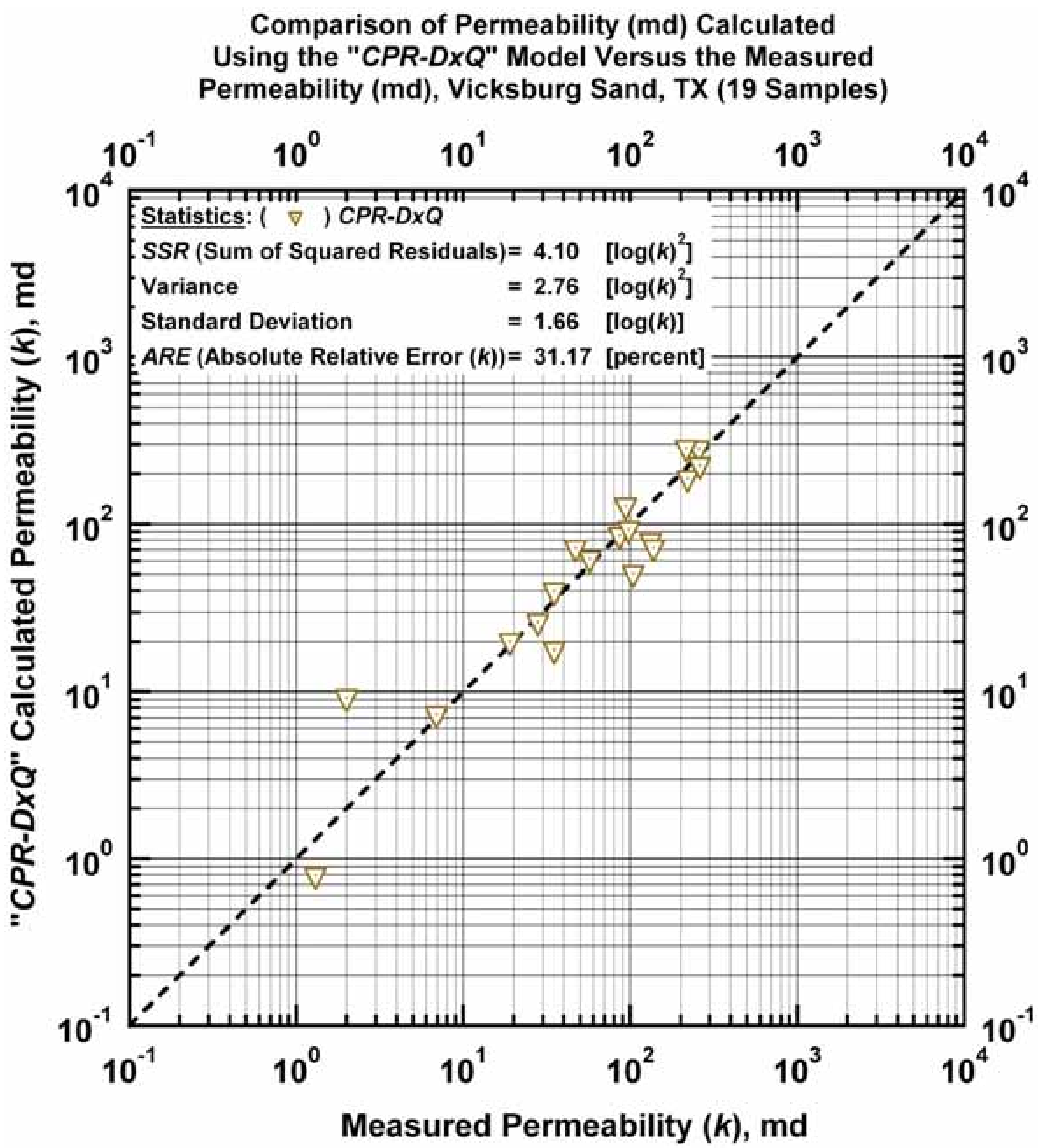

Figure D.9a — Model *CPR-DxQ*: Calculated versus measured permeability. [*Case*: Vicksburg Sand, S. TX (USA)]

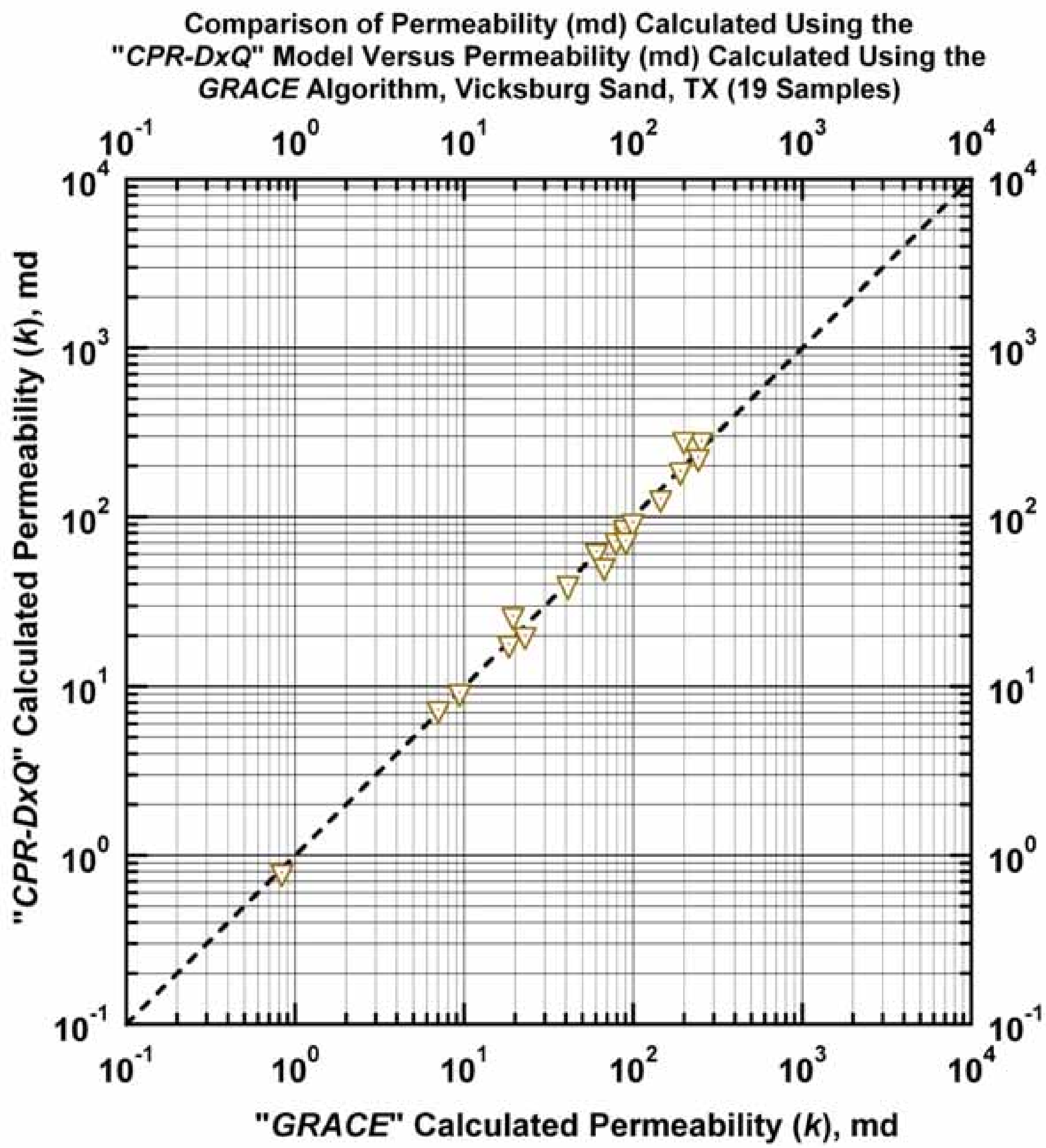

Figure D.9b — Model *CPR-DxQ*: Permeability calculated using Model *CPR-C* versus permeability calculated using the *GRACE* Algorithm. [*Case*: Vicksburg Sand, S. TX (USA)]

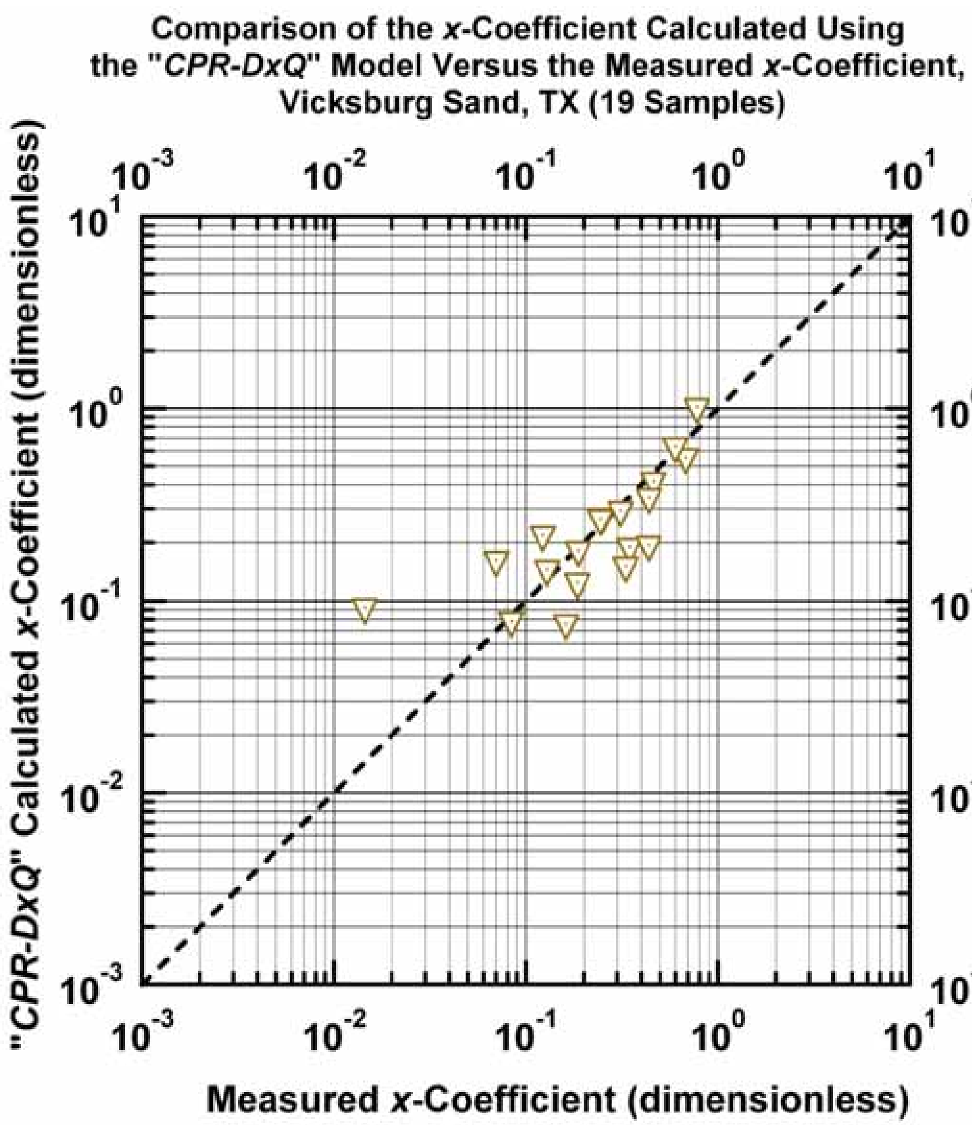

Figure D.9c — Model *CPR-DxQ*: Calculated *x*-function weight values versus measured *x*-function weight values. [*Case*: Vicksburg Sand, S. TX (USA)]

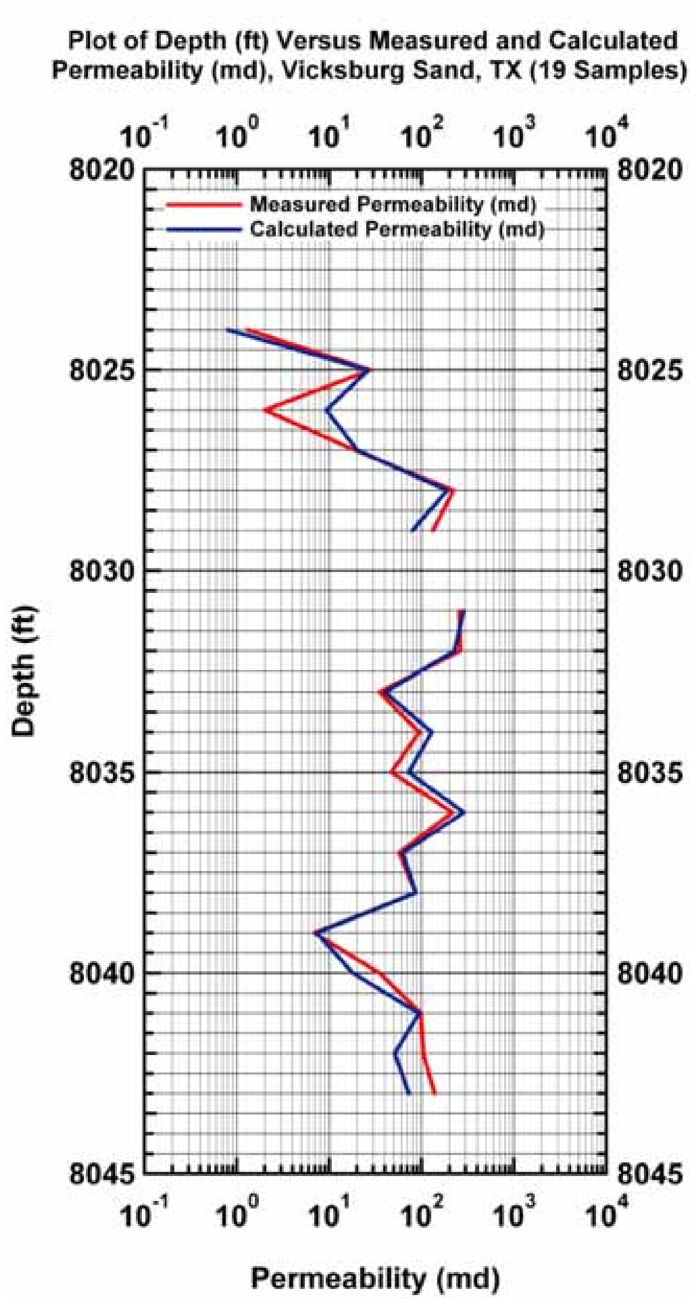

Figure D.9d — Model *CPR-A*: Calculated and measured permeability values versus depth. [*Case*: Vicksburg Sand, S. TX (USA)]

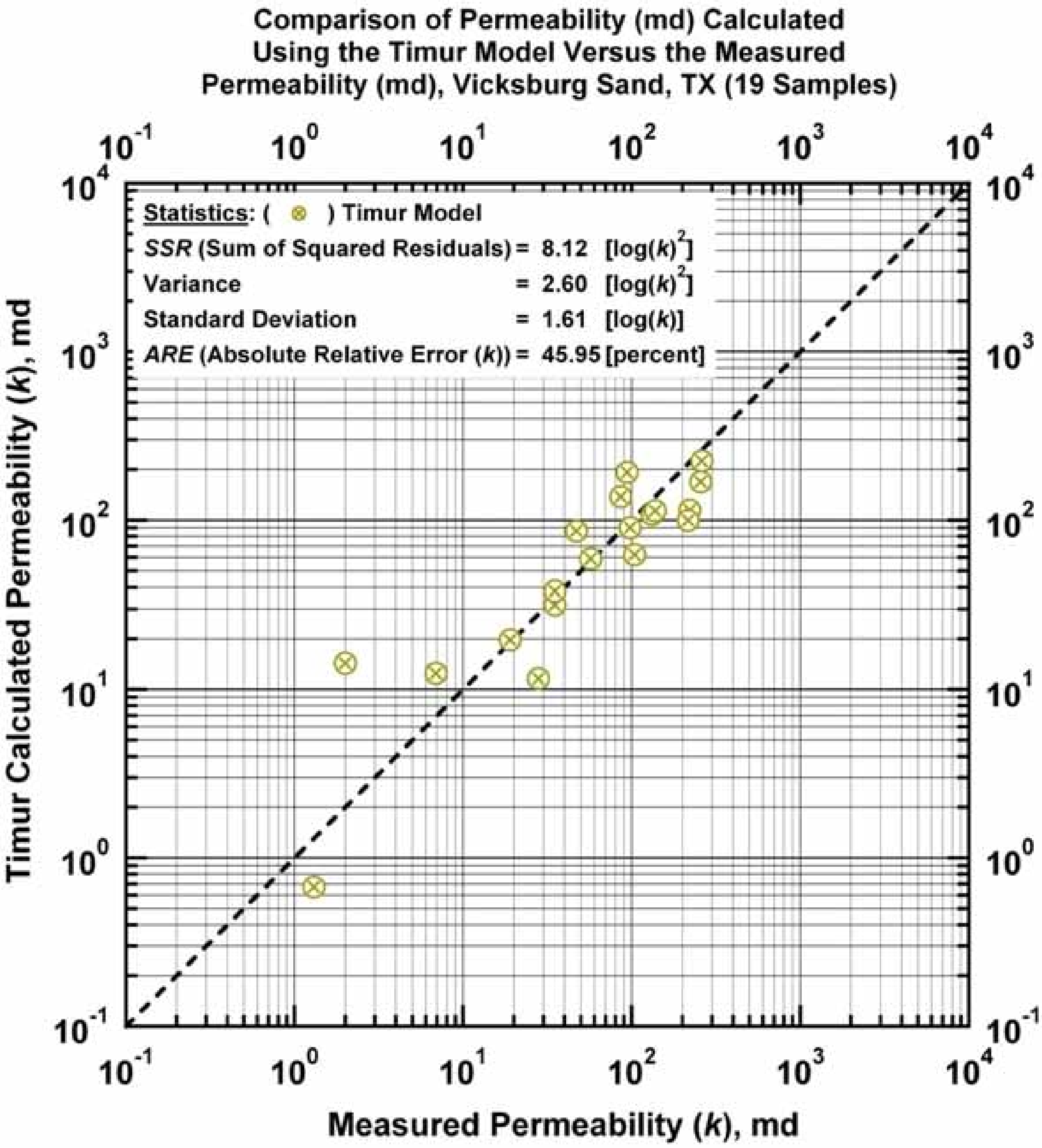

Figure D.10a — "Timur Model:" Calculated versus measured permeability. [*Case*: Vicksburg Sand, S. TX (USA)]

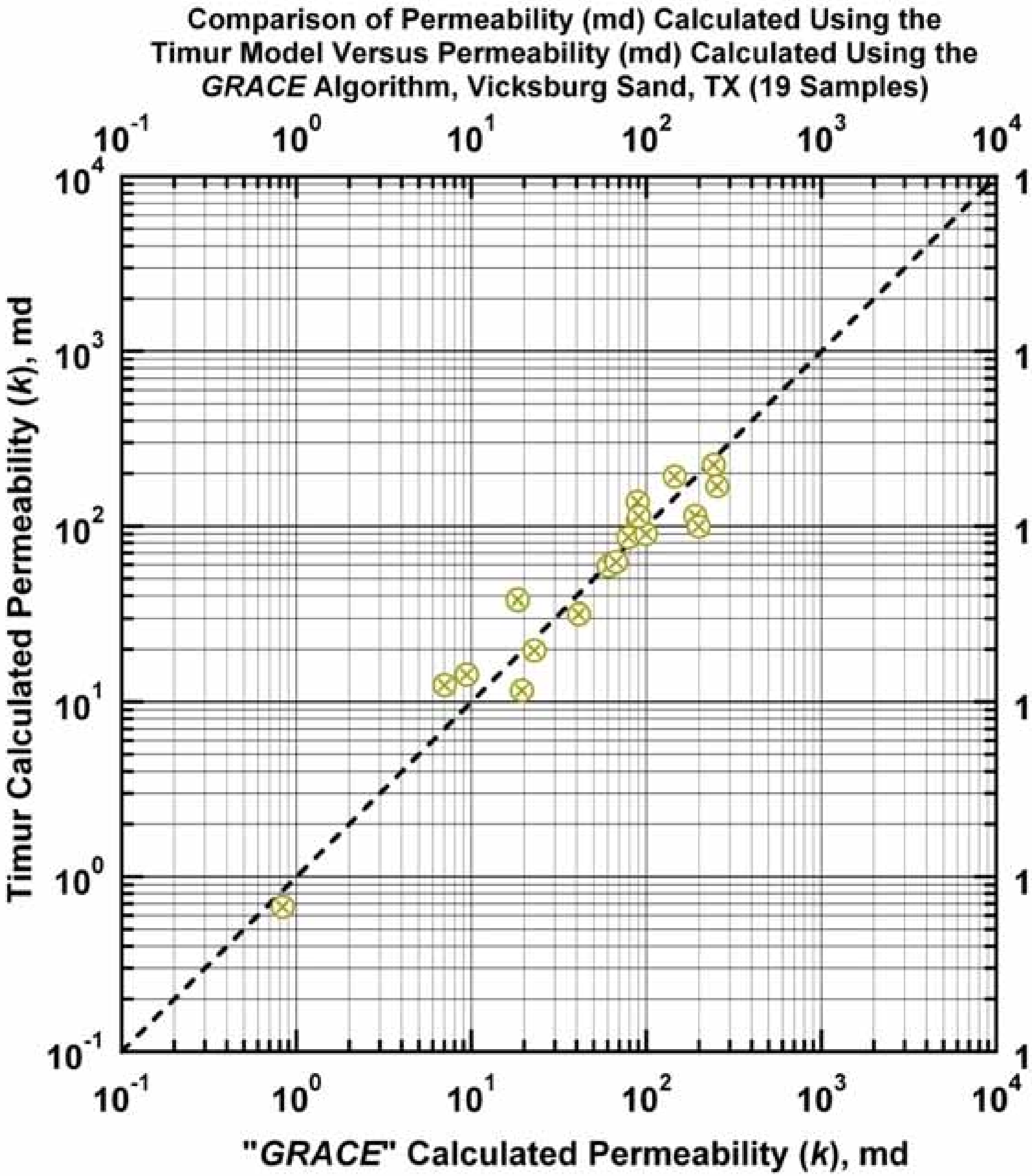

Figure D.10b — "Timur Model:" Permeability calculated using the "Timur Model" versus permeability calculated using the *GRACE* Algorithm. [*Case*: Vicksburg Sand, S. TX (USA)]

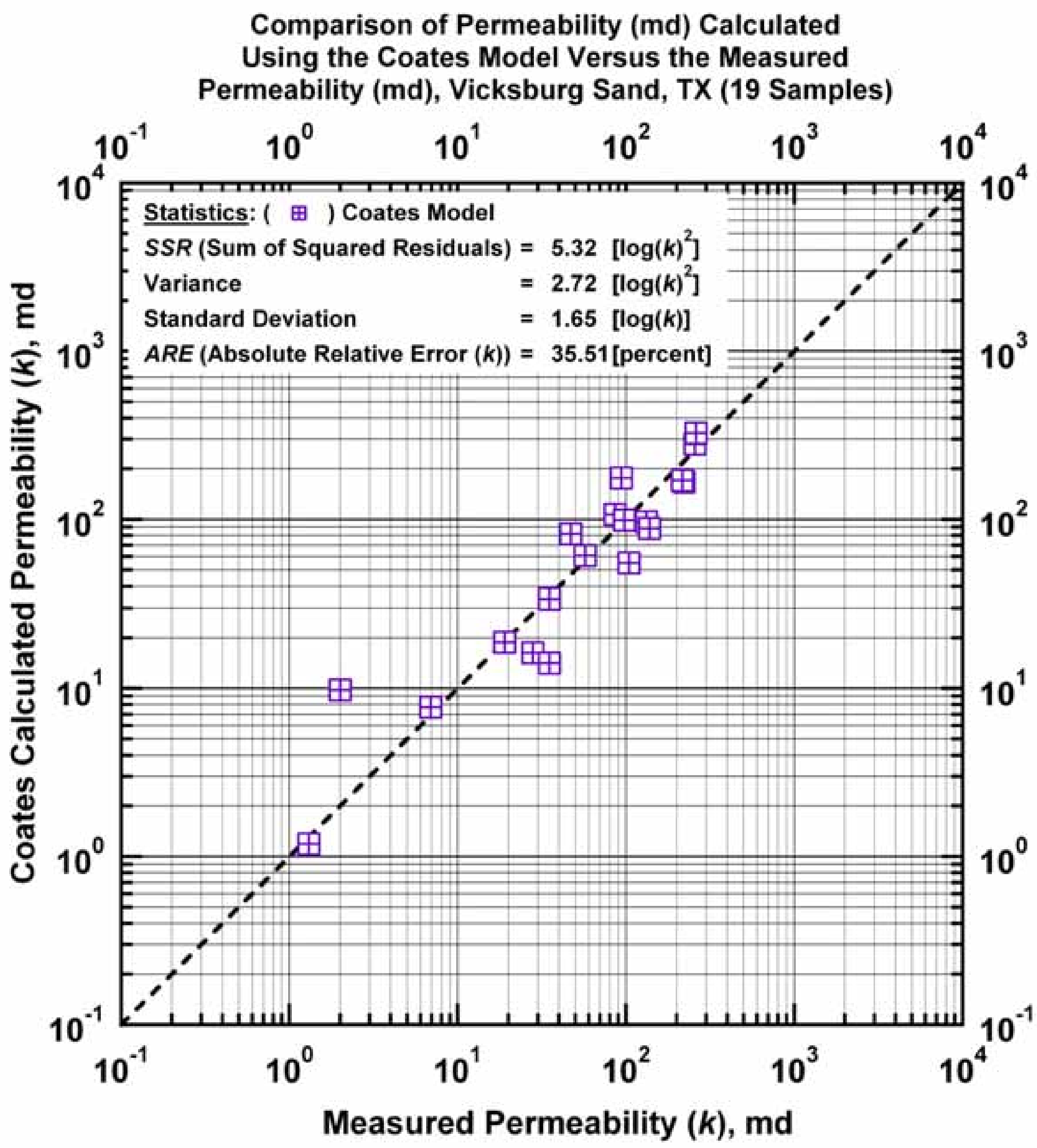

Figure D.11a — "Coates Model:" Calculated versus measured permeability. [*Case*: Vicksburg Sand, S. TX (USA)]

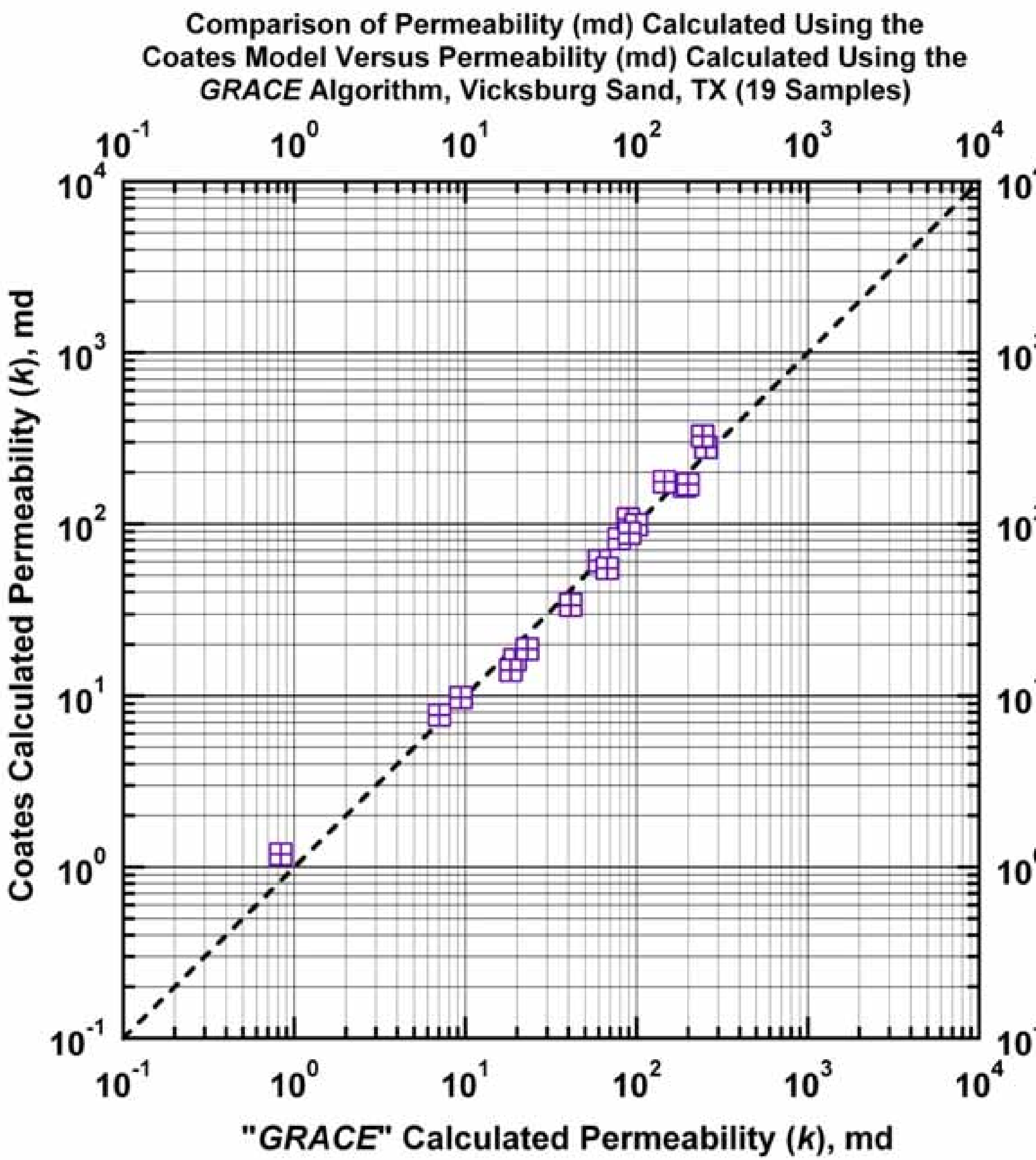

Figure D.11b — "Coates Model:" Permeability calculated using the "Coates Model" versus permeability calculated using the *GRACE* Algorithm. [*Case*: Vicksburg Sand, S. TX (USA)]

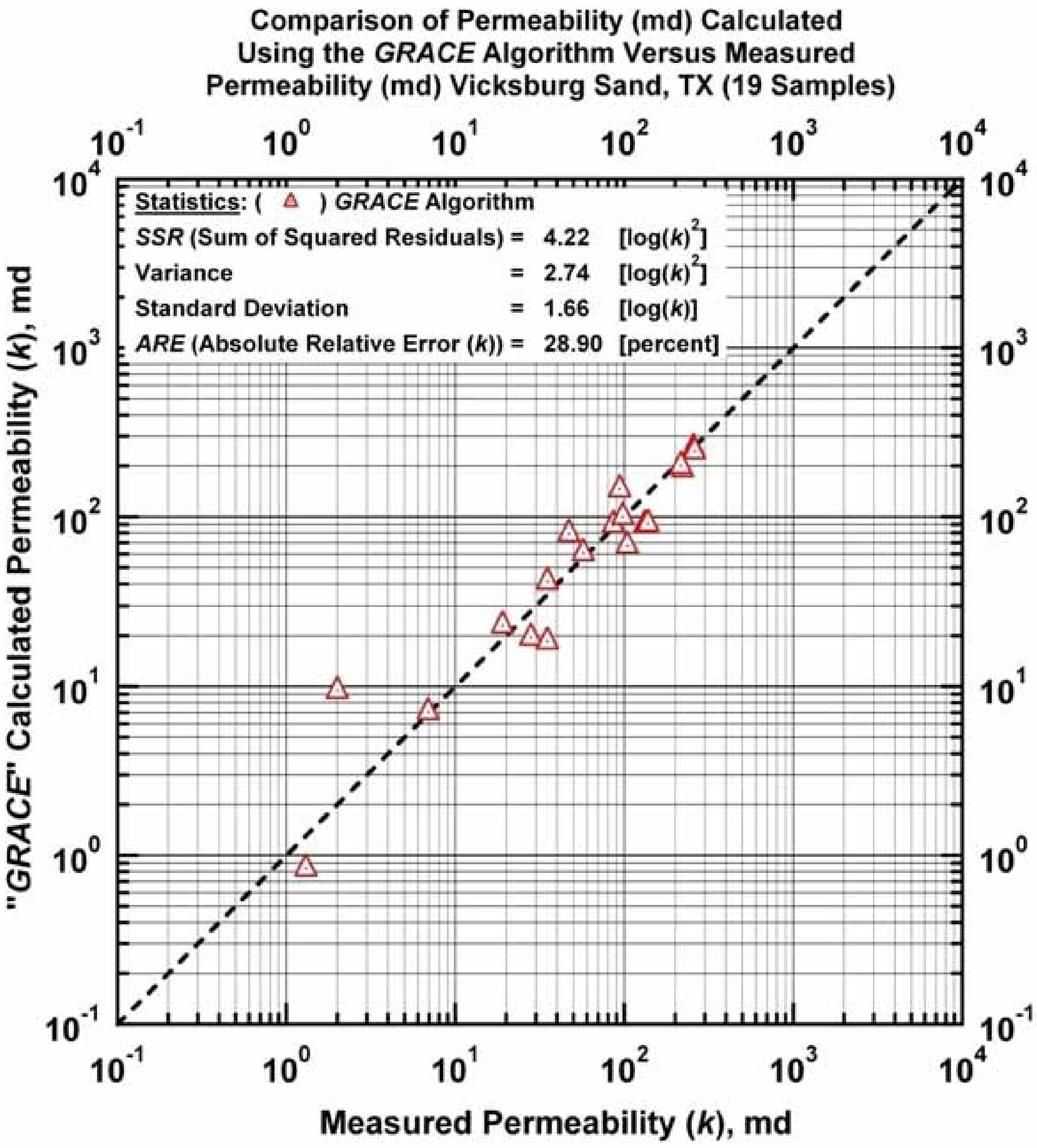

Figure D.12 — *GRACE* Model: Calculated versus measured permeability. [*Case*: Vicksburg Sand, S. TX (USA)]

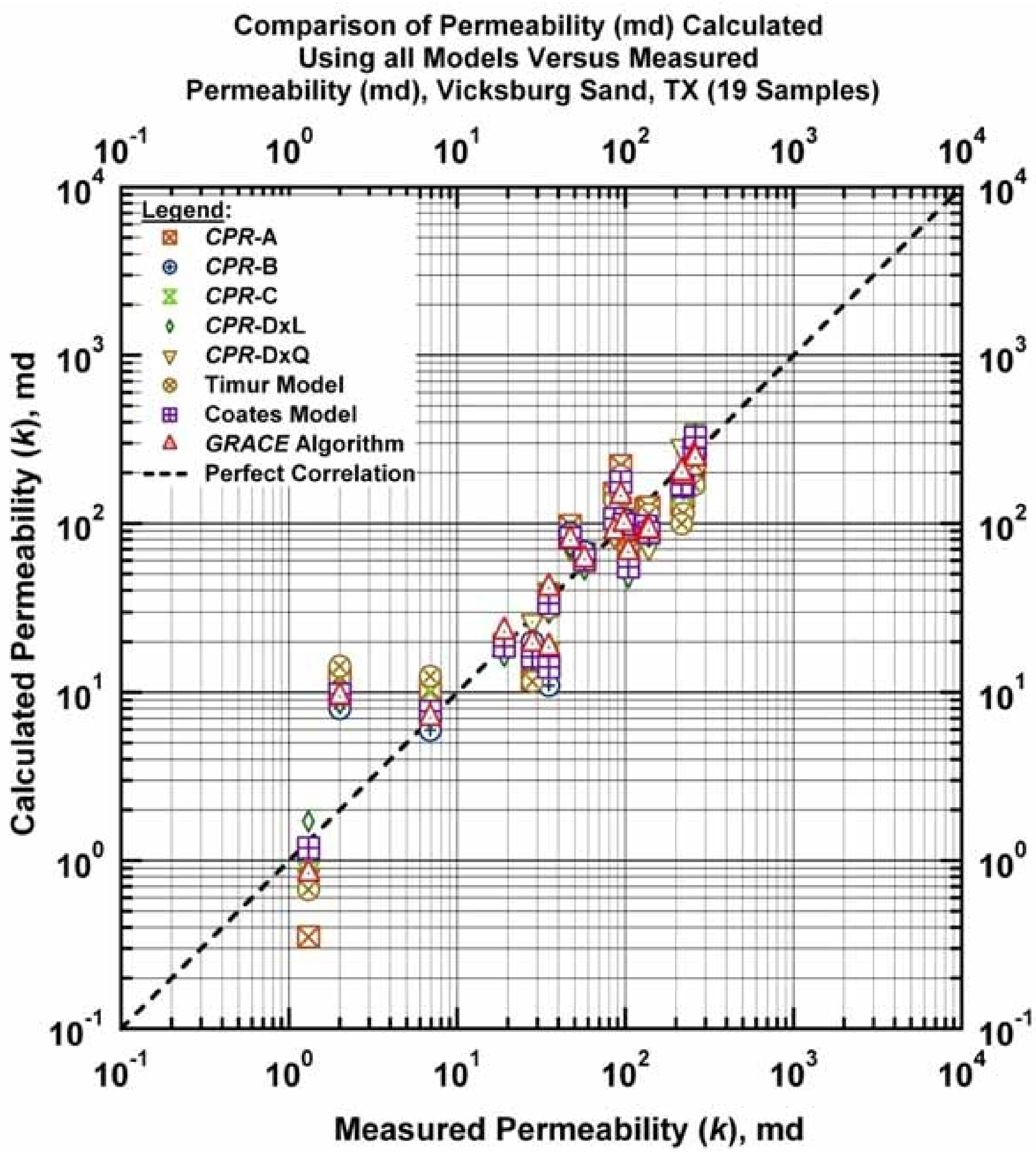

Figure D.13 — All Models: Calculated versus measured permeability. [*Case*: Vicksburg Sand, S. TX (USA)]

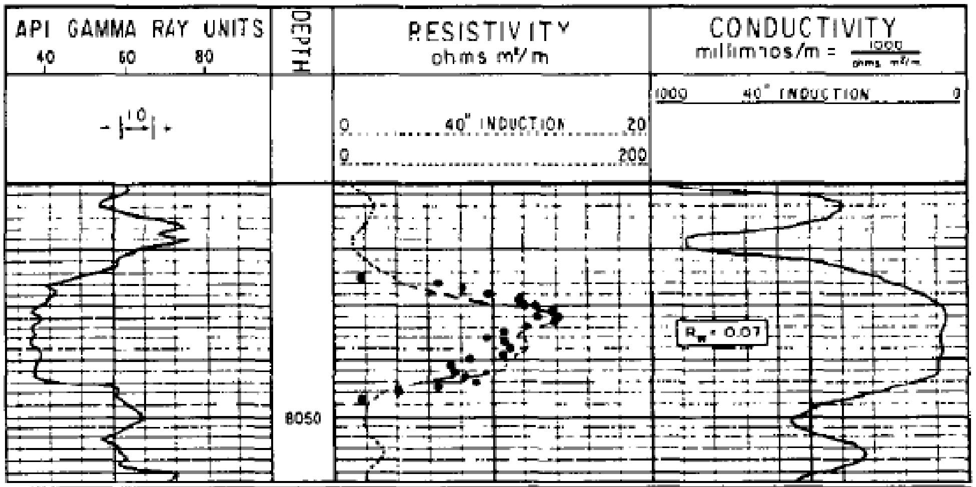

SAMP. NO.	DEPTH FEET	PERM. Md.	POR. %	% POR SAT. OIL	TOTAL WATER	PROB. PROD.	% OIL VOL.	% GAS VOL.	°API
1	8024-24.5	1.3	13.9	15.8	38.1				
2	24.5-25	28.	18.2	21.4	30.3				
3	25-26	2.0	18.9	16.9	36.5				
4	26-27	19.	19.3	25.9	32.1				
5	27-27.5	0.0	16.3	24.5	25.7				
6	27.5-28	221	22.4	26.3	22.8				
7	28-29	132	22.6	25.2	27.0				
8	29-30	.3	8.8	3.4	51.2				
9	30-31	256	23.1	34.3	20.7				
10	31-32	260	23.8	31.9	20.9				
11	32-33	35.	20.1	32.3	29.4				
12	33-34	94.	23.8	38.3	25.0				
13	34-35	47.	22.1	37.1	27.2				
14	35-36	216	22.0	31.9	21.9				
15	36-37	57.	21.3	33.3	27.7				
16	37-38	86.	23.2	31.9	27.5				
17	38-39	6.9	18.7	27.3	38.0				
18	39-40	35.	21.0	21.0	39.1				
19	40-41	98.	22.1	25.8	25.8				
20	41-42	104	21.5	23.7	28.9				
21	42-43	138.	22.8	29.4	28.1				

FIGURE 9: $R_p - R_t$ COMPARISON FOR VICKSBURG SAND IN SOUTH TEXAS

Figure D.14 — Original data from Granberry and Wilshusen (1962). [*Case*: Vicksburg Sand, S. TX (USA)]

APPENDIX E

RESULTS FOR WILCOX SAND

(S. TEXAS — USA)

In this Appendix we present the Wilcox Sand, located in S. Texas (USA), — this is a sandstone reservoir (Granberry and Wilshusen (1962)).

Model *CPR-A*: (Appendix E)

The "characteristic permeability relation" (or *CPR*) Model *CPR-A* (*i.e.*, the modified Archie "Clean Sand" Model) is given as:

$$k = a(\phi - c)^b \quad c = c_{\max} \exp[-c_1 \phi^{c_2} S_w^{c_3}] \text{ .... (E-1)}$$

Where a plot of log(k) versus log(ϕ) is used to graphically calibrate Eq. E-1 in terms of the coefficients — a, b, and $c_{\max}$. **Fig. E.1** shows that the *CPR-A* model performs quite well for this case. **Figs. E.1a and b** show the log-log and the semilog format of permeability versus porosity, respectively. In **Fig. E.2** we provide the "error" plots for this case, where the measured and computed data are compared systematically. In **Fig. E.2a** we note a good correlation of the results obtained using Model *CPR-A* versus the measured permeability data — Good agreement with the perfect correlation trend (*i.e.*, the 45-degree line) is observed. In **Fig. E.2b** we provide a comparison with the *GRACE* algorithm correlation (Xue *et al*. 1997)), and we note that the *CPR-A* model results correlate very well with the *GRACE* algorithm results for this case. **Fig. E.2c** we present the calculated and measure c-function — and again we note a reasonable correlation of the data about the perfect correlation trend. Lastly, in **Fig. E.2d** we present the measured and calculated permeability with depth.

Model *CPR-B*: (Appendix E)

The "characteristic permeability relation" (or *CPR*) Model *CPR-B* (*i.e.*, the modified Archie "Dirty Sand" Model (power-law basis)) is given as:

$$k = a(\phi + c)^b \quad c = c_{\max} \exp[-c_1 \phi^{c_2} S_w^{c_3}] \text{ .... (E-2)}$$

Where a plot of log(k) versus log(ϕ) is used to graphically calibrate Eq. E-2 in terms of the coefficients — a, b, and $c_{\max}$. The results for this case are presented in **Figs. E.3 and 4**. In **Fig. E.3a** (log-log format) we note that a very distinct "envelope" is formed by the *CPR-B* model, essentially all of the data on the right and left flanks are well-matched (*i.e.*, the "dirty sand" power law relation (applied on the right portion of the data) and its correction function (applied on the left portion of the data). Similarly, in **Fig. E.3b** (semilog format), we observe an excellent distribution of the power law model across the body of the data. The error analyses for this case are shown in **Fig. E.4**. In **Fig. E.4a** we present the results obtained using

Model *CPR-B* versus the measured permeability data and in this case there is good agreement with the perfect correlation trend (*i.e.*, the 45-degree line). We provide comparison with the *GRACE* algorithm correlation in **Fig. E.4b** — the results using Model *CPR-B* and the *GRACE* algorithm compare very well for this case. We compare the computed and data-derived values of the *c*-function for this case in **Fig. E.4c** and we note a reasonably "tight" correlation, except for the very lowest values of the *c*-function. Lastly, in **Fig. E.4d** we present the measured and calculated permeability with depth. In summary, we believe that Model *CPR-B* is an efficient correlation model for this particular data case.

Model *CPR-C*: (Appendix E)

The "characteristic permeability relation" (or *CPR*) Model *CPR-C* (*i.e.*, the modified Archie "Dirty Sand" Model (exponential basis)) is given as:

$$k = c\exp[\beta\phi] \quad c = c_{\max}\exp[-c_1\phi^{c_2} S_w^{c_3}] \text{ ......(E-3)}$$

Where a plot of log(*k*) versus ϕ is used to graphically calibrate Eq. E-3 in terms of the coefficients — β and $c_{\max}$. Model *CPR-C* is fundamentally different than Models *CPR-A* and *CPR-B*, as the basis for Model *CPR-C* is an exponential function, not a power law relation. In **Figs. E.5 and 6** we present the results of applying Model *CPR-B* for this case, and in general, we observe a very consistent performance of Model *CPR-B*. **Fig. E.5b** illustrates the excellent conformance of Model *CPR-C* for this case — again recalling that this model has an exponential relationship with porosity as its basis.

In **Figs. E.6a, E.6b, and E.6c** we review the error analyses plots for this case, and we note good performance (visually) in terms of the correlation of the results using Model *CPR-C*. The correlation of the *c*-function (see **Fig. E.6c**) appears to be very consistent. We believe that the *CPR-C* model has performed well for this case, and **Fig. E.6** confirms the value of this model as a "characteristic relation" for permeability.

Model *CPR-D*: (Appendix E)

The "characteristic permeability relation" (or *CPR*) Model *CPR-D* (*i.e.*, the weighted power law-exponential model) is given in its fundamental form as:

$$k = xa\phi^b + (1-x)\alpha\exp[\beta\phi] \quad [0 \le x \le 1]] \text{ ......(E-4a)}$$

For Eq. E-4 there are two proposed models for the *x*-function (*i.e.*, the weighting function) — these are:

$$x = \exp[-\ln(x_0) + x_1\ln(\phi) + x_2\ln(S_w) + x_3\ln(\phi)\ln(S_w)] \text{ (Model } \textit{CPR-DxL}\text{) ......(E-4b)}$$

$$x = \exp\begin{bmatrix} -\ln(x_0) + x_1\ln(\phi) + x_2\ln(S_w) + x_3\ln(\phi)\ln(S_w) \\ + x_4\ln(\phi)^2 + x_5\ln(S_w)^2 + x_6\ln(\phi)^2\ln(S_w) \\ + x_7\ln(\phi)\ln(S_w)^2 + x_8\ln(\phi)^2\ln(S_w)^2 \end{bmatrix} \text{(Model } \textit{CPR-DxL}\text{) ......(E-4c)}$$

As noted in Eq. E-4b, Model *CPR-DxL* utilizes a logarithmic linear model for the weights (*x*-values) and as seen in Eq. E-4c, Model *CPR-DxQ* utilizes a logarithmic quadratic model for the weights (*x*-values).

While these models (Eqs. E-4b and E-4c) are *empirical*, we have found generally good application of these relations for all cases. In this case, the base results using Models *CPR-DxL* and *CPR-DxQ* are presented in **Fig. E.7** — where the power law and exponential basis functions are fitted to the appropriate portion of the data. The power law equation represents the "Archie clean sand" trend and is fitted to the leftmost data as shown in **Fig. E.7a** and in contrast, the exponential equation is thought to represent the "Archie Dirty Sand" trend and the exponential is fitted to the far rightmost portion of the data (see **Fig. E.7b**).

In **Figs. E.8 and 9** we present the error analyses for this case, where we have employed the weighting functions (Eqs. E-4b and E-4c) as appropriate. In **Fig. E.8a**, we find a good correlation of permeability. The comparison of the Model *CPR-DxL* results are compared to the results obtained from the *GRACE* algorithm in **Fig. E.8b**, we note the very good results obtained using Model *CPR-DxL*. The computed weight function (x-values) shown for the *CPR-DxL* model in **Fig. E.8c** does exhibit more scatter than expected, but the trend is (relatively) centered about the perfect correlation line. **Fig. E.8d** provides the measured and calculated permeability versus depth.

The results obtained using Model *CPR-DxQ* are presented in **Fig. E.9**, and we note substantially improved behavior over that of Model *CPR-DxL*. In particular, the base correlation of computed and measured permeabilities (**Fig. E.9a**) for Model *CPR-DxQ* does indicate a slightly better correlation than that of Model *CPR-DxL*. Also, the comparison of Model *CPR-DxQ* with the results from the *GRACE* algorithm (**Fig. E.9b**) exhibits better agreement than the results of Model *CPR-DxL*. Finally, the correlation of the x-function (**Fig. E.9c**) for Model *CPR-DxQ* is better than the correlation for Model *CPR-DxL*. These comparisons suggest that Model *CPR-DxQ* (*i.e.*, the combination of Eqs. E-4a and E-4c) provides a better correlation of data, for this case, than Model *CPR-DxL*. **Fig. E.9d** provides the measured and calculated permeability versus depth.

"Timur Model": (Appendix E)

The "Timur Model" [Timur (1968)] is given as:

$$k_{\text{Timur}} = a\phi^b S_w^c \qquad \text{(E-5)}$$

In **Fig. E.10** we present the results of the "Timur Model" (Eq. E-5) which is essentially just a generalized power law function relation in terms of k, ϕ, and S_w. As shown in **Figs. E.10a and b**, the "Timur Model" also provides a good correlation of the data for this case. The comparison of results using the "Timur Model" with the results of the *GRACE* algorithm (**Fig. E.10b**).

"Coates Model": (Appendix E)

The "Coates Model" [referenced by Ahmed *et al.* (1989)] is given as:

$$k_{\text{Coates}} = \left[100\phi^2 \frac{(1-S_w)}{S_w} \right]^2 \text{.........} \quad \text{(E-6)}$$

In **Fig. E.11** we present the results of the "Coates Model" (Eq. E-6) which is essentially just a modified power function relation in terms of k, ϕ, and S_w. The results are shown in **Figs. E.11a and b** of the data for this case. The comparison of results using the "Coates Model" with the results of the *GRACE* algorithm (**Fig. E.11b**) is also shown.

***GRACE* Algorithm: (Appendix E)**

In **Fig. E.12** we present the results predicted by the *GRACE* algorithm, which is a non-parametric regression approach (see Xue *et al.* (1997) for details). In theory, the *GRACE* algorithm should provide the most *unbiased* correlation of the data — *i.e.*, the *GRACE* algorithm is designed not "fit the errors" as other regression approaches may. It is our contention that the *GRACE* algorithm is the statistical standard — and any algorithm/approach/model which achieves better regression statistics than the *GRACE* algorithm is actually "fitting the errors" in the data. *None of the cases have significantly better regression statistics than the GRACE algorithm* — hence, none of the cases are "over-fitted" in a statistical sense.

***Comparison of All Models*: (Appendix E)**

Fig. E.13, illustrates all of the models on a single plot of calculated versus measured permeability. We also present a table of all statistical results in **Table E.1**. Our last plot, **Fig. E.14**, illustrates the source of the original data set.

Table E.1 — Statistical Results for all Models (Wilcox Sand, S. TX (USA), n=27).

Model	Sum of Squared Residuals [log(k)^2]	Variance [log(k)^2]	Standard Deviation [log(k)]	Absolute Relative Error [percent]
CPR-A	8.31	2.14	1.46	43.45
CPR-B	7.92	2.21	1.49	42.18
CPR-C	7.83	2.36	1.54	40.82
CPR-DxL	7.15	2.03	1.42	44.53
CPR-DxQ	6.87	2.04	1.43	41.50
Timur	7.74	2.19	1.48	41.11
Coates	7.66	2.19	1.48	40.74
GRACE Algorithm	5.21	2.18	1.48	34.10

The coefficients for the models used in this case are provided in **Table E.2**.

Table E.2a — Model Coefficients (Wilcox Sand, S. TX (USA), n=27).

Model	a or α	b or β	c or c_{max}	c_1	c_2	c_3
CPR-A	1.00×10^{8}	8.00	0.050	0.03	-0.22	-2.73
CPR-B	5.00×10^{6}	8.00	0.070	0.09	-2.68	3.00
CPR-C	5.00×10^{-8}	110.00	3.00×10^{-6}	1109.49	2.68	1.19
Timur	2.65×10^{7}	9.66	2.999	–	–	–
Coates	2.94×10^{4}	5.20	1.835	–	–	–

Table E.2b — Model Coefficients (Wilcox Sand, S. TX (USA), n=27).

Model	a	b	α	β
CPR-DxL	1.00×10^{8}	8.00	5.00×10^{-8}	110.00
CPR-DxQ	1.00×10^{8}	8.00	5.00×10^{-8}	110.00

Model	c_0	c_1	c_2	c_3	c_4	c_5	c_6	c_7	c_8
CPR-DxL	9.54×10^{8}	-7.61	-16.93	-6.60	–	–	–	–	–
CPR-DxQ	1.76×10^{4}	3.25	14.42	16.70	1.78	8.42	1.52	-0.35	-3.63

Nomenclature: (Appendix E)

S_w = Water Saturation (fraction)
k = Formation Permeability, md (or any consistent units)
ϕ = Porosity, fraction

References: (Appendix E)

Ahmed, U., Crary, S.F., and Coates, G.R: "Permeability Estimation: The Various Sources and Their Interrelationship," paper SPE 19604 presented at the 1989 SPE Annual Technical Conference and Exhibition, San Antonio, TX, 8-11 Oct., 649-662.

Granberry, R.J., and Wilshusen, R.C.: "Improved Interpretation of Formation Productivity by Combined Use of Core Analysis and Electronic Log Data," *Trans.*, Gulf Coast Association of Geological Societies (1962) 13, 213-221.

Timur, A.: "An Investigation of Permeability, Porosity, and Residual Water Saturation Relationships," *Trans.*, SPWLA Symposium (1968) paper I.

Xue, G., Datta-Gupta, A., Valko, P., and Blasingame, T.A.: "Optimal Transformations for Multiple Regression: Application to Permeability Estimation from Well Logs," *SPEFE* (June 1997), 85-93.

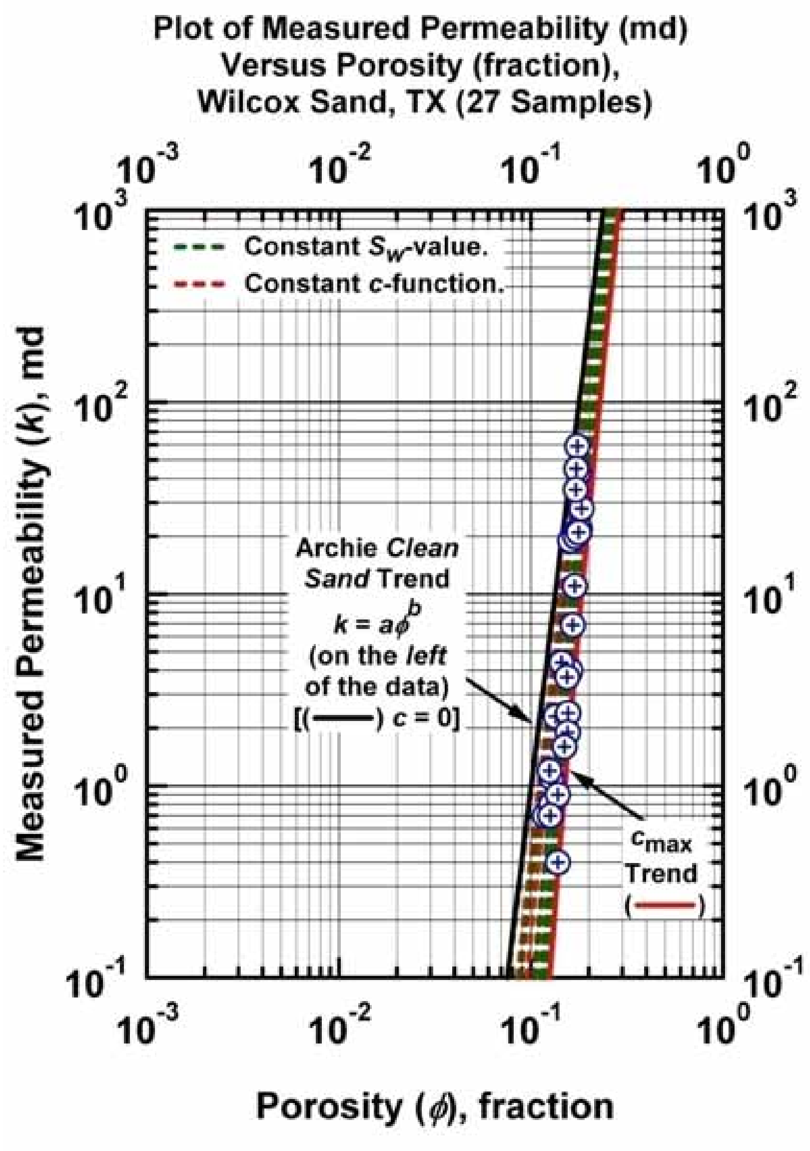

Figure E.1a — Model *CPR-A*: $k = a(\phi - c)^b \quad c = c_{\max} \exp[-c_1 \phi^{c_2} S_w^{c_3}]$ — "Clean Sand" Plot (log-log format) — Archie "Clean Sand" trend is given by the straight-line trend at the far left of the data (power law model). [*Case*: Wilcox Sand, S. TX (USA)]

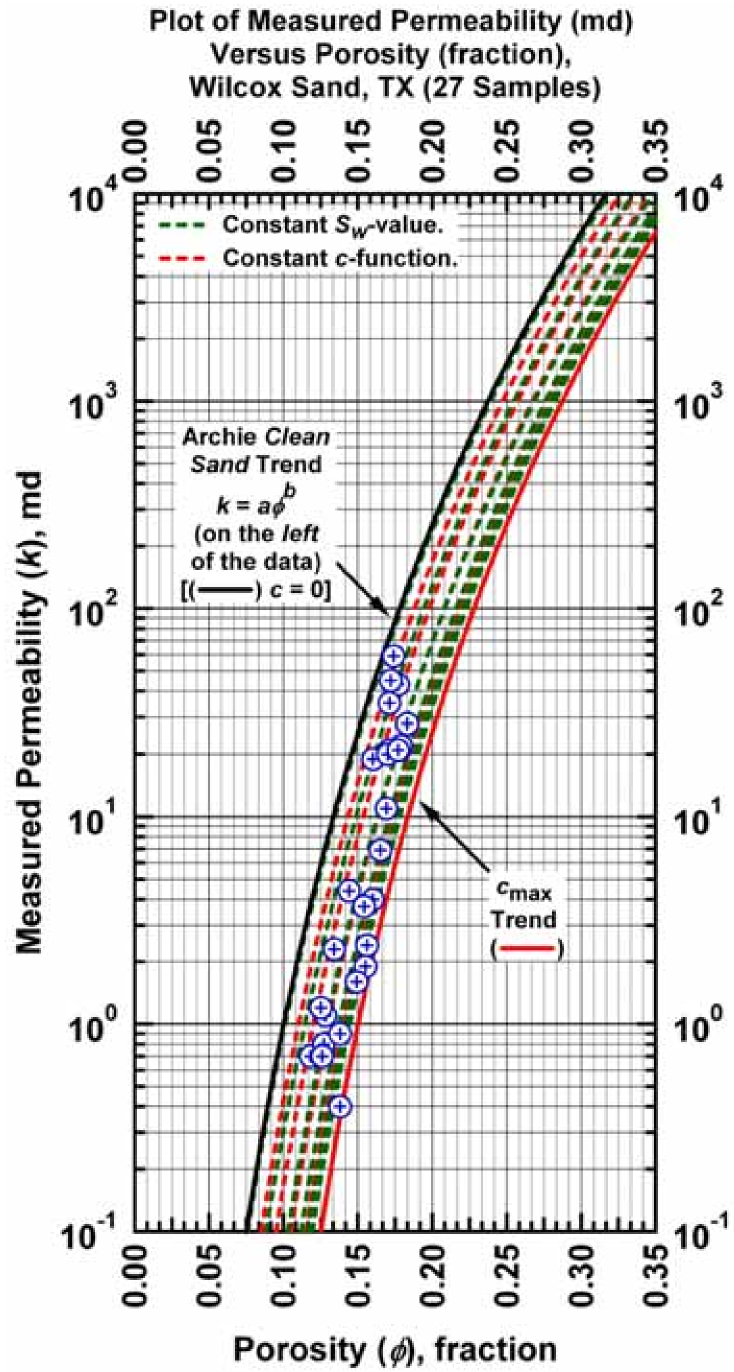

Figure E.1b — Model *CPR-A*: $k = a(\phi - c)^b \quad c = c_{max} \exp[-c_1 \phi^{c_2} S_w^{c_3}]$ — "Dirty Sand" Plot (semilog format). Archie "Clean Sand" trend is given by the curved trend at the far left of the data (power law model). [*Case*: Wilcox Sand, S. TX (USA)]

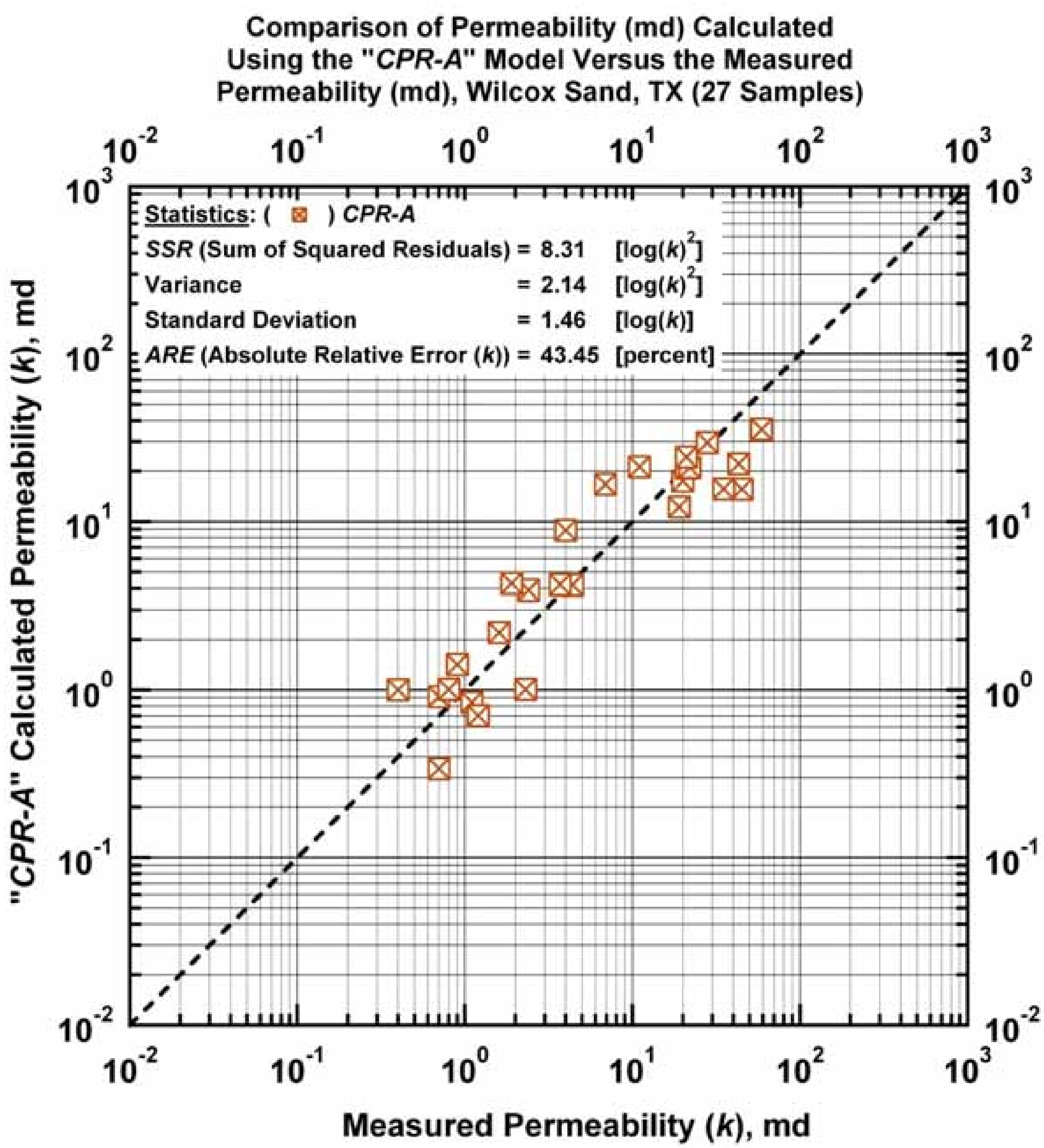

Figure E.2a — Model *CPR-A*: calculated versus measured permeability. [*Case*: Wilcox Sand, S. TX (USA)]

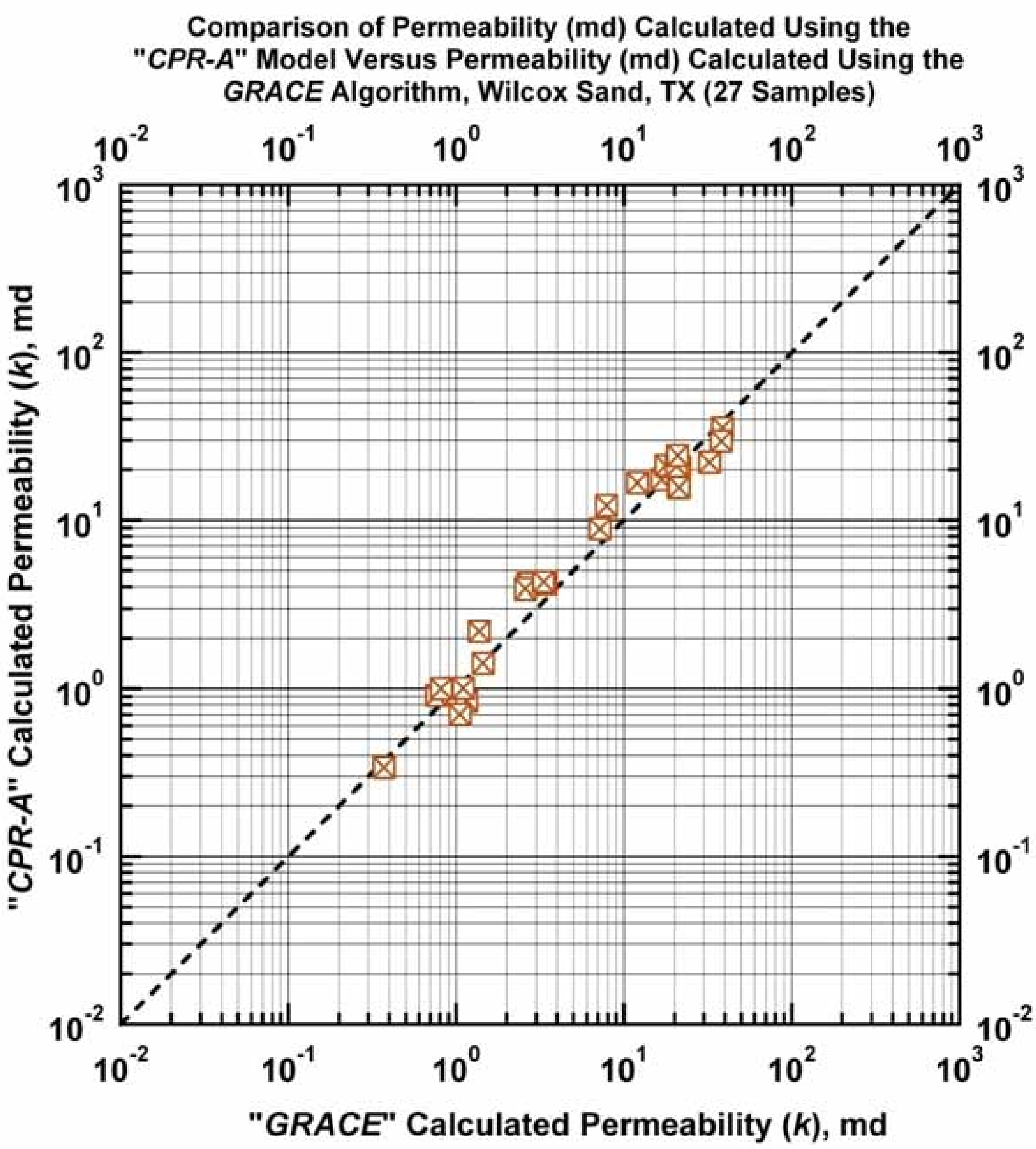

Figure E.2b — Model *CPR-A*: Permeability calculated using Model *CPR-A* versus permeability calculated using the *GRACE* Algorithm. [*Case*: Wilcox Sand, S. TX (USA)]

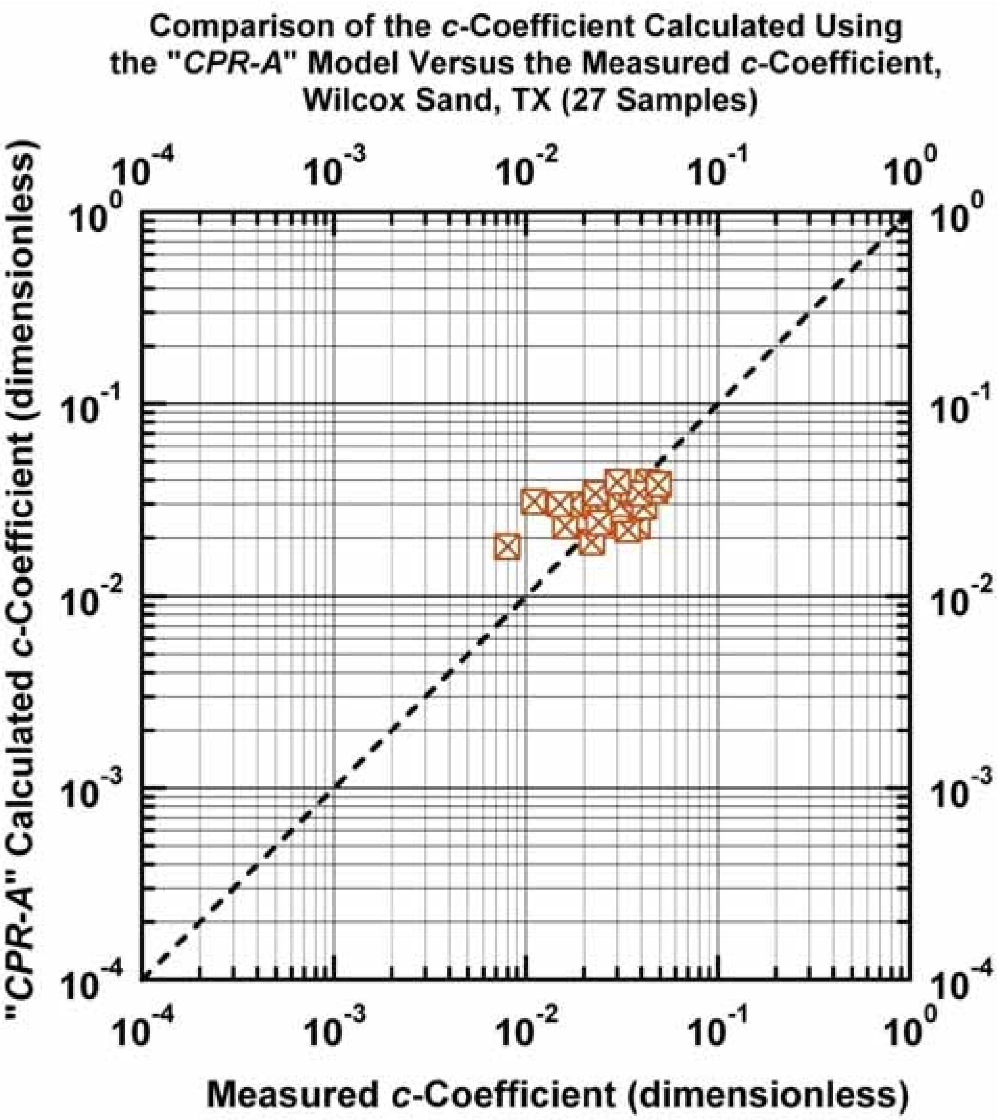

Figure E.2c — Model *CPR-A*: Calculated *c*-function values versus measured *c*-function values. [*Case*: Wilcox Sand, S. TX (USA)]

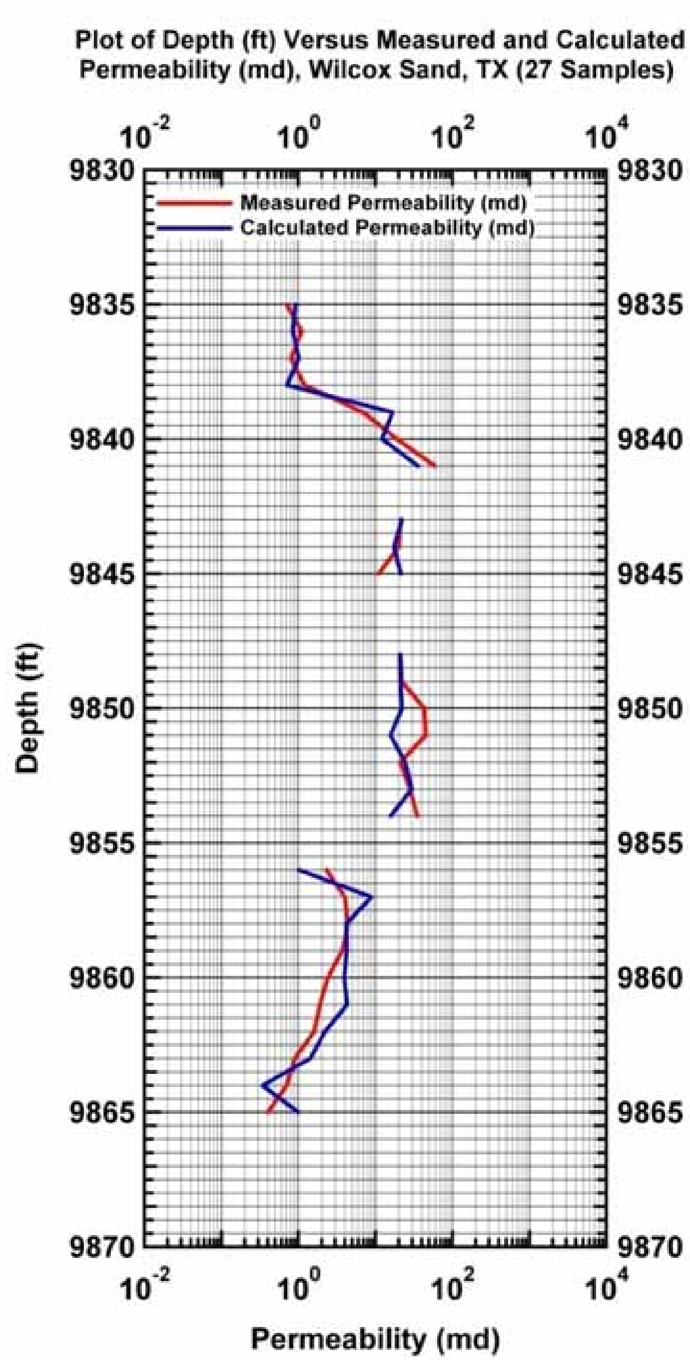

Figure E.2d — Model *CPR-A*: Calculated and measured permeability values versus deptE. [*Case*: Wilcox Sand, S. TX (USA)]

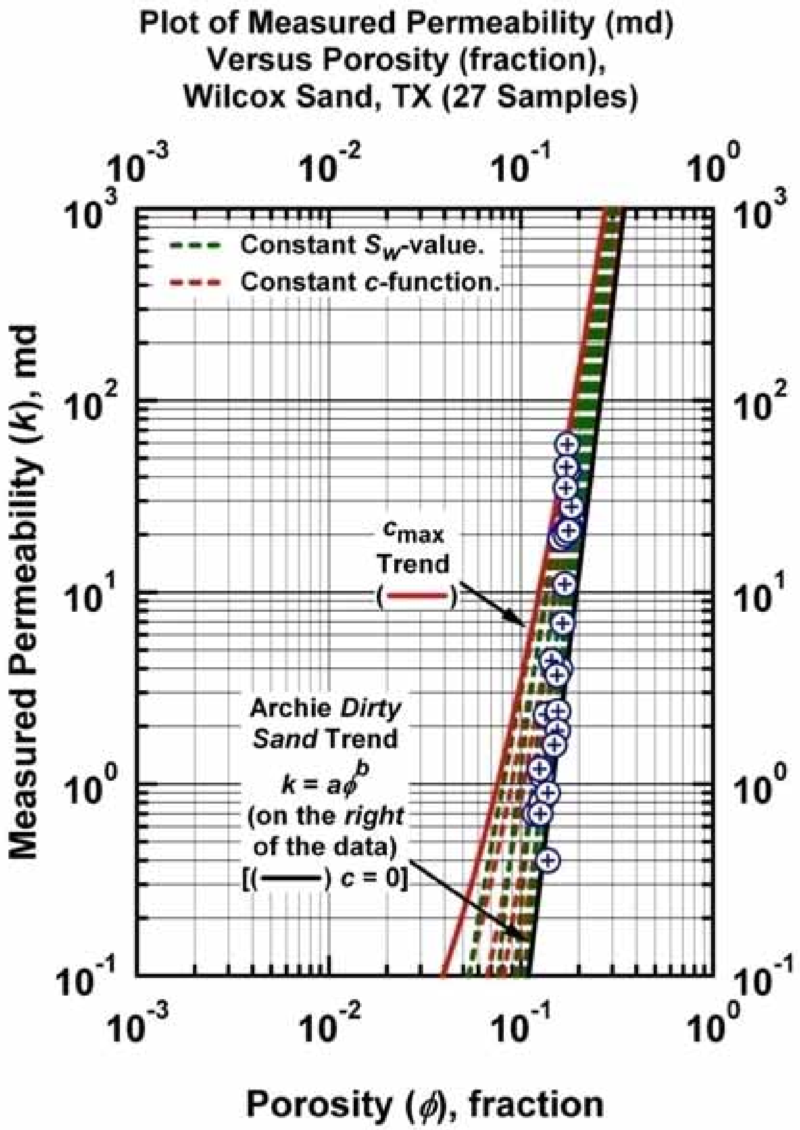

Figure E.3a — Model *CPR-B*: $k = a(\phi + c)^b$ $c = c_{\max} \exp[-c_1 \phi^{c_2} S_w^{c_3}]$ — "Clean Sand" Plot (log-log format) — Archie "Dirty Sand" trend is given by the straight-line trend at the far right of the data (power law model). [*Case*: Wilcox Sand, S. TX (USA)]

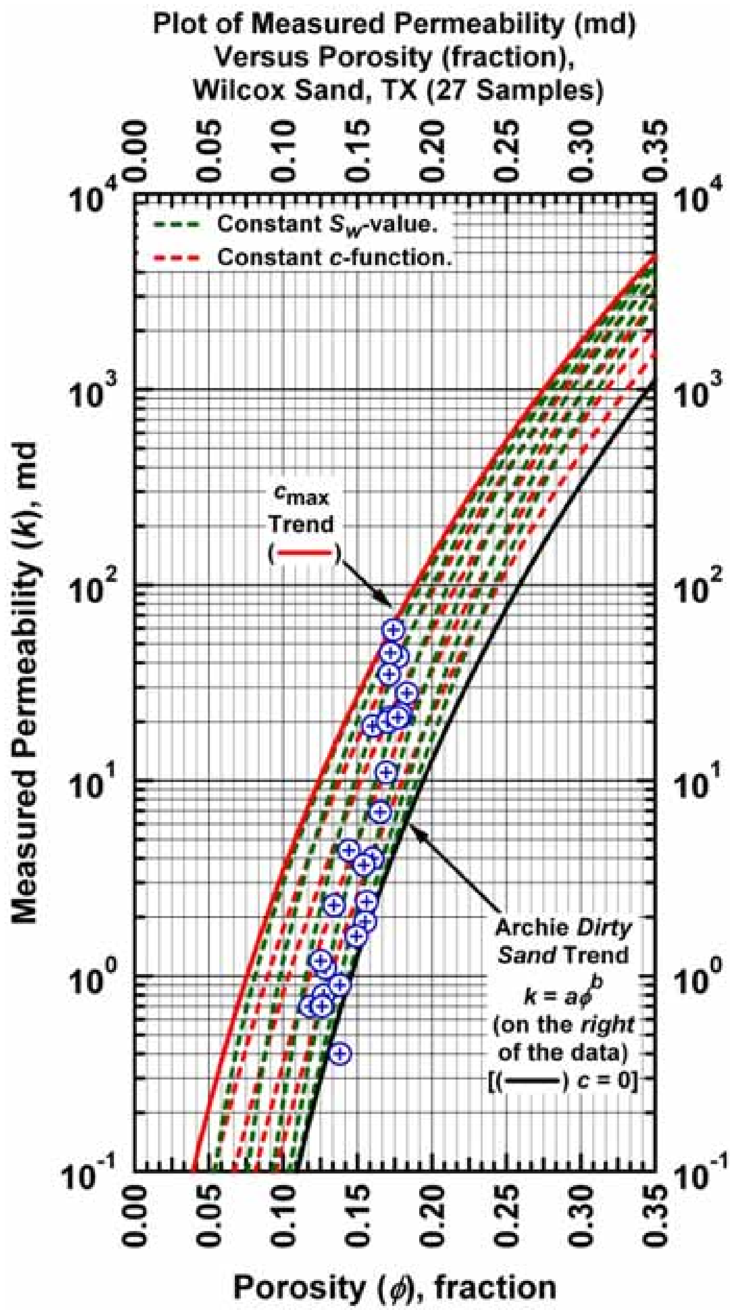

Figure E.3b — Model *CPR-B*: $k = a(\phi + c)^b$ $c = c_{max} \exp[-c_1 \phi^{c_2} S_w^{c_3}]$ — "Dirty Sand" Plot (semilog format) — Archie "Dirty Sand" trend is given by the curved trend at the far right of the data (power law model). [*Case*: Wilcox Sand, S. TX (USA)]

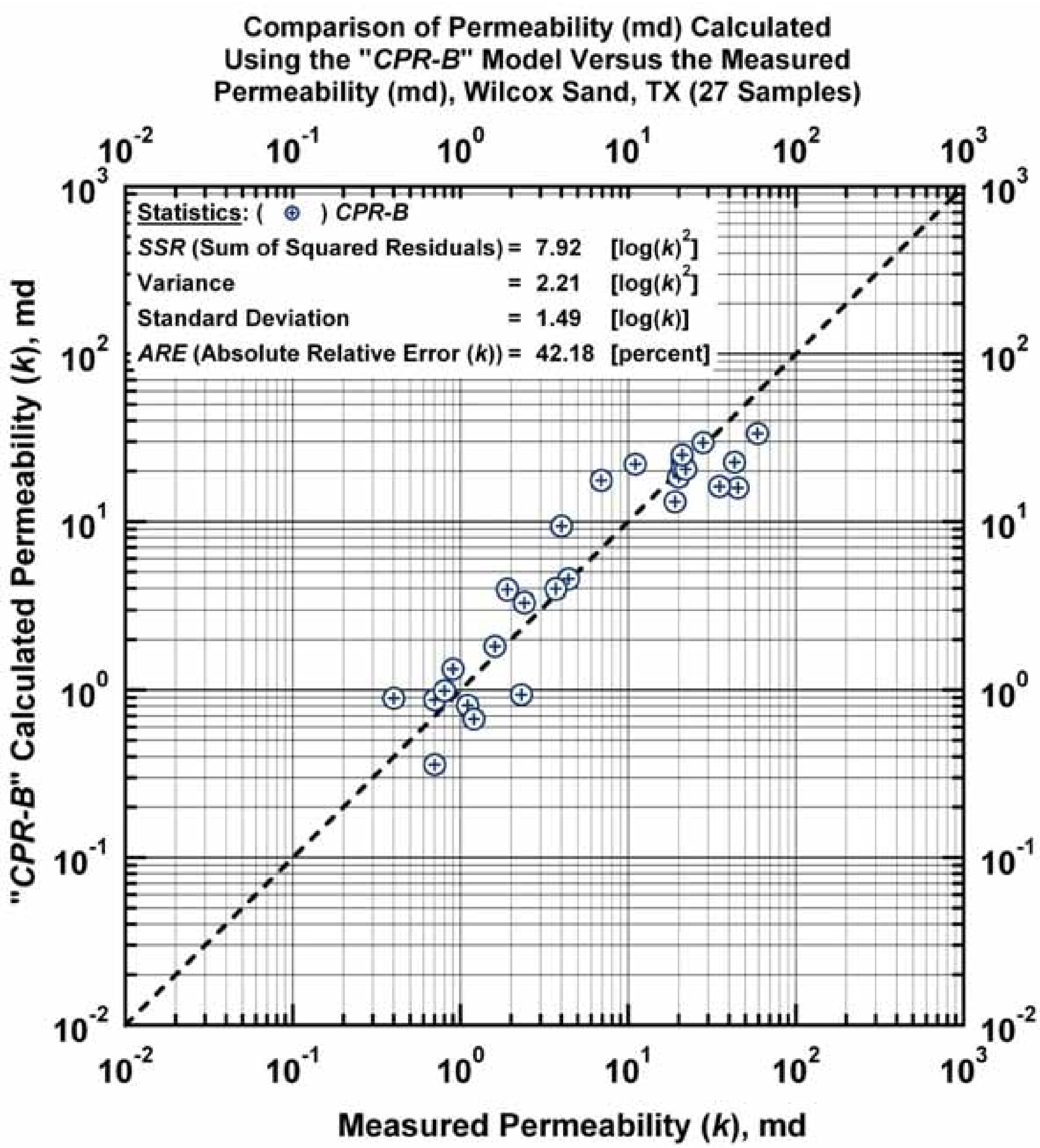

Figure E.4a — Model *CPR-B*: calculated versus measured permeability. [*Case*: Wilcox Sand, S. TX (USA)]

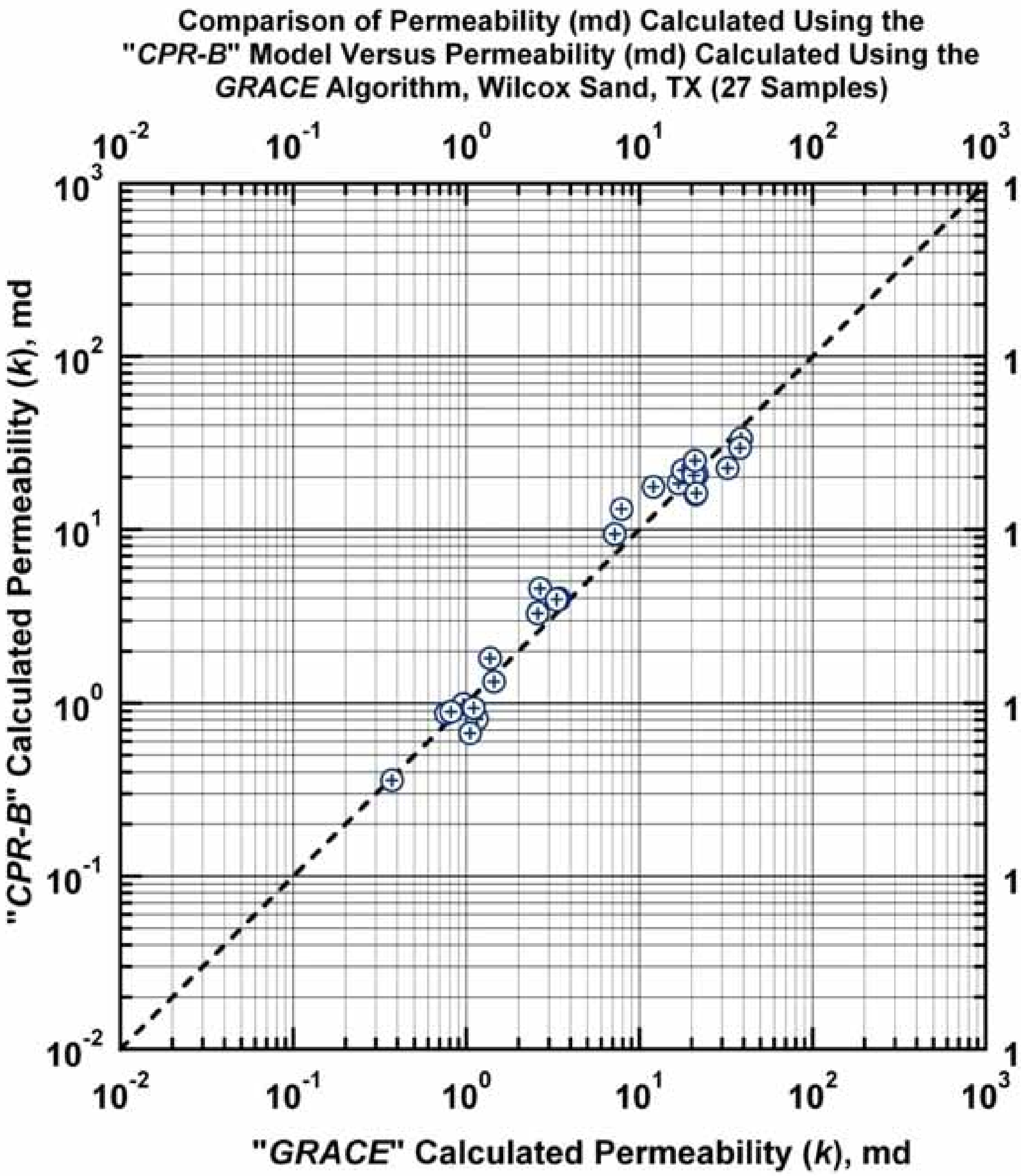

Figure E.4b — Model *CPR-B*: Permeability calculated using Model *CPR-B* versus permeability calculated using the *GRACE* Algorithm. [*Case*: Wilcox Sand, S. TX (USA)]

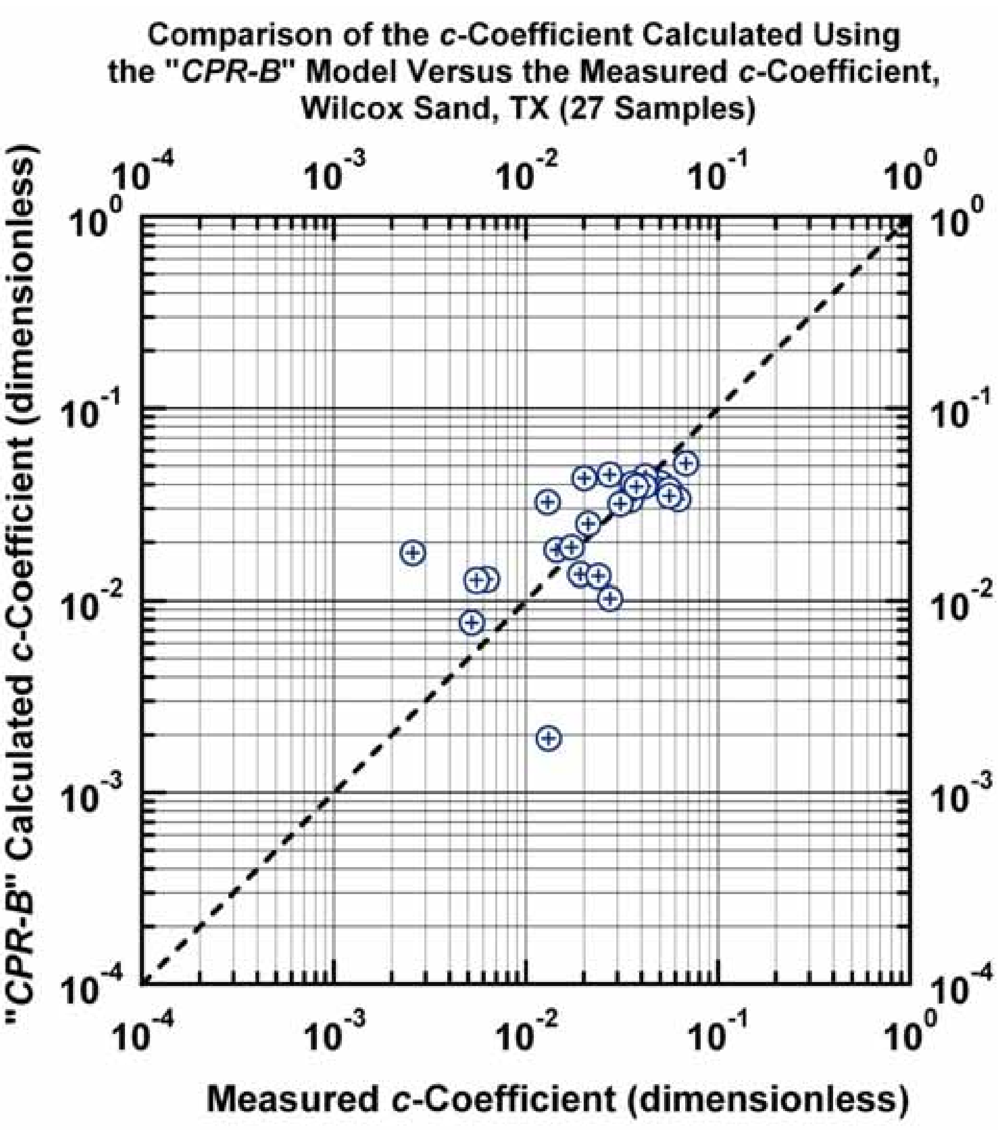

Figure E.4c — Model *CPR-B*: Calculated *c*-function values versus measured *c*-function values. [*Case*: Wilcox Sand, S. TX (USA)]

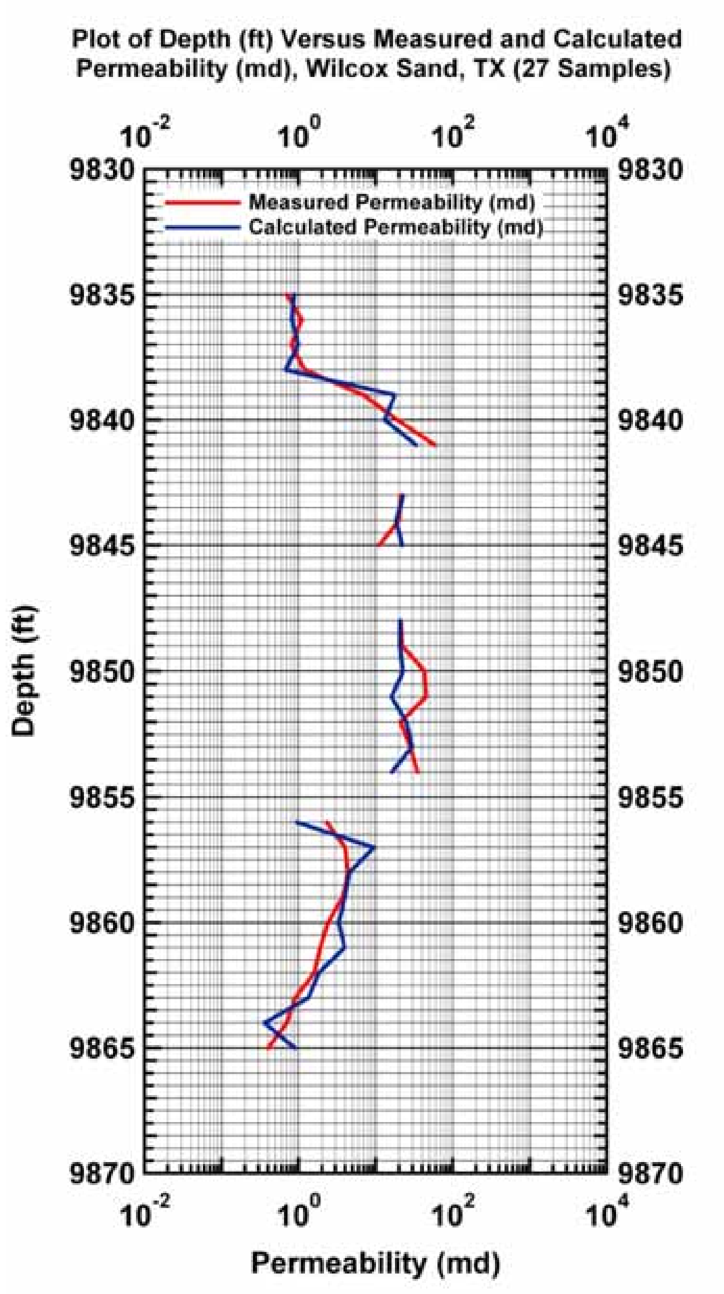

Figure E.4d — Model *CPR-A*: Calculated and measured permeability values versus depth. [*Case*: Wilcox Sand, S. TX (USA)]

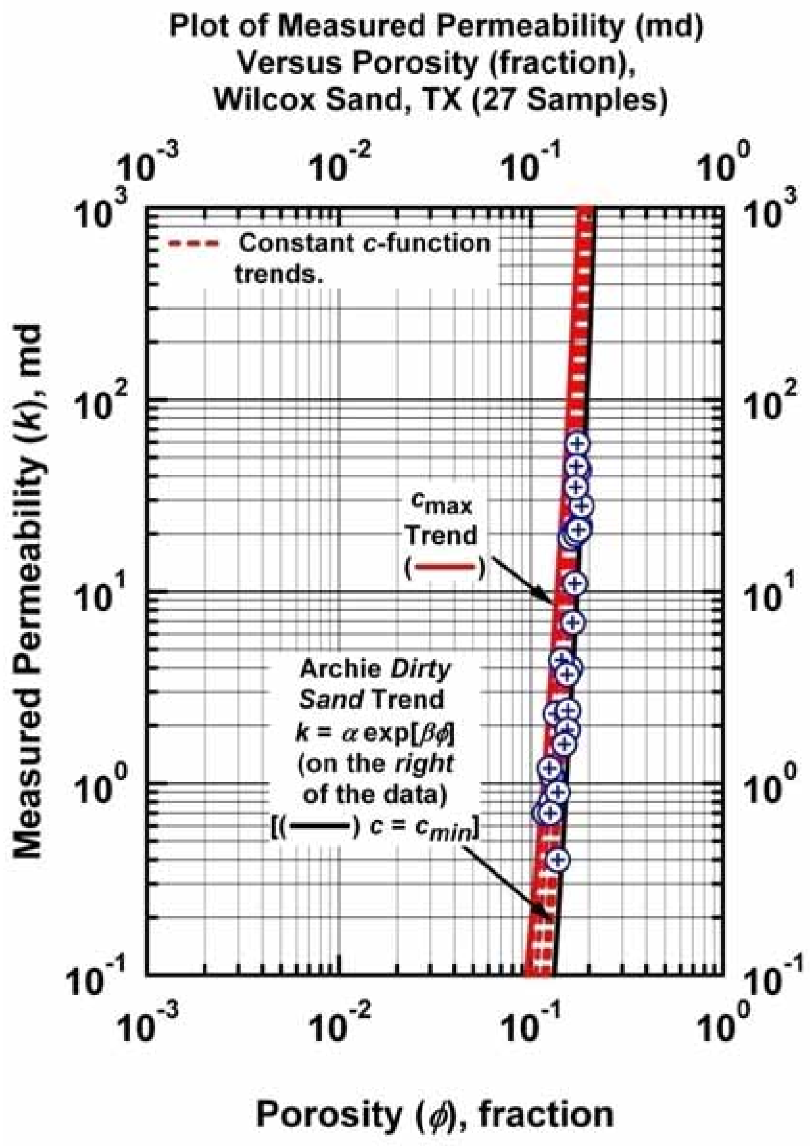

Figure E.5a — Model *CPR-C*: $k = c\exp[\beta\phi]$ $c = c_{\max}\exp[-c_1\phi^{c_2} S_w^{c_3}]$ — "Clean Sand" Plot (log-log format) — Archie "Dirty Sand" trend is given by the curved trend at the far right of the data (exponential model). [*Case*: Wilcox Sand, S. TX (USA)]

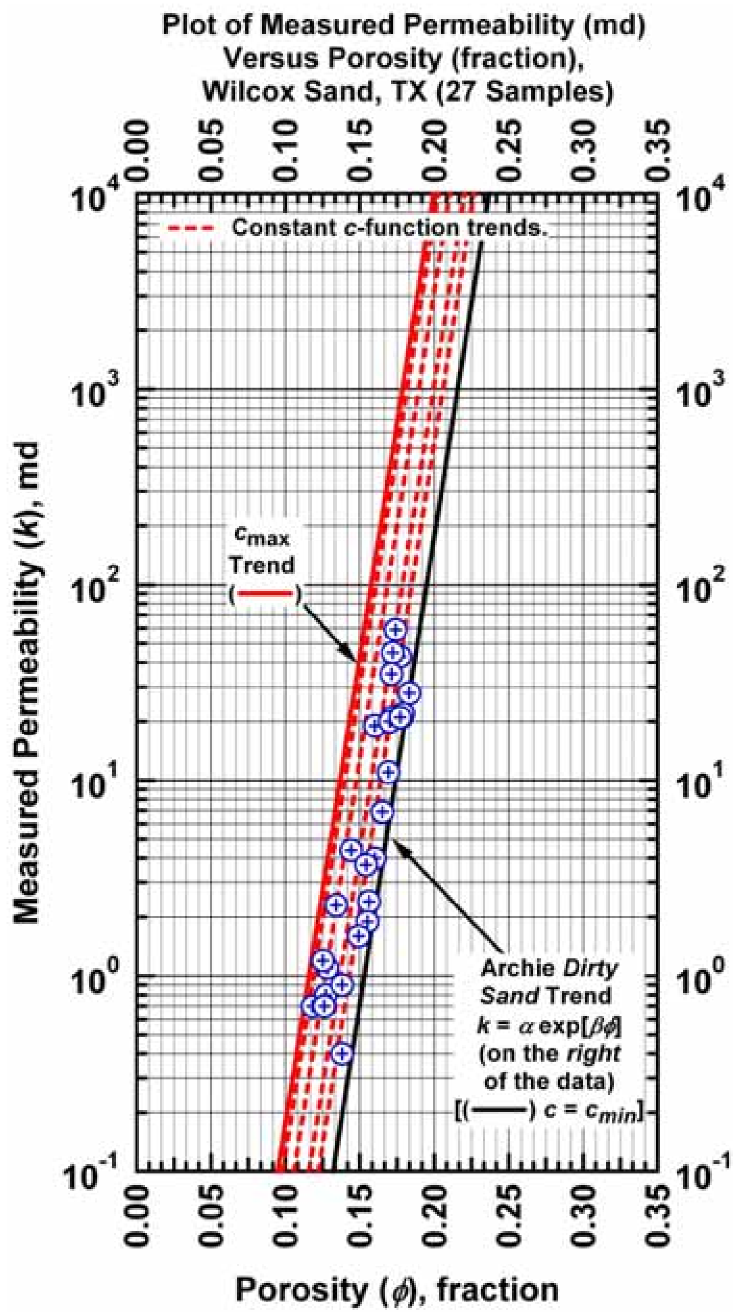

Figure E.5b — Model *CPR-C*: $k = c\exp[\beta\phi]$ $\quad c = c_{\max}\exp[-c_1\phi^{c_2}S_w^{c_3}]$ — "Dirty Sand" Plot (semilog format) — Archie "Dirty Sand" trend is given by the straight-line trend at the far right of the data (exponential model). [*Case*: Wilcox Sand, S. TX (USA)]

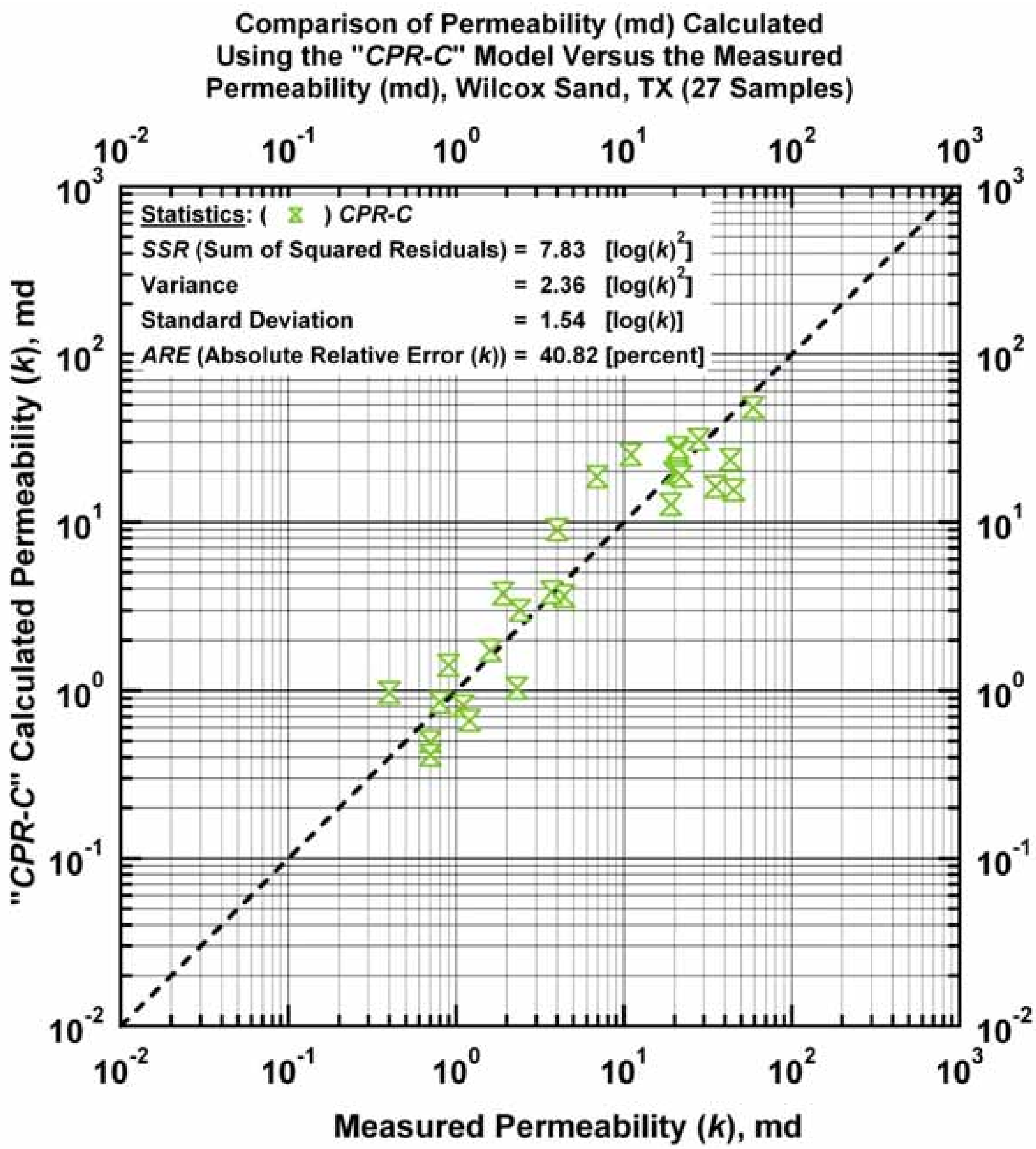

Figure E.6a — Model *CPR-C*: calculated versus measured permeability. [*Case*: Wilcox Sand, S. TX (USA)]

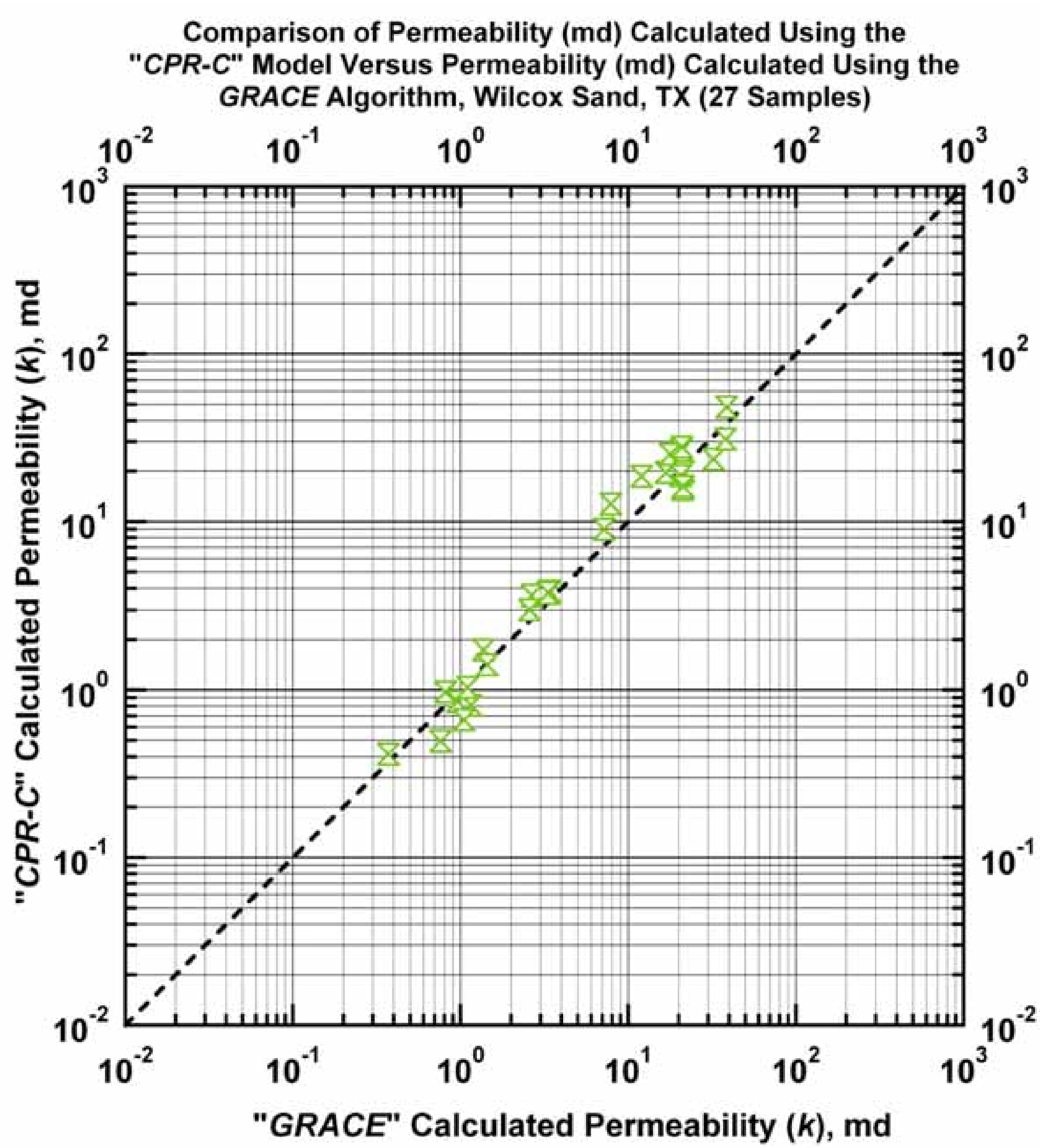

Figure E.6b — Model *CPR-C*: Permeability calculated using Model *CPR-C* versus permeability calculated using the *GRACE* Algorithm. [*Case*: Wilcox Sand, S. TX (USA)]

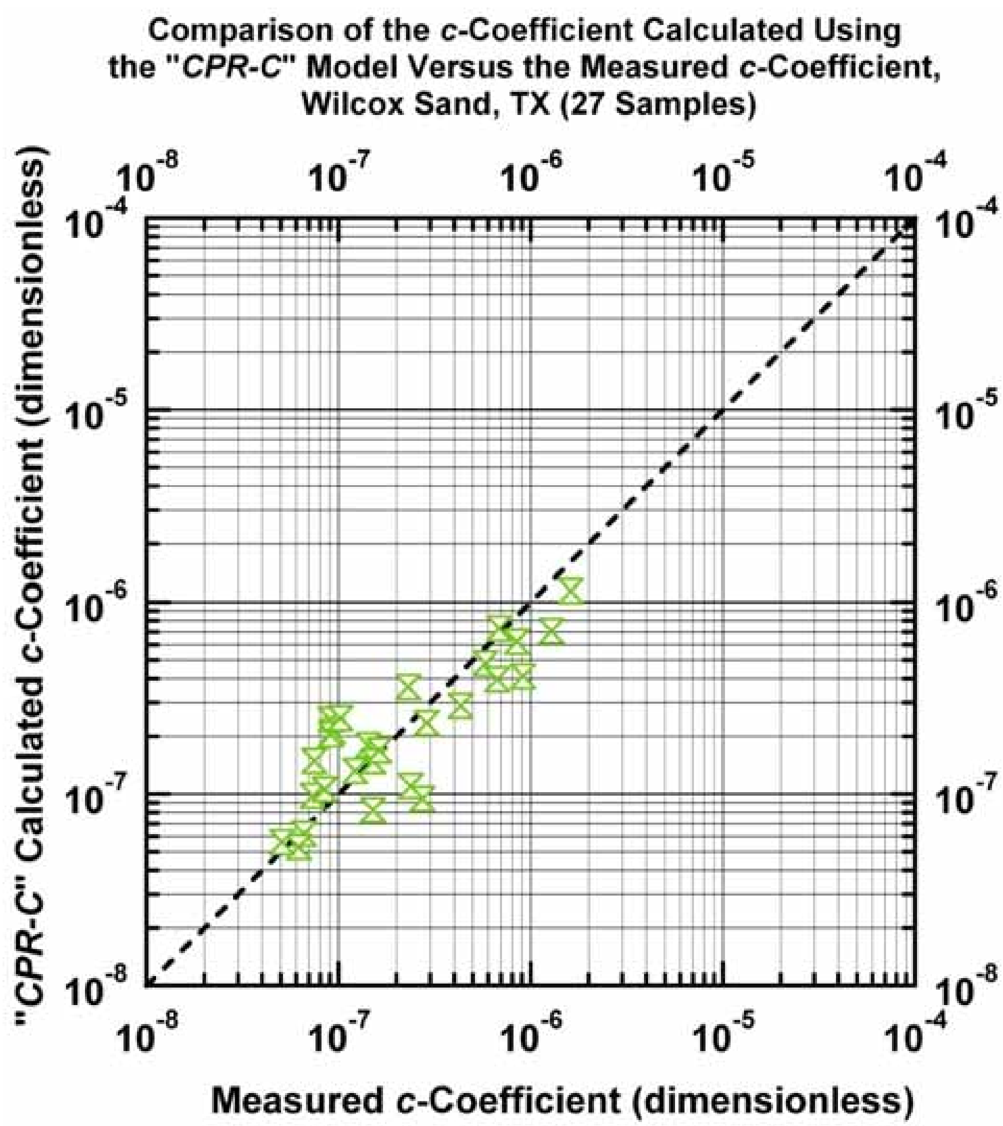

Figure E.6c — Model *CPR-C*: Calculated *c*-function values versus measured *c*-function values. [*Case*: Wilcox Sand, S. TX (USA)]

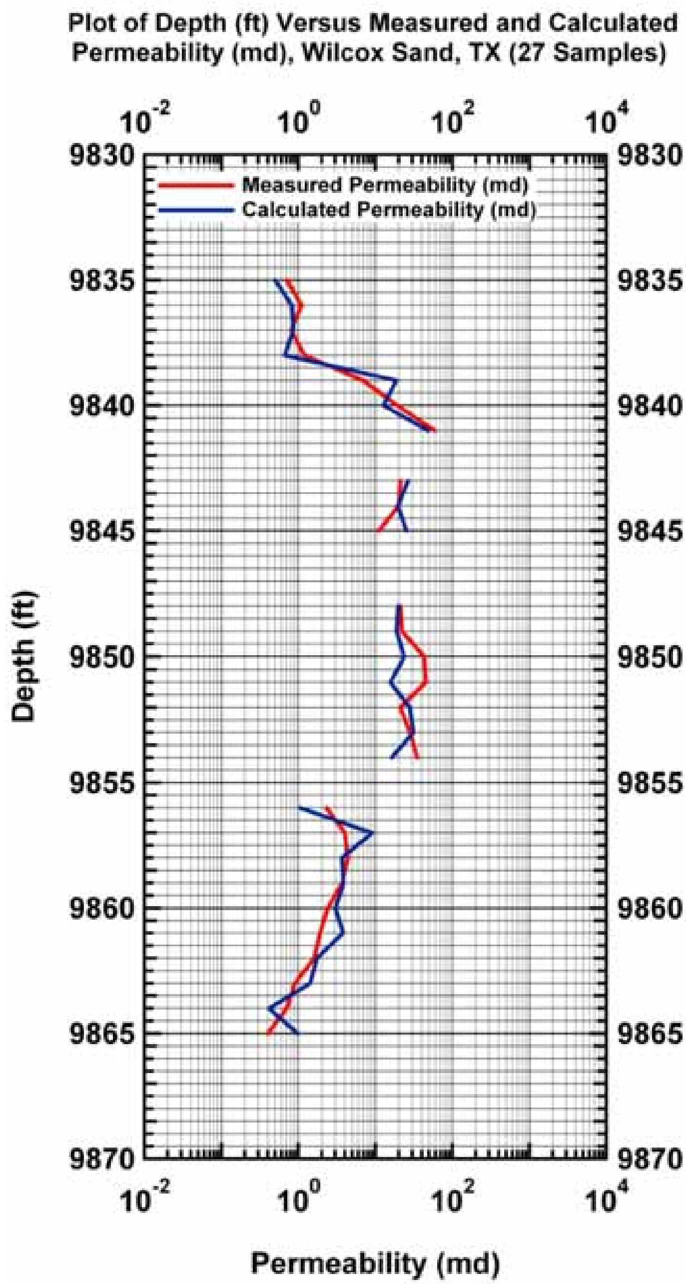

Figure E.6d — Model *CPR-A*: Calculated and measured permeability values versus depth. [*Case*: Wilcox Sand, S. TX (USA)]

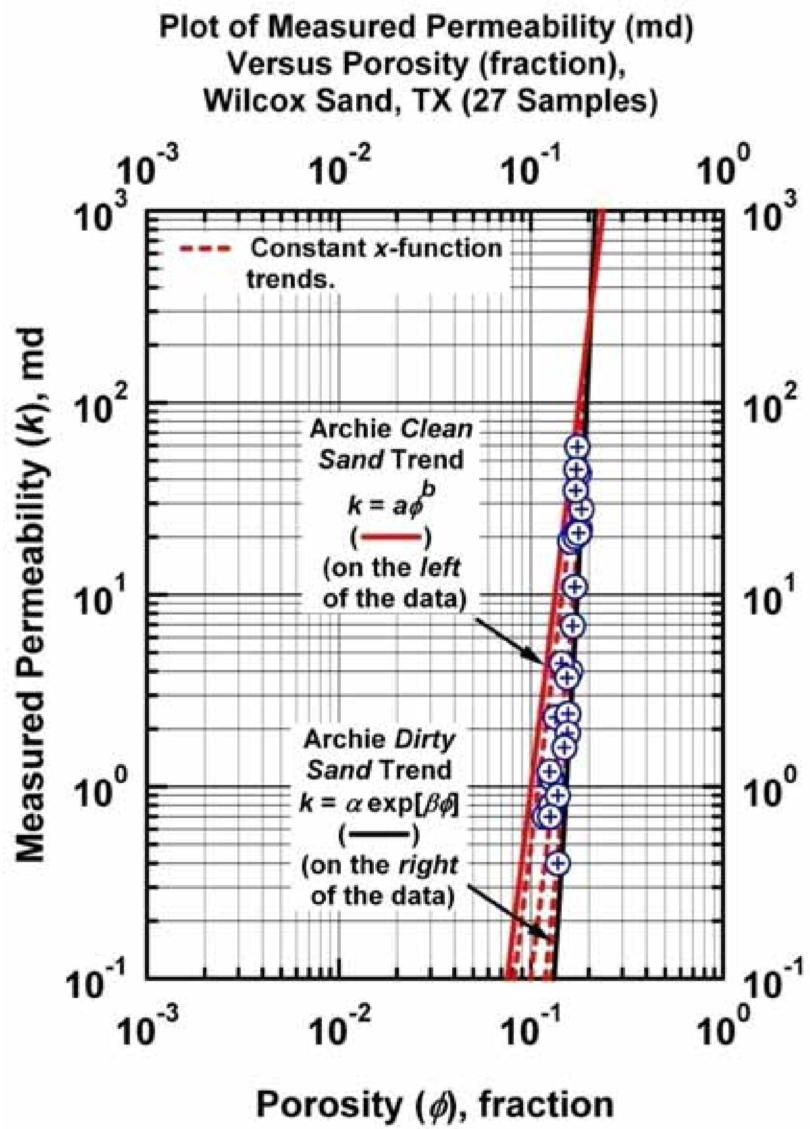

Figure E.7a — Model *CPR-D*: $k = xa\phi^b + (1-x)\alpha\exp[\beta\phi]$ $[0 \le x \le 1]$ — *Weighted Power Law-Exponential Model* used to correlate permeability (k) and porosity (ϕ). "Clean Sand" Plot — Archie "Clean Sand" trend is given by the straight-line trend at the far left of the data (power law model). [*Case*: Wilcox Sand, S. TX (USA)]

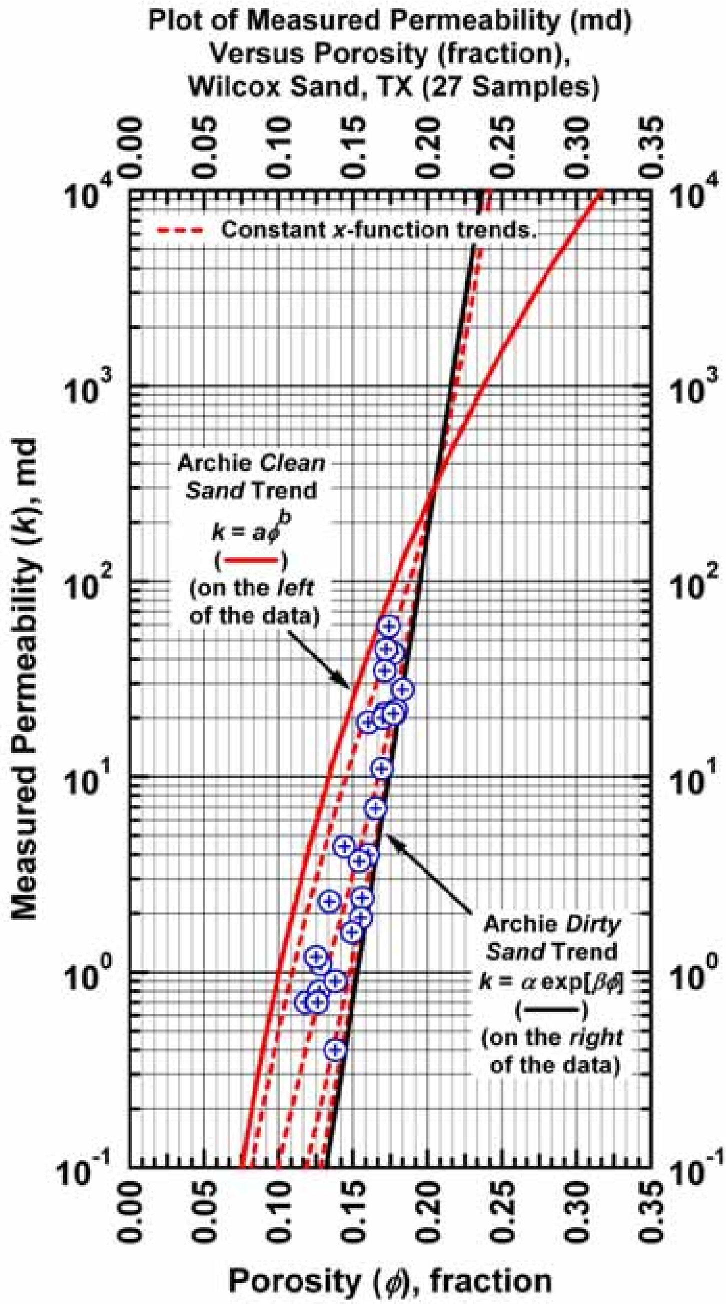

Figure E.7b — Model *CPR-D*: $k = xa\phi^b + (1-x)\alpha\exp[\beta\phi]$ $[0 \le x \le 1]$ — *Weighted Power Law-Exponential Model* used to correlate permeability (k) and porosity (ϕ). "Dirty Sand" Plot — Archie "Dirty Sand" trend is given by the straight-line trend at the far right of the data (exponential model). [*Case*: Wilcox Sand, S. TX (USA)]

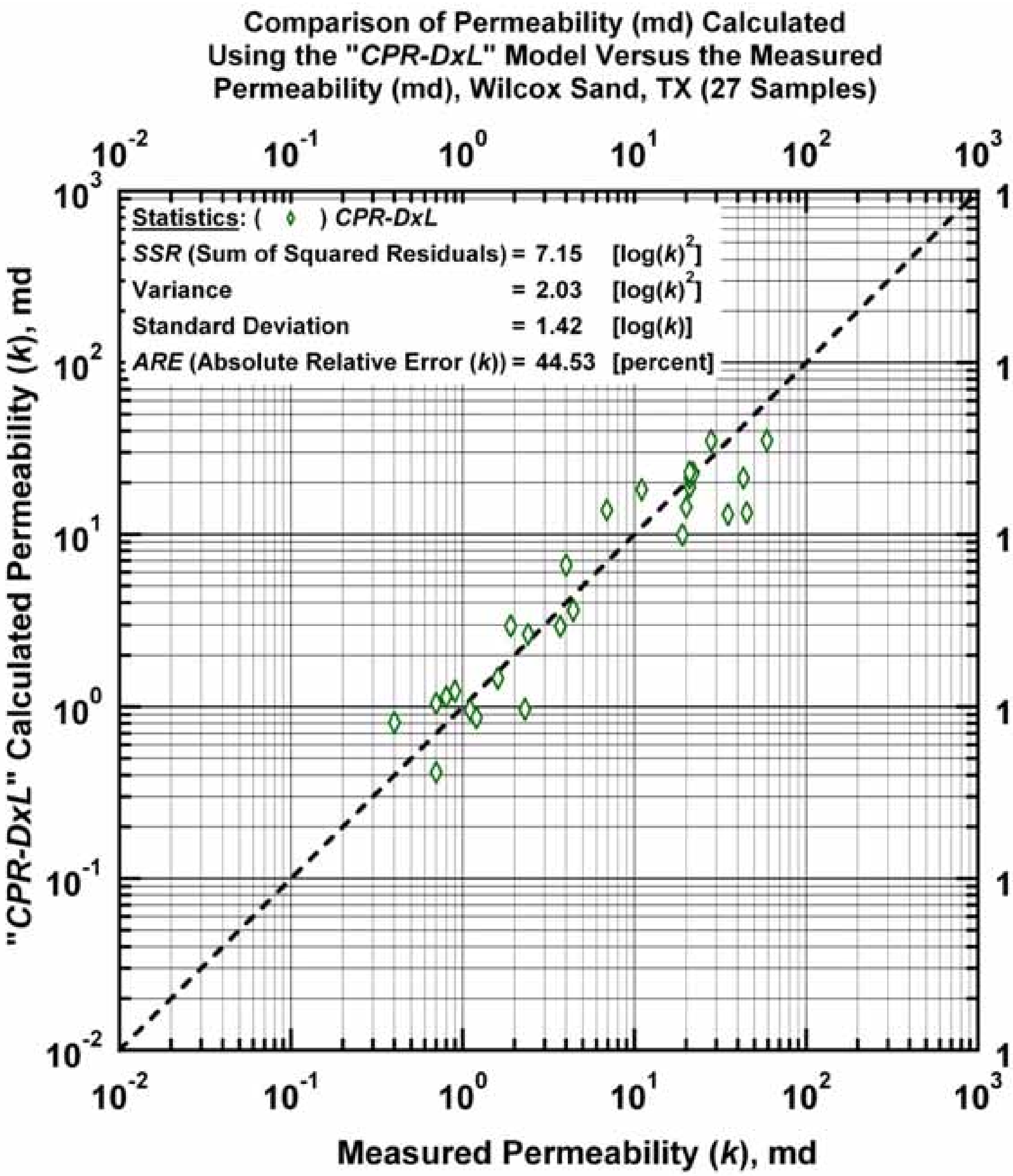

Figure E.8a — Model *CPR-DxL*: Calculated versus measured permeability. [*Case*: Wilcox Sand, S. TX (USA)]

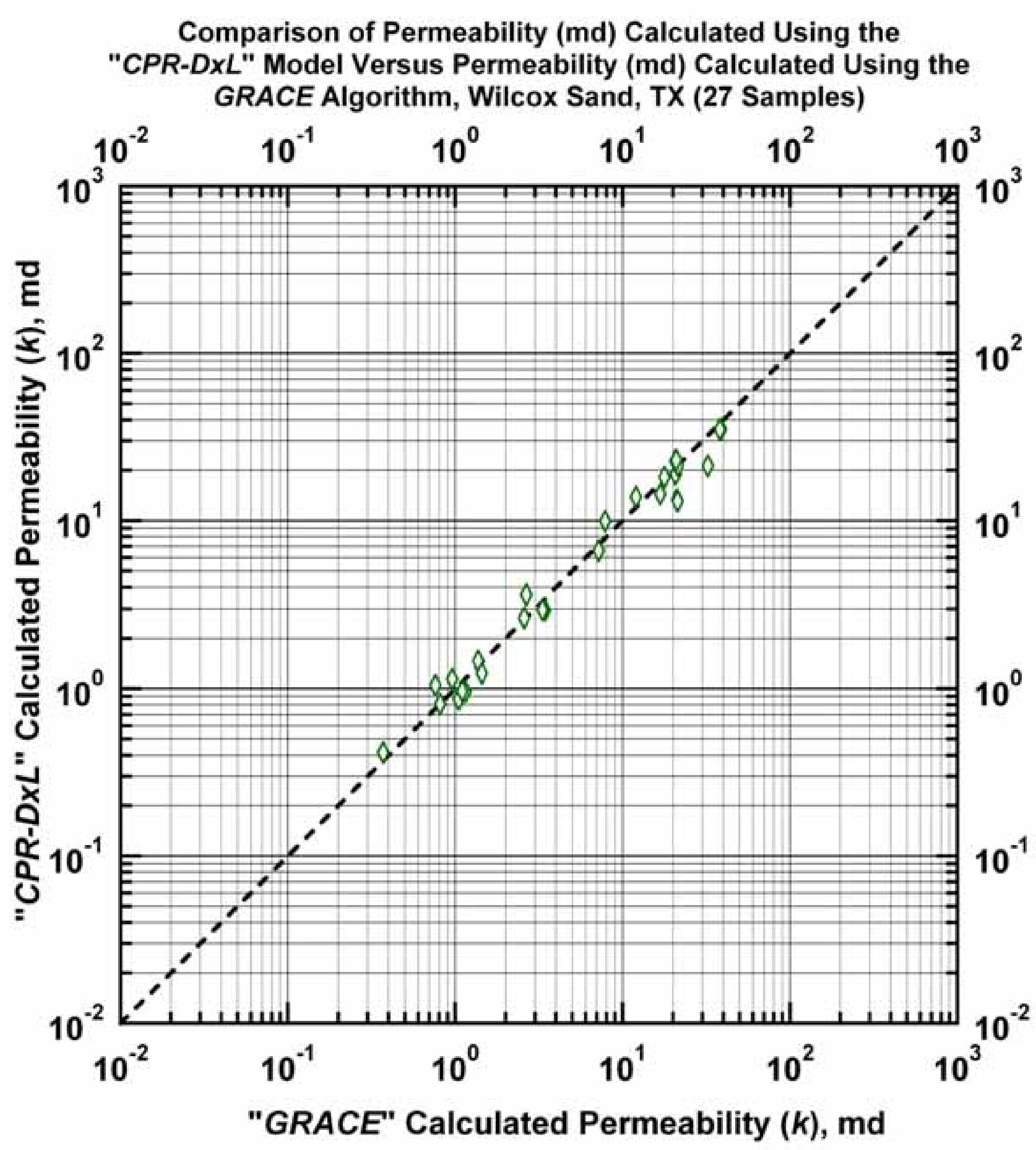

Figure E.8b — Model *CPR-DxL*: Permeability calculated using Model *CPR-C* versus permeability calculated using the *GRACE* Algorithm. [*Case*: Wilcox Sand, S. TX (USA)]

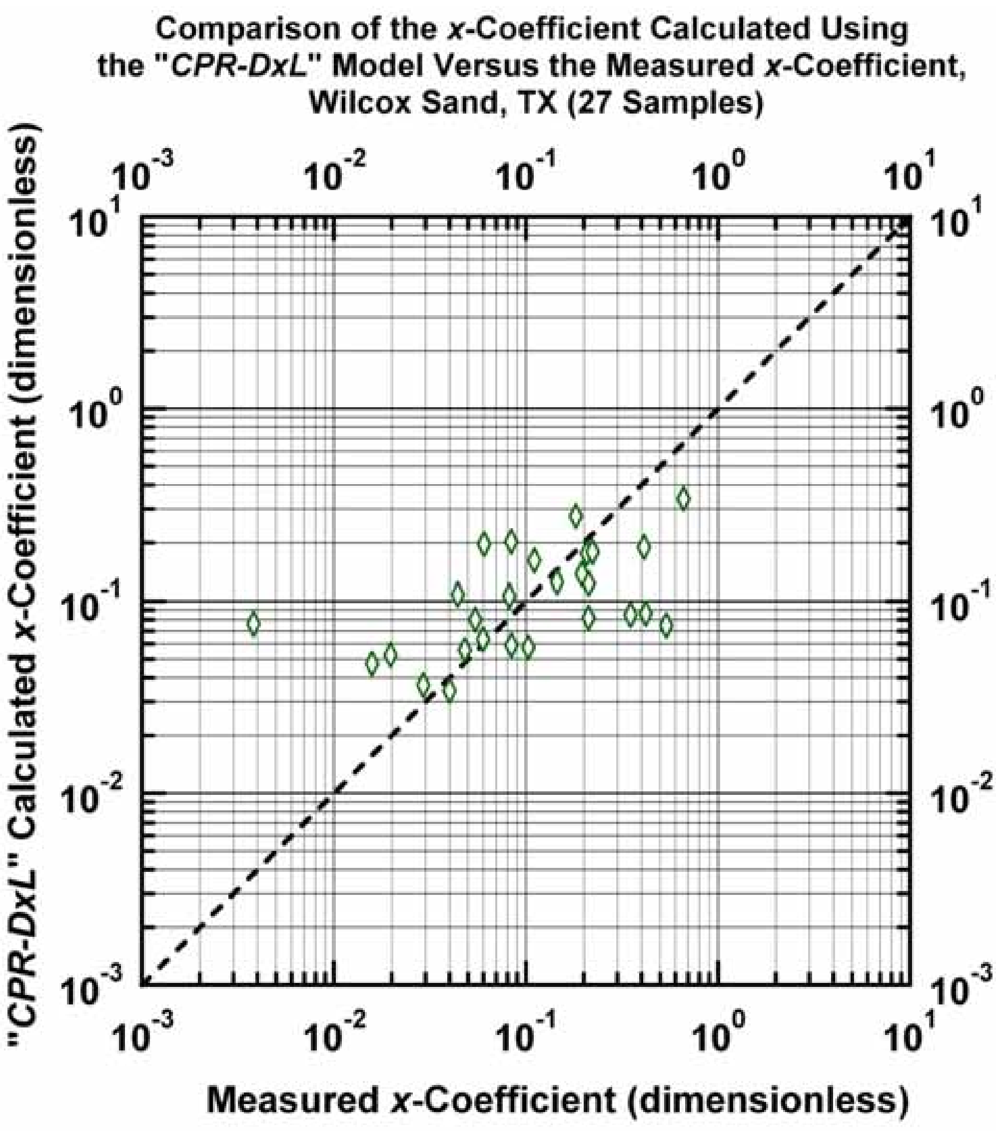

Figure E.8c — Model *CPR-DxL*: Calculated *x*-function weight values versus measured *x*-function weight values. [*Case*: Wilcox Sand, S. TX (USA)]

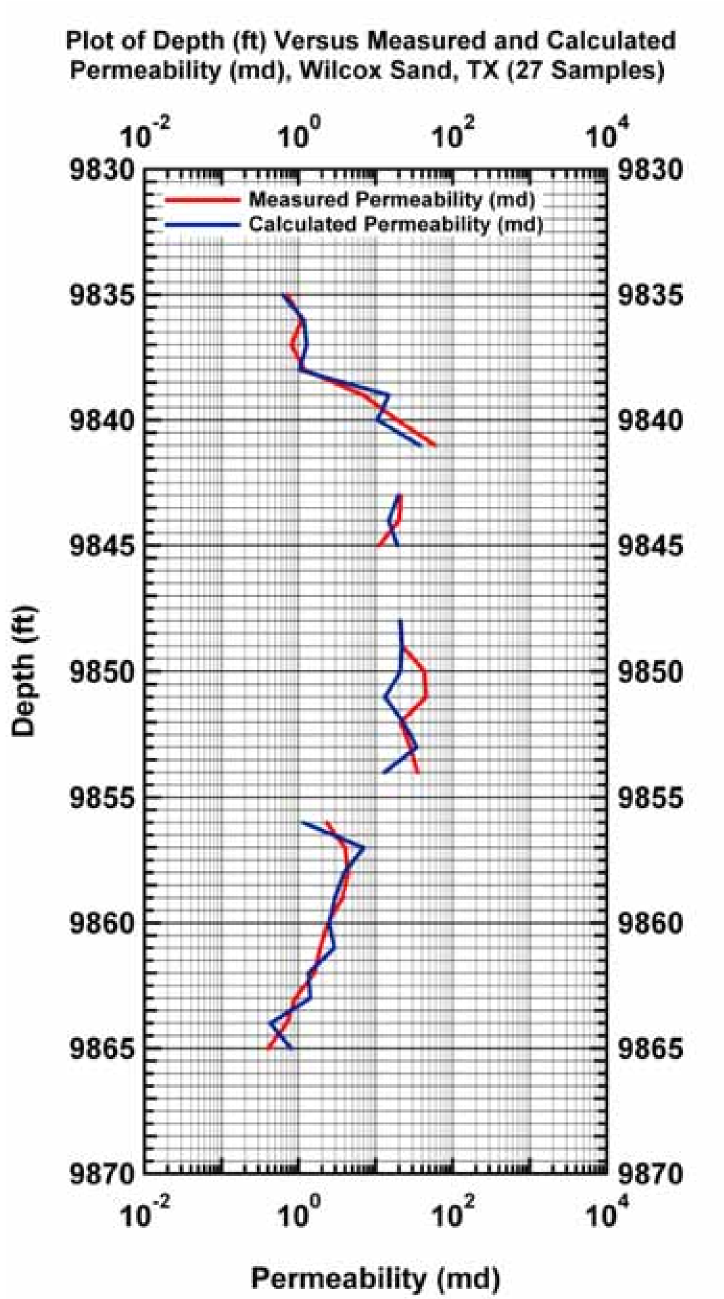

Figure E.8d — Model *CPR-A*: Calculated and measured permeability values versus depth. [*Case*: Wilcox Sand, S. TX (USA)]

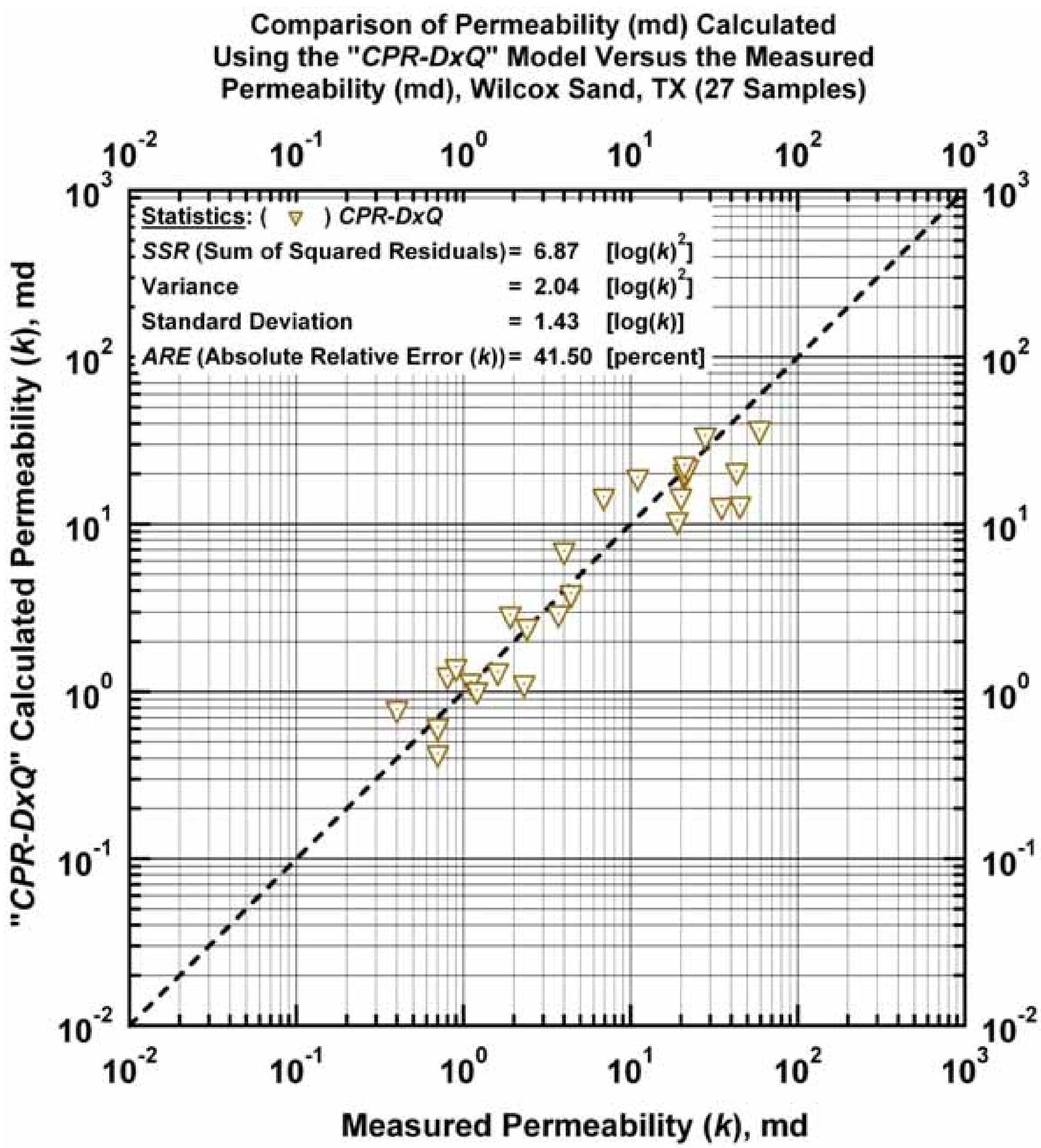

Figure E.9a — Model *CPR-DxQ*: Calculated versus measured permeability. [*Case*: Wilcox Sand, S. TX (USA)]

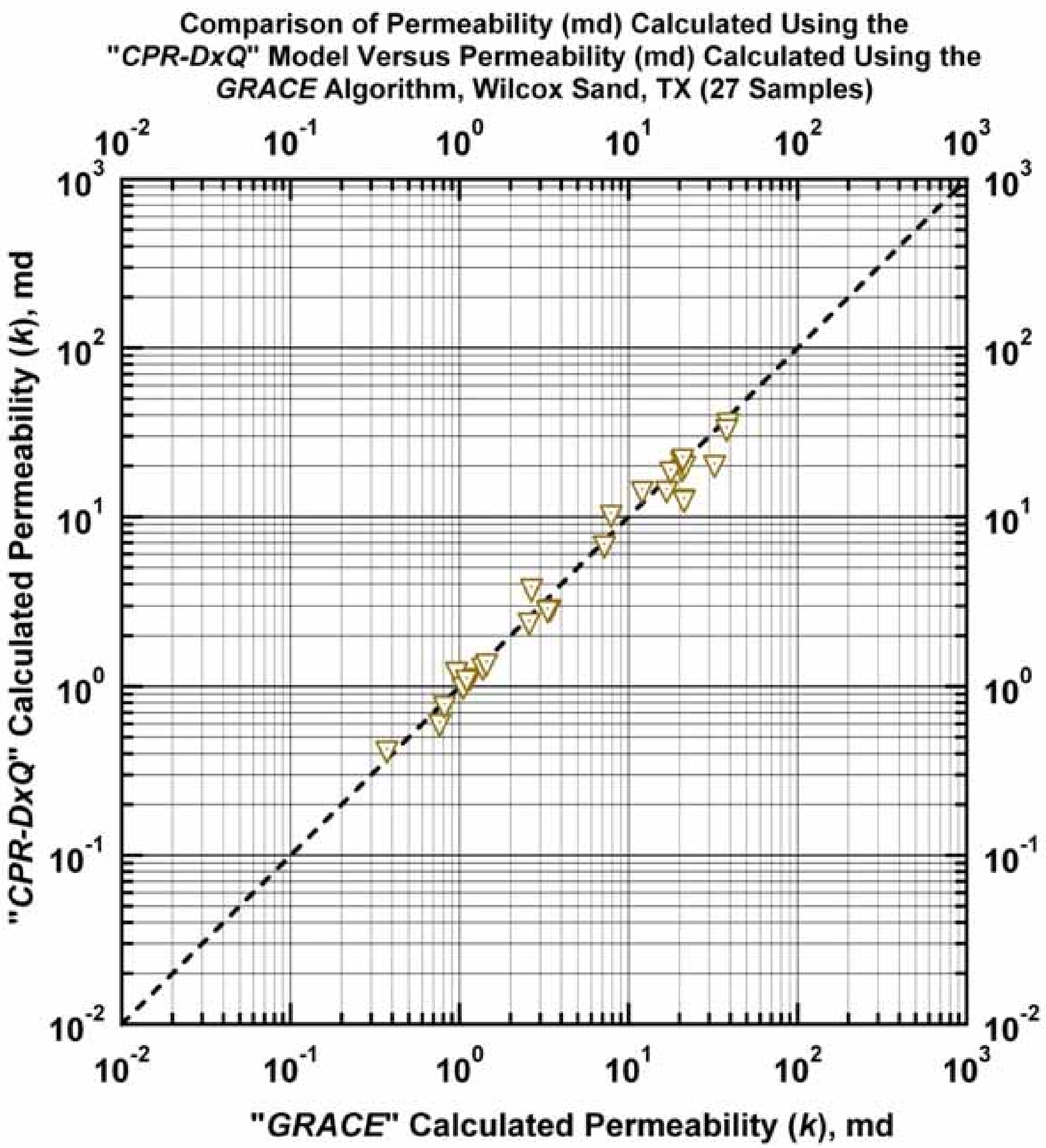

Figure E.9b — Model *CPR-DxQ*: Permeability calculated using Model *CPR-C* versus permeability calculated using the *GRACE* Algorithm. [*Case*: Wilcox Sand, S. TX (USA)]

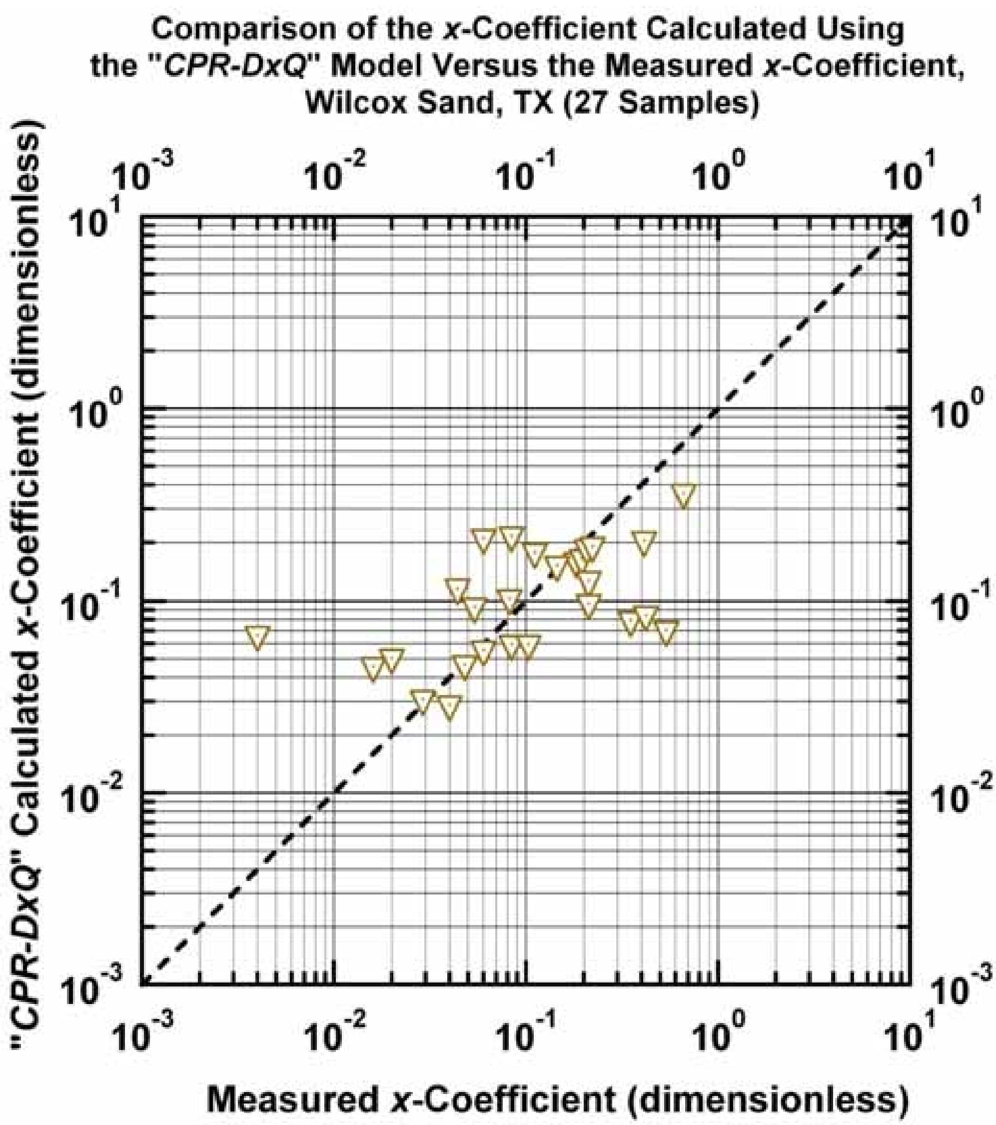

Figure E.9c — Model *CPR-DxQ*: Calculated *x*-function weight values versus measured *x*-function weight values. [*Case*: Wilcox Sand, S. TX (USA)]

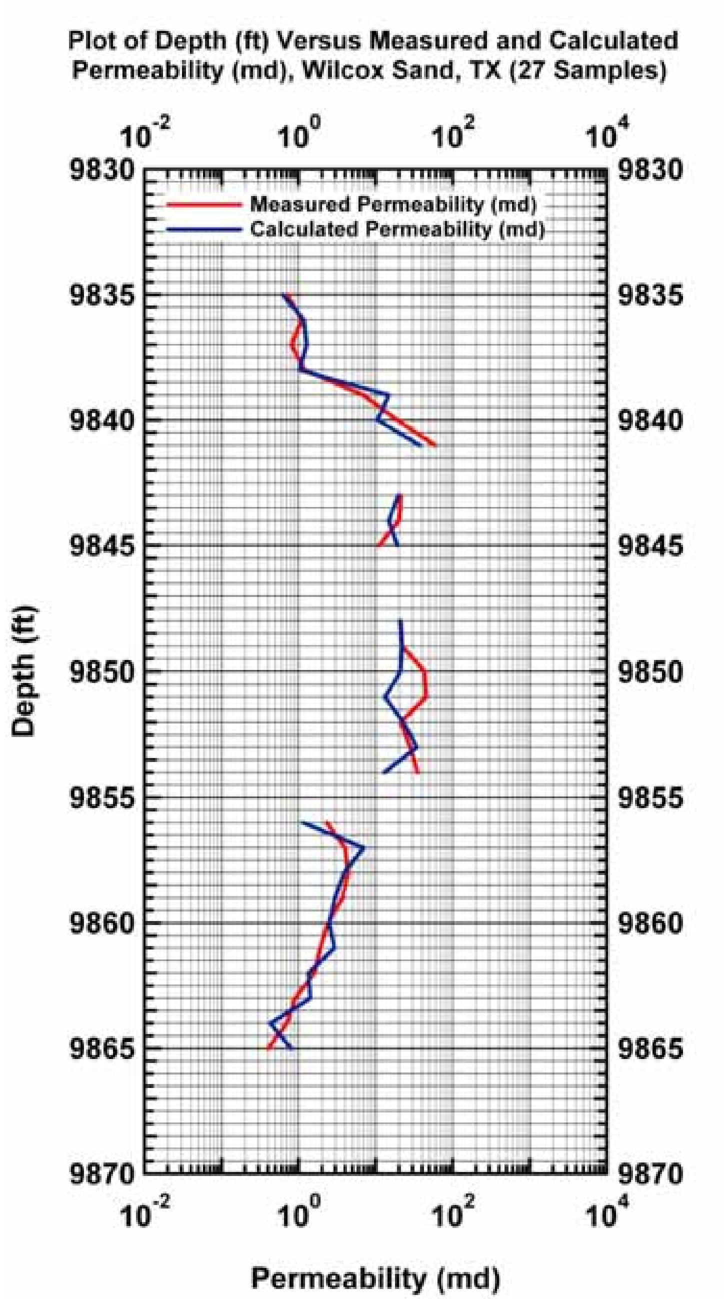

Figure E.9d — Model *CPR-A*: Calculated and measured permeability values versus depth. [*Case*: Wilcox Sand, S. TX (USA)]

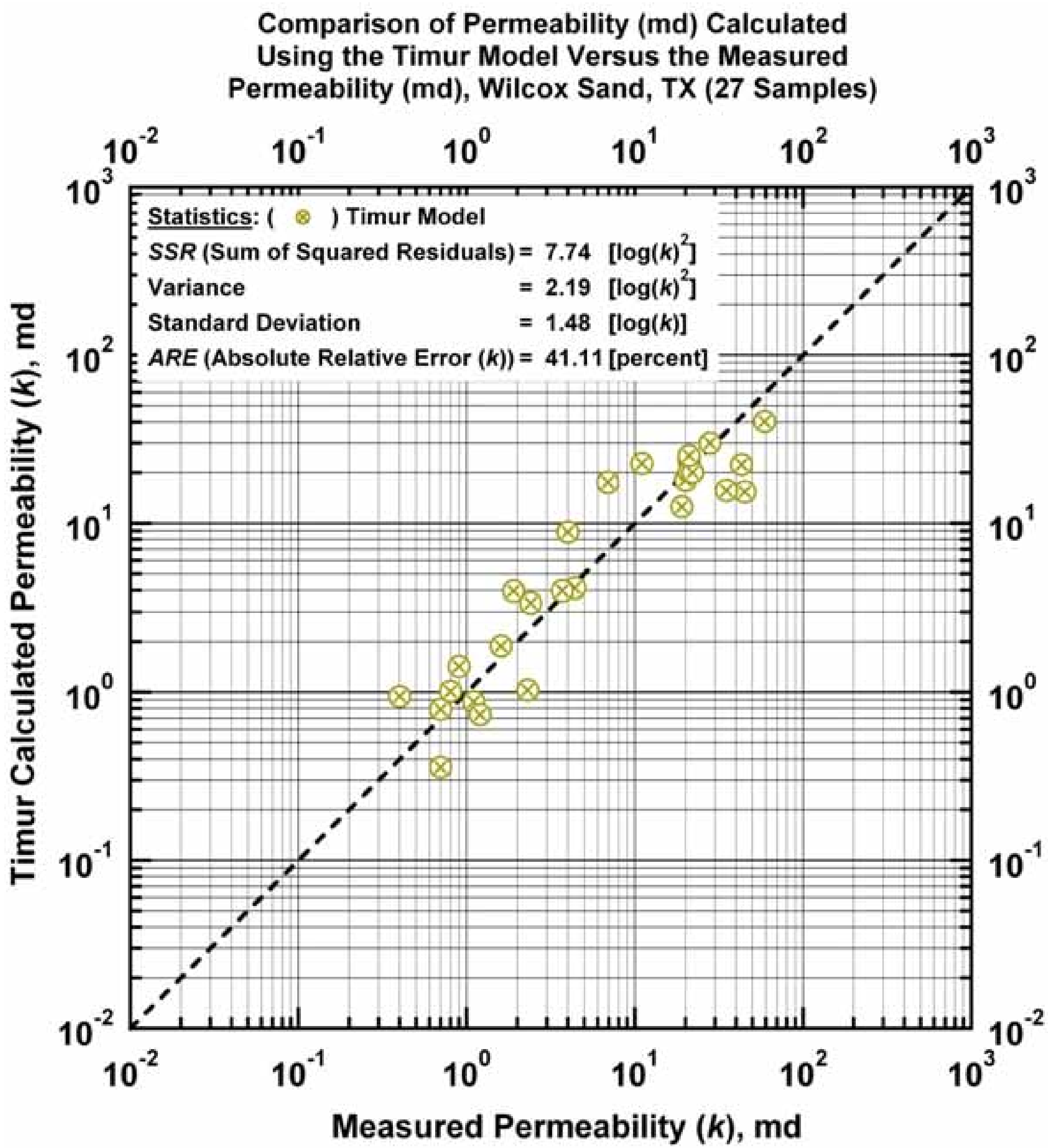

Figure E.10a — "Timur Model:" Calculated versus measured permeability. [*Case*: Wilcox Sand, S. TX (USA)]

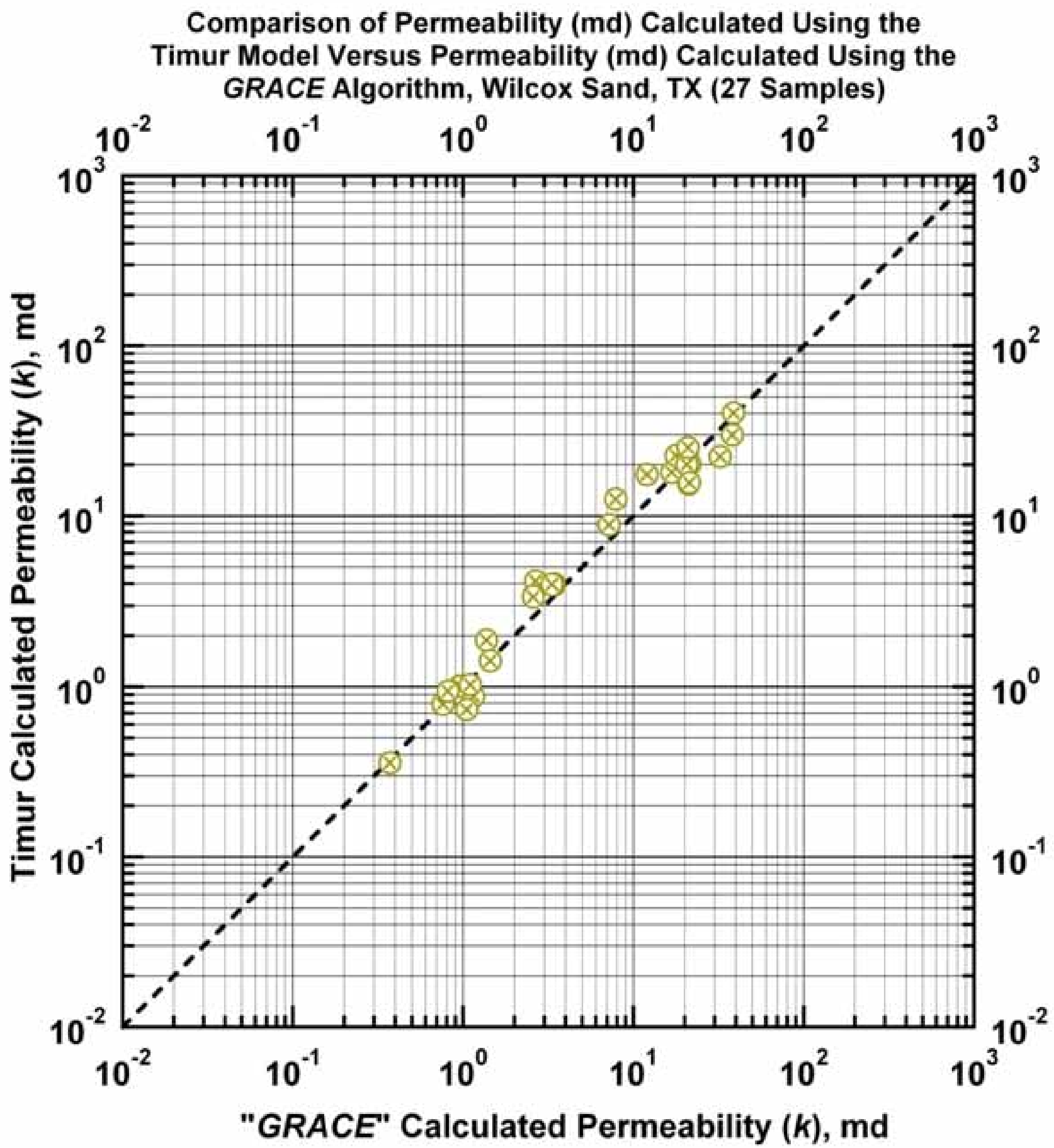

Figure E.10b — "Timur Model:" Permeability calculated using the "Timur Model" versus permeability calculated using the *GRACE* Algorithm. [*Case*: Wilcox Sand, S. TX (USA)]

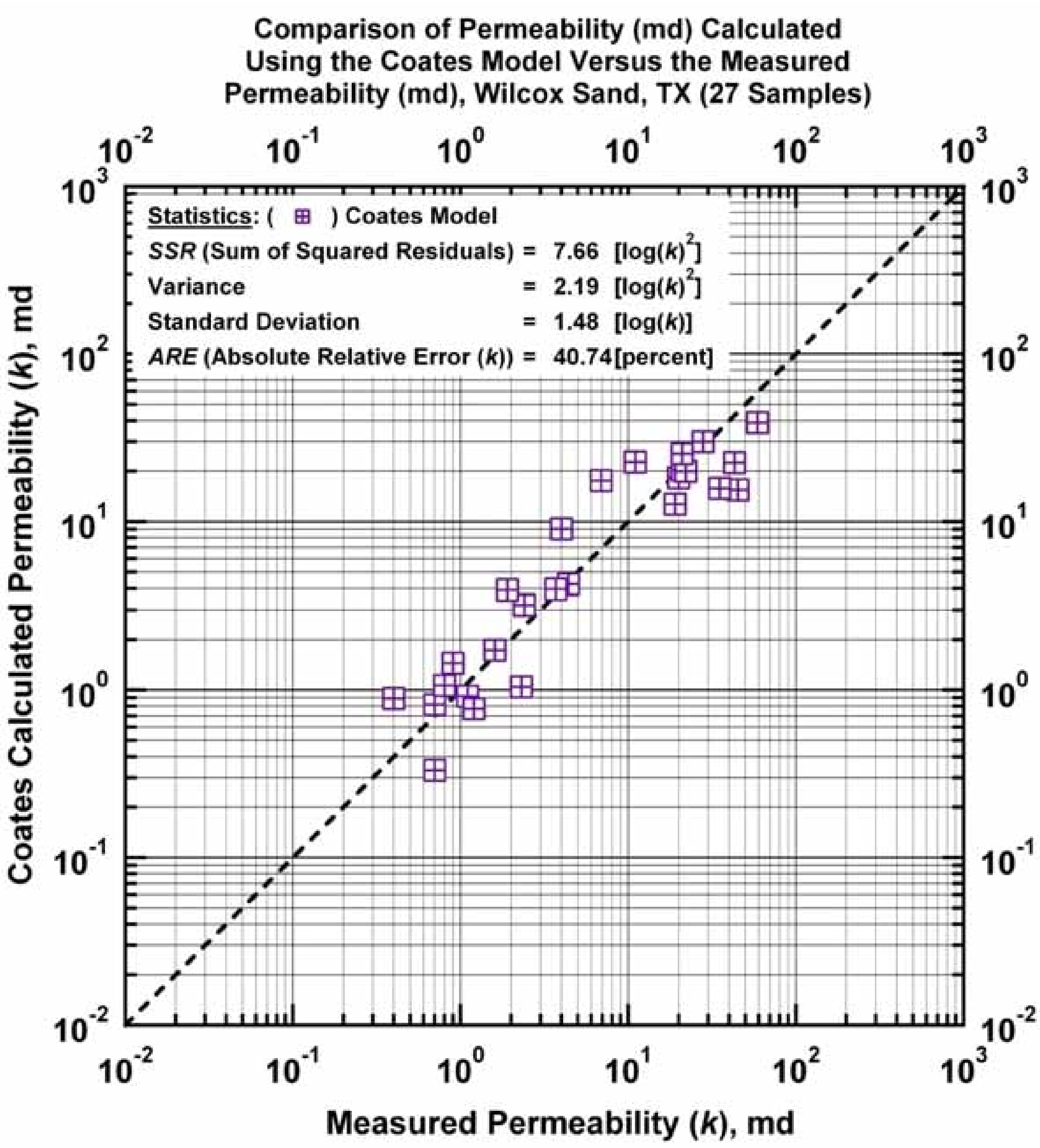

Figure E.11a — "Coates Model:" Calculated versus measured permeability. [*Case*: Wilcox Sand, S. TX (USA)]

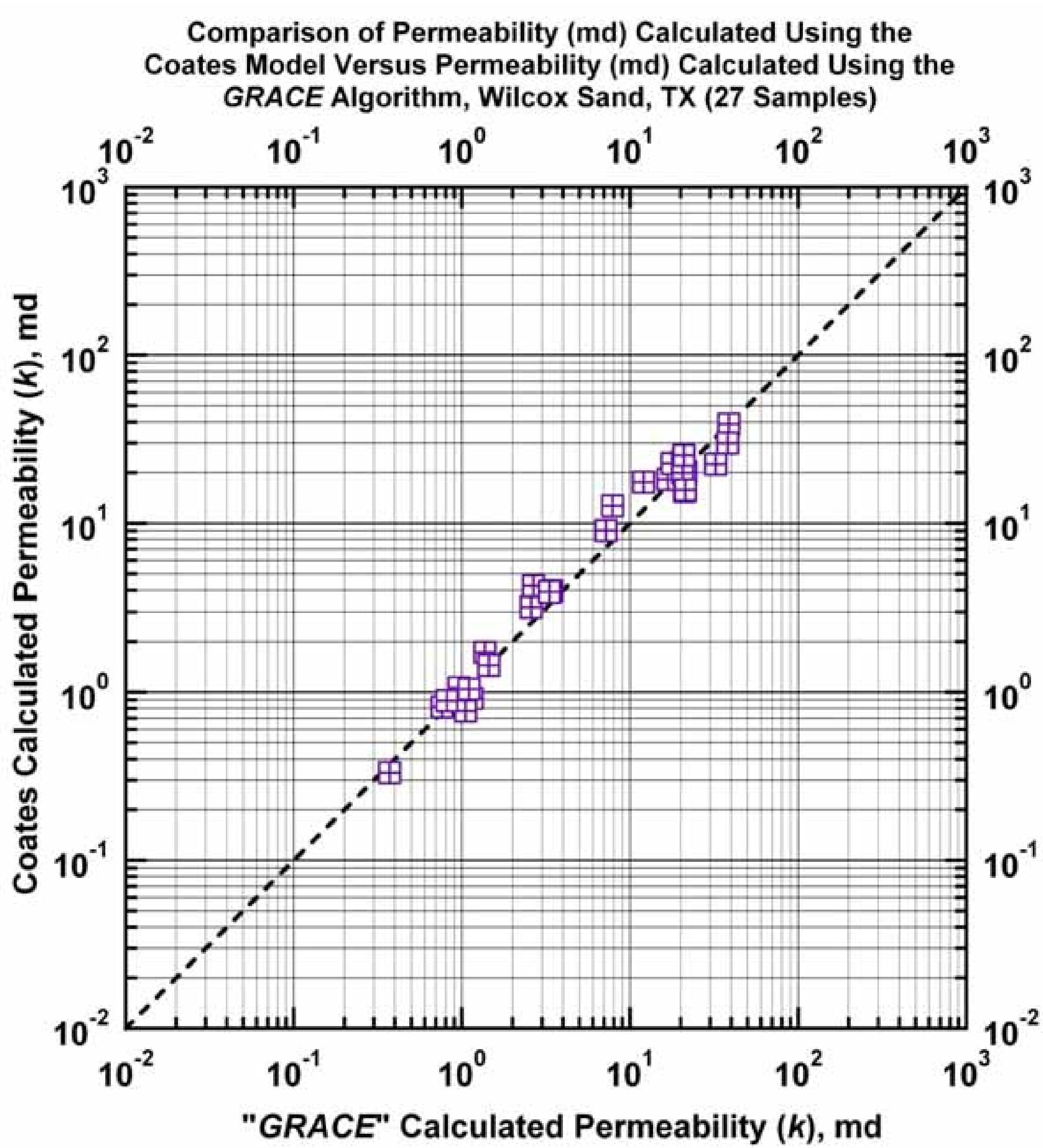

Figure E.11b — "Coates Model:" Permeability calculated using the "Coates Model" versus permeability calculated using the *GRACE* Algorithm. [*Case*: Wilcox Sand, S. TX (USA)]

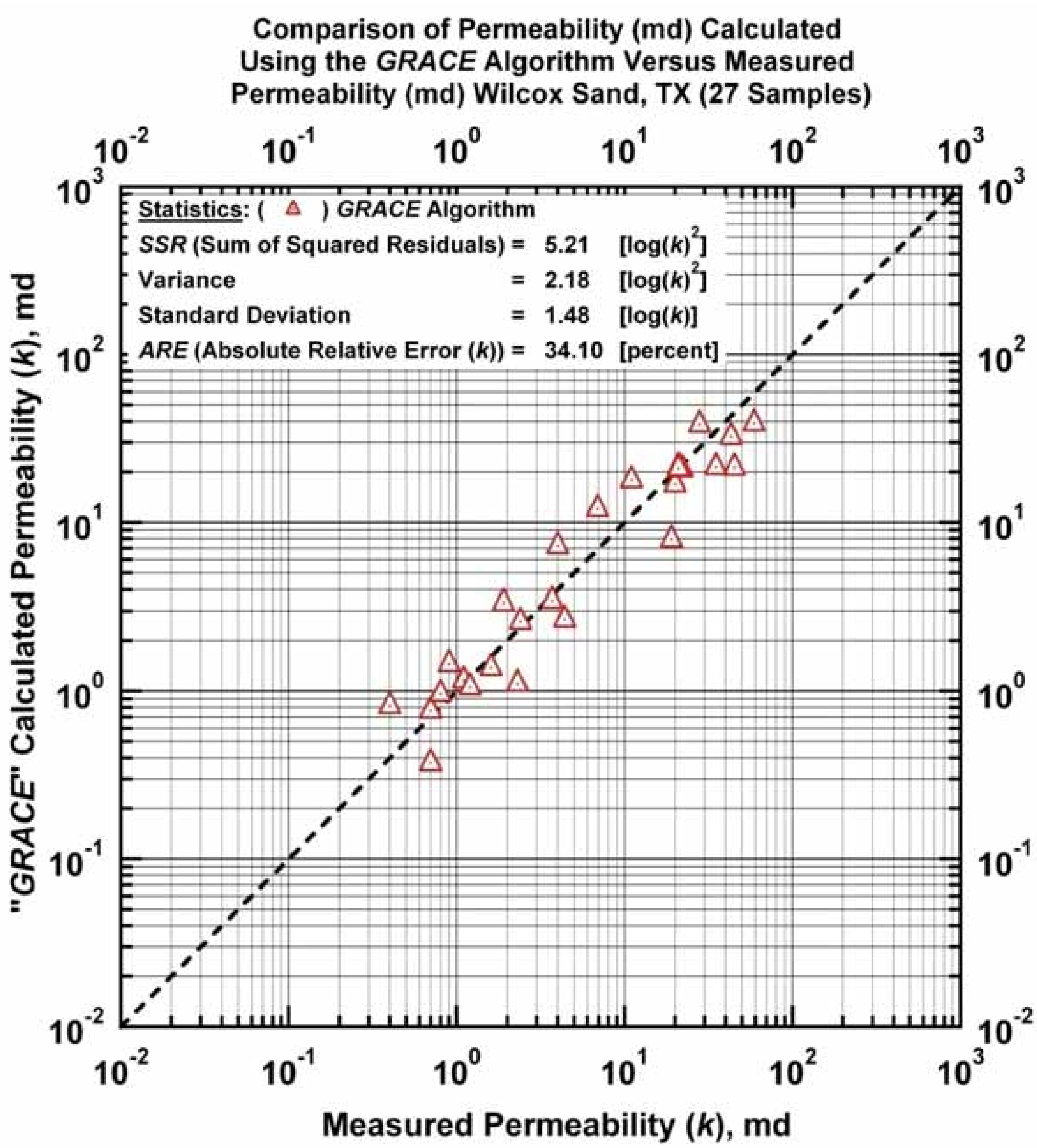

Figure E.12 — *GRACE* Model: Calculated versus measured permeability. [*Case*: Wilcox Sand, S. TX (USA)]

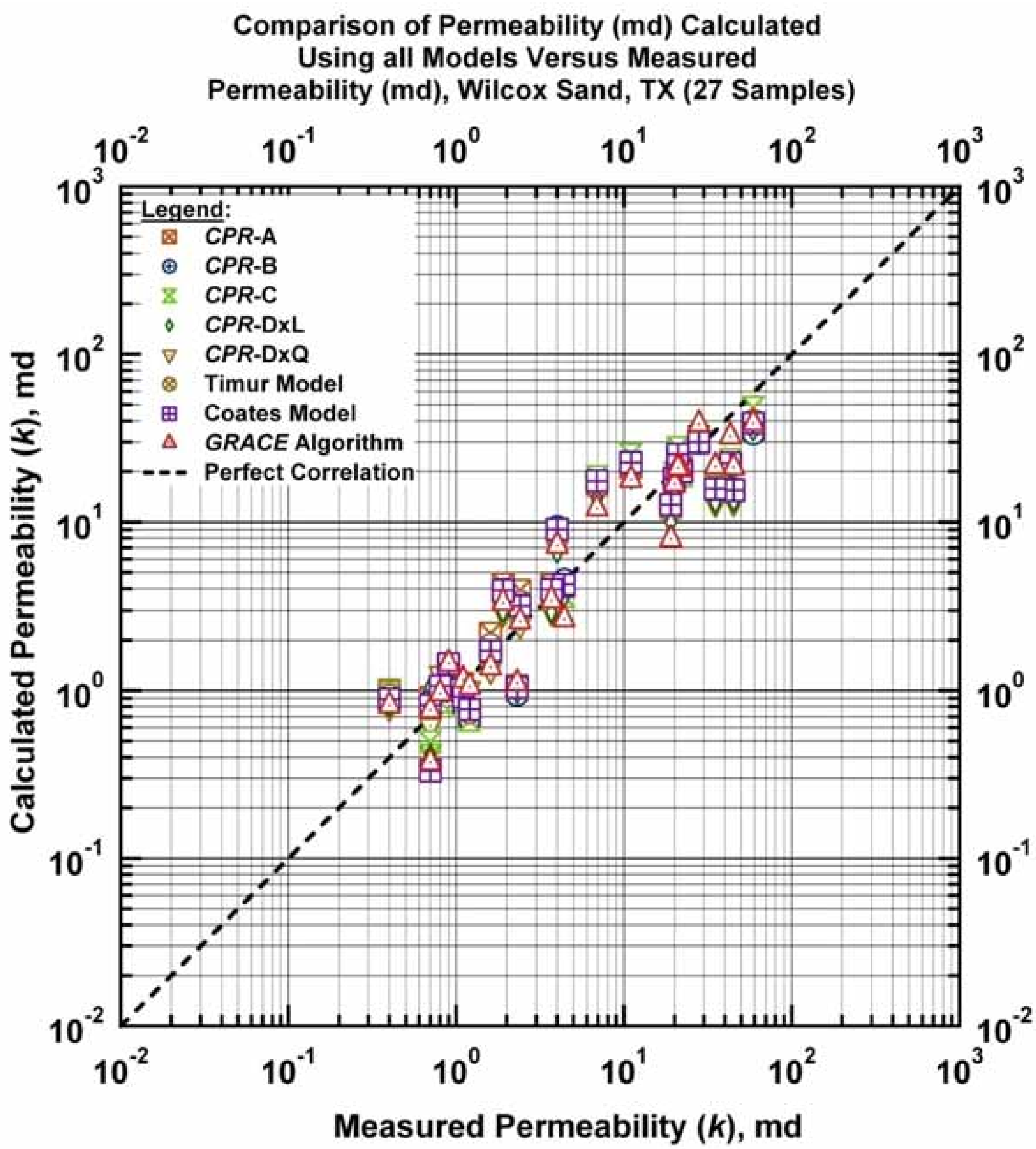

Figure E.13 — All Models: Calculated versus measured permeability. [*Case*: Wilcox Sand, S. TX (USA)]

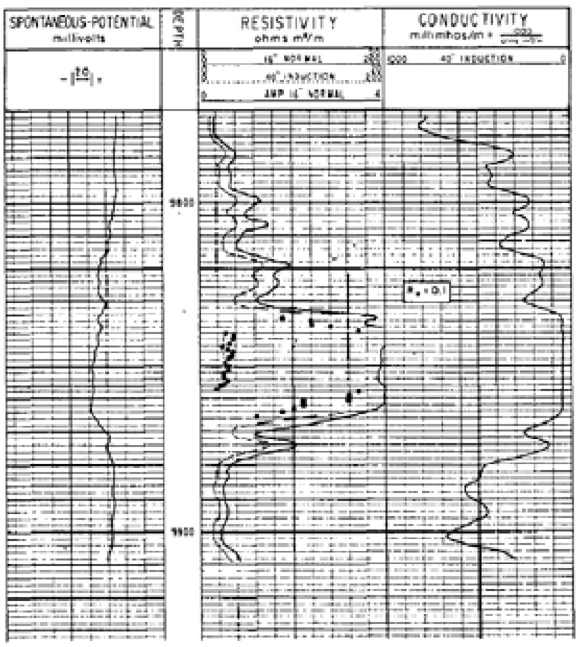

SAMP. NO.	DEPTH FEET	PERM. Md.	POR. %	% POR SAT. OIL	% POR SAT. TOTAL WATER	PROB. PROD.	% OIL VOL.	% GAS VOL.	°API
1	9834-35	00	70	00	500				
2	35-36	07	118	00	330	*			
3	36-37	1.1	128	00	414	COND *			
4	37-38	08	127	00	385	*			
5	38-39	1.2	12.5	00	407	COND *			
6	39-40	69	165	00	346	COND *			
7	40-41	19	160	1.3	350	COND			
8	41-42	59	174	2.9	31.1	COND			
9	42-43	87	15.6	1.3	30.2	COND			
10	43-44	21.	17.1	2.9	352	COND			
11	44-45	20.	170	1.2	377	COND			
12	45-46	11.	169	1.2	343	COND			
13	46-47	44	163	1.2	436	COND			
14	47-48	54	157	1.3	382	COND			
15	49-49	21	178	1.1	42.1	COND			
16	49-50	22	179	1.1	430	COND			
17	50-51	43	17.7	1.1	400	COND			
18	51-52	45	17.2	1.2	41.3	COND			
19	52-53	21.	17.7	1.1	38.4	COND			
20	53-54	28	183	1.1	40.4	COND			
21	54-55	35	171	1.2	40.3	COND			
22	55-56	20	148	1.4	480	COND			
23	56-57	2.3	134	1.5	455	COND *			
24	57-58	4.0	160	1.2	39.3	COND *			
25	58-59	44	144	1.4	36.1	COND *			
26	59-60	37	154	1.3	45.4	COND *			
27	60-61	24	156	1.3	500	COND *			
28	61-62	1.9	155	1.3	464	COND *			
29	62-63	1.6	149	1.3	524	COND *			
30	63-64	09	138	1.5	449	*			
31	64-65	07	126	1.6	53.1	*			
32	9865-66	04	138	2.2	51.5	*			

* LOW PERMEABILITY

FIGURE 10: R_w - P_f COMPARISON FOR WILCOX SAND IN SOUTH TEXAS

Figure E.14 — Original data from Granberry and Wilshusen (1962). [*Case*: Wilcox Sand, S. TX (USA)]

APPENDIX F

RESULTS FOR HAZLETT WELL 103

In this Appendix we present the "Hazlett" Well 103, (Hazlett, 1989).

Model *CPR-A*: (Appendix F)

The "characteristic permeability relation" (or *CPR*) Model *CPR-A* (*i.e.*, the modified Archie "Clean Sand" Model) is given as:

$$k = a(\phi - c)^b \quad c = c_{\max} \exp[-c_1 \phi^{c_2} F^{c_3}] \quad \text{.......(F-1)}$$

Where a plot of log(k) versus log(ϕ) is used to graphically calibrate Eq. F-1 in terms of the coefficients — a, b, and $c_{\max}$. **Fig. F.1** shows that the *CPR-A* model performs quite well for this case. **Figs. F.1a and b** show the log-log and the semilog format of permeability versus porosity, respectively. In **Fig. F.2** we provide the "error" plots for this case, where the measured and computed data are compared systematically. In **Fig. F.2a** we note a good correlation of the results obtained using Model *CPR-A* versus the measured permeability data — there is good agreement with the perfect correlation trend (*i.e.*, the 45-degree line). In **Fig. F.2b** we provide a comparison with the *GRACE* algorithm correlation (Xue *et al*. 1997)), and we note that the *CPR-A* model results correlate very well with the *GRACE* algorithm results for this case. Lastly, in **Fig. F.2c** we present the calculated and measured c-function — and again we note a reasonable correlation of the data about the perfect correlation trend.

Model *CPR-B*: (Appendix F)

The "characteristic permeability relation" (or *CPR*) Model *CPR-B* (*i.e.*, the modified Archie "Dirty Sand" Model (power-law basis)) is given as:

$$k = a(\phi + c)^b \quad c = c_{\max} \exp[-c_1 \phi^{c_2} F^{c_3}] \quad \text{.......(F-2)}$$

Where a plot of log(k) versus log(ϕ) is used to graphically calibrate Eq. F-2 in terms of the coefficients — a, b, and $c_{\max}$. The results for this case are presented in **Figs. F.3 and 4**. In **Fig. F.3a** (log-log format) we note that a very distinct "envelope" is formed by the *CPR-B* model, essentially all of the data on the right and left flanks are well-matched (*i.e.*, the "dirty sand" power law relation (applied on the right portion of the data) and its correction function (applied on the left portion of the data). Similarly, in **Fig. F.3b** (semilog format), we observe an excellent distribution of the power law model across the body of the data. The error analyses for this case are shown in **Fig. F.4**. In **Fig. F.4a** we present the results obtained using Model *CPR-B* versus the measured permeability data and in this case there is good agreement with the perfect correlation trend (*i.e.*, the 45-degree line). We provide a comparison with the *GRACE* algorithm correlation in **Fig. F.4b** — the results using Model *CPR-B* and the *GRACE* algorithm compare very well for this case. We compare the computed and data-derived values of the c-function for this case in **Fig. F.4c** and we note the computed c-function does not change much form the data-derived values of the c-function. In summary, we believe that Model *CPR-B* works well for this particular data case.

Model *CPR-C*: (Appendix F)

The "characteristic permeability relation" (or *CPR*) Model *CPR-C* (*i.e.*, the modified Archie "Dirty Sand" Model (exponential basis)) is given as:

$$k = c\exp[\beta\phi] \quad c = c_{\max}\exp[-c_1\phi^{c_2}F^{c_3}] \quad \text{(F-3)}$$

Where a plot of log(k) versus ϕ is used to graphically calibrate Eq. F-3 in terms of the coefficients — β and $c_{\max}$. Model *CPR-C* is fundamentally different than Models *CPR-A* and *CPR-B*, as the basis for Model *CPR-C* is an exponential function, not a power law relation. In **Figs. F.5 and 6** we present the results of applying Model *CPR-B* for this case, and in general, we observe a very consistent performance of Model *CPR-B*. **Fig. F.5b** illustrates the excellent conformance of Model *CPR-C* for this case — again recalling that this model has an exponential relationship with porosity as its basis.

In **Figs. F.6a, F.6b, and F.6c** we review the error analyses plots for this case, and we note good performance (visually) in terms of the correlation of the results using Model *CPR-C*. The correlation of the c-function (see **Fig. F.6c**) appears to be consistent — but scatter and a slight off-center trend is evident. However, as we are approaching this work from the perspective that the primary value of the work is the characteristic model, not the statistical "best fit" correlation, we believe that the *CPR-C* model has performed well for this case, and the plots in **Fig. F.6** confirms the value of this model as a "characteristic relation" for permeability.

Model *CPR-D*: (Appendix F)

The "characteristic permeability relation" (or *CPR*) Model *CPR-D* (*i.e.*, the weighted power law-exponential model) is given in its fundamental form as:

$$k = xa\phi^b + (1-x)\alpha\exp[\beta\phi] \quad [0 \le x \le 1]] \quad \text{(F-4a)}$$

For Eq. F-4 there are two proposed models for the x-function (*i.e.*, the weighting function) — these are:

$$x = \exp[-\ln(x_0) + x_1\ln(\phi) + x_2\ln(F) + x_3\ln(\phi)\ln(F)] \quad \text{(Model } \textit{CPR-DxL}\text{)} \quad \text{(F-4b)}$$

$$x = \exp\begin{bmatrix} -\ln(x_0) + x_1\ln(\phi) + x_2\ln(F) + x_3\ln(\phi)\ln(F) \\ + x_4\ln(\phi)^2 + x_5\ln(F)^2 + x_6\ln(\phi)^2\ln(F) \\ + x_7\ln(\phi)\ln(F)^2 + x_8\ln(\phi)^2\ln(F)^2 \end{bmatrix} \quad \text{(Model } \textit{CPR-DxL}\text{)} \quad \text{(F-4c)}$$

As noted in Eq. F-4b, Model *CPR-DxL* utilizes a logarithmic linear model for the weights (x-values) and as seen in Eq. F-4c, Model *CPR-DxQ* utilizes a logarithmic quadratic model for the weights (x-values). While these models (Eqs. F-4b and F-4c) are *empirical*, we have found generally good application of these relations for all cases. In this case, the base results using Models *CPR-DxL* and *CPR-DxQ* are presented in

Fig. F.7 — where the power law and exponential basis functions are fitted to the appropriate portion of the data. The power law equation represents the "Archie Clean Sand" trend and is fitted to the leftmost data as shown in **Fig. F.7a** and in contrast, the exponential equation is thought to represent the "Archie Dirty Sand" trend and the exponential is fitted to the far rightmost portion of the data (see **Fig. F.7b**).

In **Figs. F.8 and 9** we present the error analyses for this case, where we have employed the weighting functions (Eqs. F-4b and F-4c) as appropriate. In **Fig. F.8a** we observe a good correlation of permeability (with the out-lying points noted in the middle of the trend). The comparison of the Model *CPR-DxL* results are compared to the results obtained from the *GRACE* algorithm in **Fig. F.8b**. The computed weight function (*x*-values) shown for the *CPR-DxL* model in **Fig. F.8c** does exhibit more scatter than expected, but the trend is (relatively) centered about the perfect correlation line.

The results obtained using Model *CPR-DxQ* are presented in **Fig. F.9**, and we note substantially improved behavior over that of Model *CPR-DxL*. In particular, the base correlation of computed and measured permeabilities (**Fig. F.9a**) for Model *CPR-DxQ* does indicate a slightly better correlation than that of Model *CPR-DxL*. Also, the comparison of Model *CPR-DxQ* with the results from the *GRACE* algorithm (**Fig. F.9b**) exhibits better agreement than the results of Model *CPR-DxL*. Finally, the correlation of the *x*-function (**Fig. F.9c**) for Model *CPR-DxQ* is better than the correlation for Model *CPR-DxL*. These comparisons suggest that Model *CPR-DxQ* (*i.e.*, the combination of Eqs. F-4a and F-4c) provides a better correlation of data, for this case, than Model *CPR-DxL*.

***"Modified Timur Model"*: (Appendix F)**

The "Modified Timur Model" is given as:

$$k_{\text{Timur}} = a\phi^b F^c \quad \text{(F-5)}$$

In **Fig. F.10** we present the results of the "Modified Timur Model" (Eq. F-5) which is essentially just a generalized power-law function relation in terms of *k*, ϕ, and *F*. **Figs. F.10a and b**, provide the "Modified Timur Model" results of the data for this case.

***GRACE* Algorithm: (Appendix F)**

In **Fig. F.11** we present the results predicted by the *GRACE* algorithm, which is a noF-parametric regression approach (see Xue *et al.* (1997) for details). In theory, the *GRACE* algorithm should provide the most *unbiased* correlation of the data — *i.e.*, the *GRACE* algorithm is designed not to "fit the errors" as other regression approaches may. It is our contention that the *GRACE* algorithm is the statistical standard — and any algorithm/approach/model which achieves better regression statistics than the *GRACE* algorithm is actually "fitting the errors" in the data. *None of the cases have significantly better regression statistics than the GRACE algorithm* — hence, none of the cases are "over-fitted" in a statistical sense.

***Comparison of All Models*: (Appendix F)**

Our final graphic, **Fig. F.12**, illustrates all of the models on a single plot of calculated versus measured permeability. We also present a table of all statistical results in **Table F.1**.

Table F.1 — Statistical Results for all Models (Hazlett Well 103 Case, *n*=34).

Model	Sum of Squared Residuals $[\log(k)^2]$	Variance $[\log(k)^2]$	Standard Deviation $[\log(k)]$	Absolute Relative Error [percent]
CPR-A	20.00	4.38	2.09	70.78
CPR-B	25.76	3.76	1.94	79.06
CPR-C	21.69	4.38	2.09	72.39
CPR-DxL	25.18	4.05	2.01	75.42
CPR-DxQ	18.56	4.34	2.08	69.46
Modified Timur	28.11	4.13	2.03	83.89
GRACE Algorithm	15.21	4.45	2.11	55.57

The coefficients for the models used in this case are provided in **Table F.2**.

Table F.2a — Model Coefficients (Hazlett Well 103 Case, *n*=34).

Model	a or α	b or β	c or c_{max}	c_1	c_2	c_3
CPR-A	8.00×10^{8}	8.00	0.050	1.33×10^{-3}	-1.88	0.35
CPR-B	1.00×10^{7}	8.00	0.050	1.09	-0.32	-0.26
CPR-C	1.00×10^{-6}	100.00	5.00×10^{-4}	24.49	0.66	-0.11
Modified Timur	1.54×10^{6}	6.87	0.246	–	–	–

Table F.2b — Model Coefficients (Hazlett Well 103 Case, *n*=34).

Model	a	b	α	β
CPR-DxL	8.00×10^{8}	8.00	1.00×10^{-6}	100.00
CPR-DxQ	8.00×10^{8}	8.00	1.00×10^{-6}	100.00

Model	c_0	c_1	c_2	c_3	c_4	c_5	c_6	c_7	c_8
CPR-DxL	90.24	-0.72	-0.56	-0.25	–	–	–	–	–
CPR-DxQ	2.48×10^{7}	-12.28	3.21	3.86	0.69	0.24	-0.36	0.08	0.14

Nomenclature: (Appendix F)

F = Archie Formation Factor (dimensionless)
k = Formation Permeability, md (or any consistent units)
ϕ = Porosity, fraction

References: (Appendix F)

Hazlett, W.G.: "Correlation of Reservoir Rock Properties in Porous Media." PhD dissertation, Texas A&M U., College Station, TX (1989).

Xue, G., Datta-Gupta, A., Valko, P., and Blasingame, T.A.: "Optimal Transformations for Multiple Regression: Application to Permeability Estimation from Well Logs," *SPEFE* (June 1997), 85-93.

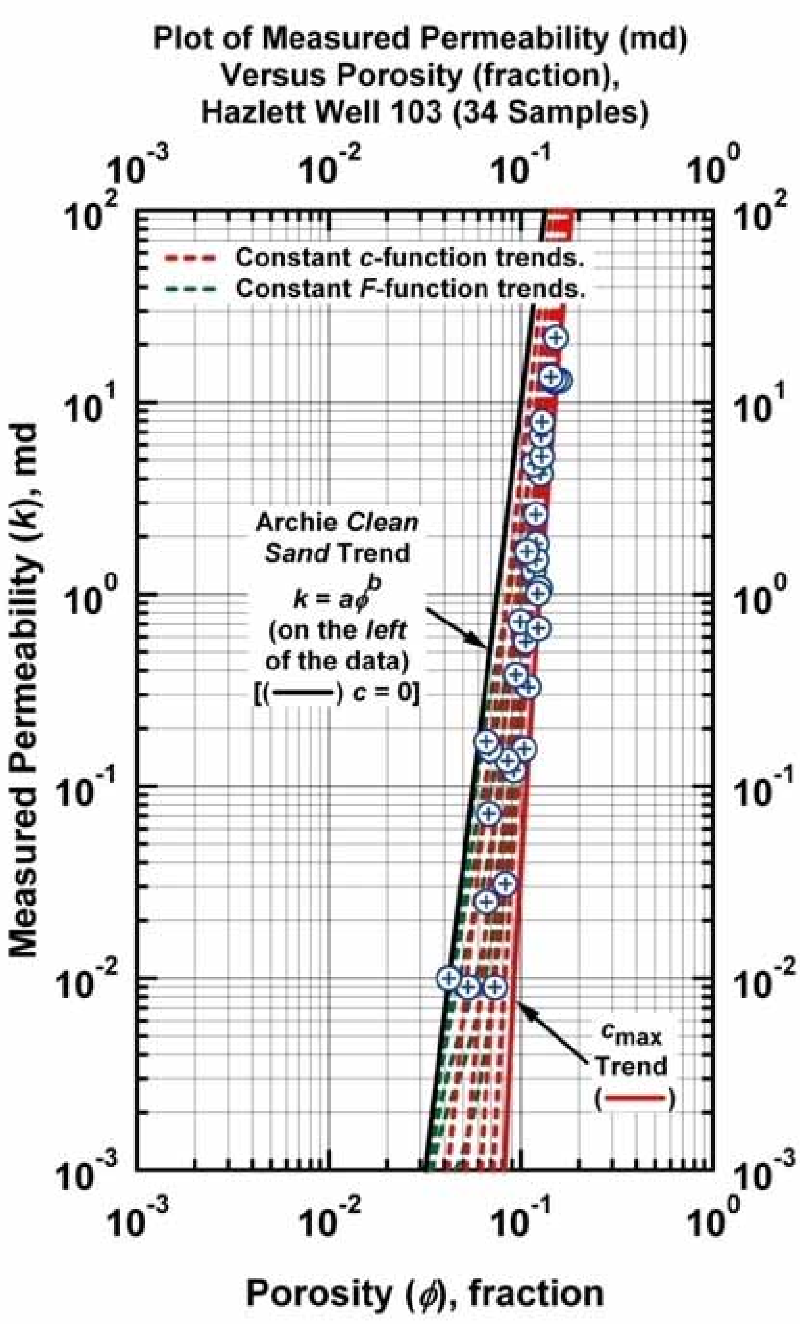

Figure F.1a — Model *CPR-A*: $k = a(\phi - c)^b$ $(c = c_{max} \exp[-c_1 \phi^{c_2} F^{c_3}])$ — "Clean Sand" Plot (log-log format) — Archie "Clean Sand" trend is given by the straight-line trend at the far left of the data (power law model). [*Case*: Hazlett Well 103]

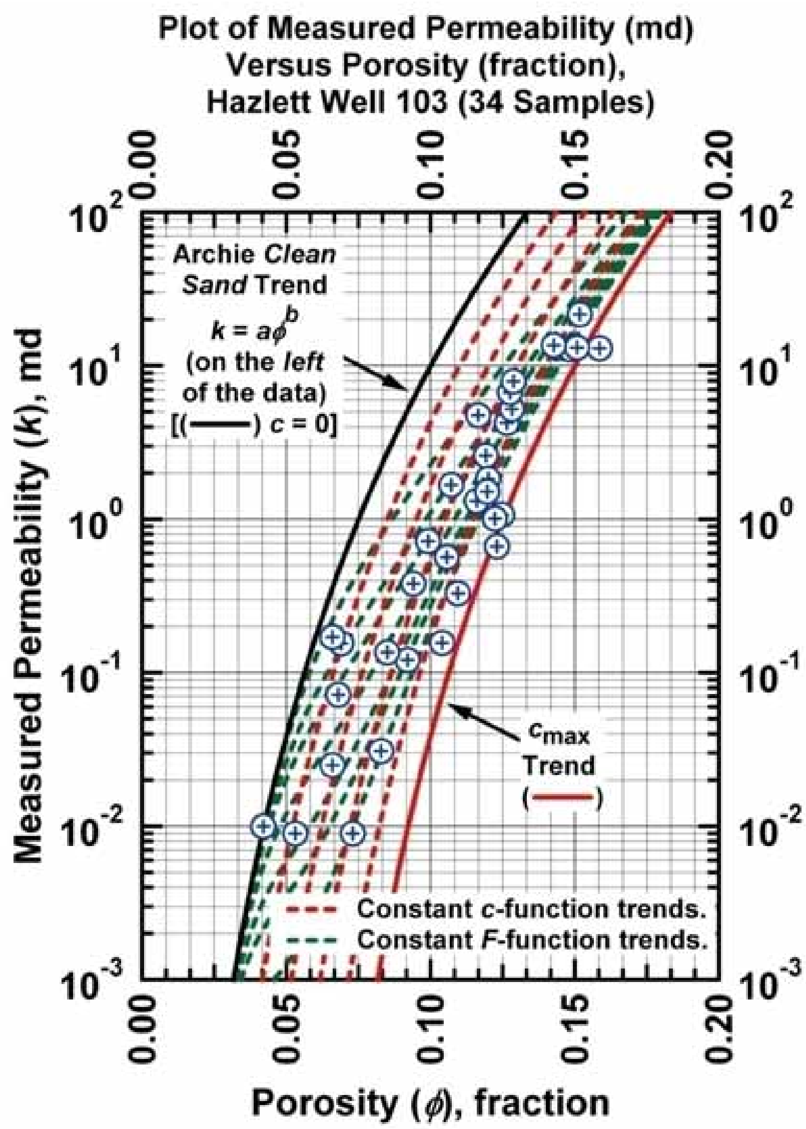

Figure F.1b — Model *CPR-A*: $k = a(\phi - c)^b$ ($c = c_{max} \exp[-c_1 \phi^{c2} F^{c3}]$) — "Dirty Sand" Plot (semilog format). Archie "Clean Sand" trend is given by the curved trend at the far left of the data (power law model). [*Case*: Hazlett Well 103]

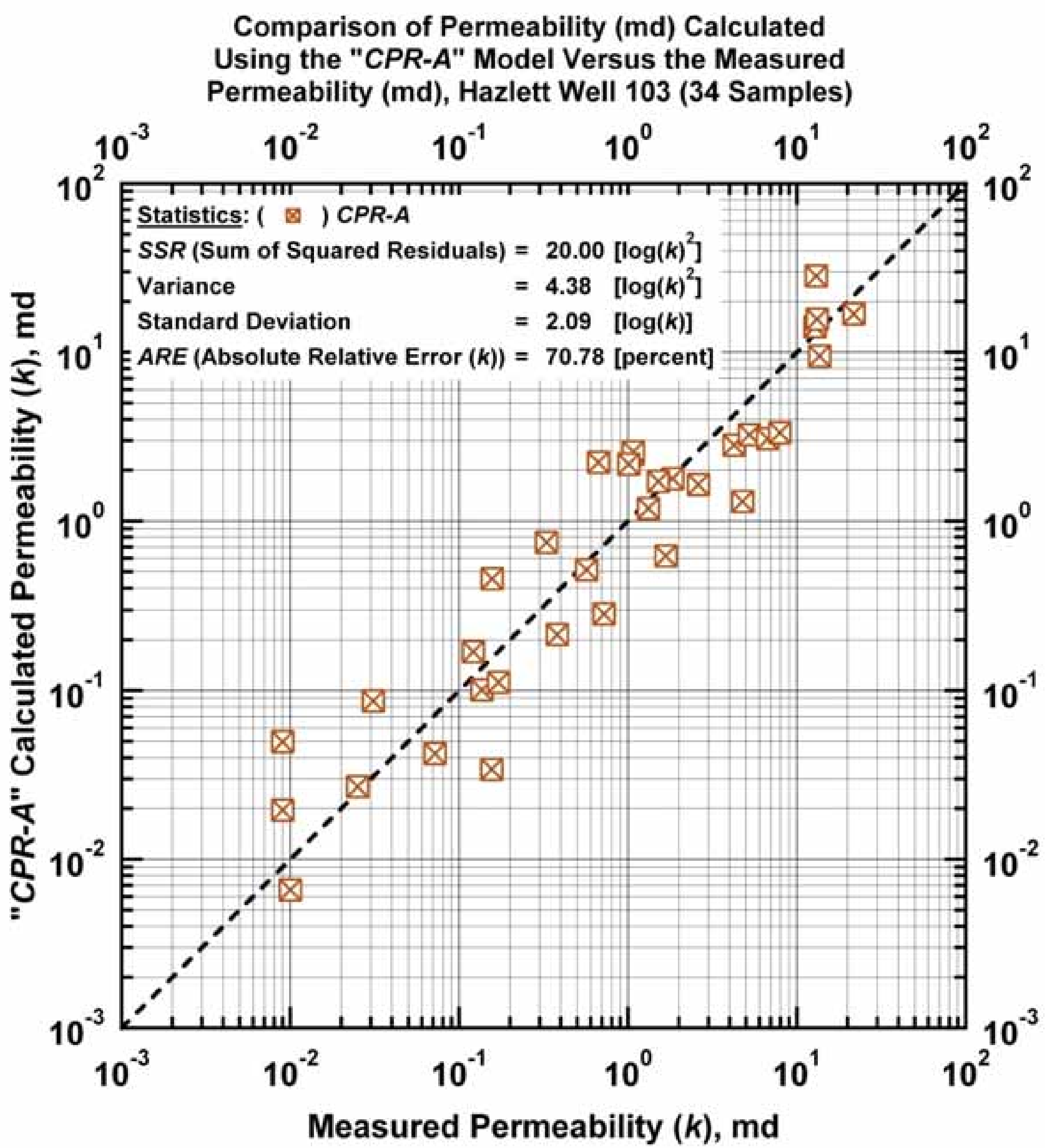

Figure F.2a — Model *CPR-A*: calculated versus measured permeability. [*Case*: Hazlett Well 103]

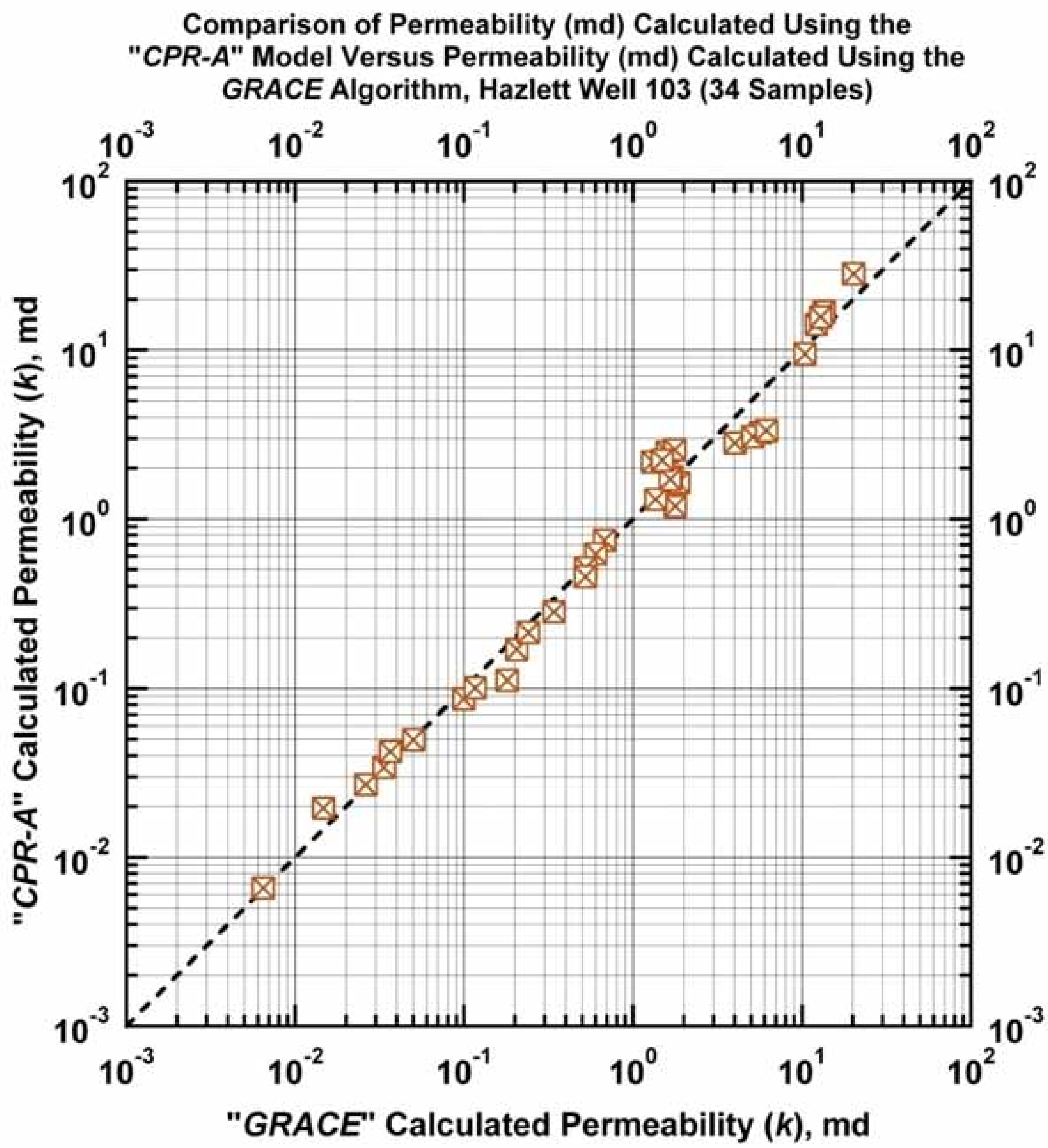

Figure F.2b — Model *CPR-A*: Permeability calculated using Model *CPR-A* versus permeability calculated using the *GRACE* Algorithm. [*Case*: Hazlett Well 103]

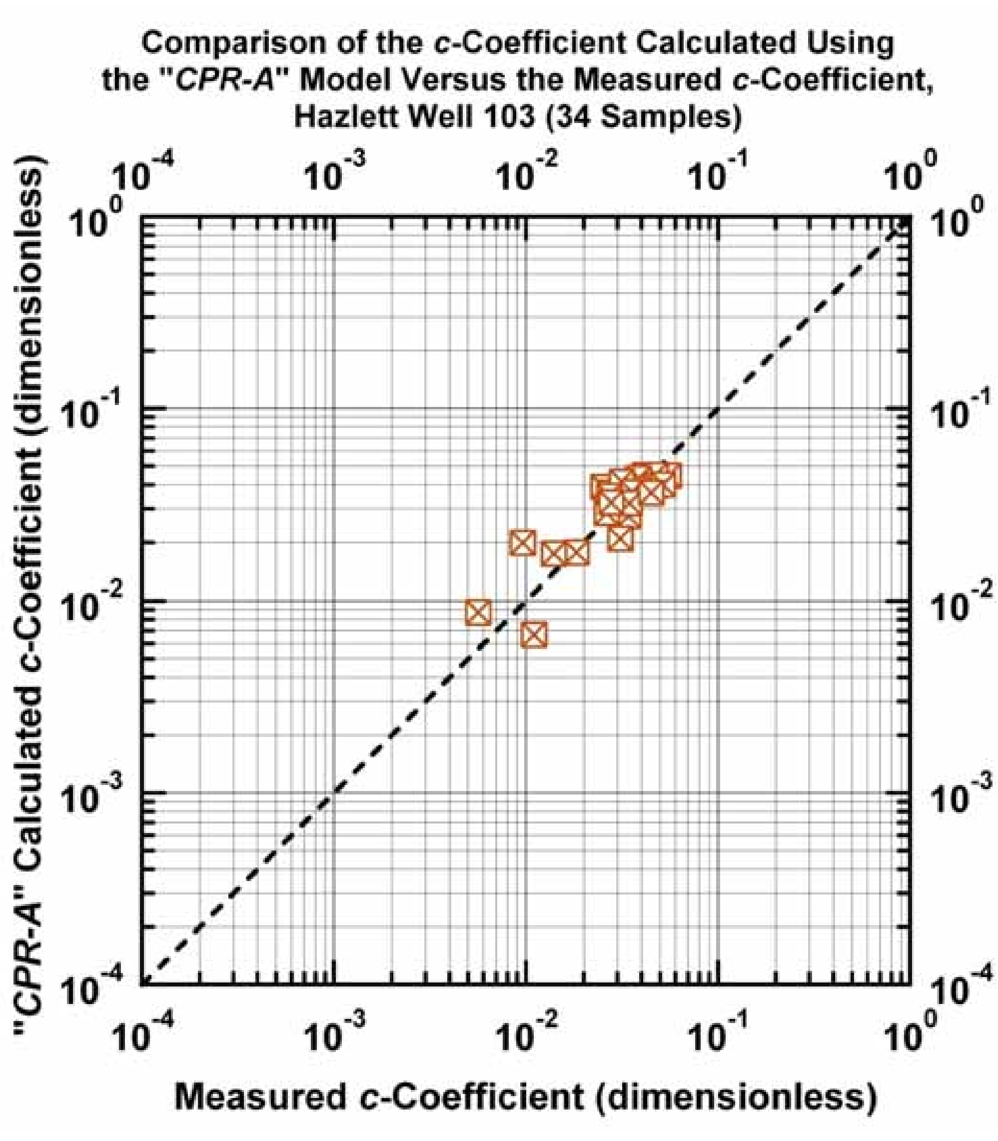

Figure F.2c — Model *CPR-A*: Calculated *c*-function values versus measured *c*-function values. [*Case*: Hazlett Well 103]

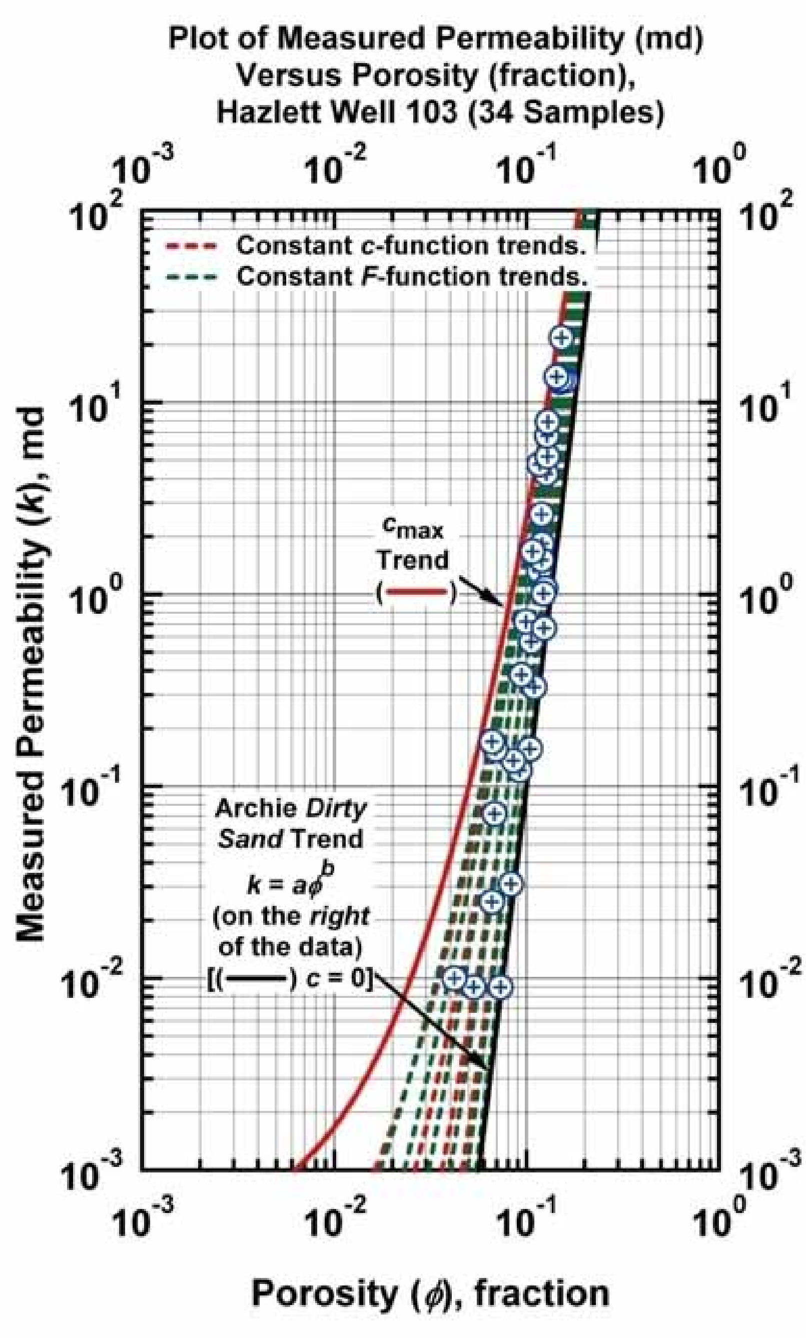

Figure F.3a — Model *CPR-B*: $k = a(\phi + c)^b$ $\quad c = c_{max} \exp[-c_1 \phi^{c_2} F^{c_3}]$ — "Clean Sand" Plot (log-log format) — Archie "Dirty Sand" trend is given by the straight-line trend at the far right of the data (power law model). [*Case*: Hazlett Well 103]

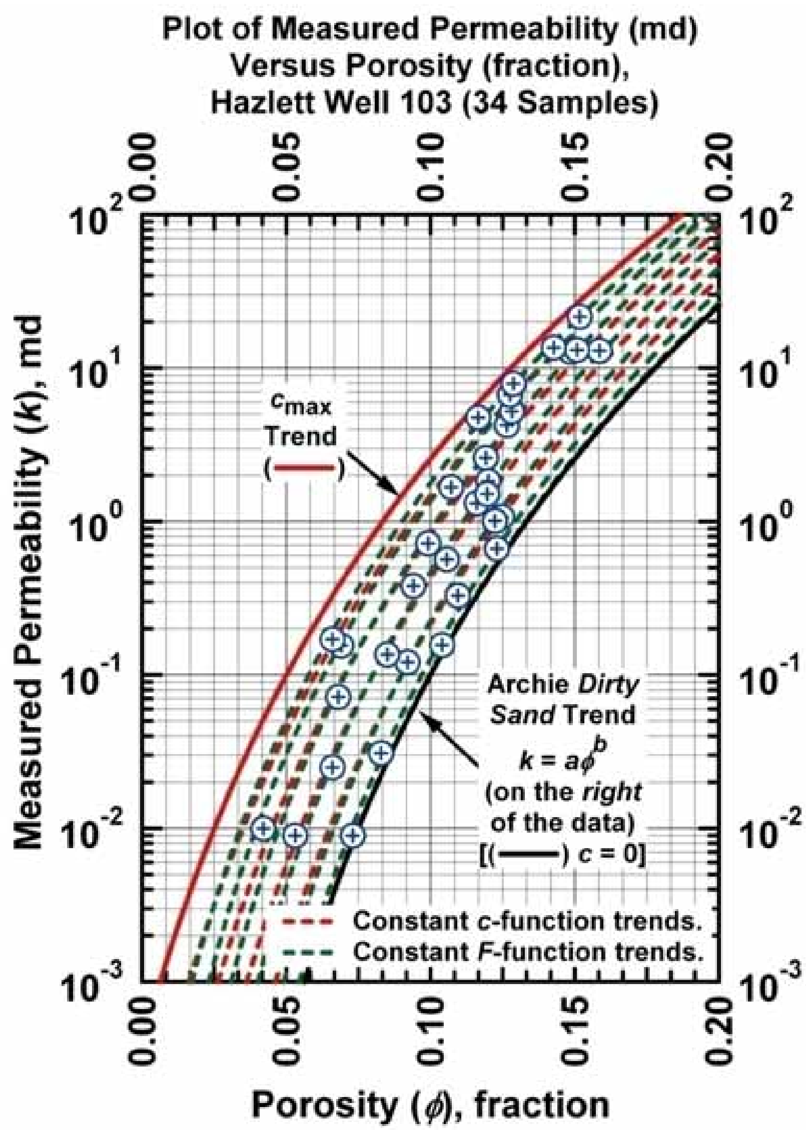

Figure F.3b — Model *CPR-B*: $k = a(\phi + c)^b \quad c = c_{max} \exp[-c_1 \phi^{c_2} F^{c_3}]$ — "Dirty Sand" Plot (semilog format) — Archie "Dirty Sand" trend is given by the curved trend at the far right of the data (power law model). [*Case*: Hazlett Well 103]

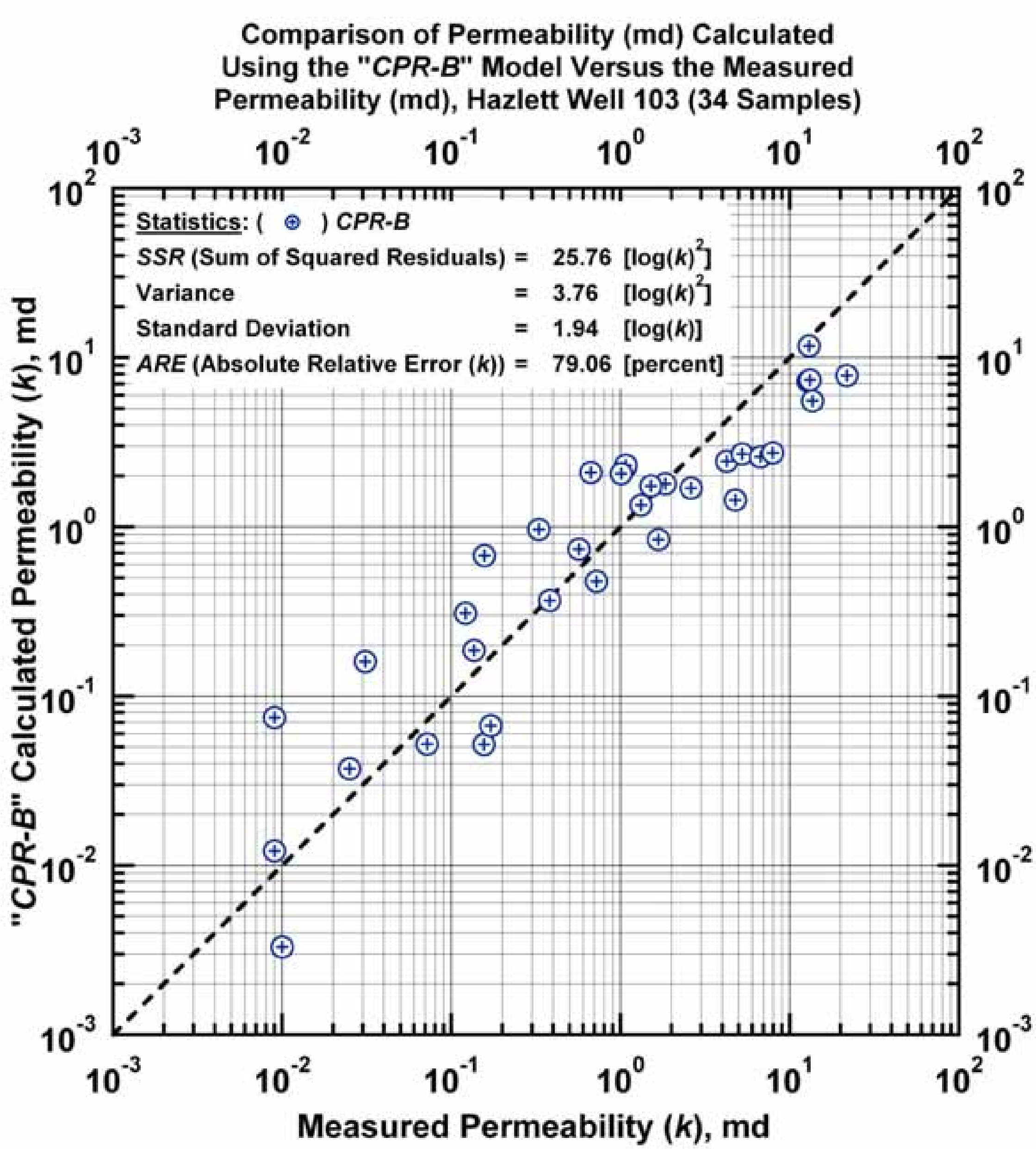

Figure F.4a — Model *CPR-B*: calculated versus measured permeability. [*Case*: Hazlett Well 103]

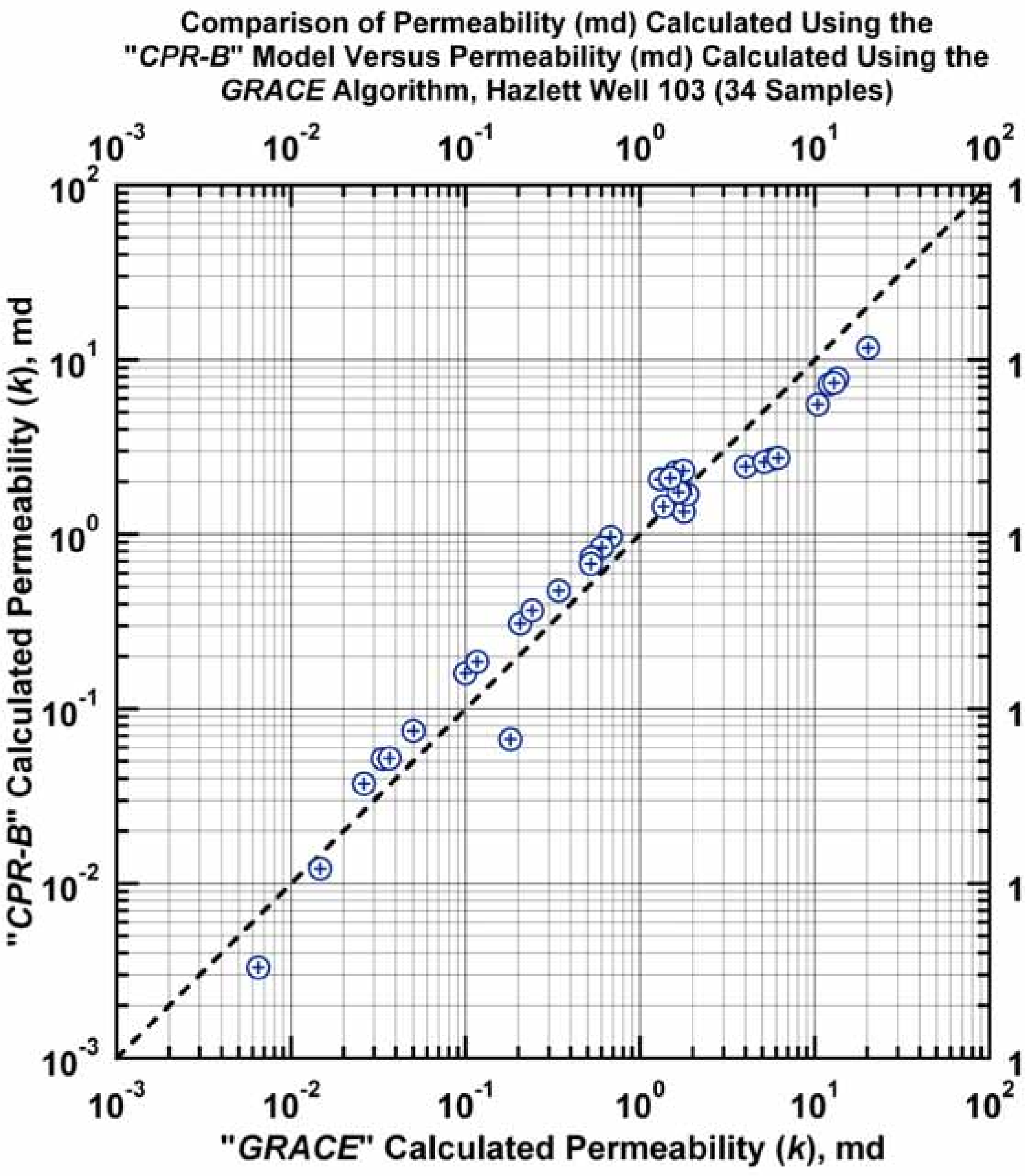

Figure F.4b — Model *CPR-B*: Permeability calculated using Model *CPR-B* versus permeability calculated using the *GRACE* Algorithm. [*Case*: Hazlett Well 103]

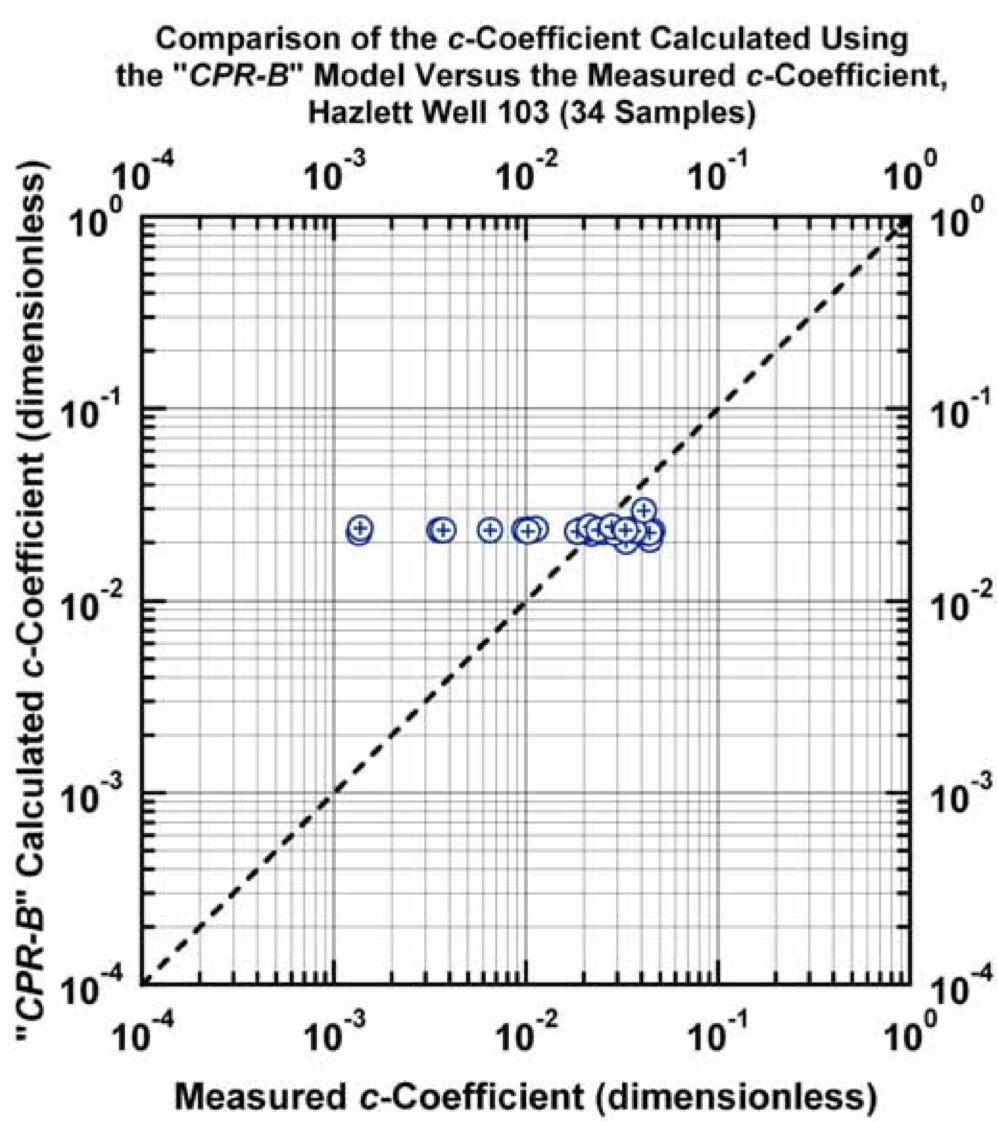

Figure F.4c — Model *CPR-B*: Calculated *c*-function values versus measured *c*-function values. [*Case*: Hazlett Well 103]

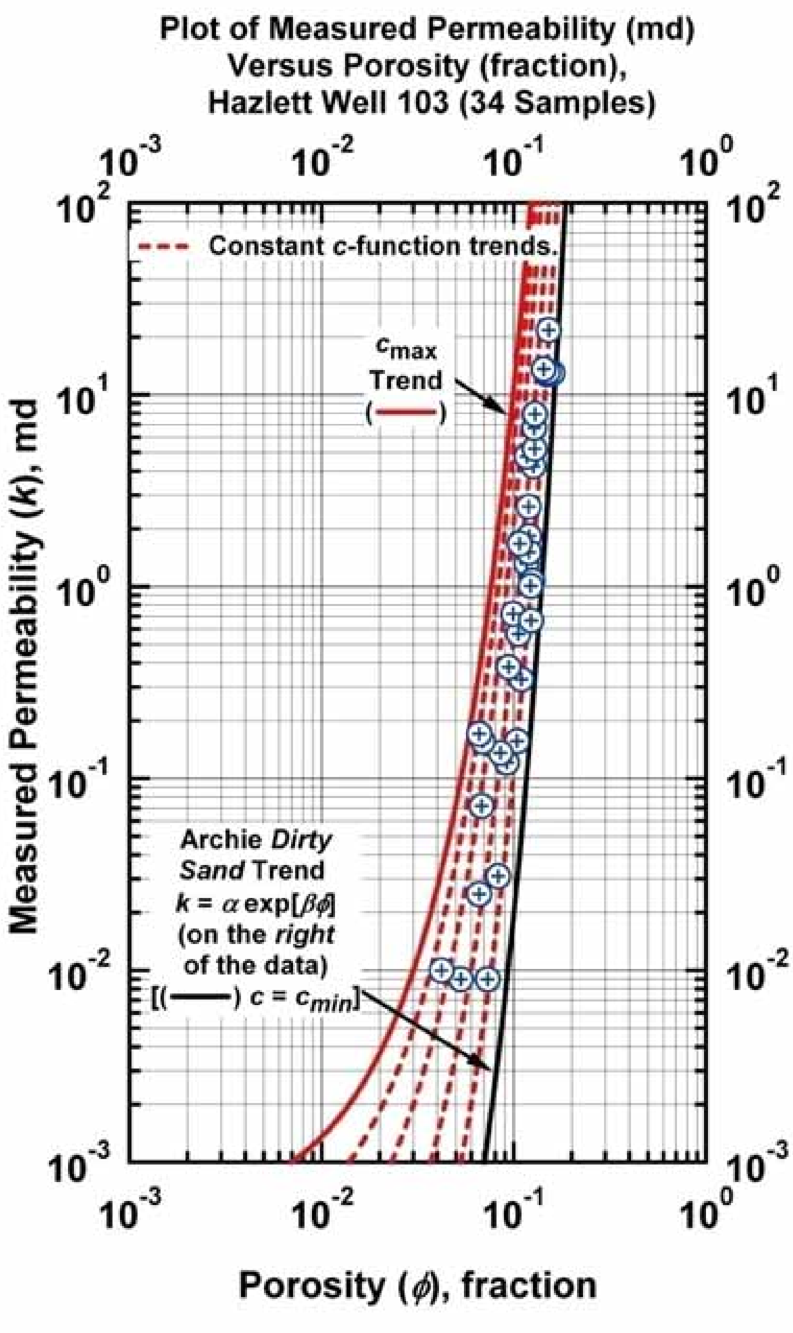

Figure F.5a — Model *CPR-C*: $k = c\exp[\beta\phi]$ $c = c_{\max}\exp[-c_1\phi^{c_2}F^{c_3}]$ — "Clean Sand" Plot (log-log format) — Archie "Dirty Sand" trend is given by the curved trend at the far right of the data (exponential model). [*Case*: Hazlett Well 103]

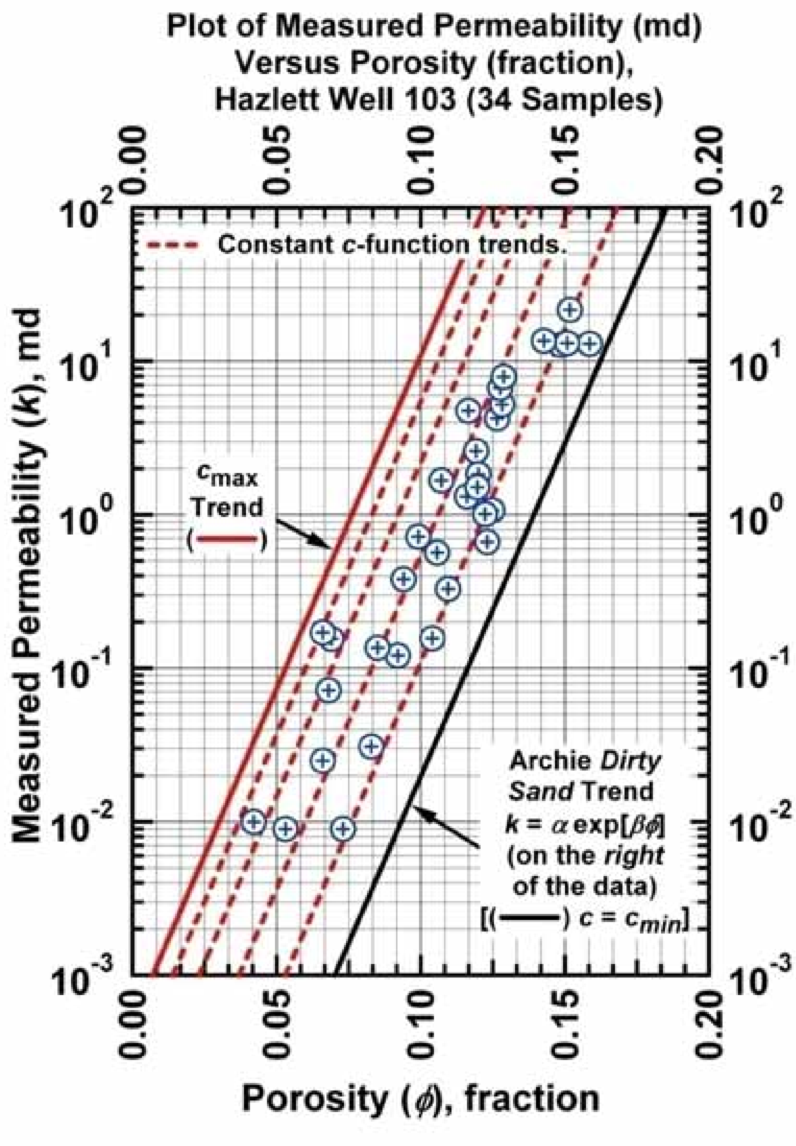

Figure F.5b — Model *CPR-C*: $k = c\exp[\beta\phi]$ $c = c_{\max}\exp[-c_1\phi^{c_2} F^{c_3}]$ — "Dirty Sand" Plot (semilog format) — Archie "Dirty Sand" trend is given by the straight-line trend at the far right of the data (exponential model). [*Case*: Hazlett Well 103]

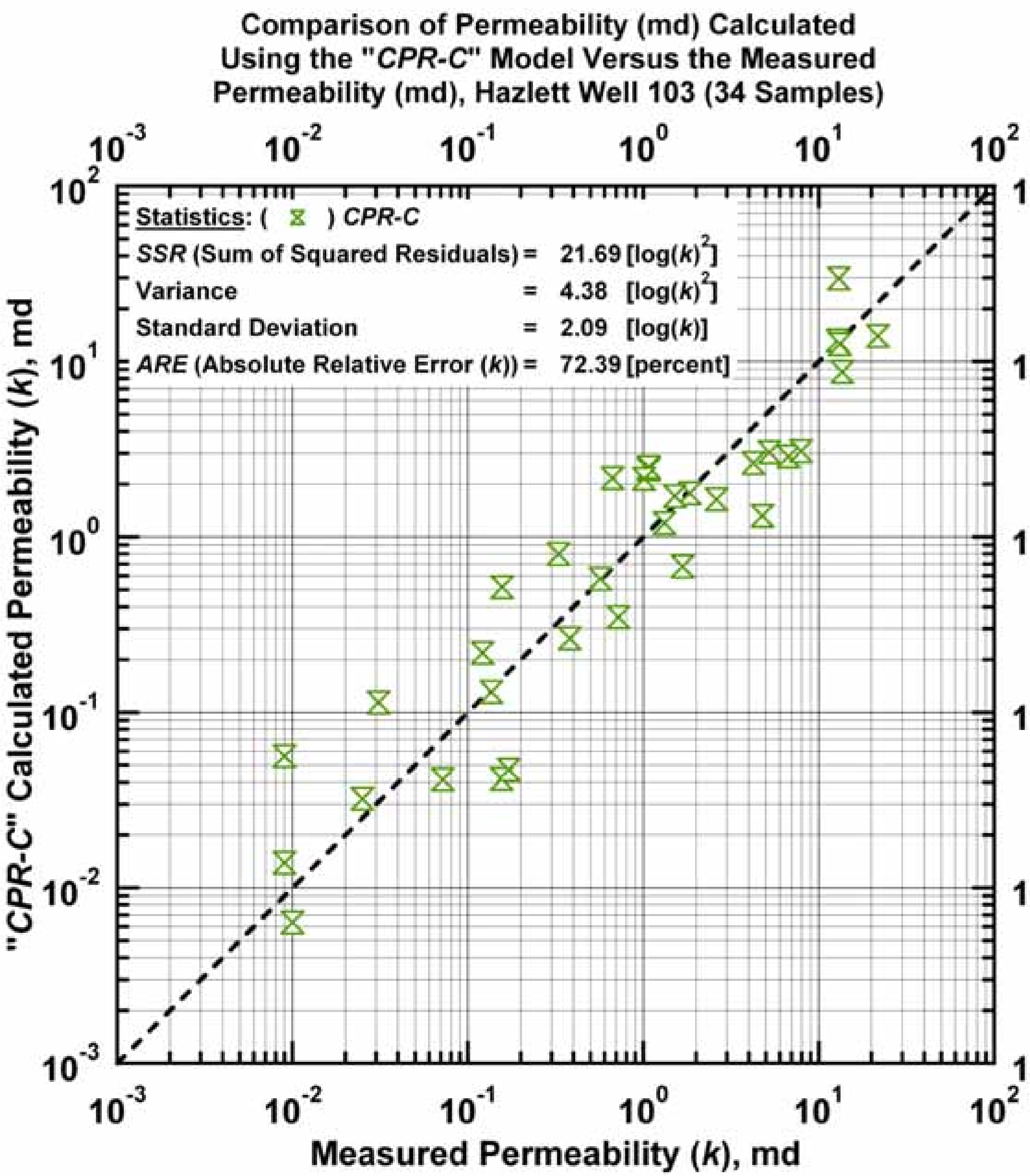

Figure F.6a — Model *CPR-C*: calculated versus measured permeability. [*Case*: Hazlett Well 103]

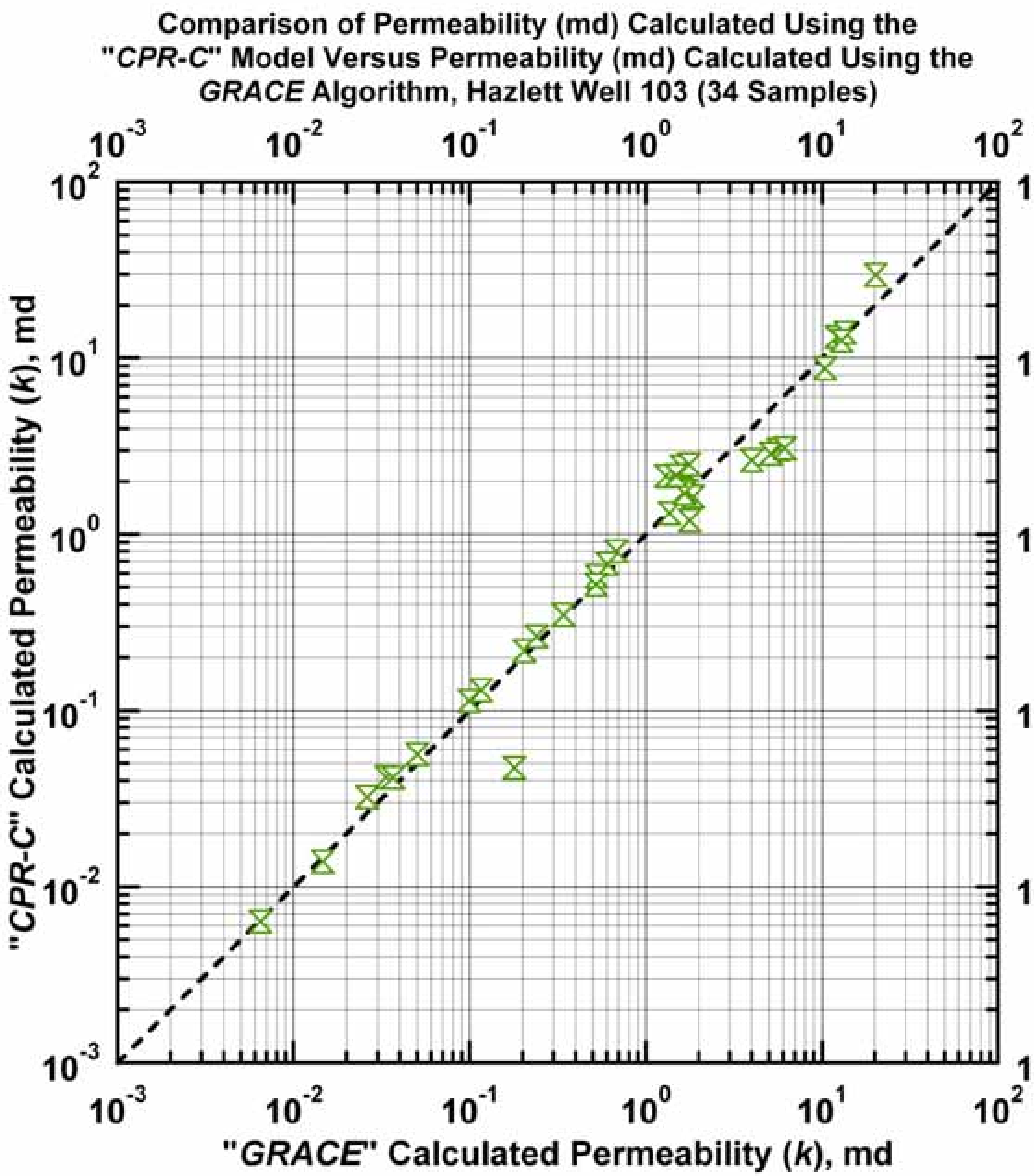

Figure F.6b — Model *CPR-C*: Permeability calculated using Model *CPR-C* versus permeability calculated using the *GRACE* Algorithm. [*Case*: Hazlett Well 103]

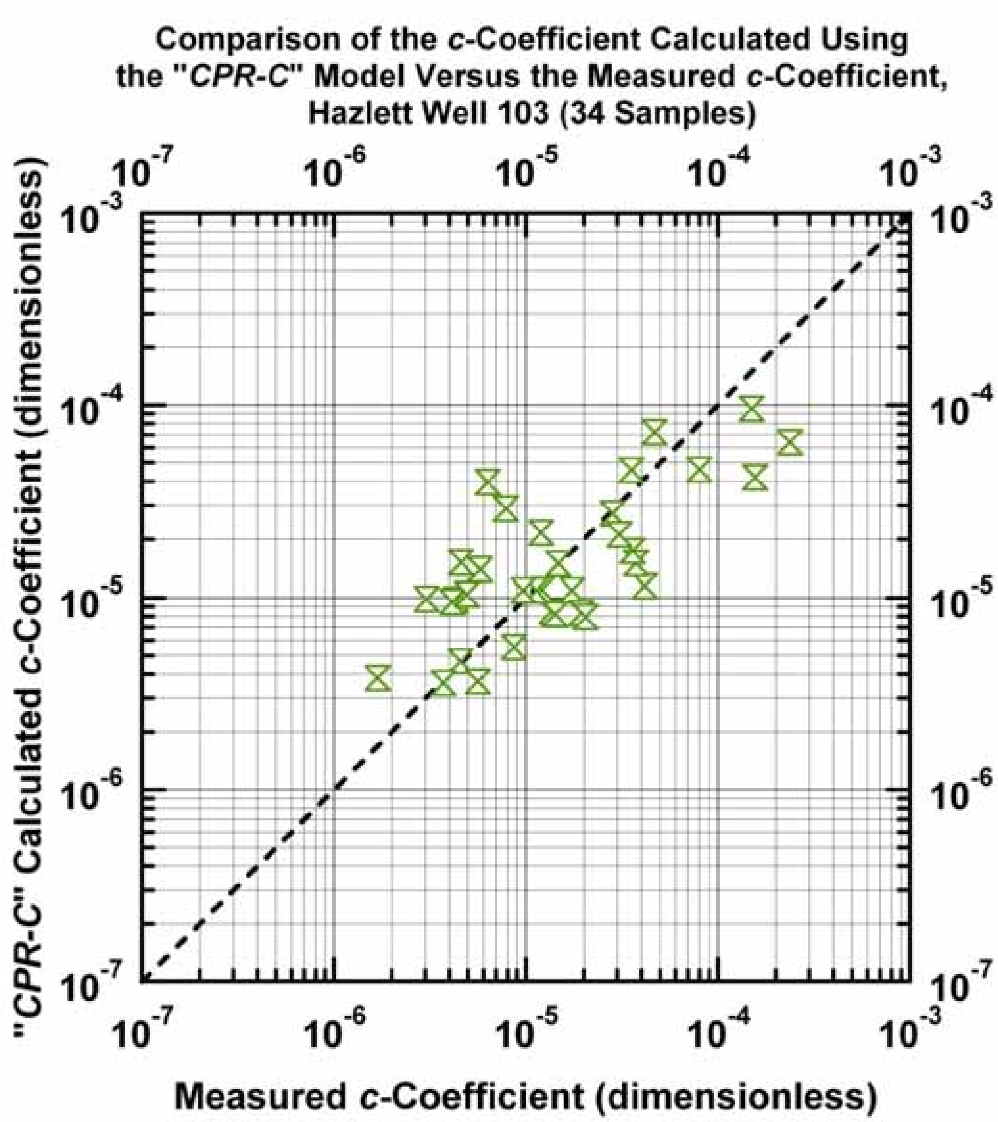

Figure F.6c — Model *CPR-C*: Calculated *c*-function values versus measured *c*-function values. [*Case*: Hazlett Well 103]

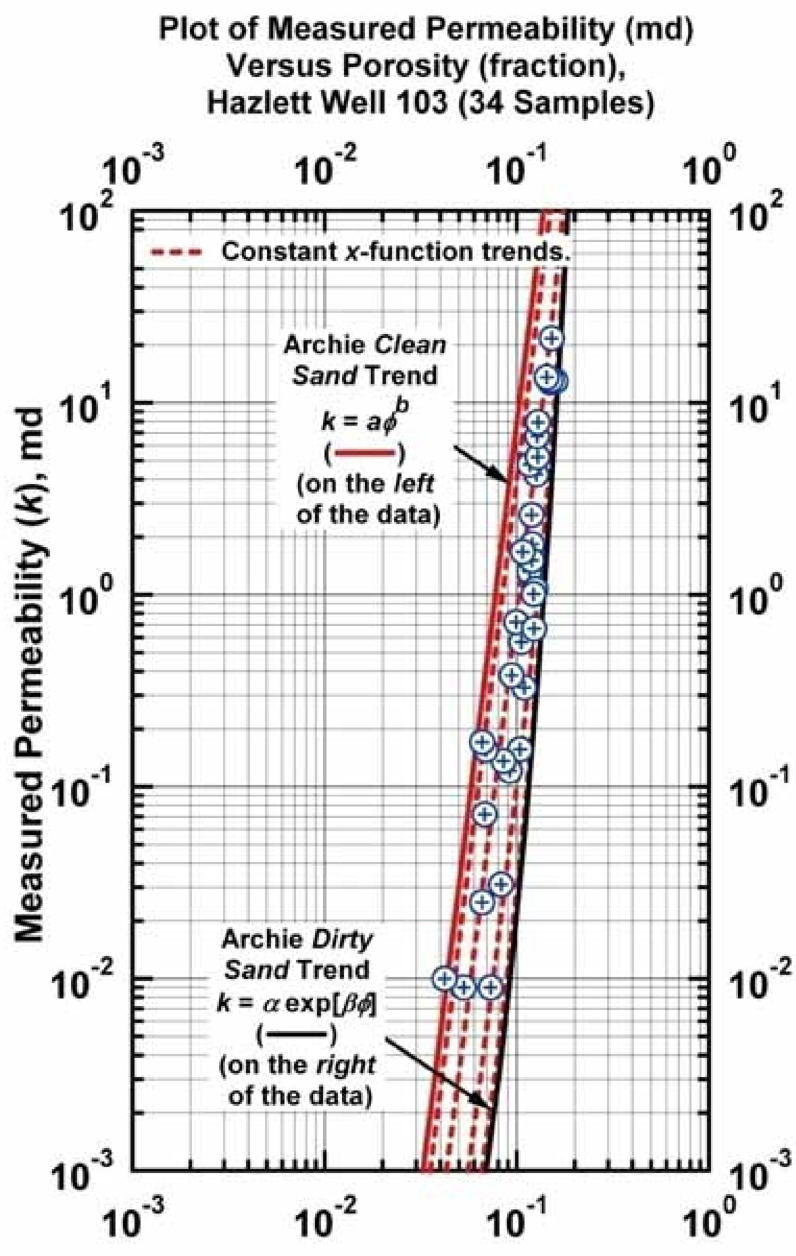

Figure F.7a — Model *CPR-D*: $k = xa\phi^b + (1-x)\alpha\exp[\beta\phi]$ $[0 \le x \le 1]$ — *Weighted Power Law-Exponential Model* used to correlate permeability (k) and porosity (ϕ). "Clean Sand" Plot — Archie "Clean Sand" trend is given by the straight-line trend at the far left of the data (power law model). [*Case*: Hazlett Well 103]

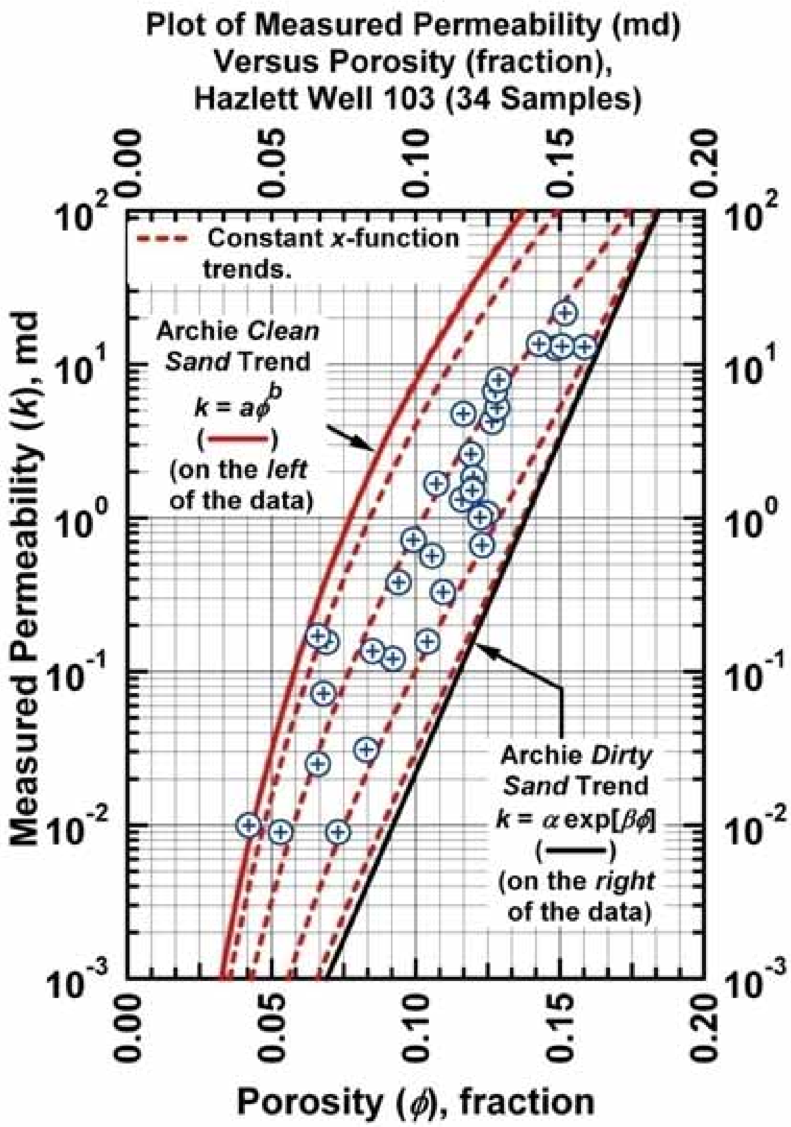

Figure F.7b — Model *CPR-D*: $k = xa\phi^b + (1-x)\alpha\exp[\beta\phi] \quad [0 \le x \le 1]$ — *Weighted Power Law-Exponential Model* used to correlate permeability (k) and porosity (ϕ). "Dirty Sand" Plot — Archie "Dirty Sand" trend is given by the straight-line trend at the far right of the data (exponential model). [*Case*: Hazlett Well 103]

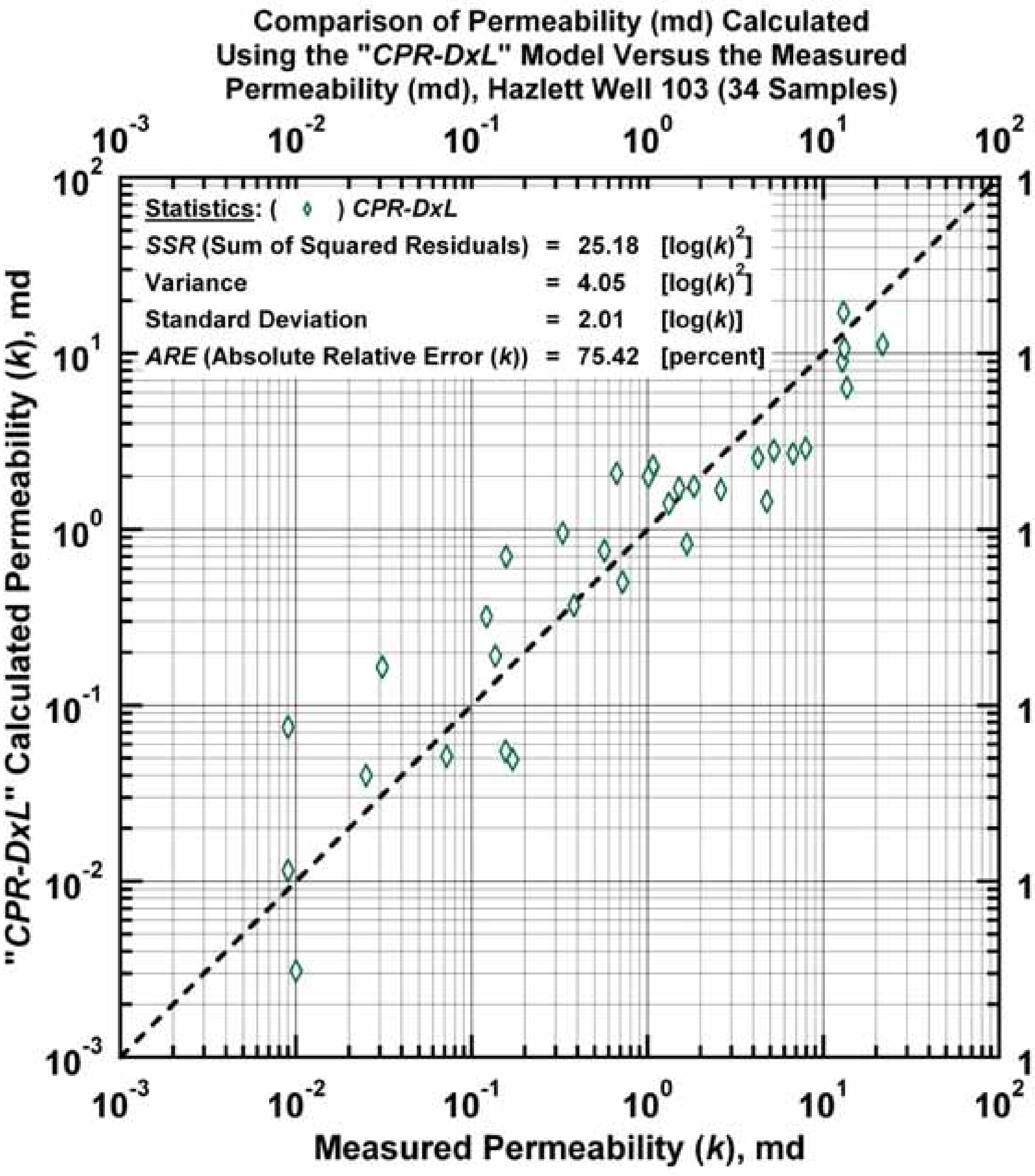

Figure F.8a — Model *CPR-DxL*: Calculated versus measured permeability. [*Case*: Hazlett Well 103]

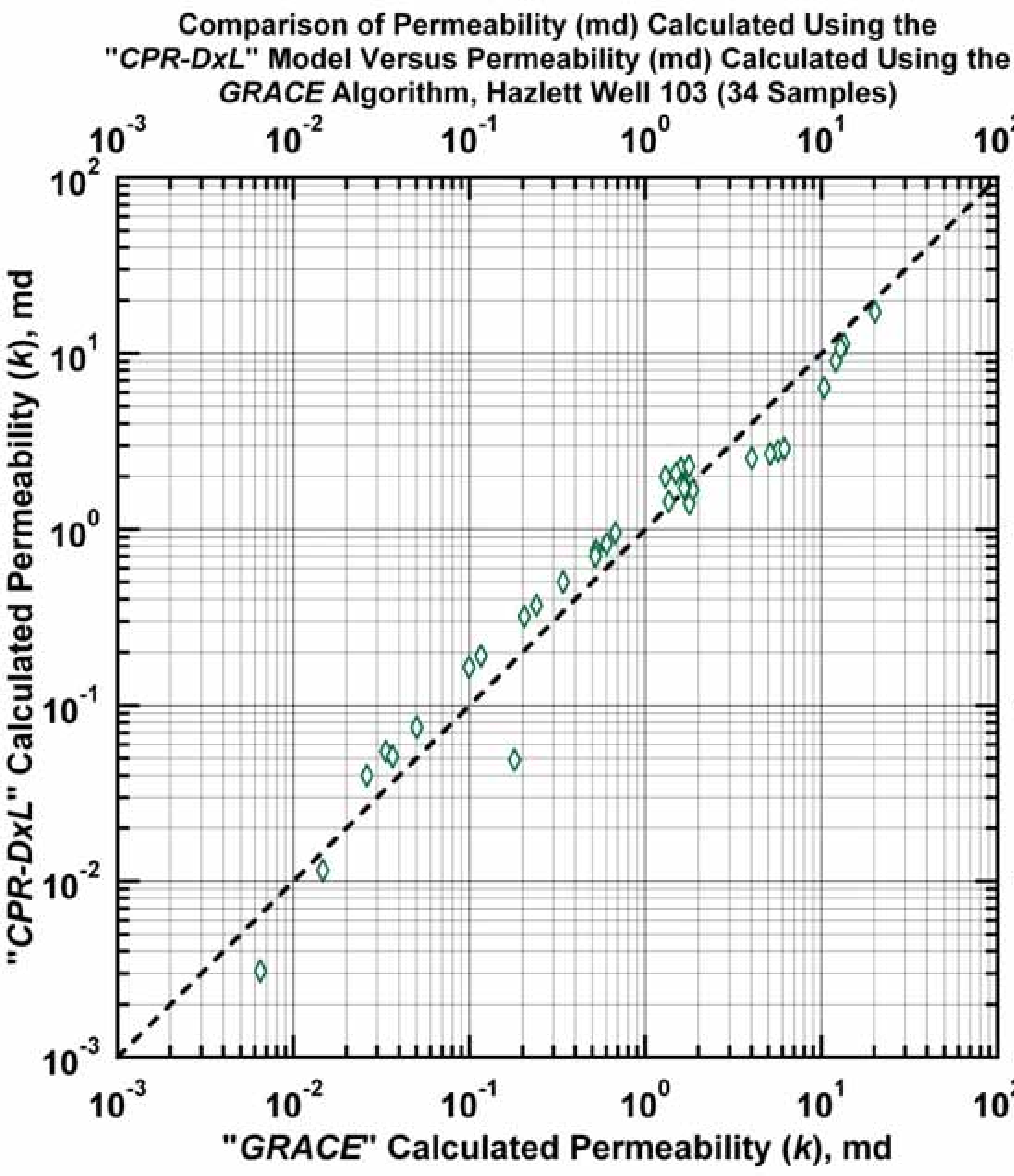

Figure F.8b — Model *CPR-DxL*: Permeability calculated using Model *CPR-C* versus permeability calculated using the *GRACE* Algorithm. [*Case*: Hazlett Well 103]

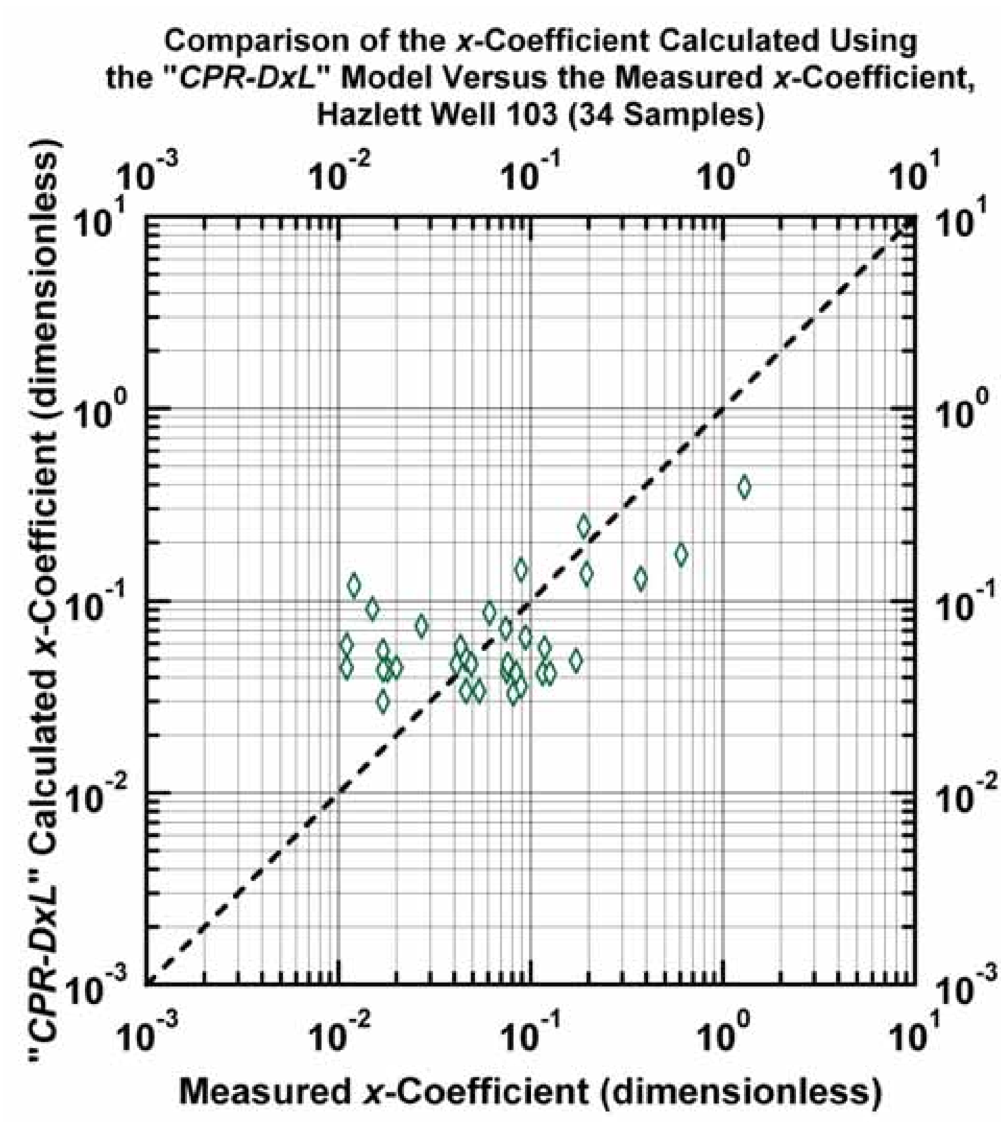

Figure F.8c — Model *CPR-DxL*: Calculated *x*-function weight values versus measured *x*-function weight values. [*Case*: Hazlett Well 103]

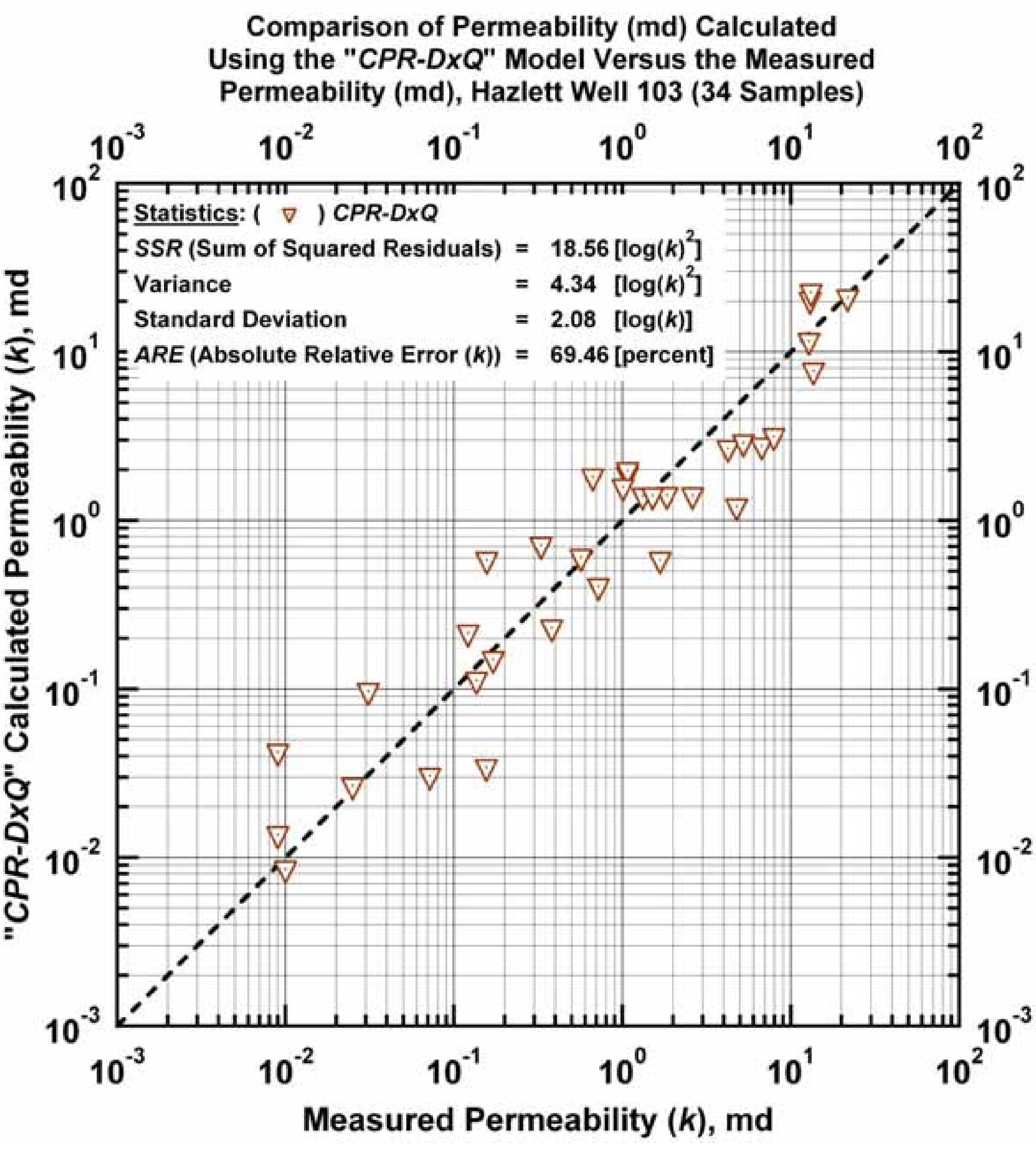

Figure F.9a — Model *CPR-DxQ*: Calculated versus measured permeability. [*Case*: Hazlett Well 103]

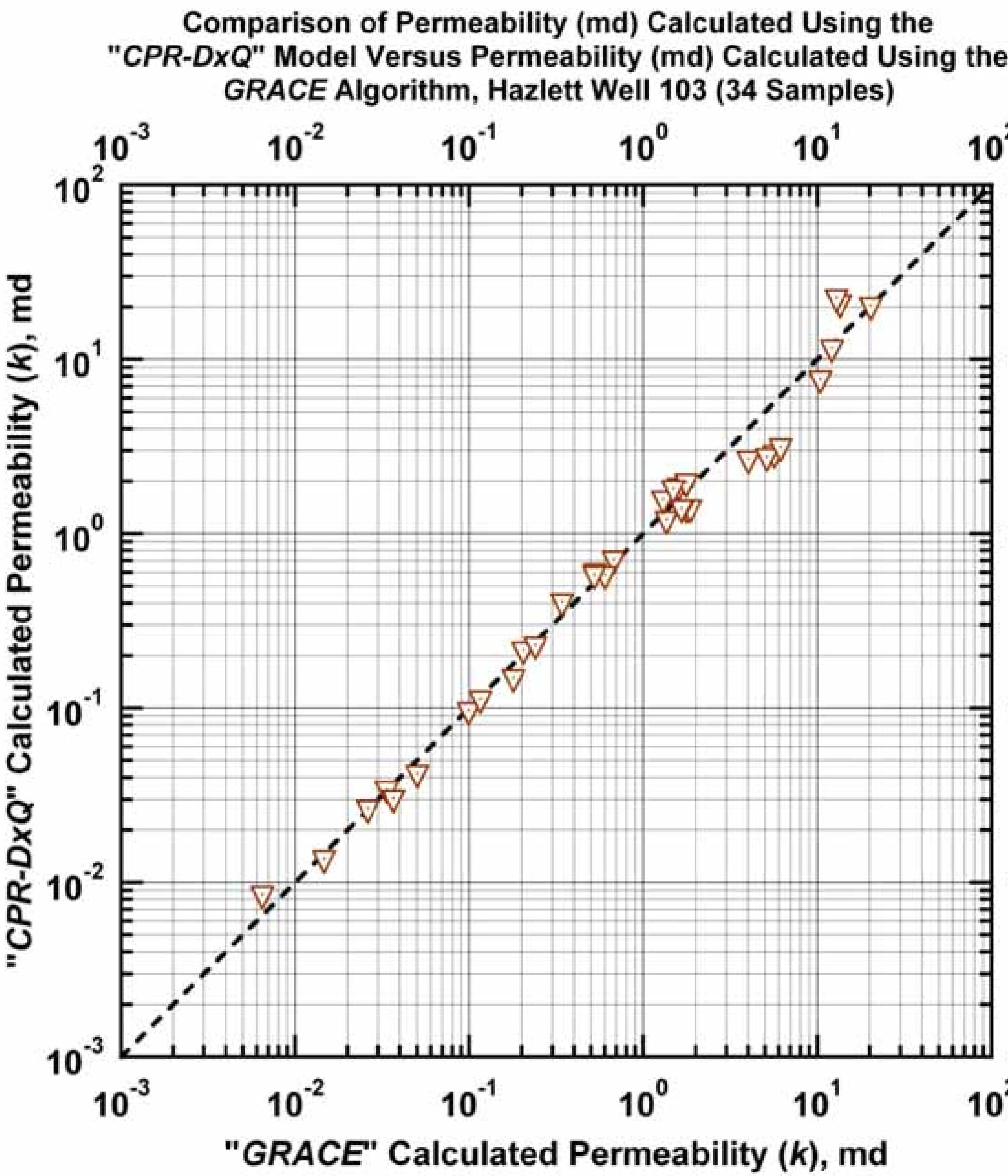

Figure F.9b — Model *CPR-DxQ*: Permeability calculated using Model *CPR-C* versus permeability calculated using the *GRACE* Algorithm. [*Case*: Hazlett Well 103]

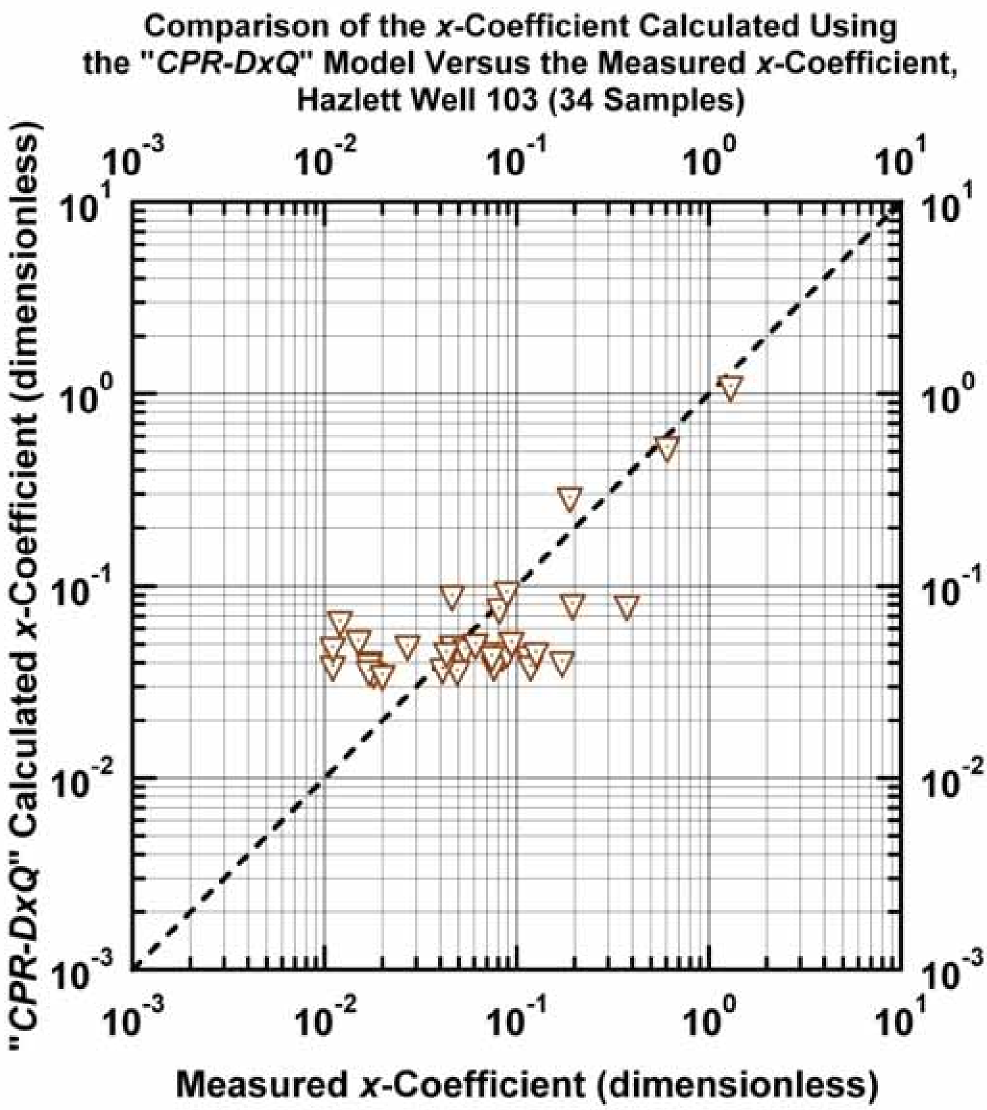

Figure F.9c — Model *CPR-DxQ*: Calculated *x*-function weight values versus measured *x*-function weight values. [*Case*: Hazlett Well 103]

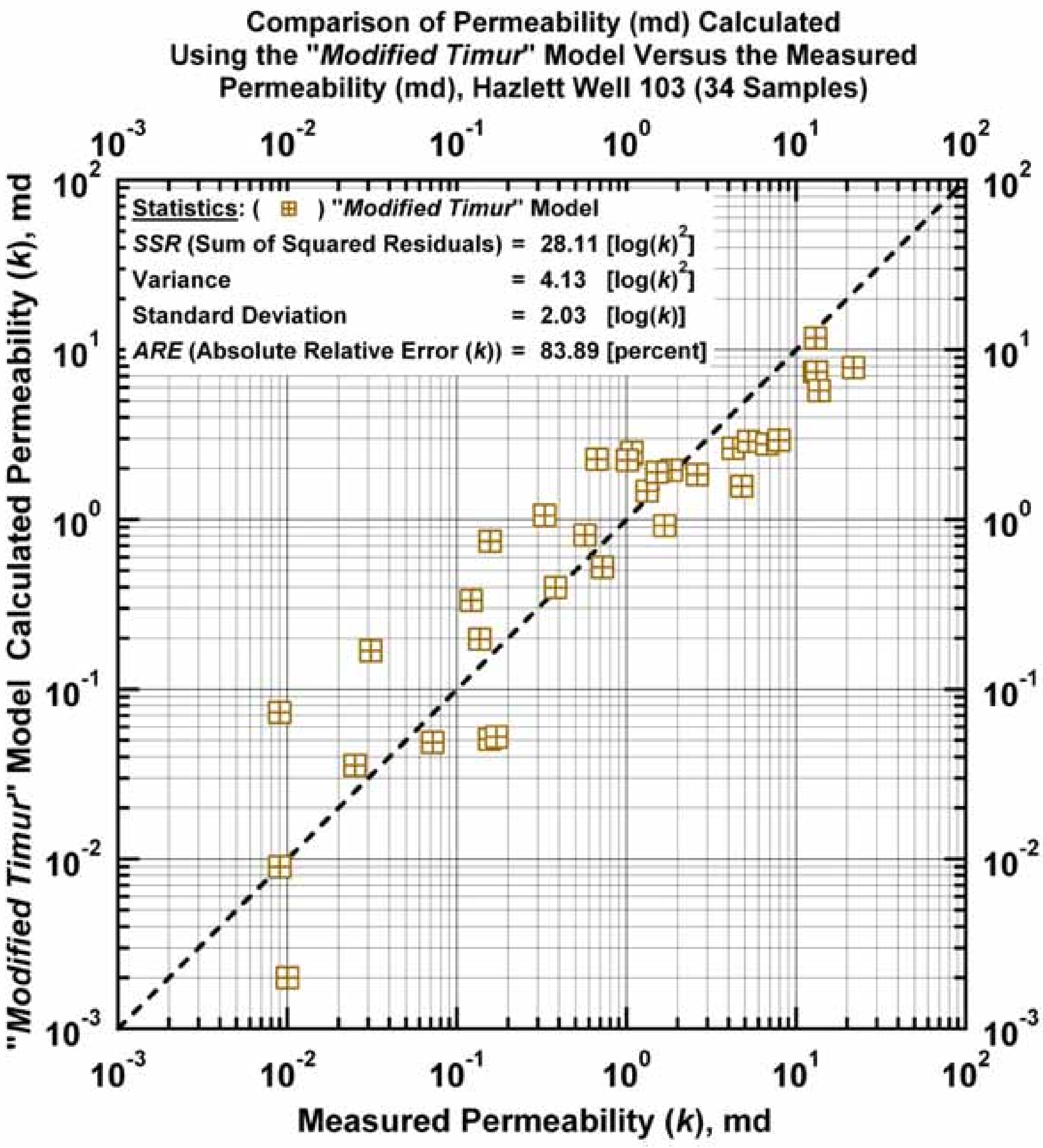

Figure F.10a — "Modified Timur Model:" Calculated versus measured permeability. [*Case*: Hazlett Well 103]

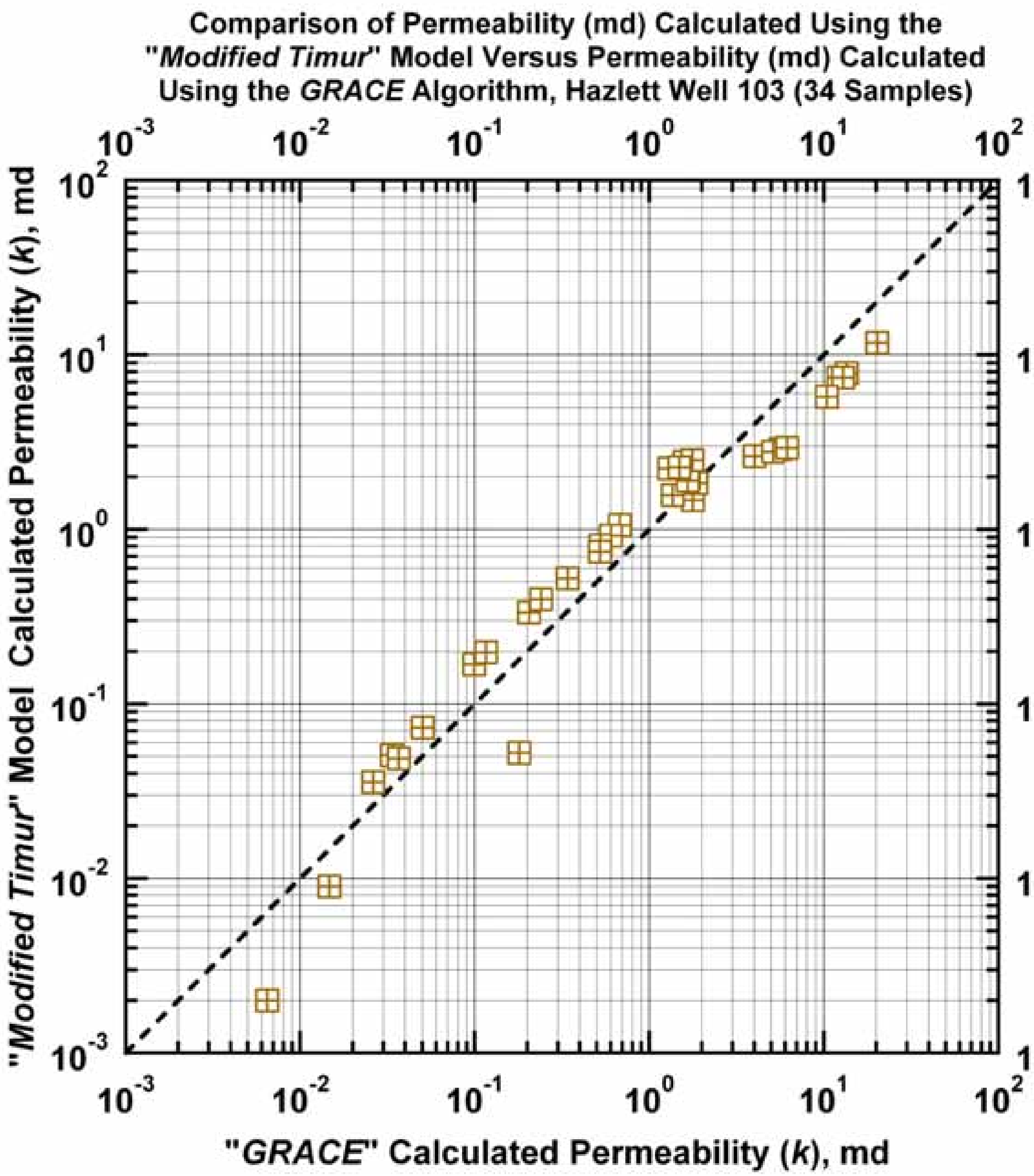

Figure F.10b — "Modified Timur Model:" Permeability calculated using the "Modified Timur Model" versus permeability calculated using the *GRACE* Algorithm. [*Case*: Hazlett Well 103]

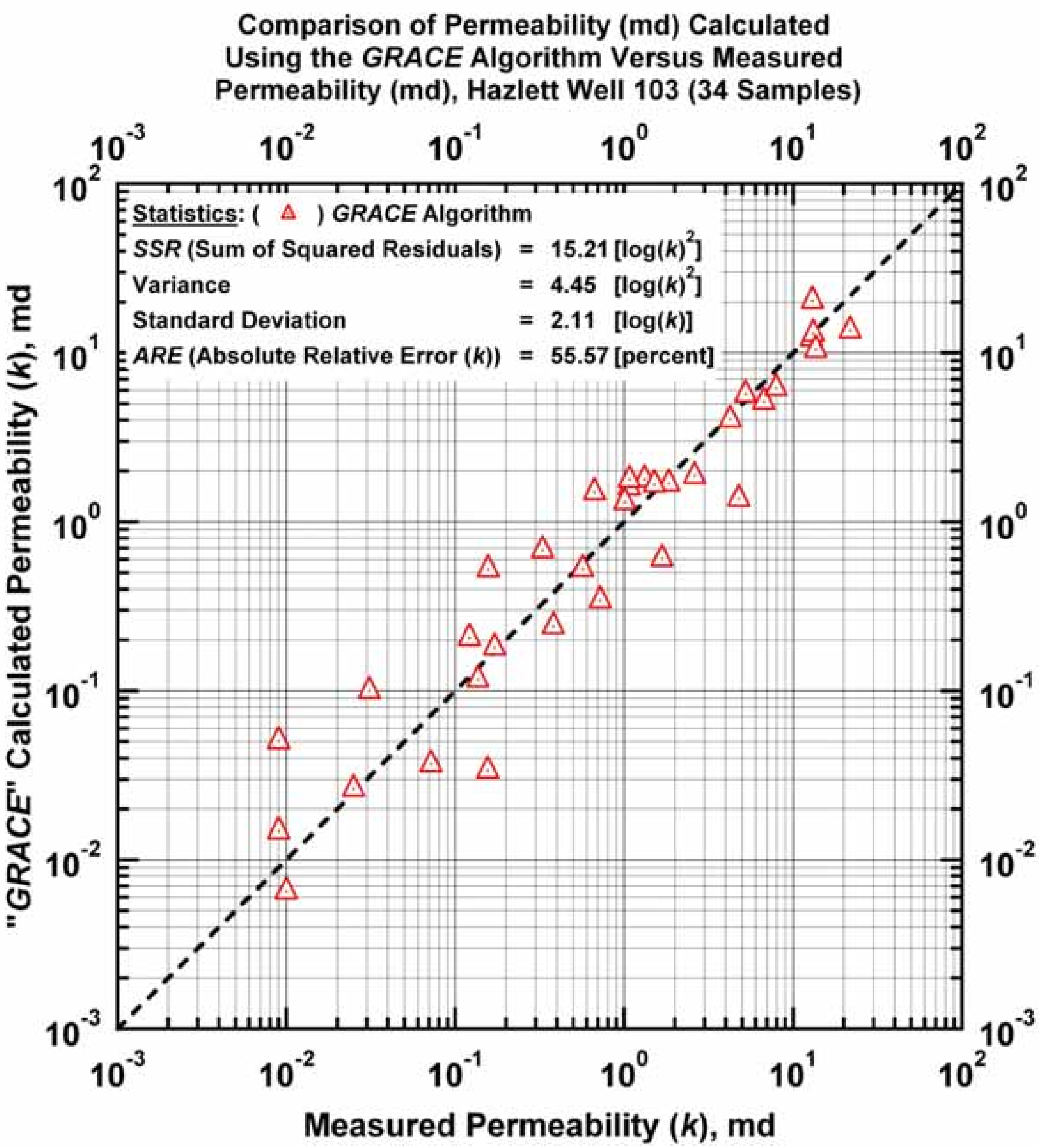

Figure F.11 — *GRACE* Model: Calculated versus measured permeability. [*Case*: Hazlett Well 103]

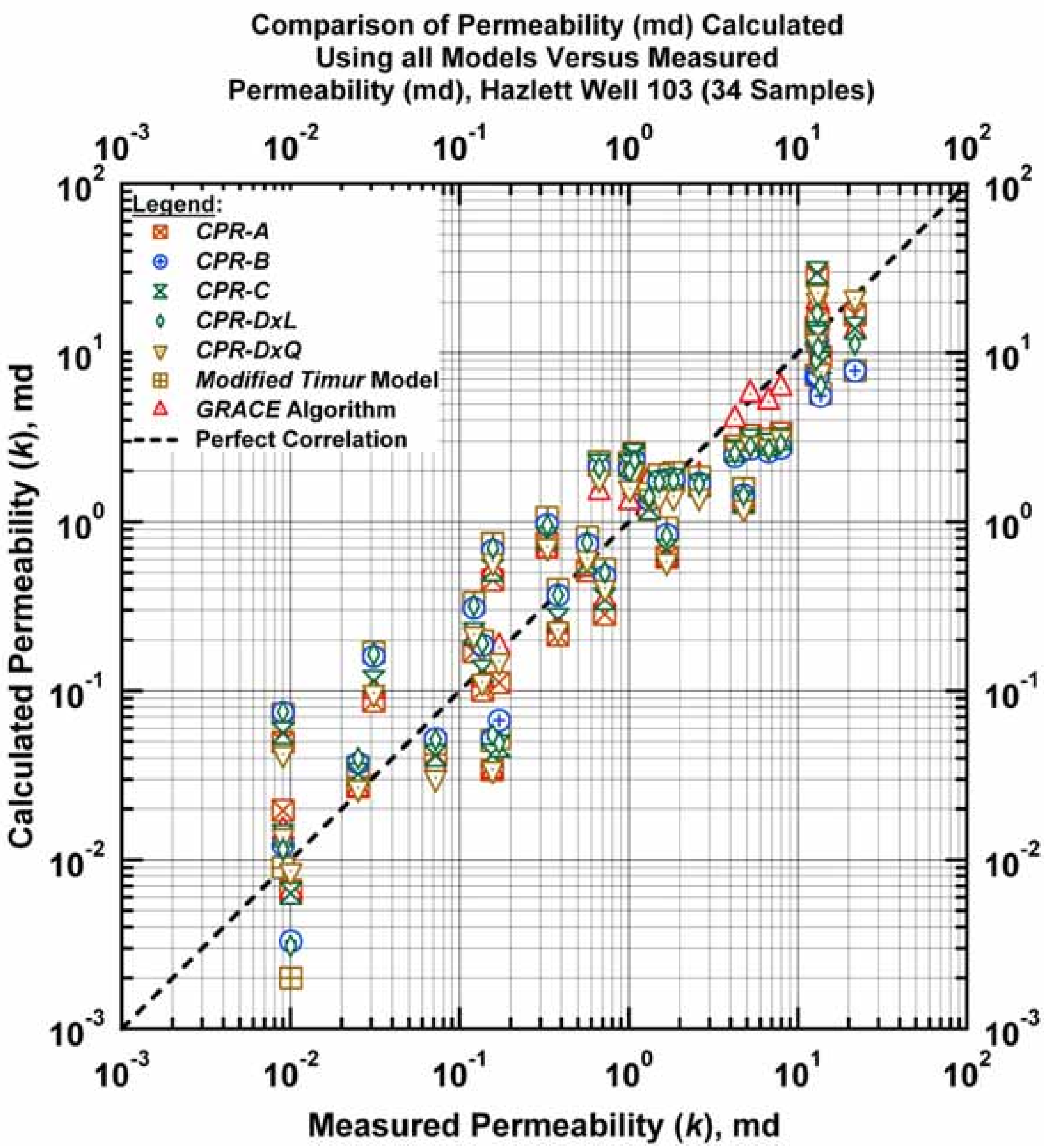

Figure F.12 — All Models: Calculated versus measured permeability. [*Case*: Hazlett Well 103]

APPENDIX G

RESULTS FOR DEVONIAN LIMESTONE (TEXAS — USA)

In this Appendix we present the "Devonian Limestone" Well, located in Texas (USA — this is a carbonate reservoir system (Ellis, 1987).

Model *CPR-A*: (Appendix G)

The "characteristic permeability relation" (or *CPR*) Model *CPR-A* (*i.e.*, the modified Archie "Clean Sand" Model) is given as:

$$k = a(\phi - c)^b \qquad c = c_{\max} \exp[-c_1 \phi^{c_2} F^{c_3}] \quad \text{(G-1)}$$

Where a plot of log(k) versus log(ϕ) is used to graphically calibrate Eq. G-1 in terms of the coefficients — a, b, and c_{max}. **Fig. G.1** shows that the *CPR-A* model performs quite well for this case. **Figs. G.1a and b** show the log-log and the semilog format of permeability versus porosity, respectively. In **Fig. G.2** we provide the "error" plots for this case, where the measured and computed data are compared systematically. In **Fig. G.2a** we note a good correlation of the results obtained using Model *CPR-A* versus the measured permeability data — there is good agreement with the perfect correlation trend (*i.e.*, the 45-degree line). In **Fig. G.2b** we provide a comparison with the *GRACE* algorithm correlation (Xue *et al*. 1997)), and we note that the *CPR-A* model results correlate very well with the *GRACE* algorithm results for this case. Lastly, in **Fig. G.2c** we present the calculated and measured c-function — and again we note a reasonable correlation of the data about the perfect correlation trend.

Model *CPR-B*: (Appendix G)

The "characteristic permeability relation" (or *CPR*) Model *CPR-B* (*i.e.*, the modified Archie "Dirty Sand" Model (power-law basis)) is given as:

$$k = a(\phi + c)^b \qquad c = c_{\max} \exp[-c_1 \phi^{c_2} F^{c_3}] \quad \text{(G-2)}$$

Where a plot of log(k) versus log(ϕ) is used to graphically calibrate Eq. G-2 in terms of the coefficients — a, b, and c_{max}. The results for this case are presented in **Figs. G.3 and 4**. In **Fig. G.3a** (log-log format) we note that a very distinct "envelope" is formed by the *CPR-B* model, essentially all of the data on the right and left flanks are well-matched (*i.e.*, the "dirty sand" power law relation (applied on the right portion of the data) and its correction function (applied on the left portion of the data). Similarly, in **Fig. G.3b** (semilog format), we observe an excellent distribution of the power law model across the body of the data. The error analyses for this case are shown in **Fig. G.4**. In **Fig. G.4a** we present the results obtained using Model *CPR-B* versus the measured permeability data and in this case there is good agreement with the perfect correlation trend (*i.e.*, the 45-degree line). We provide a comparison with the *GRACE* algorithm correlation in **Fig. G.4b** — the results using Model *CPR-B* and the *GRACE* algorithm compare very well for this case. We compare the computed and data-derived values of the *c*-function for this case in **Fig. G.4c** and we note a "tight" correlation. In summary, we believe that Model *CPR-B* is a very effective correlation model for this particular data case.

Model *CPR-C*: (Appendix G)

The "characteristic permeability relation" (or *CPR*) Model *CPR-C* (*i.e.*, the modified Archie "Dirty Sand" Model (exponential basis)) is given as:

$$k = c\exp[\beta\phi] \quad c = c_{\max}\exp[-c_1\phi^{c_2}F^{c_3}] \quad \text{(G-3)}$$

Where a plot of log(k) versus ϕ is used to graphically calibrate Eq. G-3 in terms of the coefficients — β and $c_{\max}$. Model *CPR-C* is fundamentally different than Models *CPR-A* and *CPR-B*, as the basis for Model *CPR-C* is an exponential function, not a power law relation. In **Figs. G.5 and 6** we present the results of applying Model *CPR-C* for this case, and in general, we observe a very consistent performance of Model *CPR-C*. **Fig. G.5b** illustrates the excellent conformance of Model *CPR-C* for this case — again recalling that this model has an exponential relationship with porosity as its basis.

In **Figs. G.6a, G.6b, and G.6c** we review the error analyses plots for this case, and we note good performance (visually) in terms of the correlation of the results using Model *CPR-C*. In this case, the *c*-function (in Eq. G-3) is not a correction term, but rather the instantaneous intercept for the exponential basis. The correlation of the *c*-function (see **Fig. G.6c**) appears to be consistent — but scatter and a slight off-center trend is evident. We believe that the *CPR-C* model has performed well for this case, and the **Fig. G.6** confirms the value of this model as a "characteristic relation" for permeability.

Model *CPR-D*: (Appendix G)

The "characteristic permeability relation" (or *CPR*) Model *CPR-D* (*i.e.*, the weighted power law-exponential model) is given in its fundamental form as:

$$k = xa\phi^{b} + (1-x)\alpha\exp[\beta\phi] \quad [0 \le x \le 1]] \quad \text{(G-4a)}$$

For Eq. G-4 there are two proposed models for the *x*-function (*i.e.*, the weighting function) — these are:

$$x = \exp[-\ln(x_0) + x_1\ln(\phi) + x_2\ln(F) + x_3\ln(\phi)\ln(F)] \ \text{(Model } CPR\text{-}DxL) \quad \text{(G-4b)}$$

$$x = \exp\begin{bmatrix} -\ln(x_0) + x_1\ln(\phi) + x_2\ln(F) + x_3\ln(\phi)\ln(F) \\ + x_4\ln(\phi)^2 + x_5\ln(F)^2 + x_6\ln(\phi)^2\ln(F) \\ + x_7\ln(\phi)\ln(F)^2 + x_8\ln(\phi)^2\ln(F)^2 \end{bmatrix} \text{(Model } CPR\text{-}DxL) \quad \text{(G-4c)}$$

As noted in Eq. G-4b, Model *CPR-DxL* utilizes a logarithmic linear model for the weights (*x*-values) and as seen in Eq. G-4c, Model *CPR-DxQ* utilizes a logarithmic quadratic model for the weights (*x*-values). While these models (Eqs. G-4b and G-4c) are *empirical*, we have found generally good application of these relations for all cases. In this case, the base results using Models *CPR-DxL* and *CPR-DxQ* are presented in **Fig. G.7** — where the power law and exponential basis functions are fitted to the appropriate portion of the data. The power law equation represents the "Archie Clean Sand" trend and is fitted to the leftmost data as shown in **Fig. G.7a** and in contrast, the exponential equation is thought to represent the "Archie Dirty Sand" trend and the exponential is fitted to the far rightmost portion of the data (see **Fig. G.7b**).

In **Figs. G.8 and 9** we present the error analyses for this case, where we have employed the weighting functions (Eqs. G-4b and G-4c) as appropriate. In **Fig. G.8a** we find a good correlation of permeability. The comparison of the Model *CPR-DxL* results are compared to the results obtained from the *GRACE* algorithm in **Fig. G.8b**, we note that the very good results obtained using Model *CPR-DxL*. The computed weight function (*x*-values) shown for the *CPR-DxL* model in **Fig. G.8c** does exhibit more scatter than expected, but the trend is (relatively) centered about the perfect correlation line.

The results obtained using Model *CPR-DxQ* are presented in **Fig. G.9**, and we note substantially improved behavior over that of Model *CPR-DxL*. In particular, the base correlation of computed and measured permeabilities (**Fig. G.9a**) for Model *CPR-DxQ* does indicate a slightly better correlation than that of Model *CPR-DxL*. Also, the comparison of Model *CPR-DxQ* with the results from the *GRACE* algorithm (**Fig. G.9b**) exhibits better agreement than the results of Model *CPR-DxL*. Finally, the correlation of the *x*-function (**Fig. G.9c**) for Model *CPR-DxQ* is better than the correlation for Model *CPR-DxL*. These comparisons suggest that Model *CPR-DxQ* (*i.e.*, the combination of Eqs. G-4a and G-4c) has provided a better correlation of data, for this case, than Model *CPR-DxL*.

***"Modified Timur Model"*: (Appendix G)**

The "Modified Timur Model" is given as:

$$k_{\mathrm{Timur}} = a\phi^b F^c \quad \text{(G-5)}$$

In **Fig. G.10** we present the results of the "Modified Timur Model" (Eq. G-5) which is essentially just a generalized power-law function relation in terms of k, ϕ, and F. **Figs. G.10a and b**, provide the "Modified Timur Model" results of the data for this case.

***GRACE* Algorithm: (Appendix G)**

In **Fig. G.11** we present the results predicted by the *GRACE* algorithm, which is a non-parametric regression approach (see Xue *et al.* (1997) for details). In theory, the *GRACE* algorithm should provide the most *unbiased* correlation of the data — *i.e.*, the *GRACE* algorithm is designed not to "fit the errors" as other regression approaches may. It is our contention that the *GRACE* algorithm is the statistical standard — and any algorithm/approach/model which achieves better regression statistics than the *GRACE* algorithm is actually "fitting the errors" in the data. *None of the cases have significantly better regression statistics than the GRACE algorithm* — hence, none of the cases are "over-fitted" in a statistical sense.

***Comparison of All Models*: (Appendix G)**

Our final plot, **Fig. G.12**, illustrates all of the models on a single plot of calculated versus measured permeability. We also present a table of all statistical results in **Table G.1**.

Table G.1 — Statistical Results for all Models (Devonian Limestone Case, n=58).

Model	Sum of Squared Residuals $[\log(k)^2]$	Variance $[\log(k)^2]$	Standard Deviation $[\log(k)]$	Absolute Relative Error [percent]
CPR-A	8.24	1.86	1.36	29.92
CPR-B	9.45	1.83	1.35	32.85
CPR-C	8.91	1.65	1.29	30.87
CPR-DxL	9.03	1.80	1.34	33.01
CPR-DxQ	8.99	1.87	1.37	33.21
Modified Timur	8.50	1.82	1.35	31.35
GRACE Algorithm	8.25	1.85	1.36	29.12

The coefficients for the models used in this case are provided in **Table G.2**.

Table G.2a — Model Coefficients (Devonian Limestone Case, n=58).

Model	a or α	b or β	c or c_{max}	c_1	c_2	c_3
CPR-A	$4.00\text{x}10^3$	4.00	0.110	0.15	-2.79	-0.89
CPR-B	$1.02\text{x}10^5$	8.00	0.110	10.79	3.61	0.95
CPR-C	$1.00\text{x}10^{-2}$	18.00	0.080	$2.85\text{x}10^{-2}$	1.33	1.43
Modified Timur	$1.10\text{x}10^3$	1.55	-1.185	–	–	–

Table G.2b — Model Coefficients (Devonian Limestone Case, n=58).

Model	a	b	α	β
CPR-DxL	$4.00\text{x}10^3$	4.00	$1.00\text{x}10^{-2}$	18.00
CPR-DxQ	$4.00\text{x}10^3$	4.00	$1.00\text{x}10^{-2}$	18.00

Model	c_0	c_1	c_2	c_3	c_4	c_5	c_6	c_7	c_8
CPR-DxL	61.66	-5.60	-1.12	-0.50	–	–	–	–	–
CPR-DxQ	$6.28\text{x}10^5$	-6.83	-5.88	3.98	1.02	-0.28	0.38	0.11	0.07

Nomenclature: (Appendix G)

F = Archie Formation Factor (dimensionless)
k = Formation Permeability, md (or any consistent units)
ϕ = Porosity, fraction

References: (Appendix G)

Ellis, K.W.: "Extended Correlations of Porosity, Permeability, and Formation Resistivity Factor," MS thesis, Texas A&M U., College Station, TX (1987).

Xue, G., Datta-Gupta, A., Valko, P., and Blasingame, T.A.: "Optimal Transformations for Multiple Regression: Application to Permeability Estimation from Well Logs," *SPEFE* (June 1997), 85-93.

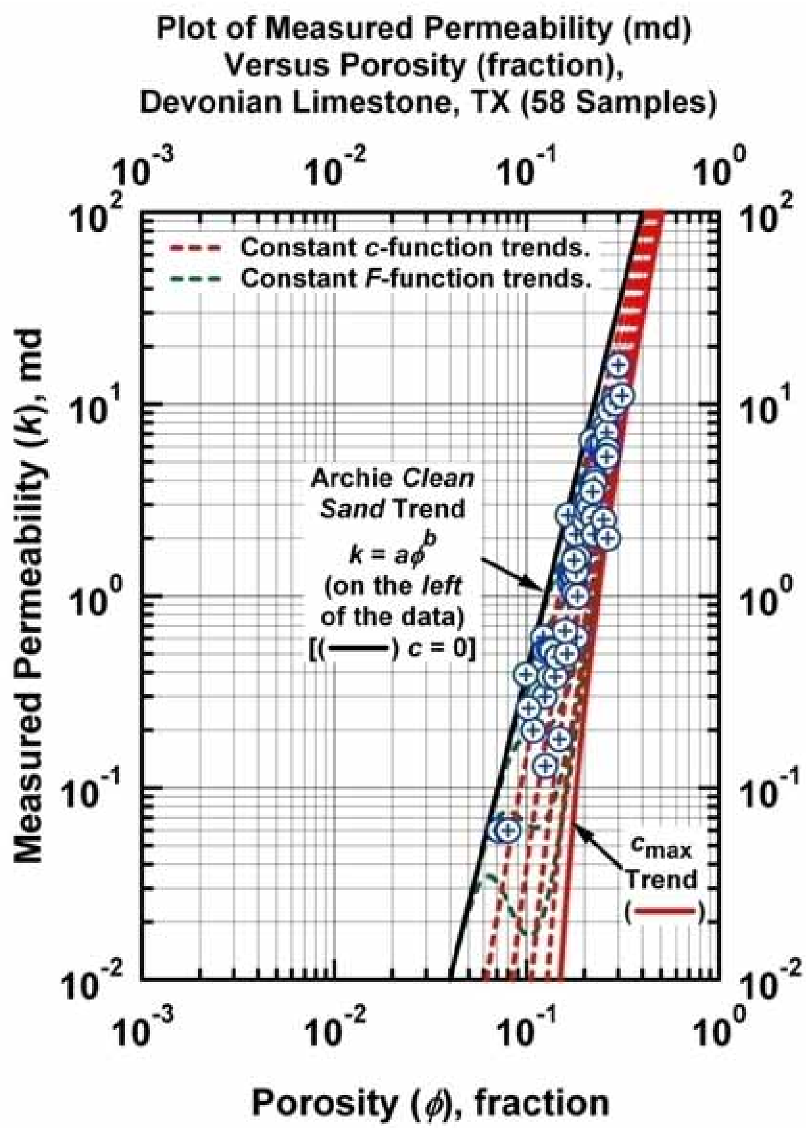

Figure G.1a — Model *CPR-A*: $k = a(\phi - c)^b$ $(c = c_{max} \exp[-c_1 \phi^{c_2} F^{c_3}])$ — "Clean Sand" Plot (log-log format) — Archie "Clean Sand" trend is given by the straight-line trend at the far left of the data (power law model). [*Case*: Devonian Limestone TX (USA)]

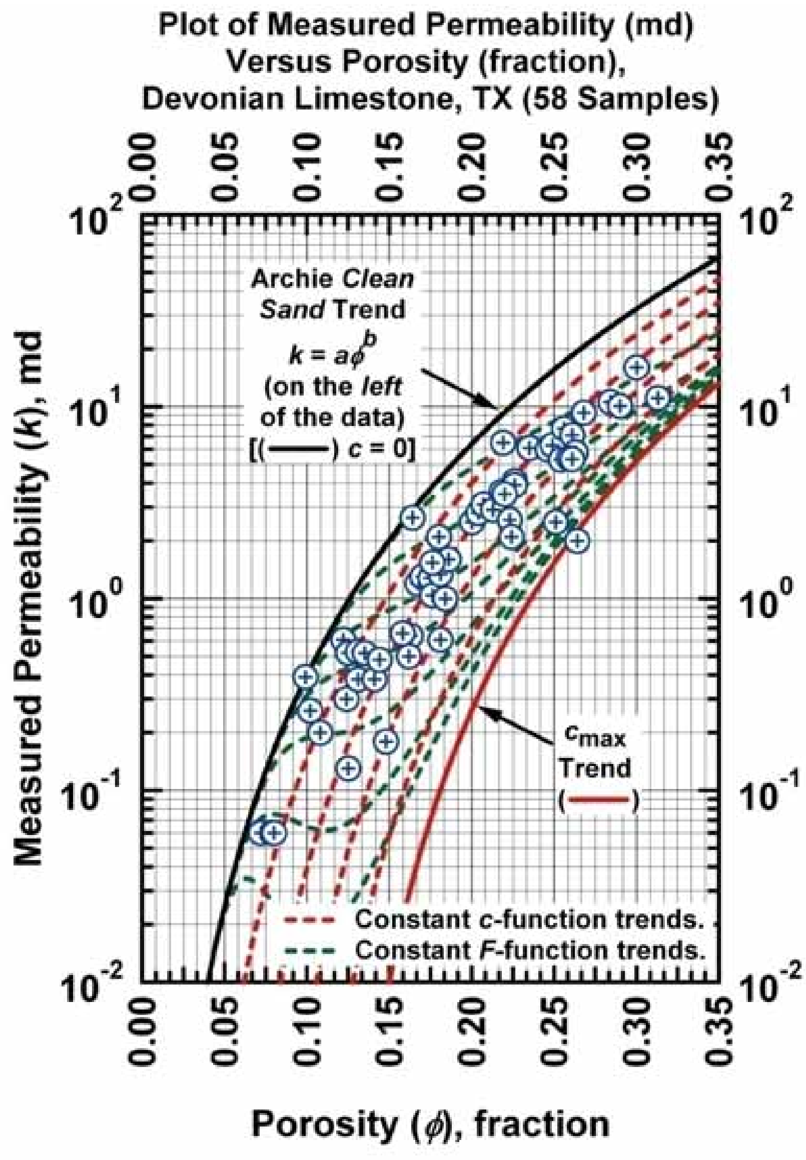

Figure G.1b — Model *CPR-A*: $k = a(\phi - c)^b$ $(c = c_{max} \exp[-c_1 \phi^{c2} F^{c3}])$ — "Dirty Sand" Plot (semilog format). Archie "Clean Sand" trend is given by the curved trend at the far left of the data (power law model). [*Case*: Devonian Limestone TX (USA)]

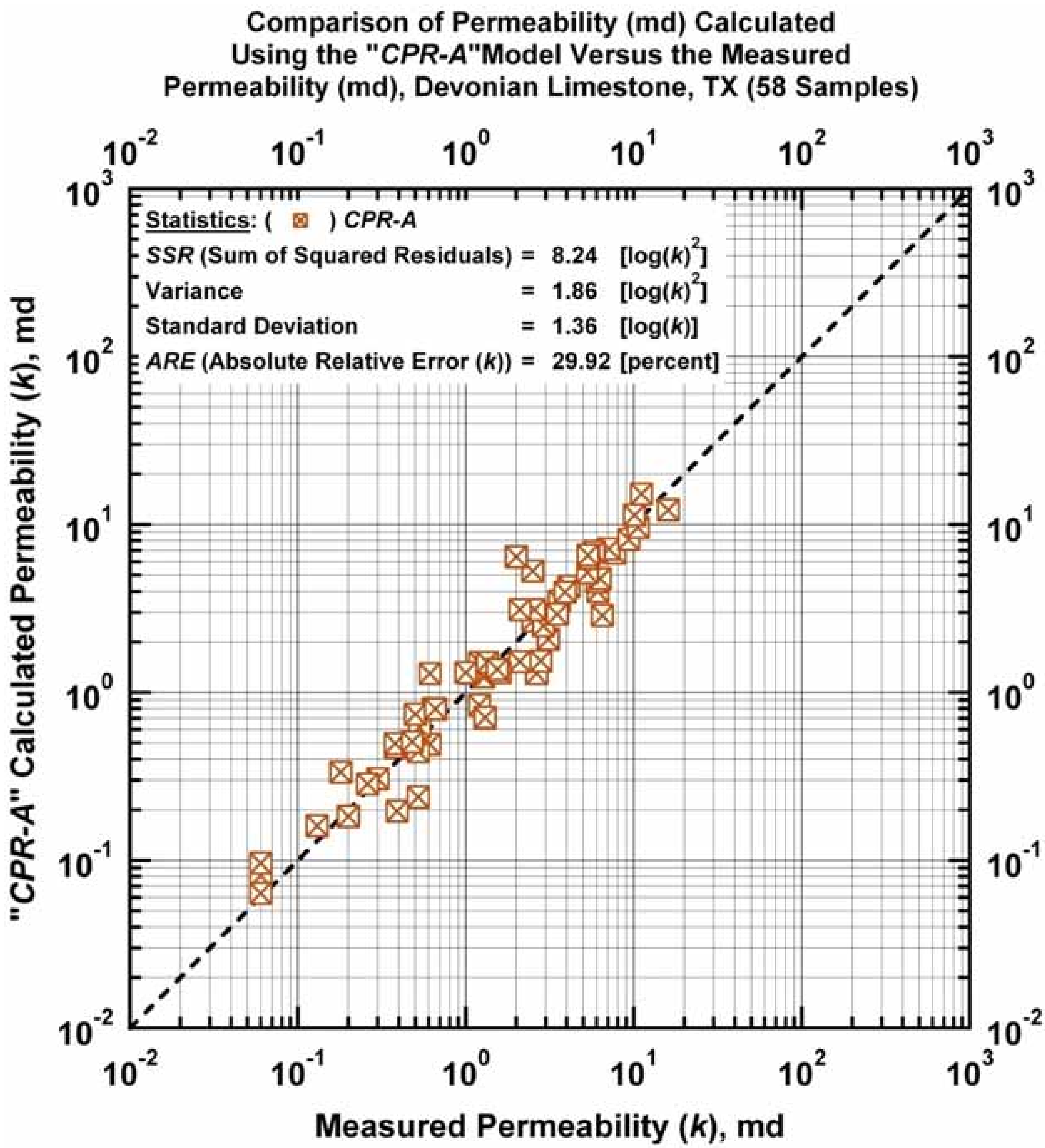

Figure G.2a — Model *CPR-A*: calculated versus measured permeability. [*Case*: Devonian Limestone TX (USA)]

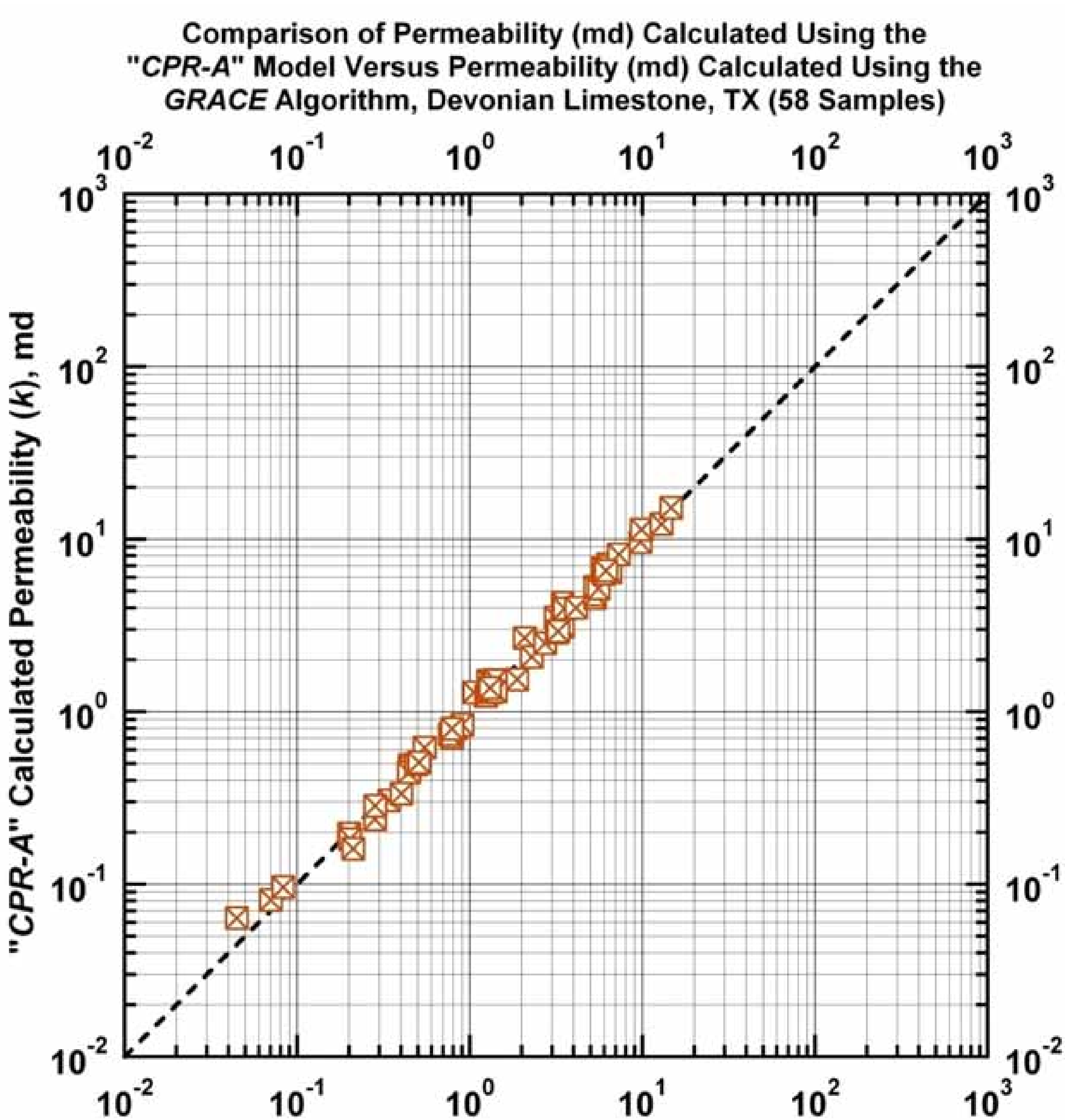

Figure G.2b — Model *CPR-A*: Permeability calculated using Model *CPR-A* versus permeability calculated using the *GRACE* Algorithm. [*Case*: Devonian Limestone TX (USA)]

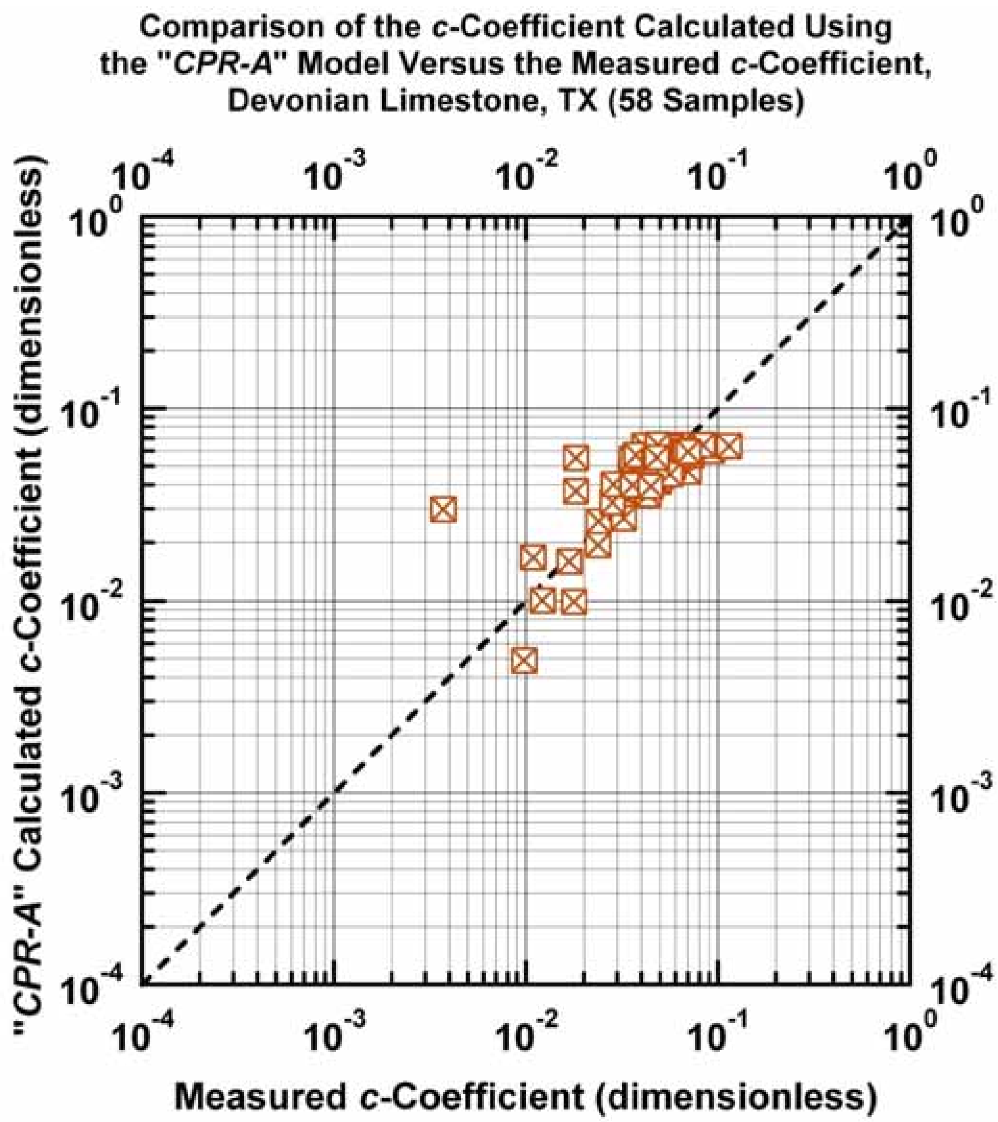

Figure G.2c — Model *CPR-A*: Calculated *c*-function values versus measured *c*-function values. [*Case*: Devonian Limestone TX (USA)]

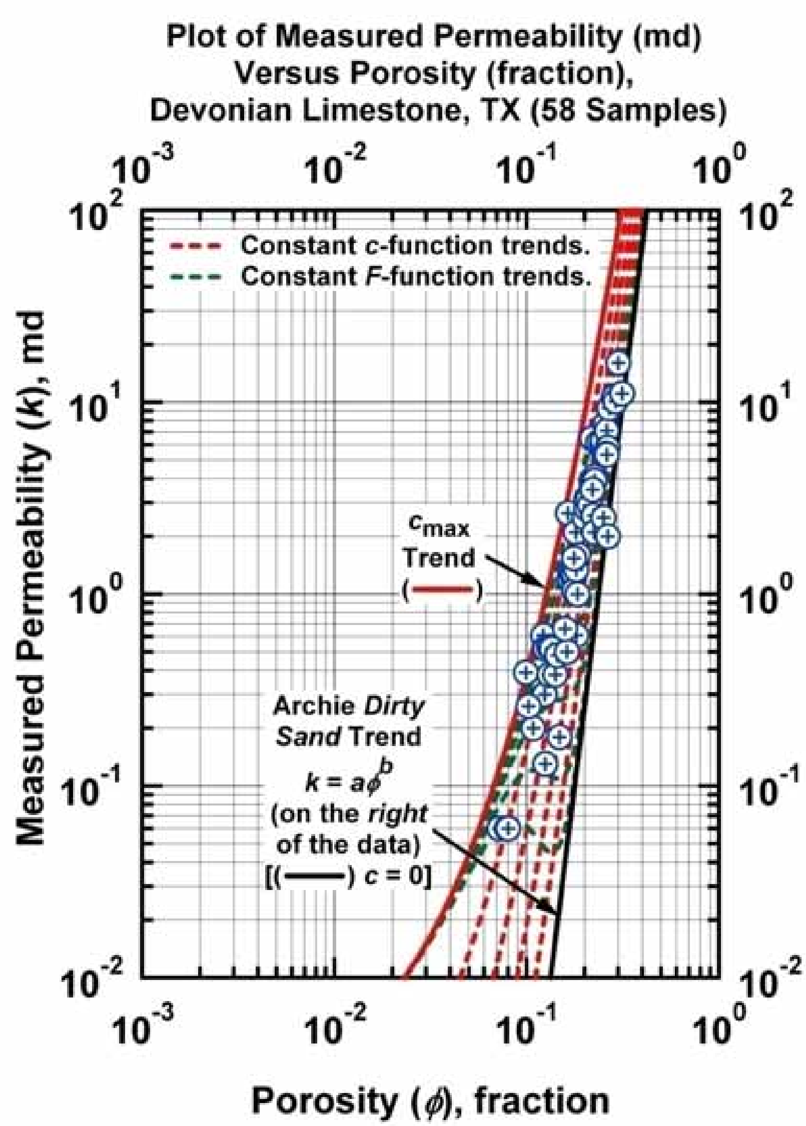

Figure G.3a — Model *CPR-B*: $k = a(\phi + c)^b \quad c = c_{max} \exp[-c_1 \phi^{c_2} F^{c_3}]$ — "Clean Sand" Plot (log-log format) — Archie "Dirty Sand" trend is given by the straight-line trend at the far right of the data (power law model). [*Case*: Devonian Limestone TX (USA)]

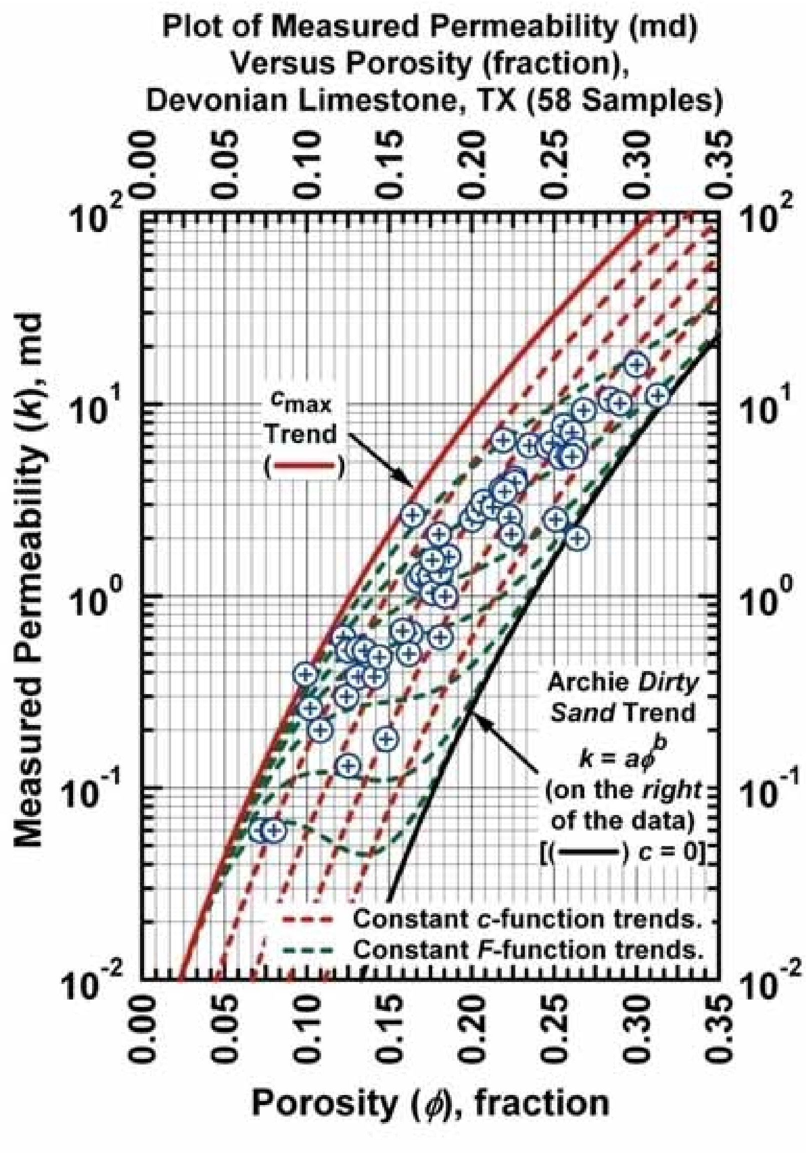

Figure G.3b — Model *CPR-B*: $k = a(\phi + c)^b \quad c = c_{\max} \exp[-c_1 \phi^{c2} F^{c3}]$ — "Dirty Sand" Plot (semilog format) — Archie "Dirty Sand" trend is given by the curved trend at the far right of the data (power law model). [*Case*: Devonian Limestone TX (USA)]

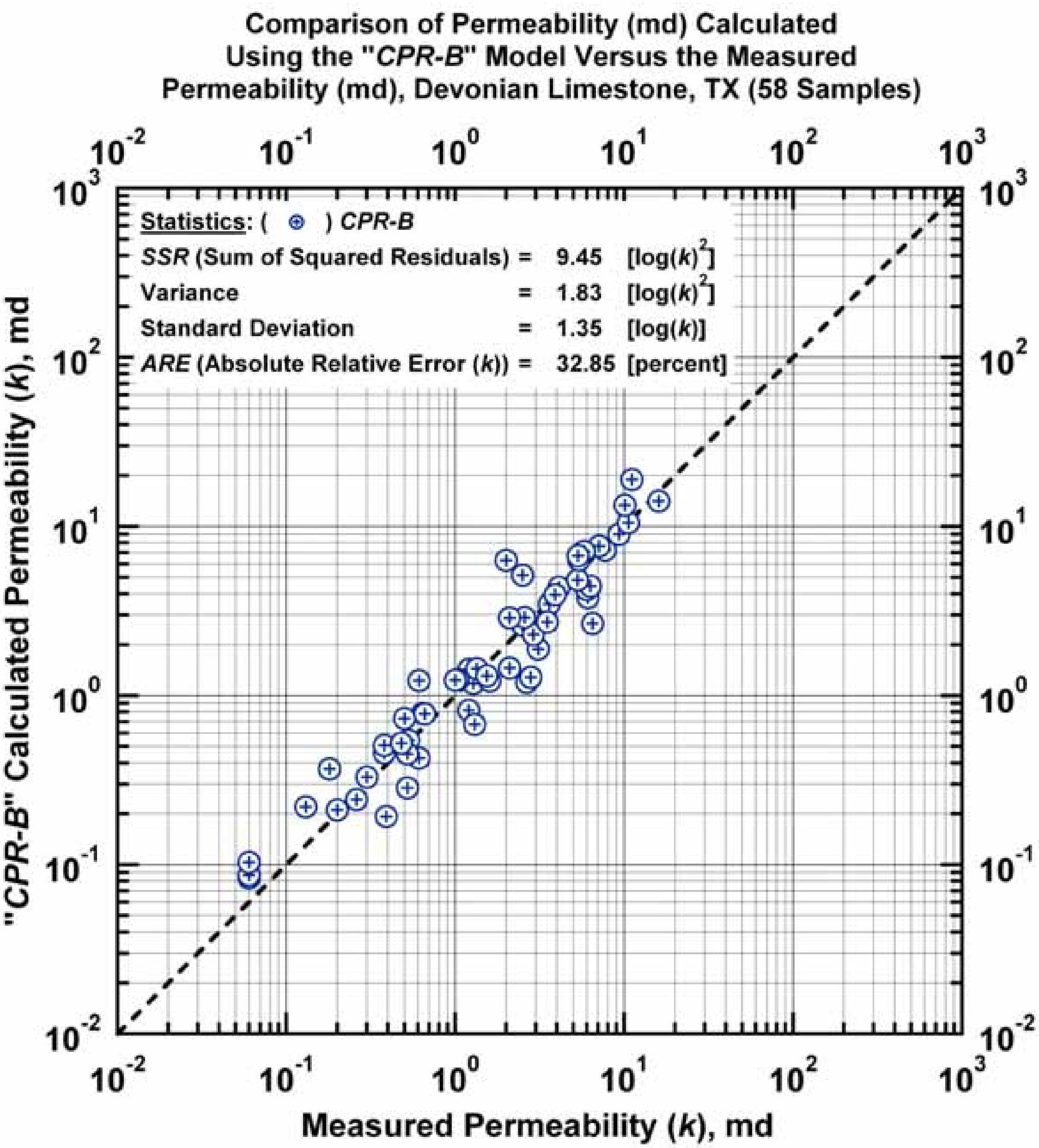

Figure G.4a — Model *CPR-B*: calculated versus measured permeability. [*Case*: Devonian Limestone TX (USA)]

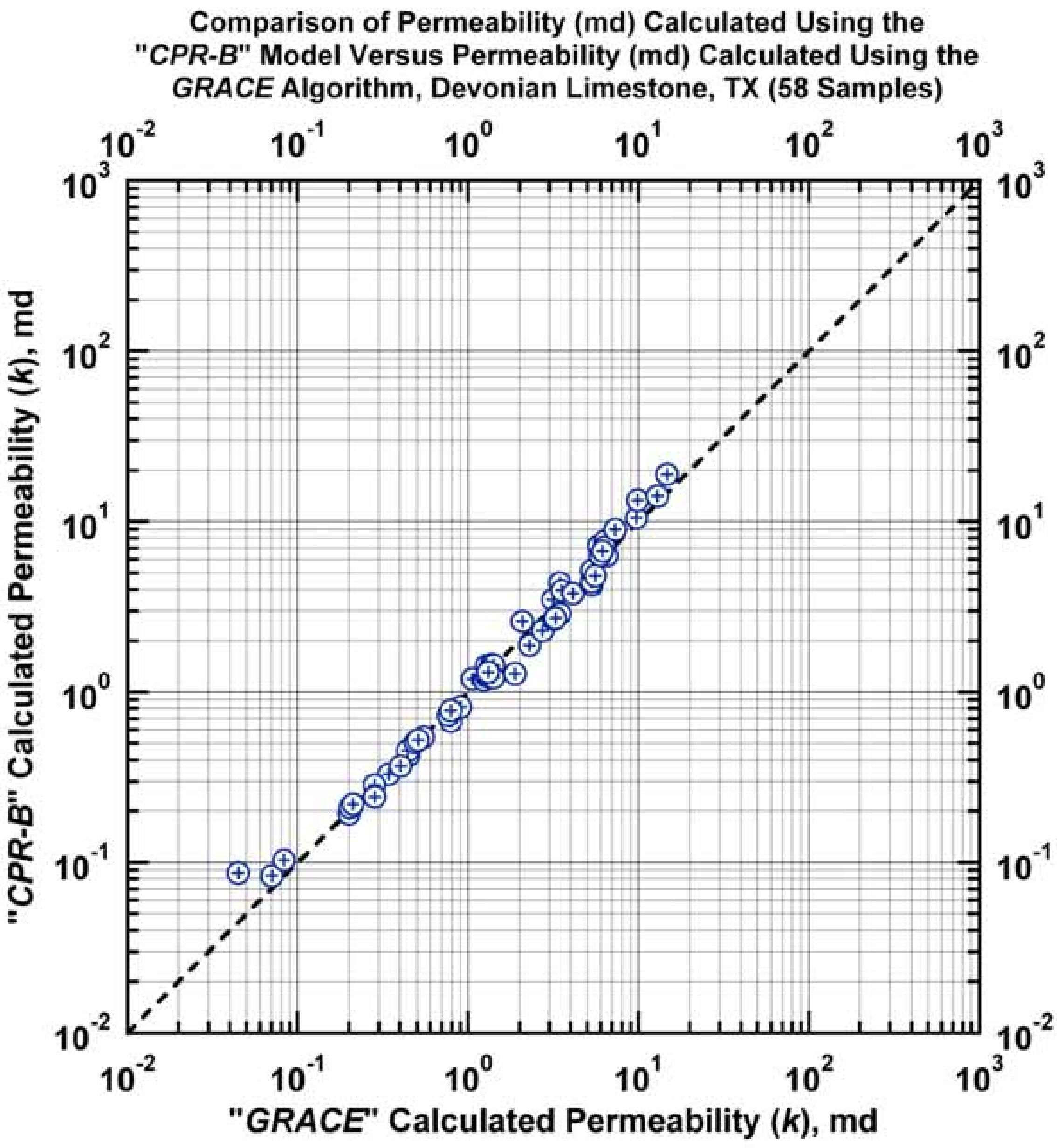

Figure G.4b — Model *CPR-B*: Permeability calculated using Model *CPR-B* versus permeability calculated using the *GRACE* Algorithm. [*Case*: Devonian Limestone TX (USA)]

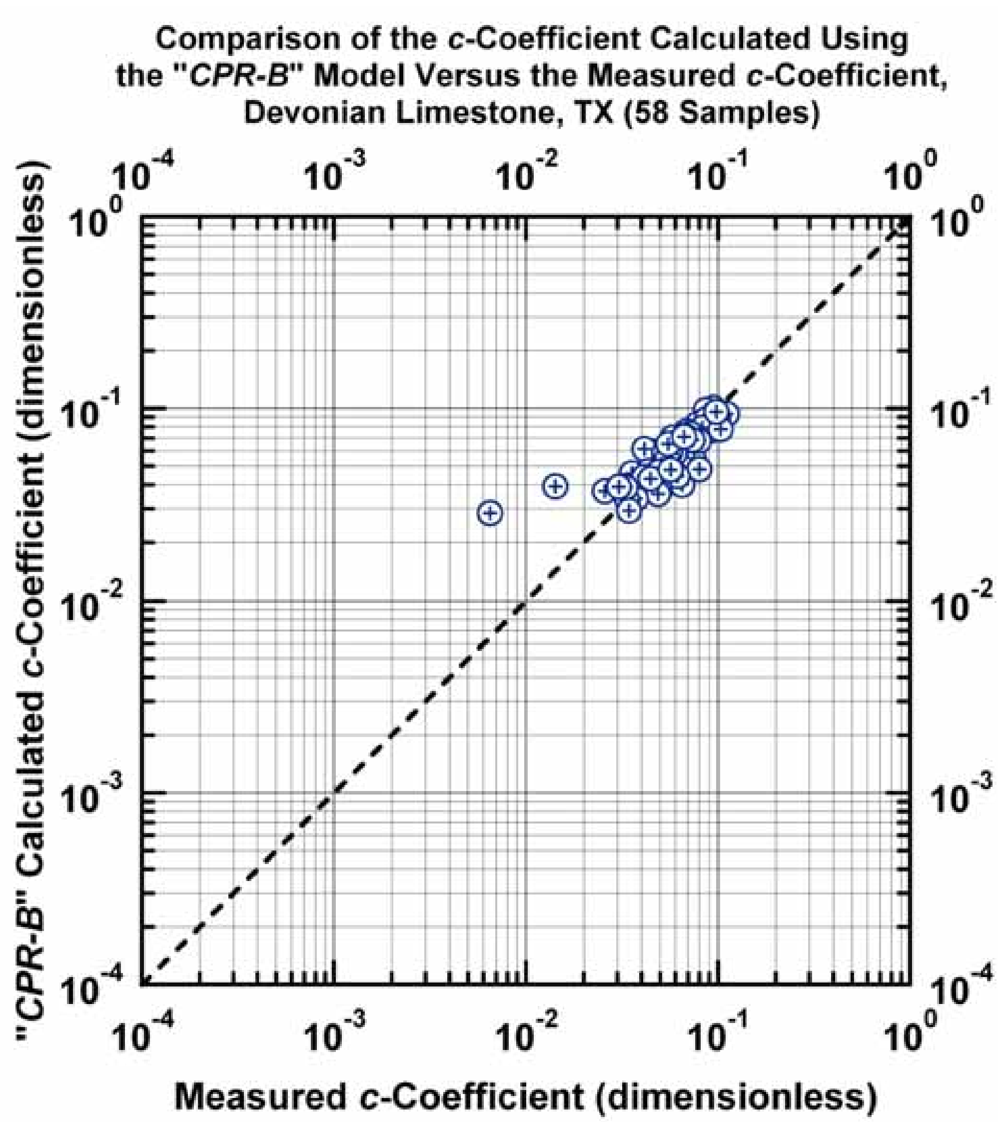

Figure G.4c — Model *CPR-B*: Calculated *c*-function values versus measured *c*-function values. [*Case*: Devonian Limestone TX (USA)]

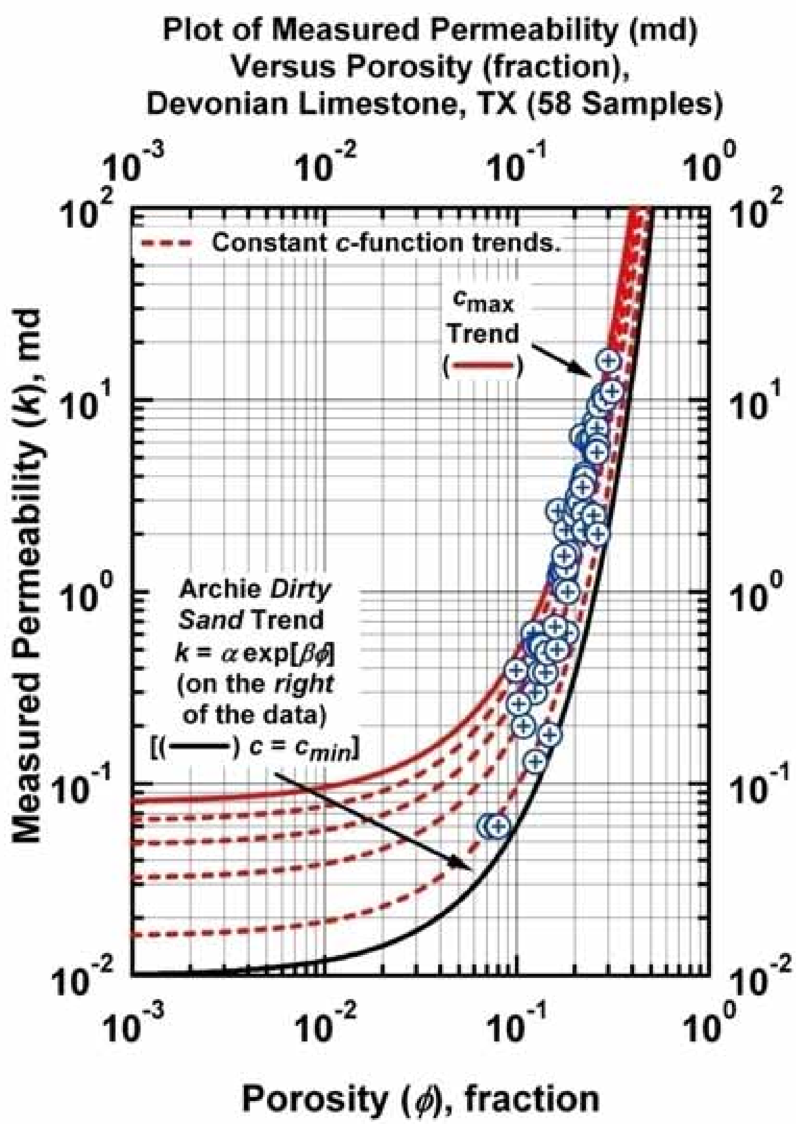

Figure G.5a — Model *CPR-C*: $k = c\exp[\beta\phi]$ $\quad c = c_{\max}\exp[-c_1\phi^{c_2}F^{c_3}]$ — "Clean Sand" Plot (log-log format) — Archie "Dirty Sand" trend is given by the curved trend at the far right of the data (exponential model). [*Case*: Devonian Limestone TX (USA)]

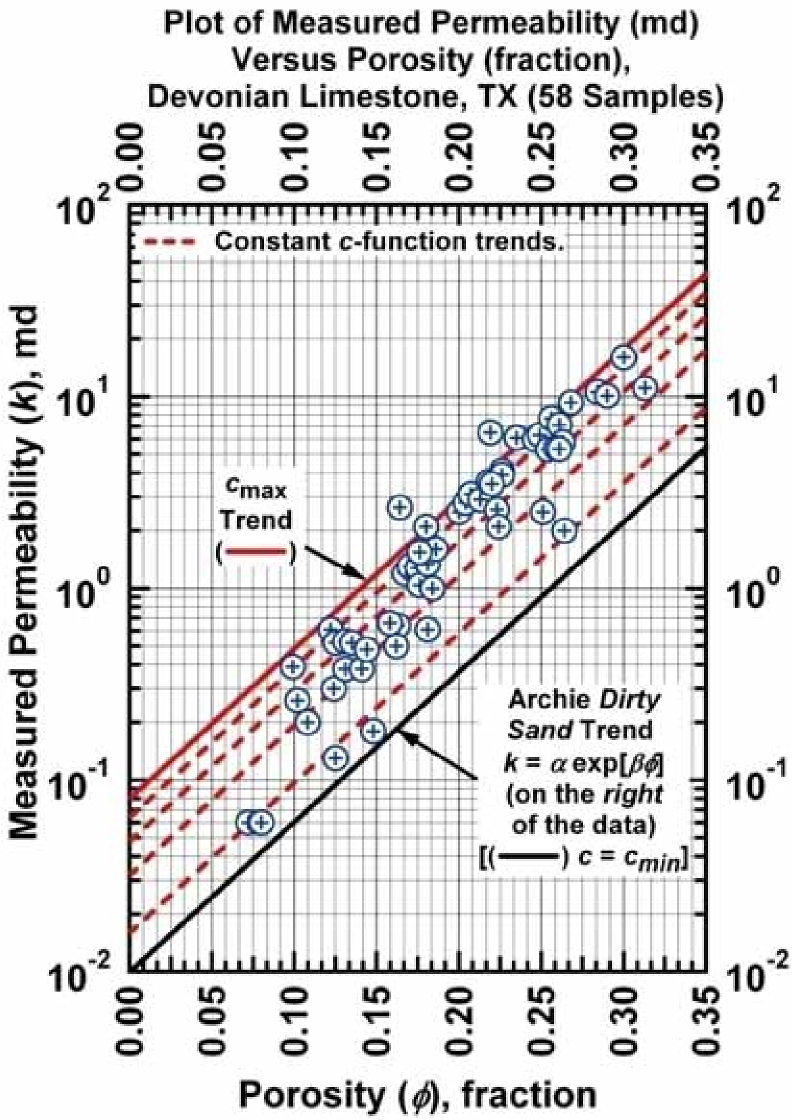

Figure G.5b — Model *CPR-C*: $k = c\exp[\beta\phi]$ $c = c_{\max}\exp[-c_1\phi^{c_2}F^{c_3}]$ — "Dirty Sand" Plot (semilog format) — Archie "Dirty Sand" trend is given by the straight-line trend at the far right of the data (exponential model). [*Case*: Devonian Limestone TX (USA)]

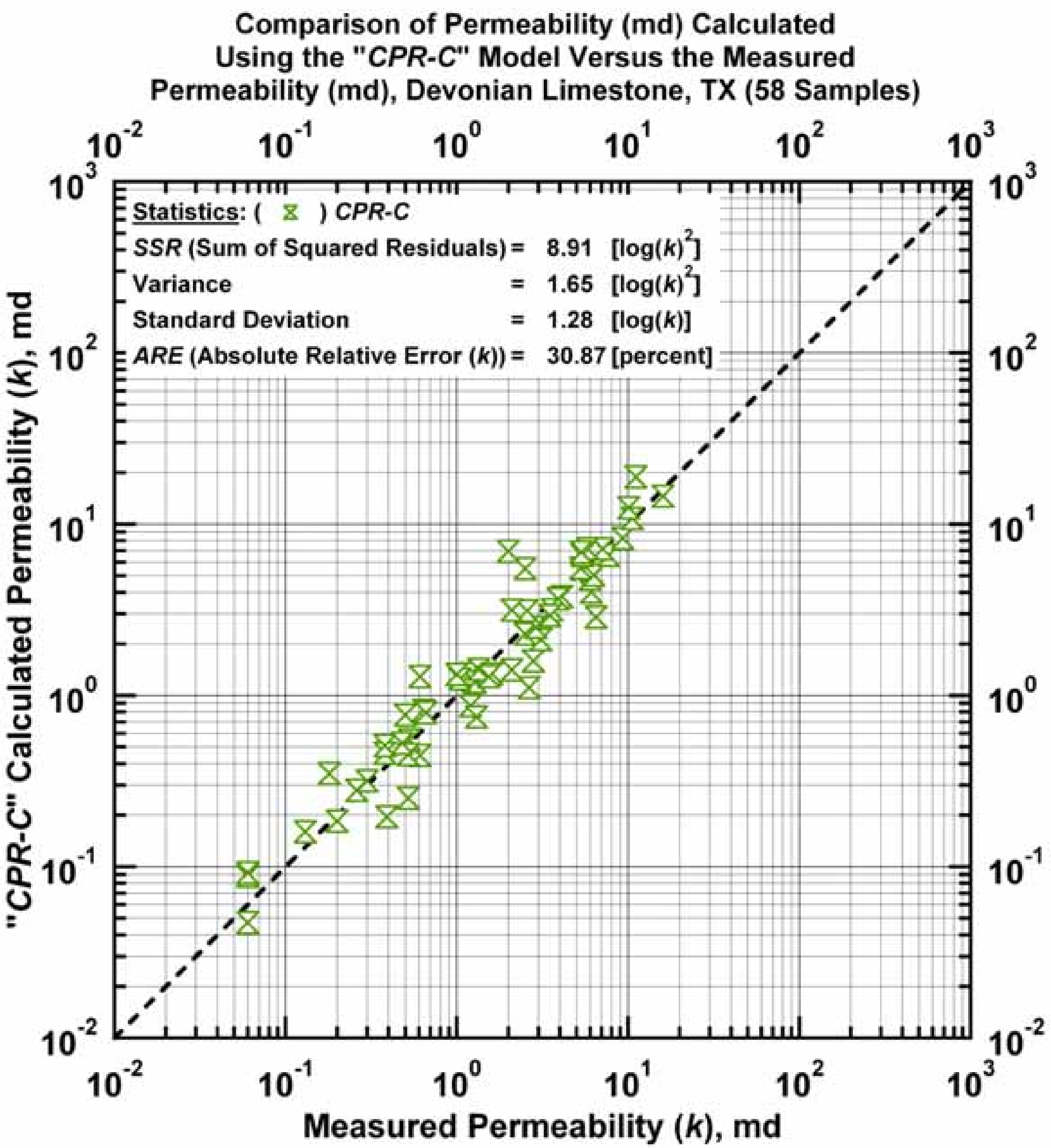

Figure G.6a — Model *CPR-C*: calculated versus measured permeability. [*Case*: Devonian Limestone TX (USA)]

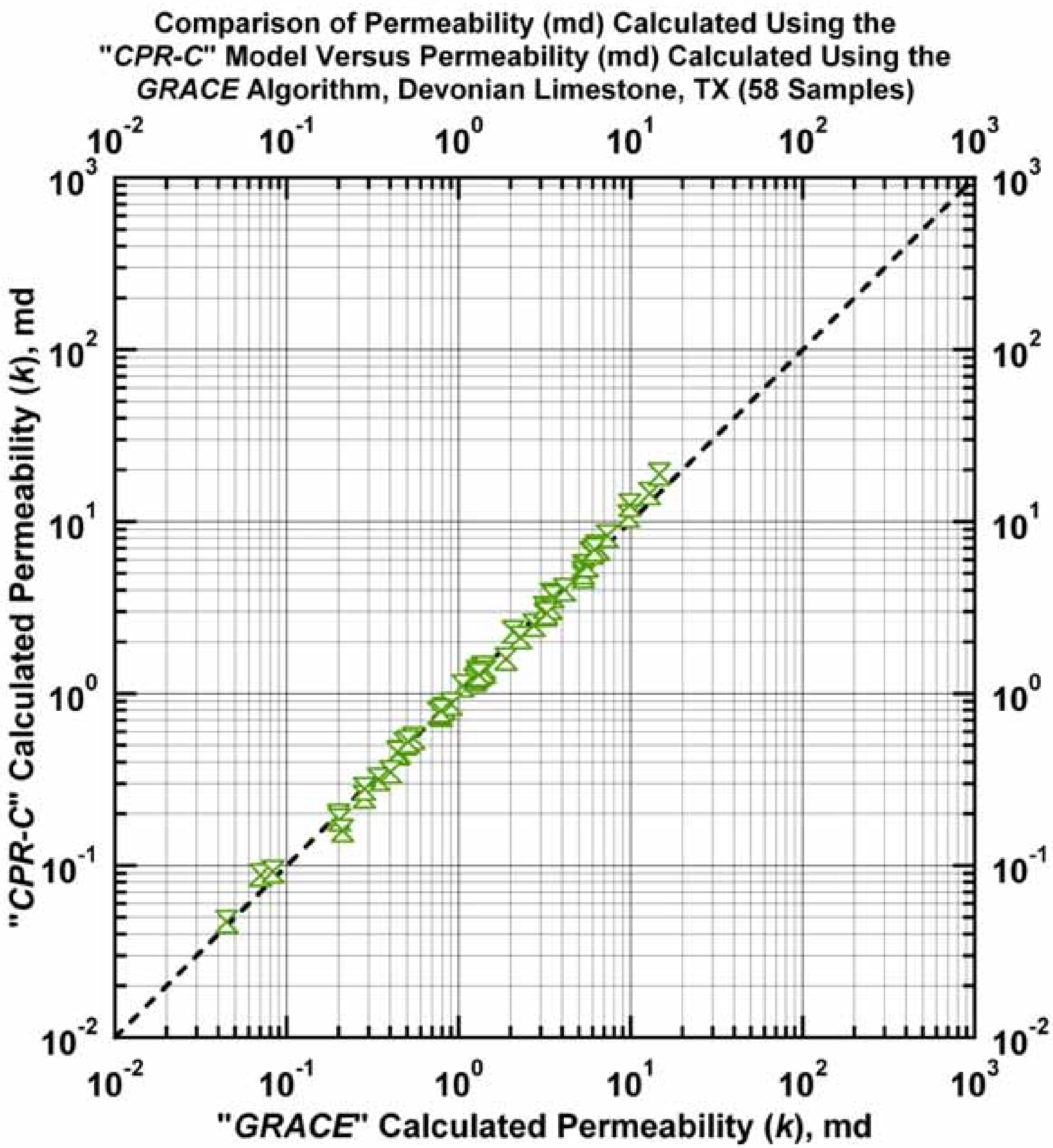

Figure G.6b — Model *CPR-C*: Permeability calculated using Model *CPR-C* versus permeability calculated using the *GRACE* Algorithm. [*Case*: Devonian Limestone TX (USA)]

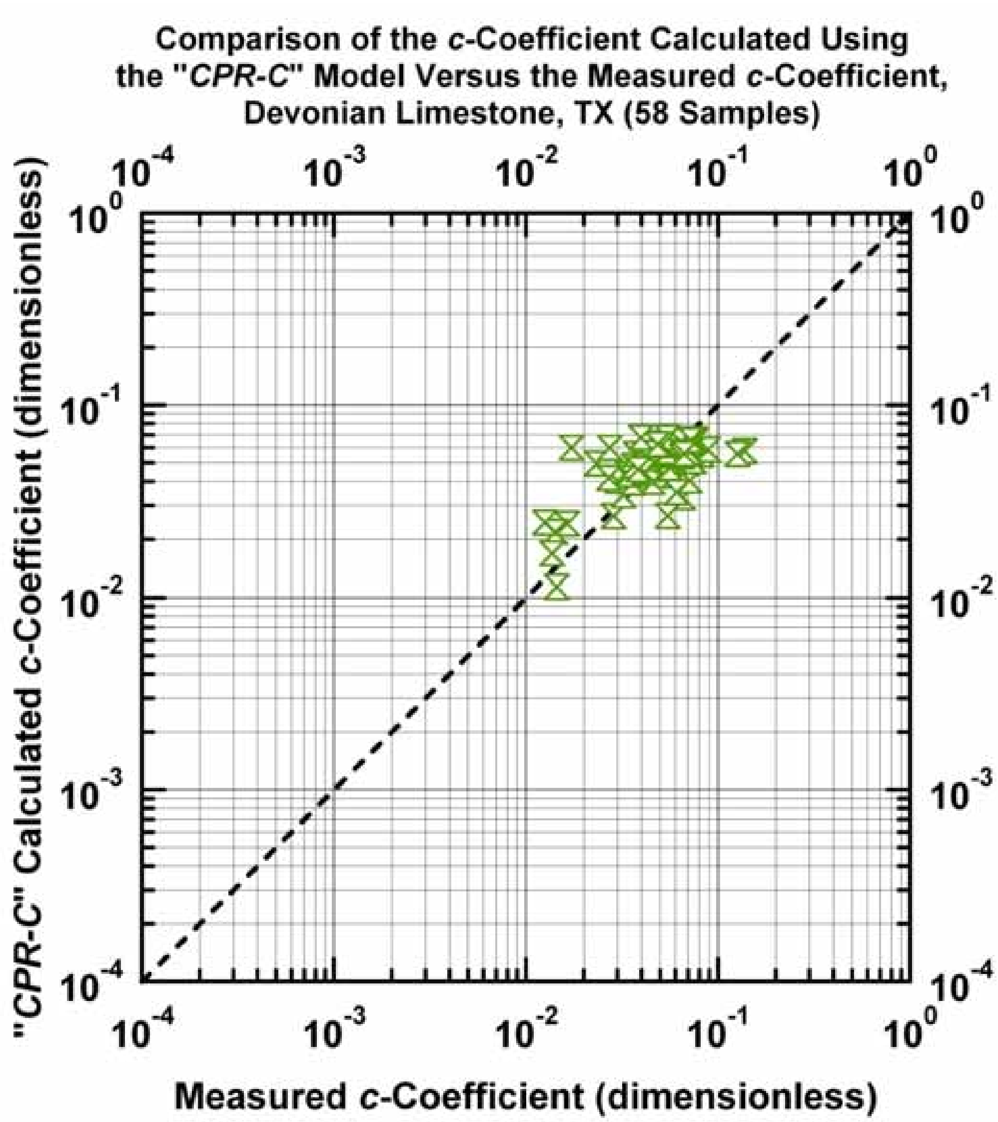

Figure G.6c — Model *CPR-C*: Calculated *c*-function values versus measured *c*-function values. [*Case*: Devonian Limestone TX (USA)]

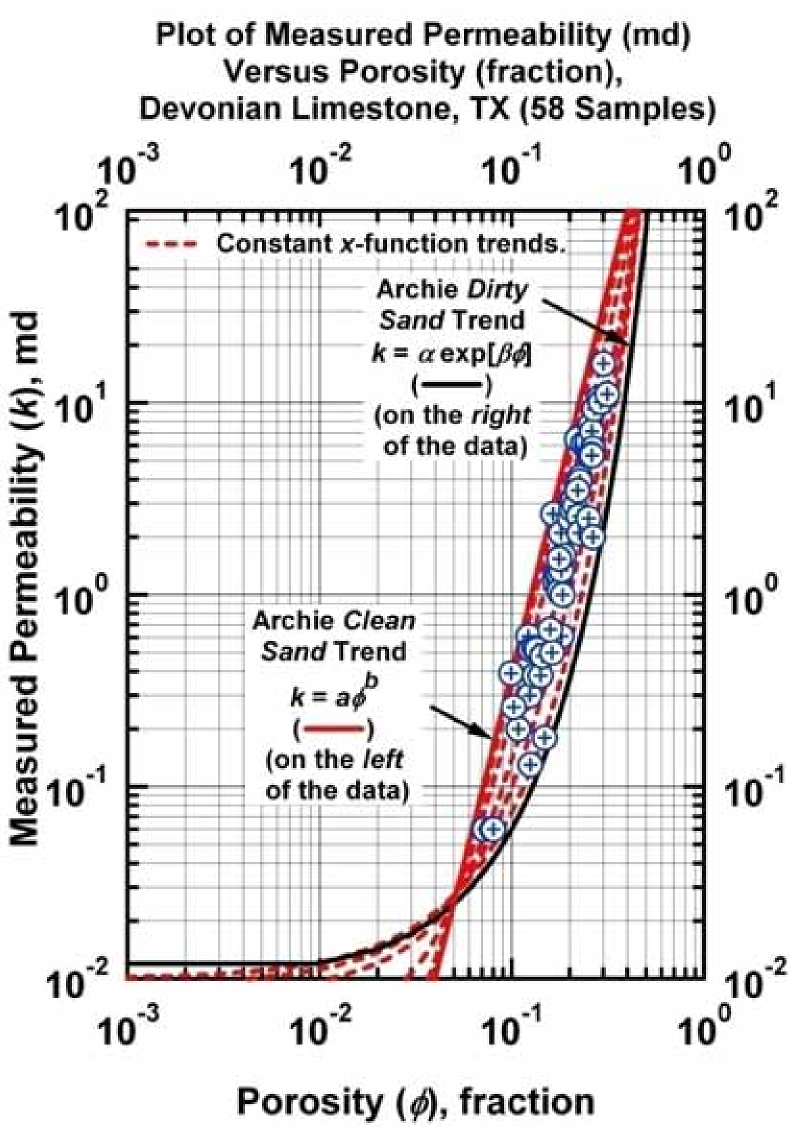

Figure G.7a — Model *CPR-D*: $k = xa\phi^b + (1-x)\alpha\exp[\beta\phi]$ $[0 \le x \le 1]$ — *Weighted Power Law-Exponential Model* used to correlate permeability (k) and porosity (ϕ). "Clean Sand" Plot — Archie "Clean Sand" trend is given by the straight-line trend at the far left of the data (power law model). [*Case*: Devonian Limestone TX (USA)]

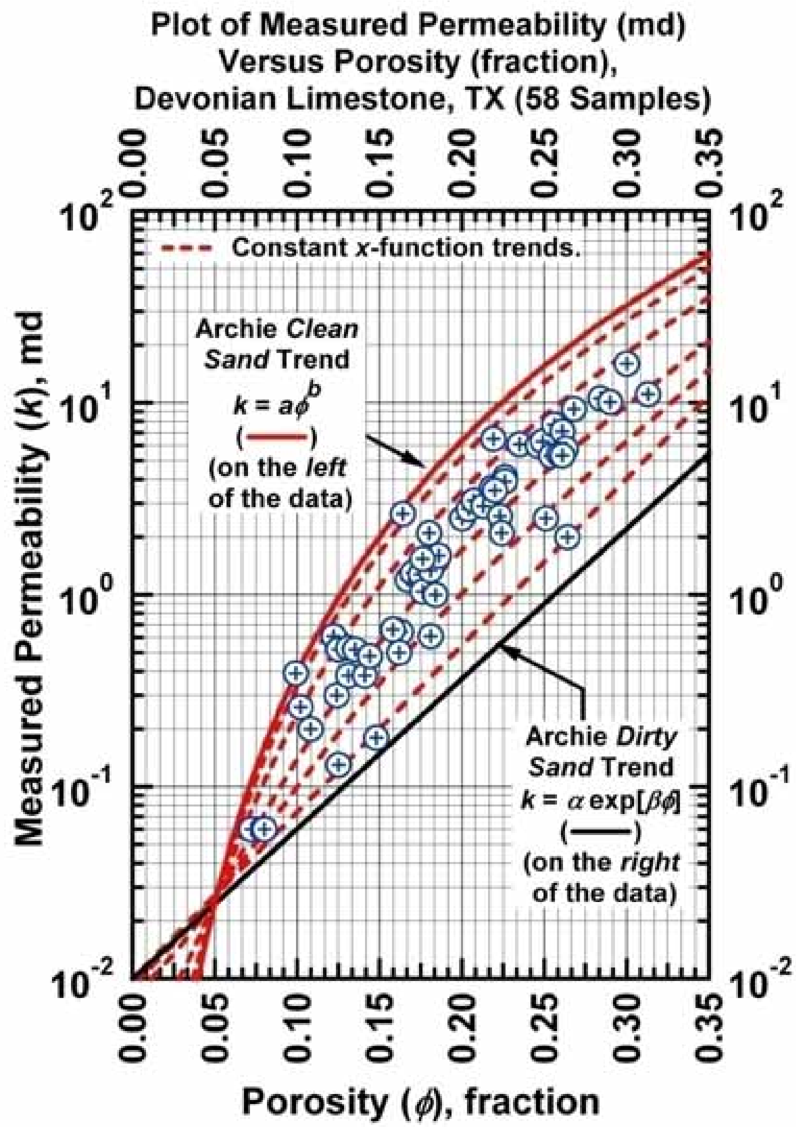

Figure G.7b — Model *CPR-D*: $k = xa\phi^b + (1-x)\alpha\exp[\beta\phi]$ $[0 \le x \le 1]$ — *Weighted Power Law-Exponential Model* used to correlate permeability (k) and porosity (ϕ). "Dirty Sand" Plot — Archie "Dirty Sand" trend is given by the straight-line trend at the far right of the data (exponential model). [*Case*: Devonian Limestone TX (USA)]

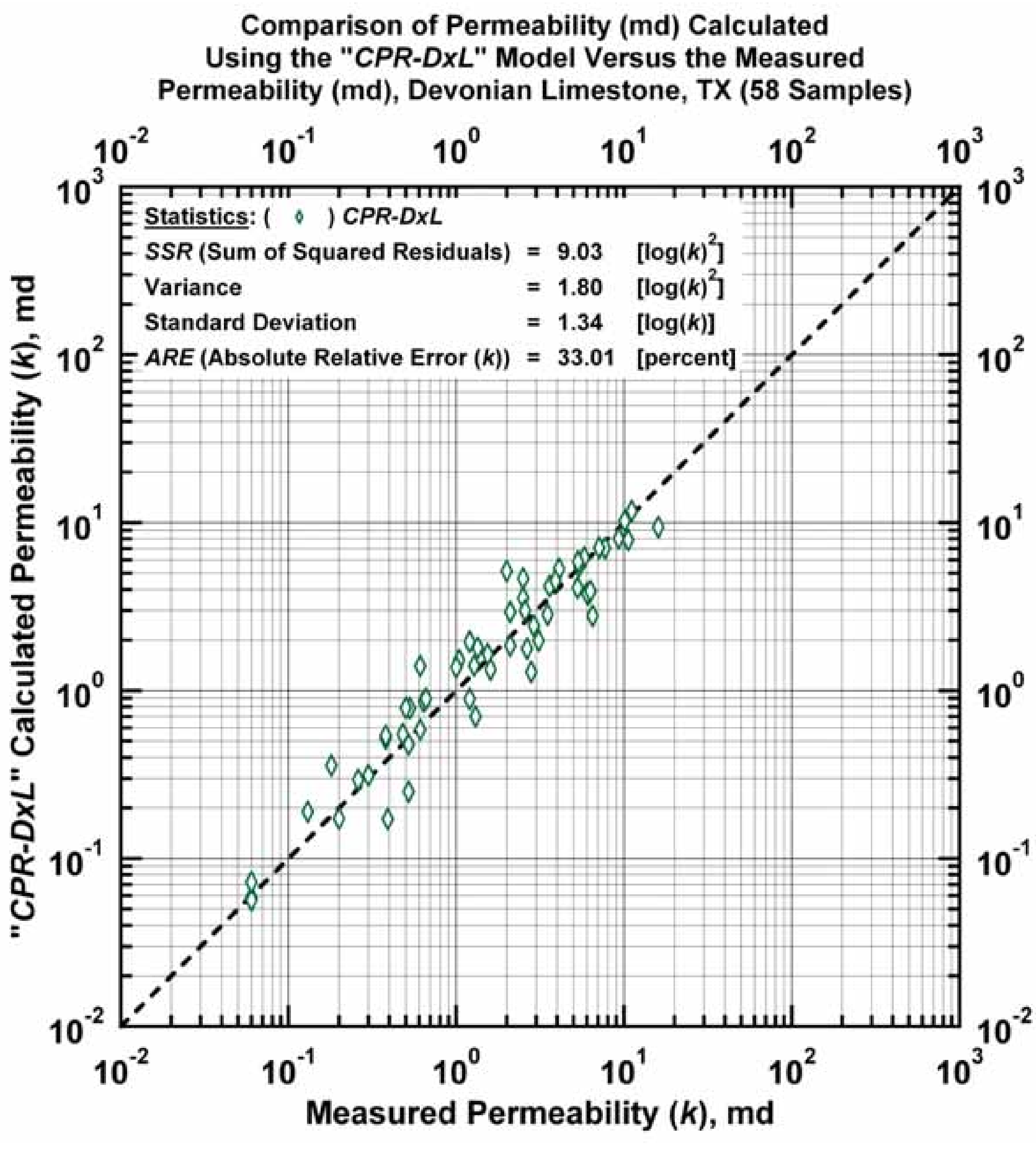

Figure G.8a — Model *CPR-DxL*: Calculated versus measured permeability. [*Case*: Devonian Limestone TX (USA)]

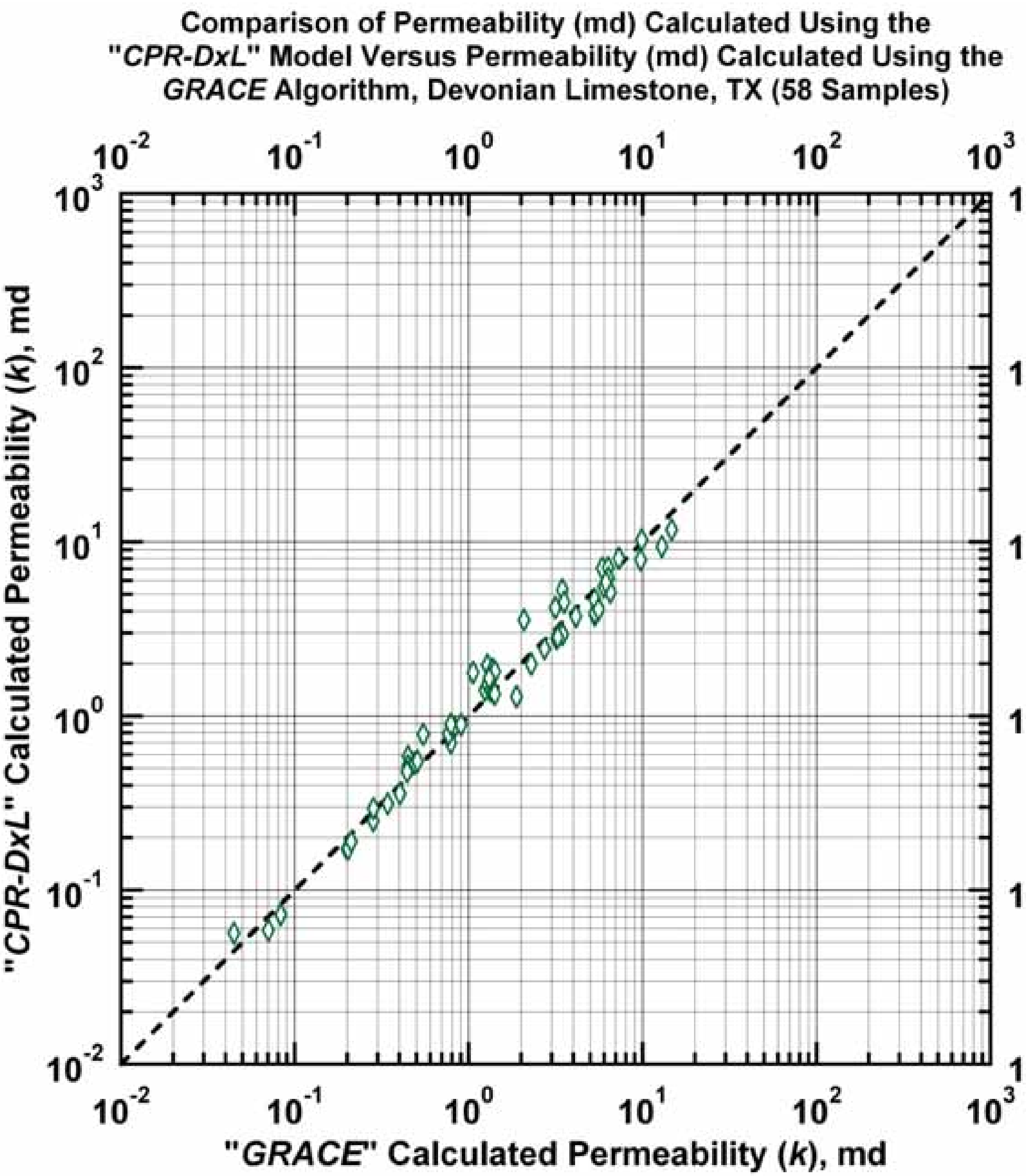

Figure G.8b — Model *CPR-DxL*: Permeability calculated using Model *CPR-C* versus permeability calculated using the *GRACE* Algorithm. [*Case*: Devonian Limestone TX (USA)]

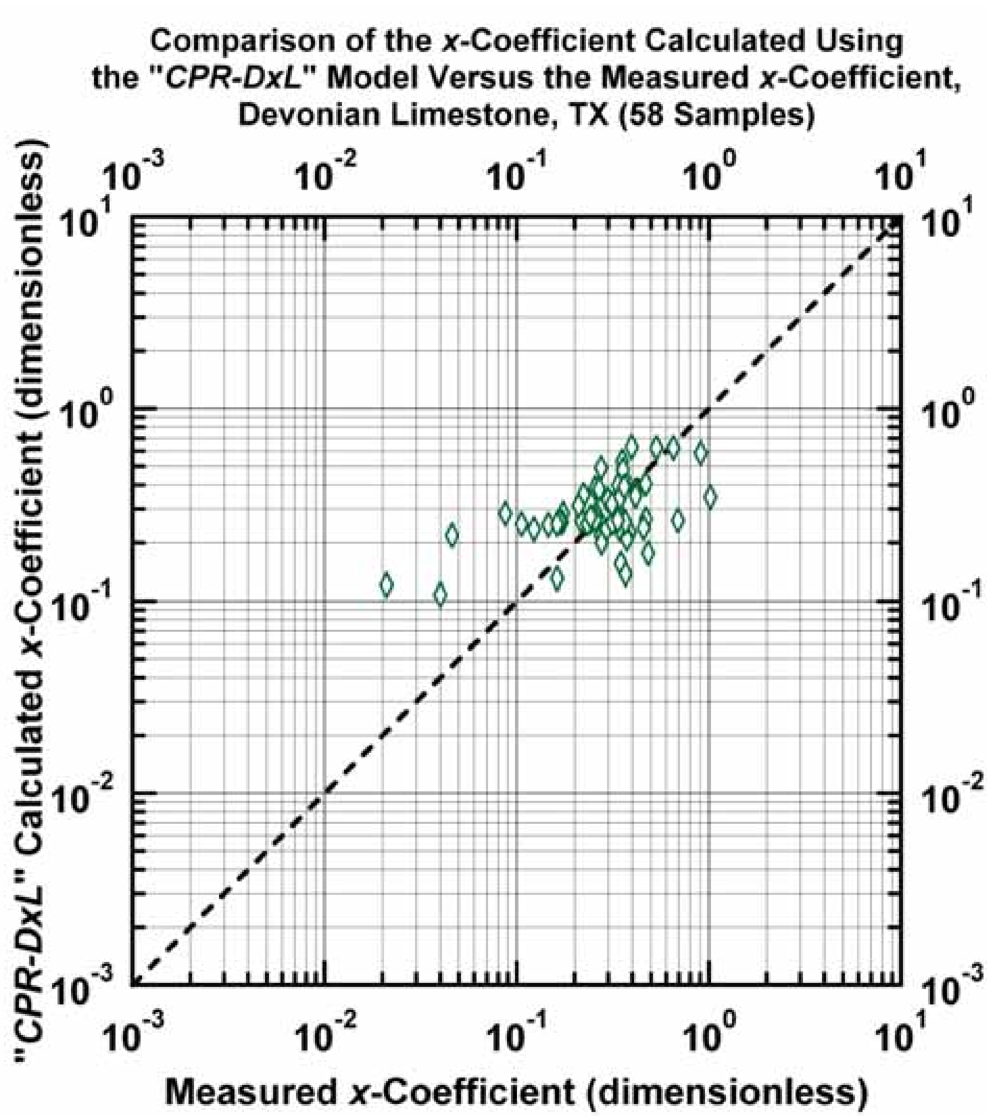

Figure G.8c — Model *CPR-DxL*: Calculated *x*-function weight values versus measured *x*-function weight values. [*Case*: Devonian Limestone TX (USA)]

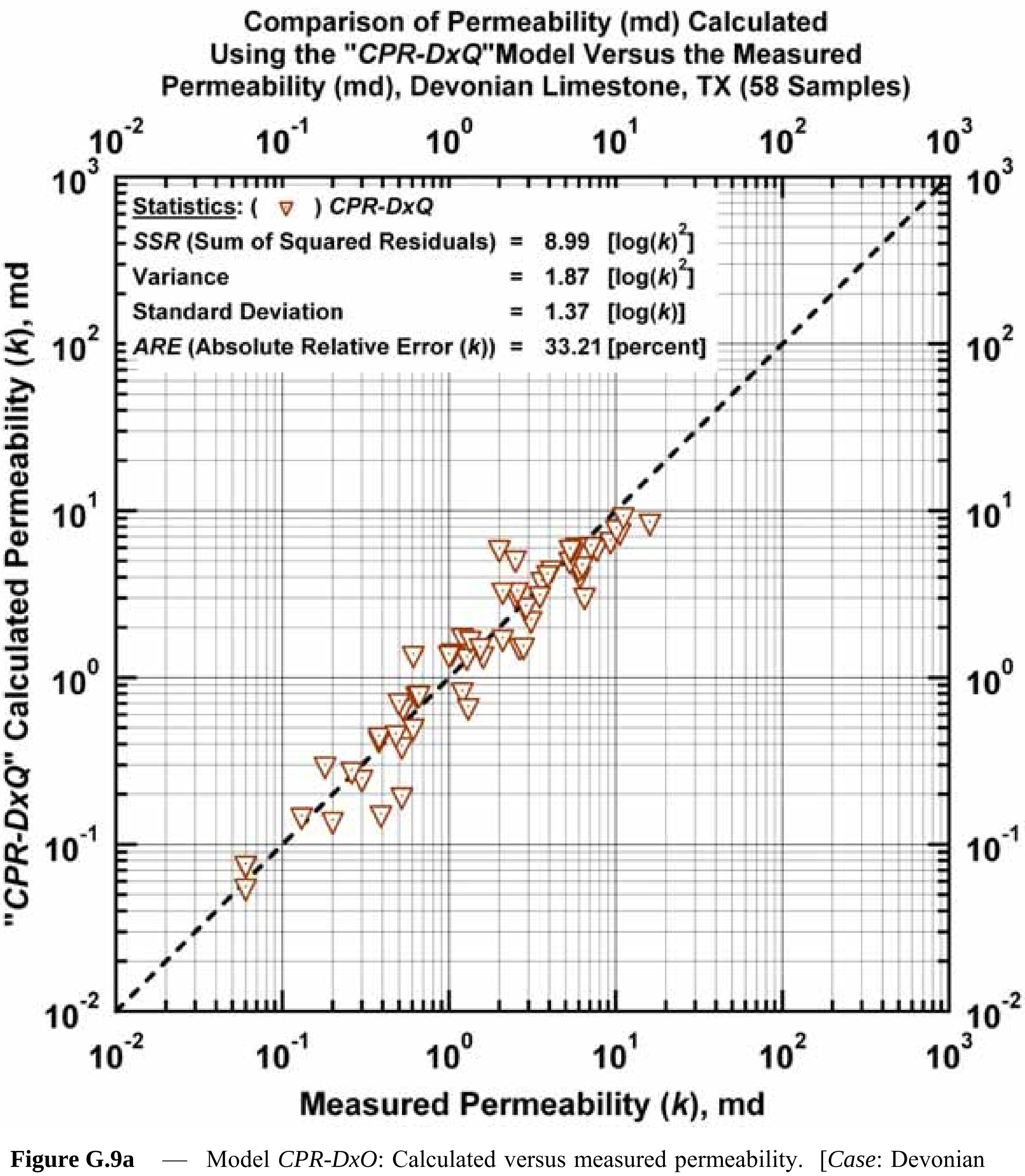

Figure G.9a — Model *CPR-DxO*: Calculated versus measured permeability. [*Case*: Devonian Limestone TX (USA)]

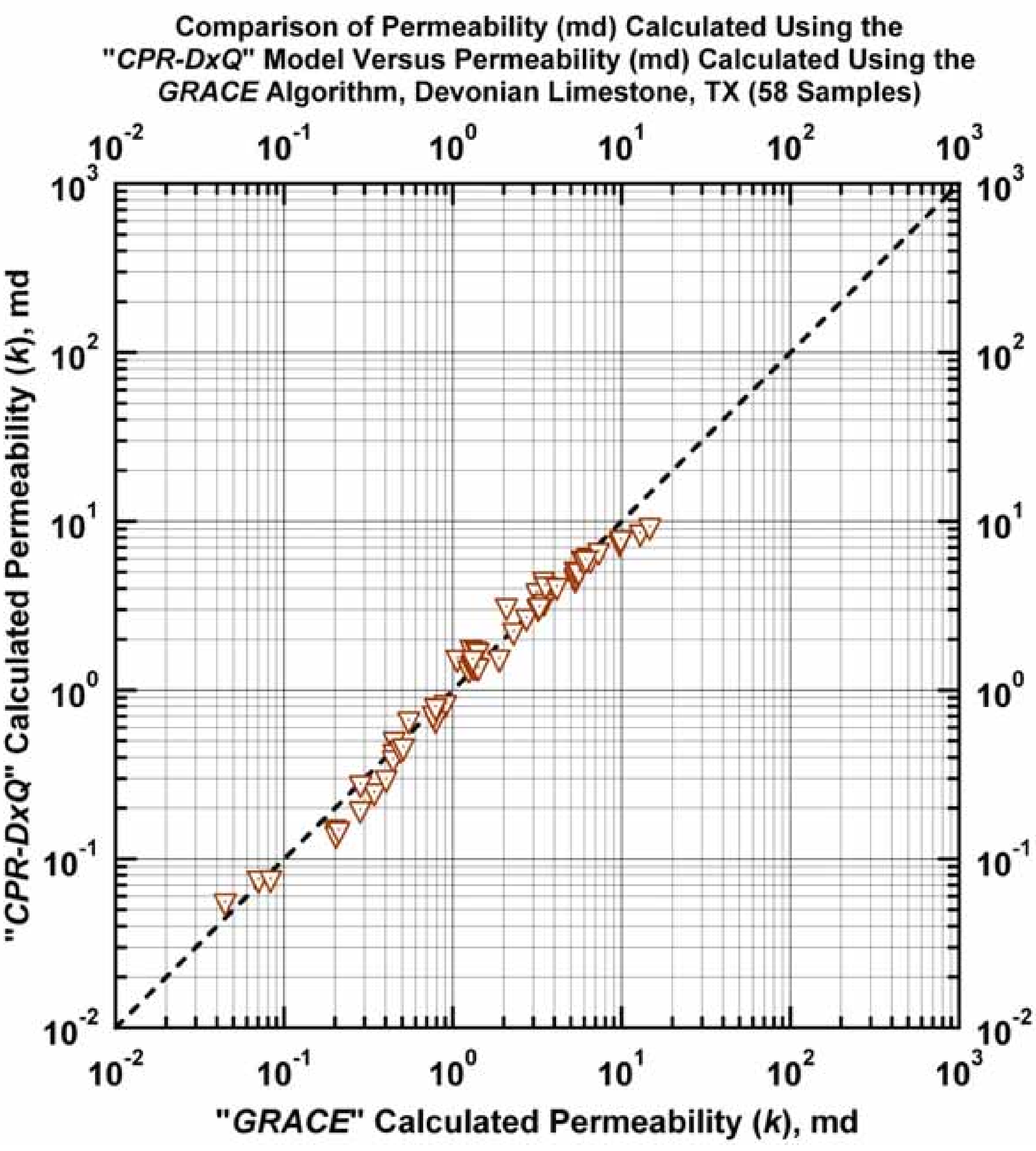

Figure G.9b — Model *CPR-DxQ*: Permeability calculated using Model *CPR-C* versus permeability calculated using the *GRACE* Algorithm. [*Case*: Devonian Limestone TX (USA)]

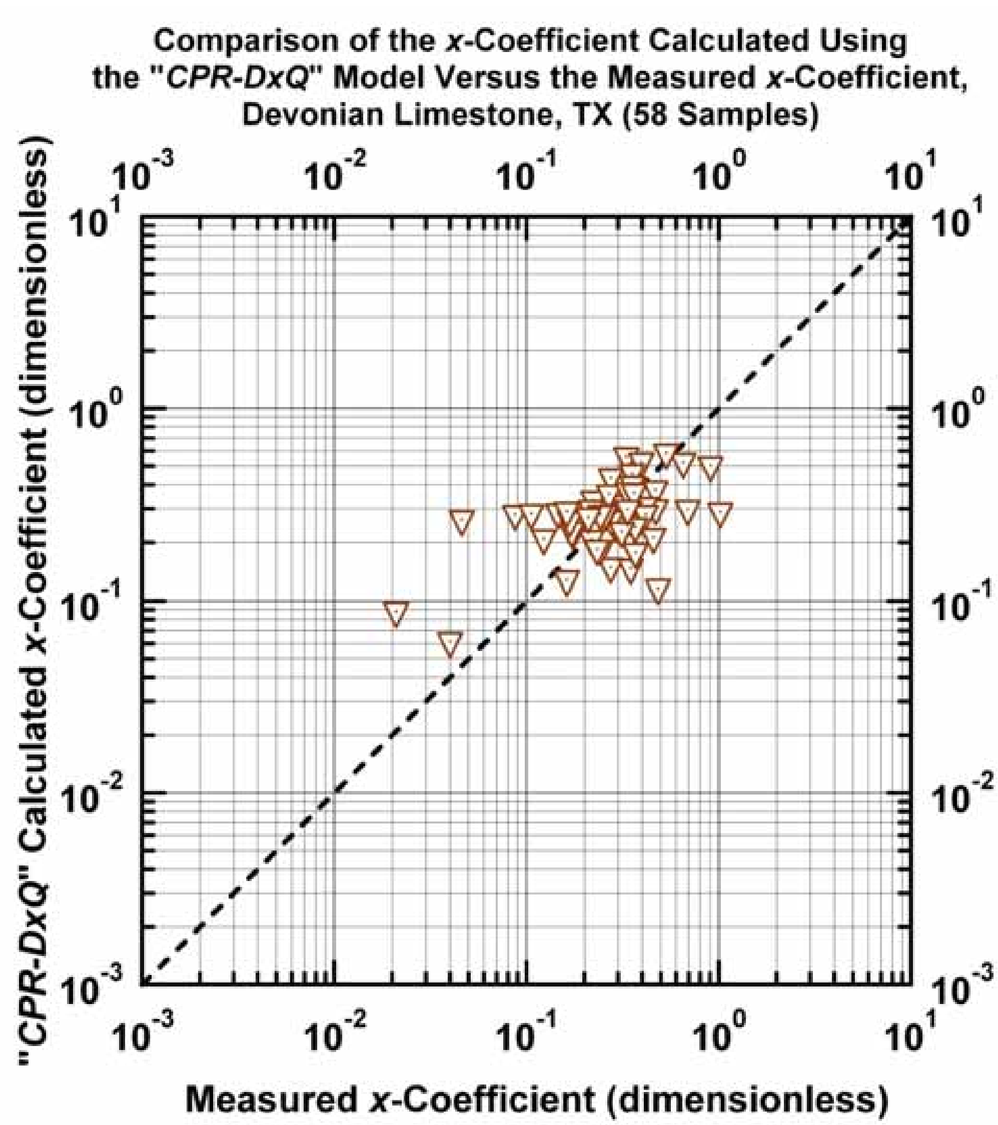

Figure G.9c — Model *CPR-DxQ*: Calculated *x*-function weight values versus measured *x*-function weight values. [*Case*: Devonian Limestone TX (USA)]

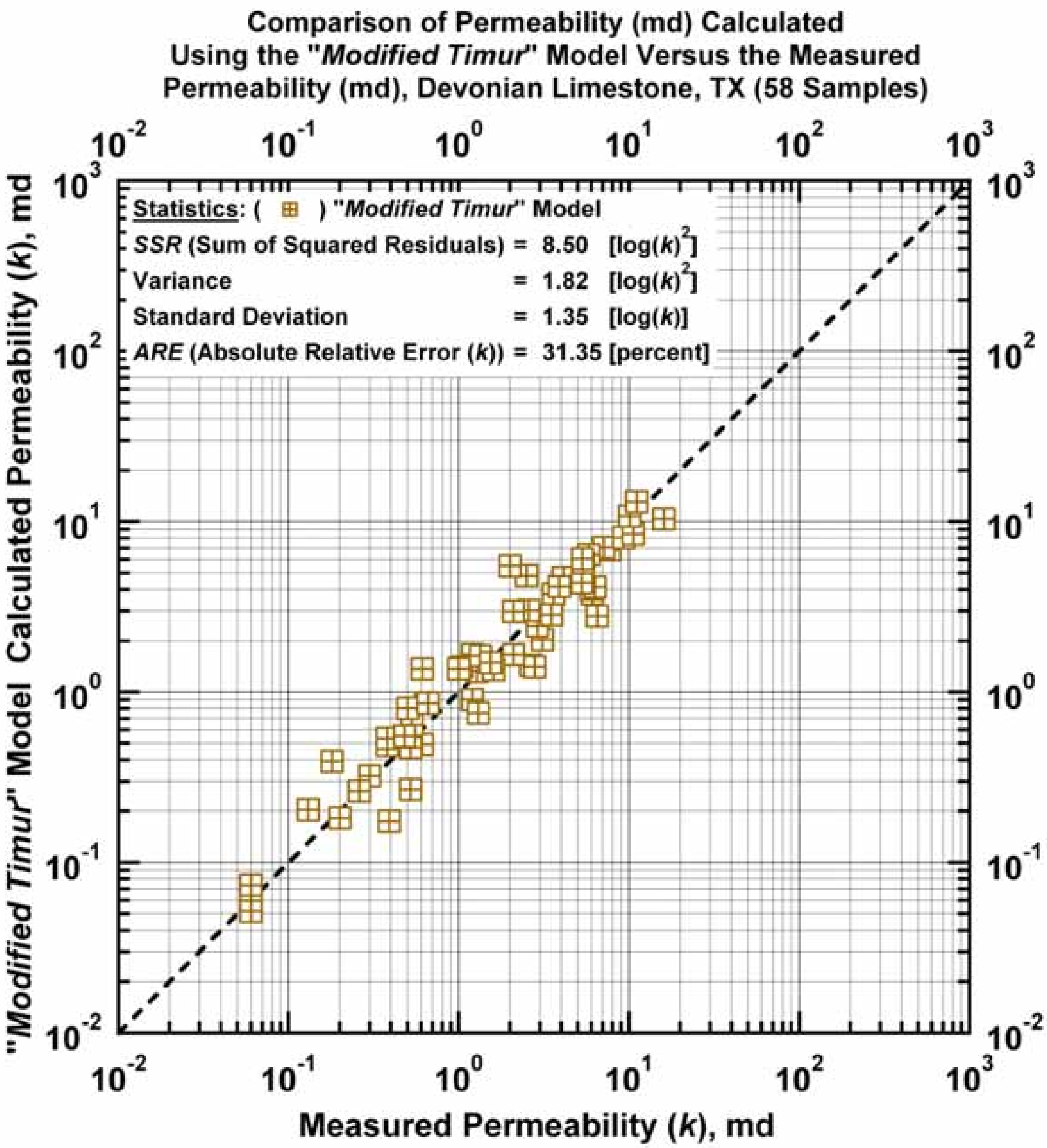

Figure G.10a — "Modified Timur Model:" Calculated versus measured permeability. [*Case*: Devonian Limestone TX (USA)]

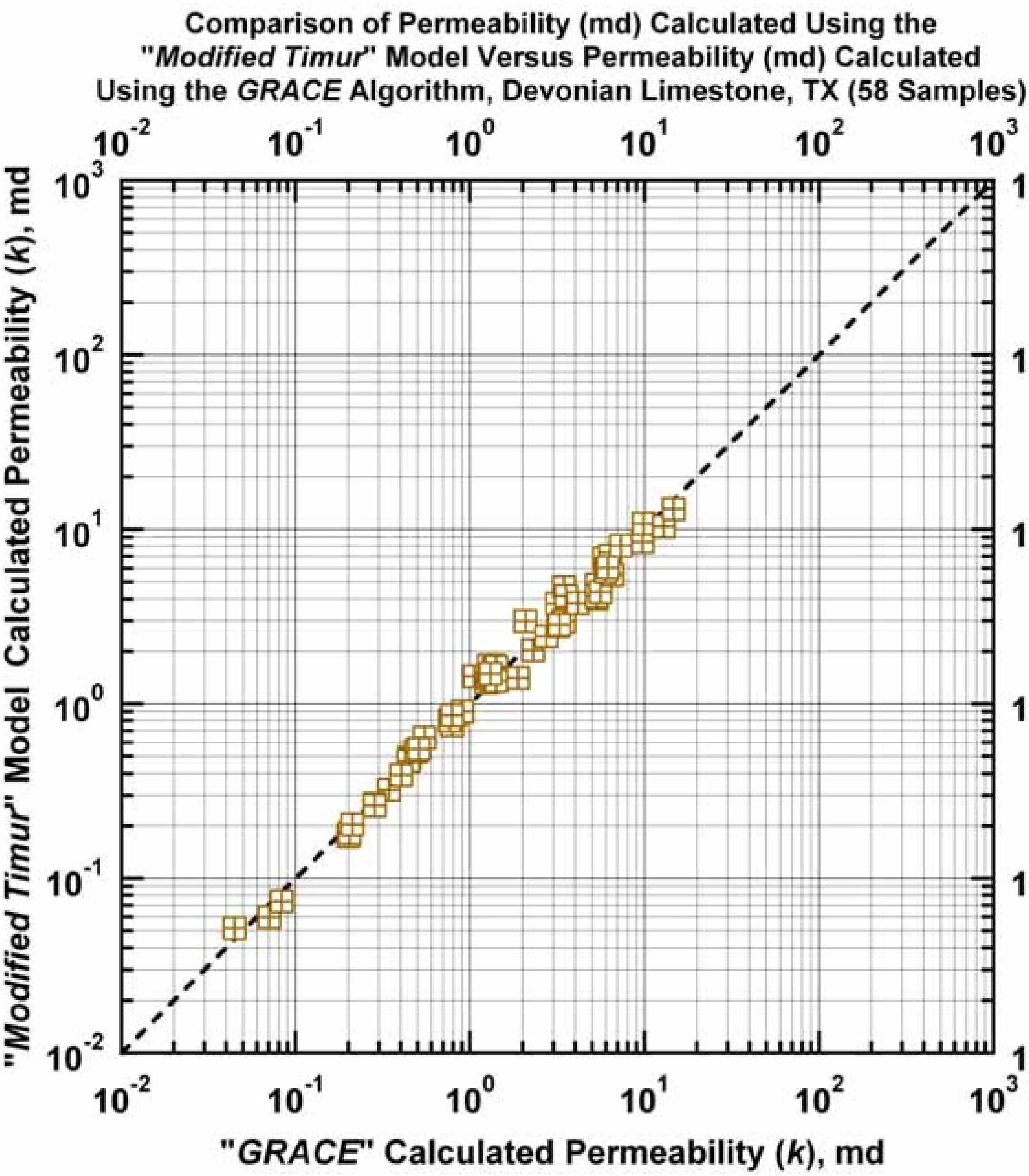

Figure G.10b — "Modified Timur Model:" Permeability calculated using the "Modified Timur Model" versus permeability calculated using the *GRACE* Algorithm. [*Case*: Devonian Limestone TX (USA)]

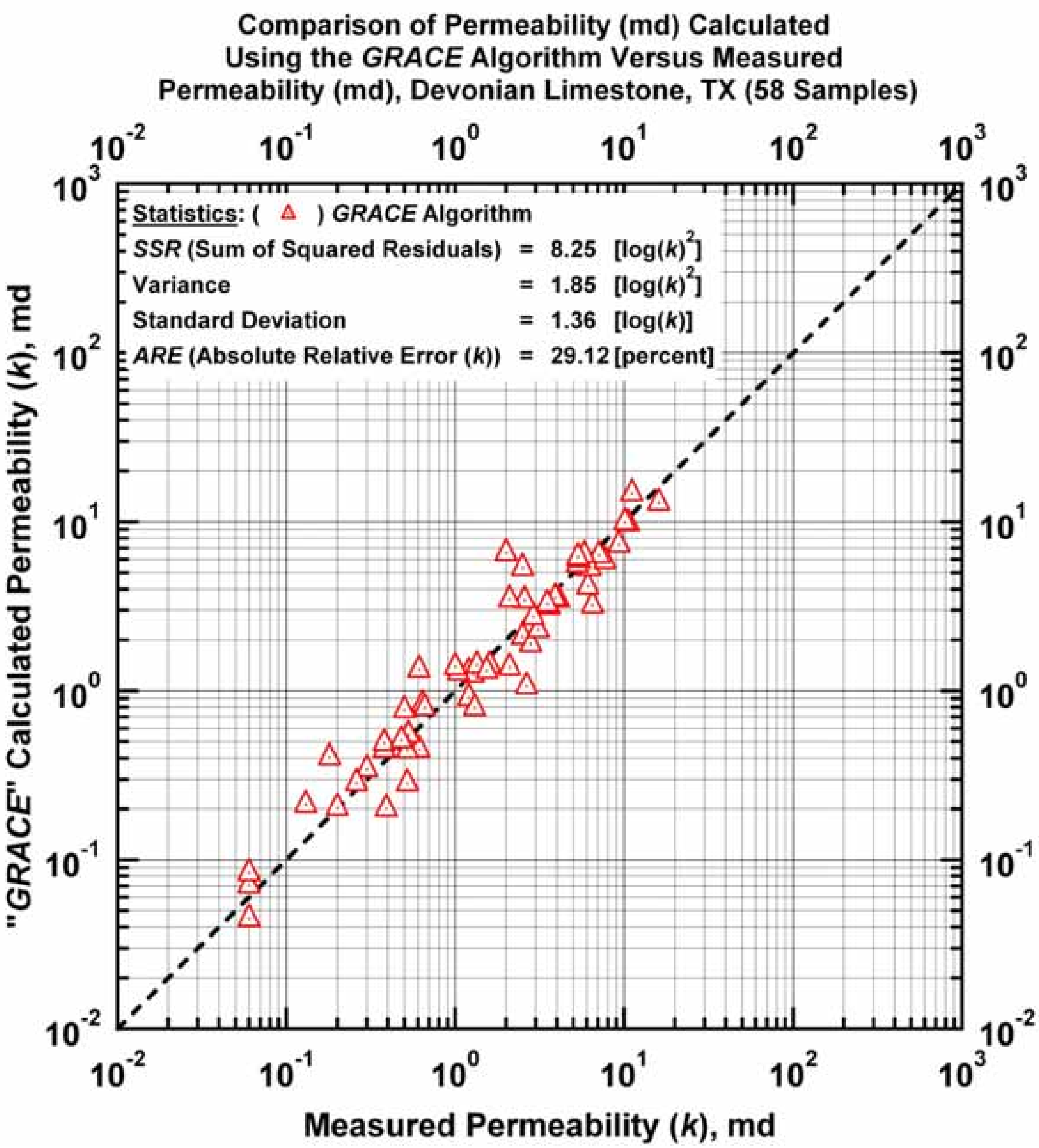

Figure G.11 — *GRACE* Model: Calculated versus measured permeability. [*Case*: Devonian Limestone TX (USA)]

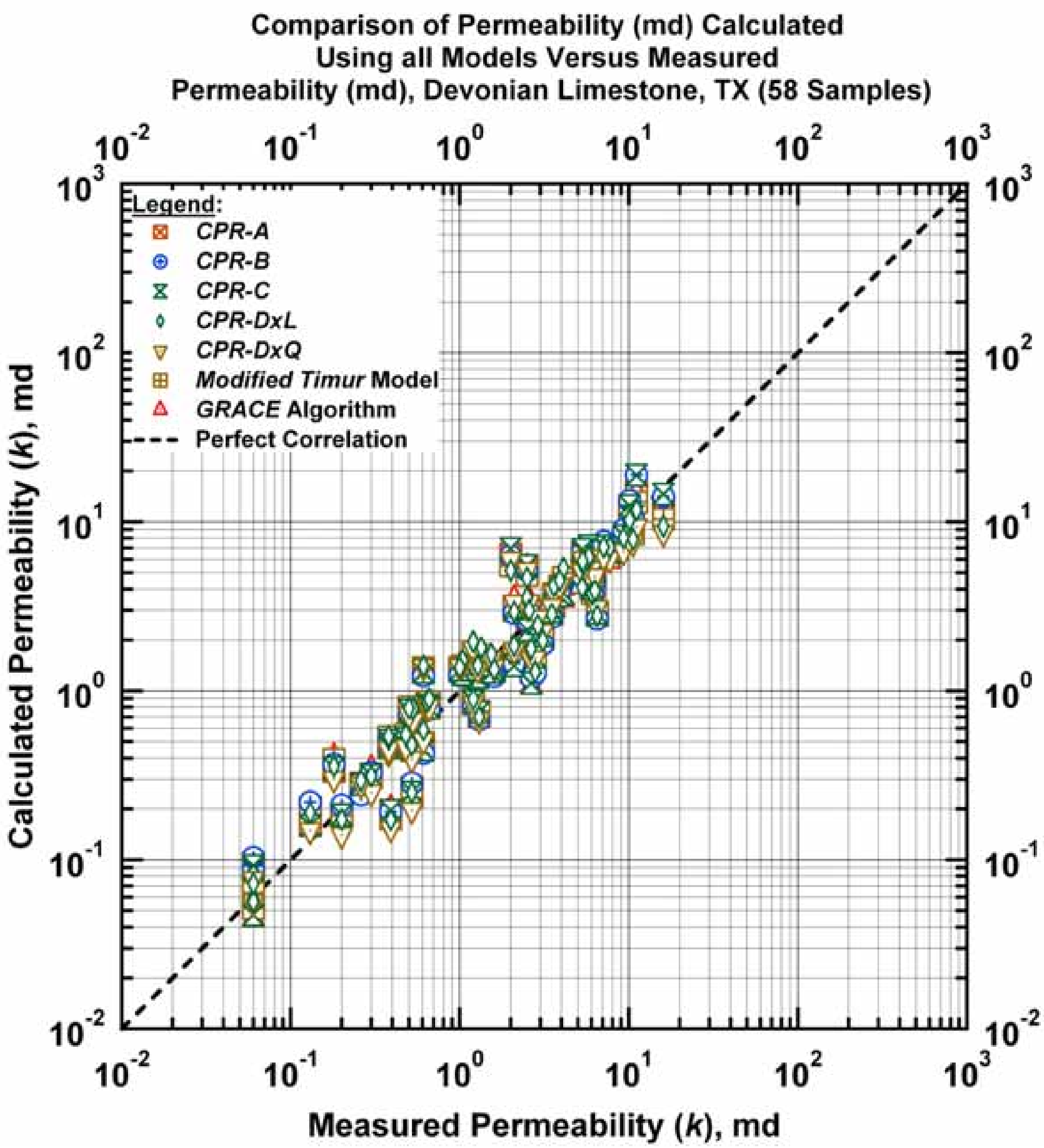

Figure G.12 — All Models: Calculated versus measured permeability. [*Case*: Devonian Limestone TX (USA)]

APPENDIX H

RESULTS FOR FRIO SHALY SANDSTONE (TEXAS — USA)

In this Appendix we present the "Frio" Well, located in Texas (USA) — this is a shaly sandstone reservoir (Ellis, 1987).

Model *CPR-A*: (Appendix H)

The "characteristic permeability relation" (or *CPR*) Model *CPR-A* (*i.e.*, the modified Archie "Clean Sand" Model) is given as:

$$k = a(\phi - c)^b \qquad c = c_{max} \exp[-c_1 \phi^{c_2} F^{c_3}] \text{ .... (H-1)}$$

Where a plot of log(k) versus log(ϕ) is used to graphically calibrate Eq. H-1 in terms of the coefficients — a, b, and c_{max}. In this case we had to remove some of the points from the original data set in order to better fit this equation. **Fig. H.1** shows that the *CPR-A* model performs quite well for this case. **Figs. H.1a and b** show the log-log and the semilog format of permeability versus porosity, respectively. In **Fig. H.2** we provide the "error" plots for this case, where the measured and computed data are compared systematically. In **Fig. H.2a** we note a good correlation of the results obtained using Model *CPR-A* versus the measured permeability data — we observe good agreement with the perfect correlation trend (*i.e.*, the 45-degree line). In **Fig. H.2b** we provide a comparison with the *GRACE* algorithm correlation (Xue *et al*. 1997)), and we note that the *CPR-A* model results correlate very well with the *GRACE* algorithm results for this case. Finally, in **Fig. H.2c** we present the calculated and measured c-function — and again we note a reasonable correlation of the data about the perfect correlation trend.

Model *CPR-B*: (Appendix H)

The "characteristic permeability relation" (or *CPR*) Model *CPR-B* (*i.e.*, the modified Archie "Dirty Sand" Model (power-law basis)) is given as:

$$k = a(\phi + c)^b \qquad c = c_{max} \exp[-c_1 \phi^{c_2} F^{c_3}] \text{ .... (H-2)}$$

Where a plot of log(k) versus log(ϕ) is used to graphically calibrate Eq. H-2 in terms of the coefficients — a, b, and c_{max}. The results for this case are presented in **Figs. H.3 and 4**. In **Fig. H.3a** (log-log format) we note that a very distinct "envelope" is formed by the *CPR-B* model, essentially all of the data on the right and left flanks are well-matched (*i.e.*, the "dirty sand" power law relation (applied on the right portion of the data) and its correction function (applied on the left portion of the data). Similarly, in **Fig. H.3b** (semilog format), we observe an excellent distribution of the power law model across the body of the data. The error analyses for this case are shown in **Fig. H.4**. In **Fig. H.4a** we present the results obtained using

Model *CPR-B* versus the measured permeability data and in this case there is good agreement with the perfect correlation trend (*i.e.*, the 45-degree line) — a few data points are out-lying, mostly in the middle of the trend. We provide a comparison with the *GRACE* algorithm correlation in **Fig. H.4b** — the results using Model *CPR-B* and the *GRACE* algorithm compare very well for this case. We compare the computed and data-derived values of the *c*-function for this case in **Fig. H.4c** and we note a reasonably "tight" correlation, except for the very lowest values of the *c*-function. In summary, we believe that Model *CPR-B* is a very effective correlation model for this particular data case.

Model *CPR-C*: (Appendix H)

The "characteristic permeability relation" (or *CPR*) Model *CPR-C* (*i.e.*, the modified Archie "Dirty Sand" Model (exponential basis)) is given as:

$$k = c\exp[\beta\phi] \quad c = c_{\max}\exp[-c_1\phi^{c_2}F^{c_3}] \text{ .... (H-3)}$$

Where a plot of log(k) versus ϕ is used to graphically calibrate Eq. H-3 in terms of the coefficients — β and $c_{\max}$. Model *CPR-C* is fundamentally different than Models *CPR-A* and *CPR-B*, as the basis for Model *CPR-C* is an exponential function, not a power law relation. In **Figs. H.5 and 6**, we present the results of applying Model *CPR-C* for this case, and in general, we observe a very consistent performance of Model *CPR-C*. **Fig. H.5b** illustrates the excellent conformance of Model *CPR-C* for this case — again recalling that this model has an exponential relationship with porosity as its basis.

In **Figs. H.6a, H.6b, and H.6c** we review the error analyses plots for this case, and we note good performance (visually) in terms of the correlation of the results using Model *CPR-C*. In this case, the *c*-function (in Eq. H-3) is not a correction term, but rather the instantaneous intercept for the exponential basis. The correlation of the *c*-function (see **Fig. H.6c**) appears to be consistent — but scatter and a slight off-center trend is evident. We believe that the *CPR-C* model has performed well for this case, and the **Fig. H.6** confirms the value of this model as a "characteristic relation" for permeability.

Model *CPR-D*: (Appendix H)

The "characteristic permeability relation" (or *CPR*) Model *CPR-D* (*i.e.*, the weighted power law-exponential model) is given in its fundamental form as:

$$k = xa\phi^{b} + (1-x)\alpha\exp[\beta\phi] \quad [0 \le x \le 1]] \text{ .... (H-4a)}$$

For Eq. H-4 there are two proposed models for the *x*-function (*i.e.*, the weighting function) — these are:

$$x = \exp[-\ln(x_0) + x_1\ln(\phi) + x_2\ln(F) + x_3\ln(\phi)\ln(F)] \text{ (Model } \textit{CPR-DxL}\text{) .... (H-4b)}$$

$$x = \exp\begin{bmatrix} -\ln(x_0) + x_1\ln(\phi) + x_2\ln(F) + x_3\ln(\phi)\ln(F) \\ + x_4\ln(\phi)^2 + x_5\ln(F)^2 + x_6\ln(\phi)^2\ln(F) \\ + x_7\ln(\phi)\ln(F)^2 + x_8\ln(\phi)^2\ln(F)^2 \end{bmatrix} \text{(Model } \textit{CPR-DxL}\text{) .... (H-4c)}$$

As noted in Eq. H-4b, Model *CPR-DxL* utilizes a logarithmic linear model for the weights (x-values) and as seen in Eq. H-4c, Model *CPR-DxQ* utilizes a logarithmic quadratic model for the weights (x-values). While these models (Eqs. H-4b and H-4c) are *empirical*, we have found generally good application of these relations for all cases. In this case, the base results using Models *CPR-DxL* and *CPR-DxQ* are presented in **Fig. H.7** — where the power law and exponential basis functions are fitted to the appropriate portion of the data. The power law equation represents the "Archie clean sand" trend and is fitted to the leftmost data as shown in **Fig. H.7a** and in contrast, the exponential equation is thought to represent the "Archie dirty sand" trend and the exponential is fitted to the far rightmost portion of the data (see **Fig. H.7b**).

In **Figs. H.8 and 9** we present the error analyses for this case, where we have employed the weighting functions (Eqs. H-4b and H-4c) as appropriate. In **Fig. H.8a** we find a good correlation of permeability (with the out-lying points noted in the middle of the trend). The comparison of the Model *CPR-DxL* results are compared to the results obtained from the *GRACE* algorithm in **Fig. H.8b**, we note the good results obtained using Model *CPR-DxL*. The computed weight function (x-values) shown for the *CPR-DxL* model in **Fig. H.8c** does exhibit more scatter than expected, but the trend is (relatively) centered about the perfect correlation line.

The results obtained using Model *CPR-DxQ* are presented in **Fig. H.9**, and we note substantially improved behavior over that of Model *CPR-DxL*. In particular, the base correlation of computed and measured permeabilities (**Fig. H.9a**) for Model *CPR-DxQ* does indicate a slightly better correlation than that of Model *CPR-DxL*. Also, the comparison of Model *CPR-DxQ* with the results from the *GRACE* algorithm (**Fig. H.9b**) exhibits better agreement than the results of Model *CPR-DxL*. Finally, the correlation of the x-function (**Fig. H.9c**) for Model *CPR-DxQ* is better than the correlation for Model *CPR-DxL*. These comparisons suggest that Model *CPR-DxQ* (*i.e.*, the combination of Eqs. H-4a and H-4c) provides a better correlation of data, for this case, than Model *CPR-DxL*.

***"Modified Timur Model"*: (Appendix H)**

The "Modified Timur Model" is given as:

$$k_{\text{Timur}} = a\phi^b F^c \qquad \text{(H-5)}$$

In **Fig. H.10** we present the results of the "Modified Timur Model" (Eq. H-5) which is essentially just a generalized power-law function relation in terms of k, ϕ, and F. **Figs. H.10a and b**, provide the "Modified Timur Model" results of the data for this case.

***GRACE* Algorithm: (Appendix H)**

In **Fig. H.11** we present the results predicted by the *GRACE* algorithm, which is a non-parametric regression approach (see Xue *et al.* (1997) for details). In theory, the *GRACE* algorithm should provide the most *unbiased* correlation of the data — *i.e.*, the *GRACE* algorithm is designed not to "fit the errors" as other regression approaches may. It is our contention that the *GRACE* algorithm is the statistical standard — and any algorithm/approach/model which achieves better regression statistics than the *GRACE* algorithm is actually "fitting the errors" in the data. *The only case which has significantly better regression statistics than the GRACE algorithm is the CPR-A* — but we must remember that for this case we used fewer number of points.

***Comparison of All Models*: (Appendix H)**

Our final graphic, **Fig. H.12**, illustrates all of the models on a single plot of calculated versus measured permeability. We also present a table of all statistical results in **Table H.1**.

Table H.1 — Statistical Results for all Models (Frio, TX (USA), *n*=64).

Model	Sum of Squared Residuals [log(k)^2]	Variance [log(k)^2]	Standard Deviation [log(k)]	Absolute Relative Error [percent]
CPR-A	59.49	4.57	2.14	78.38
CPR-B	67.78	5.76	2.40	99.21
CPR-C	57.11	5.59	2.36	100.09
CPR-DxL	58.80	5.31	2.30	103.74
CPR-DxQ	54.49	5.52	2.35	88.71
Modified Timur	71.00	6.12	2.47	134.64
GRACE Algorithm	51.94	5.50	2.35	88.99

The coefficients for the models used in this case are provided in **Table H.2**.

Table H.2a — Model Coefficients (Frio, TX (USA), *n*=64).

Model	a or α	b or β	c or c_{max}	c_1	c_2	c_3
CPR-A	5.00x10^{11}	12.00	0.100	4.14x10^{-3}	-4.89	-0.97
CPR-B	1.00x10^{14}	20.00	0.135	28.25	2.67	0.40
CPR-C	7.00x10^{-5}	50.00	5.00x10^{-3}	11.969	4.32	1.48
Modified Timur	1.00x10^{7}	0.17	-3.8271	–	–	–

Table H.2b — Model Coefficients (Frio, TX (USA), *n*=64).

Model	a	b	α	β
CPR-DxL	5.00x10^{6}	6.00	7.00x10^{-5}	50.00
CPR-DxQ	5.00x10^{6}	6.00	7.00x10^{-5}	50.00

Model	c_0	c_1	c_2	c_3	c_4	c_5	c_6	c_7	c_8
CPR-DxL	2.42x10^{-4}	1.02	-5.07	-1.37	–	–	–	–	–
CPR-DxQ	1.49x10^{6}	-53.45	-11.82	7.23	-16.87	1.90	3.40	2.65x10^{-3}	-0.12

Nomenclature: (Appendix H)

F = Archie Formation Factor (dimensionless)
k = Formation Permeability, md (or any consistent units)
ϕ = Porosity, fraction

References: (Appendix H)

Ellis, K.W.: "Extended Correlations of Porosity, Permeability, and Formation Resistivity Factor," MS thesis, Texas A&M U., College Station, TX (1987).

Xue, G., Datta-Gupta, A., Valko, H., and Blasingame, T.A.: "Optimal Transformations for Multiple Regression: Application to Permeability Estimation from Well Logs," *SPEFE* (June 1997), 85-93.

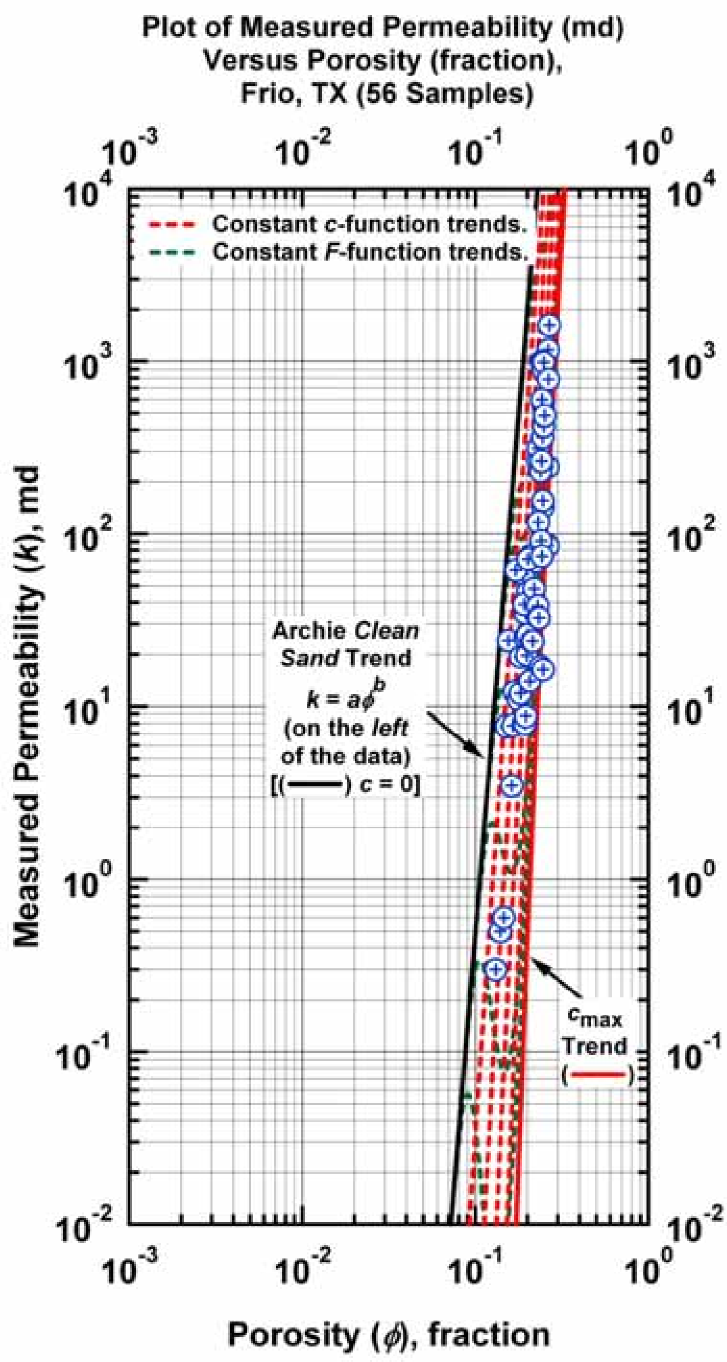

Figure H.1a — Model *CPR-A*: $k = a(\phi - c)^b$ ($c = c_{\max} \exp[-c_1 \phi^{c2} F^{c3}]$) — "Clean Sand" Plot (log-log format) — Archie "Clean Sand" trend is given by the straight-line trend at the far left of the data (power law model). [*Case*: Frio, TX (USA)]

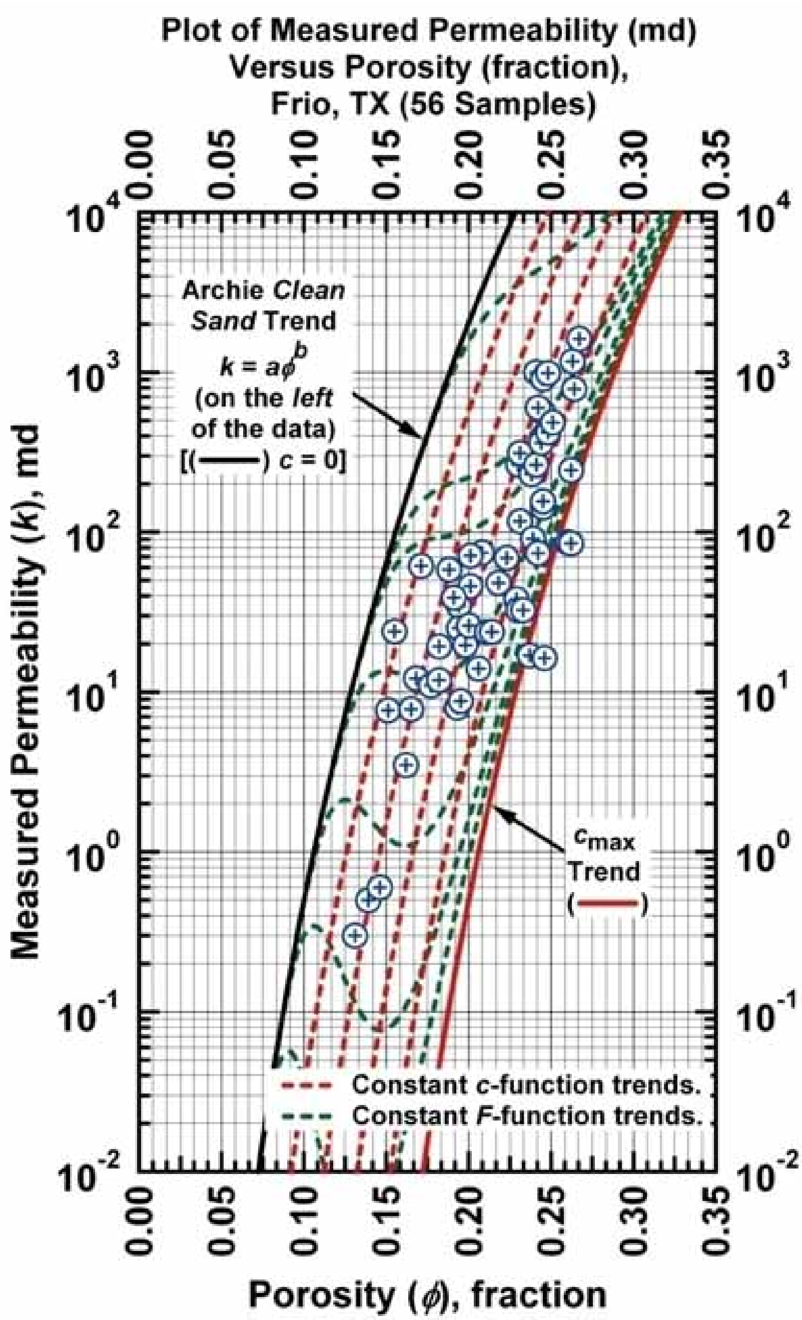

Figure H.1b — Model *CPR-A*: $k = a(\phi - c)^b$ ($c = c_{max}\exp[-c_1\phi^{c_2}F^{c_3}]$) — "Dirty Sand" Plot (semilog format). Archie "Clean Sand" trend is given by the curved trend at the far left of the data (power law model). [*Case*: Frio, TX (USA)]

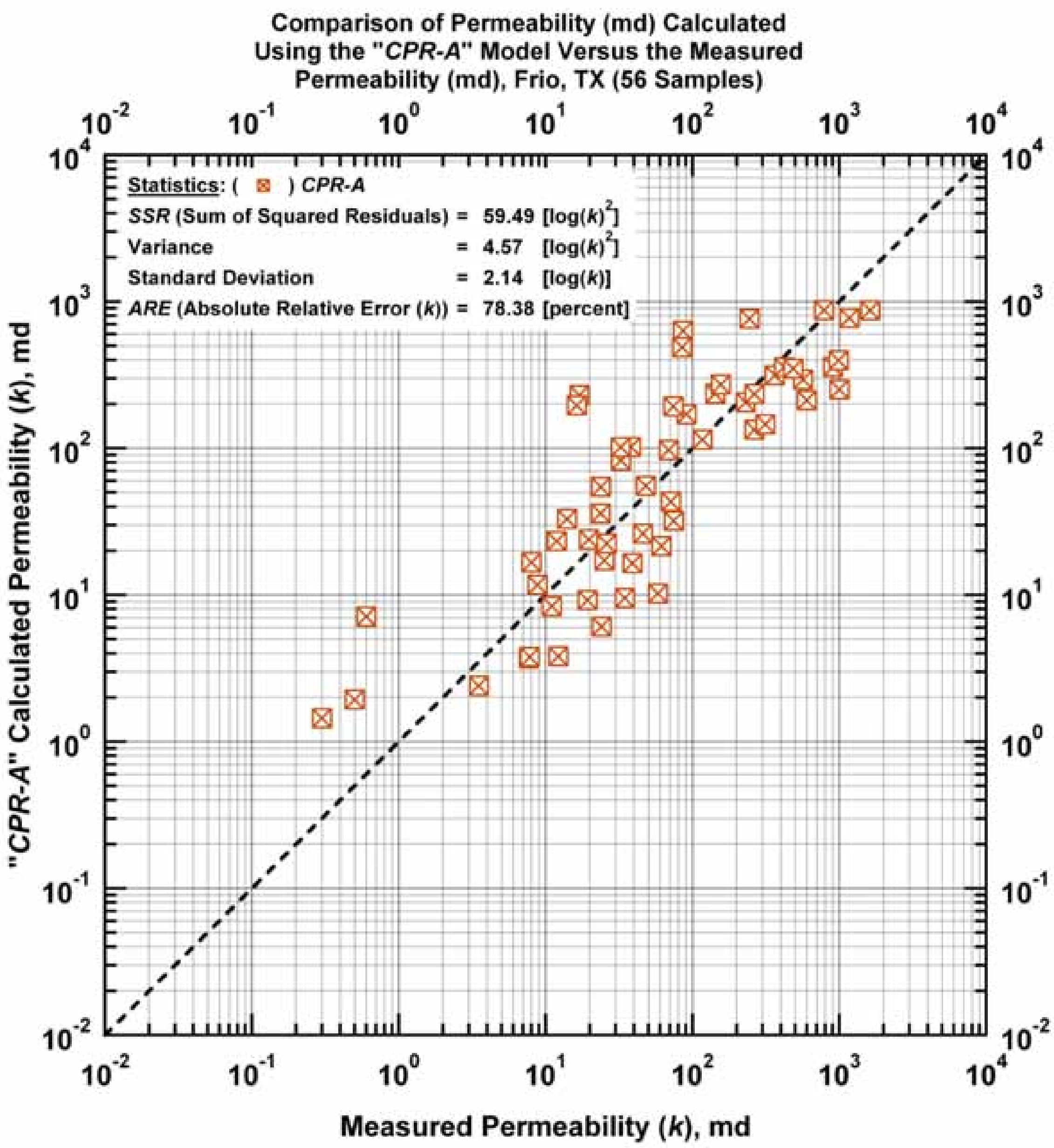

Figure H.2a — Model *CPR-A*: calculated versus measured permeability. [*Case*: Frio, TX (USA)]

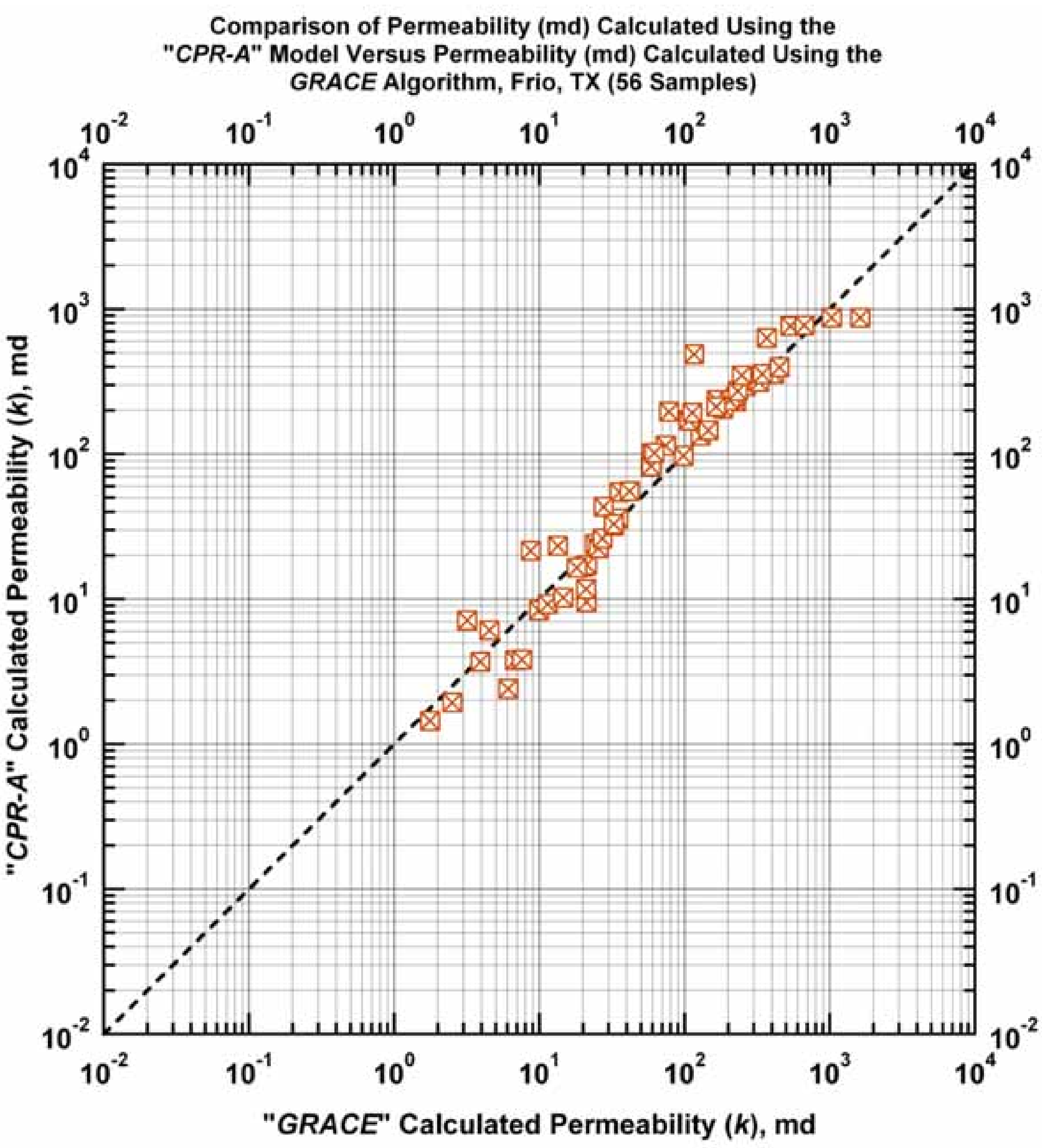

Figure H.2b — Model *CPR-A*: Permeability calculated using Model *CPR-A* versus permeability calculated using the *GRACE* Algorithm. [*Case*: Frio, TX (USA)]

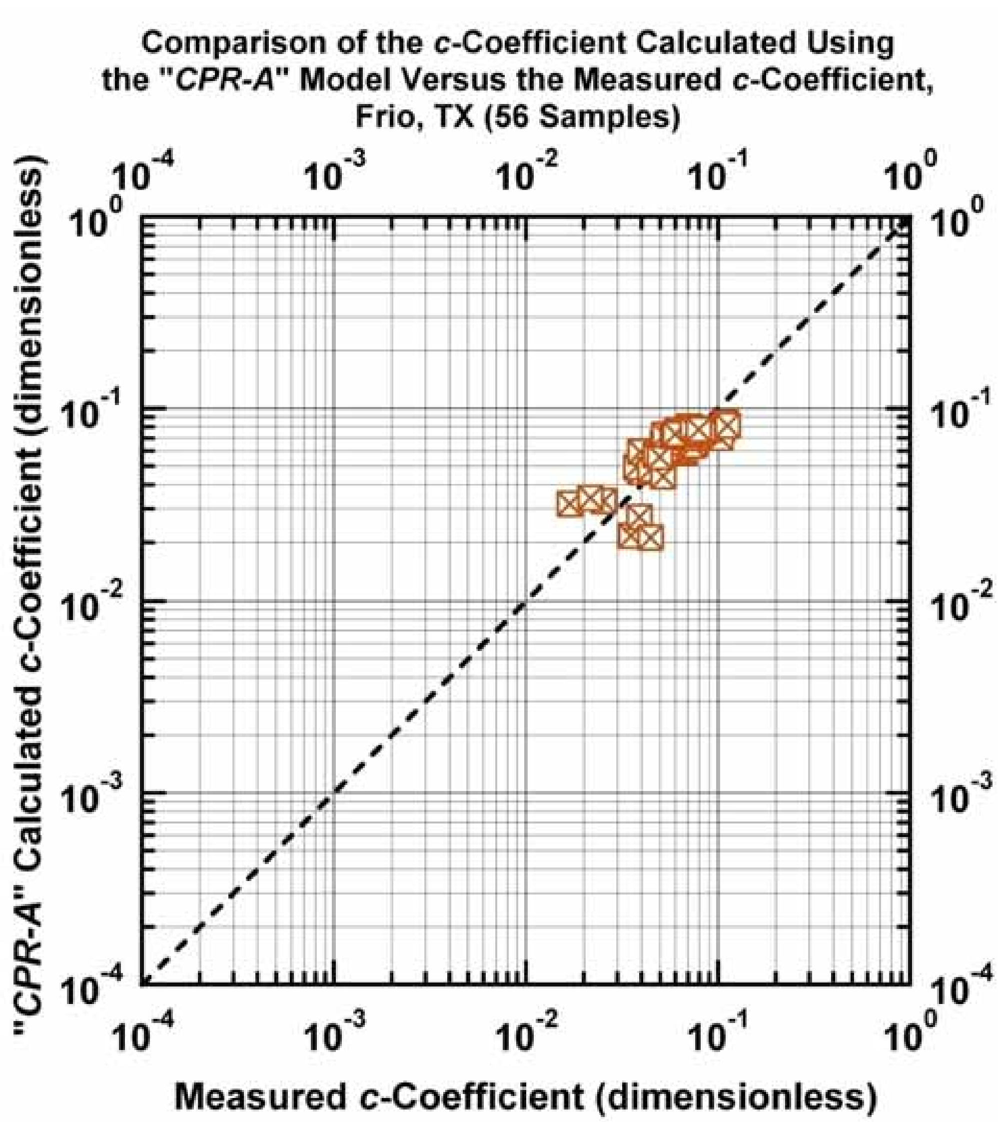

Figure H.2c — Model *CPR-A*: Calculated *c*-function values versus measured *c*-function values. [*Case*: Frio, TX (USA)]

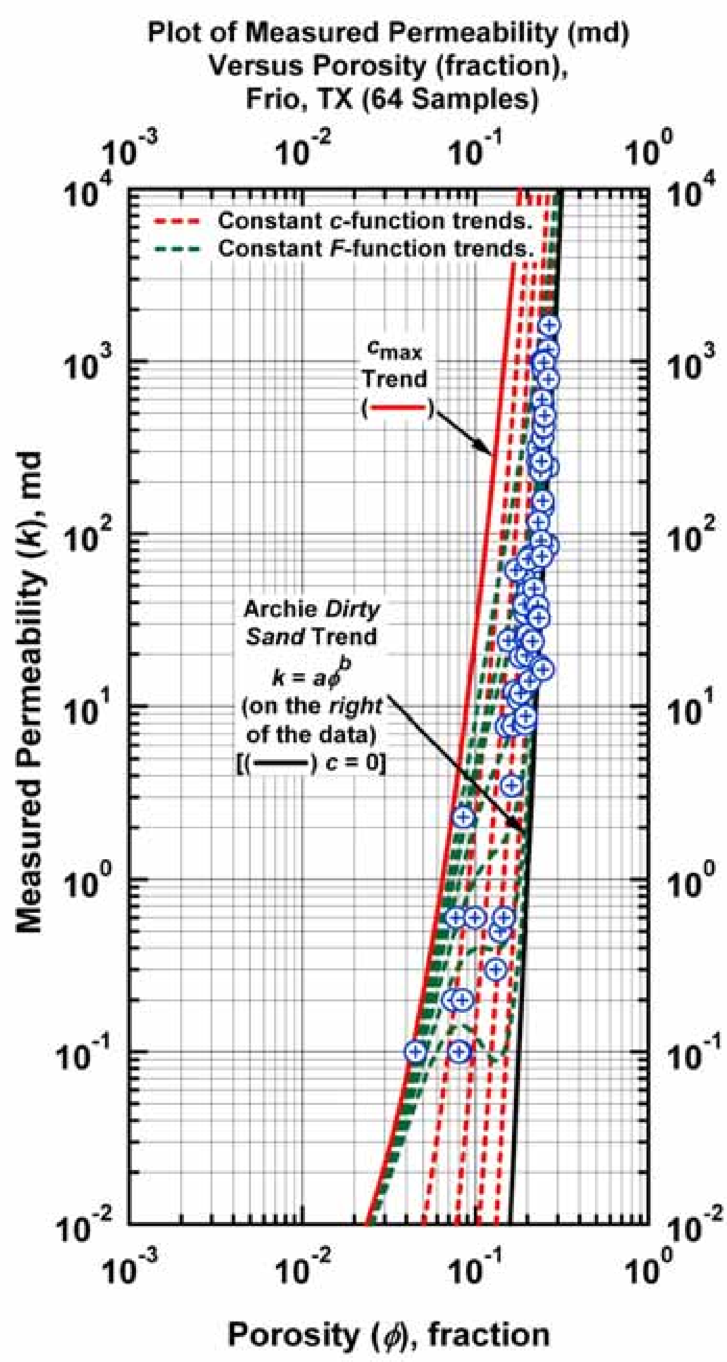

Figure H.3a — Model *CPR-B*: $k = a(\phi + c)^b \quad c = c_{max} \exp[-c_1 \phi^{c_2} F^{c_3}]$ — "Clean Sand" Plot (log-log format) — Archie "Dirty Sand" trend is given by the straight-line trend at the far right of the data (power law model). [*Case*: Frio, TX (USA)]

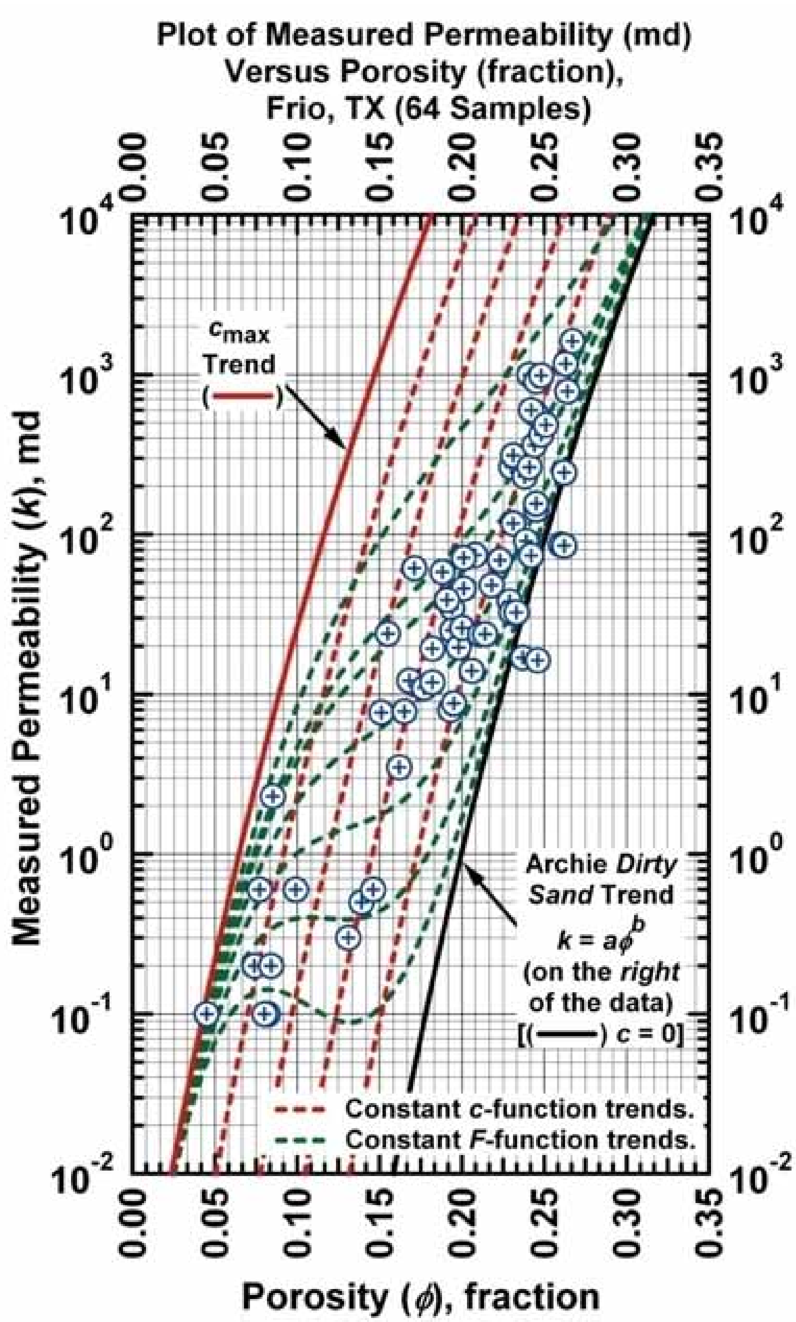

Figure H.3b — Model *CPR-B*: $k = a(\phi + c)^b$ $\quad c = c_{max} \exp[-c_1\phi^{c2} F^{c3}]$ — "Dirty Sand" Plot (semilog format) — Archie "Dirty Sand" trend is given by the curved trend at the far right of the data (power law model). [*Case*: Frio, TX (USA)]

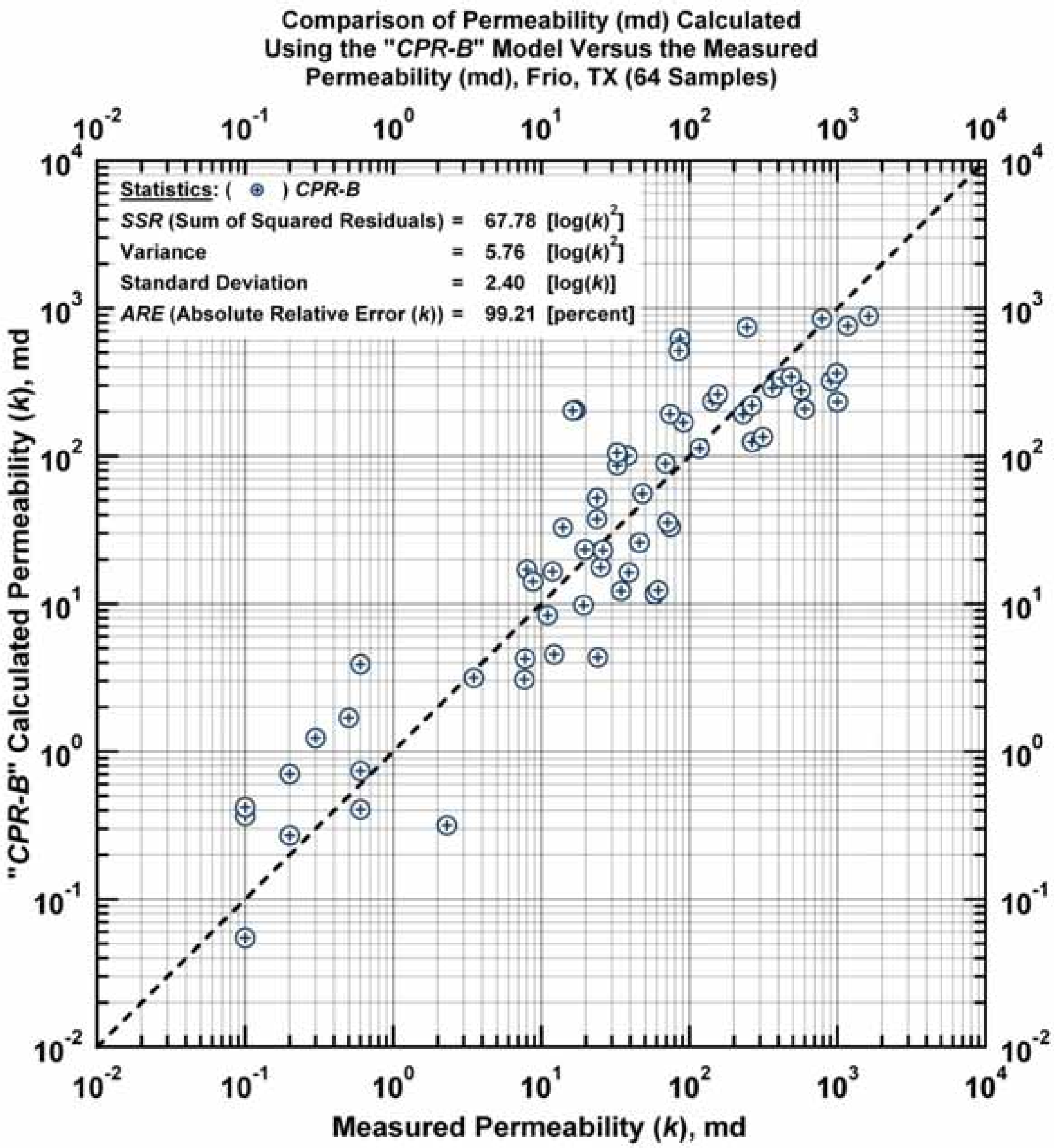

Figure H.4a — Model *CPR-B*: calculated versus measured permeability. [*Case*: Frio, TX (USA)]

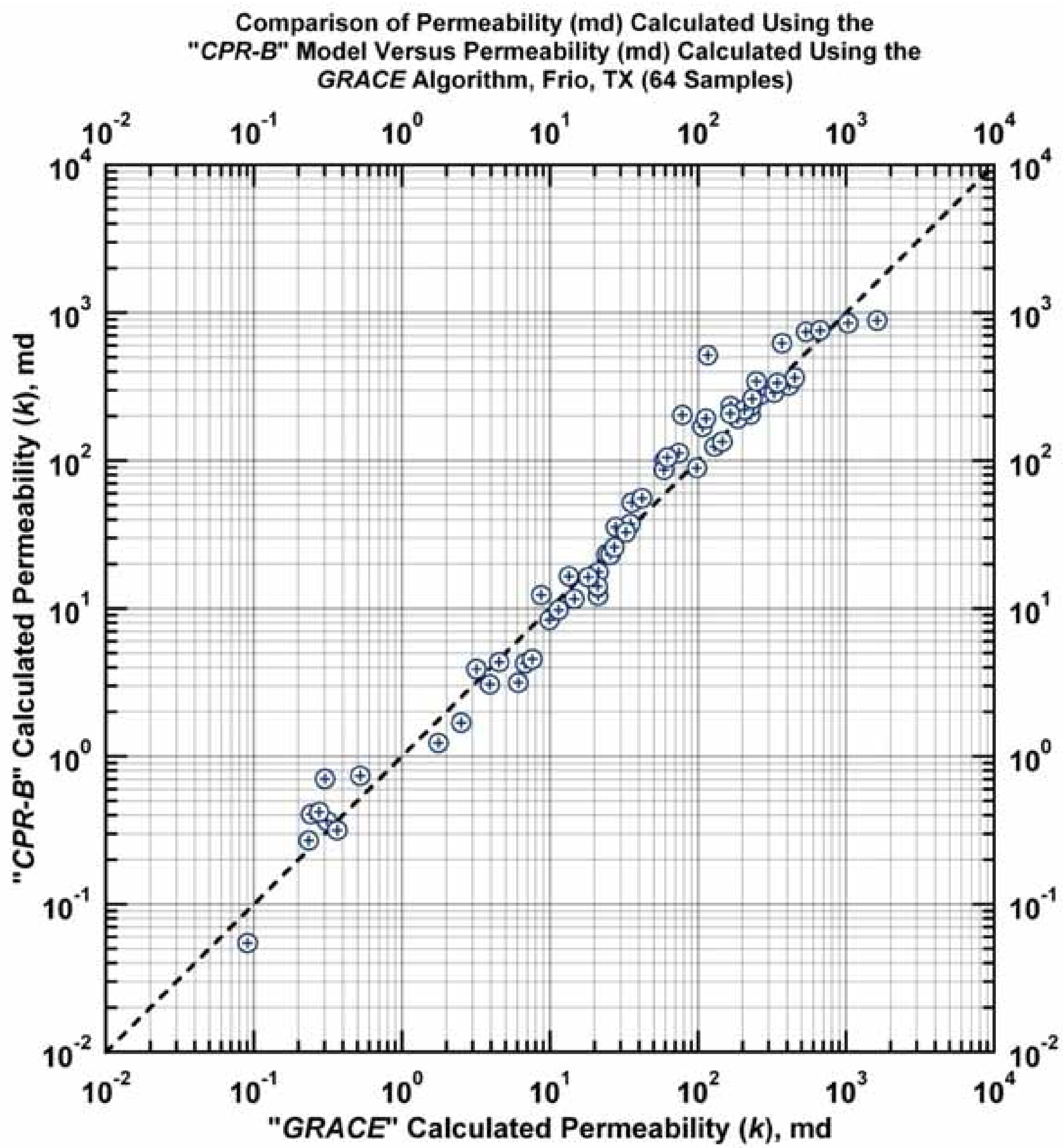

Figure H.4b — Model *CPR-B*: Permeability calculated using Model *CPR-B* versus permeability calculated using the *GRACE* Algorithm. [*Case*: Frio, TX (USA)]

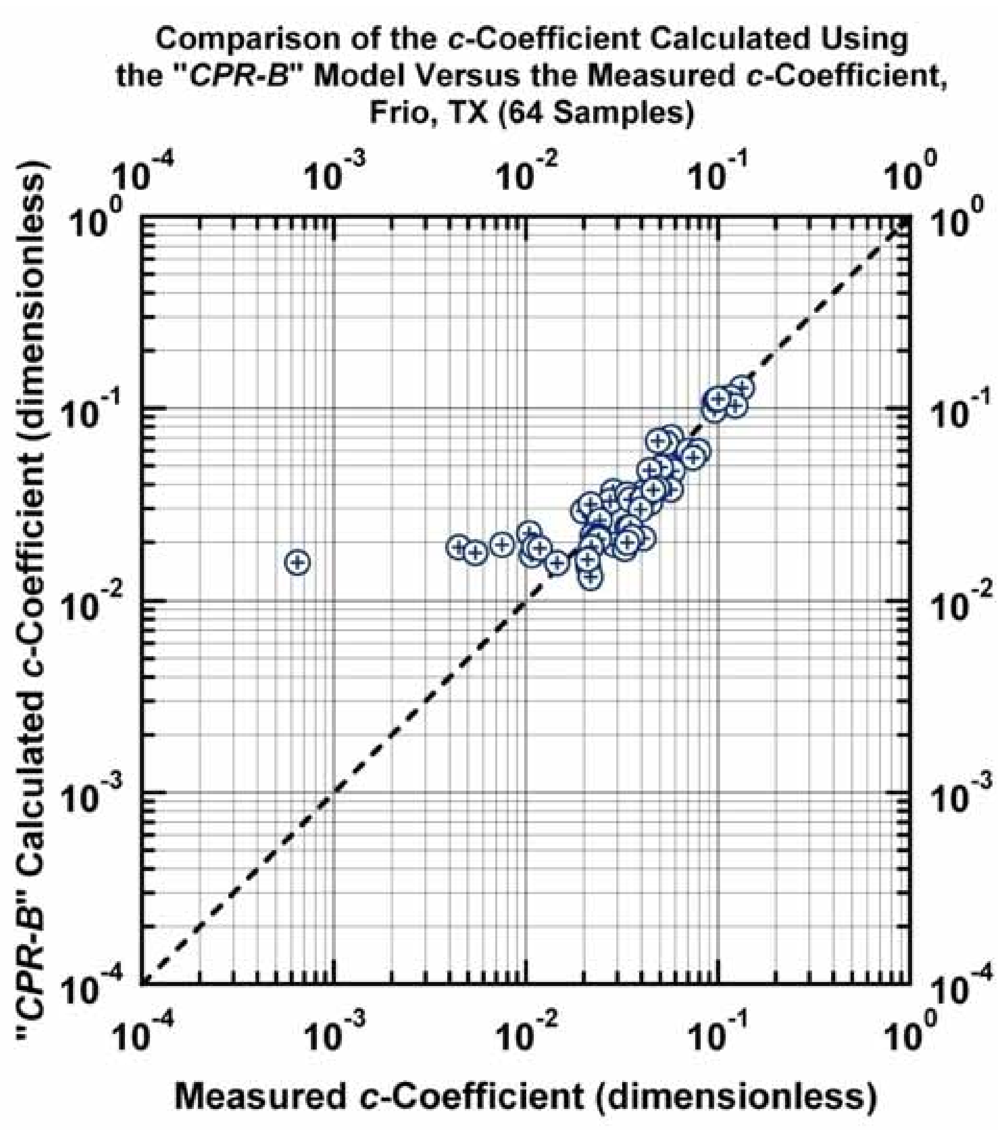

Figure H.4c — Model *CPR-B*: Calculated *c*-function values versus measured *c*-function values. [*Case*: Frio, TX (USA)]

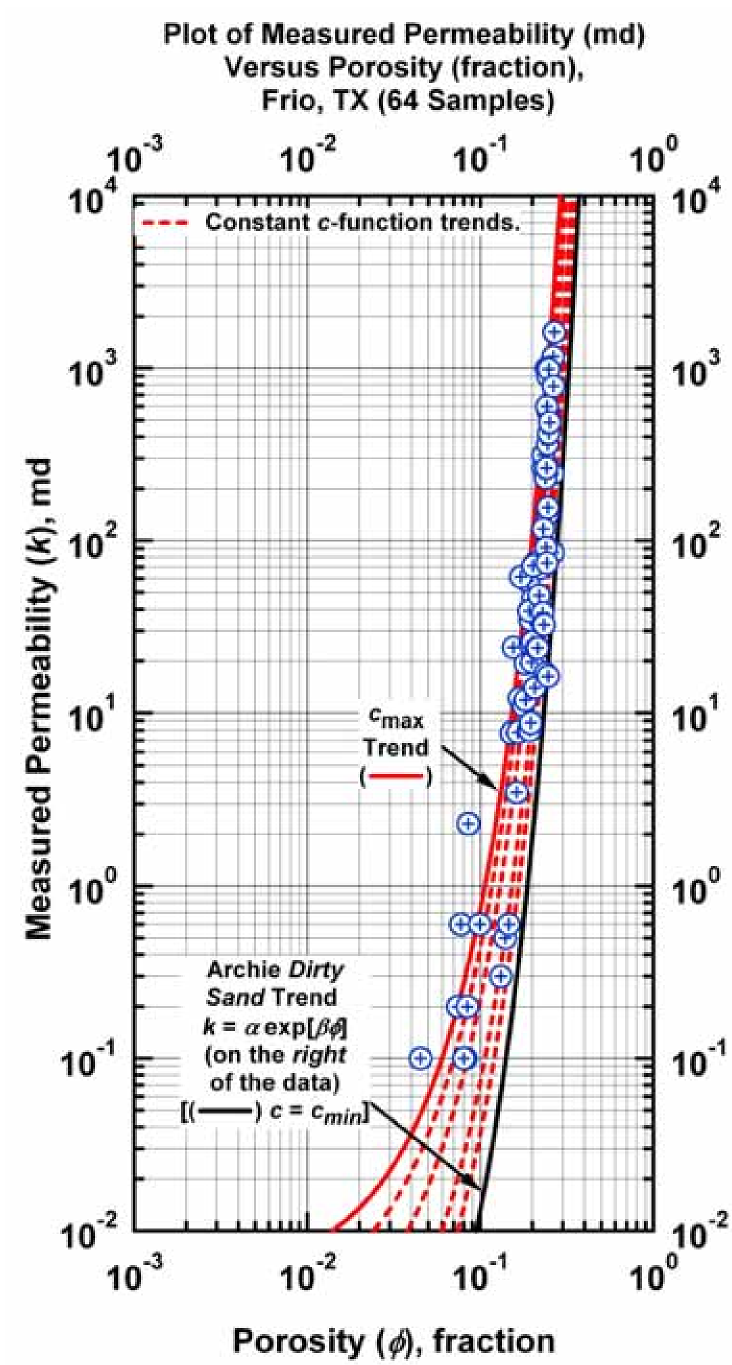

Figure H.5a — Model *CPR-C*: $k = c\exp[\beta\phi]$ $\quad c = c_{\max}\exp[-c_1\phi^{c_2}F^{c_3}]$ — "Clean Sand" Plot (log-log format) — Archie "Dirty Sand" trend is given by the curved trend at the far right of the data (exponential model). [*Case*: Frio, TX (USA)]

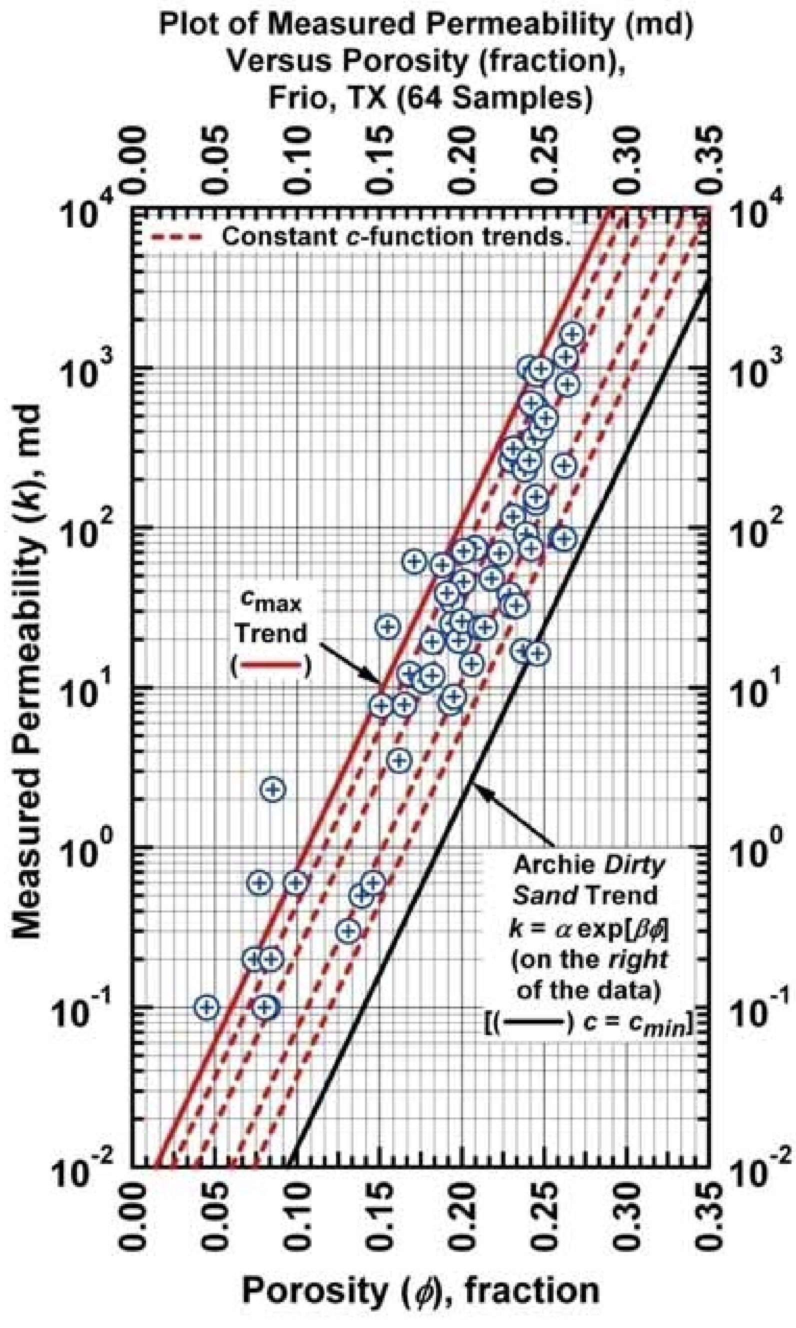

Figure H.5b — Model *CPR-C*: $k = c\exp[\beta\phi]$ $\quad c = c_{\max}\exp[-c_1\phi^{c_2}F^{c_3}]$ — "Dirty Sand" Plot (semilog format) — Archie "Dirty Sand" trend is given by the straight-line trend at the far right of the data (exponential model). [*Case*: Frio, TX (USA)]

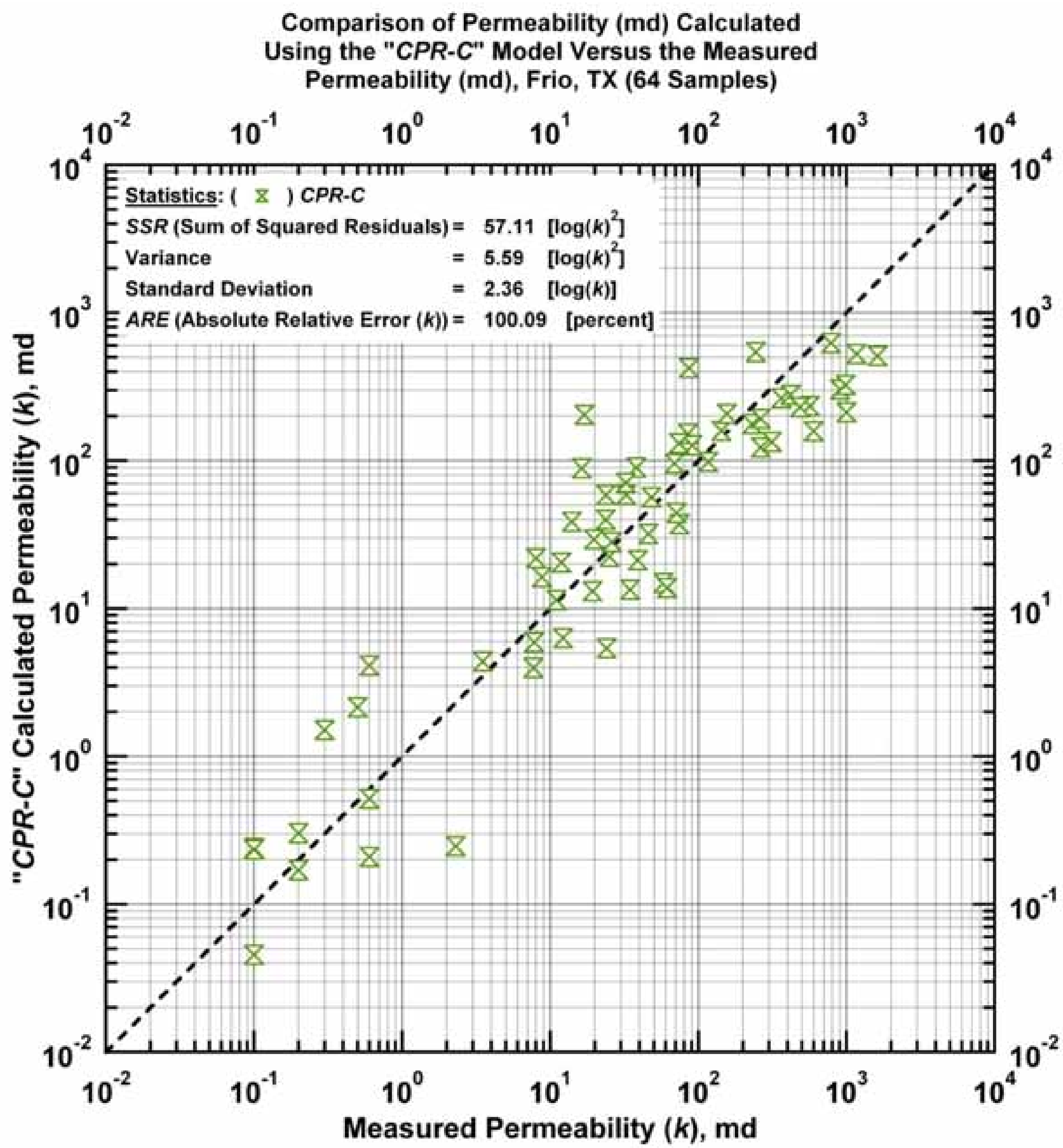

Figure H.6a — Model *CPR-C*: calculated versus measured permeability. [*Case*: Frio, TX (USA)]

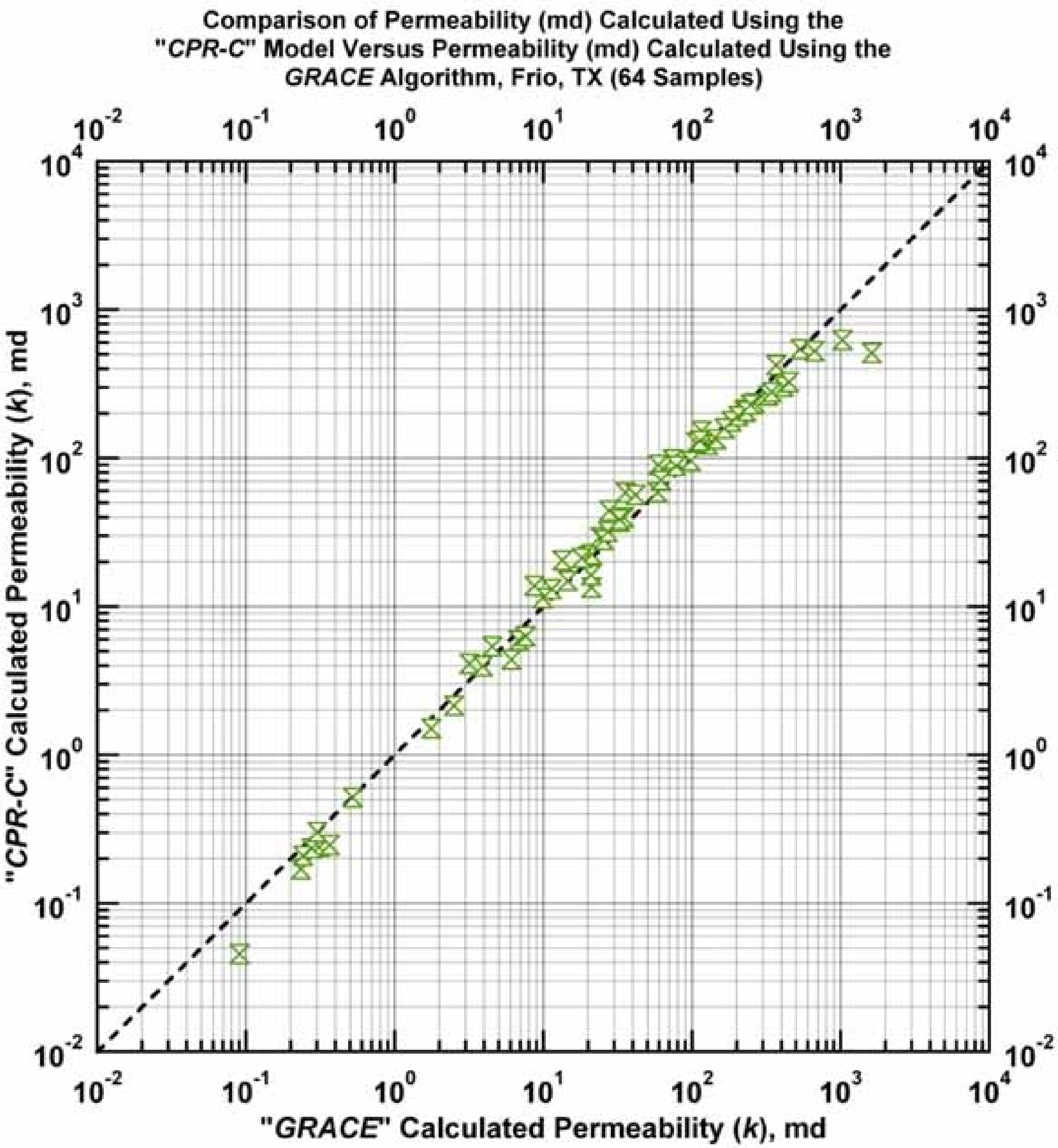

Figure H.6b — Model *CPR-C*: Permeability calculated using Model *CPR-C* versus permeability calculated using the *GRACE* Algorithm. [*Case*: Frio, TX (USA)]

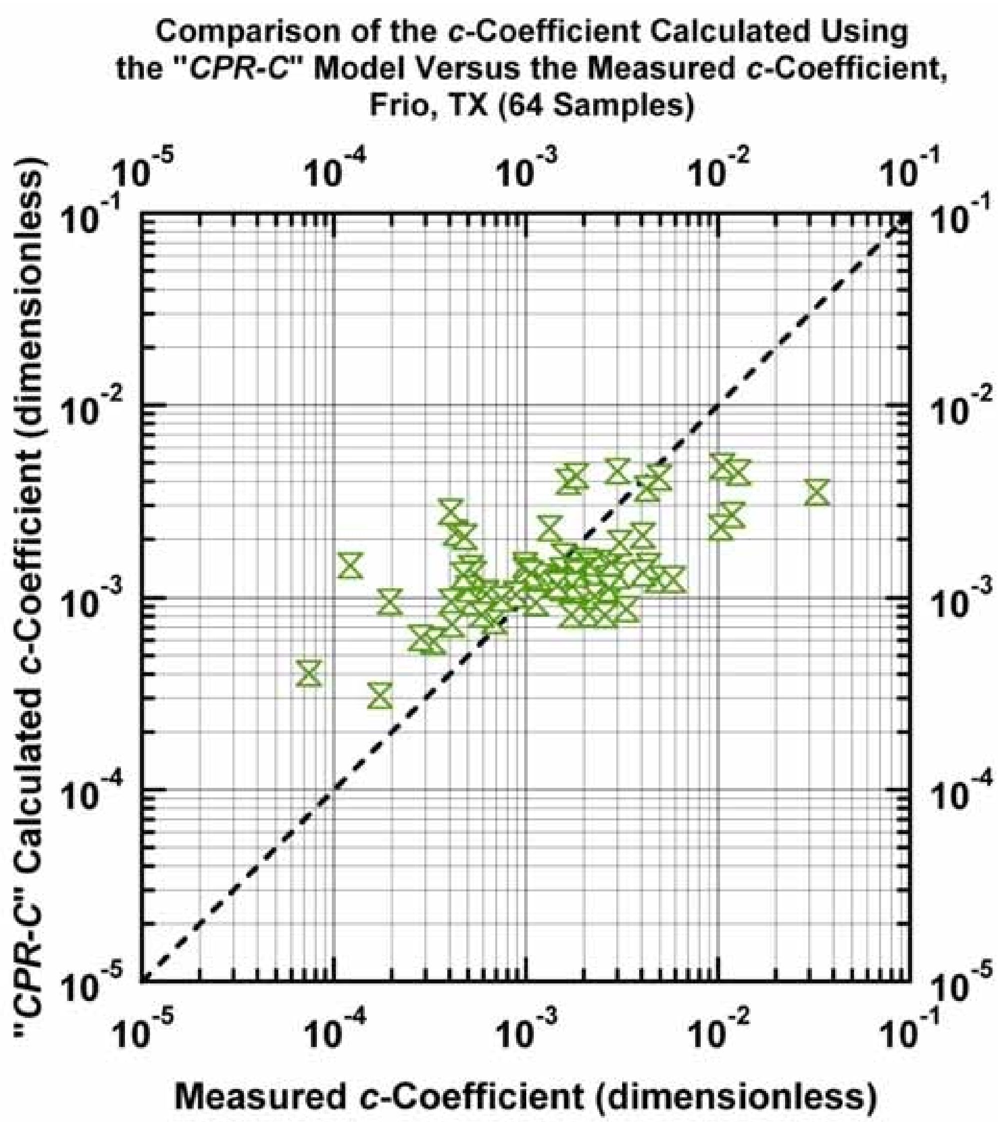

Figure H.6c — Model *CPR-C*: Calculated *c*-function values versus measured *c*-function values. [*Case*: Frio, TX (USA)]

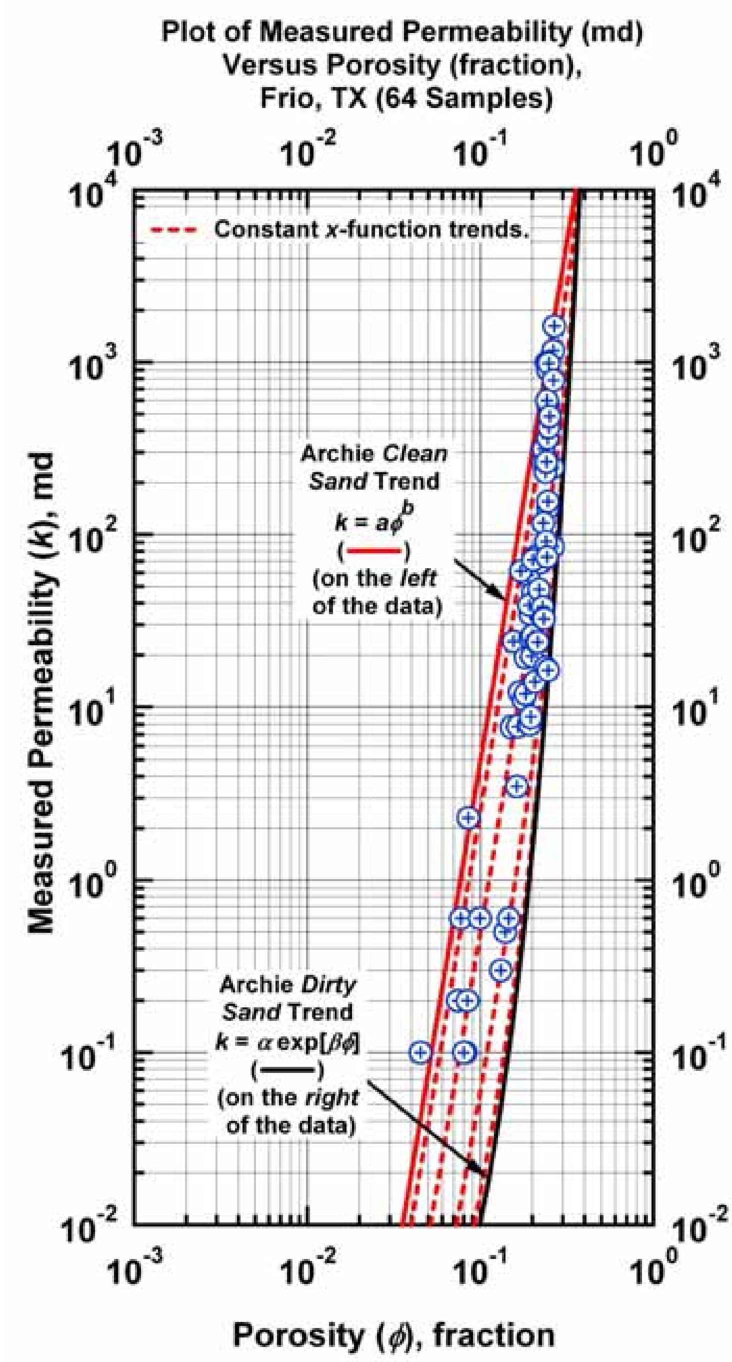

Figure H.7a — Model *CPR-D*: $k = xa\phi^b + (1-x)\alpha\exp[\beta\phi]$ $[0 \le x \le 1]$ — *Weighted Power Law-Exponential Model* used to correlate permeability (k) and porosity (ϕ). "Clean Sand" Plot — Archie "Clean Sand" trend is given by the straight-line trend at the far left of the data (power law model). [*Case*: Frio, TX (USA)]

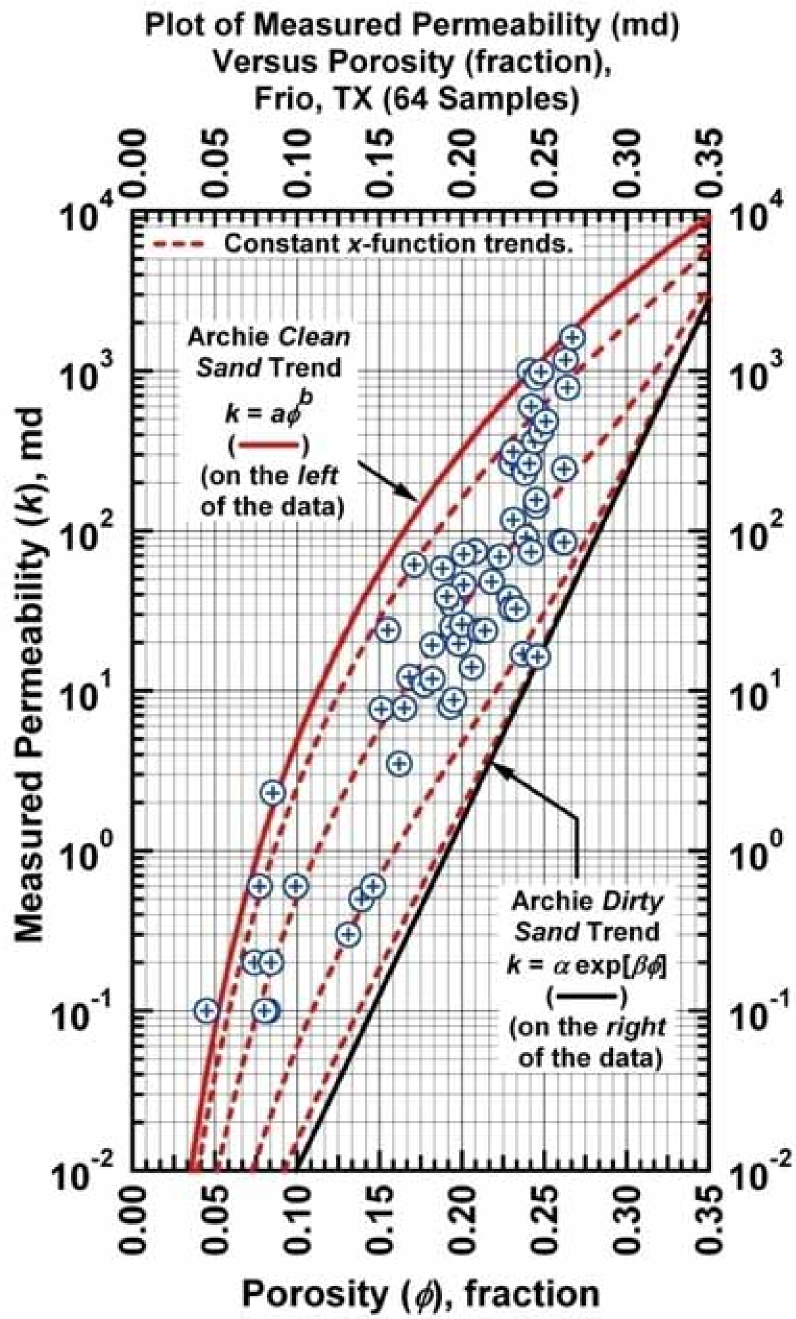

Figure H.7b — Model *CPR-D*: $k = xa\phi^b + (1-x)\alpha\exp[\beta\phi]$ $[0 \le x \le 1]$ — *Weighted Power Law-Exponential Model* used to correlate permeability (k) and porosity (ϕ). "Dirty Sand" Plot — Archie "Dirty Sand" trend is given by the straight-line trend at the far right of the data (exponential model). [*Case*: Frio, TX (USA)]

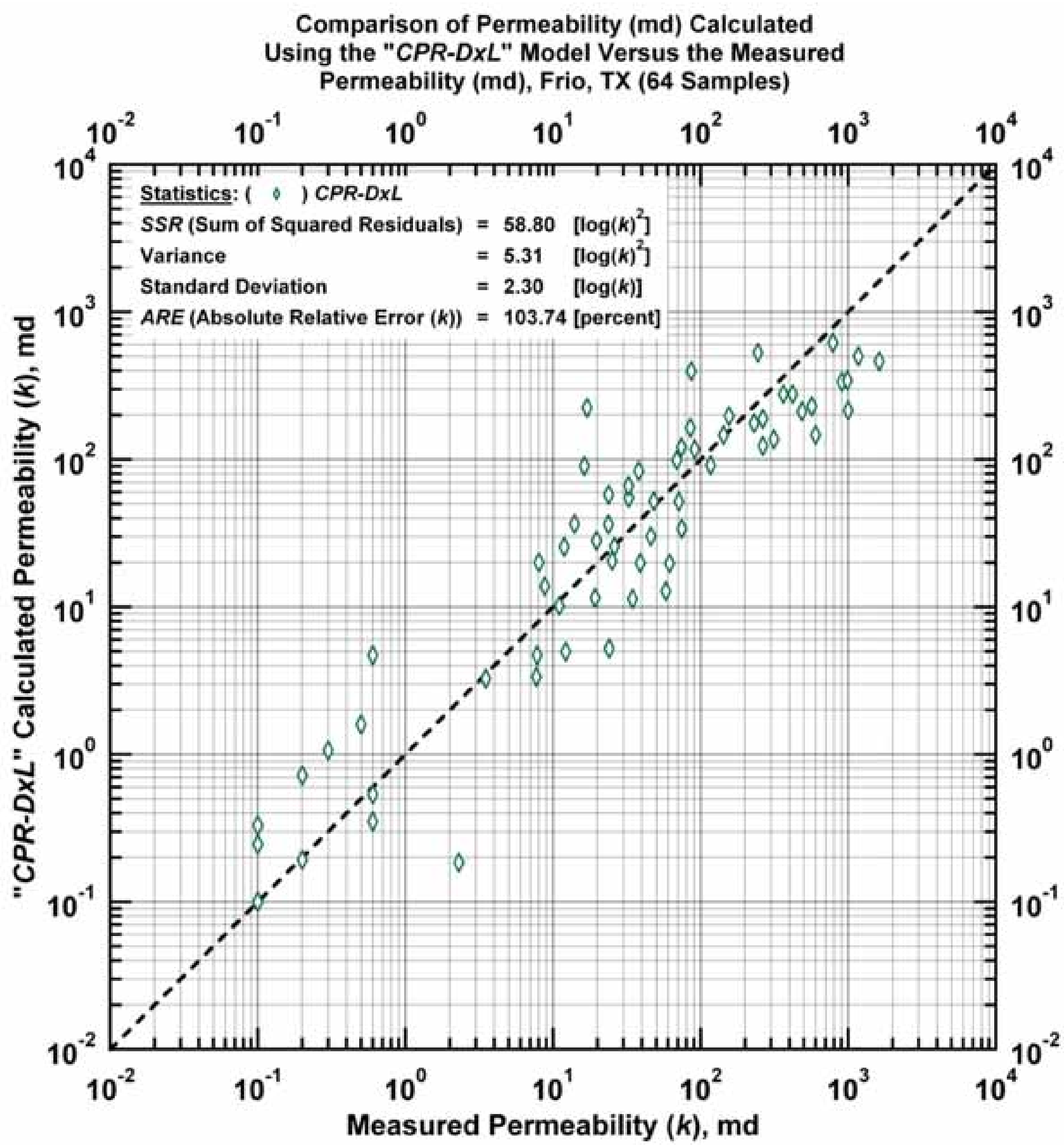

Figure H.8a — Model *CPR-DxL*: Calculated versus measured permeability. [*Case*: Frio, TX (USA)]

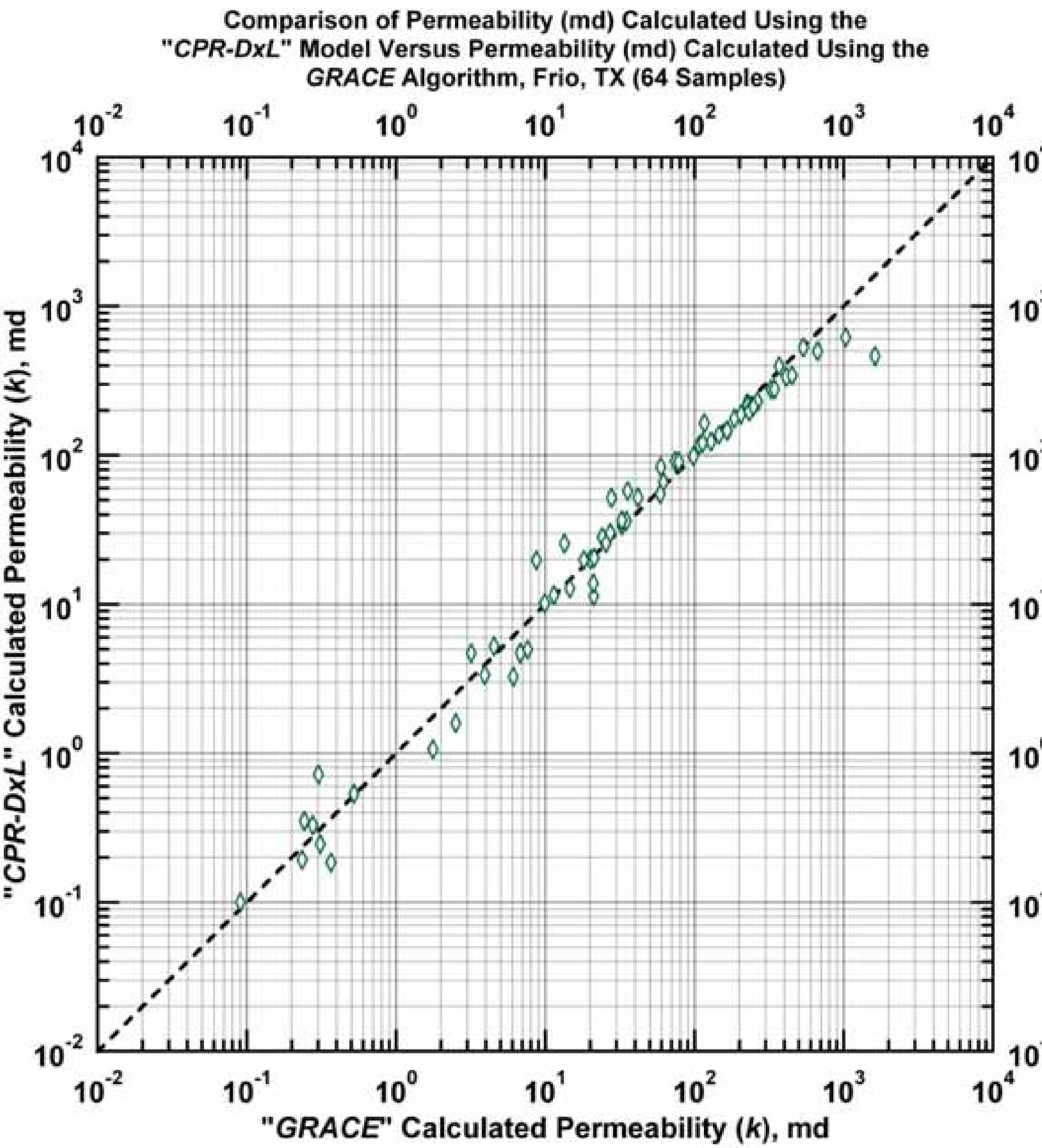

Figure H.8b — Model *CPR-DxL*: Permeability calculated using Model *CPR-C* versus permeability calculated using the *GRACE* Algorithm. [*Case*: Frio, TX (USA)]

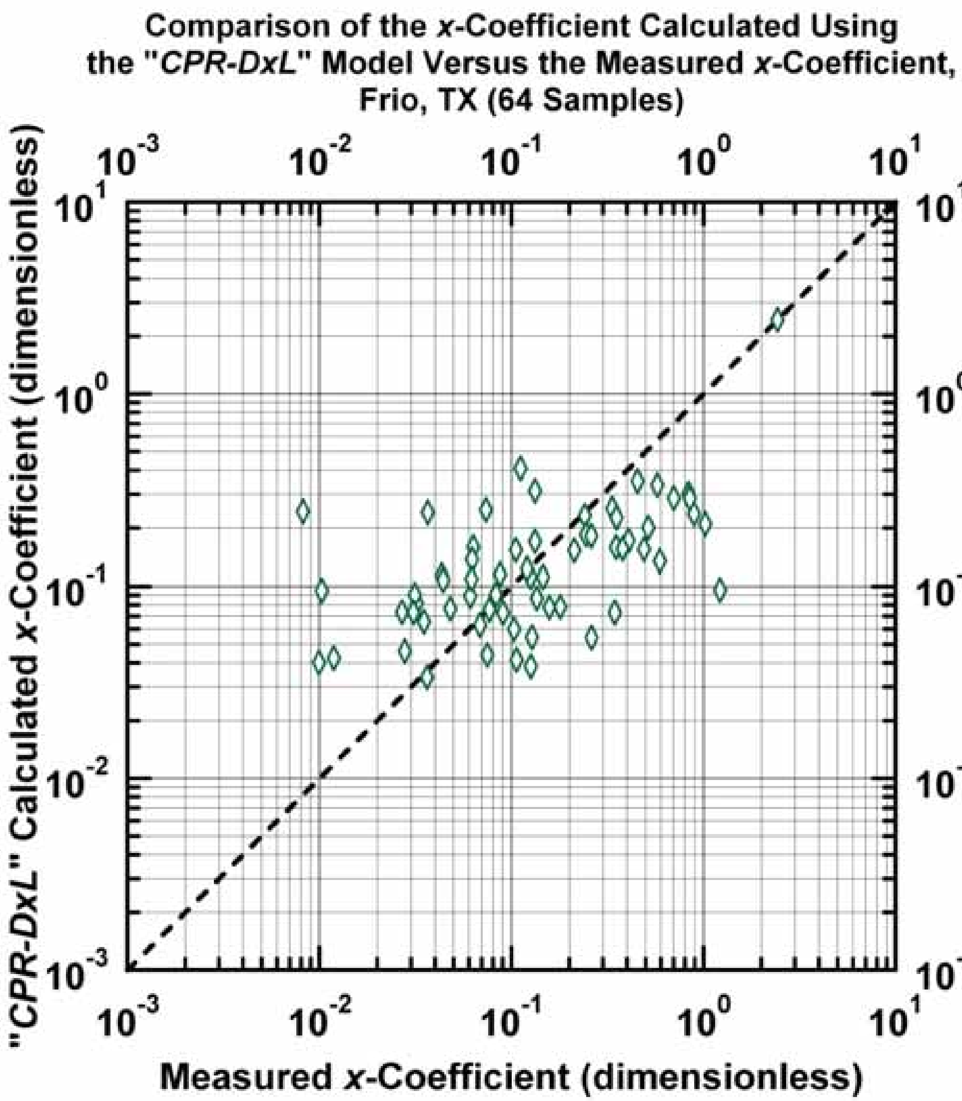

Figure H.8c — Model *CPR-DxL*: Calculated *x*-function weight values versus measured *x*-function weight values. [*Case*: Frio, TX (USA)]

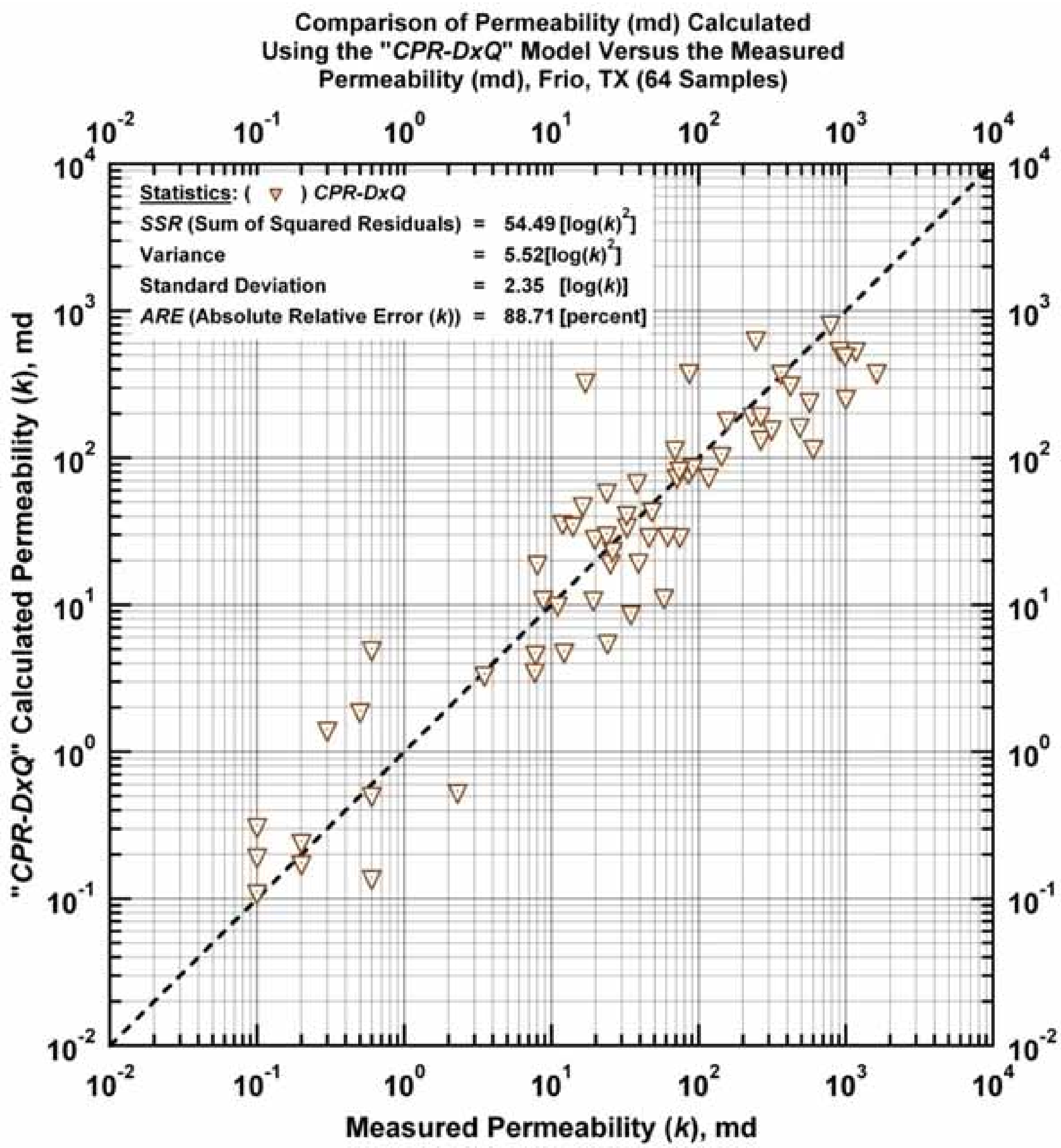

Figure H.9a — Model *CPR-DxQ*: Calculated versus measured permeability. [*Case*: Frio, TX (USA)]

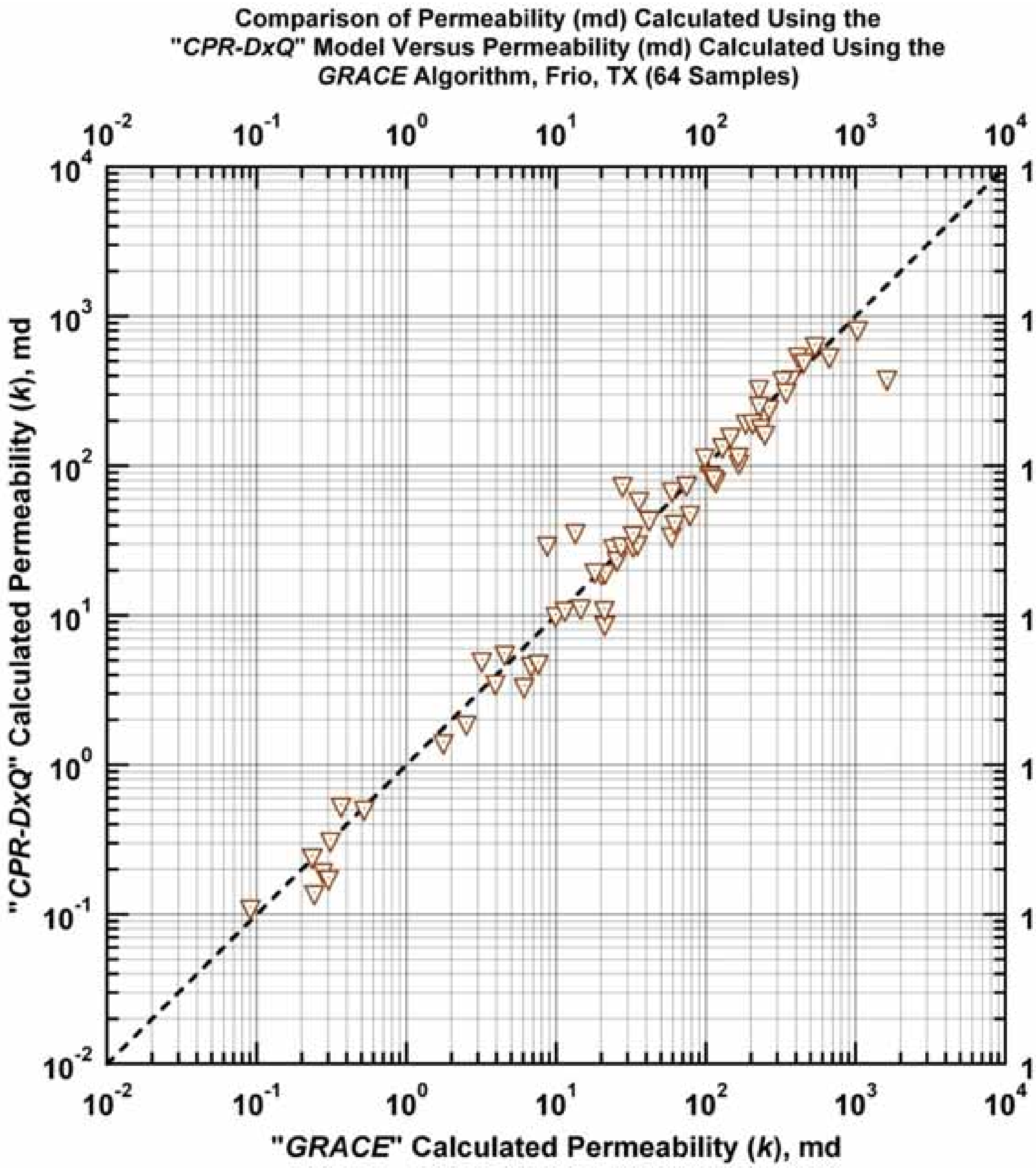

Figure H.9b — Model *CPR-DxQ*: Permeability calculated using Model *CPR-C* versus permeability calculated using the *GRACE* Algorithm. [*Case*: Frio, TX (USA)]

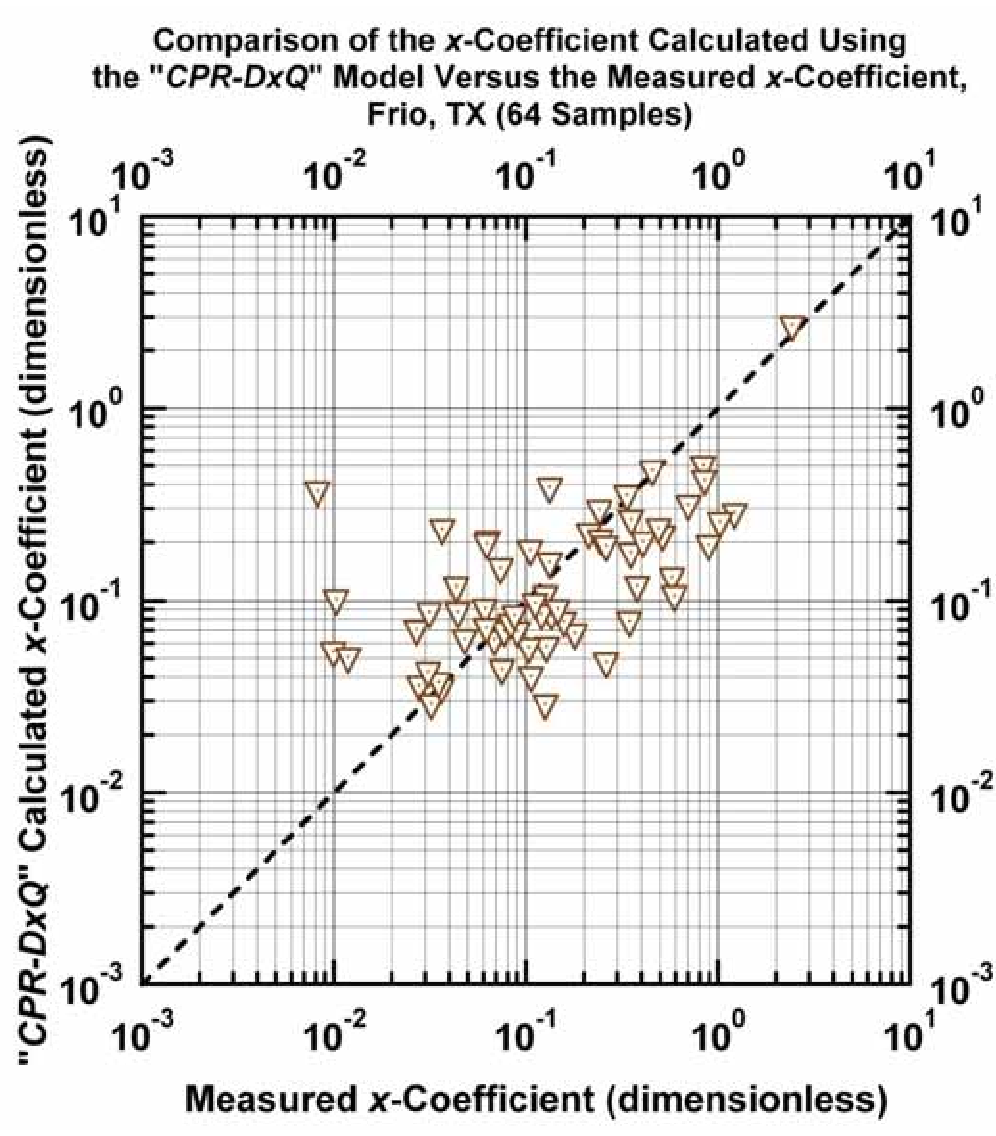

Figure H.9c — Model *CPR-DxQ*: Calculated *x*-function weight values versus measured *x*-function weight values. [*Case*: Frio, TX (USA)]

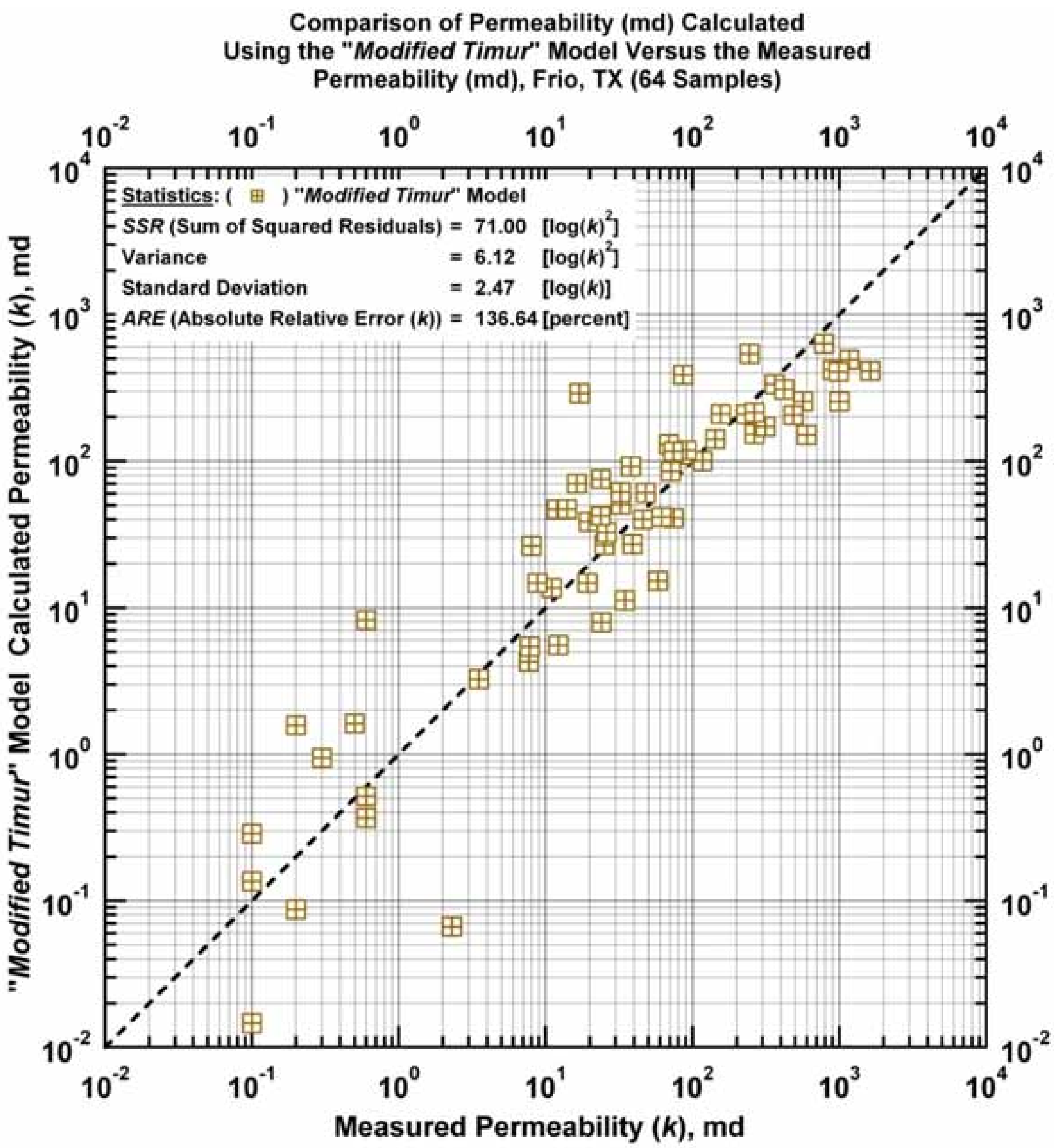

Figure H.10a — "Modified Timur Model:" Calculated versus measured permeability. [*Case*: Frio, TX (USA)]

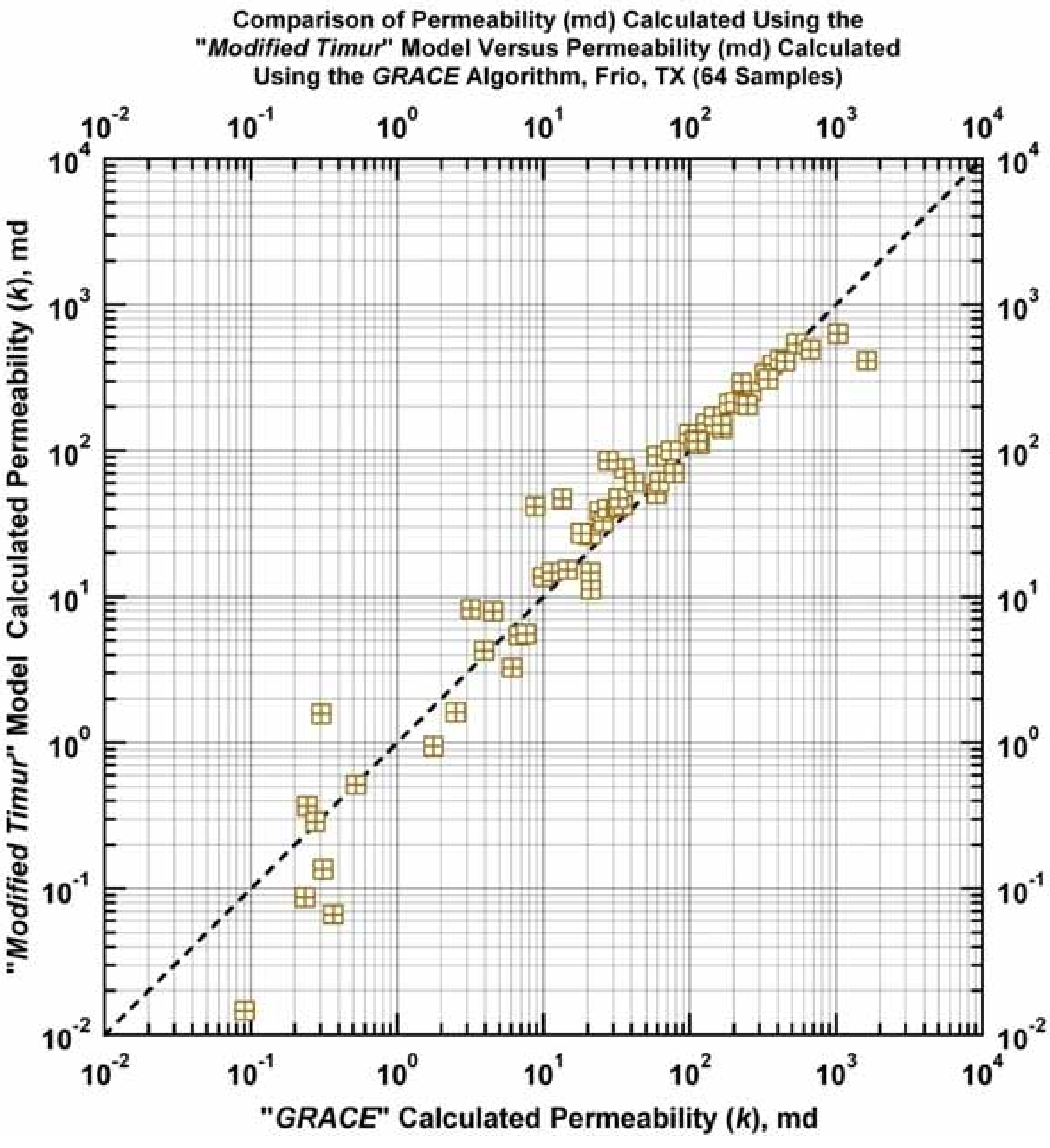

Figure H.10b — "Modified Timur Model:" Permeability calculated using the "Modified Timur Model" versus permeability calculated using the *GRACE* Algorithm. [*Case*: Frio, TX (USA)]

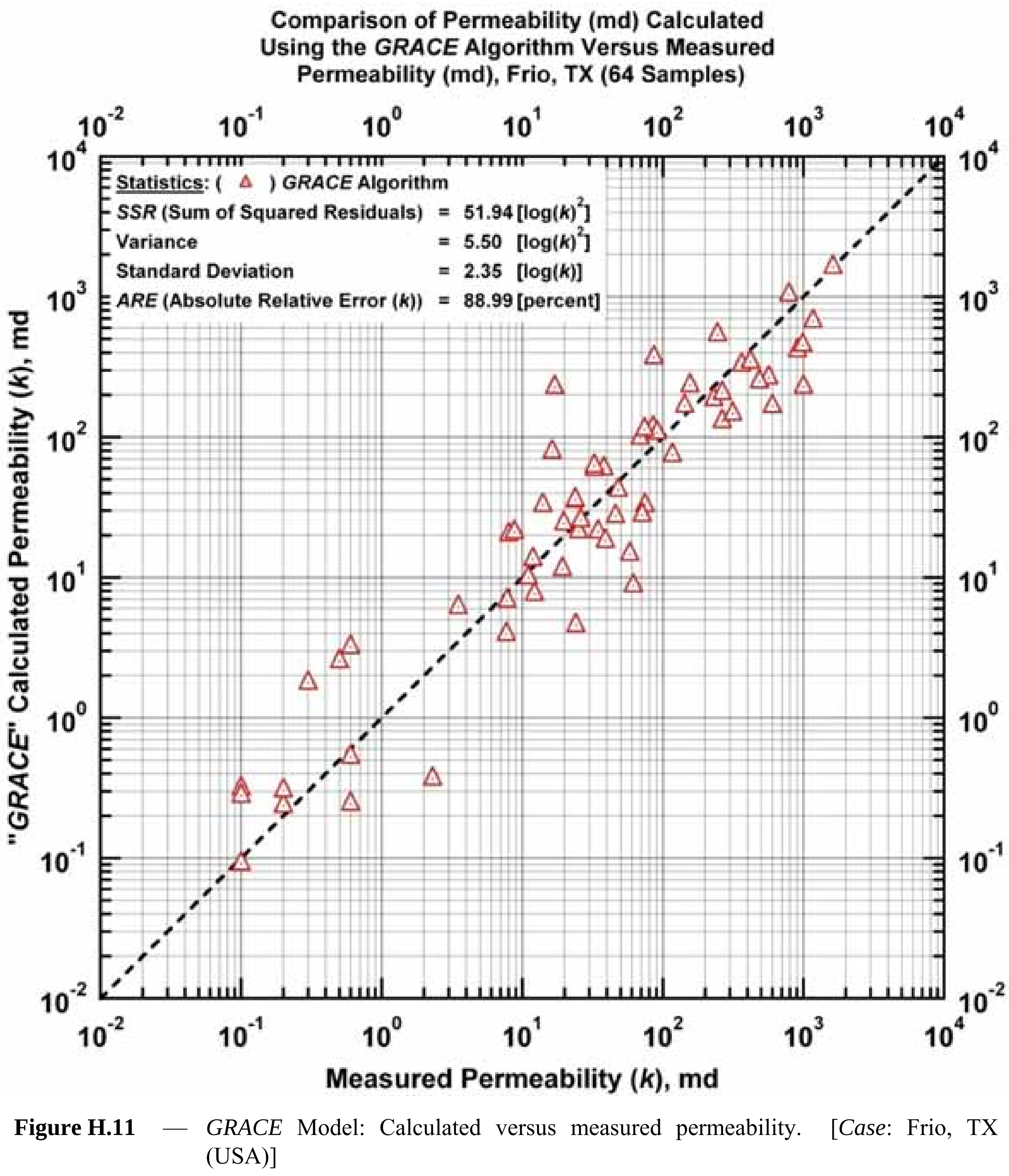

Figure H.11 — *GRACE* Model: Calculated versus measured permeability. [*Case*: Frio, TX (USA)]

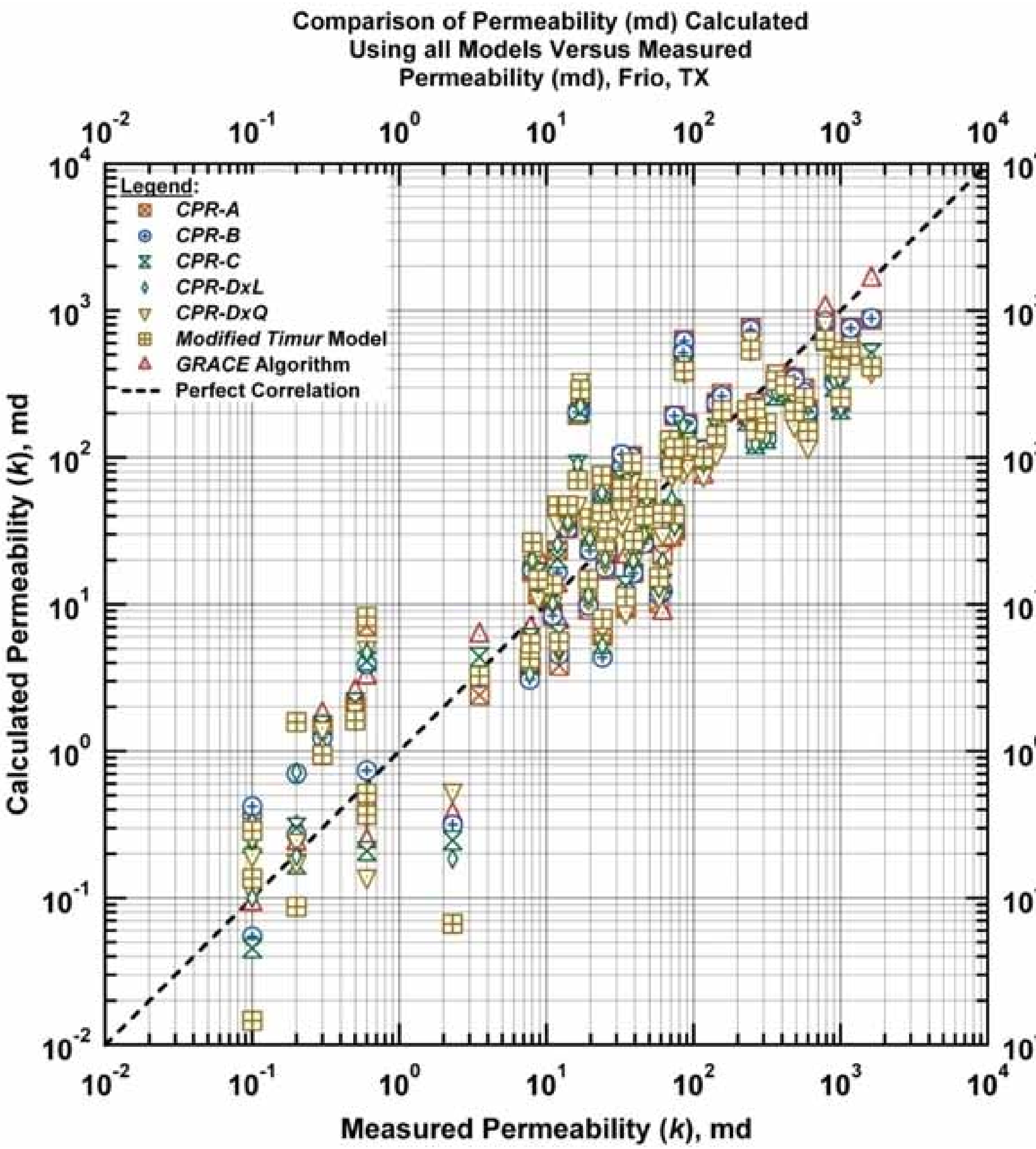

Figure H.12 — All Models: Calculated versus measured permeability. [*Case*: Frio, TX (USA)]

APPENDIX I

RESULTS FOR LOWER WILCOX SHALY SANDSTONE (TEXAS — USA)

In this Appendix we present the "Lower Wilcox" Well, located in South Texas (USA) — this is a tight gas reservoir system comprised of shaly (clastic) sediments (Ellis, 1987).

Model *CPR-A*: (Appendix I)

The "characteristic permeability relation" (or *CPR*) Model *CPR-A* (*i.e.*, the modified Archie "Clean Sand" Model) is given as:

$$k = a(\phi - c)^b \quad c = c_{\max} \exp[-c_1 \phi^{c_2} F^{c_3}] \text{ ....(I-1)}$$

Where a plot of log(k) versus log(ϕ) is used to graphically calibrate EI. I-1 in terms of the coefficients — a, b, and $c_{\max}$. **Fig. I.1** shows that the *CPR-A* model performs quite well for this case. **Figs. I.1a and b** show the log-log and the semilog format of permeability versus porosity, respectively. In **Fig. I.2** we provide the "error" plots for this case, where the measured and computed data are compared systematically. In **Fig. I.1a** we note a good correlation of the results obtained using Model *CPR-A* versus the measured permeability data — we observe good agreement with the perfect correlation trend (*i.e.*, the 45-degree line). In **Fig. I.2b** we provide a comparison with the *GRACE* algorithm correlation (Xue *et al*. 1997)), and we note that the *CPR-A* model results correlate very well with the *GRACE* algorithm results for this case. Finally, in **Fig. I.2c** we present the calculated and measured c-function — and again we note a reasonable correlation of the data about the perfect correlation trend.

Model *CPR-B*: (Appendix I)

The "characteristic permeability relation" (or *CPR*) Model *CPR-B* (*i.e.*, the modified Archie "Dirty Sand" Model (power-law basis)) is given as:

$$k = a(\phi + c)^b \quad c = c_{\max} \exp[-c_1 \phi^{c_2} F^{c_3}] \text{ ....(I-2)}$$

Where a plot of log(k) versus log(ϕ) is used to graphically calibrate Eq. I-2 in terms of the coefficients — a, b, and $c_{\max}$. The results for this case are presented in **Figs. I.3 and 4**. In **Fig. I.3a** (log-log format) we note that a very distinct "envelope" is formed by the *CPR-B* model, essentially all of the data on the right and left flanks are well-matched (*i.e.*, the "dirty sand" power law relation (applied on the right portion of the data) and its correction function (applied on the left portion of the data). Similarly, in **Fig. I.3b** (semilog format), we observe an excellent distribution of the power law model across the body of the data. The error analyses for this case are shown in **Fig. I.4**. In **Fig. I.4a** we present the results obtained using Model *CPR-B* versus the measured permeability data and in this case there is good agreement with the perfect correlation trend (*i.e.*, the 45-degree line) — a few data points are out-lying, mostly in the middle of the trend. We provide a comparison with the *GRACE* algorithm correlation in **Fig. I.4b** — the results using Model *CPR-B* and the *GRACE* algorithm compare very well for this case. We compare the computed and data-derived values of the *c*-function for this case in **Fig. I.4c** and we note a reasonably "tight" correlation, except for the very lowest values of the *c*-function. In summary, we believe that Model *CPR-B* is a very effective correlation model for this particular data case.

Model *CPR-C*: (Appendix I)

The "characteristic permeability relation" (or *CPR*) Model *CPR-B* (*i.e.*, the modified Archie "Dirty Sand" Model (exponential basis)) is given as:

$$k = c\exp[\beta\phi] \quad c = c_{\max}\exp[-c_1\phi^{c_2}F^{c_3}] \text{ ....} \text{(I-3)}$$

Where a plot of log(k) versus ϕ is used to graphically calibrate Eq. I-3 in terms of the coefficients — β and c_{max}. Model *CPR-C* is fundamentally different than Models *CPR-A* and *CPR-B*, as the basis for Model *CPR-C* is an exponential function, not a power law relation. In **Figs. I.5 and 6** we present the results of applying Model *CPR-B* for this case, and in general, we observe a very consistent performance of Model *CPR-B*. **Fig. I.5b** illustrates the excellent conformance of Model *CPR-C* for this case — again recalling that this model has an exponential relationship with porosity as its basis.

In **Figs. I.6a, I.6b, and I.6c** we review the error analyses plots for this case, and we note good performance (visually) in terms of the correlation of the results using Model *CPR-C*. We do note that in this case, the overall (statistical) error is somewhat high, but we have to remember that we are proposing "characteristic models" in this work, and as such, this case appears (again, based on visual inspections) to have good clustering of the correlated results in terms of permeability (**Figs. I.6a and I.6b**). In this case, the *c*-function (in Eq. I-3) is not a correction term, but rather the instantaneous intercept for the exponential basis. The correlation of the *c*-function (see **Fig. I.6c**) appears to be consistent — but scatter and a slight off-center trend is evident. However, as we are approaching this work from the perspective that the primary value of the work is the characteristic model, not the statistical "best fit" correlation, we believe that the *CPR-C* model has performed well for this case, and **Fig. I.6** confirms the value of this model as a "characteristic relation" for permeability.

Model *CPR-D*: (Appendix I)

The "characteristic permeability relation" (or *CPR*) Model *CPR-D* (*i.e.*, the weighted power law-exponential model) is given in its fundamental form as:

$$k = xa\phi^b + (1-x)\alpha\exp[\beta\phi] \quad [0 \le x \le 1]] \text{ ....} \text{(I-4a)}$$

For Eq. I-4 there are two proposed models for the x-function (*i.e.*, the weighting function) — these are:

$$x = \exp[-\ln(x_0) + x_1\ln(\phi) + x_2\ln(F) + x_3\ln(\phi)\ln(F)] \text{ (Model } \textit{CPR-DxL}\text{) ....} \text{(I-4b)}$$

$$x = \exp\begin{bmatrix} -\ln(x_0) + x_1 \ln(\phi) + x_2 \ln(F) + x_3 \ln(\phi)\ln(F) \\ + x_4 \ln(\phi)^2 + x_5 \ln(F)^2 + x_6 \ln(\phi)^2 \ln(F) \\ + x_7 \ln(\phi)\ln(F)^2 + x_8 \ln(\phi)^2 \ln(F)^2 \end{bmatrix} \text{(Model } CPR\text{-}DxL) \quad \text{(I-4c)}$$

As noted in Eq. I-4b, Model *CPR-DxL* utilizes a logarithmic linear model for the weights (*x*-values) and as seen in Eq. I-4c, Model *CPR-DxQ* utilizes a logarithmic quadratic model for the weights (*x*-values). While these models (Eqs. I-4c and I-4c) are *empirical*, we have found generally good application of these relations for all cases. In this case, the base results using Models *CPR-DxL* and *CPR-DxQ* are presented in **Fig. I.7** — where the power law and exponential basis functions are fitted to the appropriate portion of the data. The power law equation represents the "Archie clean sand" trend and is fitted to the leftmost data as shown in **Fig. I.7a** and in contrast, the exponential equation is thought to represent the "Archie Dirty Sand" trend and the exponential is fitted to the far rightmost portion of the data (see **Fig. I.7b**).

In **Figs. I.8 and 9** we present the error analyses for this case, where we have employed the weighting functions (Eqs. I-4c and I-4c) as appropriate. In **Fig. I.8a** we find a good correlation of permeability (with the out-lying points noted in the middle of the trend). The comparison of the Model *CPR-DxL* results are compared to the results obtained from the *GRACE* algorithm in **Fig. I.8b**, we note that the results obtained using Model *CPR-DxL* does "drift" slightly from the *GRACE* solution at lower values of permeability, indicating some inconsistency. The computed weight function (*x*-values) shown for the *CPR-DxL* model in **Fig. I.8c** does exhibit more scatter than expected, but the trend is (relatively) centered about the perfect correlation line.

The results obtained using Model *CPR-DxQ* are presented in **Fig. I.9**, and we note substantially improved behavior over that of Model *CPR-DxL*. In particular, the base correlation of computed and measured permeabilities (**Fig. I.9a**) for Model *CPR-DxQ* does indicate a slightly better correlation than that of Model *CPR-DxL*. Also, the comparison of Model *CPR-DxQ* with the results from the *GRACE* algorithm (**Fig. I.9b**) exhibits better agreement than the results of Model *CPR-DxL*. Finally, the correlation of the *x*-function (**Fig. I.9c**) for Model *CPR-DxQ* is better than the correlation for Model *CPR-DxL*. These comparisons suggest that Model *CPR-DxQ* (*i.e.*, the combination of Eqs. I-4a and I-4c) has provided a better correlation of data, for this case, than Model *CPR-DxL*.

***"Modified Timur Model"*: (Appendix I)**

The "Modified Timur Model" is given as:

$$k_{\text{Timur}} = a\phi^b F^c \text{ ....} \quad \text{(I-5)}$$

In **Fig. I.10** we present the results of the "Modified Timur Model" (EI. I-5) which is essentially just a generalized power-law function relation in terms of k, ϕ, and F. Somewhat surprisingly, as shown in **Figs. I.10a and b**, the "Modified Timur Model" provides the best correlation (in a statistical sense) of the data for this case. The comparison of results using the "Modified Timur Model" with the results of the *GRACE* algorithm (**Fig. I.10b**) is outstanding — a near perfect comparison with the *GRACE* algorithm.

***GRACE* Algorithm: (Appendix I)**

In **Fig. I.11** we present the results predicted by the *GRACE* algorithm, which is a non-parametric regression approach (see Xue *et al.* (1997) for details). In theory, the *GRACE* algorithm should provide the most *unbiased* correlation of the data — *i.e.*, the *GRACE* algorithm is designed not to "fit the errors" as other regression approaches may. It is our contention that the *GRACE* algorithm is the statistical standard — and any algorithm/approach/model which achieves better regression statistics than the *GRACE* algorithm is actually "fitting the errors" in the data. *The only case which has significantly better regression statistics than the GRACE algorithm is the "Modified Timur Model"* — hence, we must label this case as "over-fitted" in a statistical sense.

***Comparison of All Models*: (Appendix I)**

Our final plot, **Fig. I.12**, illustrates all of the models on a single plot of calculated versus measured permeability. We also present a table of all statistical results in **Table I.1**.

Table I.1 — Statistical Results for all Models (Lower Wilcox, S. TX (USA), n=62).

Model	Sum of Squared Residuals [log(k)^2]	Variance [log(k)^2]	Standard Deviation [log(k)]	Absolute Relative Error [percent]
CPR-A	48.89	2.08	1.44	86.39
CPR-B	48.78	2.11	1.45	90.10
CPR-C	57.32	2.20	1.48	99.03
CPR-DxL	51.74	2.36	1.54	102.77
CPR-DxQ	49.10	2.15	1.46	93.05
Modified Timur	47.83	2.11	1.45	84.41
GRACE Algorithm	50.47	2.17	1.47	88.14

The coefficients for the models used in this case are provided in **Table I.2**.

Table I.2a — Model Coefficients (Lower Wilcox, S. TX (USA), *n*=62).

Model	a or α	b or β	c or c_{max}	c_1	c_2	c_3
CPR-A	1.00×10^{8}	8.00	0.090	0.03	-5.71	-2.06
CPR-B	4.00×10^{5}	8.00	0.150	9.16×10^{-2}	3.49	2.38
CPR-C	9.00×10^{-9}	100.00	5.00×10^{-5}	1.49×10^{2}	3.14	0.65
Modified Timur	1.89×10^{6}	-0.92	-4.207	–	–	–

Table I.2b — Model Coefficients (Lower Wilcox, S. TX (USA), *n*=62).

Model	a	b	α	β
CPR-DxL	2.00×10^{8}	8.00	9.00×10^{-9}	100.00
CPR-DxQ	2.00×10^{8}	8.00	9.00×10^{-9}	100.00

Model	c_0	c_1	c_2	c_3	c_4	c_5	c_6	c_7	c_8
CPR-DxL	528.19	-13.36	-6.03	0.06	–	–	–	–	–
CPR-DxQ	1.23×10^{5}	-29.95	-10.55	-10.66	-15.58	-2.46	0.05	-0.19	-3.68×10^{-3}

Nomenclature: (Appendix I)

F = Archie Formation Factor (dimensionless)
k = Formation Permeability, md (or any consistent units)
ϕ = Porosity, fraction

References: (Appendix I)

Ellis, K.W.: "Extended Correlations of Porosity, Permeability, and Formation Resistivity Factor," MS thesis, Texas A&M U., College Station, TX (1987).

Xue, G., Datta-Gupta, A., Valko, P., and Blasingame, T.A.: "Optimal Transformations for Multiple Regression: Application to Permeability Estimation from Well Logs," *SPEFE* (June 1997), 85-93.

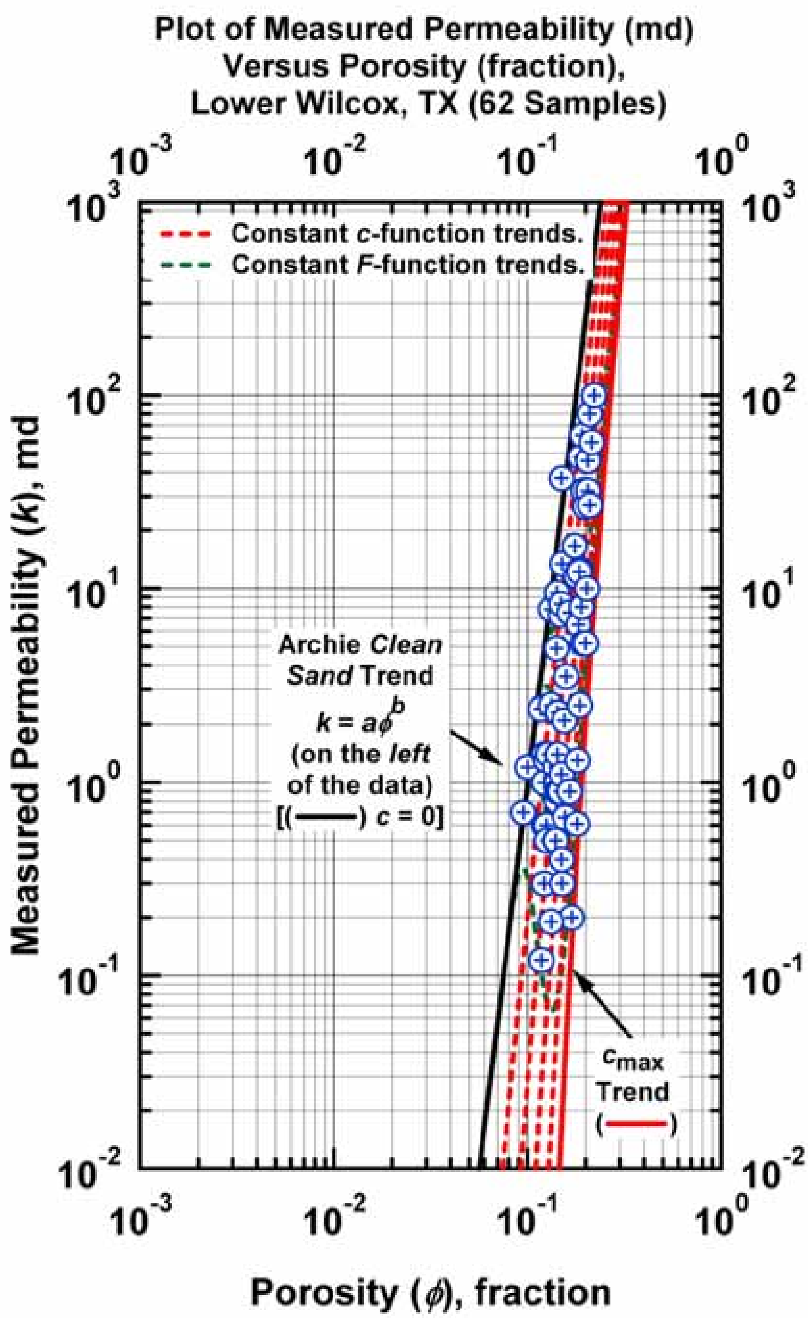

Figure I.1a — Model *CPR-A*: $k = a(\phi - c)^b$ ($c = c_{max} \exp[-c_1 \phi^{c_2} F^{c_3}]$) — "Clean Sand" Plot (log-log format) — Archie "Clean Sand" trend is given by the straight-line trend at the far left of the data (power law model). [*Case*: Lower Wilcox S. TX (USA)]

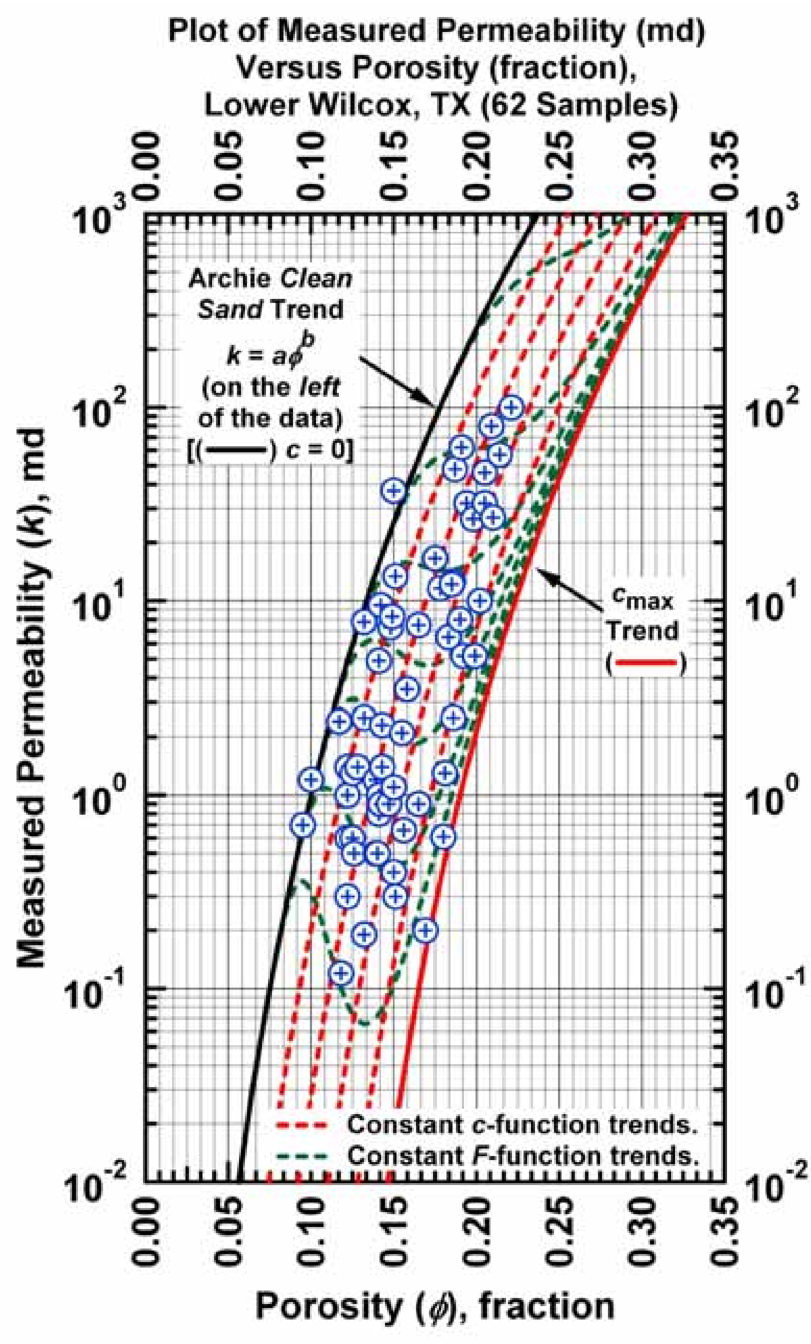

Figure I.1b — Model *CPR-A*: $k = a(\phi - c)^b$ ($c = c_{max} \exp[-c_1 \phi^{c_2} F^{c_3}]$) — "Dirty Sand" Plot (semilog format). Archie "Clean Sand" trend is given by the curved trend at the far left of the data (power law model). [*Case*: Lower Wilcox S. TX (USA)]

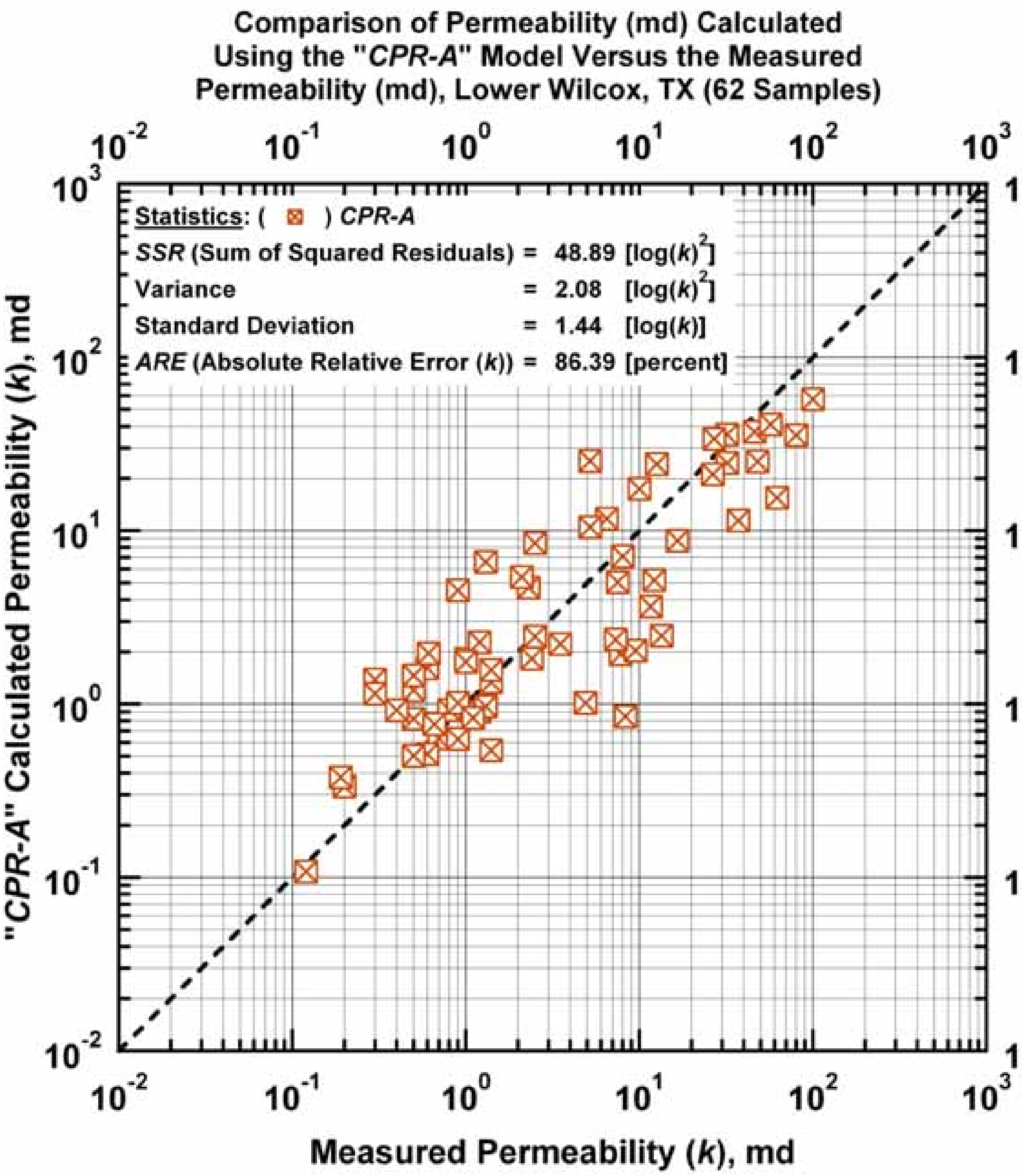

Figure I.2a — Model *CPR-A*: calculated versus measured permeability. [*Case*: Lower Wilcox S. TX (USA)]

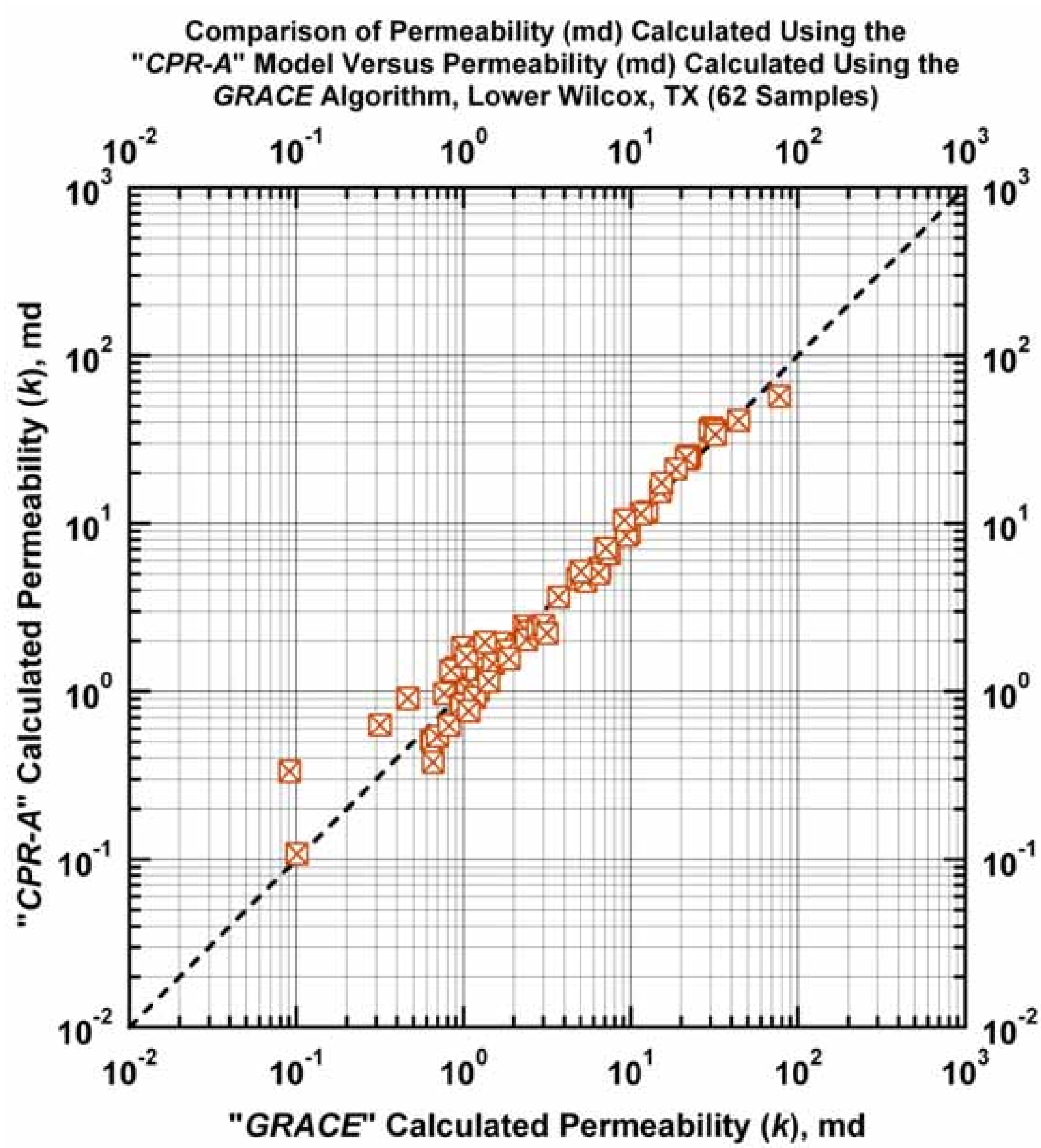

Figure I.2b — Model *CPR-A*: Permeability calculated using Model *CPR-A* versus permeability calculated using the *GRACE* Algorithm. [*Case*: Lower Wilcox S. TX (USA)]

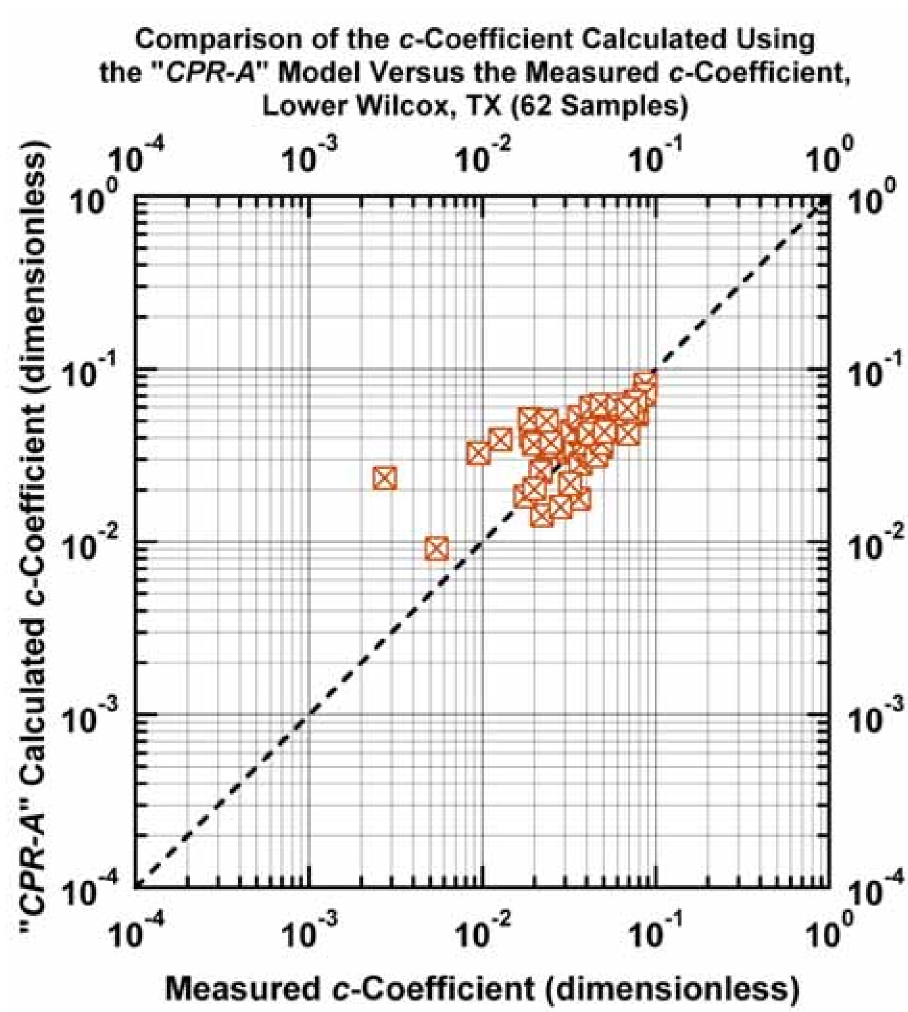

Figure I.2c — Model *CPR-A*: Calculated *c*-function values versus measured *c*-function values. [*Case*: Lower Wilcox S. TX (USA)]

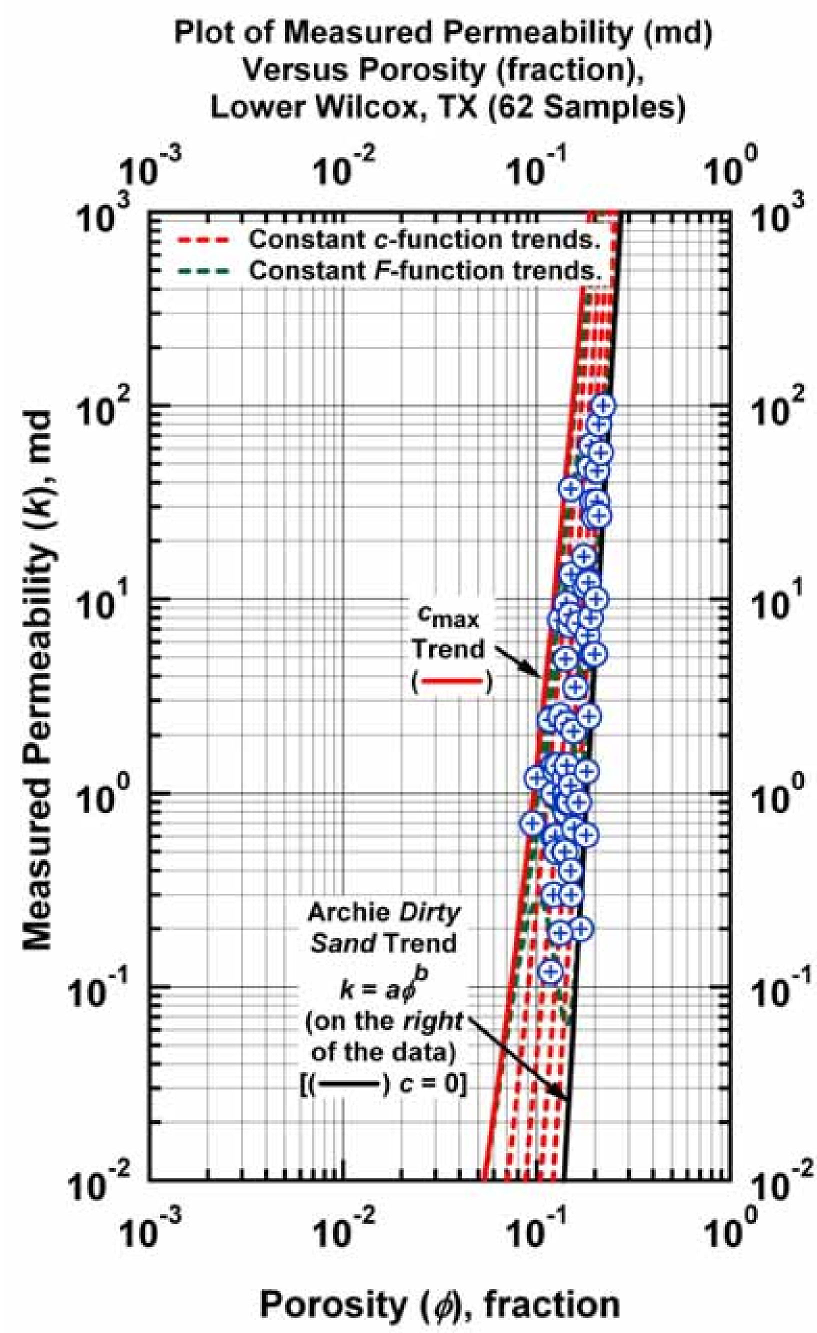

Figure I.3a — Model *CPR-B*: $k = a(\phi + c)^b \quad c = c_{max} \exp[-c_1 \phi^{c_2} F^{c_3}]$ — "Clean Sand" Plot (log-log format) — Archie "Dirty Sand" trend is given by the straight-line trend at the far right of the data (power law model). [*Case*: Lower Wilcox S. TX (USA)]

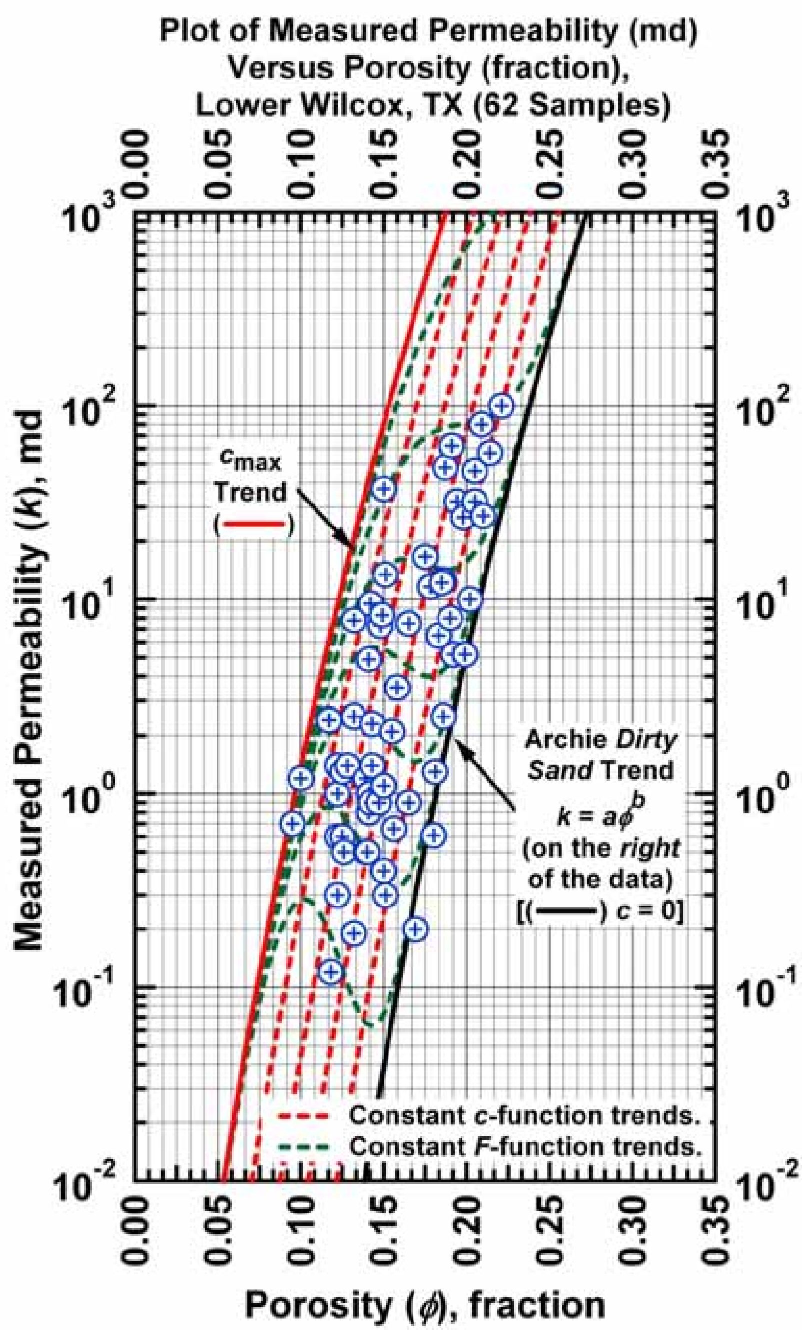

Figure I.3b — Model *CPR-B*: $k = a(\phi + c)^b$ $\quad c = c_{max}\exp[-c_1\phi^{c_2}F^{c_3}]$ — "Dirty Sand" Plot (semilog format) — Archie "Dirty Sand" trend is given by the curved trend at the far right of the data (power law model). [*Case*: Lower Wilcox S. TX (USA)]

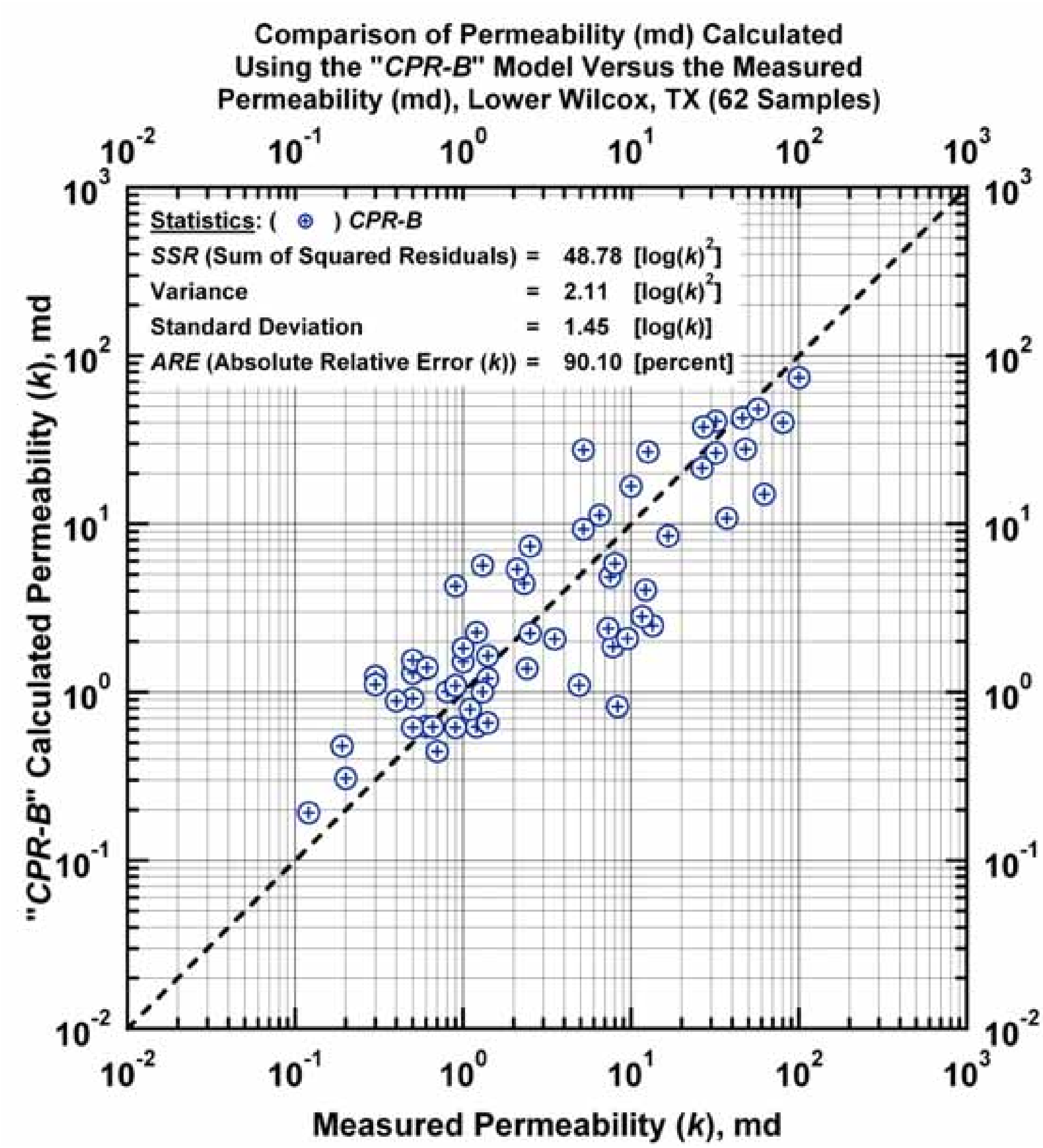

Figure I.4a — Model *CPR-B*: calculated versus measured permeability. [*Case*: Lower Wilcox S. TX (USA)]

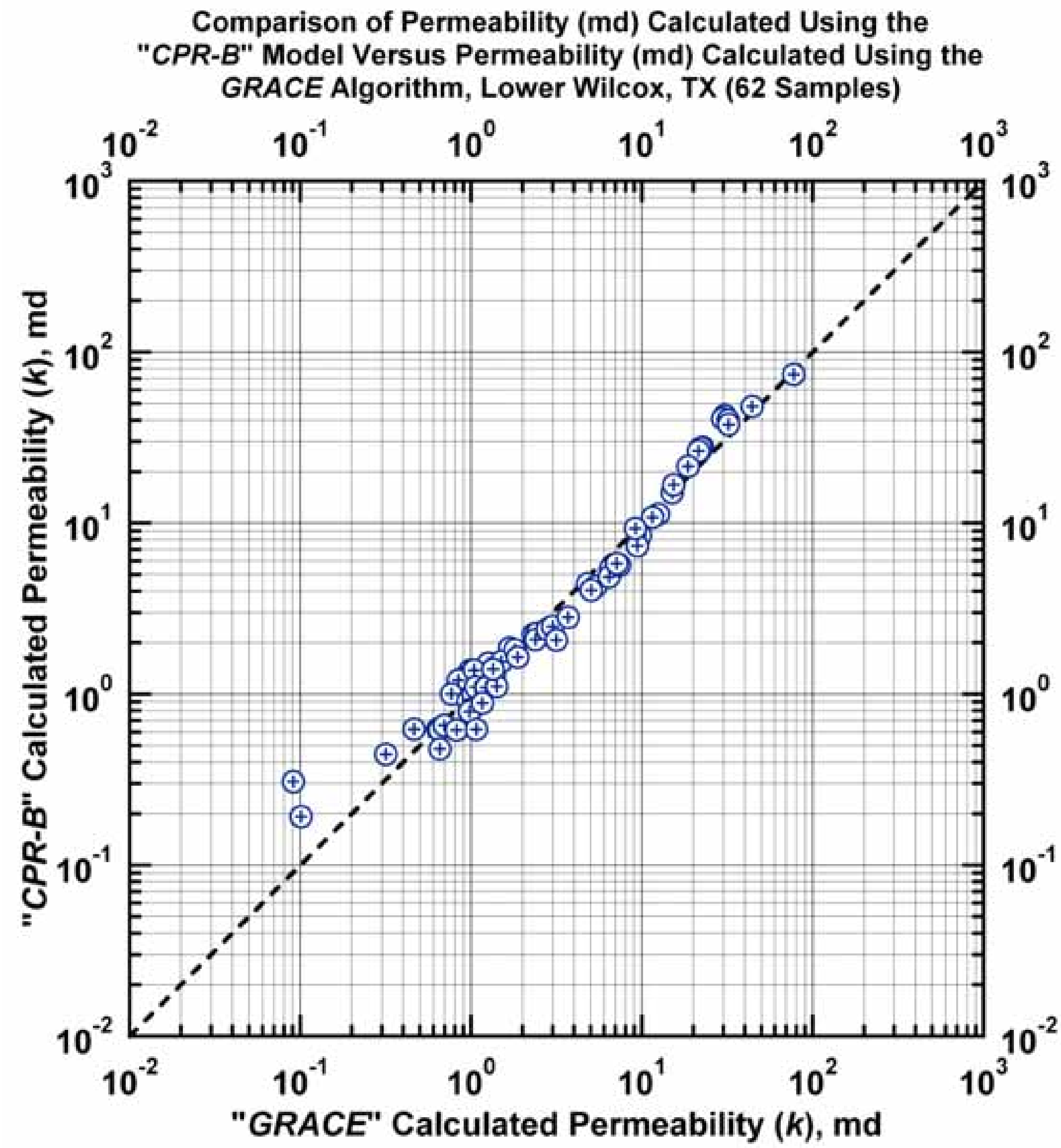

Figure I.4b — Model *CPR-B*: Permeability calculated using Model *CPR-B* versus permeability calculated using the *GRACE* Algorithm. [*Case*: Lower Wilcox S. TX (USA)]

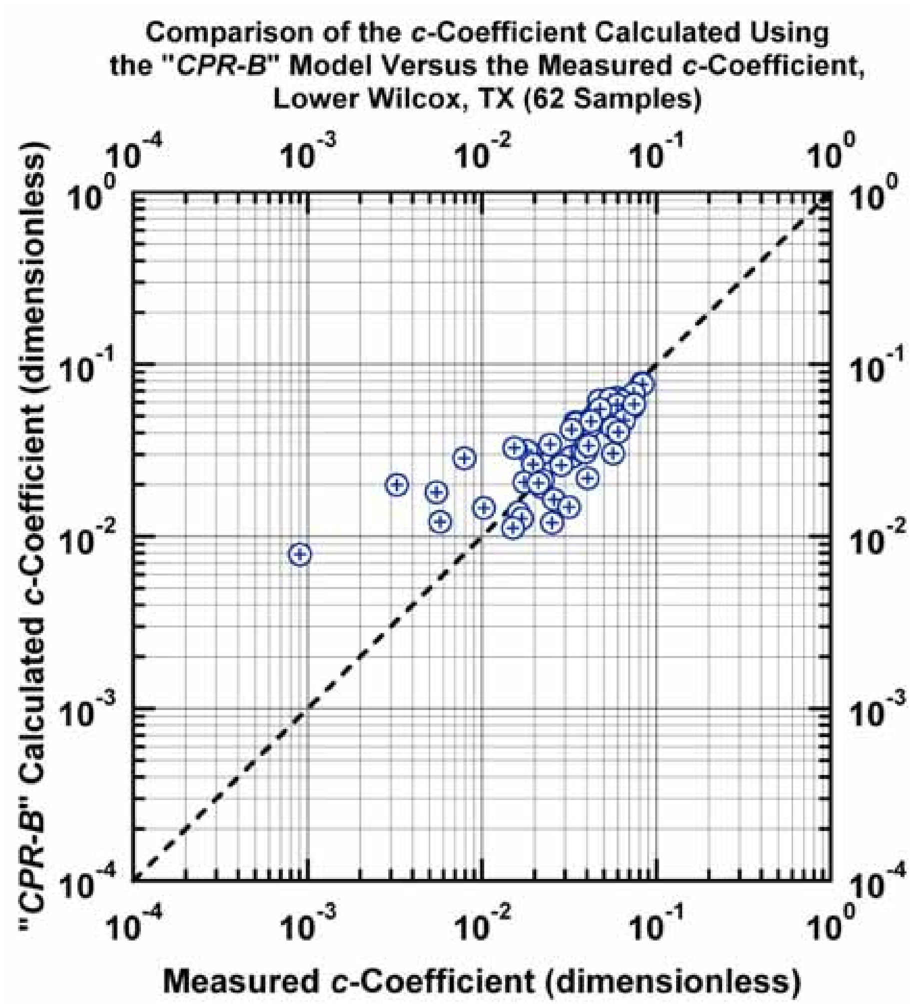

Figure I.4c — Model *CPR-B*: Calculated *c*-function values versus measured *c*-function values. [*Case*: Lower Wilcox S. TX (USA)]

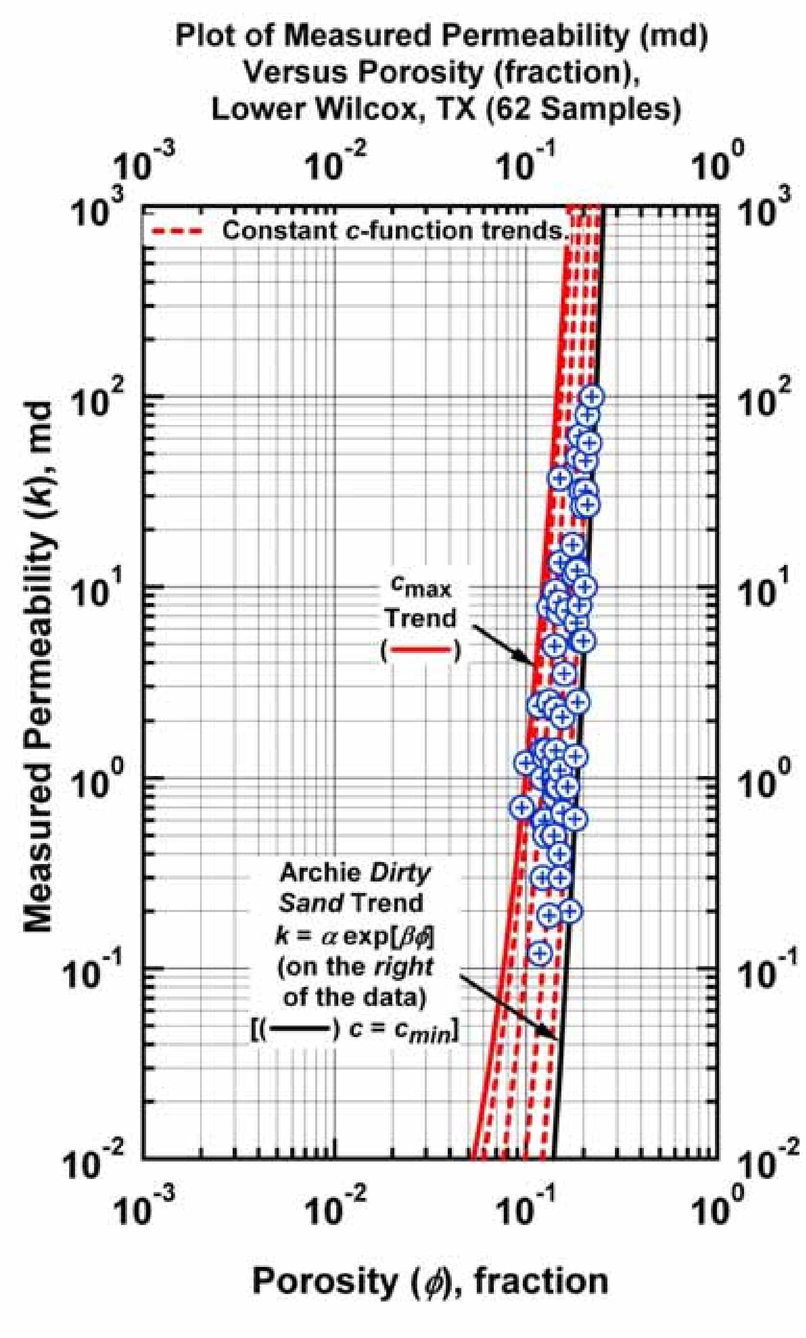

Figure I.5a — Model *CPR-C*: $k = c\exp[\beta\phi]$ $c = c_{\max}\exp[-c_1\phi^{c_2}F^{c_3}]$ — "Clean Sand" Plot (log-log format) — Archie "Dirty Sand" trend is given by the curved trend at the far right of the data (exponential model). [*Case*: Lower Wilcox S. TX (USA)]

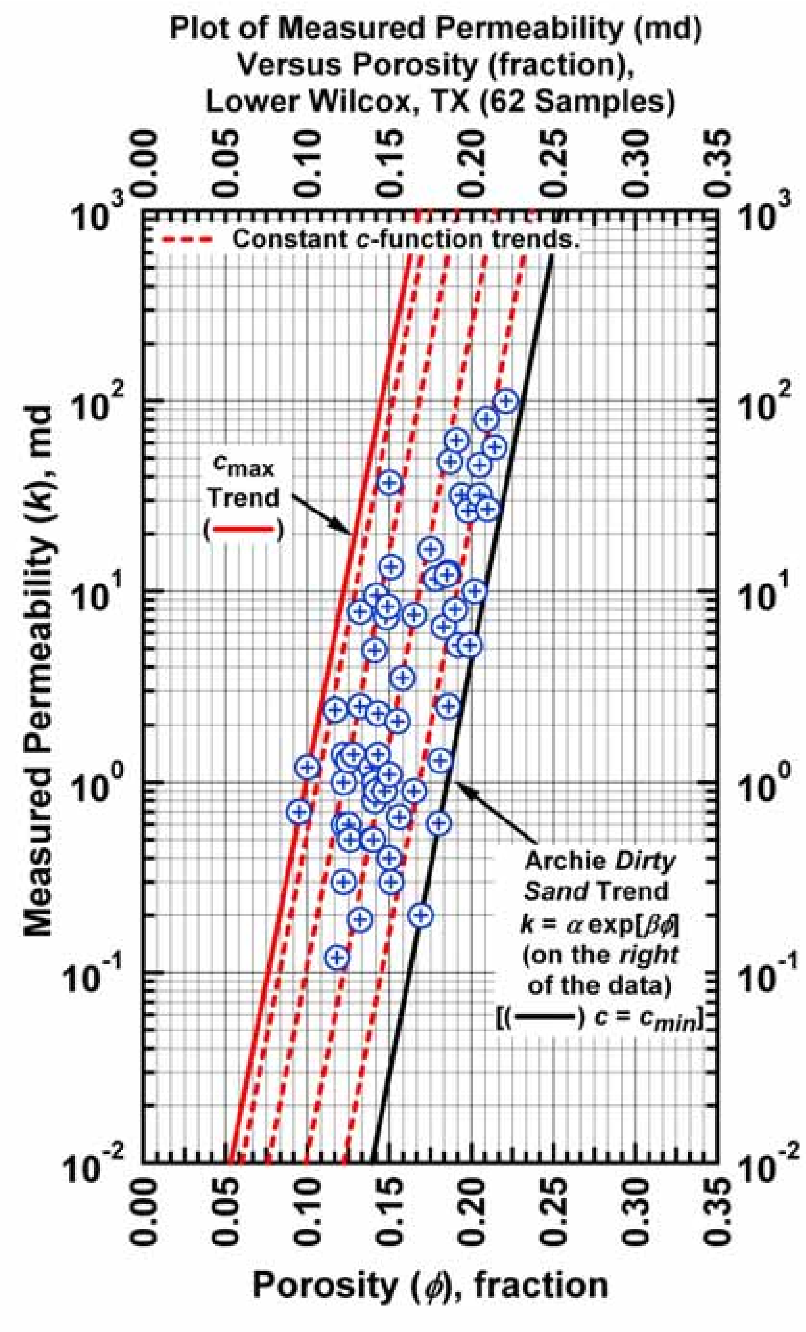

Figure I.5b — Model *CPR-C*: $k = c\exp[\beta\phi]$ $c = c_{\max}\exp[-c_1\phi^{c_2}F^{c_3}]$ — "Dirty Sand" Plot (semilog format) — Archie "Dirty Sand" trend is given by the straight-line trend at the far right of the data (exponential model). [*Case*: Lower Wilcox S. TX (USA)]

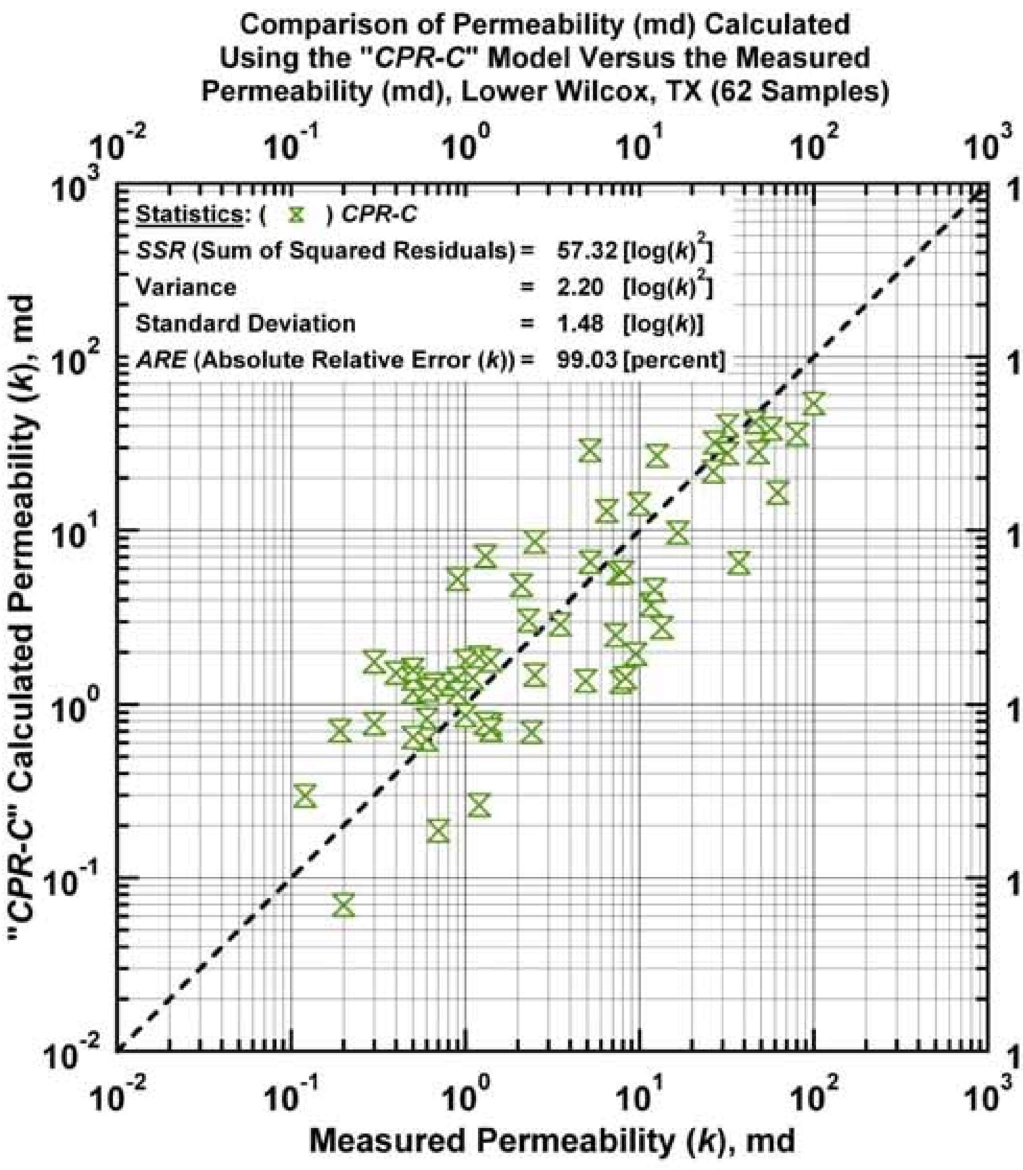

Figure I.6a — Model *CPR-C*: calculated versus measured permeability. [*Case*: Lower Wilcox S. TX (USA)]

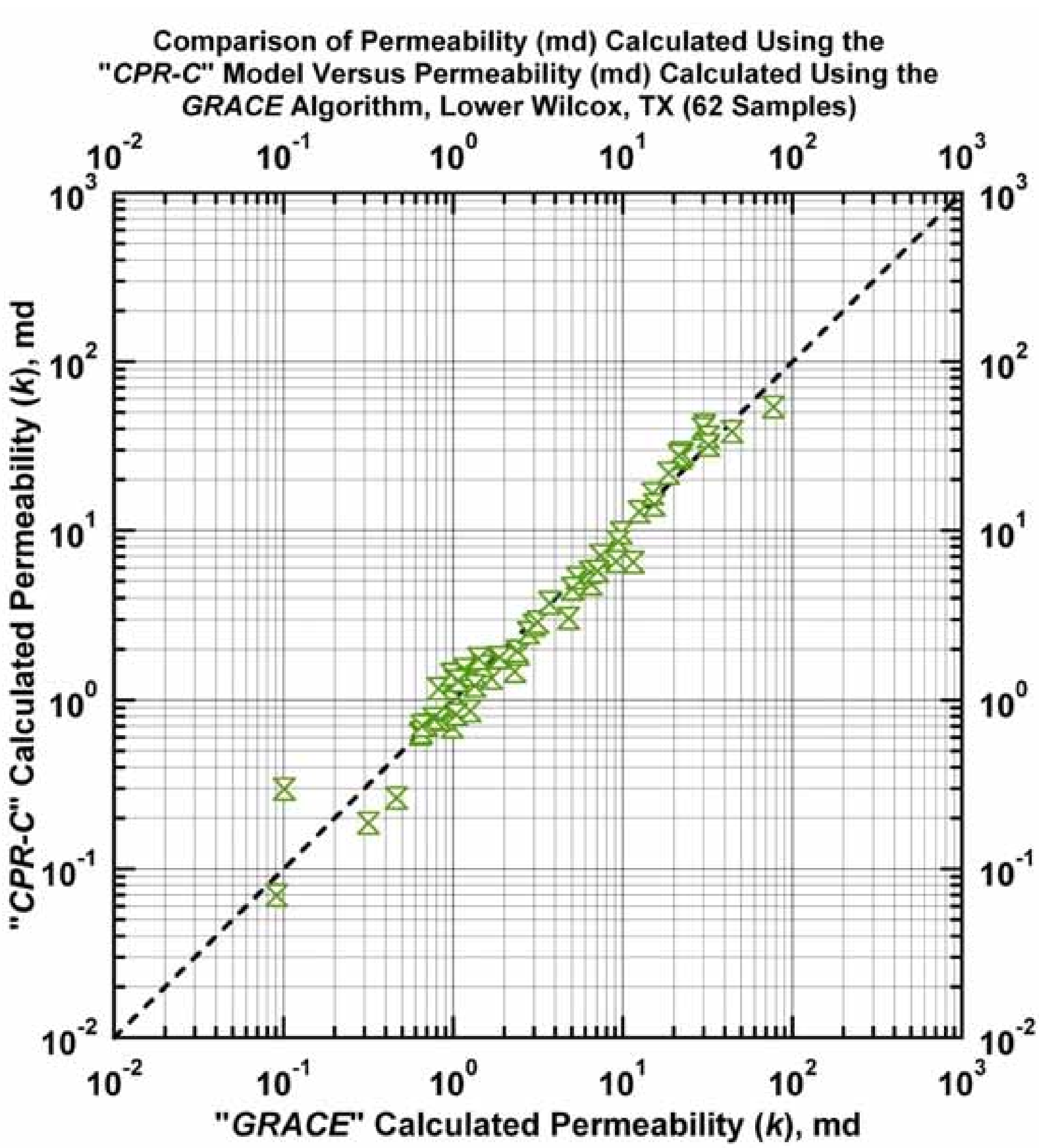

Figure I.6b — Model *CPR-C*: Permeability calculated using Model *CPR-C* versus permeability calculated using the *GRACE* Algorithm. [*Case*: Lower Wilcox S. TX (USA)]

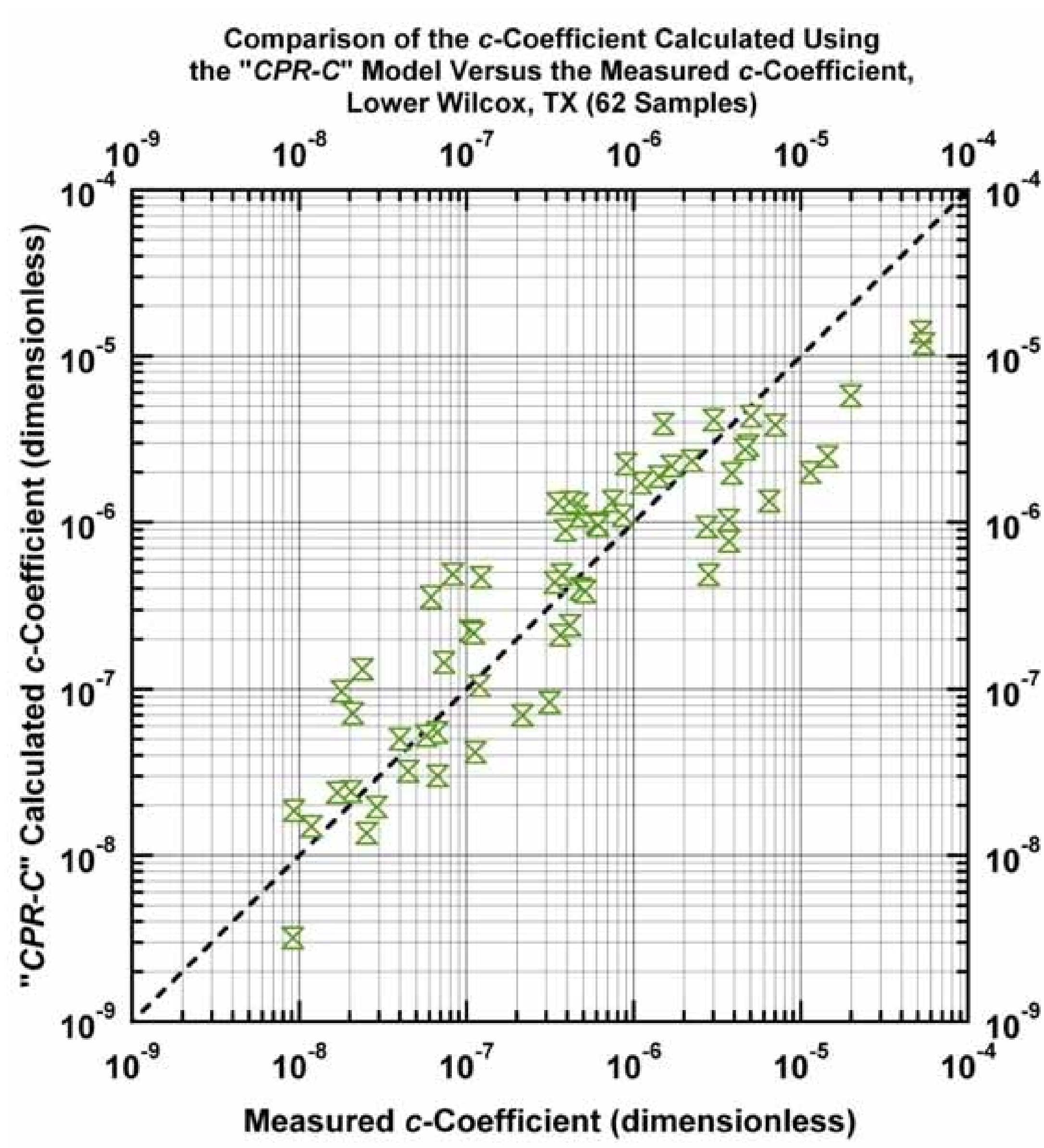

Figure I.6c — Model *CPR-C*: Calculated *c*-function values versus measured *c*-function values. [*Case*: Lower Wilcox S. TX (USA)]

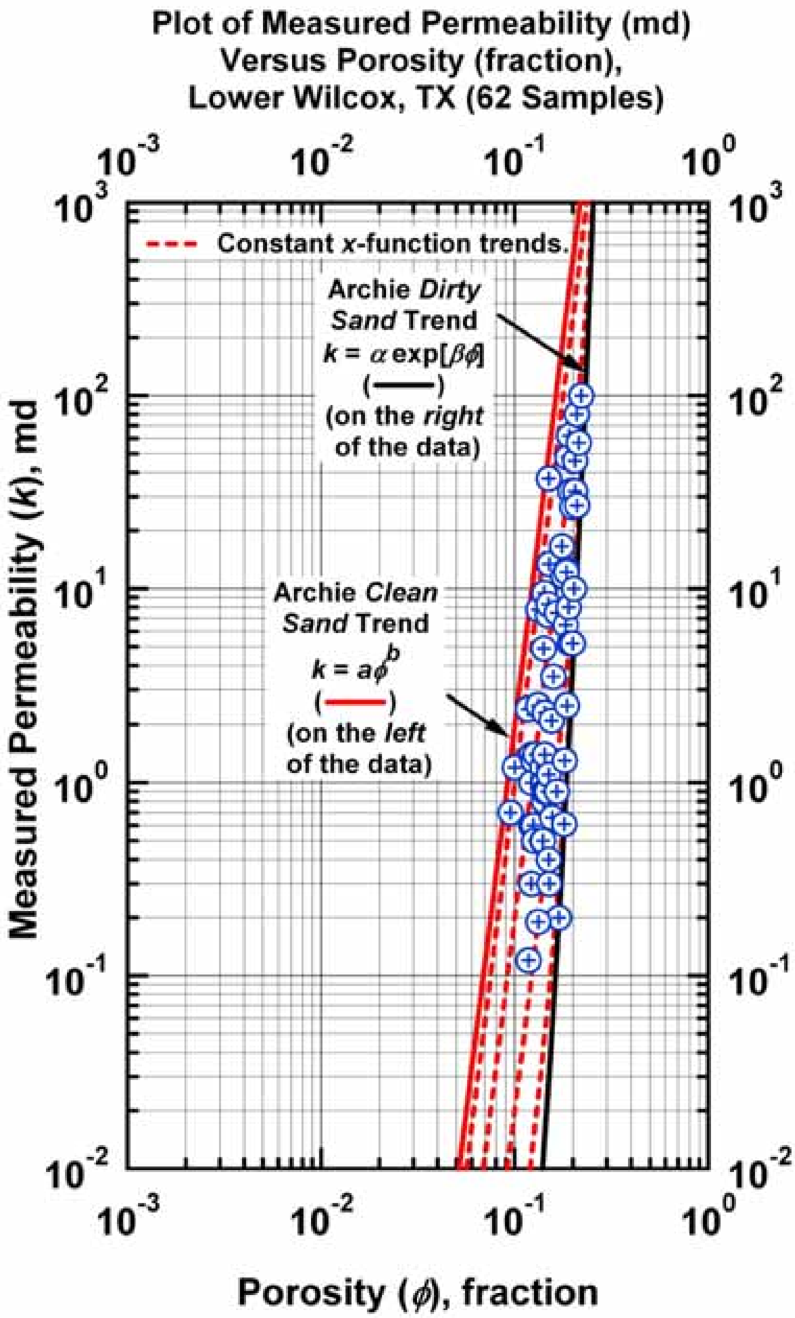

Figure I.7a — Model *CPR-D*: $k = xa\phi^{b} + (1-x)\alpha\exp[\beta\phi]$ $[0 \le x \le 1]$ — *Weighted Power Law-Exponential Model* used to correlate permeability (k) and porosity (ϕ). "Clean Sand" Plot — Archie "Clean Sand" trend is given by the straight-line trend at the far left of the data (power law model). [*Case*: Lower Wilcox S. TX (USA)]

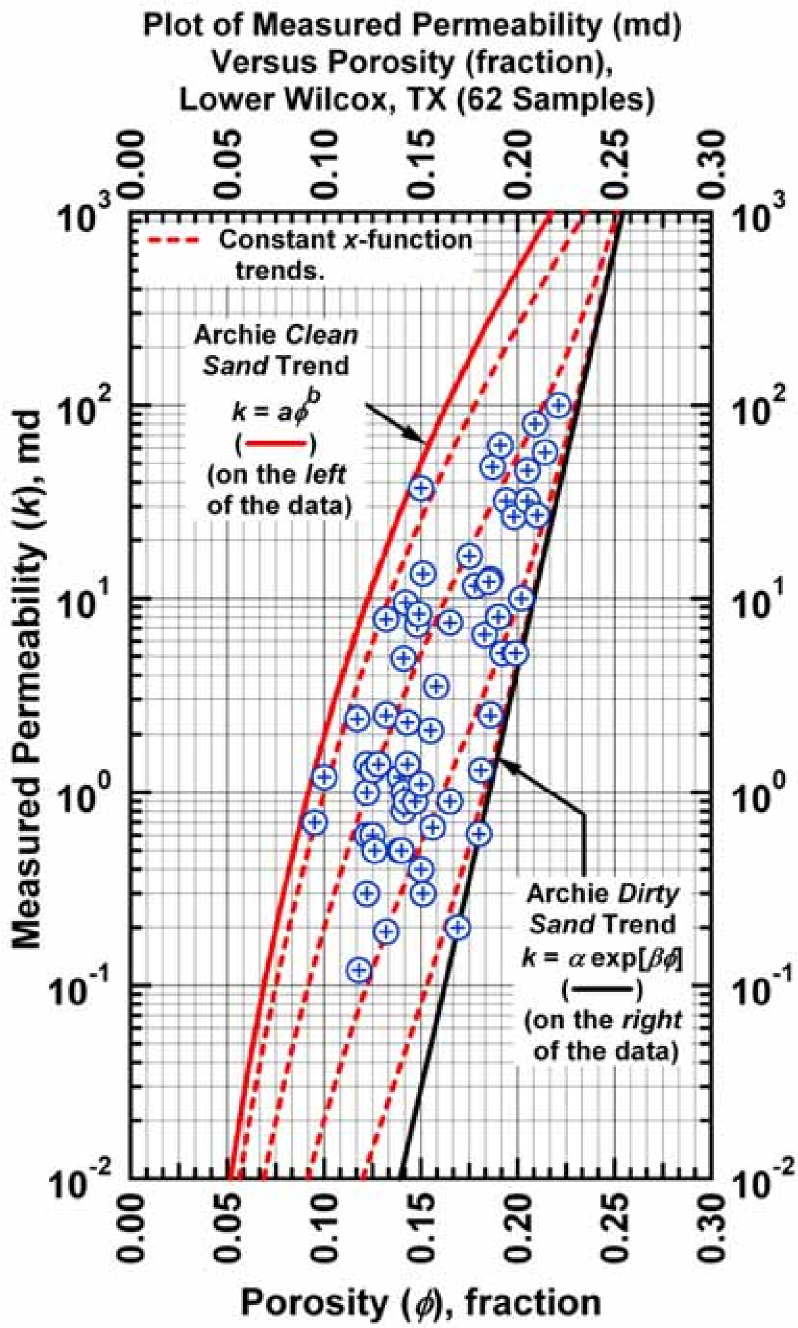

Figure I.7b — Model *CPR-D*: $k = xa\phi^b + (1-x)\alpha\exp[\beta\phi]$ $[0 \leq x \leq 1]$ — *Weighted Power Law-Exponential Model* used to correlate permeability (k) and porosity (ϕ). "Dirty Sand" Plot — Archie "Dirty Sand" trend is given by the straight-line trend at the far right of the data (exponential model). [*Case*: Lower Wilcox S. TX (USA)]

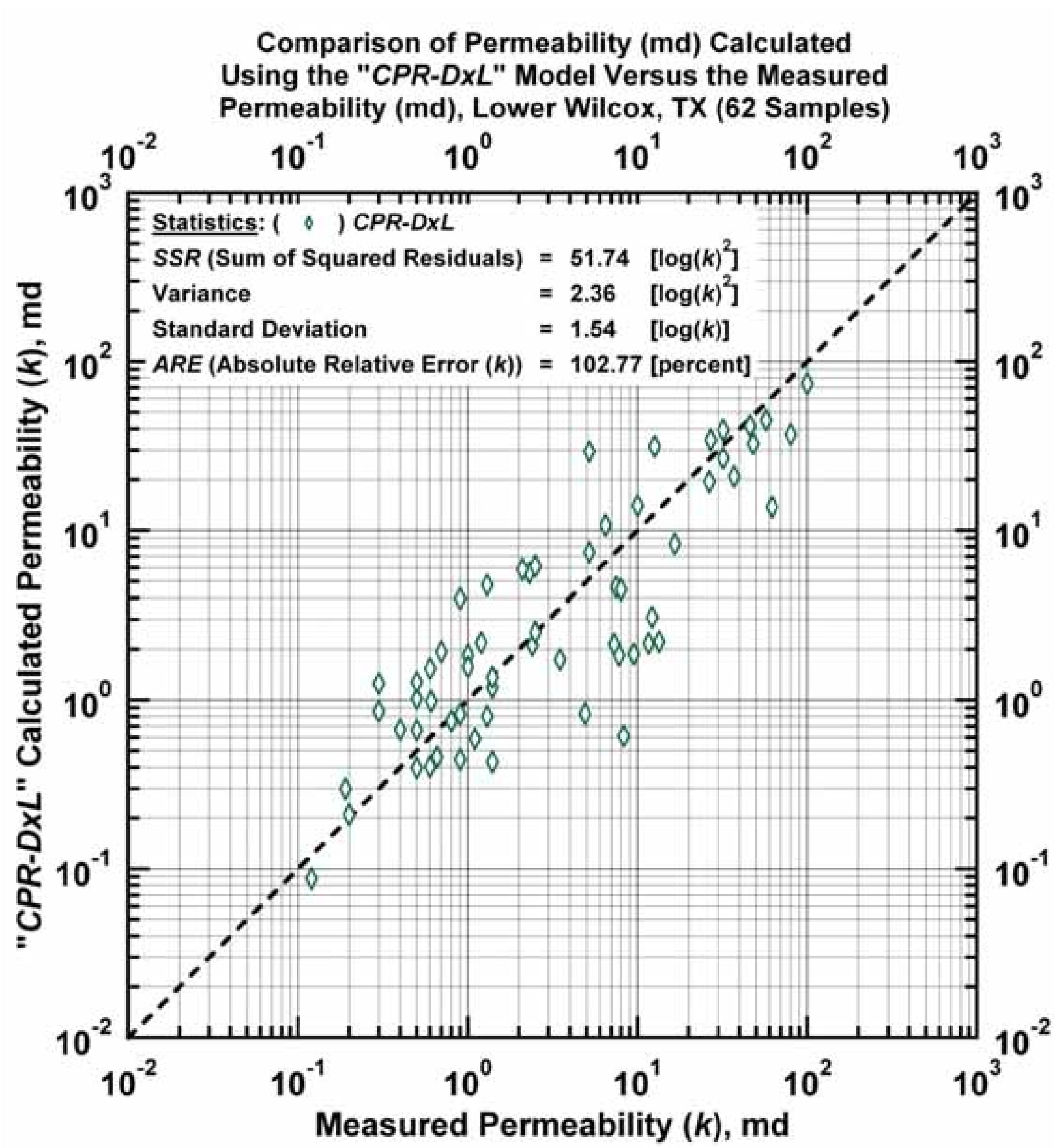

Figure I.8a — Model *CPR-DxL*: Calculated versus measured permeability. [*Case*: Lower Wilcox S. TX (USA)]

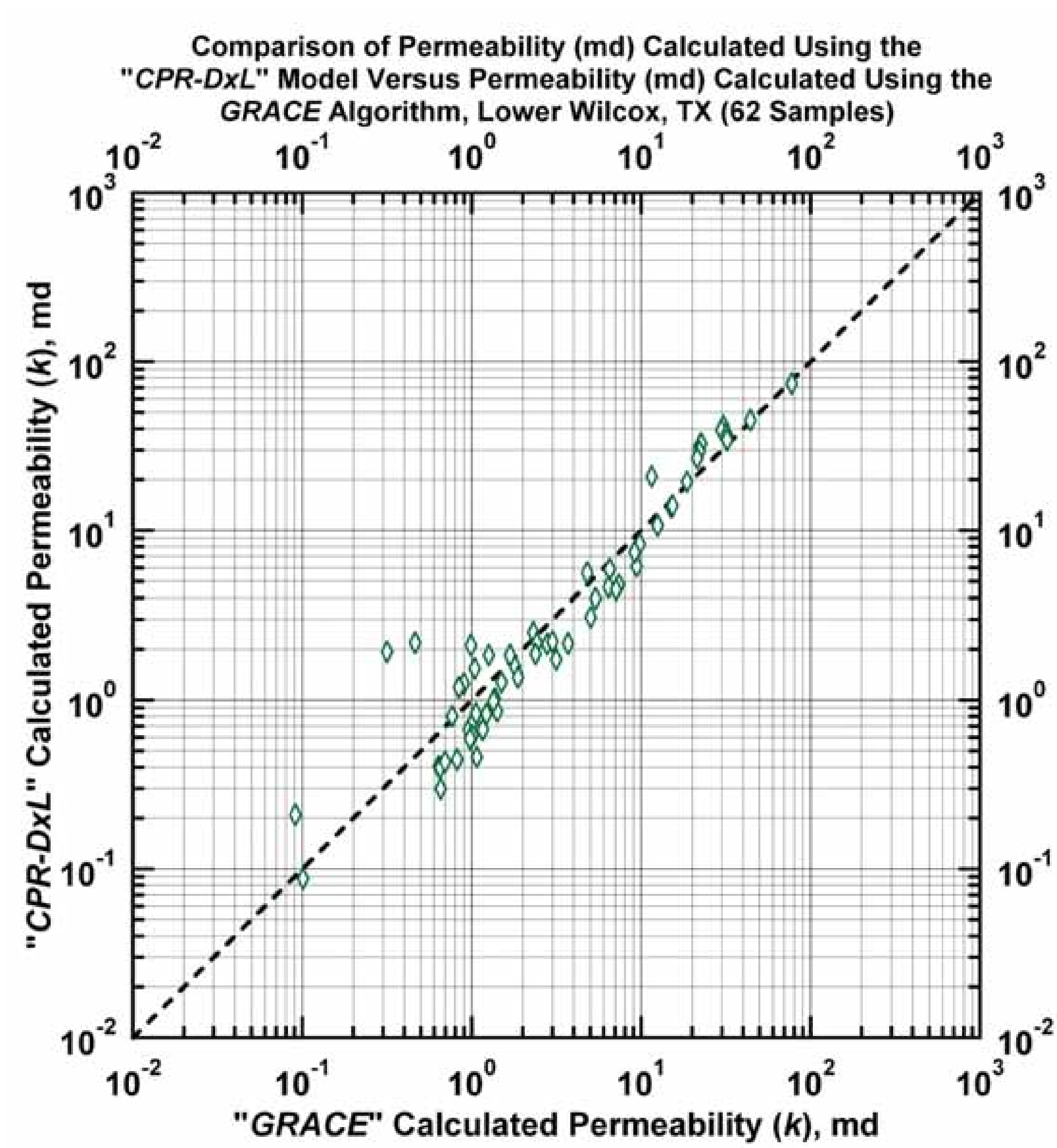

Figure I.8b — Model *CPR-DxL*: Permeability calculated using Model *CPR-C* versus permeability calculated using the *GRACE* Algorithm. [*Case*: Lower Wilcox S. TX (USA)]

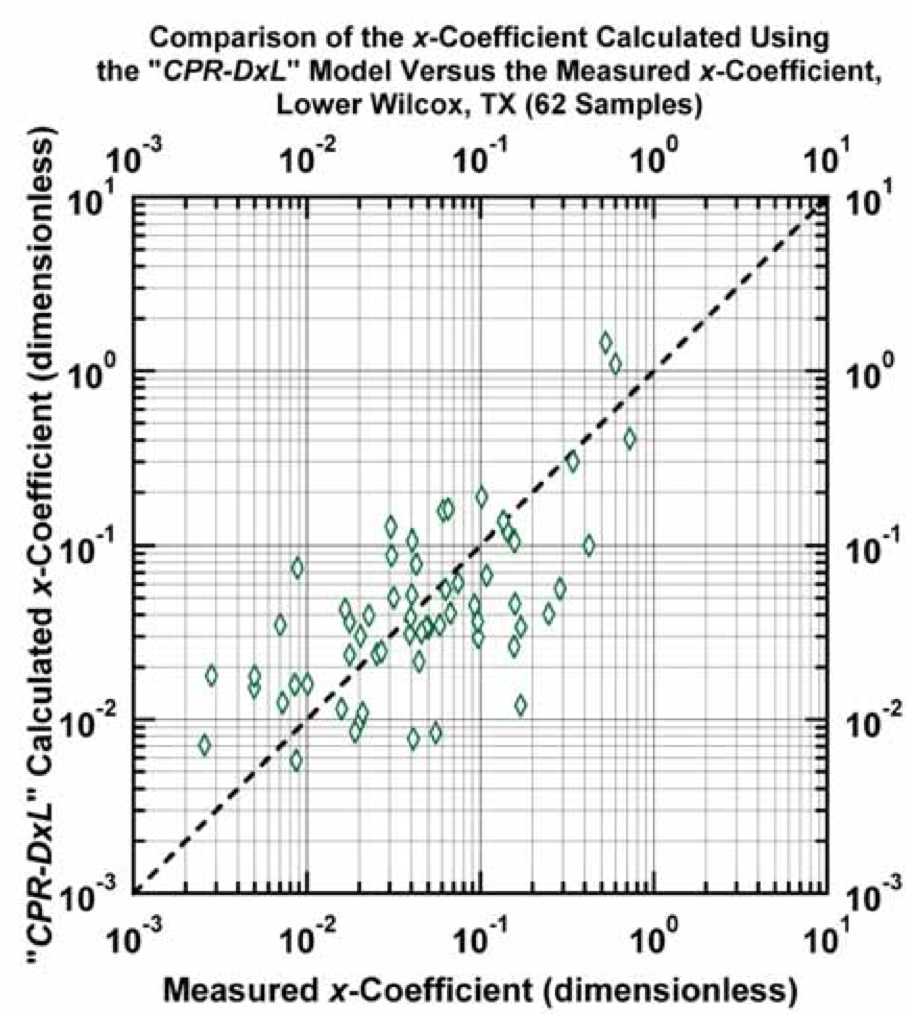

Figure I.8c — Model *CPR-DxL*: Calculated *x*-function weight values versus measured *x*-function weight values. [*Case*: Lower Wilcox S. TX (USA)]

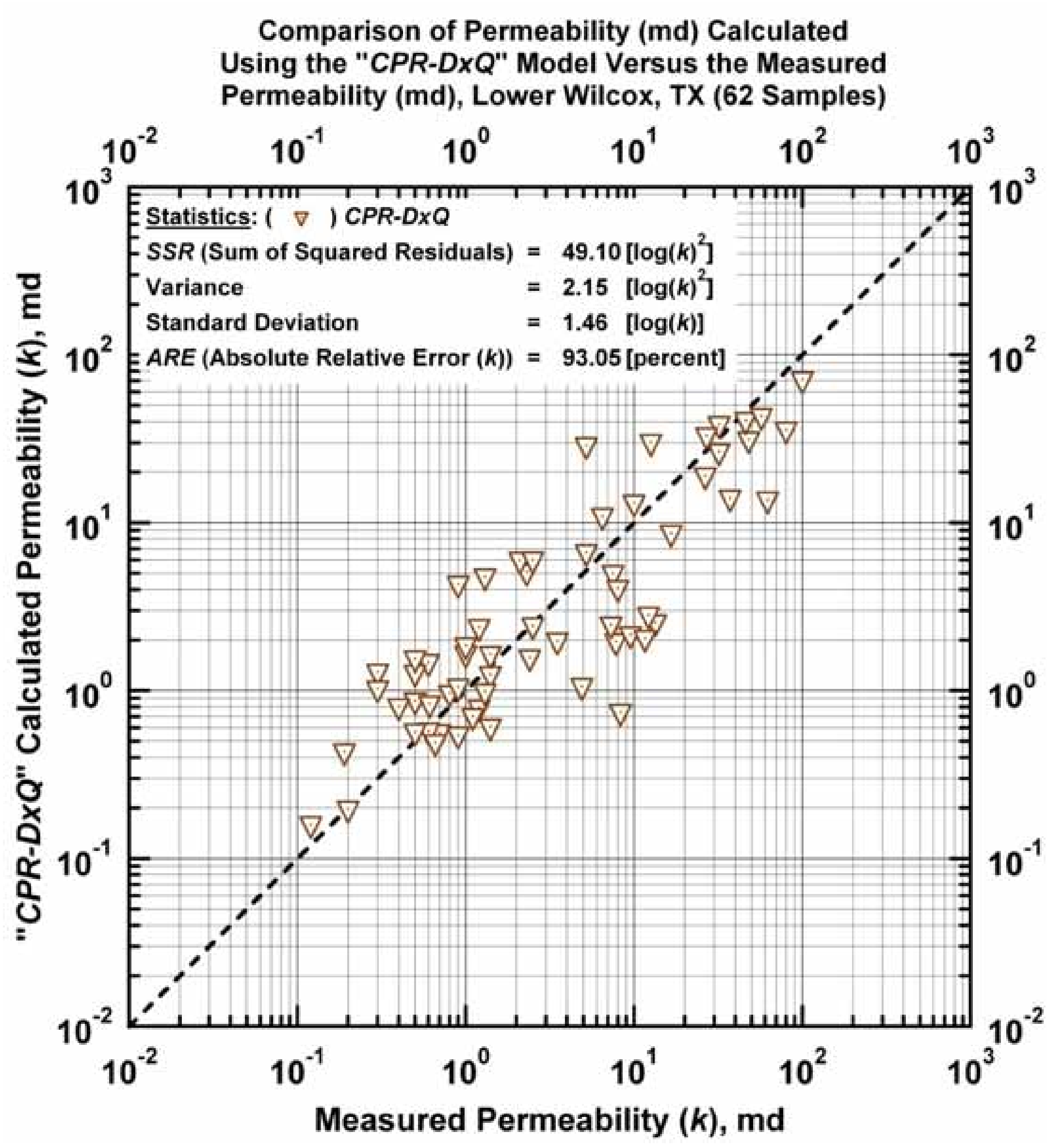

Figure I.9a — Model *CPR-DxQ*: Calculated versus measured permeability. [*Case*: Lower Wilcox S. TX (USA)]

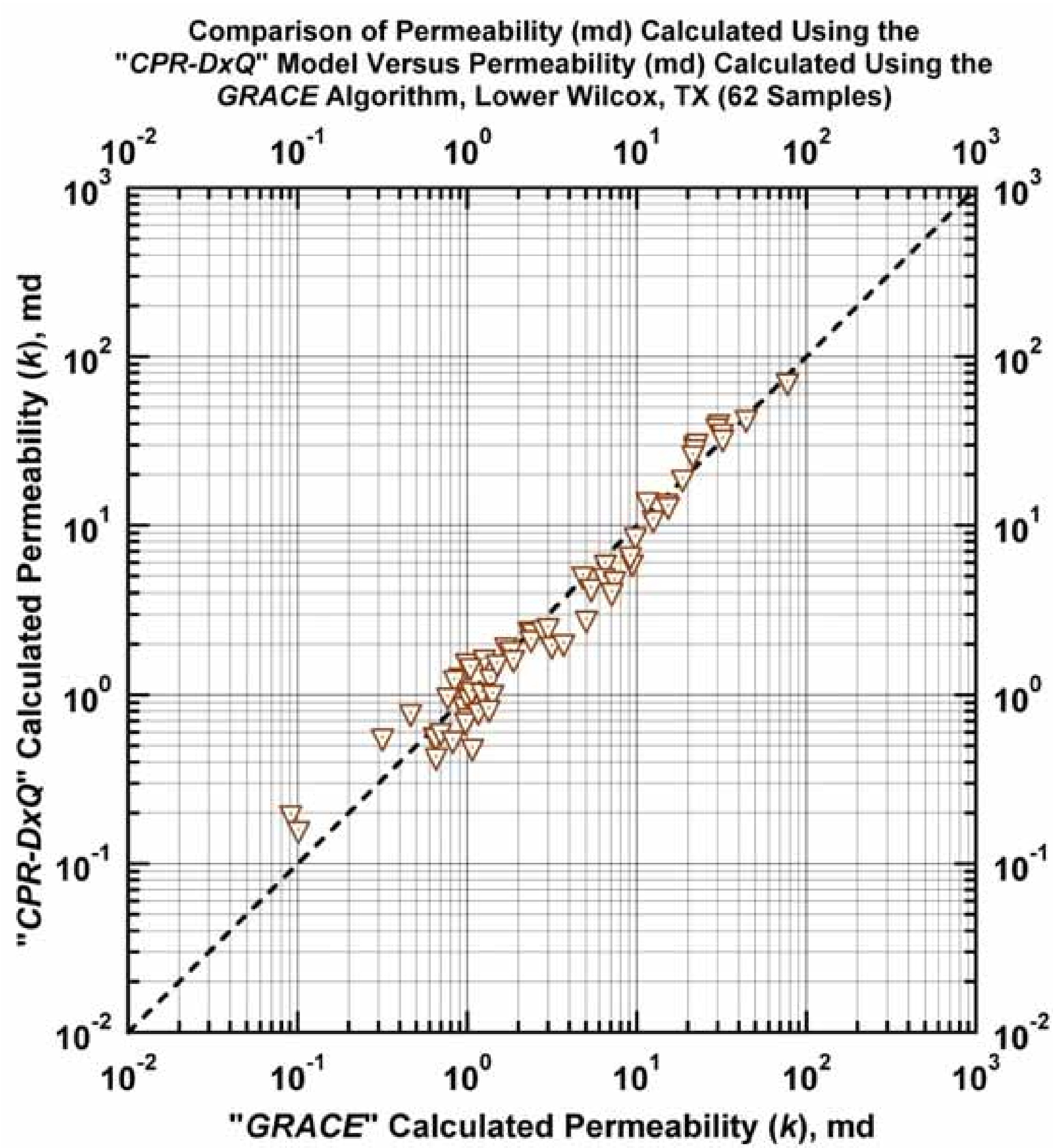

Figure I.9b — Model *CPR-DxQ*: Permeability calculated using Model *CPR-C* versus permeability calculated using the *GRACE* Algorithm. [*Case*: Lower Wilcox S. TX (USA)]

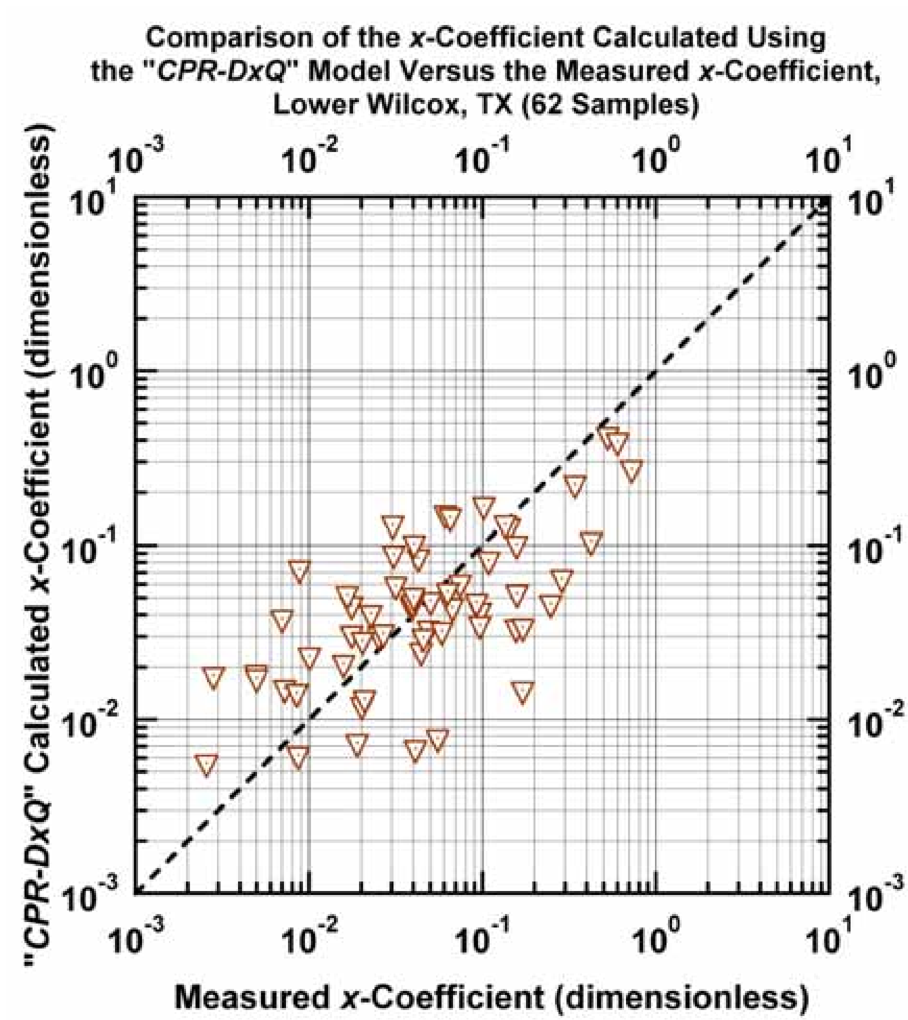

Figure I.9c — Model *CPR-DxQ*: Calculated *x*-function weight values versus measured *x*-function weight values. [*Case*: Lower Wilcox S. TX (USA)]

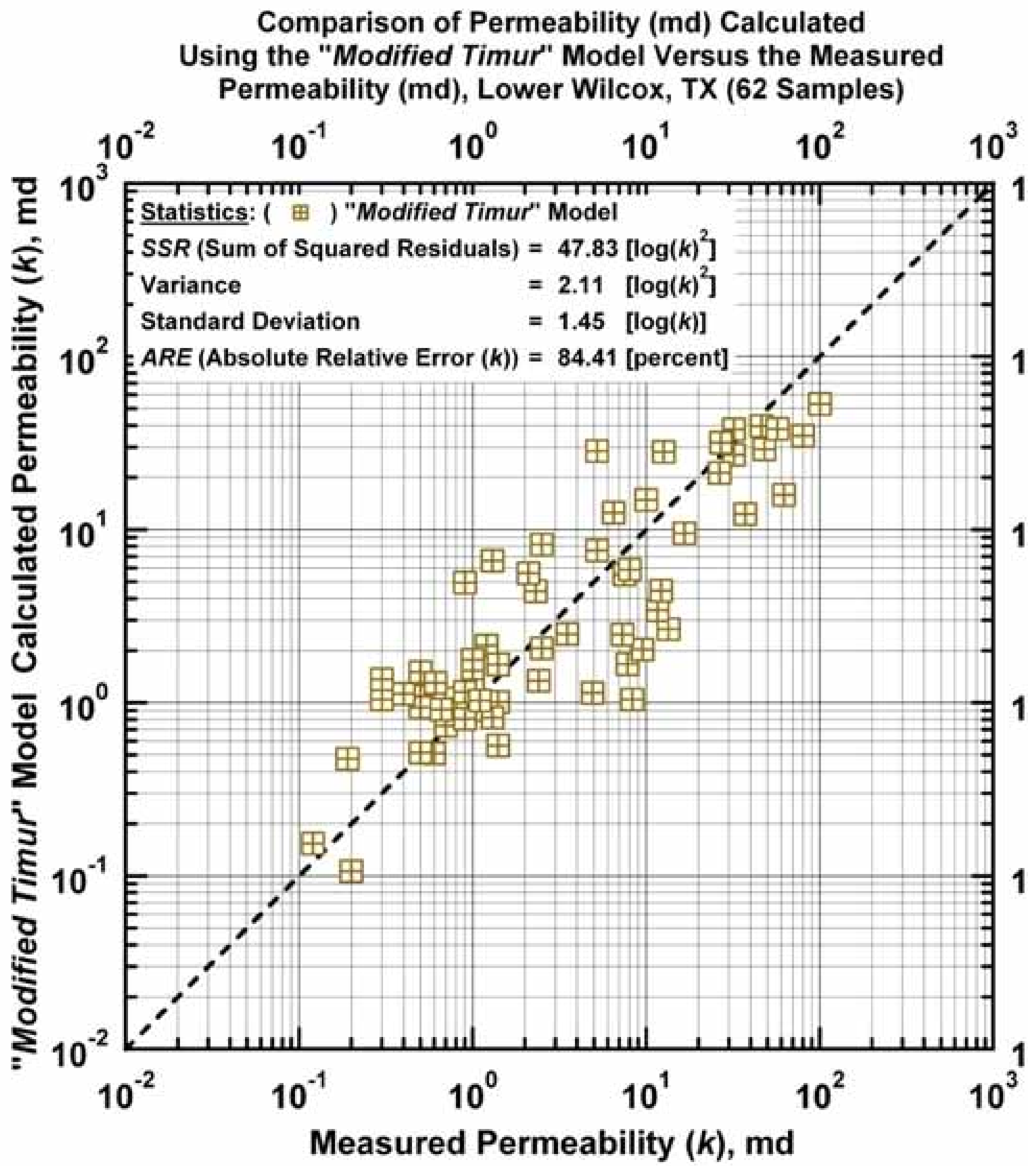

Figure I.10a — "Modified Timur Model:" Calculated versus measured permeability. [*Case*: Lower Wilcox S. TX (USA)]

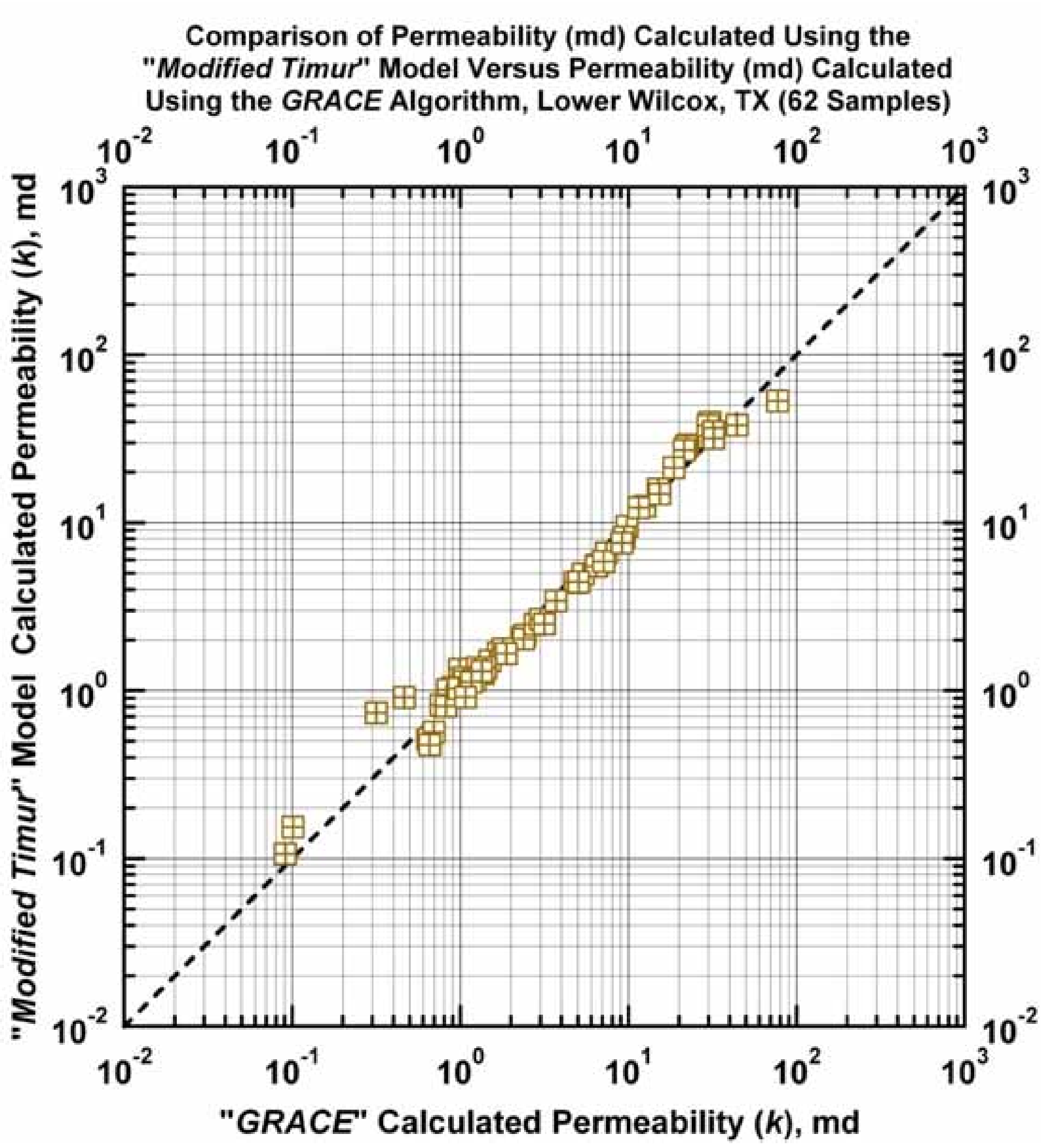

Figure I.10b — "Modified Timur Model:" Permeability calculated using the "Modified Timur Model" versus permeability calculated using the *GRACE* Algorithm. [*Case*: Lower Wilcox S. TX (USA)]

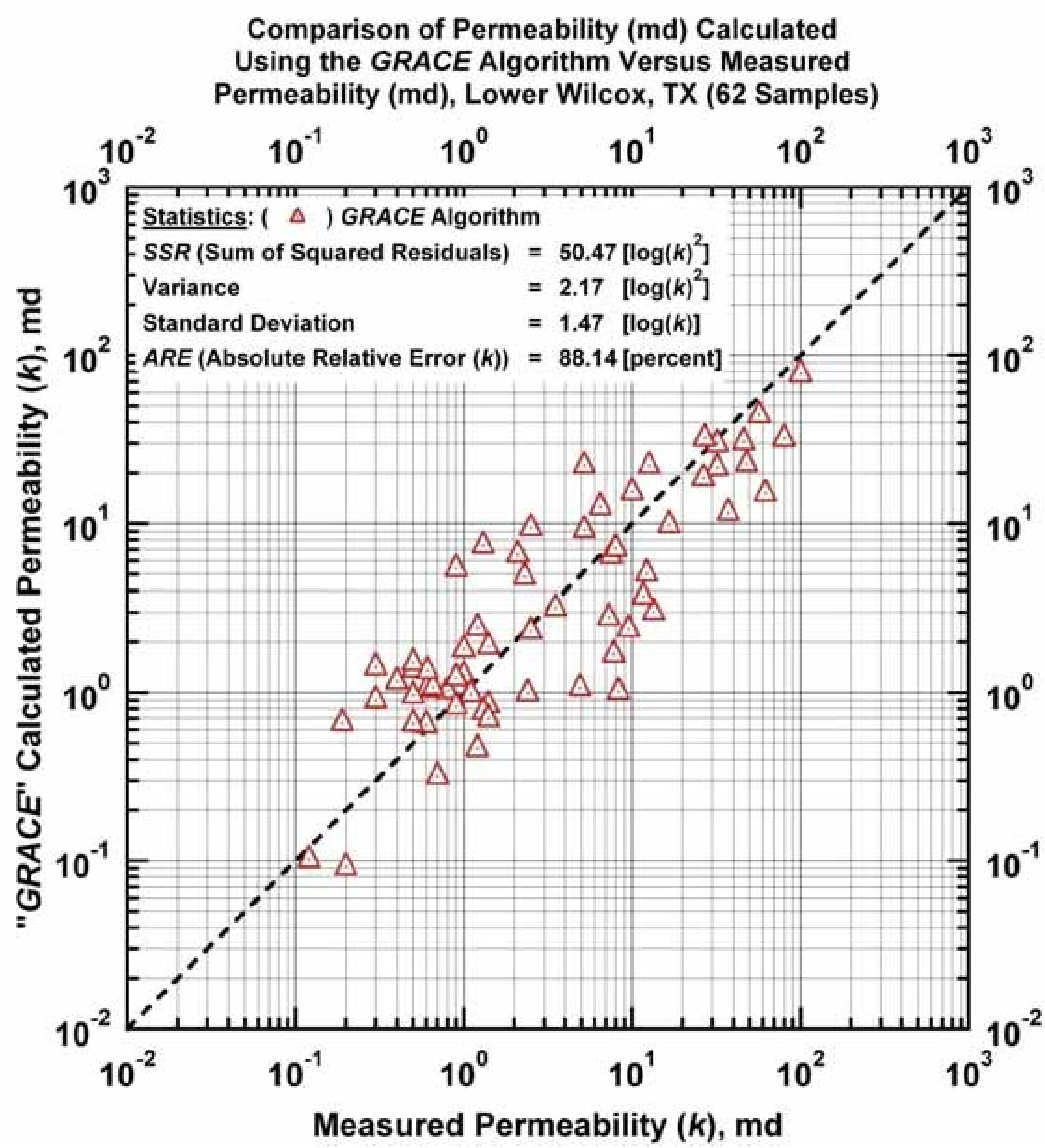

Figure I.11 — *GRACE* Model: Calculated versus measured permeability. [*Case*: Lower Wilcox S. TX (USA)]

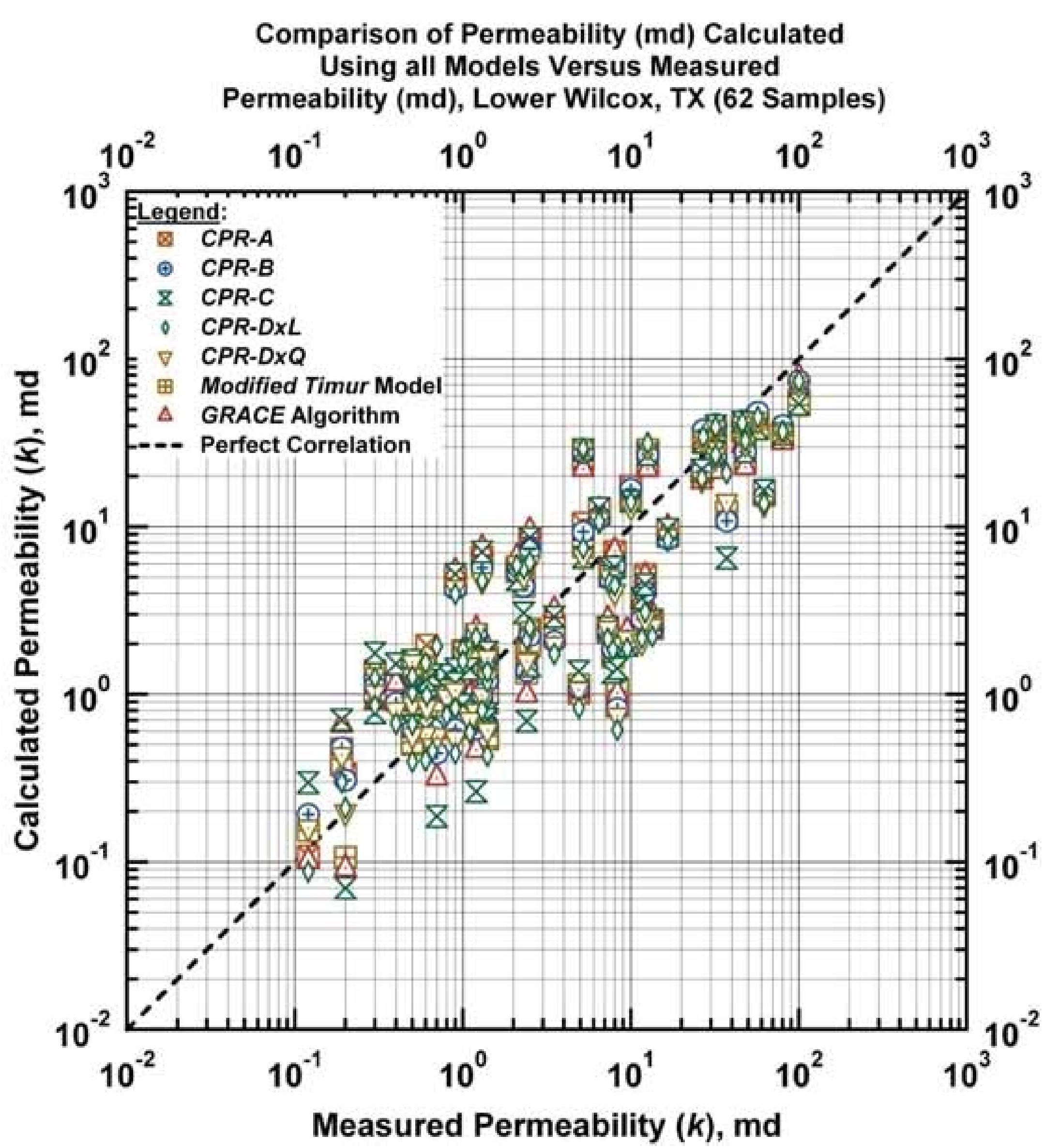

Figure I.12 — All Models: Calculated versus measured permeability. [*Case*: Lower Wilcox S. TX (USA)]

APPENDIX J

RESULTS FOR LOWER PALUXY CLEAN SANDSTONE (TEXAS — USA)

In this Appendix we present the "Paluxy" Well, located in Texas (USA) — this is a clean sandstone reservoir (Ellis, 1987).

Model *CPJ-A*: (Appendix J)

The "characteristic permeability relation" (or *CPR*) Model *CPJ-A* (*i.e.*, the modified Archie "Clean Sand" Model) is given as:

$$k = a(\phi - c)^b \quad c = c_{\max} \exp[-c_1 \phi^{c_2} F^{c_3}] \qquad \text{(J-1)}$$

Where a plot of log(k) versus log(ϕ) is used to graphically calibrate Eq. J-1 in terms of the coefficients — a, b, and $c_{\max}$. **Fig. J.1** shows that the *CPJ-A* model performs quite well for this case. **Figs. J.1a and b** show the log-log and the semilog format of permeability versus porosity, respectively. In **Fig. J.2** we provide the "error" plots for this case, where the measured and computed data are compared systematically. In **Fig. J.2a** we note a good correlation of the results obtained using Model *CPJ-A* versus the measured permeability data — there is good agreement with the perfect correlation trend (*i.e.*, the 45-degree line). In **Fig. J.2b** we provide a comparison with the *GRACE* algorithm correlation (Xue *et al*. 1997)), and we note that the *CPJ-A* model results correlate very well with the *GRACE* algorithm results for this case. Lastly, in **Fig. J.2c** we present the calculated and measured c-function — and again we note a reasonable correlation of the data about the perfect correlation trend.

Model *CPJ-B*: (Appendix J)

The "characteristic permeability relation" (or *CPR*) Model *CPJ-B* (*i.e.*, the modified Archie "Dirty Sand" Model (power-law basis)) is given as:

$$k = a(\phi + c)^b \quad c = c_{\max} \exp[-c_1 \phi^{c_2} F^{c_3}] \qquad \text{(J-2)}$$

Where a plot of log(k) versus log(ϕ) is used to graphically calibrate Eq. J-2 in terms of the coefficients — a, b, and $c_{\max}$. The results for this case are presented in **Figs. J.3 and 4**. In **Fig. J.3a** (log-log format) we note that a very distinct "envelope" is formed by the *CPJ-B* model, essentially all of the data on the right and left flanks are well-matched (*i.e.*, the "dirty sand" power law relation (applied on the right portion of the data) and its correction function (applied on the left portion of the data). Similarly, in **Fig. J.3b** (semilog format), we observe an excellent distribution of the power law model across the body of the data. The error analyses for this case are shown in **Fig. J.4**. In **Fig. J.4a** we present the results obtained using Model *CPJ-B* versus the measured permeability data. In this case we observe good agreement with the perfect correlation trend (*i.e.*, the 45-degree line). We provide a comparison with the *GRACE* algorithm correlation in **Fig. J.4b** — the results using Model *CPJ-B* and the *GRACE* algorithm compare very well for this case. We compare the computed and data-derived values of the *c*-function for this case in **Fig. J.4c** and we note a reasonably "tight" correlation, except for the very lowest values of the *c*-function. In summary, we believe that Model *CPJ-B* is a very effective correlation model for this particular data case.

Model *CPJ-C*: (Appendix J)

The "characteristic permeability relation" (or *CPR*) Model *CPJ-C* (*i.e.*, the modified Archie "Dirty Sand" Model (exponential basis)) is given as:

$$k = c\exp[\beta\phi] \quad c = c_{\max}\exp[-c_1\phi^{c_2}F^{c_3}] \qquad \text{(J-3)}$$

Where a plot of log(*k*) versus ϕ is used to graphically calibrate Eq. J-3 in terms of the coefficients — β and $c_{\max}$. Model *CPJ-C* is fundamentally different than Models *CPJ-A* and *CPJ-B*, as the basis for Model *CPJ-C* is an exponential function, not a power law relation. In **Figs. J.5 and 6** we present the results of applying Model *CPJ-C* for this case, and in general, we observe a very consistent performance of Model *CPJ-C*. **Fig. J.5b** illustrates the excellent conformance of Model *CPJ-C* for this case — again recalling that this model has an exponential relationship with porosity as its basis.

In **Figs. J.6a, J.6b, and J.6c** we review the error analyses plots for this case, and we note good performance (visually) in terms of the correlation of the results using Model *CPJ-C*. The correlation of the *c*-function (see **Fig. J.6c**) appears to be consistent — but scatter and a slight off-center trend is evident. We believe that the *CPJ-C* model has performed well for this case, and the plots in **Fig. J.6** confirm the value of this model as a "characteristic relation" for permeability.

Model *CPJ-D*: (Appendix J)

The "characteristic permeability relation" (or *CPR*) Model *CPJ-D* (*i.e.*, the weighted power law-exponential model) is given in its fundamental form as:

$$k = xa\phi^{b} + (1-x)\alpha\exp[\beta\phi] \quad [0 \le x \le 1]] \qquad \text{(J-4a)}$$

For Eq. J-4 there are two proposed models for the *x*-function (*i.e.*, the weighting function) — these are:

$$x = \exp[-\ln(x_0) + x_1\ln(\phi) + x_2\ln(F) + x_3\ln(\phi)\ln(F)] \quad \text{(Model } CPJ\text{-}DxL\text{)} \qquad \text{(J-4b)}$$

$$x = \exp\begin{bmatrix} -\ln(x_0) + x_1\ln(\phi) + x_2\ln(F) + x_3\ln(\phi)\ln(F) \\ + x_4\ln(\phi)^2 + x_5\ln(F)^2 + x_6\ln(\phi)^2\ln(F) \\ + x_7\ln(\phi)\ln(F)^2 + x_8\ln(\phi)^2\ln(F)^2 \end{bmatrix} \quad \text{(Model } CPJ\text{-}DxL\text{)} \qquad \text{(J-4c)}$$

As noted in Eq. J-4b, Model *CPJ-DxL* utilizes a logarithmic linear model for the weights (*x*-values) and as seen in Eq. J-4c, Model *CPJ-DxQ* utilizes a logarithmic quadratic model for the weights (*x*-values). While these models (Eqs. J-4b and J-4c) are *empirical*, we have found generally good application of these relations for all cases. In this case, the base results using Models *CPJ-DxL* and *CPJ-DxQ* are presented in

Fig. J.7 — where the power law and exponential basis functions are fitted to the appropriate portion of the data. The power law equation represents the "Archie clean sand" trend and is fitted to the leftmost data as shown in **Fig. J.7a** and in contrast, the exponential equation is thought to represent the "Archie dirty sand" trend and the exponential is fitted to the far rightmost portion of the data (see **Fig. J.7b**).

In **Figs. J.8 and 9** we present the error analyses for this case, where we have employed the weighting functions (Eqs. J-4b and J-4c) as appropriate. In **Fig. J.8a** we find a good correlation of permeability (with the out-lying points noted in the middle of the trend). The comparison of the Model *CPJ-DxL* results are compared to the results obtained from the *GRACE* algorithm in **Fig. J.8b**, we note that the very good results obtained using Model *CPJ-DxL*. The computed weight function (*x*-values) shown for the *CPJ-DxL* model in **Fig. J.8c** does exhibit more scatter than expected, but the trend is (relatively) centered about the perfect correlation line.

The results obtained using Model *CPJ-DxQ* are presented in **Fig. J.9**, and we note substantially improved behavior over that of Model *CPJ-DxL*. In particular, the base correlation of computed and measured permeabilities (**Fig. J.9a**) for Model *CPJ-DxQ* does indicate a slightly better correlation than that of Model *CPJ-DxL*. Also, the comparison of Model *CPJ-DxQ* with the results from the *GRACE* algorithm (**Fig. J.9b**) exhibits better agreement than the results of Model *CPJ-DxL*. Finally, the correlation of the *x*-function (**Fig. J.9c**) for Model *CPJ-DxQ* is better than the correlation for Model *CPJ-DxL*. These comparisons suggest that Model *CPJ-DxQ* (*i.e.*, the combination of Eqs. J-4a and J-4c) has provided a better correlation of data, for this case, than Model *CPJ-DxL*.

***"Modified Timur Model"*: (Appendix J)**

The "Modified Timur Model" is given as:

$$k_{\text{Timur}} = a\phi^b F^c \qquad \text{(J-5)}$$

In **Fig. J.10** we present the results of the "Modified Timur Model" (Eq. J-5) which is essentially just a generalized power-law function relation in terms of k, ϕ, and F. **Figs. J.10a and b**, provide the "Modified Timur Model" results of the data for this case.

***GRACE* Algorithm: (Appendix J)**

In **Fig. J.11** we present the results predicted by the *GRACE* algorithm, which is a non-parametric regression approach (see Xue *et al.* (1997) for details). In theory, the *GRACE* algorithm should provide the most *unbiased* correlation of the data — *i.e.*, the *GRACE* algorithm is designed not to "fit the errors" as other regression approaches may. It is our contention that the *GRACE* algorithm is the statistical standard — and any algorithm/approach/model which achieves better regression statistics than the *GRACE* algorithm is actually "fitting the errors" in the data. *Surprisingly all the cases have significantly better regression statistics than the GRACE algorithm* — hence, we must label these cases as "over-fitted" in a statistical sense.

***Comparison of All Models*: (Appendix J)**

Our final graphic, **Fig. J.12**, illustrates all of the models on a single plot of calculated versus measured permeability. We also present a table of all statistical results in **Table J.1**.

Table J.1 — Statistical Results for all Models (Paluxy TX (USA), n=43).

Model	Sum of Squared Residuals [$\log(k)^2$]	Variance [$\log(k)^2$]	Standard Deviation [$\log(k)$]	Absolute Relative Error [percent]
CPJ-A	18.60	5.10	2.26	45.26
CPJ-B	16.00	4.90	2.21	42.69
CPJ-C	15.38	5.05	2.25	44.37
CPJ-DxL	15.52	4.91	2.22	46.13
CPJ-DxQ	14.43	4.94	2.22	44.86
Modified Timur	15.28	4.98	2.23	39.75
GRACE Algorithm	15.73	4.88	2.21	47.68

The coefficients for the models used in this case are provided in **Table J.2**.

Table J.2a — Model Coefficients (Paluxy TX (USA), n=43).

Model	a or α	b or β	c or c_{max}	c_1	c_2	c_3
CPJ-A	$1.50\text{x}10^{9}$	8.00	0.090	$1.16\text{x}10^{-3}$	-6.21	-1.47
CPJ-B	$1.50\text{x}10^{7}$	8.00	0.110	2.62	3.21	1.38
CPJ-C	$1.50\text{x}10^{-3}$	50.00	0.05	$1.69\text{x}10^{2}$	4.91	1.12
Modified Timur	$5.76\text{x}10^{5}$	0.94	-2.194	–	–	–

Table J.2b — Model Coefficients (Paluxy TX (USA), n=43).

Model	a	b	α	β
CPJ-DxL	$1.50\text{x}10^{9}$	8.00	$1.50\text{x}10^{-3}$	50.00
CPJ-DxQ	$1.50\text{x}10^{9}$	8.00	$1.50\text{x}10^{-3}$	50.00

Model	c_0	c_1	c_2	c_3	c_4	c_5	c_6	c_7	c_8
CPJ-DxL	528.19	-13.36	-6.03	0.06	–	–	–	–	–
CPJ-DxQ	$9.69\text{x}10^{6}$	-16.23	0.14	7.04	3.87	-0.05	-0.56	-0.16	-0.09

Nomenclature: (Appendix J)

F = Archie Formation Factor (dimensionless)
k = Formation Permeability, md (or any consistent units)
ϕ = Porosity, fraction

References: (Appendix J)

Ellis, K.W.: "Extended Correlations of Porosity, Permeability, and Formation Resistivity Factor," MS thesis, Texas A&M U., College Station, TX (1987).

Xue, G., Datta-Gupta, A., Valko, P., and Blasingame, T.A.: "Optimal Transformations for Multiple Regression: Application to Permeability Estimation from Well Logs," *SPEFE* (June 1997), 85-93.

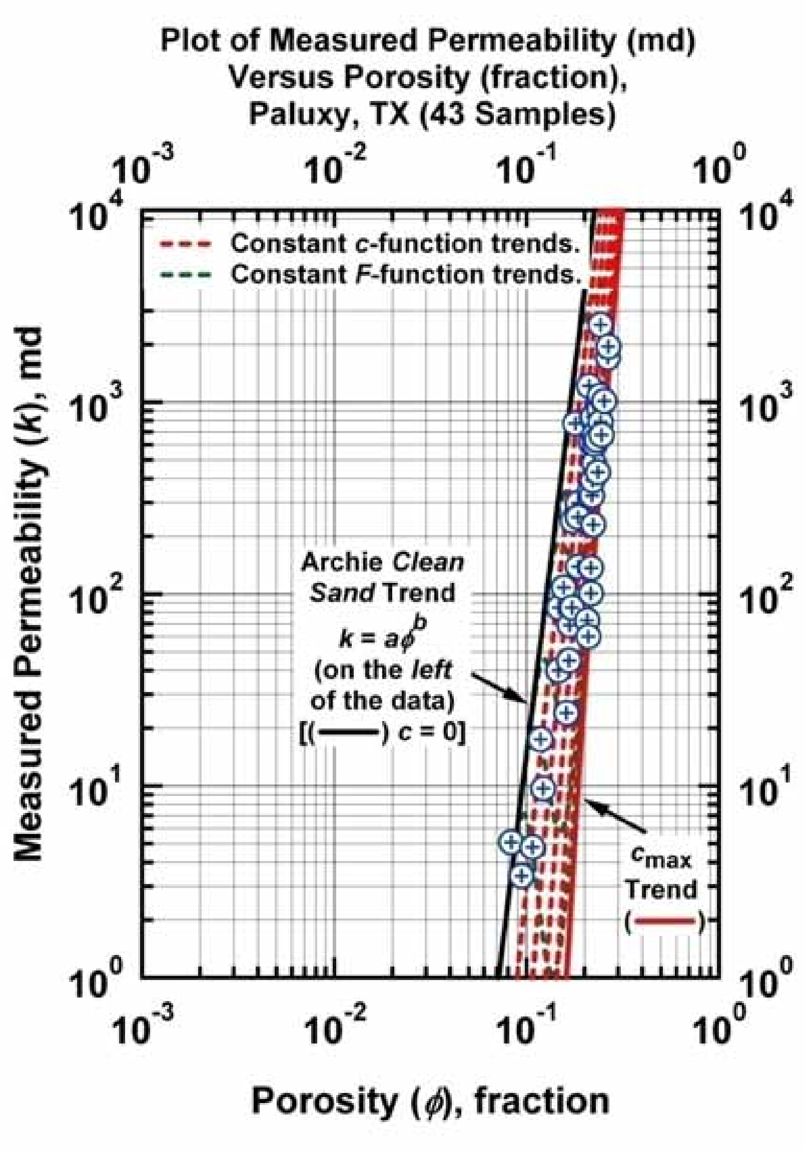

Figure J.1a — Model *CPJ-A*: $k = a(\phi - c)^b$ ($c = c_{max} \exp[-c_1 \phi^{c_2} F^{c_3}]$) — "Clean Sand" Plot (log-log format) — Archie "Clean Sand" trend is given by the straight-line trend at the far left of the data (power law model). [*Case*: Paluxy, TX (USA)]

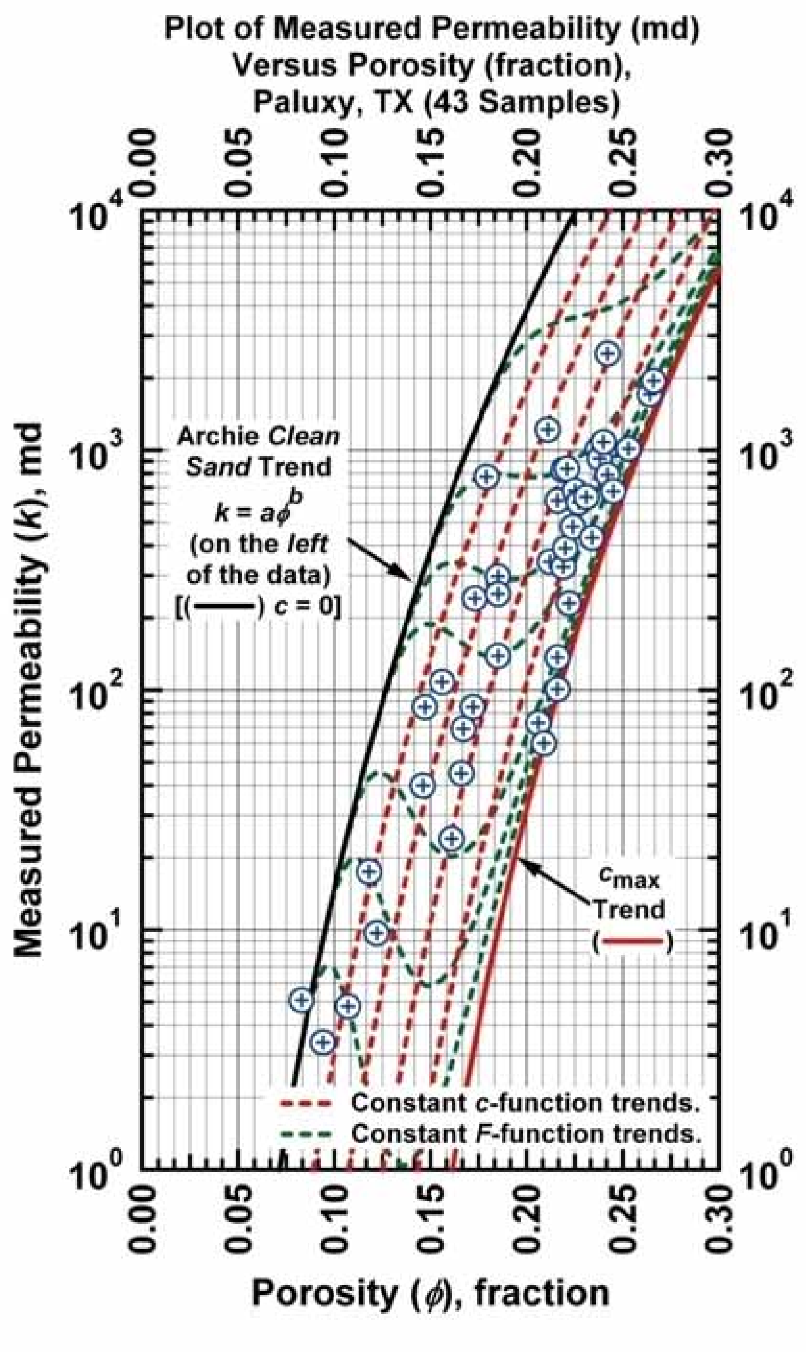

Figure J.1b — Model *CPJ-A*: $k = a(\phi - c)^b$ ($c = c_{max} \exp[-c_1 \phi^{c_2} F^{c_3}]$) — "Dirty Sand" Plot (semilog format). Archie "Clean Sand" trend is given by the curved trend at the far left of the data (power law model). [*Case*: Paluxy, TX (USA)]

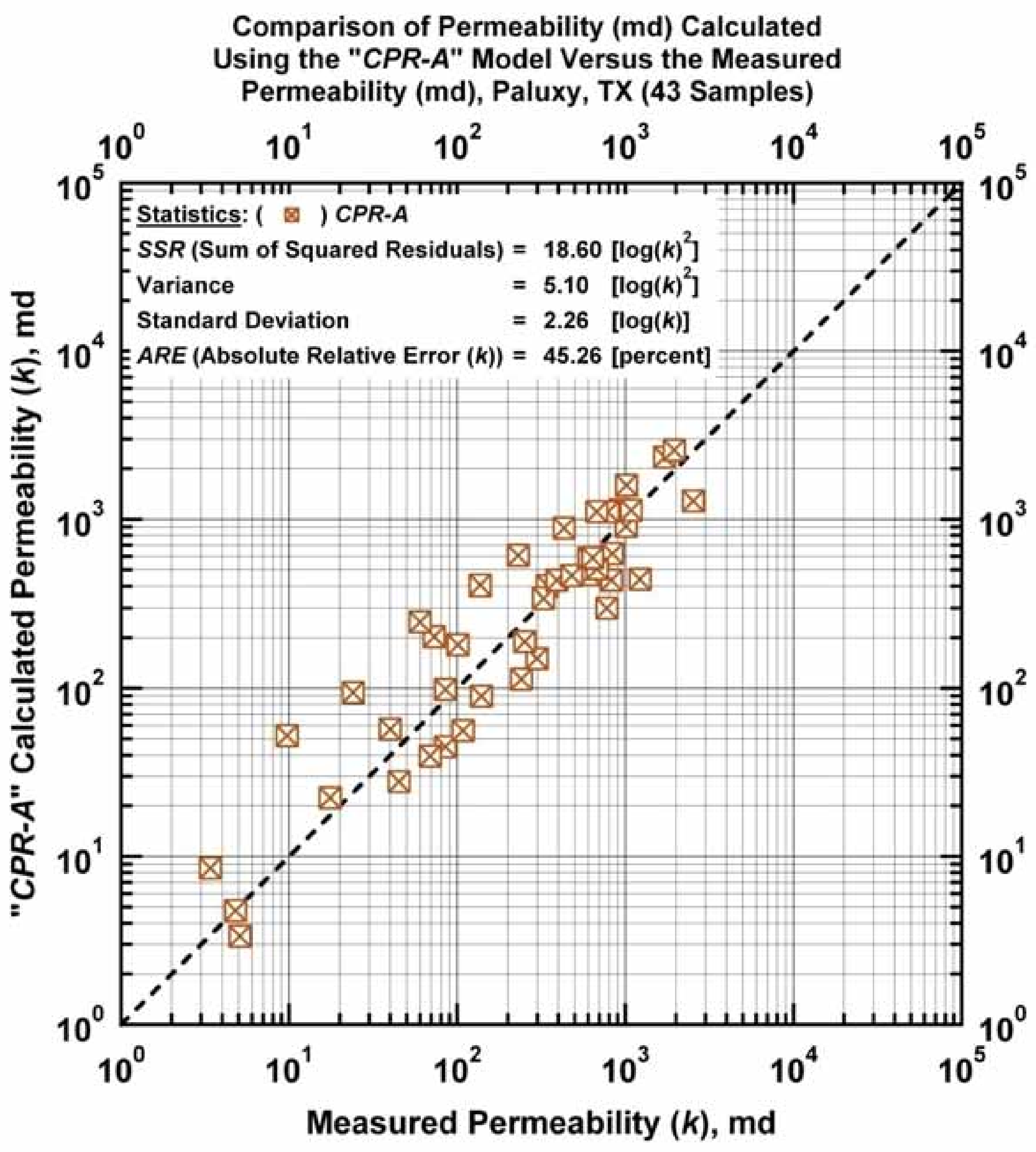

Figure J.2a — Model *CPJ-A*: calculated versus measured permeability. [*Case*: Paluxy, TX (USA)]

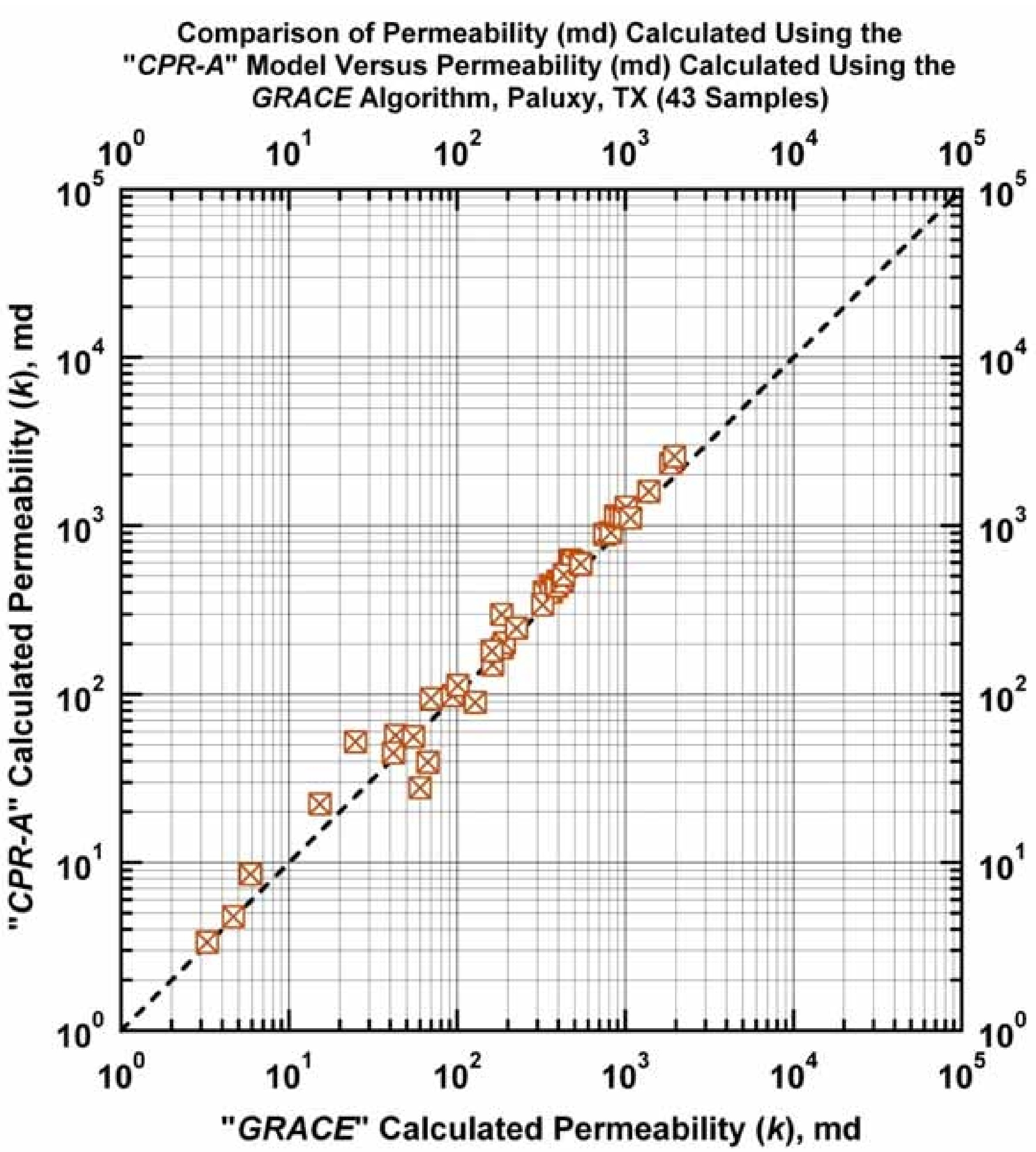

Figure J.2b — Model *CPJ-A*: Permeability calculated using Model *CPJ-A* versus permeability calculated using the *GRACE* Algorithm. [*Case*: Paluxy, TX (USA)]

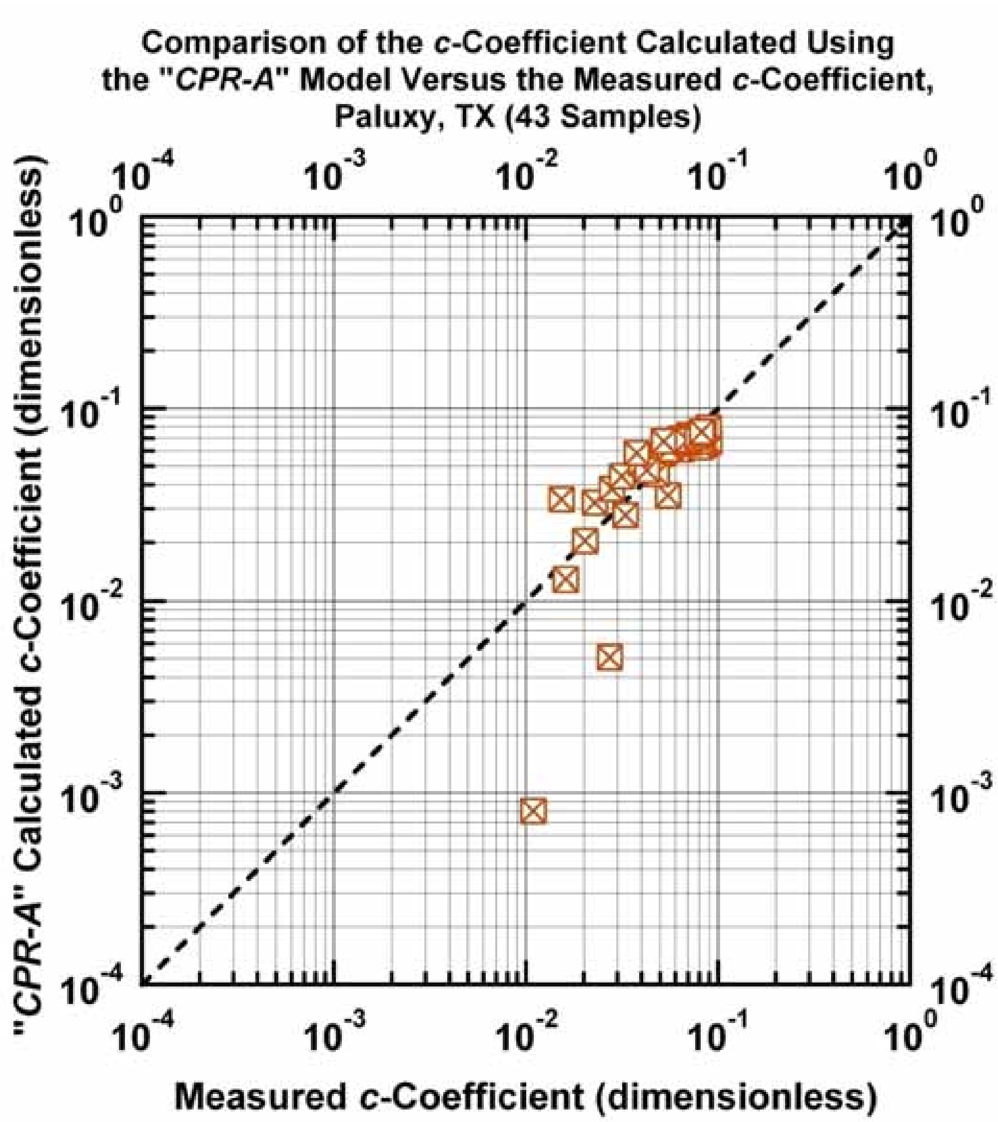

Figure J.2c — Model *CPJ-A*: Calculated *c*-function values versus measured *c*-function values. [*Case*: Paluxy, TX (USA)]

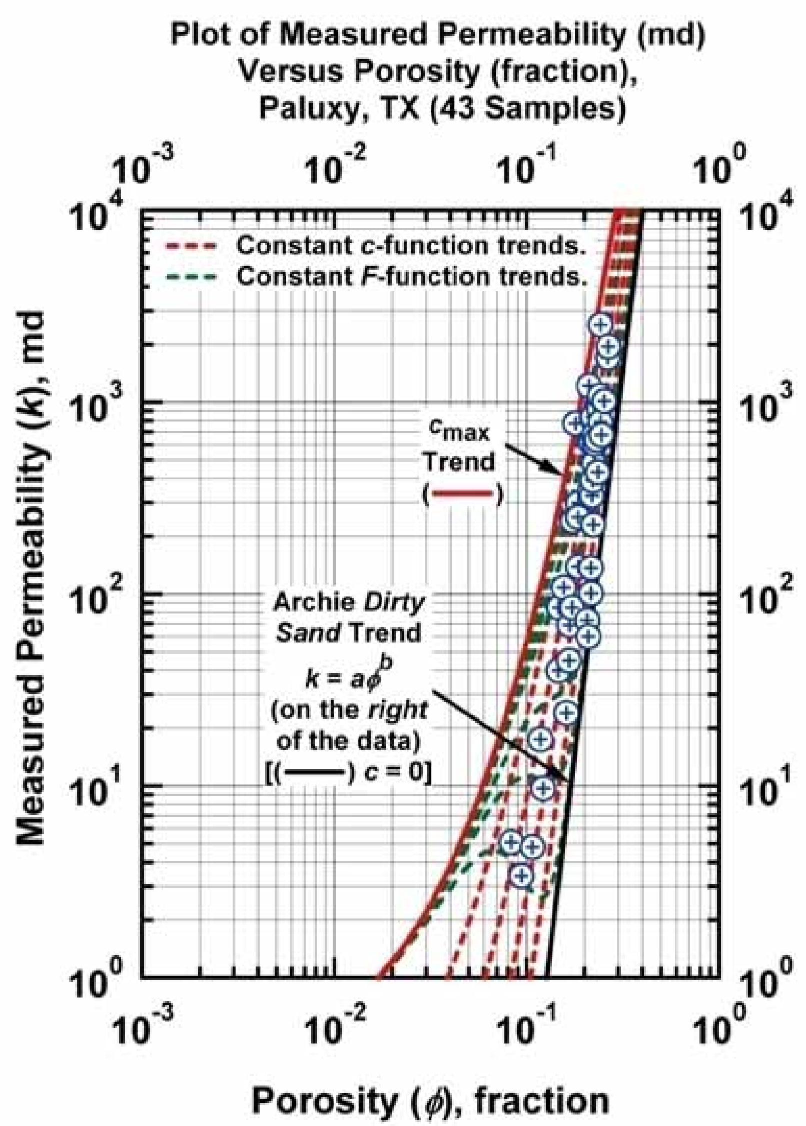

Figure J.3a — Model *CPJ-B*: $k = a(\phi + c)^b \quad c = c_{max} \exp[-c_1 \phi^{c_2} F^{c_3}]$ — "Clean Sand" Plot (log-log format) — Archie "Dirty Sand" trend is given by the straight-line trend at the far right of the data (power law model). [*Case*: Paluxy, TX (USA)]

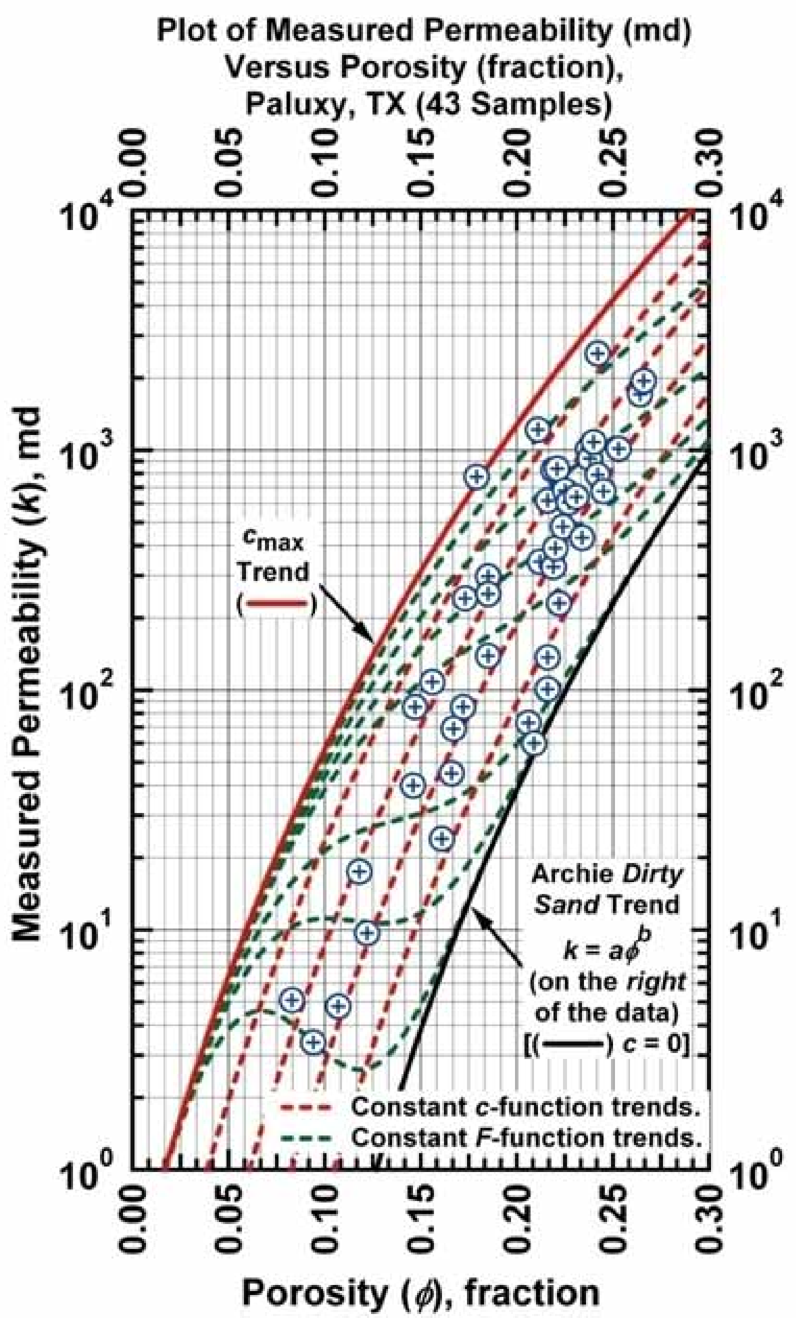

Figure J.3b — Model *CPJ-B*: $k = a(\phi + c)^b$ $\quad c = c_{\max} \exp[-c_1\phi^{c_2} F^{c_3}]$ — "Dirty Sand" Plot (semilog format) — Archie "Dirty Sand" trend is given by the curved trend at the far right of the data (power law model). [*Case*: Paluxy, TX (USA)]

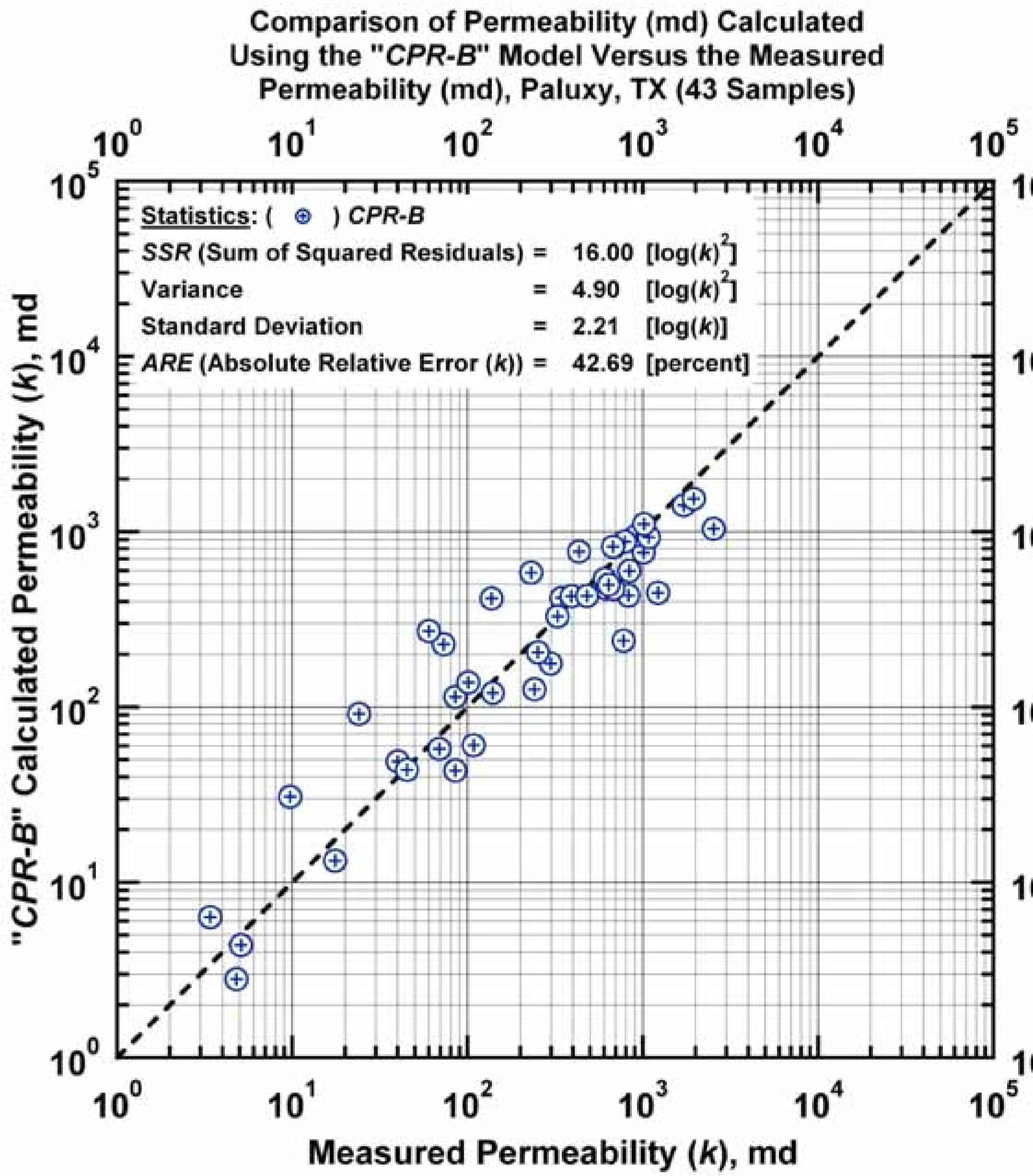

Figure J.4a — Model *CPJ-B*: calculated versus measured permeability. [*Case*: Paluxy, TX (USA)]

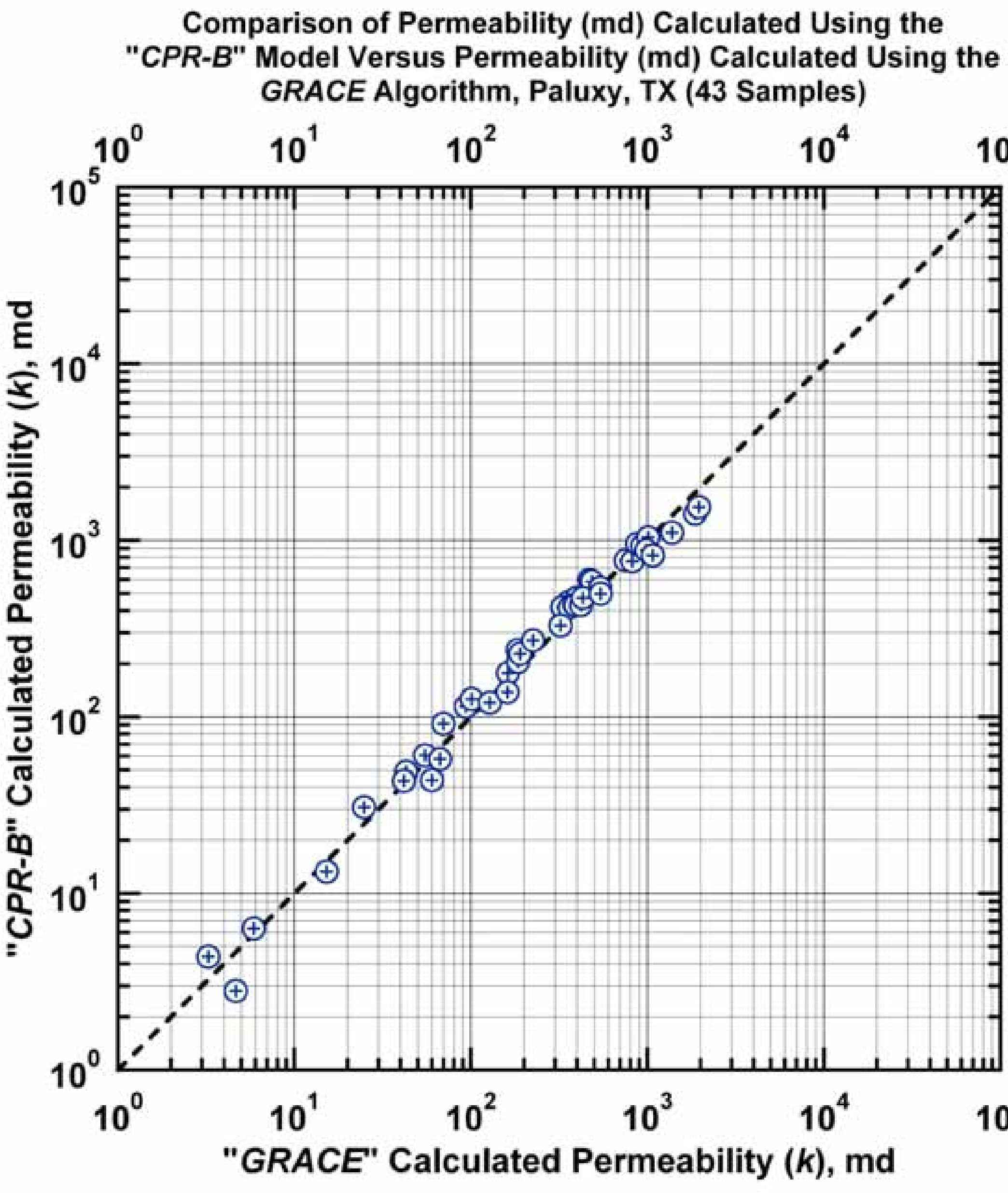

Figure J.4b — Model *CPJ-B*: Permeability calculated using Model *CPJ-B* versus permeability calculated using the *GRACE* Algorithm. [*Case*: Paluxy, TX (USA)]

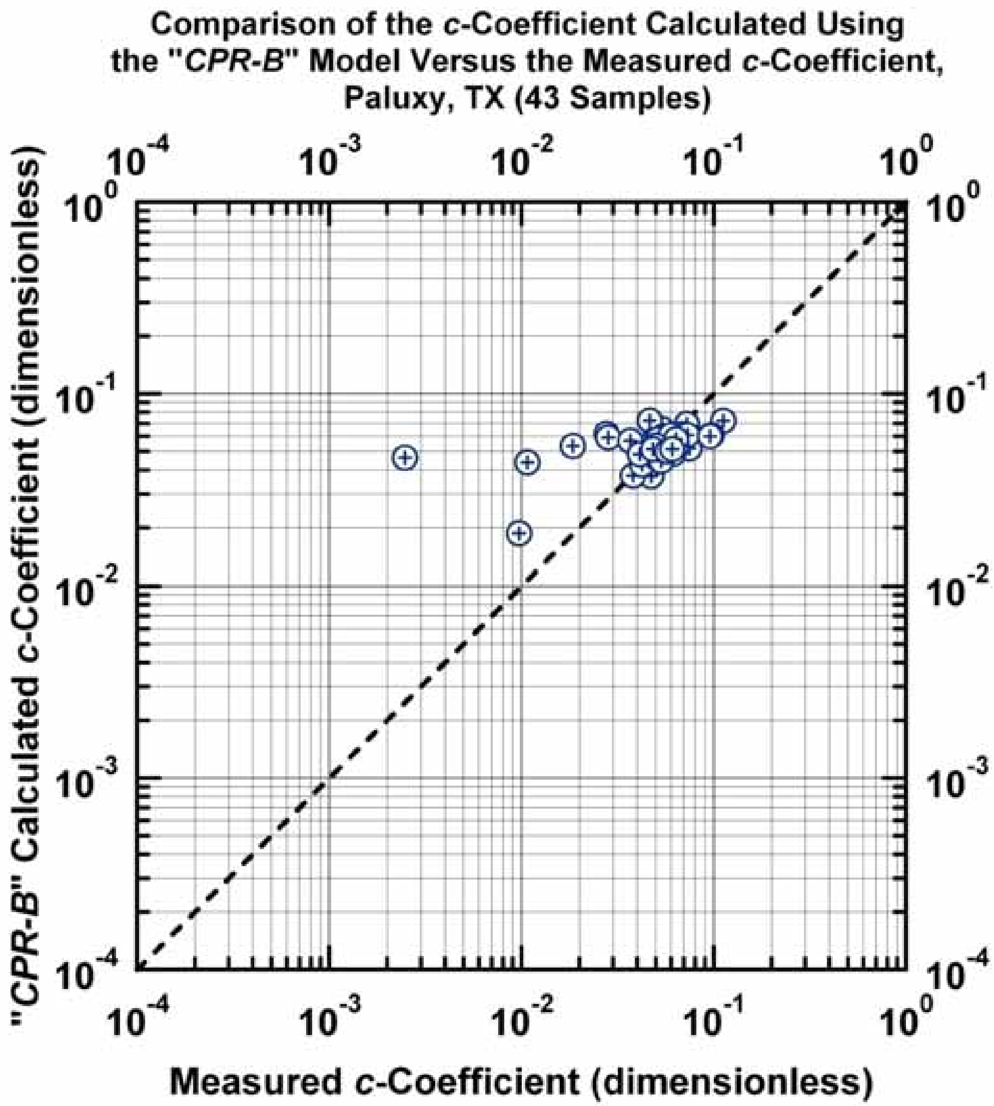

Figure J.4c — Model *CPJ-B*: Calculated *c*-function values versus measured *c*-function values. [*Case*: Paluxy, TX (USA)]

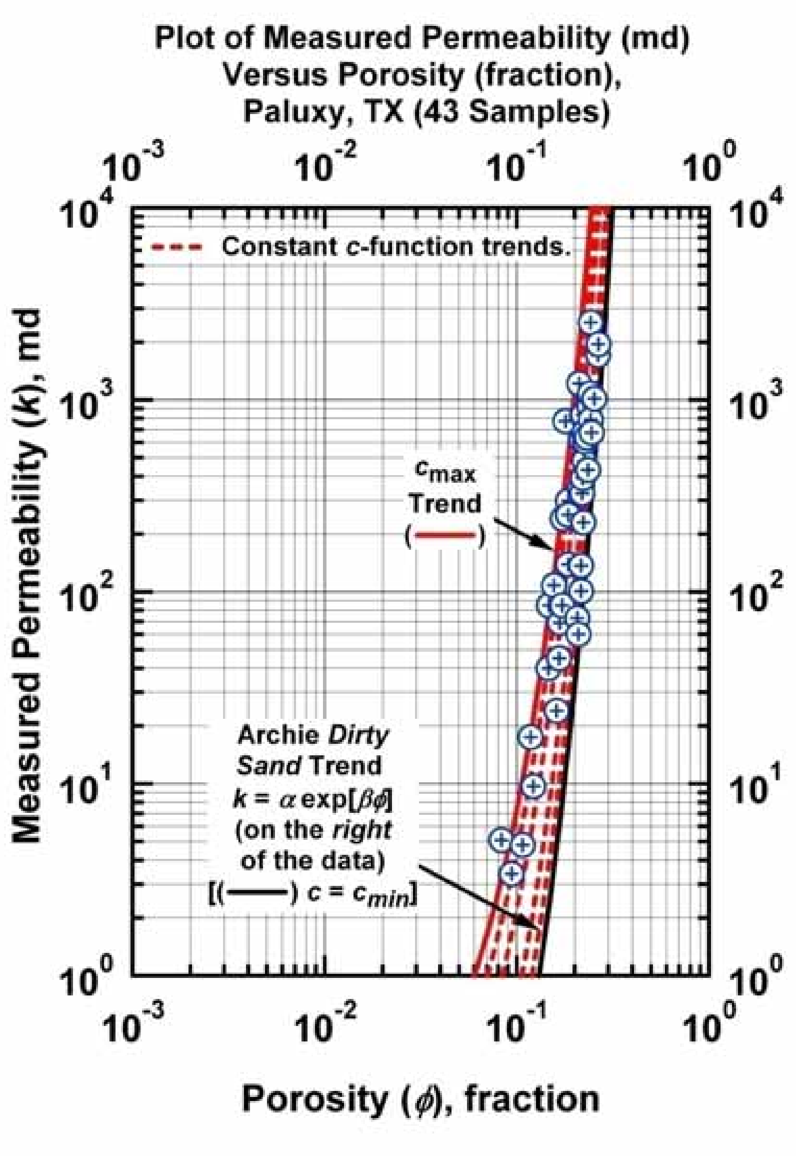

Figure J.5a — Model *CPJ-C*: $k = c\exp[\beta\phi]$ $c = c_{max}\exp[-c_1\phi^{c_2}F^{c_3}]$ — "Clean Sand" Plot (log-log format) — Archie "Dirty Sand" trend is given by the curved trend at the far right of the data (exponential model). [*Case*: Paluxy, TX (USA)]

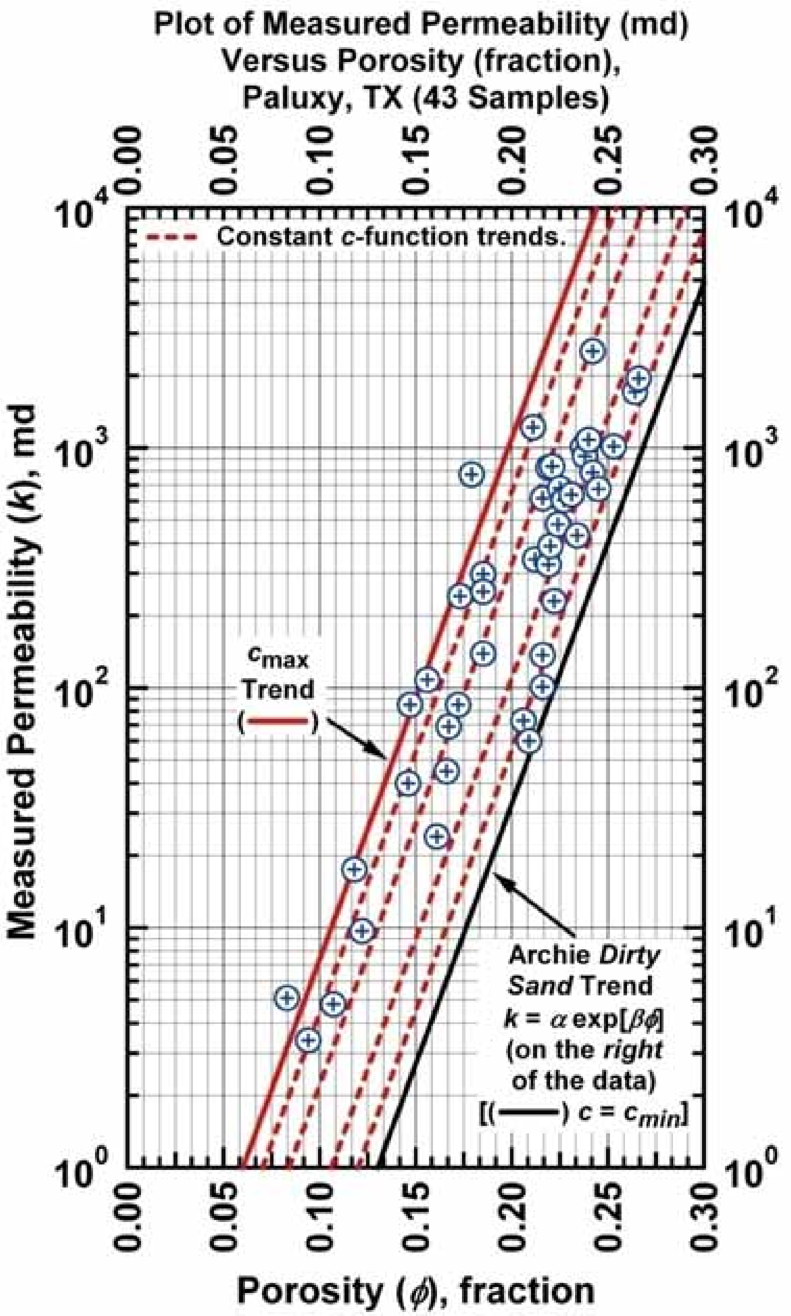

Figure J.5b — Model *CPJ-C*: $k = c\exp[\beta\phi]$ $c = c_{\max}\exp[-c_1\phi^{c_2}F^{c_3}]$ — "Dirty Sand" Plot (semilog format) — Archie "Dirty Sand" trend is given by the straight-line trend at the far right of the data (exponential model). [*Case*: Paluxy, TX (USA)]

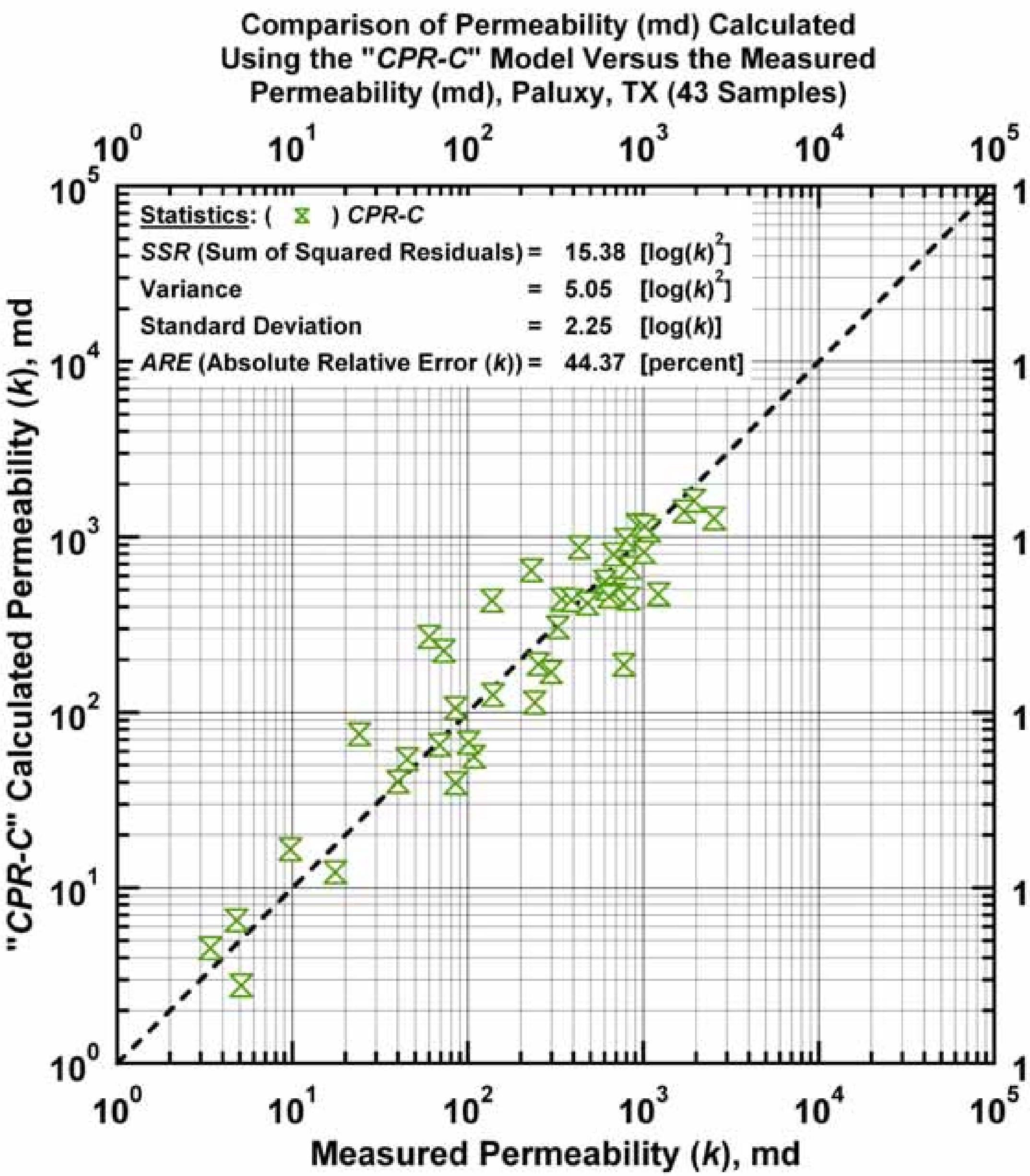

Figure J.6a — Model *CPJ-C*: calculated versus measured permeability. [*Case*: Paluxy, TX (USA)]

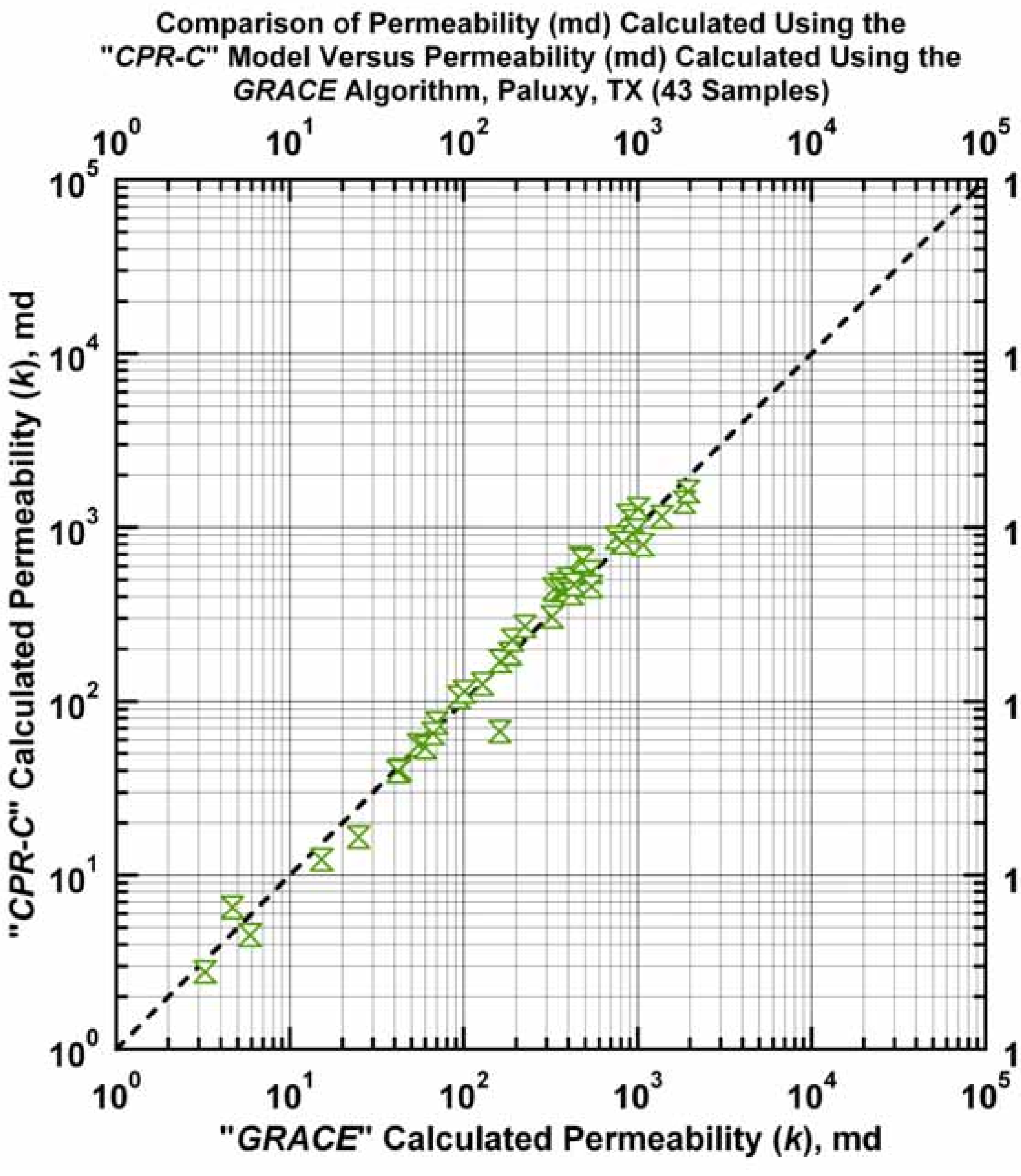

Figure J.6b — Model *CPJ-C*: Permeability calculated using Model *CPJ-C* versus permeability calculated using the *GRACE* Algorithm. [*Case*: Paluxy, TX (USA)]

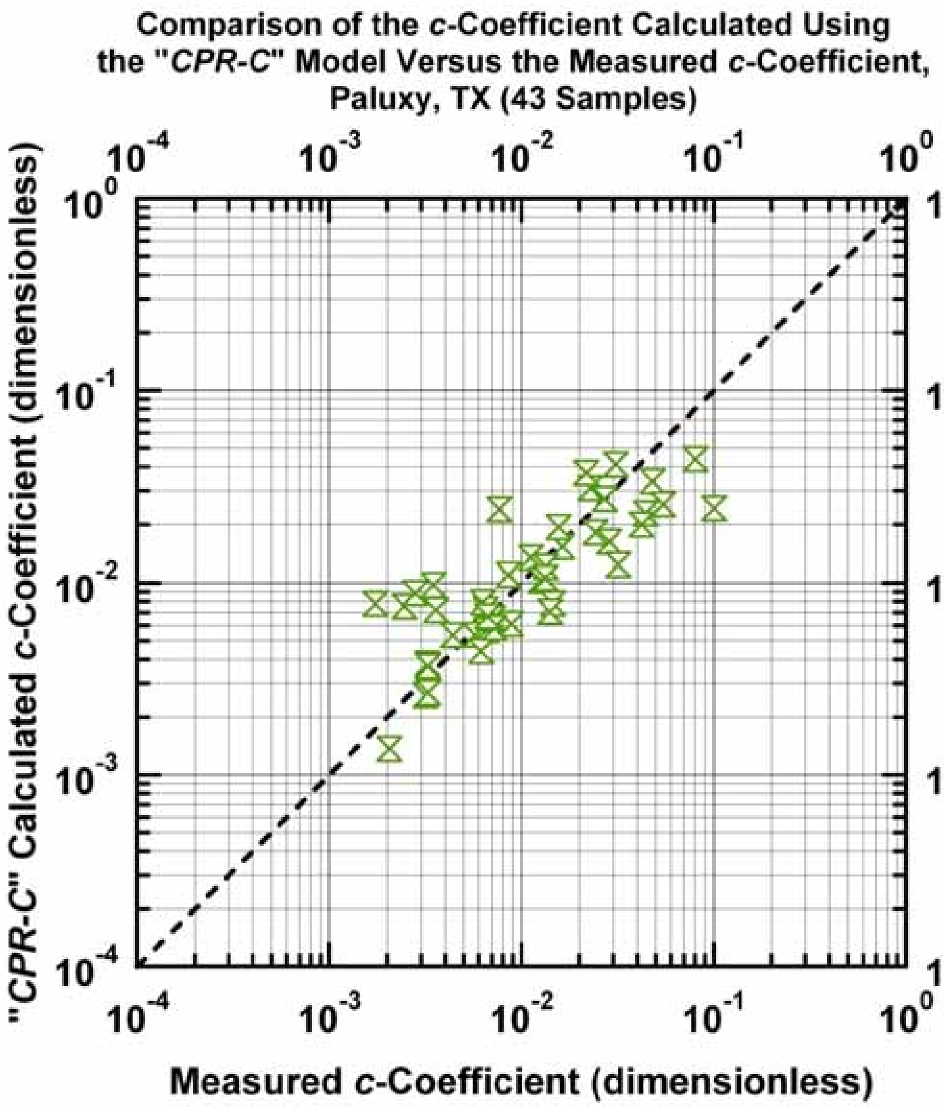

Figure J.6c — Model *CPJ-C*: Calculated *c*-function values versus measured *c*-function values. [*Case*: Paluxy, TX (USA)]

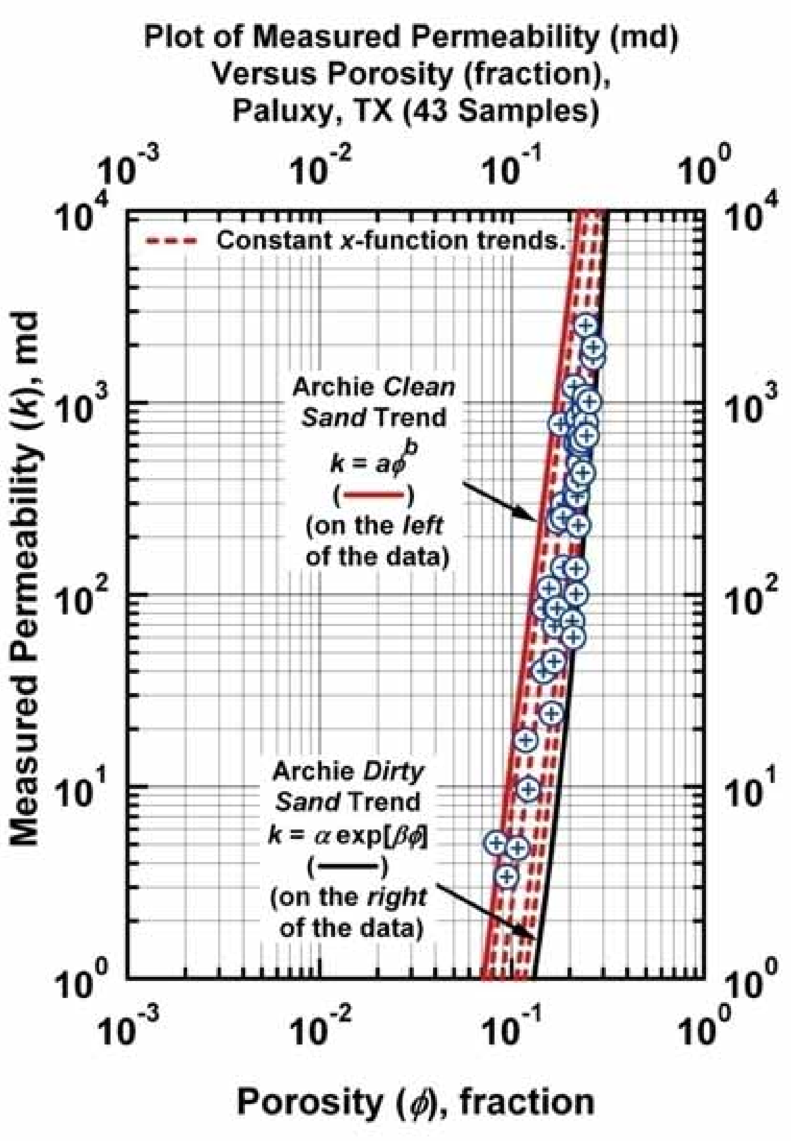

Figure J.7a — Model *CPJ-D*: $k = xa\phi^b + (1-x)\alpha \exp[\beta\phi] \quad [0 \le x \le 1]$ — *Weighted Power Law-Exponential Model* used to correlate permeability (k) and porosity (ϕ). "Clean Sand" Plot — Archie "Clean Sand" trend is given by the straight-line trend at the far left of the data (power law model). [*Case*: Paluxy, TX (USA)]

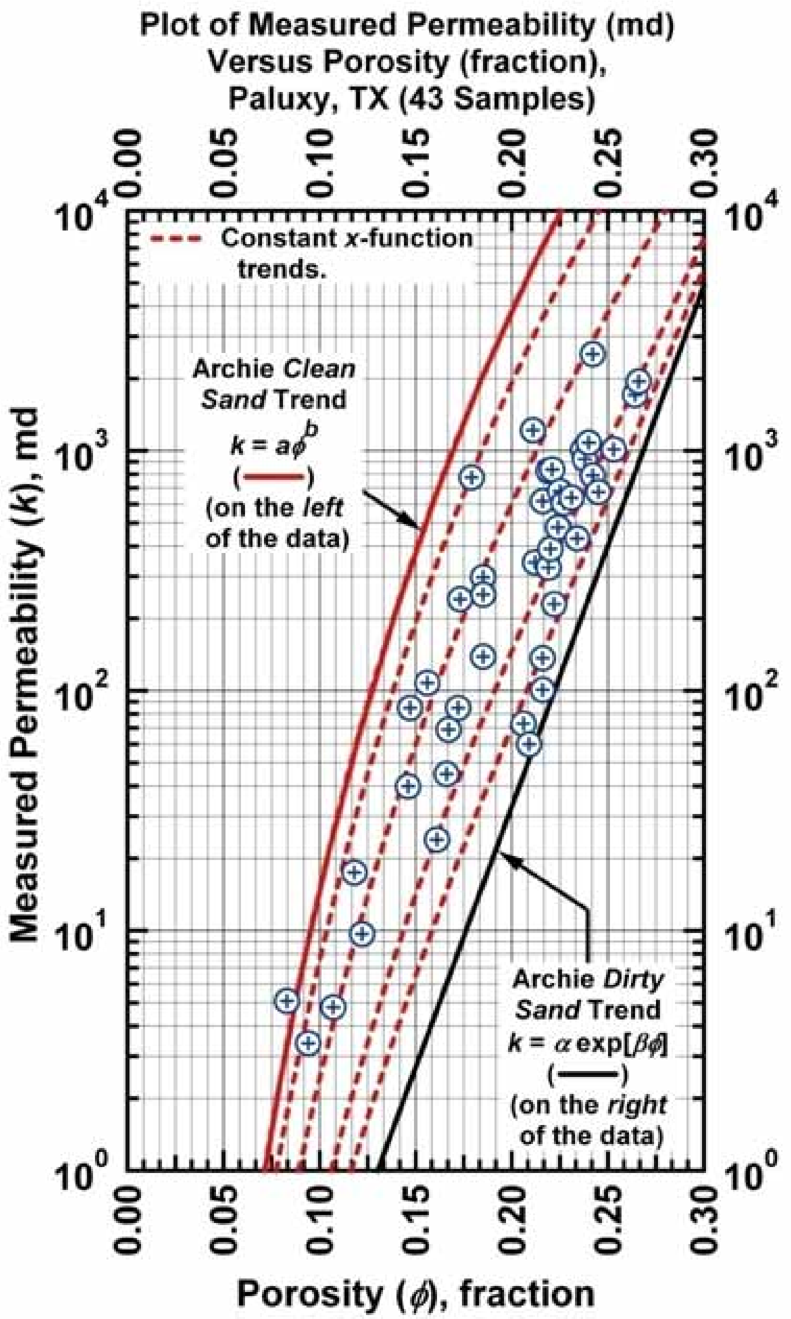

Figure J.7b — Model *CPJ-D*: $k = xa\phi^b + (1-x)\alpha\exp[\beta\phi]$ $[0 \le x \le 1]$ — *Weighted Power Law-Exponential Model* used to correlate permeability (k) and porosity (ϕ). "Dirty Sand" Plot — Archie "Dirty Sand" trend is given by the straight-line trend at the far right of the data (exponential model). [*Case*: Paluxy, TX (USA)]

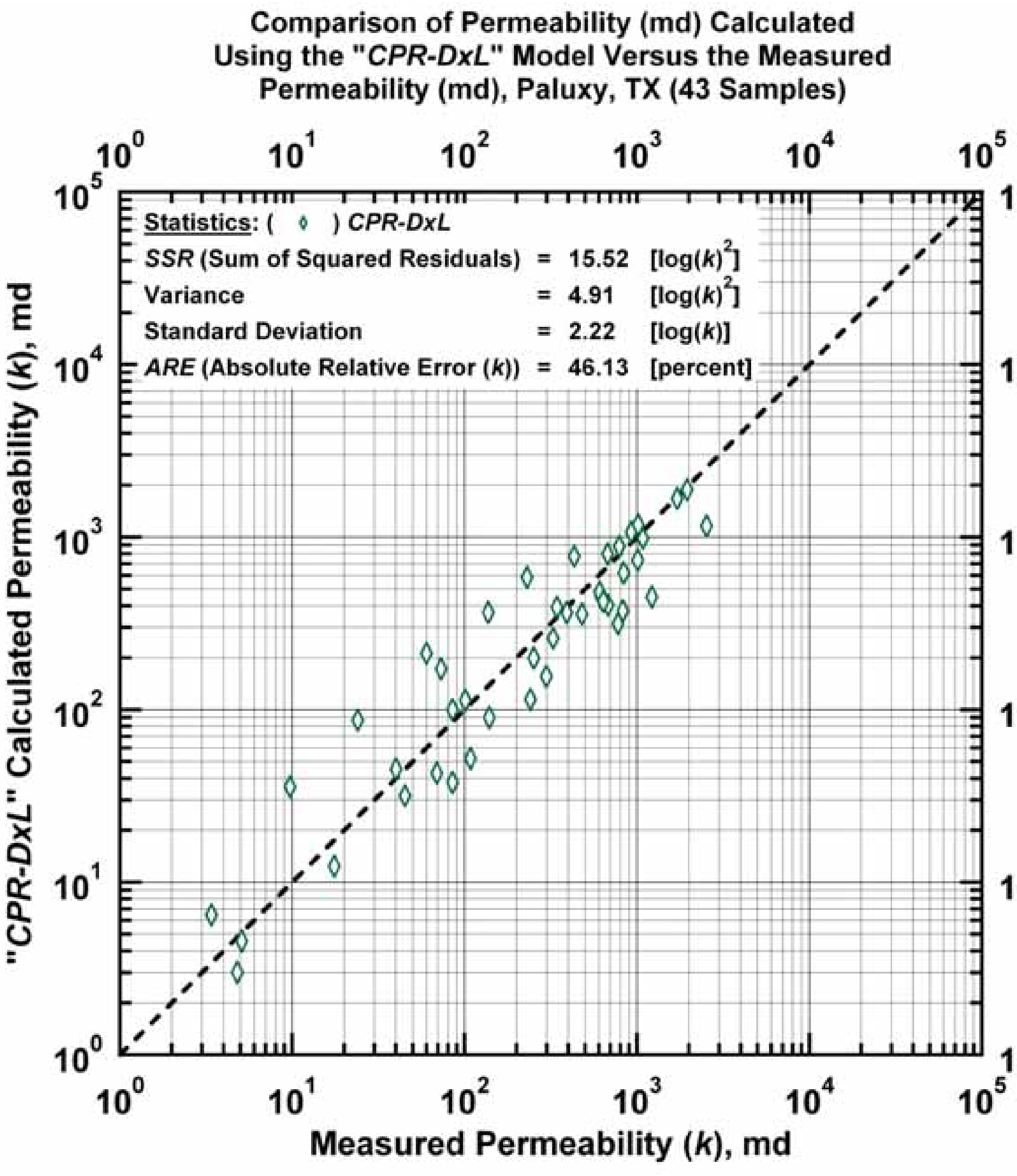

Figure J.8a — Model *CPJ-DxL*: Calculated versus measured permeability. [*Case*: Paluxy, TX (USA)]

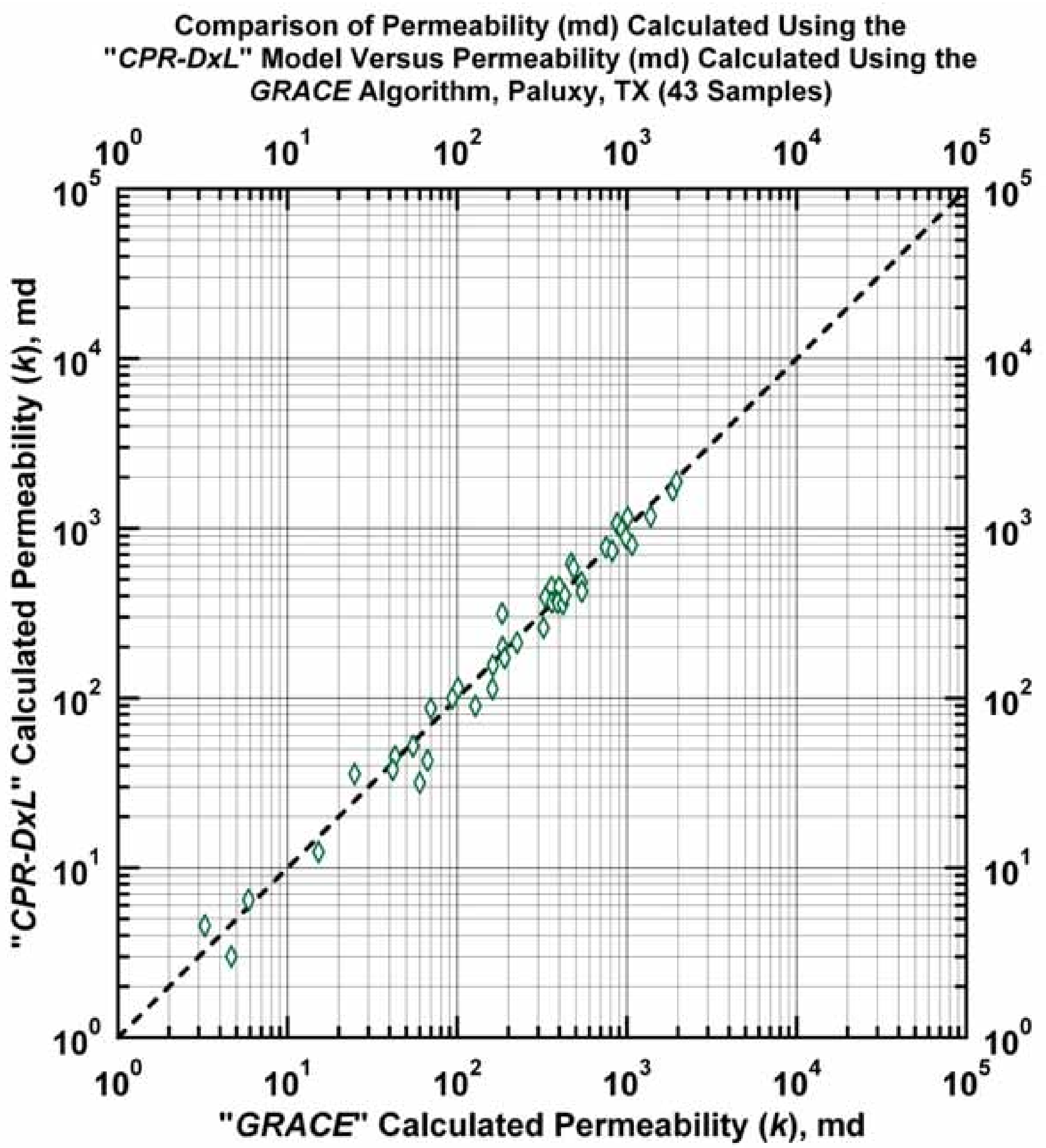

Figure J.8b — Model *CPJ-DxL*: Permeability calculated using Model *CPJ-C* versus permeability calculated using the *GRACE* Algorithm. [*Case*: Paluxy, TX (USA)]

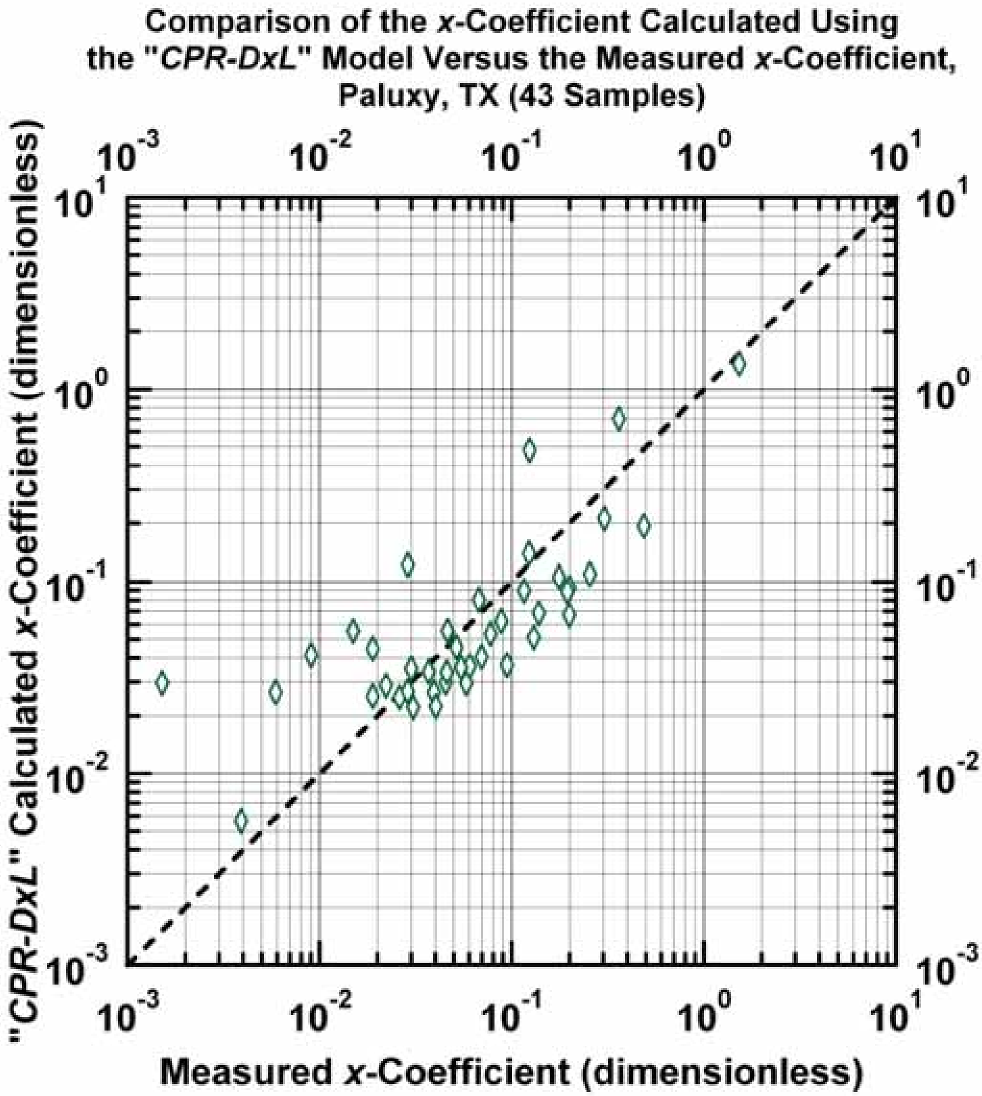

Figure J.8c — Model *CPJ-DxL*: Calculated *x*-function weight values versus measured *x*-function weight values. [*Case*: Paluxy, TX (USA)]

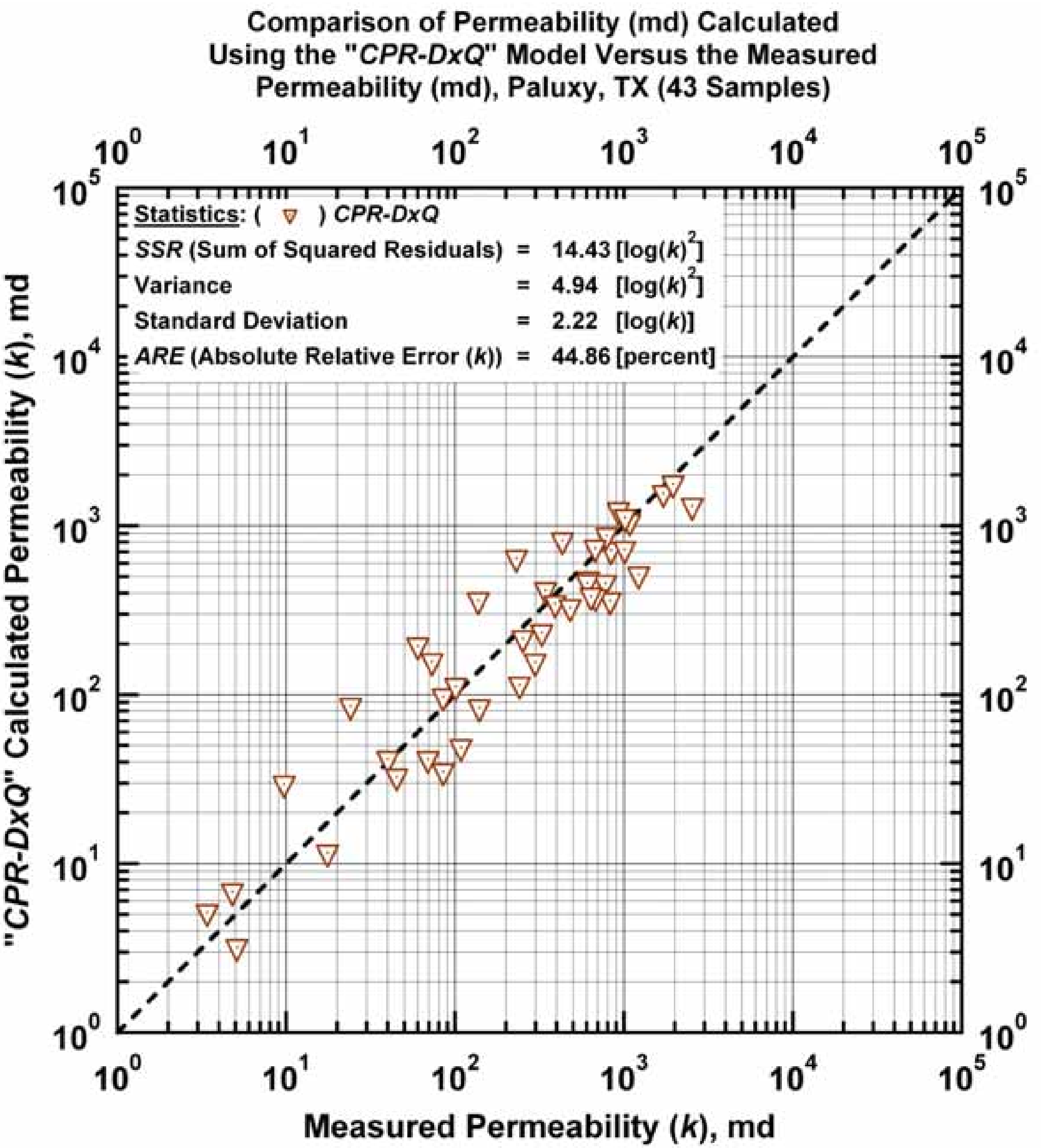

Figure J.9a — Model *CPJ-DxQ*: Calculated versus measured permeability. [*Case*: Paluxy, TX (USA)]

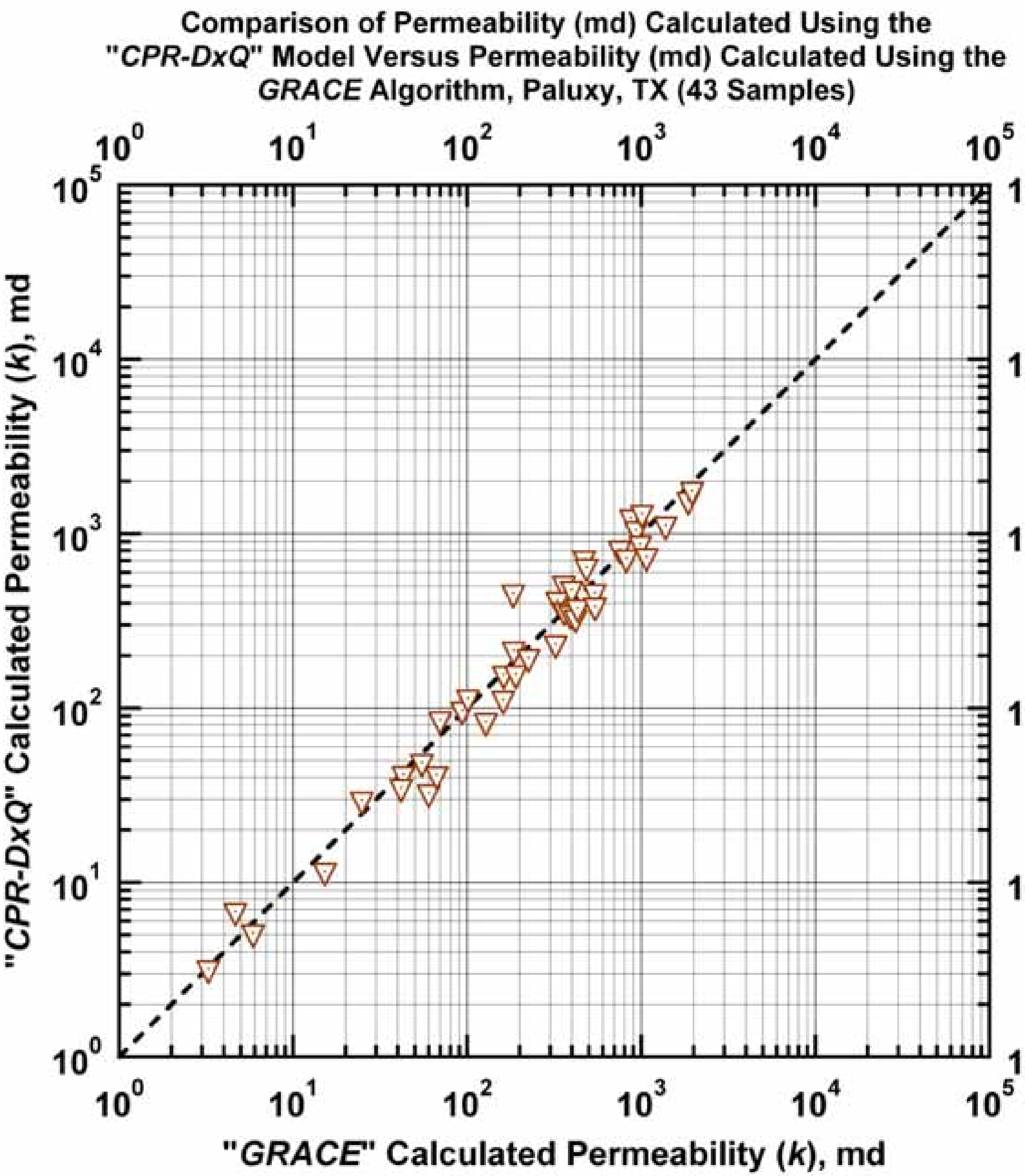

Figure J.9b — Model *CPJ-DxQ*: Permeability calculated using Model *CPJ-C* versus permeability calculated using the *GRACE* Algorithm. [*Case*: Paluxy, TX (USA)]

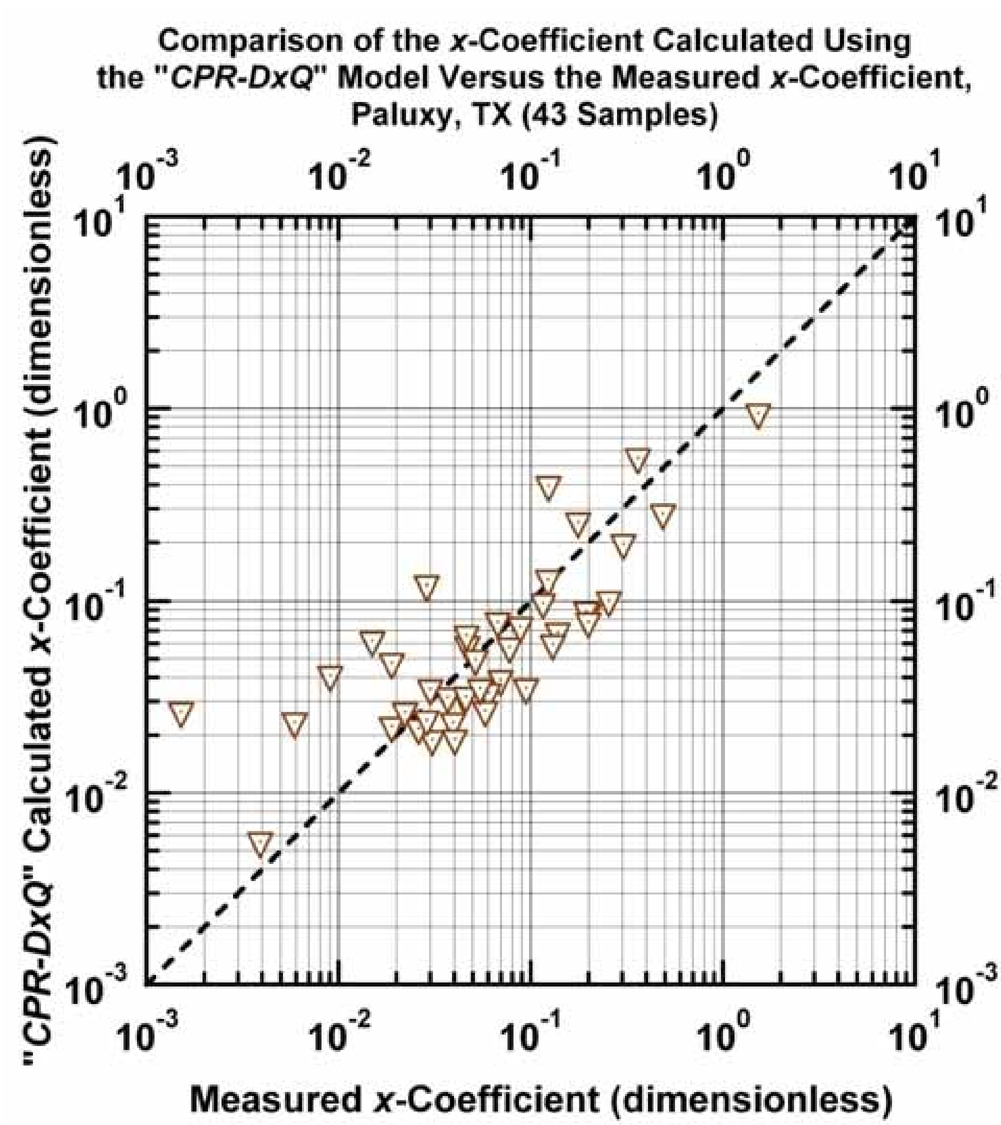

Figure J.9c — Model *CPJ-DxQ*: Calculated *x*-function weight values versus measured *x*-function weight values. [*Case*: Paluxy, TX (USA)]

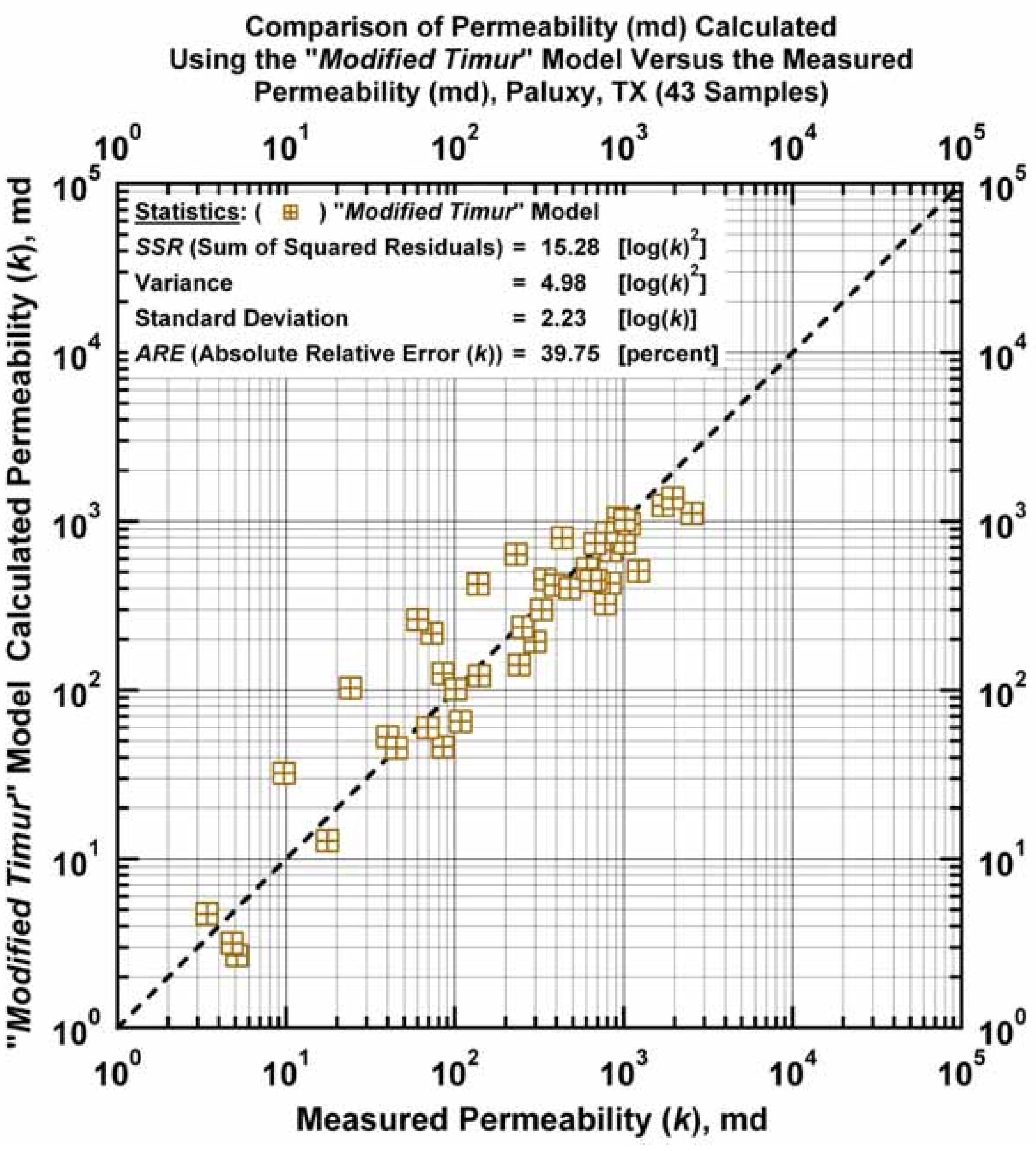

Figure J.10a — "Modified Timur Model:" Calculated versus measured permeability. [*Case*: Paluxy, TX (USA)]

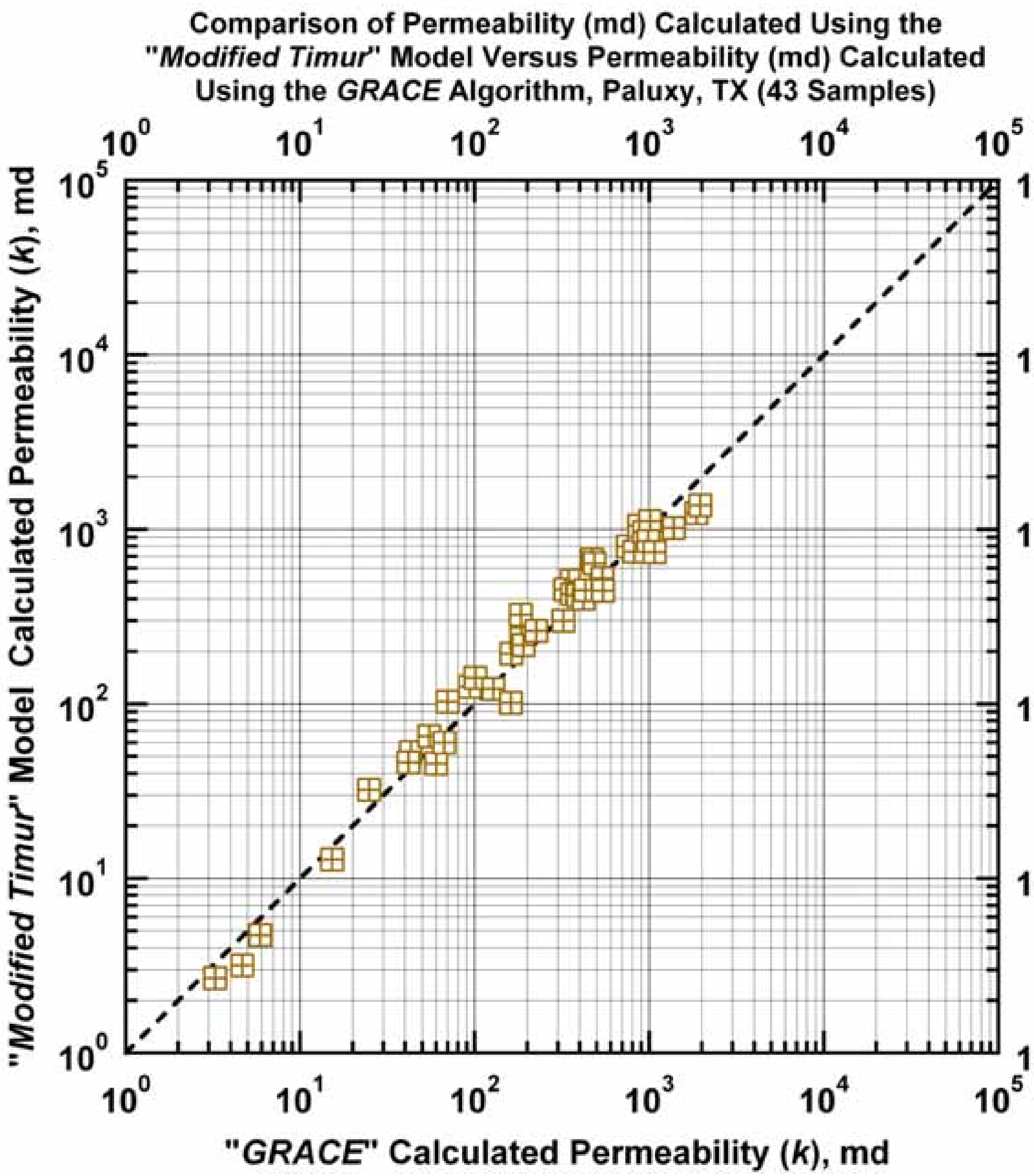

Figure J.10b — "Modified Timur Model:" Permeability calculated using the "Modified Timur Model" versus permeability calculated using the *GRACE* Algorithm. [*Case*: Paluxy, TX (USA)]

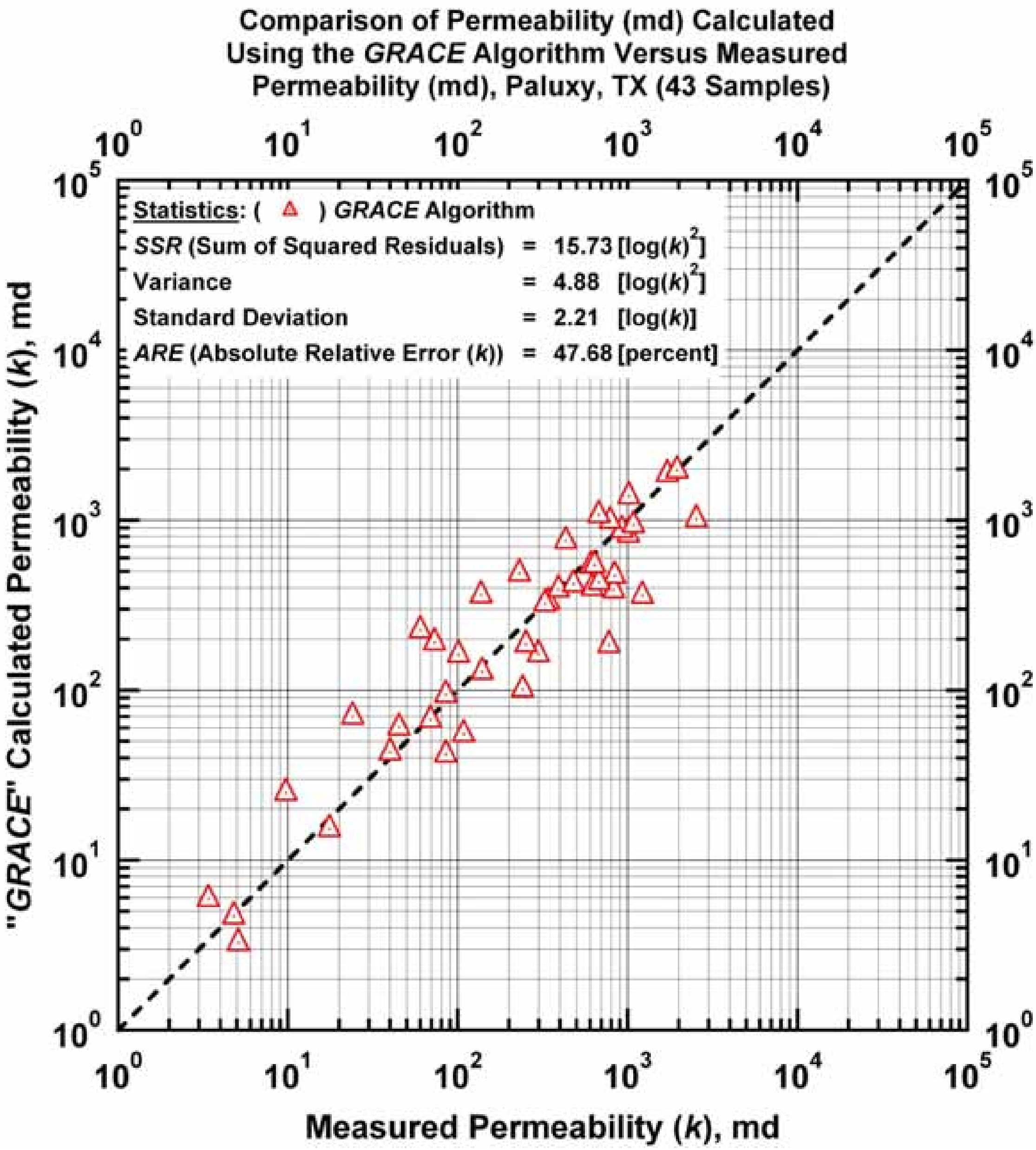

Figure J.11 — *GRACE* Model: Calculated versus measured permeability. [*Case*: Paluxy, TX (USA)]

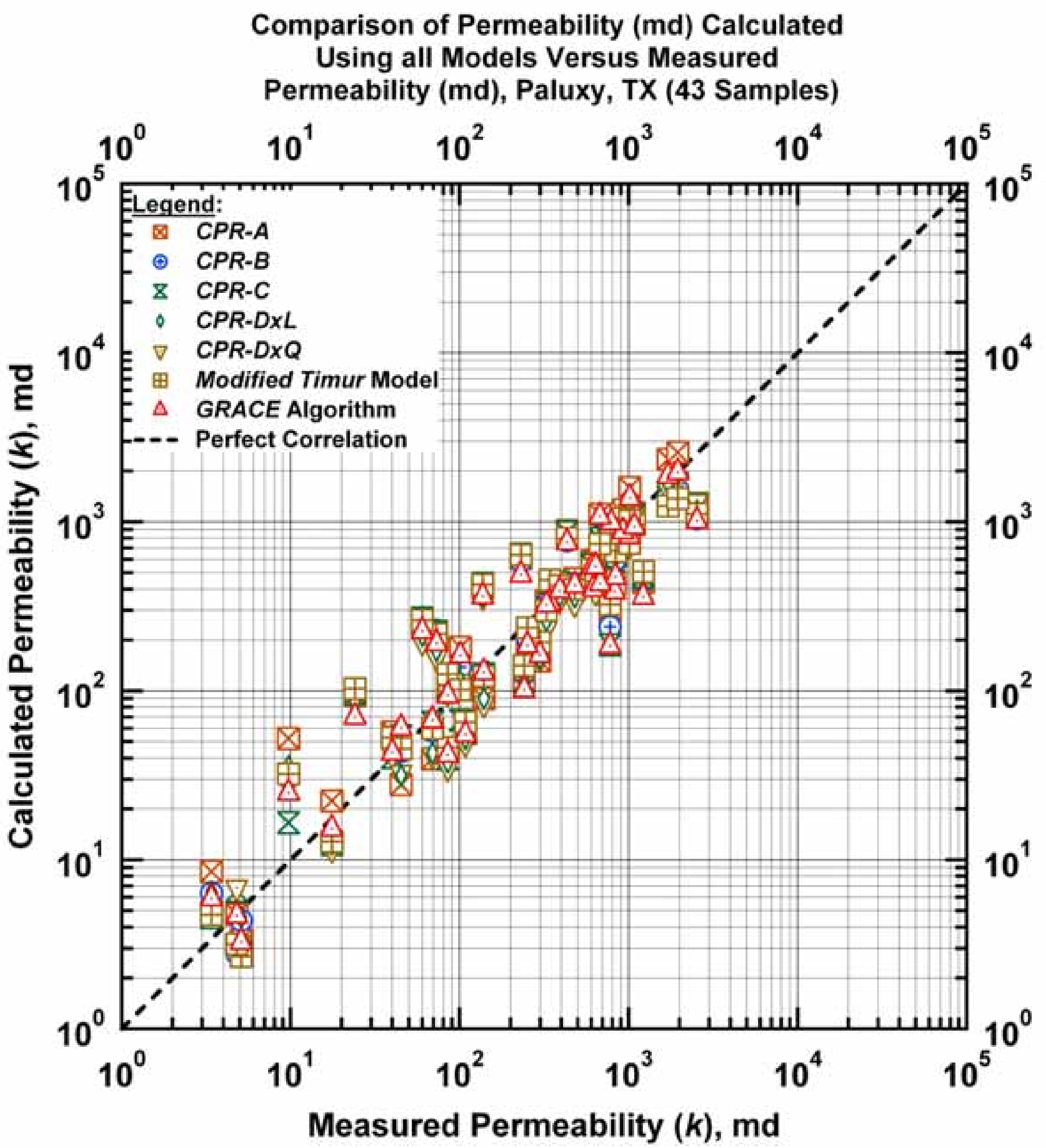

Figure J.12 — All Models: Calculated versus measured permeability. [*Case*: Paluxy, TX (USA)]

VITA

Name: Adil Ahmed Siddiqui

Permanent Address: A-301/C, Grey Garden,
Gulistan-e-Jauhar, Block-16
Karachi, 75290
PAKISTAN

E-mail Address: sir_adilahmed@yahoo.com

Education: Texas A&M University, College Station, Texas, USA
Master of Science Degree in Petroleum Engineering
August 2008

IFP School, Rueil-Malmaison, France
Master of Science Degree in Reservoir Geoscience and Engineering
Expected September 2008

National University of Sciences & Technology, Karachi, Pakistan
Bachelor of Engineering Degree in Mechanical Engineering
June 2005

Affiliations: Society of Petroleum Engineers